



Universitat Autònoma de Barcelona

LOOKING FOR NEW PHYSICS IN THE

$\bar{B}_d^0 \rightarrow \bar{K}^{*0}(\rightarrow K\pi) \ell^+\ell^-$ DECAY MODE

AT LARGE RECOIL

Marc Ramon Bohigas

ADVERTIMENT. L'accés als continguts d'aquesta tesi doctoral i la seva utilització ha de respectar els drets de la persona autora. Pot ser utilitzada per a consulta o estudi personal, així com en activitats o materials d'investigació i docència en els termes establerts a l'art. 32 del Text Refós de la Llei de Propietat Intel·lectual (RDL 1/1996). Per altres utilitzacions es requereix l'autorització prèvia i expressa de la persona autora. En qualsevol cas, en la utilització dels seus continguts caldrà indicar de forma clara el nom i cognoms de la persona autora i el títol de la tesi doctoral. No s'autoritza la seva reproducció o altres formes d'explotació efectuades amb finalitats de lucre ni la seva comunicació pública des d'un lloc aliè al servei TDX. Tampoc s'autoritza la presentació del seu contingut en una finestra o marc aliè a TDX (framing). Aquesta reserva de drets afecta tant als continguts de la tesi com als seus resums i índexs.

ADVERTENCIA. El acceso a los contenidos de esta tesis doctoral y su utilización debe respetar los derechos de la persona autora. Puede ser utilizada para consulta o estudio personal, así como en actividades o materiales de investigación y docencia en los términos establecidos en el art. 32 del Texto Refundido de la Ley de Propiedad Intelectual (RDL 1/1996). Para otros usos se requiere la autorización previa y expresa de la persona autora. En cualquier caso, en la utilización de sus contenidos se deberá indicar de forma clara el nombre y apellidos de la persona autora y el título de la tesis doctoral. No se autoriza su reproducción u otras formas de explotación efectuadas con fines lucrativos ni su comunicación pública desde un sitio ajeno al servicio TDR. Tampoco se autoriza la presentación de su contenido en una ventana o marco ajeno a TDR (framing). Esta reserva de derechos afecta tanto al contenido de la tesis como a sus resúmenes e índices.

WARNING. The access to the contents of this doctoral thesis and its use must respect the rights of the author. It can be used for reference or private study, as well as research and learning activities or materials in the terms established by the 32nd article of the Spanish Consolidated Copyright Act (RDL 1/1996). Express and previous authorization of the author is required for any other uses. In any case, when using its content, full name of the author and title of the thesis must be clearly indicated. Reproduction or other forms of for profit use or public communication from outside TDX service is not allowed. Presentation of its content in a window or frame external to TDX (framing) is not authorized either. These rights affect both the content of the thesis and its abstracts and indexes.




Universitat Autònoma de Barcelona


LOOKING FOR NEW PHYSICS IN THE


$\bar{B}_d^0 \rightarrow \bar{K}^{*0}(\rightarrow K\pi)\ell^+\ell^-$ DECAY MODE

AT LARGE RECOIL

Marc Ramon Bohigas

ADVERTIMENT. L'accés als continguts d'aquesta tesi queda condicionat a l'acceptació de les condicions d'ús establertes per la següent llicència Creative Commons:  http://cat.creativecommons.org/?page_id=184

ADVERTENCIA. El acceso a los contenidos de esta tesis queda condicionado a la aceptación de las condiciones de uso establecidas por la siguiente licencia Creative Commons:  <http://es.creativecommons.org/blog/licencias/>

WARNING. The access to the contents of this doctoral thesis it is limited to the acceptance of the use conditions set by the following Creative Commons license:  <https://creativecommons.org/licenses/?lang=en>

LOOKING FOR NEW PHYSICS IN THE
 $\overline{B}_d^0 \rightarrow \overline{K}^{*0}(\rightarrow K\pi) \ell^+ \ell^-$ DECAY MODE
AT LARGE RECOIL

Marc Ramon Bohigas

Doctoral thesis carried out under the supervision of Dr. Joaquim Matias Espona

Unitat de Física Teòrica
Departament de Física
Universitat Autònoma de Barcelona

September 2012



Submitted in partial fulfilment of the requirements for the degree of Doctor of Philosophy.

Contents

Preface	1
Introduction	3
I Theoretical background	9
1 Effective Hamiltonians in B physics	11
1.1 The weak effective Hamiltonian	11
1.1.1 Energy scales	11
1.1.2 The weak effective Hamiltonian in the Standard Model	11
1.1.3 The weak effective Hamiltonian beyond the Standard Model	13
1.2 Introduction to heavy quark effective theory	14
1.2.1 Derivation of the heavy quark effective theory Lagrangian	14
1.2.2 Remarks	17
1.2.3 The Isgur-Wise function	17
1.3 Introduction to large energy effective theory	19
1.3.1 Derivation of the large energy effective theory Lagrangian	19
1.3.2 Remarks	22
2 Hard exclusive processes, light-cone distribution amplitudes and sum rules	23
2.1 Introduction to hard exclusive processes	23
2.2 Light-cone distribution amplitudes	26
2.2.1 Scale dependence	26
2.2.2 Conformal partial waves expansion and asymptotic limit	27
2.2.3 Meson light-cone distribution amplitudes	28
2.3 Introduction to QCD sum rules	30
2.3.1 Path A	31
2.3.2 Path B	33

2.3.3	The quark-hadron duality and the matching of paths A and B	35
2.3.4	Final considerations	37
2.4	Introduction to light-cone sum rules	38
2.4.1	Path A	38
2.4.2	Path B	41
2.4.3	The quark-hadron duality and the matching of paths A and B	41
2.4.4	Final considerations	42
3	The non-perturbative quantities: form factors and decay amplitudes	43
3.1	Meson form factors	43
3.1.1	Introduction	43
3.1.2	Guidelines for the calculation of $B \rightarrow P, V$ form factors from LCSRs . . .	46
3.1.3	Using effective field theories to establish relations among form factors . .	47
3.1.4	Heavy-to-light form factors in HQET/LEET	49
3.2	Meson decay constants	51
4	Factorisation of matrix elements	53
4.1	Overview of processes involving a heavy meson decay	53
4.2	Naïve factorisation	55
4.2.1	Framework	55
4.2.2	Drawbacks and theoretical justification	56
4.2.3	Generalised factorisation approaches	57
4.3	General concepts on QCD factorisation	58
4.3.1	QCDF at work for purely hadronic decays	60
4.4	Interaction scales	63
4.5	Strong points and shortcomings of QCD factorisation	64
II	The $\bar{B}_d^0 \rightarrow \bar{K}^{*0}(\rightarrow K\pi)\ell^+\ell^-$ decay mode at large recoil	67
5	Kinematics of a 4-body decay	69
5.1	Definitions	69
5.2	Relations	72
5.2.1	General relations	72
5.2.2	Relations in the rest frame of the decaying particle	73
5.2.3	Relations in the rest frame of a diparticle	73
5.2.4	Relations involving θ_{ij}	75
5.2.5	Relations involving ϕ	76
5.2.6	Summary of Lorentz invariant scalar products of P and Q	78
5.3	Phase space integration	78

6	Dynamics	83
6.1	The weak effective $b \rightarrow s \ell^+ \ell^-$ Hamiltonian	83
6.1.1	Standard Model contributions	84
6.1.2	New physics contributions	88
6.2	The $\bar{B}_d^0 \rightarrow \bar{K}^{*0}(\rightarrow K\pi) \ell^+ \ell^-$ matrix element	90
6.2.1	Building the matrix element	90
6.2.2	The resonant decay	91
6.3	The $\bar{B} \rightarrow \bar{K}^*$ form factors	95
6.4	The transversity amplitudes	99
6.4.1	The origin of the transversity amplitudes	99
6.4.2	Transversity amplitudes at large recoil	104
6.5	The full angular decay distribution	105
6.5.1	How to obtain it	105
6.5.2	The full angular decay distribution for $\bar{B}_d^0 \rightarrow \bar{K}^{*0}(\rightarrow K^- \pi^+) \ell^+ \ell^-$ and its CP -conjugate process	108
6.5.3	The angular coefficients	109
6.6	The $O(\alpha_s)$ corrections from QCD factorisation	111
6.6.1	Motivation and general aspects	111
6.6.2	Assumptions and range of applicability of QCDF to the $\bar{B}_d^0 \rightarrow \bar{K}^{*0} \ell^+ \ell^-$ decay mode	113
6.6.3	Diagrams contributing to CKM-allowed terms	114
6.6.4	The non-perturbative amplitudes $\mathcal{T}_{\parallel}^{(i)}(q^2)$ and $\mathcal{T}_{\perp}^{(i)}(q^2)$	116
6.6.5	The inclusion of power-suppressed corrections to $\mathcal{T}_{\perp, \parallel}^{(i)}(q^2)$	121
6.6.6	Final expressions for $\mathcal{T}_{\perp, \parallel}^{(i)}(q^2)$ including power-suppressed corrections	122
6.6.7	Final considerations	123
6.7	Including the $O(\alpha_s)$ corrections from QCDF into the transversity amplitudes	125
6.7.1	Comparison with other approaches	127
III	Epilogue and conclusions	129
7	Epilogue	131
7.1	Forerunners of this thesis	131
7.2	Overview of the papers published	132
8	Conclusions and Outlook	137

Bibliography	138
Acknowledgements	147
IV Published papers	151

Preface

This lengthy thesis is not intended to torment the reader with a cumbersome text. However, at the moment of start its writing I was in a bind. I could have chosen to do a "standard" thesis with just a short introduction and the contents of the papers published more or less rearranged. But this posed several "technical" problems. Firtsly, the values used for the Wilson coefficients were computed from the scratch in our third paper, and were a bit different from those used in our first papers, so this meant that a curve computed using these an other new parameters was not directly comparable with the experimental predictions from our first two papers and therefore the work would have been lacking consistency. Furthermore, in view of the recent experimental data made available to the community at Moriond 2012, all plots in our third paper required an update and the conclusions extracted from them also demanded a rewriting. Lastly, and maybe the worst drawback to me, this thesis would have been just a mere formality to get a degree without any other aim than having a piece of paper stating that I had a PhD.

The other option was much more time consuming, but at least it gave a purpose to all these years spent working on particle physics. I could write a thesis trying to review the many different areas of particle physics that the decay mode $\bar{B}_d \rightarrow \bar{K}^{*0} \ell^+ \ell^-$ requires to understand to deal with it properly. I have tried to summarise all the contents in the most didactical way I could, so that a master student dealing with this subject or an experimentalist trying to understand a theoretical aspect of this exclusive B channel could grasp the main points about it. In doing so I had to gain some knowledge about the many topics involved in this decay channel, gathering the key concepts from different sources and assembling them like pieces of a jigsaw. I do not know if I have succeeded, the members of the committee and the possible readers of this thesis will decide on this. Nevertheless I am happy with the effort put on this thesis and this alone is already a reward to me. A particle physicist finding any part of it useful would already mean a success to me.

Marc Ramon

Introduction

There is a general consensus among particle physicists in considering that the Standard Model is not the complete theory of elementary particles and interactions. There are several reasons for this. First of all, there are well established *observational facts* like the discovery of the *mass of neutrinos*, the presence of large galaxy halos (producing strong gravitational fields that cannot be explained if it does not exist a kind of matter in the universe that interacts extremely weakly with the Standard Model fields, i.e. *dark matter*), the probable existence of *dark energy* (which is a constant energy density for the vacuum that could account for the current measured value of the cosmological constant), or the amount of charge-parity (*CP*) violation required to describe the current asymmetry between the particle and antiparticle content in the observable universe, which cannot be explained by the Standard Model either. Furthermore, there are *aesthetic or unnatural* reasons such as the *hierarchy problem* (the instability of Higgs mass to radiative corrections requires that the difference between the electroweak and the Plank mass scales to be tuned to a part in 10^{30}), or the *strong CP problem*, related to the absence of a *CP*-violating term in the strong sector. Finally, there is a third category related to unanswered questions such as how to include the gravity in an unified particle physics models, why there are so many free parameters in the Standard Model or why quark and lepton masses and Cabibbo-Kobayashi-Maskawa (CKM) matrix elements (see below) display such hierarchies.

All these unanswered questions have led theoretician particle physics to develop families of models during many decades, trying to find a framework that could solve all the aforementioned problems and some more, while recovering the Standard Model formalism at low enough energies. The collection of these families of models is usually known as "physics Beyond the Standard Model" or simply "New Physics".

Flavour physics is the part of particle physics that deals with the flavour structure of matter. Flavour is a set of global symmetries of quantum chromodynamics that have a certain quantum numbers associated; in the quark sector these are *isospin*, *strangeness*, *charm*, *bottomness* and *topness*. Electroweak interactions, however, break these flavour symmetries introducing mixing between different flavours in mass eigenstates of the kinetic and strong interaction terms of the Lagrangian. In the Standard Model, the transformation from flavour basis to mass basis for quarks is given by the CKM matrix, which is a 3×3 unitary matrix that can be expressed in terms of three angles (usually known as α , β and γ) and a single *CP*-violating weak phase. This

allows the simultaneous use of several observables to over-constrain these four parameters in the CKM-matrix. The result of all these measurements is usually represented as a fit to the apex of the so-called *unitary triangle* (UT) displayed in Fig. 1. Nowadays this fit is very constrained and allows only marginal departures from the Standard Model predictions, providing the following results for the real ($\bar{\rho}$) and imaginary ($\bar{\eta}$) parts of the UT apex [1]:

$$\bar{\rho} = 0.136 \pm 0.018 \quad \bar{\eta} = 0.348 \pm 0.014. \quad (1)$$

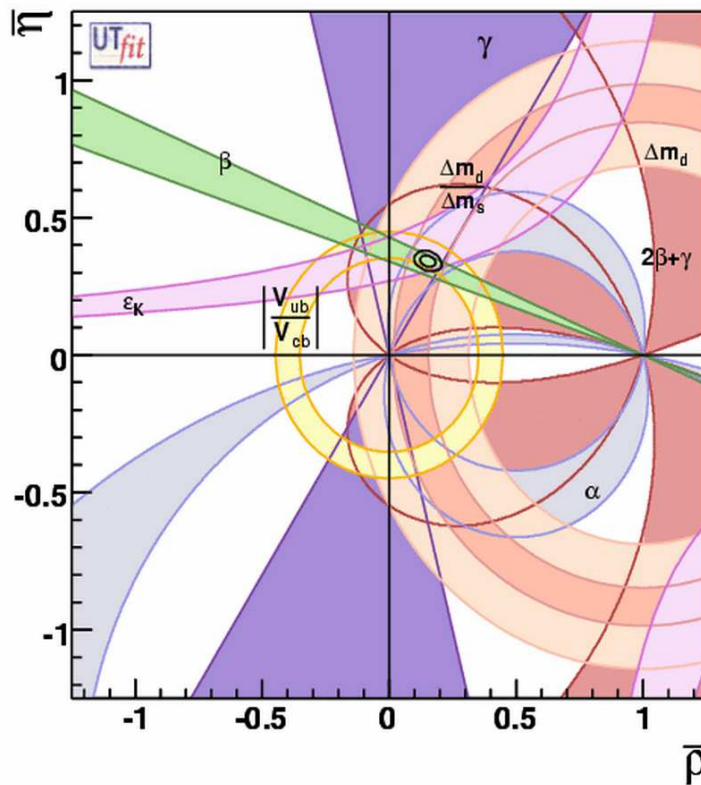


Figure 1: Fit to the apex of the standard UT as of March 2012. The inner black elliptical line corresponds to 68% CL and the outer to 95% CL. Source: *UT-fit*.

It is manifest in Fig. 1 that there is not much room for New Physics at the energies explored so far, and therefore flavour physics provides the Standard Model with very restrictive *precision measurements*. Hence, any beyond the Standard Model one might figure out must also fulfil these constraints stemming from the flavour sector of the Lagrangian at energies low enough. Another problem that any NP model should deal with is the suppression of the flavour-changing neutral

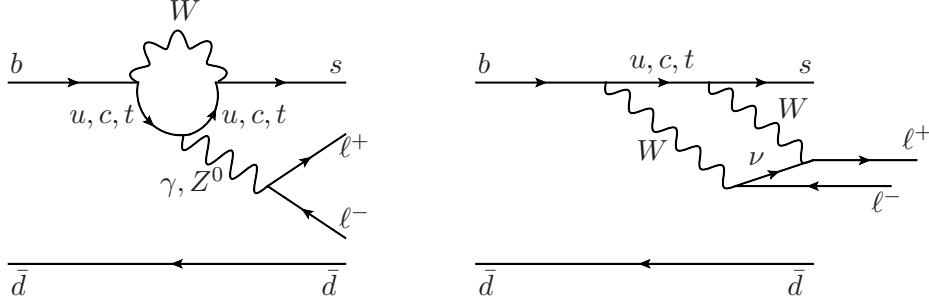


Figure 2: Lowest-order Standard Model process for the $\bar{B}_d^0 \rightarrow \bar{K}^{*0} \ell^+ \ell^-$ decay mode; (left) penguin loop and (right) weak box diagram.

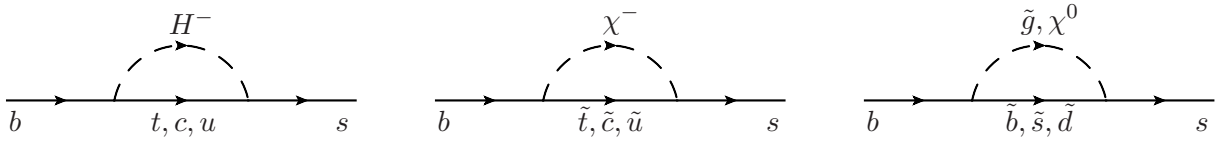


Figure 3: Examples of Beyond the Standard Model contributions arising from loops containing a charged Higgs boson and other supersymmetric particles.

currents (FCNCs) in the Standard Model, which stems from the fact that in the Standard Model Lagrangian there appear terms proportional to $\bar{Q}_L Z^\mu \gamma_\mu Q_L$ (with Q_L representing either the *up-type* or the *down-type* left-handed quark doublets), that are invariant under the unitary transformations used to diagonalise the Yukawa terms and give physical meaning to quark masses preventing, at leading order in perturbation theory, the transitions between quarks of different flavours mediated by neutral currents. Without any mechanism capable of suppressing FCNC processes, a generic Beyond the Standard Model scenario should be forbidden up to 10^3 TeV: this is commonly known as the *New Physics flavour problem*. In spite of this, these FCNCs are very interesting from the point of view of phenomenology as they occur at next-to-leading order in perturbation theory of the strong interaction in the Standard Model and, as virtual particles in the loop can have any momenta between 0 and ∞ , they are able to explore, albeit indirectly, energies much higher than the ones provided by the experimental colliders. So the advantage of such kind of decays is twofold: they allow precision tests of the Standard Model at the energies provided by the experiment and, at the same time, they constitute an interesting hunting ground to look for New Physics.

In this thesis one of these FCNCs will be studied: the $\bar{B}_d^0 \rightarrow \bar{K}^{*0} \ell^+ \ell^-$ decay mode (where ℓ denote leptons) and its *CP*-conjugated channel, which at lowest order in the Standard Model occurs through the diagrams in Fig. 2, although it might also receive non-negligible New Physics contributions (see, for instance, Fig. 3). It is one of the rarest *B* decays ever observed, with a branching ratio (\mathcal{B}) of $(9.9_{-1.1}^{+1.2}) \cdot 10^{-7}$ [1], which precludes the possibility of collecting a large

amount of data in a short period of time. This requires either waiting for a large integrated luminosity to have statistics good enough to compare experimental data with theoretical predictions or using smart techniques such as folding one angle in the angular distribution of the corresponding decay amplitude to search selectively for relevant data with the few statistics available [2].

The theoretical analysis of exclusive decay modes is not straightforward at all either. Quantum Chromodynamics (QCD), the theory of strong interactions, has proven to work extremely well during almost forty years in the high-energy regime, where a perturbative expansion in the strong coupling constant α_s is allowed as α_s is small at such high energies; this phenomenon constitutes the basis for the *asymptotic freedom* of the quarks inside a hadron. However, at sufficiently low energies α_s is large enough to spoil the perturbative treatment of QCD and cause the quark *confinement*. When one enters the non-perturbative regime things are much more involved. In this case one needs to resort to either dedicated approximate frameworks with a limited degree of accuracy, such as large-N expansions or QCD sum rules, or to QCD calculations on the lattice (if they are already available for the process studied).

Strong interactions in exclusive B decays have been traditionally dealt with using the Heavy Quark Effective Theory (HQET), developed about two decades ago. HQET assumes that the mass of the whole B meson can be assimilated to the b quark mass (up to corrections arising from lighter degrees of freedom) and that a perturbative expansion in the small parameter Λ_{QCD}/m_b can be performed. Likewise, the Large Energy Effective Theory (LEET) was developed a decade later to deal with the light energetic mesons produced in heavy-to-light meson decays, supposing that the recoiling light meson moves with an energy E large enough to enable another perturbative expansion in Λ_{QCD}/E . The QCD factorisation (QCDF) framework for heavy-to-light exclusive processes (such as the $b \rightarrow s\ell^+\ell^-$ decay) evolved from the $O(1)$ term in the Λ_{QCD}/m_b and Λ_{QCD}/E expansions in HQET and LEET in combination with the hard-exclusive formalism of Brodsky and Lepage.

This thesis deals with the study of the $\bar{B}_d^0 \rightarrow \bar{K}^{*0}\ell^+\ell^-$ decay mode at next-to-leading order in α_s using QCD factorisation. It also deals with the construction of observables for this exclusive channel that maximise the sensitivity to certain kinds of New Physics (while minimising the hadronic uncertainties stemming from the $B \rightarrow K^*$ form factors) and with the "symmetries" identified in the differential decay distribution and their practical implications. It is divided in four major parts. The first part is a summary of the theoretical knowledge needed to understand the rest of the work. Reviewing the Standard Model and the renormalisation techniques was avoided on purpose, as there are complete Master subjects dedicated to them, so the building of effective theories in Flavour Physics was sketched and some notions on HQET and LEET were also given in the first chapter. A whole chapter was dedicated to QCD sum rules and light-cone sum rules as it was an unknown field to me, but very important for some aspects of the calculation of the non-perturbative inputs entering the $\bar{B}_d^0 \rightarrow \bar{K}^{*0}\ell^+\ell^-$. These non-perturbative inputs also deserved a chapter for themselves. The final chapter was dedicated to explain the birth, fundamentals, range of applicability and drawbacks of QCD factorisation.

The second part is devoted to the study of the decay itself. The first chapter contains a general study of the kinematics of 4-body decays, while the second chapter is fully devoted to the dynamics of this decay mode, from the $b \rightarrow s\ell^+\ell^-$ weak effective Hamiltonian to the computation of the matrix element of the decay in terms of the so-called *transversity amplitudes* and the inclusion of $O(\alpha_s)$ and power-suppressed corrections from QCDf.

The third part contains a summary of all publications contained in this thesis, the final conclusions and the acknowledgements. The fourth part is composed by the published articles.

Part I

Theoretical background

Chapter 1

Effective Hamiltonians in B physics

This chapter contains a brief summary dealing with the construction of effective theories for particle decays involving weak interactions in the SM and beyond it, to focus immediately afterwards on the two effective theories that will play a central role in the forthcoming chapters of this thesis: the heavy quark effective theory (HQET) and the large energy effective theory (LEET). Only a few brushstrokes of each one will be given here in order to introduce the concepts that will be needed later on. Helpful references to very good books and reviews can be found along this chapter.

1.1 The weak effective Hamiltonian

1.1.1 Energy scales

Weak decays of heavy mesons involve simultaneously at least three energy scales: the scale of strong interactions that keep the quarks bound inside the meson, set by Λ_{QCD} ; the scale of the decaying heavy quark Q that characterizes the energy of the process, given by the mass of Q (m_Q); and the scale of the weak interactions, depicted by the mass of the W boson, M_W . The order of magnitude of these scales is

$$O(\Lambda_{\text{QCD}}) \sim 0.2 \text{ GeV}, \quad O(m_Q) \sim 5 \text{ GeV (for } b \text{ quarks)}, \quad O(M_W) \sim 90 \text{ GeV}.$$

The three scales are strongly hierarchized: $\Lambda_{\text{QCD}} \ll m_Q \ll M_W$ so the physical processes they describe are almost independent one of another. In this context, an *effective field theory* may be constructed and employed as a tool to account for the relevant phenomena at the scale considered.

1.1.2 The weak effective Hamiltonian in the Standard Model

The weak effective Hamiltonian (WEH) describes weak interactions at energies much lower than $2M_W$, where the virtual weak gauge bosons and top quark fields can be removed (or "integrated

out") from the Standard Model (SM) Lagrangian as explicit dynamical degrees of freedom. It has the structure of an *Operator Product Expansion* (OPE)

$$\mathcal{H}_{\text{eff}} = \frac{G_F}{\sqrt{2}} \sum_i C_i(\mu) \mathcal{O}_i. \quad (1.1)$$

This expansion may be regarded as a generalisation of the Fermi theory of weak interaction to include all quarks and leptons described by the SM. Using Eq. (1.1) the amplitude of a meson decay process can be expressed as

$$A(i \rightarrow f) = \langle f | \mathcal{H}_{\text{eff}} | i \rangle = \frac{G_F}{\sqrt{2}} \sum_i C_i(\mu) \langle f | \mathcal{O}_i | i \rangle(\mu) \equiv \frac{G_F}{\sqrt{2}} \sum_i C_i(\mu) \langle \mathcal{O}_i(\mu) \rangle. \quad (1.2)$$

The *Wilson coefficients* $C_i(\mu)$ are calculable functions of α_s , $2M_W$ and a *renormalisation scale* μ . They may be interpreted as the running coupling constants for the *effective operators* \mathcal{O}_i , which constitute the effective interaction terms. An important comment related to the appearance of a renormalisation scale is in order here: amplitudes must be scale- and scheme-independent however, since neither the operators \mathcal{O}_i nor the initial or final states depend on renormalisation scale and scheme, the dependence of the coefficients $C_i(\mu)$ on these unphysical parameters must be canceled by the matrix elements $\langle \mathcal{O}_i(\mu) \rangle$ to the order in the perturbation theory included in the calculation, as shown in Eq. (1.2). This cancellation will involve, in general, several terms of the OPE.

When computing the Wilson coefficients there are two ways to proceed. On the one hand, they can be treated as unknown phenomenological parameters to be measured through experiment, and then the effective theory can be tested by checking its predictions over different observables. On the other hand, if the underlying theory is known (i.e. a certain model is assumed to be valid), they can also be computed in terms of its fundamental parameters. When the latter approach is used, there are some standard steps that should be followed to obtain the corresponding effective Hamiltonian¹:

- (1) The amplitudes A are computed using the full theory up to some order in α_s expansion. When doing so some divergencies arise. These divergencies can be absorbed by conventional renormalisation introducing the high scale $\mu_0 \sim O(2M_W)$, suitable for perturbative treatment because the coupling constant is small at this scale.
- (2) The operators generated at the scale μ_0 are identified and the relevant OPE for the theory written.
- (3) An *operator matrix elements renormalisation* must be performed to remove the divergencies that arise from QCD effects. This process introduces a *mixing* between different operators

¹This is just a brief qualitative overview of the technique. A more detailed review can be found in [3, 4] and a throughout explanation in [5, 6].

in the OPE that carry the same quantum numbers, generating new effective interactions mediated by local operators with the same or lower dimension than their "parent" operators.

- (4) The full theory is *matched* into the effective theory to find the Wilson coefficients at the scale μ_0 .
- (5) The Wilson coefficients are computed at a lower scale μ using *renormalisation group equations* (RGEs). Since μ can be chosen at will, it is a matter of choice what belongs to $C_i(\mu)$ and what to $\langle \mathcal{O}_i(\mu) \rangle$, but is usual to assign different energy ranges to these quantities, in such manner that the $C_i(\mu)$ contain the QCD *short-distance* perturbative effects with energies between μ and $2M_W$ while the $\langle \mathcal{O}_i(\mu) \rangle$ include the *long-distance* non-perturbative QCD effects with virtualities below μ , which are the ones responsible for the binding of quarks inside the asymptotic hadronic states. For an effective field theory with five flavours $\mu = \mu_b \sim O(m_b)$, so μ has to be "run down" from $2M_W$ to m_b . The large difference between the two scales causes the appearance of powers of the large logarithms $\ln(\mu_0^2/\mu_b^2)$ which spoil the convergence of the perturbative series. However, *renormalisation group improved perturbation theory* can then be used to resume these large logarithms to all orders in α_s [7].

The reduction in complexity achieved by transforming the non-local heavy particle exchanges in the SM Lagrangian into local effective interactions in the WEH is exact up to corrections suppressed by inverse powers of the heavy mass scales (M_W and m_t) and also up to the order in α_s chosen in (1). The WEH is also process-independent but the matching conditions imposed in (4) make it model-dependent.

1.1.3 The weak effective Hamiltonian beyond the Standard Model

The effective theory approach may be used to deal with contributions of new physics (NP) at low energies in a general and model independent way. In some cases, in presence of NP, many new operators will appear that will have to be added to the SM operators of Eq. (1.1). Then, the Wilson coefficients will be shifted away from their SM values when performing the matching so, if we are able to design experiments that allow us to extract observables related to these Wilson coefficients, the presence of NP can be tested and NP contributions constrained.

The starting point for the construction of a NP effective weak Hamiltonian is to assume the existence of a new energy scale Λ_{NP} at which the SM breaks down as an effective theory; this scale is supposed to be of $O(\Lambda_{\text{NP}}) \sim \text{few TeV}$, so the strong hierarchisation that motivates the use of an effective field theory holds. Moreover, the building blocks of $\mathcal{H}_{\text{eff}}^{\text{NP}}$ at energies of the order of $2M_W$ and lower must be the SM fields relevant to the process considered and the operators must be gauge-invariant under $SU(3)_c \otimes SU(2)_L \otimes U(1)_Y$. In principle we might have an infinite set of such operators, so a prescription must also be taken to curtail this set to a manageable size: a suppression factor $\Lambda_{\text{NP}}^{D-6}$ is added to the NP effective Hamiltonian so that

the larger D becomes the smaller are the factors $C_i^{[D]}/\Lambda_{\text{NP}}^{D-6}$ preceding the effective operators. As Λ_{NP} is large, this factor effectively constrains the dimension of the operators that may play a role in $\mathcal{H}_{\text{eff}}^{\text{NP}}$. With all these considerations, the most general form it may have is:

$$\mathcal{H}_{\text{eff}}^{\text{NP}} = \sum_{D=7}^{\infty} \sum_i \frac{C_i^{[D]}}{\Lambda_{\text{NP}}^{D-6}} \mathcal{O}_i^{[D]}. \quad (1.3)$$

Despite of using this procedure, Eq. (1.3) contains still too many operators. So, to further reduce the complexity of the effective Hamiltonian, one must restrict oneself to a model or family of models that can be obtained with the same set of operators. Part of this thesis will be devoted to the construction of observables sensitive to certain types of NP contributions, coming either from the chirality flipped operators $\mathcal{O}'_7, \mathcal{O}'_9, \mathcal{O}'_{10}$ (which might arise, for instance, in left-right models or in supersymmetry [8, 9]) or from scalar or pseudo-scalar operators (also possible in supersymmetry [10]).

1.2 Introduction to heavy quark effective theory

1.2.1 Derivation of the heavy quark effective theory Lagrangian

The heavy-quark effective theory (HQET) is an effective field theory² aimed at providing a simplified description of mesons containing a single heavy-quark (with $m_Q \rightarrow \infty$) and one or more "light degrees of freedom" (quarks, antiquarks and/or gluons) with the restriction that QCD interactions between them are mainly mediated by low energy or soft gluons. In this situation, the high and low energy scales are set, respectively, by the mass of the heavy quark m_Q and the typical momenta of gluons exchanged in a bound state (Λ_{QCD}). If $\Lambda_{\text{QCD}}/m_Q \sim 0.1 \ll 1$, as in $Q = b$, a technique somewhat analogous to OPE can be performed to exploit the presence of such small parameters. However, in HQET the heavy quark can not be removed from the theory by integration in the fashion described in Sec. (1.1.2), as it is not a virtual particle and carries a flavour charge. What can be "integrated out" and incorporated into the Wilson coefficients are the hard perturbative contributions, with virtualities larger than a factorisation scale μ but smaller than the high scale m_Q , which can take the heavy quark field far from its "mass shell". The soft non-perturbative contributions (with scales below μ) will remain in the matrix elements of HQET operators. This can be done order by order in powers of Λ_{QCD}/m_Q , obtaining a covariantly formulated effective field theory for a static heavy quark.

The formulation of HQET at first order in Λ_{QCD}/m_Q will be presented here following [13]. The heavy quark Q is almost on-shell inside a meson that moves with four-velocity v^μ , so Q also has a mean velocity v^μ . Therefore, its four momentum can be written as

$$p_Q^\mu = m_Q v^\mu + k^\mu \quad (1.4)$$

²Refer to [11] and [12] for in-depth monographs on the subject.

where $m_Q v^\mu$ is the *on-shell* part and k^μ is the *residual momentum* that represents the fluctuations in p_Q^μ due to the exchange of soft gluons with the rest of the meson. Hence $k \sim \Lambda_{\text{QCD}}$ and the corresponding changes in the heavy quark velocity vanish as $\Lambda_{\text{QCD}}/m_Q \rightarrow 0$.

Let $h(x)$ denote the heavy quark field in the QCD Lagrangian. With the definitions³

$$h_v(x) \equiv e^{imv \cdot x} P_+ h(x), \quad (1.5)$$

$$H_v(x) \equiv e^{imv \cdot x} P_- h(x) \quad (1.6)$$

it can be rewritten as

$$h(x) = e^{-imv \cdot x} [h_v(x) + H_v(x)], \quad (1.7)$$

where we have defined $P_\pm \equiv (1 \pm \not{v})/2$. Given that v^μ is a four velocity (so $v^2 = 1$), it is easy to check that both P_+ and P_- are projection operators, whose action represents the covariant generalisation of decomposing $h(x)$ into upper and lower components. This can be seen in the heavy quark rest frame using Dirac's representation of γ -matrices: there, the four-velocity of Q is given by $v^\mu = (1, 0, 0, 0)$, so that $\not{v} = \gamma_0$ and hence h_v corresponds to the upper two components of the heavy quark whereas H_v corresponds to the lower ones (it would be absent if the heavy quark were exactly on-shell). Moreover, h_v and H_v have been constructed in a way that the exponential factor $e^{imv \cdot x}$ removes the large-frequency part of the x -dependence in $h(x)$ resulting from the large momentum mv [see Eqs. (1.5)-(1.7)]. Therefore, the residual x -dependence of h_v and H_v is governed by the small momentum k^μ , so derivatives acting on both fields count as $O(\Lambda_{\text{QCD}})$ [11].

The Lagrangian density of the HQET can be obtained starting from the QCD Lagrangian

$$\mathcal{L}_{\text{QCD}} = \bar{\Psi}(x) i \not{D} \Psi(x) - m_Q \bar{\Psi}(x) \Psi(x), \quad (1.8)$$

where $\Psi(x)$ represents any quark field and D_μ is the covariant derivative

$$D_\mu \equiv \partial_\mu - ig T^a A_\mu^a. \quad (1.9)$$

Substituting Eq. (1.7) into the QCD equation of motion

$$(i \not{D} - m_Q) \Psi(x) = 0 \quad (1.10)$$

one obtains

$$e^{-imv \cdot x} [i \not{D} - (1 - \not{v})m] [h_v(x) + H_v(x)] = 0. \quad (1.11)$$

From Eq. (1.5), Eq. (1.6) and the projection operators properties it is easy to check that

$$\not{v} h_v(x) = h_v(x), \quad (1.12)$$

$$\not{v} H_v(x) = -H_v(x); \quad (1.13)$$

³These sign conventions are suited to a heavy *quark*. To describe a heavy *antiquark* the sign of v must be reversed.

now substituting Eq. (1.12) and Eq. (1.13) into Eq. (1.11) one obtains

$$i \not{D} h_v(x) + (i \not{D} - 2m) H_v(x) = 0. \quad (1.14)$$

Performing the product of P_{\pm} by Eq. (1.14) and employing the relation

$$P_{\pm} \not{D} = \not{D} P_{\mp} \pm v \cdot D \quad (1.15)$$

and the definition

$$D_{\perp}^{\mu} \equiv D^{\mu} - v^{\mu} v \cdot D, \quad (1.16)$$

the coupled system of equations

$$iv \cdot D h_v(x) = -i \not{D}_{\perp} H_v(x) \quad \text{for } P_+, \quad (1.17a)$$

$$i \not{D}_{\perp} h_v(x) = (iv \cdot D + 2m_Q) H_v(x) \quad \text{for } P_- \quad (1.17b)$$

can be derived. The second of these equations can be solved, giving

$$H_v(x) = \frac{i \not{D}_{\perp} h_v(x)}{iv \cdot D + 2m_Q - i\epsilon}, \quad (1.18)$$

which shows that $H_v(x) \sim O(\Lambda_{\text{QCD}}/m_Q) h_v(x)$, as the numerator is proportional to a derivative of a field and the denominator contains m_Q . Hence $H_v(x)$ is suppressed with respect to $h_v(x)$ in the heavy-quark limit. In other words, $h_v(x)$ contains the large components and $H_v(x)$ the small components of $h(x)$ with mass $2m_Q$.

Inserting Eq. (1.18) into Eq. (1.17a) we obtain the equation of motion for $h_v(x)$

$$iv \cdot D h_v(x) = -i \not{D}_{\perp} \frac{1}{iv \cdot D + 2m_Q - i\epsilon} i \not{D}_{\perp} h_v(x). \quad (1.19)$$

The HQET Lagrangian can hence be written down

$$\mathcal{L}_{\text{HQET}} = \bar{h}_v(x) iv \cdot D h_v(x) + \bar{h}_v(x) i \not{D}_{\perp} \frac{1}{iv \cdot D + 2m_Q - i\epsilon} i \not{D}_{\perp} h_v(x), \quad (1.20)$$

as can be easily checked upon variation with respect to $\bar{h}_v(x)$ (i.e. $\delta \mathcal{L}_{\text{HQET}} / \delta \bar{h}_v(x) = 0$). In terms of an expansion in powers of Λ_{QCD}/m_Q , the HQET Lagrangian reduces to

$$\mathcal{L}_{\text{HQET}} = \bar{h}_v(x) iv \cdot D h_v(x) + O\left(\frac{\Lambda_{\text{QCD}}}{m_Q}\right). \quad (1.21)$$

It should be also stated here that, using the $\mathcal{L}_{\text{HQET}}$ as it appears in (1.21), HQET can be expanded perturbatively to all orders in $\alpha_s(m_Q)$ (being m_Q the *pole mass* -see Sec. 6.6.7-) via Wilson coefficients, but just to 0-th order in Λ_{QCD}/m_Q .

on the heavy quark changing its velocity to v' , so that the whole meson undergoes an elastic scattering. If $v = v'$ the light degrees of freedom do not realize the action of the current; they only "feel" the velocity of the heavy quark which remains unchanged in its reference frame. But if $v \neq v'$, there is a velocity change with respect to the former heavy quark frame; now the soft degrees of freedom can "see" the movement of the colour source. Hence, soft gluons must be exchanged inside the meson to rearrange into a heavy pseudoscalar meson with velocity v' [$H(v')$]. The more different v and v' are, the less likely is an elastic scattering of this kind, so a dimensionless suppression factor ξ must be present in the transition matrix that describes this process. In the limit $m_Q \rightarrow \infty$, ξ will only depend on the Lorentz boost that connects the rest frames of $H(v)$ and $H(v')$, which is a function of just $v \cdot v'$; therefore $\xi = \xi(v \cdot v')$. This is the so-called *Isgur-Wise function* [14].

Since the limit $m_Q \rightarrow \infty$ has been employed, the hadronic matrix element that describes the scattering process can be written using the HQET framework⁴

$$\frac{1}{m_H} \langle H(v') | \bar{h}_{v'} \gamma^\mu h_v | H(v) \rangle = \xi(v \cdot v') (v + v')^\mu, \quad (1.24)$$

where the factor $1/m_H$ on the left-hand side has been added to compensate for the trivial dependence on the heavy-meson mass introduced by the relativistic normalisation of heavy-meson states $\langle H(p') | H(p) \rangle = 2 m_H v^0 (2\pi)^3 \delta^3(\vec{p} - \vec{p}')$, with $p^{(\prime)} = m_H v^{(\prime)}$.

The matrix element in Eq. (1.24) is conventionally written in full QCD in terms of an elastic form factor $F_{\text{el}}(q^2)$, where $q^2 = (p - p')^2 = -2m_H^2(v \cdot v' - 1)$ is the momentum transfer:

$$\langle H(v') | \bar{h} \gamma^\mu h | H(v) \rangle = F_{\text{el}}(q^2) (p + p')^\mu. \quad (1.25)$$

Comparing this with (1.24) one finds

$$F_{\text{el}}(q^2) = \xi(v \cdot v'). \quad (1.26)$$

As the current must be conserved for equal initial and final velocities, the elastic form factor is normalized to unity at $q^2 = 0$. As $q^2 = -2m_H^2(v \cdot v' - 1)$, this condition automatically implies the normalisation of the Isgur-Wise function to unity at $v \cdot v' = 1$, i.e. for $v = v'$:

$$\xi(1) = 1. \quad (1.27)$$

This result agrees with the intuitive argument that the probability for an elastic transition is unity if there is no velocity change. Since for $v = v'$ the final-state meson is at rest in the rest frame of the initial meson, the point $v \cdot v' = 1$ is referred to as the *zero-recoil limit*.

⁴Using Eq. (1.12) and its barred partner for v' , $\bar{h}_{v'} \not{v}' = \bar{h}_{v'}$, it can be easily checked that the contraction of the matrix element with $(v - v')_\mu$ gives 0, so there is no term proportional to $(v - v')^\mu$ in Eq. (1.24).

1.3 Introduction to large energy effective theory

1.3.1 Derivation of the large energy effective theory Lagrangian

The large energy effective theory (LEET) is an effective field theory developed to deal with the decay of a heavy meson into an energetic lighter meson (in the rest frame of the parent meson) through a weak current. In this situation, HQET can then be applied to the heavy quark of the parent meson, but not to the fast recoiling light quark of the daughter meson since, due to its high energy, its worldline is almost light-like with small fluctuations coming from soft and collinear infrared QCD interactions with light degrees of freedom (as hard-gluon exchange contributions between the quark that suffers the transition and the light quark of the heavy meson are neglected). Hence the LEET formalism is also built under a *soft contribution dominance* assumption.

Here the high energy scale will be determined by the energy of the light meson (E), and the low scale by Λ_{QCD} . If E is high enough, the condition $\Lambda_{\text{QCD}}/E \ll 1$ will be also satisfied and an OPE may be carried out: "hard" momenta, with virtualities between a factorisation scale μ and E , will be "integrated out" into the perturbative Wilson coefficients and "soft" momenta, with characteristic scales well below μ , will be kept in the matrix elements of the LEET operators.

The construction of LEET is very similar to that of HQET, assuming the heavy-quark limit for the initial meson and the large energy limit for the final one

$$(\Lambda_{\text{QCD}}, m) \ll (M, E) \quad (1.28)$$

where m and E are the mass and the energy of the light meson respectively, and M is the mass of the heavy meson.

The four-momentum of the heavy meson is taken to be

$$P^\mu \equiv Mv^\mu. \quad (1.29)$$

A nearly light-like four-vector n^μ ($n^2 \simeq 0$) is defined so that the momentum of the light meson is $p^\mu = En^\mu$ and the condition $v \cdot n = 1$ holds. Thus,

$$E = v \cdot p \quad (1.30)$$

is just the energy of the light meson in the rest frame of the heavy meson.

Since only the low-energy QCD interactions with the soft degrees of freedom of the light meson are taken into account, the momentum p_q^μ of the energetic light quark is close to that of the light meson

$$p_q^\mu = En^\mu + k^\mu \quad (1.31)$$

up to corrections $k \sim O(\Lambda_{\text{QCD}}/E)$ coming from these soft interactions, which vanish as $E \rightarrow \infty$.

If $q(x)$ denotes the light energetic quark field, then using the definitions

$$q_n(x) \equiv e^{iEn \cdot x} P_+ q(x), \quad (1.32)$$

$$Q_n(x) \equiv e^{iEn \cdot x} P_- q(x), \quad (1.33)$$

it can be written

$$q(x) = e^{-iEn \cdot x} [q_n(x) + Q_n(x)], \quad (1.34)$$

with P_{\pm} defined as

$$P_+ \equiv \frac{\not{n} \not{v}}{2}, \quad P_- \equiv \frac{\not{v} \not{n}}{2}. \quad (1.35)$$

These are projection operators since, with the normalisation conditions

$$v^2 = 1, \quad v \cdot n = 1 \quad \text{and} \quad n^2 \simeq 0, \quad (1.36)$$

it can be easily shown that P_{\pm} verify the projector properties

$$P_{\pm}^2 = P_{\pm}, \quad P_{\pm} P_{\mp} = 0 \quad \text{and} \quad P_+ + P_- = \frac{\{\not{n}, \not{v}\}}{2} = 1. \quad (1.37)$$

The statements made after Eq. (1.7) concerning the heavy-quark fields $h_v(x)$ and $H_v(x)$ also apply here to $q_n(x)$ and $Q_n(x)$ respectively, enforcing the parallelism in the derivation of both effective theories.

The next step is the construction of the LEET Lagrangian density. The QCD equation of motion (1.10) (with the change $m_Q \rightarrow m_q$, where m_q is the mass of the light quark) can be expressed in terms of $q_n(x)$ and $Q_n(x)$ by means of Eq. (1.34) as

$$e^{-iEn \cdot x} [i \not{D} - m_q + E \not{n}] [q_n(x) + Q_n(x)] = 0. \quad (1.38)$$

Using the algebra of Dirac for γ -matrices ($\{\gamma^{\mu}, \gamma^{\nu}\} = 2g^{\mu\nu}$) and (1.32) it can be shown that $\not{v} q_n(x) = 0$; therefore, Eq. (1.38) becomes

$$[i \not{D} - m_q] q_n(x) + [i \not{D} - m_q + E \not{n}] Q_n(x) = 0. \quad (1.39)$$

Multiplying the previous equation by P_{\pm} , substituting the expressions

$$P_{\pm} \not{D} = \pm \not{v} \cdot D \mp \not{n} \cdot D + \not{D} P_{\pm} \quad (1.40)$$

and employing Eqs. (1.37) and $\not{v} q_n(x) = 0$ it is straightforward to obtain the coupled system of equations

$$(i \not{D} - m_q - \not{v} i n \cdot D) q_n(x) + \left(E \frac{\not{n} \not{v}}{2} \not{n} + i v \cdot D \not{n} - i n \cdot D \not{v} \right) Q_n(x) = 0, \quad (1.41a)$$

$$\not{v} i n \cdot D q_n(x) + \left(i \not{D} - m_q - \not{v} i v \cdot D + \not{v} i n \cdot D + E \frac{\not{v} \not{n}}{2} \not{n} \right) Q_n(x) = 0. \quad (1.41b)$$

The second term of these equations may be further simplified by using the slashed form of the first and the third expressions in Eq. (1.36):

$$\not{v}^2 = 1 \quad \text{and} \quad \not{n}^2 \simeq 0. \quad (1.42)$$

Hence, the identities

$$\frac{\not{n} \not{v}}{2} \not{n} Q_n(x) = \not{n} \frac{\not{v} \not{n}}{2} Q_n(x) = \not{n} Q_n(x) = \not{v}^2 \not{n} Q_n(x) = 2 \not{v} \frac{\not{v} \not{n}}{2} Q_n(x) = 2 \not{v} Q_n(x) \quad (1.43)$$

may be inserted into Eq. (1.41a) and Eq. (1.41b) to give

$$\not{v} i n \cdot D q_n(x) + [i \not{D} - m_q - \not{v}(2i v \cdot D - i n \cdot D)] Q_n(x) = 0, \quad (1.44a)$$

$$(i \not{D} - m_q - \not{v} i n \cdot D) q_n(x) + \not{v}(2E + 2i v \cdot D - i n \cdot D) Q_n(x) = 0. \quad (1.44b)$$

The latter equation can be solved to express $Q_n(x)$ in terms of $q_n(x)$:

$$Q_n(x) = \not{v} \frac{i \not{D} - m_q - \not{v} i n \cdot D}{2E + 2i v \cdot D - i n \cdot D + i\epsilon} q_n(x) \quad (1.45)$$

showing that $Q_n(x) \sim O(\Lambda_{\text{QCD}}/E) q_n(x)$ because the numerator contains a derivative and the denominator an E . Therefore, $Q_n(x)$ is suppressed with respect to $q_n(x)$ in the large-energy limit. Since in the rest frame of the heavy meson (with the z direction along p) $v = (1, 0, 0, 0)$ and $n \simeq (1, 0, 0, 1)$, the projection operators acquire the form⁵ $P_{\pm} = \pm \gamma_3 \gamma_0 = (1 \pm \alpha_z)/2$. The field $Q_n(x)$ corresponds to the negative energy solutions so, since these are suppressed, pair creation is also suppressed in the LEET.

The equation of motion for $q_n(x)$ can be obtained from Eq. (1.45) and Eq. (1.44a)

$$\not{v} i n \cdot D q_n(x) = - [i \not{D} - m_q - \not{v}(2i v \cdot D - i n \cdot D)] \not{v} \frac{i \not{D} - m_q - \not{v} i n \cdot D}{2E + 2i v \cdot D - i n \cdot D + i\epsilon} q_n(x) \quad (1.46)$$

and the LEET Lagrangian may be constructed just as it was done previously for HQET. In terms of an expansion in powers of Λ_{QCD}/E it becomes

$$\mathcal{L}_{\text{LEET}} = \bar{q}_n(x) \not{v} i n \cdot D q_n(x) + O\left(\frac{\Lambda_{\text{QCD}}}{E}\right). \quad (1.47)$$

The LEET/HQET joint framework is usually employed to describe weak heavy-to-light quark decays (mainly $b \rightarrow u, d, s$) in those situations where the dominance of QCD soft interactions can be taken for granted. It can be expanded perturbatively to all orders of α_s to account for short-distance corrections, while non-perturbative corrections will contribute with terms of $O(\Lambda_{\text{QCD}}/m_Q)$ from HQET and $O(\Lambda_{\text{QCD}}/E)$ from LEET. This will have an impact on theoretical uncertainties of QCD factorisation (QCdf) computations, as it will be seen later on.

⁵ $\alpha_i = \gamma_0 \gamma_i = \begin{pmatrix} 0 & \sigma_i \\ \sigma_i & 0 \end{pmatrix}$ as appears in the non-covariant form of Dirac equation $i \partial_t q(x) = (-i \alpha_i \partial^i + \gamma_0 m) q(x)$.

1.3.2 Remarks

The term $\bar{q}_n(x) \not{v} i n \cdot D q_n(x)$ displays no mass dependence, hence it is *flavour symmetric*. However, it contains γ -matrices that break the spin symmetry but, as these γ 's are not coupled to the covariant derivative D^μ , and the LEET Lagrangian is invariant under the chiral transformation

$$q_n(x) \rightarrow e^{i\alpha\gamma^5} q_n(x), \quad (1.48)$$

it can be shown [15] that $\mathcal{L}_{\text{LEET}}$ also possesses a *global $SU(2)$ symmetry*.

Using the full expression of the covariant derivative in Eq. (1.9) into Eq. (1.47) it can be obtained

$$\bar{q}_n(x) \not{v} i n \cdot D q_n(x) = \bar{q}_n(x) \not{v} i n^\mu \partial_\mu q_n(x) + \bar{q}_n(x) g_s \not{v} T^a n^\mu A_\mu^a q_n(x), \quad (1.49)$$

which allows the deduction of the Feynman rules for the LEET:

$$\text{LEET quark propagator :} \quad \frac{i \not{v}}{n \cdot k} \frac{\not{v}}{2} \delta_{ji}; \quad (1.50)$$

$$\text{LEET quark – gluon vertex :} \quad i g_s \not{v} (T_a)_{ji} n^\alpha. \quad (1.51)$$

Chapter 2

Hard exclusive processes, light-cone distribution amplitudes and sum rules

As explained previously, the matrix elements of the operators in the effective Hamiltonian contain the long-distance contributions that cannot be computed perturbatively. Although some of them may be extracted by fitting the data available from different experiments, it is essential to have frameworks in which these non-perturbative inputs can be computed reliably and in a systematic way. Nowadays there are two theoretical approaches to deal with them: *lattice QCD* and *QCD sum rules*. Despite the recent successes of lattice QCD [16], it is clear that some of the quantities describing structural properties of B mesons relevant for this work are still afflicted with one or several sources of systematic errors [17, 18, 19] and hence not reliable enough yet. Therefore, one must resort to the *light-cone sum rule* formalism, a combination of the theory of hard exclusive processes with classical QCD sum rules. The aim of this chapter is to provide the reader with an overview of both methods to ease the understanding of the literature referenced later on. Also notice that, since this thesis will focus mainly on the weak decay $\bar{B}_d \rightarrow \bar{K}^{*0} \ell^+ \ell^-$, the heavy meson will be identified with \bar{B} from now on.

2.1 Introduction to hard exclusive processes

Exclusive processes are defined as those scattering reactions or decays in which all initial and final state particles are specified. Exclusive processes at large momentum transfer Q^2 , also known as *hard exclusive processes*, can be described by the formalism devised by Brodsky and Lepage more than thirty years ago [21, 20, 22], the *hard scattering approach*. The basis of this picture is the factorisation of the hard amplitude into an *elementary hard kernel*, which contains the short-distance dynamics of the process, and hadron *light-cone distribution amplitudes* (LCDAs) (one for each hadron involved in the process), which account for non-perturbative long-distance dynamics. Besides, as only hard processes are considered, it is usual to replace the full meson by the so-called

valent Fock state, an approximation in which meson constituents are constrained to be collinear and both quark (antiquark) and meson masses are neglected [23]. This is the classic *standard hard scattering approach* (sHSA), in contrast to the later *modified hard scattering approach* (mHSA) which takes also into account the transverse momenta of the hadron constituents and the Sudakov suppression of end-point regions [24].¹

The hard scattering amplitude is represented by the general formula:

$$\mathcal{M}(Q^2) = T_H(u_j, Q^2, \mu) \otimes \prod_{h_i} \Phi_{h_i}(u_j, \mu) \equiv \int_0^1 [du] T_H(u_j, Q^2, \mu) \prod_{h_i} \Phi_{h_i}(u_j, \mu), \quad (2.1)$$

where T_H is the process-dependent elementary amplitude (usually known as "hard kernel") that can be computed using perturbation theory, Φ_{h_i} is the process-independent LCDA of the hadron h_i (see Sec. 2.2), Q^2 denotes the large momentum transfer and the scale μ plays the role of the factorisation scale, separating the contributions at $x^2 < 1/\mu^2$ that enter the hard kernel from the long-distance effects at $x^2 > 1/\mu^2$ parametrized by the LCDA.² The symbol " \otimes " denotes the convolution³ of T_H with $\prod_{h_i} \Phi_{h_i}$; the variable u_j is the momentum fraction of the quark (antiquark) parallel to the light cone (i.e., the infinite momentum reference frame), with j running from 1 to n_{h_i} (where n_{h_i} is the maximum number of valence quarks and antiquarks present in the meson h_i), so u_j can only take values from 0 to 1. Therefore, the convolution of T_H with $\prod_{h_i} \Phi_{h_i}$ is an integral between these two limits. Besides, the full expression of phase-space element $[du]$ reads

$$[du] = \prod_{j=1}^{n_{h_i}} du_j \delta(1 - \sum_{k=1}^{n_{h_i}} u_k). \quad (2.2)$$

The basic ideas behind the Brodsky and Lepage formalism can be best understood by studying the classic example of the proton magnetic form factor, $G_M(Q^2)$, at large $-q^2 = Q^2$ [22]. It will be assumed that a proton is struck by a highly virtual photon carrying a transverse momentum $Q^2 \gg \Lambda_{\text{QCD}}^2$, so that all transverse momentum fluctuations of the quarks and all particle masses can be neglected, and will describe the whole process in the light cone. For a proton, the lowest

¹The Sudakov form factor is an exponential of a double logarithm (see [25]) that arises from the virtual correction to the $\bar{q}\Gamma q$ vertex (being Γ a Dirac structure) when the quark legs are nearly on-shell. Physically, the Sudakov suppression of end-point contributions to form factors appears since the struck, near on-shell quark that suffers the large Q^2 transfer tends to radiate gluons but gluon radiation in the final state of an exclusive process cannot occur [26].

²The parallelism between hard kernels (LCDAs) in hard exclusive processes and Wilson coefficients (matrix elements of effective operators) in amplitudes computed using WEHs is obvious: both hard kernels and Wilson coefficients contain the contributions of gluons with virtualities above the running scale μ (being μ different in both frameworks) so they can be calculated perturbatively, whereas LCDAs and matrix elements account for the non-perturbative phenomena due to soft-gluon interactions in the process studied.

³In other words, " \otimes " means the integration of T_H over the longitudinal momenta of the partons described by Φ , which is the only component of the momenta allowed in the sHSA approach.

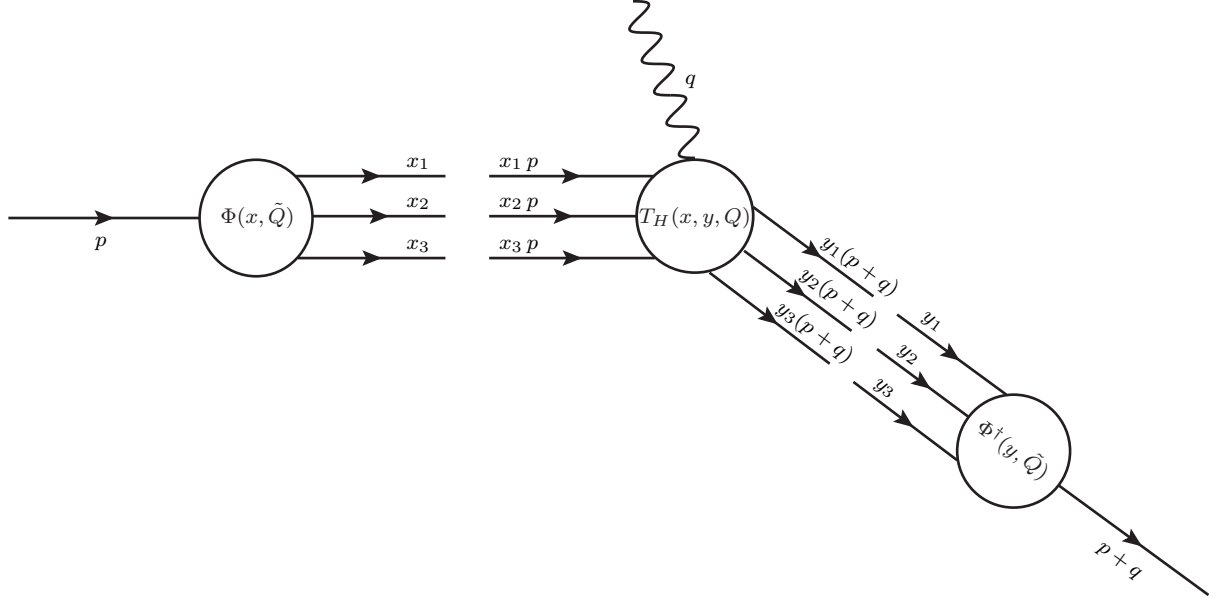


Figure 2.1: Schematic diagram of factorisation for the scattering of a p struck by a hard γ^* [22].

Fock state can be written as (omitting helicity and color indices)

$$|p\rangle = \psi(x_1, x_2, x_3) |uud\rangle, \quad (2.3)$$

being x_i the light-cone momentum fraction of the i^{th} valence quark, so that $\sum_{i=1}^3 x_i = 1$ [27]. Higher Fock states, such as $|uudg\rangle$ or $|uudq\bar{q}\rangle$, lead to contributions which are $O(1/Q^2)^n$ (with $n \geq 3$) smaller in cross sections. This suppression arises from the necessity to redistribute the large $O(Q^2)$ momentum transfer to all constituents, which costs additional very off-shell quark and gluon propagators in typical Feynman diagrams.

Physically $G_M(Q^2)$ is interpreted as the amplitude for the composite hadron to absorb the large transverse momentum delivered by the virtual photon while remaining intact, so it can be written as the product of three probability amplitudes, namely:

- (a) the amplitude Φ for finding the three-quark valence state in the incoming proton,
- (b) the amplitude T_H for this quark state to scatter with the virtual photon producing three quarks in the final state with collinear momenta, and
- (c) the amplitude Φ^\dagger for this final quark state to reconstruct an outgoing proton.

Therefore, the magnetic form factor can be written as (see Fig. 2.1)

$$G_M(Q^2) = \int_0^1 [dx] \int_0^1 [dy] \Phi^\dagger(y_i, \tilde{Q}_y) T_H(x_i, y_i, Q) \Phi(x_i, \tilde{Q}_x) [1 + O(m^2/Q^2)], \quad (2.4)$$

where $\tilde{Q}_a \equiv \min(a_i Q)$.

Since the final quarks are collinear, momentum of $O(Q^2)$ must be transferred from quark line to quark line via hard gluons in the hard kernel, so T_H is of $O(\alpha_s)$ at least and the use of perturbation theory in computing is justified. To leading order in $\alpha_s(Q^2)$, the hard scattering amplitude T_H is the sum of all Born diagrams for $\gamma^* + 3q \rightarrow 3q$ in perturbative QCD. In Fig. 2.1 it is apparent that each quark after the first, scattered from the incident to the final direction, "costs" a factor $\alpha_s(Q^2)/Q^2$. Hence, T_H admits an expansion to all orders in $\alpha_s(Q^2)$ given by

$$T_H(x_i, y_i, Q) = \left(\frac{\alpha_s(Q^2)}{Q^2} \right) [T_0(x_i, y_i) + \alpha_s(Q^2) T_1(x_i, y_i) + \dots]. \quad (2.5)$$

2.2 Light-cone distribution amplitudes

Light-cone distribution amplitudes are universal (i.e. process independent) non-perturbative objects that encode the long distance dynamics of the hadron considered in high momentum transfer exclusive reactions [28]. Physically, they account for the probability amplitude of finding a certain valence quark and antiquark momentum configuration inside the hadron probed at large Q^2 , so it is usual to find them normalised to unity in the literature. LCDAs are defined through the vacuum-hadron matrix elements of nonlocal operators composed of a certain number of quark and gluon fields taken at light-like separations [see Eqs. (2.14)-(2.16) below]. These operators emerge in the light-cone OPE of the T -product of currents, as explained in Sec. 2.4.1 where this technique is applied to a pion.

2.2.1 Scale dependence

While the LCDA is a nonperturbative input at lower scale μ_{low} , its evolution to the factorization scale μ is governed by perturbative QCD. The distribution amplitude can hence be written in the form [24]

$$\Phi(u, \mu) = \phi_V(u, v, \mu, \mu_{\text{low}}) \otimes \Phi(v, \mu_{\text{low}}), \quad (2.6)$$

where ϕ_V denotes the evolution part of the LCDA. ϕ_V is obtained by solving the evolution equation

$$\mu^2 \frac{\partial}{\partial \mu^2} \phi_V = V \otimes \phi_V, \quad (2.7)$$

and resumming the $\alpha_s \ln(\mu^2/\mu_0^2)^n$ terms, being

$$V = \frac{\alpha_s(\mu)}{4\pi} V_1 + \frac{\alpha_s^2(\mu)}{(4\pi)^2} V_2 + \dots \quad (2.8)$$

the perturbatively calculable evolution kernel.

2.2.2 Conformal partial waves expansion and asymptotic limit

Light-cone distribution amplitudes can be expanded in conformal partial waves employing the conformal theory of massless QCD [28]. The conformal spin (partial wave) decomposition allows to represent each DA as a sum of certain orthogonal polynomials that are function of the quark or antiquark longitudinal momentum fraction u . The trick is analogous to the partial wave expansion of the wave function in usual quantum mechanics. There, the rotational symmetry of the potential allows to separate the radial coordinate, governed by a one-dimensional Schrödinger equation, from the angular degrees of freedom, which are contained in spherical harmonics. Likewise, the conformal expansion of LCDAs in QCD aims to separate longitudinal degrees of freedom from transverse ones. For the pion leading twist 2 DA (see Sec. 2.4 for a definition of *twist*), this expansion has the simple form

$$\Phi_\pi(u, \mu) = 6u(1-u) \left[1 + \sum_{n=2,4,\dots} a_n(\mu) C_n^{3/2}(2u-1) \right], \quad (2.9)$$

where, aside from the prefactor, all the dependence in u is included in the Gegenbauer polynomials $C_n^{3/2}$, while the transverse momentum dependence (the scale dependence) is contained in the coefficients a_n which are given by [29]

$$a_n(\mu) = a_n(\mu_{\text{low}}) \left(\frac{\alpha_s(\mu)}{\alpha_s(\mu_{\text{low}})} \right)^{\gamma_n/\beta_0}, \quad (2.10)$$

being

$$\gamma_n = C_F \left[-3 - \frac{2}{(n+1)(n+2)} + 4 \sum_{k=1}^{n+1} \frac{1}{k} \right] \quad (2.11)$$

the anomalous dimensions. At $\mu \rightarrow \infty$ all $a_n(\mu)$ vanish and the asymptotic distribution amplitude

$$\Phi_\pi^{(\text{as})} = 6u(1-u), \quad (2.12)$$

is obtained, which is often taken as a contour condition of the LCDA at some given momentum much larger than the scale μ_{low} where Φ_π becomes non-perturbative.

The different partial waves, labeled by different "conformal spins" $j = n + 2$, do not mix with each other to leading logarithmic accuracy. Although conformal invariance is broken in QCD by higher-order quantum corrections, the conformal spin turns out to be a good quantum number in hard processes, up to small corrections of order α_s^2 , and it is therefore natural to expect that the hierarchy of contributions of different partial waves is preserved at sufficiently low scales. This means that only a few first "harmonics" are numerically important in B decays (which are the

ones important for this thesis). Besides, the coefficients a_n are multiplicatively renormalisable, as shown in Eq. (2.10), and have growing anomalous dimension so that, at sufficiently large normalisation scale μ , only the first few terms in the expansion are relevant too. Moreover, as high-order Gegenbauer polynomials oscillate rapidly, their convolution with smooth and well-behaved hard scattering kernels is strongly suppressed. Therefore, unless the coefficients a_n are abnormally large, all contributions from polynomials with $n \geq 4$ can be safely neglected when dealing with B decays. Consequently, the series in Eq. (2.9) can be safely truncated at $n = 2$ rendering

$$\Phi_\pi(u, \mu) \simeq 6u(1-u) \left[1 + a_2(\mu_0) \left(\frac{\alpha_s(\mu)}{\alpha_s(\mu_{\text{low}})} \right)^{50/81} C_2^{3/2}(2u-1) \right], \quad (2.13)$$

where $a_2(\mu_{\text{low}})$ (or any other $a_n(\mu_{\text{low}})$ coefficient) can be estimated either from two-point sum rules or from light-cone sum rules for measured hadronic quantities.

2.2.3 Meson light-cone distribution amplitudes

Light mesons

The leading twist light-cone distribution amplitudes for light pseudoscalar mesons (P), light longitudinally polarised vector mesons (V_{\parallel}) and light transversely polarized vector mesons (V_{\perp}) with flavour content $\bar{q}q'$ are defined through the following matrix elements of two-particle operators evaluated at light-cone points [30]:

$$\langle P(q) | \bar{q}_i(y)_\alpha [\dots] q'_j(x)_\beta | 0 \rangle \Big|_{(x-y)^2=0} = \frac{if_P}{4\kappa} \delta_{ij} (\not{q}\gamma_5)_{\beta\alpha} \int_0^1 du e^{i[(1-u)qx+uqy]} \Phi_P(u, \mu), \quad (2.14)$$

$$\langle V_{\parallel}(q) | \bar{q}_i(y)_\alpha [\dots] q'_j(x)_\beta | 0 \rangle \Big|_{(x-y)^2=0} = -\frac{if_{V_{\parallel}}}{4\kappa} \delta_{ij} \not{q}_{\beta\alpha} \int_0^1 du e^{i[(1-u)qx+uqy]} \Phi_{V_{\parallel}}(u, \mu), \quad (2.15)$$

$$\begin{aligned} \langle V_{\perp}(q) | \bar{q}_i(y)_\alpha [\dots] q'_j(x)_\beta | 0 \rangle \Big|_{(x-y)^2=0} &= -\frac{if_{V_{\perp}}(\mu_h)}{8\kappa} \delta_{ij} [\not{\epsilon}_{\perp}^*, \not{q}]_{\beta\alpha} \\ &\times \int_0^1 du e^{i[(1-u)qx+uqy]} \Phi_{V_{\perp}}(u, \mu), \end{aligned} \quad (2.16)$$

where the equality sign is to be understood as "equal up to higher-twist terms", i and j are colour indices, the parameter μ is the renormalisation scale of the light-cone operators of the left-hand side, $\kappa = \sqrt{2}$ ($\kappa = 1$) for π^0 and ρ^0 (for other mesons), and f_P , $f_{V_{\parallel}}$ and $f_{V_{\perp}}(\mu_h)$ are the corresponding meson decay constants (see Sec. 3.2). The helicity structure is determined by the angular momentum of the meson and the fact that the spinor of an energetic quark has only two large components. The dots in Eqs. (2.14)–(2.16) represent path-ordered exponentials that connect the two quark fields at different positions (x and y) and make the matrix element gauge invariant (see [31]). With these definitions the three distribution amplitudes (Φ_P , $\Phi_{V_{\parallel}}$ and $\Phi_{V_{\perp}}$) are normalised to unity and have the asymptotic form of Eq. (2.12).

The *boundary conditions* of light-meson LCDAs may be estimated with the assumption that, at a given scale, the distribution amplitude has the same behaviour at the end points than the asymptotic distribution amplitude of Eq. (2.12). This condition will be fulfilled approximately only if this scale is much larger than μ_{low} , which is precisely what occurs in a heavy-to-light meson decay if the B momentum and the momentum of the light meson in the B meson rest frame are both of $O(m_b)$. As all computations have an uncertainty of $O(\Lambda_{\text{QCD}}/m_b)$ coming from the HQET and LEET Lagrangians (see Sec. 3.1.4), one can count

$$\Phi_X(u) \sim \begin{cases} 1 & \text{generic } u, \\ \Lambda_{\text{QCD}}/m_b & u, 1-u \sim \Lambda_{\text{QCD}}/m_b. \end{cases} \quad \text{with } X = P, V_{\parallel}, V_{\perp}. \quad (2.17)$$

Eq. (2.17) shows that when the longitudinal light-cone momentum fraction u is not of the same order as the uncertainty, the LCDA does contribute to the convolution integral. Furthermore, when u and $1-u \sim O(\Lambda_{\text{QCD}}/m_b)$ then the light outgoing meson momentum q is of $O(\Lambda_{\text{QCD}})$, which is the typical scale of valence quark and antiquark momenta. Therefore there is a high probability that the outgoing meson is already hadronised, so the LCDA must be very suppressed (in fact it is of $O(\Lambda_{\text{QCD}}^2/m_b^2)$ at end points [30]).

The B meson

The B meson is heavy. However, the momentum distribution of its valence quarks can be probed by a hard gluon connecting one of the two quarks of the final light meson with the quark inside the B that does not decay (known as *spectator quark*), and hence the B meson LCDA must also be taken into account. The spectator quark bound to the b quark is light, so it carries a momentum of $O(\Lambda_{\text{QCD}})$ and will have a longitudinal light-cone momentum fraction χ of order Λ_{QCD}/m_b , whereas the b quark will have the largest part of the light-cone momentum of the B meson p , and hence $p_{b,\parallel} = (1-\chi)p_{\parallel} \approx p_{\parallel}$.

At leading order in $1/m_b$, the distribution of χ inside the B meson is described in terms of two LCDAs. In the case in which the transverse momentum of the spectator quark may be neglected when computing the hard-scattering amplitude, these LCDAs can be defined through [30]

$$\begin{aligned} \langle 0 | \bar{q}_i(z)_{\alpha} [\dots] b_j(0)_{\beta} | \bar{B}_d(p) \rangle \Big|_{z_{+,\perp}=0} &= -\frac{if_B}{4} \delta_{ij} [(\not{p} + m_b)\gamma_5]_{\beta\gamma} \\ &\times \int_0^1 d\chi e^{-i\chi p+z-} [\Phi_{B1}(\chi) + \not{n}_- \Phi_{B2}(\chi)]_{\gamma\alpha}, \end{aligned} \quad (2.18)$$

where $n_- \equiv (1, 0, 0, -1)$ and the subscripts $+$, $-$ denote, respectively, the positive and the

negative longitudinal light-cone components⁴, whereas the subscript \perp is reserved for the two transverse components of the spectator quark momentum that have been ignored. Moreover, f_B is the decay constant of the \bar{B} meson (see Sec. 3.2).

Φ_{B1} and Φ_{B2} are normalised as

$$\int_0^1 d\chi \Phi_{B1}(\chi) = 1, \quad \int_0^1 d\chi \Phi_{B2}(\chi) = 0. \quad (2.19)$$

At leading power in α_s the hard spectator contribution depends only on Φ_{B1} [30]. This dependence is of the form

$$\int_0^1 d\chi \frac{\Phi_{B1}(\chi)}{\chi} \equiv \frac{m_B}{\lambda_B}, \quad (2.20)$$

which defines the first inverse moment of Φ_{B1} , the hadronic parameter λ_B of $O(\Lambda_{\text{QCD}})$ [32]. The asymptotic LCDA can not be used to estimate the contribution of Φ_{B1} at end points because the typical scale of a B meson is already m_b , so the requisite $\mu \rightarrow \infty$ is not fulfilled. Fortunately, the first normalisation condition in Eq. (2.19) may be employed instead to obtain the following counting:

$$\Phi_{B1}(\chi) \sim \begin{cases} m_b/\Lambda_{\text{QCD}} & \chi \sim \Lambda_{\text{QCD}}/m_b, \\ 0 & \chi \sim 1. \end{cases} \quad (2.21)$$

The meaning of Eq. (2.21) is clear: when the momentum of the spectator quark is of order Λ_{QCD} , the momentum of the b quark will be of order m_b as one would expect intuitively, but is practically impossible to find the light spectator quark with momentum of order m_b , as there is only a marginal probability for hard fluctuations that transfer a large momentum to the spectator quark.

2.3 Introduction to QCD sum rules

The QCD sum rules method was developed more than thirty years ago by Shifman, Vainshtein and Zakharov [33]. Over this time, it has become a powerful tool in particle physics phenomenology, being able to reproduce many hadronic observables that are in good agreement with both experimental data and QCD lattice computations, such as decay constants, form factors and parton distributions. Moreover, QCD sum rules (QCDSRs), used together with experimental data on hadronic experimental densities, have been employed to determine quark masses and some universal non-perturbative parameters (such as vacuum condensates).

⁴Given a four vector $k^\mu = (k^0, k^1, k^2, k^3)$, the longitudinal light-cone components may be defined as

$$k_\pm = \frac{k^0 \pm k^3}{\sqrt{2}}.$$

This section will be devoted to sketch the procedure of constructing a simple QCD sum rule. Two different pathways (named *A* and *B*) will be followed and the final outcome from each route will be then matched to the other using the quark-hadron duality assumption. Once this goal has been accomplished our focus will move to *light-cone sum rules* (LCSRs). Although there are several excellent reviews on QCD sum rules (see, for instance, [34]), this summary is based mainly on [29] with contributions of [28] on the LCSR part.

2.3.1 Path A

A.1 - Construction of a correlation function of quark currents

The amplitude of a hadronic process can be written as the Fourier transform of a correlation function of quark currents propagating at different points of space-time. For simplicity, the derivation of a QCDSR for the amplitude

$$\Pi_{\mu\nu}(q) = i \int d^4x e^{iq \cdot x} \langle 0 | T \{ j_\mu(x), j_\nu(0) \} | 0 \rangle = (q_\mu q_\nu - q^2 g_{\mu\nu}) \Pi(q^2) \quad (2.22)$$

will be reviewed. This amplitude corresponds, for instance, to the quark-antiquark loop created by the virtual photon in a lepton-lepton scattering. In Eq. (2.22) q is the four-momentum of the virtual photon with $q^2 < 0$ and $j_\mu = -e\bar{\psi}\gamma_\mu\psi$ is the colourless quark current with a given flavour $\psi = u, d, s, c, \dots$. $\Pi(q^2)$ is the part of the amplitude (devoid of Lorentz structure) that encodes all dynamical effects, whereas the factor $q_\mu q_\nu - q^2 g_{\mu\nu}$ stems from the conservation of the electromagnetic current.

A.2 - Computation of the correlation function at large Q^2

If the four-momentum squared transferred to hadron constituents (*partons*) in the final state is large, $Q^2 \equiv -q^2 \gg \Lambda_{\text{QCD}}^2$, at least some of the quarks or gluons will become highly virtual and will travel very short distances. This condition guarantees the smallness of the corresponding effective quark-gluon coupling $\alpha_s = g_s^2/4\pi$ and, thereby, legitimates the perturbative expansion of the correlation function. Therefore, the computation of the correlation function can be split in two parts:

- The *LO term* in α_s gives the main contribution to the perturbative series. At very large $Q^2 = -q^2$ the virtual quarks in the correlation function can be replaced by the free-quark propagators inferred directly from the QCD Lagrangian. The computation of $\Pi^{(0)}(q^2)$ can be then performed following the standard steps: starting from free quark two-point correlation function, one has to integrate over the space-time coordinate x , shift to $D \neq 4$ dimensions, take traces, perform the momentum integration in D dimensions, the Wick rotation and the angular integration in the four-dimensional integral.

- The *radiative corrections* to the former term, which may be sizeable depending on the process considered.

For the correlation function in Eq. (2.22) it can be obtained [29]:

$$\text{Im } \Pi^{(pert)}(s) = \text{Im } \Pi^{(0)}(s) \left\{ 1 + \alpha_s C_F \left[\frac{\pi}{2v} - \frac{v+3}{4} \left(\frac{\pi}{2} - \frac{3}{4\pi} \right) \right] \right\}, \quad (2.23)$$

where $v = \sqrt{1 - 4m^2/s}$, m is the mass of the quark in the loop and $\text{Im } \Pi^{(pert)}(s)$ is related to $\Pi(s)$ via the dispersion relation (see Sec. B.2 below).

A.3 - Vacuum condensates and operator product expansion

The complete calculation of $\Pi(q^2)$ has to include also the effects due to the fields of soft gluons and quarks that populate the QCD vacuum, fluctuating with typical long-distance scales $\Lambda_{\text{vac}} \sim \Lambda_{\text{QCD}}$. At $Q^2 \gg \Lambda_{\text{QCD}}^2$, the average distance between the points of emission and absorption of a quark-antiquark pair is smaller than Λ_{vac} , so the pair traveling in the QCD vacuum is expected to perceive only the mean fields created by soft vacuum gluons and quarks. In the case of light quarks several important effects occur: vacuum gluons are emitted and absorbed by virtual quarks, virtual quarks and antiquarks are interchanged with their vacuum counterparts and a combined quark-gluon interaction also takes place, whereas for heavy quarks only the interactions with vacuum gluons are important.

These long-distance interactions can be incorporated into $\Pi_{\mu,\nu}(q)$ in the same footing as short-distance effects using a generalised Wilson OPE

$$\Pi_{\mu,\nu}(q) = (q_\mu q_\nu - q^2 g_{\mu\nu}) \sum_d C_d(q^2, \mu) \langle 0 | \mathcal{O}_d(\mu) | 0 \rangle. \quad (2.24)$$

In this expansion:

- The operators in Eq. (2.24) are ordered according to their dimension d . The operator with $d = 0$ is the unit operator associated with the perturbative contribution $C_0(q^2)$ computed in Sec A.2. Higher-dimension operators are composed of quark ($\psi, \bar{\psi}$) and gluon ($G_{\mu\nu}^a$) fields and their vacuum expectation values are named *vacuum condensates*. The contributions of high-dimensional condensates, corresponding to diagrams with multiple insertions of vacuum gluons and quarks, are suppressed by large powers of $\Lambda_{\text{vac}}^2/Q^2$, so the OPE is usually truncated after the first six terms (even at $Q^2 \sim 1 \text{ GeV}^2$), which are given by:

$$\mathcal{O}_3 = \bar{\psi}\psi \quad \mathcal{O}_4 = G_{\mu\nu}^a G^{a\mu\nu} \quad \mathcal{O}_5 = \bar{\psi} \sigma_{\mu\nu} \frac{\lambda^a}{2} G^{a\mu\nu} \psi, \quad (2.25)$$

$$\mathcal{O}_6^\psi = (\bar{\psi} \Gamma_r \psi) (\bar{\psi} \Gamma_s \psi) \quad \mathcal{O}_6^G = f_{abc} G_{\mu\nu}^a G_\sigma^{b\nu} G^{c\sigma\mu}. \quad (2.26)$$

- Short-distance dynamics related to the quark currents is contained in the Wilson coefficients $C_d(q^2, \mu)$ in Eq. (2.24), whereas long-distance effects are represented by the universal condensates $\langle 0 | O_d(\mu) | 0 \rangle$ with $d \neq 0$, which are independent of the properties of the quark currents. The scale μ that separates these regions of short ($p^2 < \mu^2$) and long ($p^2 > \mu^2$) distance interactions must be large enough to justify the perturbative calculation of $C_d(q^2, \mu)$ in QCD.

The Wilson coefficients $C_d(q^2)$ are computed using the procedure sketched in Sec. 1.1.2. The computation of the vacuum condensates introduced in the OPE is much more involved, as these are non-perturbative parameters that have to be obtained on a case-by-case basis. The quark condensate given by \mathcal{O}_3 in Eq. (2.26) is special, as it is responsible for the observed spontaneous breaking of the chiral symmetry in QCD and, therefore, was well determined long before it was used in QCDSRs. Very little is known about the other condensates though. They have been computed either on the lattice or fitting certain QCDSRs to experimental data but, being universal, the condensates extracted from one SR can be used in many others.

2.3.2 Path B

B.1 - Unitarity relation and summation of hadronic states

If q^2 is shifted from large negative to positive values, the average distance between the space-time points in the correlation function grows. Consequently, long-distance quark-gluon interactions become important and, eventually, the quarks form hadrons. Therefore, the perturbative QCD result must be combined with certain wave functions or momentum distribution functions that describe QCD dynamics at distances of the order of the hadron size ($R_{hadr} \sim 1/\Lambda_{QCD}$), a scale at which perturbation theory in α_s is not applicable.

Physically, the hadrons formed are observed as resonances in $\ell^+\ell^-$ annihilation processes, the first of these resonances being at energy $\sqrt{q^2} = m_V$. This hadronic content of $\Pi_{\mu\nu}$ at $q^2 > 0$ can be quantified using the *unitarity relation*, i.e. by inserting a complete set of intermediate hadronic states $|n\rangle$ in Eq. (2.22)

$$2 \operatorname{Im} \Pi(q^2) = \sum_n \langle 0 | j_\mu | n \rangle \langle n | j_\nu | 0 \rangle d\tau_n (2\pi)^4 \delta^{(4)}(q - p_n), \quad (2.27)$$

where the summation spans over all possible hadronic states $|n\rangle$ created by the quark current j_μ and includes sums over polarisations, while $d\tau_n$ denotes the integration over the phase space volume of these states.

It is convenient to single out the contribution from the ground-state to $\Pi(q^2)$ from the rest of contributions, which include excited states and the continuum of two- and many-body hadron states that contribute to the amplitude, on the basis of the q^2 dependence of quark current matrix elements between the vacuum and the state $|n\rangle$, obtaining:

$$\frac{1}{\pi} \operatorname{Im} \Pi(q^2) = f_V^2 \delta(q^2 - m_V^2) + \rho^h(q^2) \theta(q^2 - s_0^h), \quad (2.28)$$

where f_V is the decay constant of the particle (assumed to be a vector meson), m_V is the mass of the one-particle ground state, $\rho^h(q^2)$ is related to hadronic matrix elements for multiparticle states $\langle n | j_\mu | 0 \rangle$ and s_0^h depicts the threshold of the lowest continuum state (which is lower than m_V in the light quark channels but higher than several quarkonium resonances in the heavy quark channels, and so $\text{Im } \Pi(q^2) \rightarrow \sum_{\text{res}} \text{Im } \Pi^{\text{res}}(q^2)$ in the latter). Notice that, in Eq. (2.28), the total decay width of the ground state has been neglected for simplicity.

B.2 - Derivation of the dispersion relation

From the above discussion it has become clear that the correlation function in Eq. (2.22) is an object of *dual* nature. At large $q^2 < 0$ it represents a short distance quark-antiquark fluctuation that can be computed in QCD, whereas at $q^2 > 0$ it has a decomposition in terms of hadronic observables.

The next step is to derive a *dispersion relation* linking $\Pi(q^2)$ in Eq. (2.22) to the hadronic sum in Eq. (2.28). As $\Pi(q^2)$ is analytic, a convenient integration contour⁵ in the plane of the complex variable $q^2 = z$ can be chosen and the Cauchy formula used on it:

$$\Pi(q^2) = \frac{1}{2\pi i} \oint_C dz \frac{\Pi(z)}{z - q^2} = \frac{1}{2\pi i} \oint_{|z|=R} dz \frac{\Pi(z)}{z - q^2} + \frac{1}{2\pi i} \int_0^R dz \frac{\Pi(z + i\epsilon) - \Pi(z - i\epsilon)}{z - q^2}. \quad (2.29)$$

The contour integral in Eq. (2.29) tends to zero if $\Pi(q^2)$ vanishes fast enough at $|q^2| \sim R \rightarrow \infty$, whereas the last integral can be modified using the Schwartz reflection principle, since $\Pi(q^2)$ is imaginary at $q^2 > t_{\min} = \min\{m_V^2, s_0^h\}$. After this replacement, the *dispersion relation*

$$\Pi(q^2) = \frac{1}{\pi} \int_{t_{\min}}^{\infty} ds \frac{\text{Im}\Pi(s)}{s - q^2 - i\epsilon} \quad (2.30)$$

is obtained. After transforming Eq. (2.30) (see [29] for further details), the modified dispersion relation

$$\Pi(q^2) = \frac{q^2}{\pi} \int_{t_{\min}}^{\infty} ds \frac{\text{Im}\Pi(s)}{s(s - q^2)} + \Pi(0) \quad (2.31)$$

can be found, where the infinitesimal $-i\epsilon$ has been dropped to lighten the notation.

As a final step, substituting Eq. (2.28) into Eq. (2.31) a non-trivial constraint on the sum over hadronic parameters

$$\Pi(q^2) = \frac{q^2 f_V^2}{m_V^2(m_V^2 - q^2)} + q^2 \int_{s_0^h}^{\infty} ds \frac{\rho^h(s)}{s(s - q^2)} + \Pi(0) \quad (2.32)$$

can be deduced. Relations of this kind constitute the central objects of QCDSRs.

⁵This contour should surround the positions of hadronic thresholds at $q^2 > 0$ but contain the $q^2 < 0$ reference point for the QCD calculation.

B.3 - Using the Borel transformation

The Borel transformation is an operator defined as

$$\mathcal{B}_{M^2} \equiv \lim_{\substack{-q^2, n \rightarrow \infty \\ -q^2/n = M^2}} \frac{(-q^2)^n}{(n+1)!} \left(\frac{d}{dq^2} \right)^n \Pi(q^2). \quad (2.33)$$

where M^2 is the *Borel parameter*, which reflects the average virtuality in the correlator [35]. It can be shown that

$$\mathcal{B}_{M^2} \left[\left(\frac{1}{-q^2} \right)^n \right] = \frac{1}{(n-1)!} \left(\frac{1}{M^2} \right)^n \quad \text{and} \quad \mathcal{B}_{M^2} [\ln(-q^2)] = -1, \quad (2.34)$$

which in turn entails

$$\mathcal{B}_{M^2} \left(\frac{1}{s-q^2} \right) = \frac{1}{M^2} e^{-s/M^2}, \quad (2.35)$$

so the Borel-transformed dispersion relation in Eq. (2.30) takes the form

$$\Pi(M^2) \equiv \mathcal{B}_{M^2}(q^2) = \frac{1}{\pi M^2} \int_{s_0^h}^{\infty} ds \operatorname{Im} \Pi(s) e^{-s/M^2}. \quad (2.36)$$

When applied to both sides of Eq. (2.32), a more convenient form of the sum rule is obtained:

$$\Pi(M^2) = f_V^2 e^{-m_V^2/M^2} + \int_{s_0^h}^{\infty} ds \rho^h(s) e^{-s/M^2}. \quad (2.37)$$

Therefore, the Borel transformation can be regarded a mathematical object that removes subtraction terms in the dispersion relation and suppresses exponentially the contributions from excited resonances and continuum states heavier than m_V , enhancing the ground-state V meson contribution.

2.3.3 The quark-hadron duality and the matching of paths A and B

In the spacelike region $q^2 \rightarrow -\infty$, where all power-suppressed condensate contributions can be safely neglected, the limit $\Pi(q^2) \rightarrow \Pi^{(pert)}(q^2)$ is valid, yielding an approximate equation of the corresponding dispersion integrals:

$$q^2 \int_{t_{min}}^{\infty} ds \frac{\operatorname{Im} \Pi(s)}{s(s-q^2)} \simeq q^2 \int_{4m^2}^{\infty} ds \frac{\operatorname{Im} \Pi^{(pert)}(s)}{s(s-q^2)}. \quad (2.38)$$

To satisfy Eq. (2.38), the integrands of the l.h.s. and the r.h.s. must have the same asymptotic behaviour:

$$\operatorname{Im} \Pi(s) \xrightarrow{s \rightarrow +\infty} \operatorname{Im} \Pi^{(pert)}(s). \quad (2.39)$$

Eqs. (2.38) and (2.39) are known as *global* and *local quark hadron duality* respectively. From these expressions it has been postulated (and checked experimentally in [36]) that at sufficiently large $Q^2 = -q^2$,

$$q^2 \int_{s_0^h}^{\infty} ds \frac{\rho^h(s)}{s(s-q^2)} \simeq \frac{1}{\pi} q^2 \int_{s_0}^{\infty} ds \frac{\text{Im} \Pi^{(pert)}(s)}{s(s-q^2)}, \quad (2.40)$$

is a valid approximation. s_0 is a threshold parameter that does not necessarily coincide with s_0^h , but it is expected to be close to the mass squared of the first excited state of V .

Eq. (2.40) can be Borel transformed to obtain

$$\int_{s_0^h}^{\infty} ds \rho^h(s) e^{-s/M^2} \simeq \frac{1}{\pi} \int_{s_0}^{\infty} ds \text{Im} \Pi^{(pert)}(s) e^{-s/M^2}. \quad (2.41)$$

The relation (2.40) and its Borel transformed version (2.41) represent the quark-hadron duality approximation used in QCDSRs to replace the integrals over continuum and excited states.

To finish with this example, the result from path A has to be matched with that of path B . Using Eq. (2.37) on the l.h.s. and the Borel transformed OPE of the perturbative part that is obtained at the end of Sec. A.3 on the r.h.s. (see [29] for a derivation of this equation) one arrives to

$$\begin{aligned} f_V^2 e^{-m_V^2/M^2} + \int_{s_0^h}^{\infty} ds \rho^h(s) e^{-s/M^2} &= \\ &= \frac{1}{4\pi^2} \left(1 + \frac{\alpha_s(M)}{\pi} \right) \int_0^{\infty} ds e^{-s/M^2} + \frac{2m \langle \bar{\psi}\psi \rangle}{M^2} + \frac{\langle \frac{\alpha_s}{\pi} G_{\mu\nu}^a G^{a\mu\nu} \rangle}{12M^2} - \frac{112\pi \alpha_s \langle \bar{\psi}\psi \rangle^2}{81 M^4}, \end{aligned} \quad (2.42)$$

Using the quark-duality approximation (2.41) in Eq. (2.43), the integral over $\rho^h(s)$ can be subtracted from the perturbative part on the r.h.s. The resulting QCDSR for the parameters of the ground-state hadron V , which is assumed to be a ρ meson for definiteness, reads:

$$\begin{aligned} f_\rho^2 = M^2 e^{m_\rho^2/M^2} \left[\frac{1}{4\pi^2} \left(1 - e^{-s_0^p/M^2} \right) \left(1 + \frac{\alpha_s(M)}{\pi} \right) \right. \\ \left. + \frac{(m_u + m_d) \langle \bar{\psi}\psi \rangle}{M^4} + \frac{1}{12} \frac{\langle \frac{\alpha_s}{\pi} G_{\mu\nu}^a G^{a\mu\nu} \rangle}{M^4} - \frac{112\pi \alpha_s \langle \bar{\psi}\psi \rangle^2}{81 M^6} \right], \end{aligned} \quad (2.43)$$

s_0^p being the duality threshold for the ρ meson channel.

From a practical point of view Eq. (2.43) is used in the following way. A range for M^2 is carefully chosen. If M^2 is too small, the missing terms with higher-dimensional condensates and the short distance non-perturbative effects may become too important to be neglected, as they are all proportional to large powers of $1/M^2$, whereas a too large M^2 would render the quark-hadron approximation untrustworthy. Then, both f_ρ and s_0^p are fitted by demanding the maximal stability of f_ρ within the chosen energy range and m_ρ is fixed by its experimental value.

2.3.4 Final considerations

The use of QCDSRs entails several benefits but also has its drawbacks [29, 28], namely

Advantages

- Hadrons can be studied without the need of a model-dependent treatment in terms of their constituent quarks.
- Theoretical uncertainties can be estimated quite accurately and are typically of the order of 10 – 15 % [29]. Dependence on the Borel parameter, inaccurate knowledge of the condensate densities, neglect of $d > 6$ terms in the OPE and limited accuracy of perturbative contributions constitute the main sources of theoretical uncertainty.
- They can be used within the framework of EFTs, such as the HQET.
- They have many applications to the obtention of hadron physics-related quantities [29]. Those relevant for this thesis are the decay constants of light and heavy mesons and the heavy-to-light meson form factors, which can be computed from three-point correlation functions.

Drawbacks

- QCDSRs are always approximate and their accuracy cannot be improved beyond certain limits. The choice of s_0^h , for instance, introduces a certain model-dependence (or systematic error) in the final result that cannot be avoided [29, 37, 10].
- In the QCDSRs obtained for some meson form factors, high-dimension condensates are accompanied by increasing powers of Q^2 so that, as the momentum transferred increases, the form factor starts to diverge. This signals the break down of the OPE, showing that the expansion in slowly varying vacuum fields is inadequate if a short-distance subprocess is involved. Three-point sum rules for heavy-to-light meson form factors have similar problems at large recoils but with Q^2 replaced by $m_b^{1/2}$ [28].
- In some QCDSRs, transitions from the ground state to excited states ("non-diagonal" transitions) produce single-pole terms that are not suppressed by the Borel transformation. Double dispersion relations and double Borel transformations have been used to get rid of these "parasitic terms" but this way of proceeding seems to lead to more problems than solutions [28].

2.4 Introduction to light-cone sum rules

The method of light-cone sum rules (LCSRs) was developed in late eighties by Braun *et al.* [38, 39, 40]. Technically, the LCSR approach is a hybrid of the theory of hard exclusive processes and QCDSRs so that, within this framework, one is able to take into account both hard scattering and soft (end-point) contributions. The defining feature of a generic LCSR is to replace the short-distance OPE by an expansion in powers of the transverse distance between partons in light-cone coordinates. This kind of expansion rearranges the relevant operators in terms of their *twist*⁶ rather than their dimension. For a given twist, the expansion in local operators is replaced by an expansion in conformal partial waves, each of which takes into account a subset of operators of all dimensions.

The LCSR approach has two main advantages over QCDSRs:

- Additional information on QCD correlation functions related to approximate conformal symmetry of the theory is incorporated into the sum rule.
- QCDSRs vacuum condensates are substituted by light-cone hadron distribution functions of increasing twist, which have a direct physical significance (see below).

As in the case of QCDSRs, we will try to sketch briefly the steps that must be followed in order to construct a LCSR for a particular process [29].

2.4.1 Path A

A.1 - Construction of a correlation function of quark currents

The starting object of a LCSR is different than that of a QCSR. One considers a correlation function which is a T -product of two quark currents sandwiched between vacuum and an on-shell state (either a light-quark hadron or a photon). A simple physical example is provided by the process $e^-e^+ \rightarrow \pi^0 e^+e^-$, where the π^0 results from the fusion of two γ^* via quark electromagnetic currents. The corresponding amplitude is given by

$$\begin{aligned} F_{\mu\nu}(p, q) &= i \int d^4x e^{-iq \cdot x} \langle \pi^0(p) | T \{ j_\mu^{em}(x) j_\nu^{em}(0) \} | 0 \rangle \\ &= \epsilon_{\mu\nu\alpha\beta} p^\alpha q^\beta F(Q^2, (p-q)^2), \end{aligned} \quad (2.44)$$

where p is the pion momentum, q and $(p-q)$ are the photon momenta, $Q^2 = -q^2$, j_μ^{em} is the quark electromagnetic current and F is the invariant amplitude encoding the dynamics of the process. For simplicity, the chiral limit is adopted and $p^2 = m_\pi^2 = 0$.

⁶The *twist* of a traceless and totally symmetric operator is defined as the difference between its dimension and spin.

A.2.3 - Expansion of the correlation function in local operators around the light-cone

At sufficiently large $Q^2 = -q^2$ and $|(p - q)^2|$ ($|(p - q)^2| \sim Q^2 \gg \Lambda_{\text{QCD}}^2$), the dominant part of the integral in Eq. (2.44) must stem from the region near the light cone ($x^2 \sim 0$) to avoid strong oscillations arising from the term $e^{-iq \cdot x}$ [29], so the expansion of the T -product quark currents near the light-cone is well justified.

As a first step the LO contribution to the light-cone OPE of the correlator in Eq. (2.44) will be calculated. For simplicity, only the u -quark part of the currents will be considered and the electromagnetic charge factor will be omitted. Contracting the u quark fields in Eq. (2.44), using the propagator of the free massless quark

$$iS_0(x, 0) = \langle 0 | T\{u(x)\bar{u}(0)\} | 0 \rangle = \frac{i \not{x}}{2\pi^2 x^4}, \quad (2.45)$$

and transforming $\gamma_\mu \gamma_\alpha \gamma_\nu \rightarrow -i\epsilon_{\mu\alpha\nu\rho} \gamma^\rho \gamma_5 + \dots$, it can be obtained [29]

$$F_{\mu\nu}(p, q) = -i\epsilon_{\mu\nu\alpha\rho} \int d^4x \frac{x^\alpha}{\pi^2 x^4} e^{-iq \cdot x} \langle \pi^0(p) | \bar{u}(x) \gamma^\rho \gamma_5 u(0) | 0 \rangle. \quad (2.46)$$

The nonlocal quark-antiquark operator in Eq. (2.46) can be expanded in local operators around $x = 0$

$$\bar{u}(x) \gamma_\rho \gamma_5 u(0) = \sum_r \frac{1}{r!} \bar{u}(0) (\overleftarrow{D} \cdot x)^r \gamma_\rho \gamma_5 u(0). \quad (2.47)$$

The matrix elements of these operators have the following general decomposition

$$\begin{aligned} \langle \pi^0(p) | \bar{u} \overleftarrow{D}_{\alpha_1} \overleftarrow{D}_{\alpha_2} \dots \overleftarrow{D}_{\alpha_r} \gamma_\rho \gamma_5 u | 0 \rangle &= (-i)^r p_{\alpha_1} p_{\alpha_2} \dots p_{\alpha_r} p_\rho M_r \\ &+ (-i)^r g_{\alpha_1 \alpha_2} p_{\alpha_3} \dots p_{\alpha_r} p_\rho M'_r + \dots, \end{aligned} \quad (2.48)$$

where M_r, M'_r, \dots are matrix elements of local operators. The first term is totally symmetric and traceless (at $p^2 = 0$) and contains only 4-vectors while other terms contain one or more $g_{\alpha_i \alpha_j}$. Substituting the decomposition in Eq. (2.47) in Eq. (2.46), integrating over x and using Eq. (2.48) and $\xi \equiv |2q \cdot p|/Q^2$ one obtains

$$F(Q^2, (p - q)^2) = \frac{1}{Q^2} \sum_{r=0}^{\infty} \xi^r M_r + \frac{4}{Q^4} \sum_{r=2}^{\infty} \frac{\xi^{r-2}}{r(r-1)} M'_r + \dots. \quad (2.49)$$

As $|2q \cdot p| = |q^2 - (p - q)^2| \sim Q^2$ then $\xi \sim 1$ in a generic exclusive process with $p \neq 0$, so all terms in each series of Eq. (2.49) must be kept or, in other words, the expansion F in local operators cannot be truncated at any finite order. On the other hand, there is a hierarchy on the r.h.s. of Eq. (2.49), as the second term containing M'_r and further similar terms are suppressed by powers of the small parameter $1/Q^2$ when compared with the first term containing M_r . The difference between the local operators entering the first and the second terms in Eq. (2.49) turns

out to be in their twist. The lowest twist of the operators entering Eq. (2.48) is 2 because the operator without derivatives has dimension 3 and Lorentz spin 1. Furthermore, after taking the matrix elements, the twist 2 components of the operators contribute only to the first term of Eq. (2.48), containing M_r . If both sides of Eq. (2.48) are multiplied by $g_{\alpha_1\alpha_2}$ it becomes clear that the matrix elements M'_r receive their contributions from the twist 4 operators, the lowest-dimension operator among them being $\bar{u}(\overleftarrow{D})^2\gamma_\rho\gamma_5u$, and so on and so forth. Therefore, the nonlocal operator in Eq. (2.46) has to be treated by expanding it near the light cone ($x^2 = 0$) in components corresponding to different twists.

In the leading order of this expansion, at $x^2 = 0$ (and $p^2 = 0$), the matrix element in Eq. (2.46) has the following parametrisation:

$$\langle\pi^0(p)|\bar{u}(x)\gamma_\mu\gamma_5u(0)|0\rangle_{x^2=0} = -ip_\mu\frac{f_\pi}{\sqrt{2}}\int_0^1 du e^{iup\cdot x}\Phi_\pi(u,\mu), \quad (2.50)$$

where the function $\Phi_\pi(u,\mu)$ is the pion light-cone distribution amplitude of twist 2. The renormalisation scale μ emerges due to the logarithmic dependence on x^2 and reflects the light-cone separation between the quark and antiquark fields in the operator. At $x = 0$, Eq. (2.50) is simply reduced to the matrix element that defines the pion decay constant (see Sec. 3.2). Furthermore, expanding both sides of Eq. (2.50) and comparing the l.h.s. with the expansions in Eq. (2.47) and Eq. (2.48) it is found that the moments of $\Phi_\pi(u)$ are related to the matrix elements of local twist-2 operators:

$$M_r = -i\frac{f_\pi}{\sqrt{2}}\int_0^1 du u^r\Phi_\pi(u,\mu). \quad (2.51)$$

As already stated in Sec. 2.2, the function $\Phi_\pi(u)$ multiplied by f_π , is a universal non-perturbative object that encodes the long-distance dynamics of the pion which, together with the higher-twist terms, plays a similar role as the vacuum condensates do in QCDSRs. Now, with the knowledge gained in Sec. 2.2, Eq. (2.48) can be interpreted as the expansion in conformal partial waves mentioned at the beginning of this section.

Substituting Eq. (2.50) in Eq. (2.46), integrating over x , restoring the electromagnetic charge factor and adding the d -quark part the correlation function in the twist 2 approximation is obtained:

$$F^{(tw2)}(Q^2,(p-q)^2) = \frac{\sqrt{2}f_\pi}{3}\int_0^1 \frac{du\Phi_\pi(u,\mu)}{\bar{u}Q^2 - u(p-q)^2}, \quad (2.52)$$

where the definition $\bar{u} \equiv 1 - u$ has been used. It is important to notice that this representation has the form of a convolution

$$F^{(tw2)}(Q^2,(p-q)^2) = \frac{\sqrt{2}f_\pi}{3}\int_0^1 du\Phi_\pi(u,\mu)T_H(Q^2,(p-q)^2,u,\mu) \quad (2.53)$$

of the hard scattering amplitude T_H with the distribution amplitude ϕ_π , and also that T_H does not depend on μ at zeroth order in α_s .

2.4.2 Path B

B.1,2 - Using unitarity and deriving the dispersion relation

Using unitarity in the channel of the current j_ν^{em} with momentum $p - q$, a dispersion relation for Eq. (2.44) in the variable $(p - q)^2$ keeping the variable Q^2 fixed can be derived [29] :

$$F_{\mu\nu}(p, q) = 2 \frac{\langle \pi^0(p) | j_\mu^{em} | \rho^0(p - q) \rangle \langle \rho^0(p - q) | j_\nu^{em} | 0 \rangle}{m_\rho^2 - (p - q)^2} + \frac{1}{\pi} \int_{s_0^h}^{\infty} ds \frac{\text{Im} F_{\mu\nu}(Q^2, s)}{s - (p - q)^2}. \quad (2.54)$$

The first term in Eq. (2.54) corresponds to the ground-state contribution of the ρ meson. It contains the hadronic matrix element that determines the $\gamma^* \rho \rightarrow \pi$ transition form factor multiplied by the ρ meson decay constant: $\langle \rho^0(p - q) | j_\nu^{em} | 0 \rangle = (f_\rho / \sqrt{2}) m_\rho \epsilon_\nu^{(\rho)*}$. The dispersion integral includes the contributions of excited and continuum states at $s > s_0^h$ and the coefficient 2 takes into account the contribution of ω meson, which is approximately equal to that of ρ .

2.4.3 The quark-hadron duality and the matching of paths A and B

Representing Eq. (2.52) in a form of the dispersion integral

$$F^{(tw2)}(Q^2, (p - q)^2) = \int_0^\infty ds \frac{\frac{1}{\pi} \text{Im} F^{(tw2)}(Q^2, s)}{s - (p - q)^2} \quad (2.55)$$

with

$$\frac{1}{\pi} \text{Im} F^{(tw2)}(Q^2, s) = \frac{\sqrt{2} f_\pi}{3} \int_0^1 du \Phi_\pi(u) \delta(\bar{u} Q^2 - us), \quad (2.56)$$

the duality approximation for the contribution of excited and continuum states is obtained:

$$\int_{s_0^h}^\infty ds \frac{\frac{1}{\pi} \text{Im} F(Q^2, s)}{s - (p - q)^2} = \int_{s_0^p}^\infty ds \frac{\frac{1}{\pi} \text{Im} F^{(tw2)}(Q^2, s)}{s - (p - q)^2} = \frac{\sqrt{2} f_\pi}{3} \int_0^{u_0^p} \frac{du \Phi_\pi(u)}{\bar{u} Q^2 - u(p - q)^2}, \quad (2.57)$$

where $u_0^p = Q^2 / (s_0^p + Q^2)$ and the duality threshold parameter s_0^p can be taken from Eq. (2.43).

The matching of the light-cone expansion (path A) with the dispersion relation (path B) allows us to compute the LCSR for the form factor of the $\gamma^* \rho \rightarrow \pi$ transition, which is defined through

$$\langle \pi^0(p) | j_\mu^{em} | \rho^0(p - q) \rangle = F^{\rho\pi}(Q^2) \frac{1}{m_\rho} \epsilon_{\mu\nu\alpha\beta} \epsilon^{(\rho)\nu} q^\alpha p^\beta. \quad (2.58)$$

Therefore, combining eqs. (2.52) and (2.54) and substituting Eq. (2.58) one arrives to

$$\frac{\sqrt{2} f_\rho F^{\rho\pi}(Q^2)}{m_\rho^2 - (p - q)^2} + \int_{s_0^h}^\infty ds \frac{\frac{1}{\pi} \text{Im} F(Q^2, s)}{s - (p - q)^2} = \frac{\sqrt{2} f_\pi}{3} \int_0^1 \frac{du \Phi_\pi(u)}{\bar{u} Q^2 - u(p - q)^2}, \quad (2.59)$$

where the integral on the l.h.s. of Eq. (2.59) can be subtracted from the r.h.s. using Eq. (2.57). Performing the Borel transformation, it can be obtained, to leading twist 2: [41]

$$F^{\rho\pi}(Q^2) = \frac{f_\pi}{3f_\rho} \int_{u_0}^1 \frac{du}{u} \Phi_\pi(u, \mu) \exp\left(-\frac{\bar{u}Q^2}{uM^2} + \frac{m_\rho^2}{M^2}\right). \quad (2.60)$$

To improve the accuracy of Eq. (2.60), both perturbative QCD corrections to the hard scattering amplitude T_H and higher twist effects must be included. The former have already been discussed in Sec. 2.1 so the latter will be reviewed briefly. Higher twist effects take into account both the transverse momentum of the quark-antiquark state and the contributions of higher Fock states in the pion meson wave function. There are several sources of such higher twist corrections in the light-cone expansion, for instance: twist 4 terms arising from the expansion of Eq. (2.50) at $x^2 = 0$ beyond the leading order, three and four particle contributions to twist 6 corrections stemming from the quark propagator expansion near the light-cone, etc.

2.4.4 Final considerations

LCSRs have been used successfully to compute the form factors of several exclusive processes involving pions and also those of heavy (B, D) to light (π, K, ρ, K^*, \dots) meson transitions, which will be the ones interesting for this work (see Sec. 3.1.2). However, they share with QCDSRs the characteristic of being approximate, displaying typical overall uncertainties of 10 – 15 % [29].

Chapter 3

The non-perturbative quantities: form factors and decay amplitudes

We have learned that the most reliable tools to compute the non-perturbative quantities relevant for this work are the QCDSRs and the LCSRs until lattice-QCD calculations are able to supersede them completely. In this chapter these quantities, the meson form factors and the decay amplitudes will be reviewed with some detail, emphasizing the ones relevant for the study of the decay $\bar{B}_d \rightarrow \bar{K}^{*0} \ell^+ \ell^-$.

3.1 Meson form factors

3.1.1 Introduction

A *form factor* is a function of scalar variables that accompanies the independent terms in the most general decomposition of the matrix element of a current consistent with Lorentz and gauge invariance [42]. In the processes relevant for B physics, *transition* form factors¹ appear in the decomposition of the matrix elements that characterise the weak decay of a heavy meson H (a B particle in our case) into a lighter meson (or mesons) L . Roughly speaking, it could be said that they describe the overlap between the initial and final state mesons during the weak decay. Therefore, a generic form factor F can be represented schematically as

$$\langle L | \bar{q} \Gamma Q | H \rangle \sim F^{H \rightarrow L}, \quad (3.1)$$

where q and Q represent, respectively, the final light quark in L and the heavy quark in H , while Γ is the irreducible Dirac matrix that appears after the contraction of the weak vertex into a

¹Although they have no relation with the "form" of the initial heavy meson or the final ones, the name *form factor* has preserved its historical roots since the time it referred only to the Fourier transforms of the electric charge and magnetic moment distributions of a non-relativistic particle. They were named so because they indeed gave information about the form of the particle under consideration.

local one. As form factors receive leading contributions from the soft gluon exchanges that take place during the decay and the ensuing hadronisation, they constitute purely non-perturbative objects.

Depending on the spin of the final meson, two different "families" can be distinguished: form factors for $B \rightarrow P$ transitions (where P stands for a pseudoscalar meson) and form factors for $B \rightarrow V$ transitions (with V symbolising a vector meson).

$B \rightarrow P$ form factors

These are defined as follows [43, 31]:

$$\kappa \langle P(p') | \bar{q} \gamma_\mu b | \bar{B}(p) \rangle = \left[(p + p')_\mu - \frac{m_B^2 - m_P^2}{q^2} q_\mu \right] f_+(q^2) + \left[\frac{m_B^2 - m_P^2}{q^2} q_\mu \right] f_0(q^2), \quad (3.2)$$

$$\kappa \langle P(p') | \bar{q} \sigma_{\mu\nu} q^\nu b | \bar{B}(p) \rangle = \frac{i}{m_B + m_P} [q^2 (p + p')_\mu - (m_B^2 - m_P^2) q_\mu] f_T(q^2, \mu), \quad (3.3)$$

where m_B is the \bar{B} meson mass, m_P the mass of the pseudoscalar meson and the momentum transfer is given by $q_\mu = p_\mu - p'_\mu$. f_+ , f_0 , f_T are the three pseudoscalar meson form factors. The former two are independent on the renormalisation scale μ since $\bar{q} \gamma_\mu b$ is a physical current, whereas the latter is related to the penguin current $\bar{q} \sigma_{\mu\nu} q^\nu b$. In the above $\kappa = \sqrt{2}$ for π^0 and $\kappa = 1$ for the other pseudoscalar mesons.

$B \rightarrow V$ form factors

The form factors relevant for $B \rightarrow V$ transitions can be defined through the matrix elements [31]

$$\kappa \langle V(p', \varepsilon^*) | \bar{q} \gamma_\mu b | \bar{B}(p) \rangle = \frac{2iV(q^2)}{m_B + m_V} \epsilon_{\mu\nu\rho\sigma} \varepsilon^{*\nu} p'^\rho p^\sigma, \quad (3.4)$$

$$\begin{aligned} \kappa \langle V(p', \varepsilon^*) | \bar{q} \gamma_\mu \gamma_5 b | \bar{B}(p) \rangle &= 2m_V A_0(q^2) \frac{\varepsilon^* \cdot q}{q^2} q_\mu + (m_B + m_V) A_1(q^2) \left[\varepsilon_\mu^* - \frac{\varepsilon^* \cdot q}{q^2} q_\mu \right] \\ &\quad - A_2(q^2) \frac{\varepsilon^* \cdot q}{m_B + m_V} \left[(p + p')_\mu - \frac{m_B^2 - m_V^2}{q^2} q_\mu \right], \end{aligned} \quad (3.5)$$

$$\kappa \langle V(p', \varepsilon^*) | \bar{q} \sigma_{\mu\nu} q^\nu b | \bar{B}(p) \rangle = -2T_1(q^2) \epsilon_{\mu\nu\rho\sigma} \varepsilon^{*\nu} p'^\rho p^\sigma, \quad (3.6)$$

$$\begin{aligned} \kappa \langle V(p', \varepsilon^*) | \bar{q} \sigma_{\mu\nu} q^\nu \gamma_5 b | \bar{B}(p) \rangle &= (-i) T_2(q^2) [(m_B^2 - m_V^2) \varepsilon_\mu^* - (\varepsilon^* \cdot q) (p + p')_\mu] \\ &\quad + (-i) T_3(q^2) (\varepsilon^* \cdot q) \left[q_\mu - \frac{q^2}{m_B^2 - m_V^2} (p + p')_\mu \right], \end{aligned} \quad (3.7)$$

with $T_1(0) = T_2(0)$. m_V and ε^μ are the mass and polarisation vector of the final-state vector meson respectively, while $\kappa = \sqrt{2}$ for ρ^0 and $\kappa = 1$ for the other vector mesons. V , A_0 , A_1 , A_2 , T_1 , T_2 and T_3 are the seven independent vector meson form factors and all of them are function of the square of the momentum transfer q^2 . While V and A_i are scale-independent, the T_j depend on the renormalisation scale [32, 10]. The sign convention is fixed by $\epsilon^{0123} = -\epsilon_{0123} = -1$ and $\gamma_5 = i\gamma^0\gamma^1\gamma^2\gamma^3$.

Eqs. (3.4)–(3.7) may be set up in specific combinations of bilinear quark current operators. These combinations will be useful later one, when the process $\bar{B}_d \rightarrow \bar{K}^{*0} \ell^+ \ell^-$ is studied in detail using the weak effective Hamiltonian:

$$\begin{aligned} \kappa \langle V(p', \varepsilon^*) | \bar{q} \gamma_\mu P_{L,R} b | B(p) \rangle = \varepsilon^{*\nu} \left\{ -i\epsilon_{\nu\mu\rho\sigma} p'^\rho q^\sigma \frac{V(q^2)}{m_B + m_V} \mp \frac{1}{2} \left[\frac{2m_V}{q^2} q_\nu q_\mu A_0(q^2) \right. \right. \\ \left. \left. + (m_B + m_V) \left(g_{\nu\mu} - \frac{q_\nu q_\mu}{q^2} \right) A_1(q^2) \right. \right. \\ \left. \left. - \frac{q_\nu}{m_B + m_V} \left((2p' + q)_\mu - \frac{m_B^2 - m_V^2}{q^2} q_\mu \right) A_2(q^2) \right] \right\}, \quad (3.8) \end{aligned}$$

$$\begin{aligned} \kappa \langle V(p', \varepsilon^*) | \bar{q} i \sigma_{\mu\nu} q^\nu P_{L,R} b | B(p) \rangle = \varepsilon^{*\nu} \left\{ i\epsilon_{\nu\mu\rho\sigma} p'^\rho q^\sigma T_1(q^2) \right. \\ \left. \pm \frac{1}{2} \left[((m_B^2 - m_V^2) g_{\nu\mu} - q_\nu (2p' + q)_\mu) T_2(q^2) \right. \right. \\ \left. \left. + q_\nu \left(q_\mu - \frac{q^2}{m_B^2 - m_V^2} (2p' + q)_\mu \right) T_3(q^2) \right] \right\}, \quad (3.9) \end{aligned}$$

where the definition $P_{L,R} \equiv (1 \mp \gamma_5)/2$ have been used. Both sides of Eq. (3.8) can be multiplied by q^μ to obtain

$$\kappa \langle V(p', \varepsilon^*) | \bar{q} \not{q} P_{L,R} b | B(p) \rangle = \varepsilon^{*\nu} \left\{ \mp m_V q_\nu A_0(q^2) \right\}, \quad (3.10)$$

but using that the momentum transfer is $q_\mu = p_\mu - p'_\mu$, the Dirac γ property $\{\gamma_\mu, \gamma_5\} = 0$ and the equations of motion for the quark b [$(\not{p} - m_b)b = 0$] and for the antiquark \bar{q} [$\bar{q}(\not{p}' - m_q) = 0$], the quark current in the l.h.s. of Eq. (3.10) can be rewritten as

$$\bar{q} \not{p} P_{L,R} b = m_b \bar{q} P_{R,L} b - m_q \bar{q} P_{L,R} b. \quad (3.11)$$

Hence, from Eq. (3.10) one can obtain

$$\kappa \langle V(p', \varepsilon^*) | \bar{q} P_{L,R} b | B(p) \rangle \simeq \varepsilon^{*\nu} \left\{ \pm \frac{m_V}{m_b} q_\nu A_0(q^2) \right\}, \quad (3.12)$$

where it has been assumed that $m_q \ll m_b$ (i.e. $q = u, d, s$). Therefore Eq. (3.12) is only valid for heavy-to-light meson decays.

For completeness, we can rearrange Eqs. (2.13-2.14) in [44] into

$$\begin{aligned} \kappa \langle V(p', \varepsilon^*) | \bar{q} \sigma_{\mu\nu} \gamma_5 b | B(p) \rangle = & \frac{1}{2} i \epsilon_{\mu\nu\rho\sigma} \epsilon_{\alpha\beta}^{\rho\sigma} \left\{ \varepsilon^{*\alpha} (2p' + q)^\beta T_1(q^2) \right. \\ & - \frac{m_B^2 - m_V^2}{q^2} \varepsilon^{*\alpha} q^\beta [T_1(q^2) - T_2(q^2)] \\ & \left. + \frac{2(\varepsilon^* \cdot q)}{q^2} p'^\alpha q^\beta \left[T_1(q^2) - T_2(q^2) - \frac{q^2}{m_B^2 - m_V^2} T_3(q^2) \right] \right\} \end{aligned} \quad (3.13)$$

from which, using the identity $\sigma_{\mu\nu} \gamma_5 = -\frac{i}{2} \epsilon_{\mu\nu\alpha\beta} \sigma^{\alpha\beta}$ on the l.h.s. of Eq. (3.13) and renaming the index $\nu \rightarrow \lambda$, one can find

$$\begin{aligned} \kappa \langle V(p', \varepsilon^*) | \bar{q} \sigma_{\mu\nu} b | B(p) \rangle = & \varepsilon^{*\nu} \left\{ -\epsilon_{\nu\mu\lambda\beta} (2p' + q)^\beta T_1(q^2) \right. \\ & + \epsilon_{\nu\mu\lambda\beta} q^\beta \frac{m_B^2 - m_V^2}{q^2} [T_1(q^2) - T_2(q^2)] \\ & \left. - q_\nu \epsilon_{\mu\lambda\alpha\beta} p'^\alpha q^\beta \frac{2}{q^2} \left[T_1(q^2) - T_2(q^2) - \frac{q^2}{m_B^2 - m_V^2} T_3(q^2) \right] \right\}. \end{aligned} \quad (3.14)$$

Notice that Eqs. (3.8)–(3.9) deduced from Eqs. (3.4)–(3.7) coincide with those in [8, 45, 46] but display an overall extra $(-i)$ factor when compared to the corresponding form factor definitions in [44, 47, 10]. This extra factor has been also included in Eq. (3.12) and Eqs. (3.13)–(3.14) for consistency but, being a global phase is unphysical, so both sets of definitions lead to the same observable quantities.

3.1.2 Guidelines for the calculation of $B \rightarrow P, V$ form factors from LCSRs

$B \rightarrow P, V$ form factors may be calculated using the classical *light-meson LCSRs* (i.e. the ones explained in Sec. 2.4). The starting point of this kind of sum rules is the OPE of a dedicated correlation function near the light-cone. The result of this OPE is then combined with the hadronic dispersion relation and quark-hadron duality. In this approach, the correlation function is taken between the vacuum and light P - or V -meson state, whereas the B meson is interpolated by a heavy-to-light quark current. As a result, the long-distance dynamics in the correlation function is described by a set of meson DAs of different twists. The main uncertainties this kind of LCSRs originate from the limited accuracy of the DA parameters, but also a sort of "systematic" uncertainty is brought in by the quark-hadron duality approximation in the B

meson channel [35]. A detailed computation of $B \rightarrow P, V$ form factors using LCSRs, including radiative and higher twist corrections can be found in [44, 43, 37] and references therein.

However, another approach is also possible: the so-called *B-meson LCSR* [35]. The starting point for this kind of computation is a generic correlation function of two quark currents "sandwiched" between the vacuum and the on-shell \bar{B} meson state

$$F_{a,b}^{(B)}(p, q) = i \int d^4x e^{-ikx} \langle 0 | T \{ \bar{q}_2(x) \Gamma_a q_1(x), \bar{q}_1(0) \Gamma_b b(0) \} | \bar{B}(p) \rangle \propto \Pi(q^2), \quad (3.15)$$

where $\bar{q}_1 \Gamma_b b$ is a heavy-to-light weak current with momentum q , $\bar{q}_2 \Gamma_a q_1$ is the interpolating current for a P or V meson with momentum k and flavour content determined by the valence quarks $q_{1,2}$ and the proportionality factor contains four vectors with open indices and/or mass factors which are irrelevant for dynamics. The next step is to make sure that the OPE near the light-cone is applicable for Eq. (3.15) when the variables q^2 and k^2 are far below the hadronic thresholds in the channels of the corresponding currents (i.e., to prove the light-cone dominance of the OPE). Then $\Pi(q^2)$, calculated for unphysical p^2 , is written as a dispersion relation over its physical cut and Borel transformed to enhance the B meson ground state. Finally, quark-hadron duality is invoked to approximate the contributions of hadrons other than the ground-state \bar{B} meson by the imaginary part of the light-cone expansion of Π and the integral containing these is subtracted from both sides of the LCSR (as in Sec. 2.4.3). The LCSR obtained in this way depend on the parameters determining the B meson DAs (being λ_B the most important one), but they are independent of the DAs of light mesons. These light mesons are now interpolated by the light quark currents and hence the B -meson LCSRs rely on the quark-hadron duality in the channels of these currents. The duality-threshold parameter in each channel is determined from the corresponding two-point QCDSR for the light-meson decay constant.

3.1.3 Using effective field theories to establish relations among form factors

Form factors in Eqs. (3.2)–(3.3) and in Eqs. (3.4)–(3.7) are independent but, in the framework of an effective theory, some useful relations can be established among them at leading order. Two relevant examples are discussed below.

Heavy-to-heavy form factors in HQET

Let us consider a $b \rightarrow c$ transition in HQET. As long as the velocity transfer from the decaying b quark to the final c quark remains of order 1, it may be assumed that the heavy quark interacts with soft degrees of freedom (including the spectator quark) exclusively via soft-gluon exchanges, which are characterised by momentum transfers much smaller than the heavy quark masses. In this context HQET may be used successfully.

The invariance of the HQET Lagrangian under heavy-quark flavor symmetry in the infinite mass limit can be used to rewrite Eq. (1.24), replacing the generic h_v quark in the initial-state

meson by a b quark, and the generic h'_v in the final-state meson by a c quark. Then the scattering process turns into a weak decay process mediated by a flavor-changing vector current:

$$\frac{1}{\sqrt{m_B m_D}} \langle D(v') | \bar{c}_{v'} \gamma^\mu b_v | \bar{B}(v) \rangle = \xi(v \cdot v') (v + v')^\mu, \quad (3.16)$$

where the matrix element is still determined by the Isgur-Wise function $\xi(v \cdot v')$.

Defining a new form factor

$$f_-(q^2) \equiv \frac{m_B^2 - m_D^2}{q^2} [f_+(q^2) - f_0(q^2)] \quad (3.17)$$

and substituting it into Eq. (3.2) one obtains

$$\langle D(v') | \bar{c}_{v'} \gamma^\mu b_v | \bar{B}(v) \rangle = f_+(q^2)(p + p')^\mu - f_-(q^2)(p - p')^\mu. \quad (3.18)$$

Finally, comparing Eq. (3.16) with Eq. (3.18) it can be found that

$$f_\pm(q^2) = \frac{m_B \pm m_D}{2\sqrt{m_B m_D}} \xi(v \cdot v'), \quad (3.19)$$

where $q^2 = m_B^2 + m_D^2 - 2m_B m_D v \cdot v'$. Thus, the heavy-quark flavor symmetry relates two a priori independent form factors to $\xi(v \cdot v')$. Moreover, the normalisation of the Isgur-Wise function at $v \cdot v' = 1$ now implies a non-trivial normalisation of the form factors $f_\pm(q^2)$ at the point of maximum momentum transfer², $q_{\text{max}}^2 = (m_B - m_D)^2$ [14]:

$$f_\pm(q_{\text{max}}^2) = \frac{m_B \pm m_D}{2\sqrt{m_B m_D}}. \quad (3.20)$$

A similar process may be accomplished on the other pseudoscalar form factor defined in Eq. (3.3). Furthermore, the spin-symmetry invariance of the HQET Lagrangian can be used to relate pseudoscalar and vector mesons, so the seven vector form factors defined in Eqs. (3.4)–(3.7) may be also expressed as functions of $\xi(v \cdot v')$. Therefore, all heavy-to-heavy form factors end up being related to a single form factor: the Isgur-Wise function [48, 49, 32].

Heavy symmetries are violated by radiative corrections. Fortunately, their effects can be taken into account by multiplicatively renormalising the heavy quark current in HQET just as

²This is indeed the maximum value of the momentum transfer. When no momentum is transferred between the two mesons $q^2 = 0$, then

$$v \cdot v'(q^2 = 0) = \frac{1}{2} \left(\frac{m_B}{m_D} + \frac{m_D}{m_B} \right),$$

but in the heavy-quark limit both m_B and m_D masses are infinite, so by variation of the mass ratio the product $v \cdot v'$ can take any value in the interval $[1, \infty]$. Therefore, the value $v \cdot v' = 1$ corresponds to q_{max}^2 [48].

was done with the weak effective Hamiltonian; thus these short-distance effects will be contained in some Wilson coefficients that multiply matrix elements in HQET:

$$[\bar{c}\Gamma b]_{\text{QCD}} = \sum_{\Gamma'} C_{\Gamma'}(v \cdot v', \alpha_s) [\bar{c}_{v'} \Gamma' b_v]_{\text{HQET}} \quad (3.21)$$

Hence, neglecting $1/m_Q$ corrections, there remain nine parameter-free relations between the pseudoscalar and vector form factors [32].

3.1.4 Heavy-to-light form factors in HQET/LEET

Now we turn our attention to $b \rightarrow u, d, s$ weak decays, where initial and final quarks (whether u, d or s) are assumed to interact with the spectator quark and other light degrees of freedom only via soft-gluon exchanges. Hence the HQET framework can be used on the b quark and the LEET formalism on the light energetic quark resulting from the decay. Using Eq. (1.29) and Eq. (1.31) with $k^\mu \simeq 0$, the momentum transferred to the light meson can then be written as

$$q^\mu = p^\mu - p'^\mu = m_B v^\mu - E n^\mu, \quad (3.22)$$

so

$$q^2 = m_B^2 - 2m_B E + m^2 \quad \Longleftrightarrow \quad E = \frac{m_B}{2} \left(1 - \frac{q^2}{m_B^2} + \frac{m^2}{m_B^2} \right) \quad (3.23)$$

where m is the mass of the meson that picks up quark resulting from the weak decay.

The subsequent analysis will be performed at *large recoil* so the light meson is required to have an energy of $O(m_B/2)$. More precisely we demand $|E - m_B/2| \ll m_B$ or, equivalently, $q^2 \ll m_B^2$. Since with this constrain $E \sim m_B \sim m_b \gg \Lambda_{\text{QCD}}$, all errors due to restricting ourselves to the leading order when computing the HQET and LEET Lagrangians (see Eq. (1.21) and Eq. (1.47)) may be regrouped in a single $O(\Lambda_{\text{QCD}}/m_b)$ term.

The LEET can be applied only to those light mesons in which the quark resulting from the weak decay of b carries almost all of the meson momentum: this is known as *soft or Feynman mechanism*. As the preferred configuration for hadronisation is that in which the quark and antiquark in the outgoing meson have nearly equal momentum, this asymmetrical momentum distribution will be an atypical one (even for light-cone dominated processes) and hence the probability of hadronisation into a light meson will be a function of its energy. Therefore, the heavy-to-light form factors will be energy-dependent functions with unknown absolute normalisation: they are called *soft form factors* and are symbolised by $\xi(E)$. On the other hand, the interaction in Eq. (1.47) is not spin symmetric, so in this case there will be no relation between the soft form factors corresponding to P and to V mesons.

The derivation of the large recoil soft form factors is not straightforward. A complete description of their construction can be found in [15, 31]. The three pseudoscalar form factors in Eqs. (3.2)–(3.3) end up being related to a single function $\xi_P(E)$, while the seven vector form

factors in Eqs. (3.4)–(3.7) are all related to two different functions: $\xi_{\parallel}(E)$ and $\xi_{\perp}(E)$. The subindices " \perp " and " \parallel " denote that only $\xi_{\perp}(E)$ will contribute to the form factors for a transversely polarised vector meson whereas only $\xi_{\parallel}(E)$ will contribute in the case of a longitudinally polarised vector meson. Neglecting some m_V^2/m_B^2 terms that must be rejected at leading order in $1/m_b$, one finds

$$\langle P(p') | \bar{q} \gamma^\mu b | \bar{B}(p) \rangle = 2E \xi_P(E) n^\mu, \quad (3.24)$$

$$\langle P(p') | \bar{q} \sigma^{\mu\nu} q_\nu b | \bar{B}(p) \rangle = 2iE \xi_P(E) [(m_B - E) n^\mu - m_B v^\mu], \quad (3.25)$$

for pseudoscalar mesons, and

$$\langle V(p', \varepsilon^*) | \bar{q} \gamma^\mu b | \bar{B}(p) \rangle = 2iE \xi_{\perp}(E) \varepsilon^{\mu\nu\rho\sigma} \varepsilon_\nu^* n_\rho v_\sigma, \quad (3.26)$$

$$\langle V(p', \varepsilon^*) | \bar{q} \gamma^\mu \gamma_5 b | \bar{B}(p) \rangle = 2E [\xi_{\perp}(E) (\varepsilon^{*\mu} - \varepsilon^* \cdot v n^\mu) + \xi_{\parallel}(E) \varepsilon^* \cdot v n^\mu], \quad (3.27)$$

$$\langle V(p', \varepsilon^*) | \bar{q} \sigma^{\mu\nu} q_\nu b | \bar{B}(p) \rangle = 2Em_B \xi_{\perp}(E) \varepsilon^{\mu\nu\rho\sigma} \varepsilon_\nu^* v_\rho n_\sigma, \quad (3.28)$$

$$\begin{aligned} \langle V(p', \varepsilon^*) | \bar{q} \sigma^{\mu\nu} \gamma_5 q_\nu b | \bar{B}(p) \rangle = & (-2iE) \left\{ \xi_{\perp}(E) m_B (\varepsilon^{*\mu} - \varepsilon^* \cdot v n^\mu) \right. \\ & \left. + \xi_{\parallel}(E) \varepsilon^* \cdot v [(m_B - E) n^\mu - m_B v^\mu] \right\}, \end{aligned} \quad (3.29)$$

for vector mesons. Comparing Eqs. (3.2)–(3.7) with Eqs. (3.24)–(3.29), the following form factor relations may be found:

$$f_+(q^2) = \frac{m_B}{2E} f_0(q^2) = \frac{m_B}{m_B + m_P} f_T(q^2) = \xi_P(E) \quad (3.30)$$

for pseudoscalar mesons and

$$\frac{m_B}{m_B + m_V} V(q^2) = \frac{m_B + m_V}{2E} A_1(q^2) = T_1(q^2) = \frac{m_B}{2E} T_2(q^2) = \xi_{\perp}(E), \quad (3.31)$$

$$\frac{m_V}{E} A_0(q^2) = \frac{m_B + m_V}{2E} A_1(q^2) - \frac{m_B - m_V}{m_B} A_2(q^2) = \frac{m_B}{2E} T_2(q^2) - T_3(q^2) = \xi_{\parallel}(E), \quad (3.32)$$

for vector mesons. These relations are only valid for the soft contribution to the form factors at large recoil, neglecting corrections of order Λ_{QCD}/m_b and α_s .

$O(\alpha_s)$ corrections may come from two sources: *hard-vertex corrections* and *hard-spectator scattering*. The former have a high-energy part that can be accounted for by multiplicatively renormalising the current $[\bar{q}_n \Gamma b_n]_{\text{eff}}$ in the effective theory, in the same way as done previously on the weak effective Hamiltonian and heavy-to-heavy transitions, but there is also a long-distance part from gluons whose momentum is collinear to the light quark that can not be

computed perturbatively; fortunately, this part preserves the HQET/LEET symmetries and can be absorbed into a redefinition of ξ_P , ξ_\perp and ξ_\parallel [31]. The latter will allow the meson to be formed in a preferred configuration in which the momentum is distributed almost evenly between the two quarks, if a hard gluon is absorbed by the spectator quark; this contribution may be computed by means of the hard-scattering approach to exclusive processes.

Therefore, a generic form factor for a heavy-to-light meson decay can be factorised as

$$F(q^2) = D \xi_a(E) + \Phi_B \otimes T_H \otimes \Phi_a(\text{light}) \quad \text{with } a = P, V_\parallel, V_\perp, \quad (3.33)$$

where $\xi_a(E)$ is the soft form factor, T_H is the hard-scattering kernel convoluted with the LCDAs of the B meson (Φ_B) and the light meson (Φ_{light}) and $D = 1 + O(\alpha_s)$ is a factor that includes perturbative corrections to the hard vertex. Eq. (3.33) is valid to all orders in α_s but just to leading order in a Λ_{QCD}/m_b expansion, as the soft and hard corrections suppressed by powers of $1/m_b$ that should also be present in the factorisation formula are unknown to date.

3.2 Meson decay constants

A *meson decay constant* is a fundamental hadronic parameter that provides a measure of the attraction strength between the valence quark q and antiquark \bar{q}' inside a given meson [50] or, stated differently, of the likelihood that the q and \bar{q}' are at same space-time position and annihilate [51]. Consequently, it will appear as a factor whenever a transition amplitude from a meson M in the initial state to a non-hadronic final state is computed, so the formula

$$\langle 0 | \bar{q}' \Gamma q | M \rangle \sim f_M \quad (3.34)$$

can be used to define a generic decay constant. In fact, meson decay constants are actually defined through the matrix elements of such transitions mediated by a certain weak current:

- the decay constant f_P of a pseudoscalar meson P with four-momentum p' is given by [31]

$$\kappa \langle P(p') | \bar{q} \gamma_\mu \gamma_5 q' | 0 \rangle = -i f_P p'_\mu, \quad (3.35)$$

- while for a vector meson V with four-momentum p and polarisation vector ε_μ^* , the longitudinal ($f_{V,\parallel}$) and transverse ($f_{V,\perp}$) decay constants are defined through [31]

$$\kappa \langle V(p', \varepsilon_\mu^*) | \bar{q} \gamma_\mu q' | 0 \rangle = -i f_{V,\parallel} m_V \varepsilon_\mu^*, \quad (3.36)$$

$$\kappa \langle V(p', \varepsilon_\mu^*) | \bar{q} \sigma_{\mu\nu} q' | 0 \rangle = f_{V,\perp} (\mu_h) (p'_\mu \varepsilon_\nu^* - p_\nu \varepsilon_\mu^*). \quad (3.37)$$

The meson decay constants in Eqs. (3.35)–(3.37) are related to the twist-2 LCDAs $\Phi_{P,V_\parallel,V_\perp}$ defined in Eqs. (2.14)–(2.16). This relationship was already pointed out in Sec. 2.4.1 in the case of a π^0 when the LCSR framework was reviewed. For more details, the reader should refer to

Eqs. (80)-(81) and Eqs. (85)-(90) in [31] taking into account that, to obtain the matrix elements Eqs. (3.35)–(3.37), one must set $x = y = 0$.

Meson decay constants have been traditionally computed using two-point QCDSRs [35, 37], as illustrated in Sec. 2.3 for f_ρ . However, the progress of lattice QCD techniques over the past ten years has led to a steady reduction of uncertainties [52] and nowadays the best determinations of some of these decay constants are being obtained within this non-perturbative approach [16, 53, 54].

Chapter 4

Factorisation of matrix elements

In Sec. 1.1.2 we learned that the amplitude of a physical process, a heavy meson decay for instance, can be computed to a given order in α_s using the weak effective Hamiltonian. Very energetic gluons with momenta much larger than m_b are accounted for inside the Wilson coefficients, which are process-independent, so the hadronic state reached after the decay cannot depend on them. This final state depends both on the final quark and lepton content and how the former is organised into hadrons. It is possible that several light quarks are produced in the decay. Then there are different hadronic final-state configurations available, all of them possible with a certain probability. The mechanism responsible for rearranging these quarks to obtain different hadronic final states is called *rescattering* and it is due to long-distance QCD interactions, which are contained inside the hadronic matrix elements. Therefore it is of paramount importance to have a systematic and model-independent treatment of two-body heavy meson decays capable of dealing with the non-perturbative input stemming from these matrix elements while allowing, at the same time, a perturbative treatment of the high-energy QCD effects. This chapter will deal in the first place with the birth of matrix-element factorisation to focus, afterwards, on one of such successful frameworks, usually known as *QCD factorisation* (QCDF), from a qualitative point of view. The reader interested in learning in-depth the quantitative details of QCDF should refer to the excellent PhD theses by Stephan Bosch [42] and Guido Bell [55].

4.1 Overview of processes involving a heavy meson decay

There are many decay channels available to a B meson and they can be classified in four main categories, namely:

- *Leptonic decays*

These are the weak decays of a heavy meson into a lepton pair of the type $l\nu$. Since leptons do not interact strongly, all QCD effects occurring within the meson are contained in the

matrix element that defines the meson decay constant, which can be computed either from QCDSRs or lattice QCD or extracted from experimental data.

- *Strict semi-leptonic decays*

In these processes, a heavy meson decays weakly into a pair of leptons of the type $l\nu$ and a lighter meson at tree level. Again the leptonic vertex is not affected by strong interactions, which can only take place inside the initial meson, during the decay and the process of hadronisation of the final meson and inside the final light meson. Therefore, non-perturbative QCD physics can be singled out and described by a form factor.

- *Radiative decays*

In such transitions, the heavy quark inside a heavy meson decays weakly into a lighter one with the emission of a photon, whether real or virtual. If it is real the process will be *purely radiative* whereas if it is virtual the photon will decay electromagnetically into a particle-antiparticle pair. This pair can be leptonic or composed by a quark-antiquark pair. The former is easy to tag at detectors and it is often referred to as "*semileptonic decay*" (not to be confused with the one described just above), while the latter cannot be distinguished from a purely hadronic decay.

These processes are very suppressed in the SM (with branching fractions ranging from 10^{-4} for pure radiative decays to 10^{-6} for "semi-leptonic" ones), as they proceed entirely through loop effects and the chirality nature of weak decays implies additional suppression factors. Hence if radiative decays turn out to be enhanced by new virtual effects that cannot be explained within the SM this would signal that some kind of NP that violates chirality is realised in Nature.

Radiative decays demand a careful treatment of matrix elements factorization involving the simultaneous use of perturbation theory for short-distance strong interactions and the full machinery, developed in Chapters 2 and 3, necessary to deal with non-perturbative soft gluons. A detailed explanation of these processes can be found in Part II of this thesis, as it is devoted to study the exclusive decay $\bar{B}_d \rightarrow \bar{K}^{*0} \ell^+ \ell^-$.

- *Purely hadronic decays*

They are characterised by the weak decay of a heavy meson into two lighter mesons so, as in the previous case, the matrix elements must be studied carefully to be able to account for both long- and short-distance QCD interactions while obtaining physically meaningful amplitudes (free from divergencies, gauge independent, scale- and scheme- independent, etc.) for the decay. The necessity to give theoretical predictions for this kind of processes is what motivated the whole line of research that has evolved from *naïve* or *strict factorisation*.

4.2 Naïve factorisation

4.2.1 Framework

The idea of factorisation applied to heavy meson decays was suggested a long time ago in [56]. It was the first attempt to shed light to exclusive non-leptonic decays of heavy mesons. Its purpose was to find a prescription for reducing the hadronic matrix elements of weak effective Hamiltonian four-quark operators to products of current matrix elements that could be related to a form factor and a decay constant.

To fix ideas let us examine the weak decay of a \bar{B} meson into two light mesons M_1 and M_2 mediated by dimension six operators of the SM weak effective Hamiltonian \mathcal{O}_i

$$\langle M_2 M_1 | \mathcal{H}_{\text{eff}} | \bar{B} \rangle. \quad (4.1)$$

In the naïve factorisation approach this matrix element is assumed to decompose (factorise) into two factors of matrix elements of bilinear currents with colour-singlet structure and appropriate flavour content $(q_1, q_2, q, b)^1$ and Lorentz configuration $(\Gamma, \tilde{\Gamma})$ as

$$\langle M_1 M_2 | (\bar{q}_1 \Gamma q_2) (\bar{q} \tilde{\Gamma} b) | \bar{B} \rangle \simeq \langle M_2 | \bar{q}_1 \Gamma q_2 | 0 \rangle \langle M_1 | \bar{q} \tilde{\Gamma} b | \bar{B} \rangle \sim f_{M_2} \cdot F^{\bar{B} \rightarrow M_1}, \quad (4.2)$$

but this decomposition is not unique so

$$\langle M_1 M_2 | (\bar{q}_1 \Gamma q_2) (\bar{q} \tilde{\Gamma} b) | \bar{B} \rangle \simeq \langle M_1 | \bar{q}_1 \Gamma q_2 | 0 \rangle \langle M_2 | \bar{q} \tilde{\Gamma} b | \bar{B} \rangle \sim f_{M_1} \cdot F^{\bar{B} \rightarrow M_2} \quad (4.3)$$

is also allowed. In general, however, pairs of operators with the same quark and current content but different colour state are found in the weak effective Hamiltonian:

$$\mathcal{O}_i = (\bar{q}_\alpha \tilde{\Gamma} b_\alpha) (\bar{q}_{1\beta} \Gamma q_{2\beta}) \quad \text{and} \quad \mathcal{O}_j = (\bar{q}_\alpha \tilde{\Gamma} b_\beta) (\bar{q}_{1\beta} \Gamma q_{2\alpha}), \quad (4.4)$$

where α and β are colour indices. These operators can be Fierz-transformed into

$$\mathcal{O}'_i = (\bar{q}_{1\beta} \tilde{\Gamma}' b_\alpha) (\bar{q}_\alpha \Gamma' q_{2\beta}) \quad \text{and} \quad \mathcal{O}'_j = (\bar{q}_{1\alpha} \tilde{\Gamma}' b_\alpha) (\bar{q}_\beta \Gamma' q_{2\beta}) \quad (4.5)$$

with different Lorentz structures $\tilde{\Gamma}'$ and Γ' . Depending on the flavour structure of the decay it is possible that the matrix elements can be decomposed according to \mathcal{O}_i (as shown in Eqs. (4.2)–(4.3)), in the rearranged form given by \mathcal{O}'_j or in both configurations. In the latter case, there are two different ways to reorder the quarks to reach the same final state $|M_1 M_2\rangle$ and, since both are possible from a quantum mechanical point of view, they must be taken into account. Therefore, the factorised matrix elements can be defined as

$$\langle \mathcal{O}_i \rangle_F \equiv \langle M_2 | \bar{q}_1 \Gamma q_2 | 0 \rangle \langle M_1 | \bar{q} \tilde{\Gamma} b | \bar{B} \rangle + \langle M_1 | \bar{q}_1 \Gamma q_2 | 0 \rangle \langle M_2 | \bar{q} \tilde{\Gamma} b | \bar{B} \rangle, \quad (4.6)$$

$$\langle \mathcal{O}'_j \rangle_F \equiv \langle M_2 | \bar{q} \Gamma' q_2 | 0 \rangle \langle M_1 | \bar{q}_1 \tilde{\Gamma}' b | \bar{B} \rangle + \langle M_1 | \bar{q} \Gamma' q_2 | 0 \rangle \langle M_2 | \bar{q}_1 \tilde{\Gamma}' b | \bar{B} \rangle. \quad (4.7)$$

¹We assume that the valence quarks q_1 and q_2 are common to both M_1 and M_2 .

Using these operators, the weak effective Hamiltonian can be written as

$$\mathcal{H}_{\text{eff}} = C_i \mathcal{O}_i + C_j \mathcal{O}_j = C_i \mathcal{O}'_i + C_j \mathcal{O}'_j. \quad (4.8)$$

For the naïve factorisation hypothesis to hold, the two bilinear quark currents must be colour singlets. As shown in Eqs. (4.4)–(4.5) neither \mathcal{O}_j nor \mathcal{O}_i have such colour structures. In fact, they correspond to *colour suppressed* diagrams, which need a gluon exchange among the quarks involved in the decay to be rearranged into a colour-singlet, so one expects that²

$$C_j \mathcal{O}_j = \frac{1}{N_c} C_j \mathcal{O}_i + O(\alpha_s), \quad \text{and} \quad C_i \mathcal{O}'_i = \frac{1}{N_c} C_i \mathcal{O}'_j + O(\alpha_s). \quad (4.11)$$

This reasoning leads to the conclusion that, in naïve factorisation, the matrix element in Eq. (4.1) admits the decomposition

$$C_i(\mu) \langle \mathcal{O}_i \rangle + C_j(\mu) \langle \mathcal{O}_j \rangle = a_i(\mu) \langle \mathcal{O}_i \rangle_F + a_j(\mu) \langle \mathcal{O}'_j \rangle_F \quad (4.12)$$

where

$$a_i(\mu) = C_i(\mu) + \frac{1}{N_c} C_j(\mu), \quad a_j(\mu) = C_j(\mu) + \frac{1}{N_c} C_i(\mu). \quad (4.13)$$

4.2.2 Drawbacks and theoretical justification

Inspecting Eqs. (4.12)–(4.13) it can be concluded that naïve factorisation cannot be correct, as the matrix elements of the bilinear quark currents that result from factorising the full hadronic matrix element in Eq. (4.1) do not display any scale dependence that could cancel the renormalisation

²This can be proven straightforwardly in the singlet-octet basis for the local effective operators [7]

$$\begin{aligned} \mathcal{O}_i &= (\bar{q}_\alpha \delta_{\alpha\delta} b_\delta)_\Gamma (\bar{q}_{1\beta} \delta_{\beta\gamma} q_{2\gamma})_{\bar{\Gamma}} = (\bar{q}_\alpha b_{2\alpha})_\Gamma (\bar{q}_{1\beta} q_{2\beta})_{\bar{\Gamma}} \\ \mathcal{O}_i^8 &= (\bar{q}_\alpha T_{\alpha\beta}^a b_\beta)_\Gamma (\bar{q}_{1\gamma} T_{\gamma\delta}^a q_{2\delta})_{\bar{\Gamma}} = \frac{1}{2} \left(\delta_{\alpha\delta} \delta_{\beta\gamma} - \frac{1}{N_c} \delta_{\alpha\beta} \delta_{\gamma\delta} \right) (\bar{q}_\alpha b_\beta)_\Gamma (\bar{q}_{1\gamma} q_{2\delta})_{\bar{\Gamma}} = \frac{1}{2} \left(\mathcal{O}_j - \frac{1}{N_c} \mathcal{O}_i \right). \end{aligned} \quad (4.9)$$

The relation (A.38) in [25] has been used to obtain the second equality in \mathcal{O}_i^8 , where N_c denotes the number of colours. From the last of these equations one obtains

$$\mathcal{O}_j = \frac{1}{N_c} \mathcal{O}_i + 2\mathcal{O}_i^8, \quad (4.10)$$

so that

$$\begin{aligned} C_i \mathcal{O}_i + C_j \mathcal{O}_j &= \left(C_i + \frac{1}{N_c} C_j \right) \mathcal{O}_i + 2C_j \mathcal{O}_i^8 \\ C_i \mathcal{O}'_i + C_j \mathcal{O}'_j &= \left(C_j + \frac{1}{N_c} C_i \right) \mathcal{O}'_j + 2C_j \mathcal{O}_i^8, \end{aligned}$$

where it is obvious that the octet operators change the color structure and therefore they should start contributing at $O(\alpha_s)$.

scale dependence in the Wilson coefficients [50]. Hence, in general, a magnitude obtained from an amplitude computed using this approach would be unphysical for any renormalisation scale, although one might hope to find a single suitable *factorisation scale* μ_f , usually expected to be of $O(m_b)$, for which Eq. (4.12) is a good approximation. This "pathological" behaviour was already pointed out in [57], along with the facts that this framework does not hold even at one loop in perturbation theory and that it also neglects any interaction between initial or final-state particles (*rescattering*). However, for many years naïve factorisation has proven to be a useful tool to obtain estimates for the amplitudes of those SM processes where the LO contribution is clearly dominant or where certain computations in improved factorisation frameworks have not been worked out yet (see for instance [58]). The accuracy of these estimates for certain heavy meson decays, already stated in [56], depends on how closely the following two arguments can be applied to the process studied.

In [59] it was justified that naïve factorisation of four-quark operator matrix elements holds to LO in an $1/N_c$ expansion in the large- N_c limit of QCD, but this is hardly an approximation scheme that one would trust in all phenomenological applications, as corrections to just the LO could be of $O \sim 1/3$.

Another argument that supports naïve factorisation is the *color transparency* hypothesis [60] which, although intuitive, it is not strictly derived from QCD [57]. In an energetic two-body transition, hadronisation occurs when the decay products have already traveled some distance away from each other. Once quarks have grouped into colour-singlet pairs which are about to hadronise, soft gluons cannot probe the inner structure of these pairs and hence their exchange is ineffective to rearrange the quarks in them. In this situation, one expects the factorisable part of the decay amplitude (the one that can be decomposed as a product of hadronic matrix elements of colour-singlet quark currents) to give the dominant contribution to the full amplitude [50]. Color transparency can be explained in a systematic and model-independent way within the combined HQET/LEET approaches as follows [61]: when a high kinetic energy meson is produced in a point-like source (i.e. a local operator in the WEH), the couplings of soft gluons to this meson can be studied using a multipole expansion, and the first contribution of this expansion (from the color dipole) turns out to be suppressed by a power of Λ_{QCD}/m_b . Since in the $m_b \rightarrow \infty$ limit $\Lambda_{\text{QCD}}/m_b \rightarrow 0$, this effectively decouples the meson from soft QCD interactions.

4.2.3 Generalised factorisation approaches

Unsuccessful proposals

Different proposals of factorisation capable of solving the aforementioned problems were suggested over the years, but all of them turned out to have some "loophole" that also rendered unphysical any magnitude computed from the resulting amplitude. In [50] for instance, the scale dependency issued was sorted out, but the scheme dependence that acquire the Wilson coefficients at NLO in the improved RG perturbation theory could not be compensated by the

factorised matrix elements [62]; a wonderful summary of this approach can be found in [7]. In [63, 64, 65, 66], on the other hand, the matrix elements of the Hamiltonian effective operators between the quark states that participate in the decay (either in the initial or in the final states, but neglecting any spectator quark contribution) were computed using perturbation theory up to one loop, so that their scale and scheme dependence could be extracted and combined with the scale and scheme dependency of Wilson coefficients to obtain effective Wilson coefficients free from these unphysical parameters; however, as noted in [62], the perturbative evaluation of the scheme-dependent finite contributions to the matrix elements generated a "concealed" gauge and infrared regulator dependency on the effective Wilson coefficients and therefore any meaningful result was again unphysical.

Successful analytical frameworks

A few analytical frameworks have been developed to deal with hadronic matrix elements in purely hadronic and radiative B weak decays and succeeded in understanding the dynamics of these processes, which may be very involved due to the simultaneous exchange of soft and hard gluons. In these frameworks both factorisable and non-factorisable effects are accounted for and computed from first principles, that is, starting from QCD and performing a controlled set of approximations to obtain theoretically accurate results within a dynamical range of validity. One of these frameworks is the so-called *perturbative QCD* (pQCD) [67, 68, 69, 70, 71], which aims to separate soft- and hard-gluon effects in the matrix elements of the decaying B meson. However, in pQCD it is assumed that soft contributions to the $B \rightarrow M$ form factors are strongly suppressed by Sudakov effects. Hence, these form factors become perturbatively calculable and are counted as being of $O(\alpha_s)$ which, among other consequences, prevents the recovery of naïve factorisation at any limit.

Whether the Sudakov suppression of long-distance effects is enough to compute the $B \rightarrow M$ form factors perturbatively or not is a controversial issue [61, 72], so this thesis will focus on the QCD factorisation approach (QCdf), also known as "BBNS" after its authors (Beneke, Buchalla, Neubert and Sachrajda). This framework was introduced in [73] for $B \rightarrow \pi\pi$ decays and later extended to general purely hadronic decays [30, 74, 75] and also to radiative decays [32, 76, 77].

4.3 General concepts on QCD factorisation

QCdf is a theoretical tool designed to compute the transition matrix elements of the local operators $\langle \mathcal{O}_i \rangle$ that appear in the amplitudes of certain types of decays when these amplitudes are written in terms of the weak effective Hamiltonian [Eq. (1.2)], being specially suited to study weak decays of heavy mesons³ in the heavy-quark limit using the standard QCD language. It was

³A meson is called "light" in QCdf if its mass m remains finite in the heavy-quark limit, and "heavy" if it is made up by a heavy and a light quark and its mass scales with the heavy quark mass m_Q in the heavy-quark

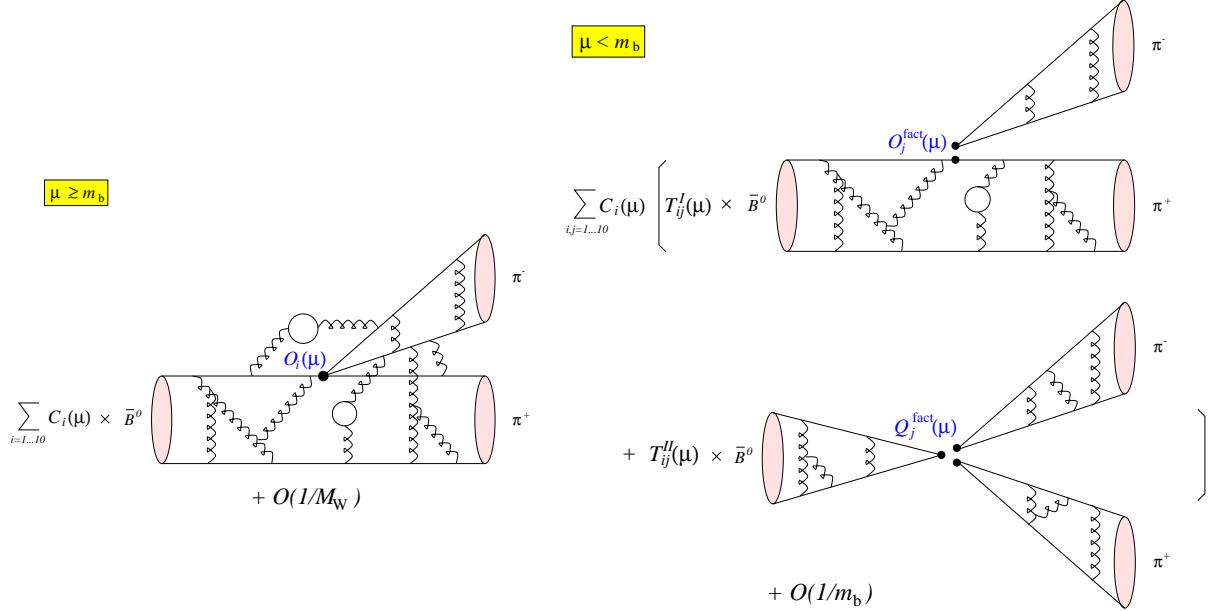


Figure 4.1: Example of factorisation of short- and long-distance contributions in the hadronic $\bar{B}^0 \rightarrow \pi^+\pi^-$ decay. Left: factorization of short-distance effects into Wilson coefficients of the WEH. Right: Factorization of hard gluon exchanges into hard-scattering kernels (QCD factorization) [61].

built to exploit the strengths of HQET/LEET and hard-scattering approaches, while avoiding their individual weaknesses, using a joint implementation of both frameworks that allows the computation of hard-gluon corrections below the scale $\mu \sim m_Q$ in a systematic manner.

The basic idea of QCdf is to take advantage of the fact that the mass m_b of the decaying b quark is much larger than the typical scale of QCD interactions (Λ_{QCD}) to disentangle the physics associated with these two scales [78]. On the one hand, at scales $\mu \geq m_b$ the physics relevant to the decay is described by the WEH: short-distance contributions, coming from gluons with virtualities much higher than m_b factorise⁴ and can be computed perturbatively in an $\alpha_s(m_b)$ expansion of the Wilson coefficients. However, the resulting picture is not straightforward at all, as $O(m_b)$ gluon exchanges between any of the quarks in the external meson states are still possible (see Fig. 4.1). Fortunately, when the renormalisation scale is lowered further into the region $\mu \simeq m_b \Lambda_{\text{QCD}}$, then color transparency comes into play and implies certain systematic cancella-

limit, so that m/m_Q stays fixed. In principle, $m \gg \Lambda_{\text{QCD}}$ would still be possible for a light meson (charm mesons could be regarded as light in this sense), but in the literature it is assumed that $m \sim \Lambda_{\text{QCD}}$ for a light meson. Thus bottom and charm mesons are considered heavy in QCdf [30]; however, since we will be dealing with B meson decays only, from now on $m_Q \equiv m_b$ for us.

⁴The word *factorisation* in QCD refers to the separation of long-distance contributions to a process from the short-distance part that depends only on the large scale, which in this case is m_b .

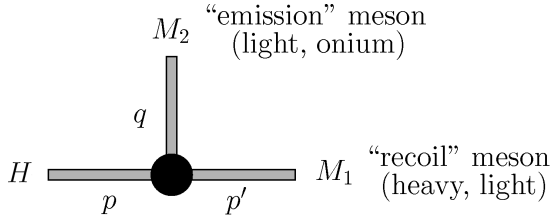


Figure 4.2: Kinematics and notation for a non-leptonic decay [30].

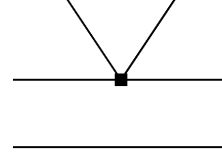


Figure 4.3: Leading order contribution to $H \rightarrow M_1 M_2$. The weak decay of the heavy quark through a four-fermion operator of the weak effective Hamiltonian is represented by the black square [30].

tions of soft and collinear gluons involved in the process [61]. As a result, some of the previously non-factorisable gluon interactions (those that connect the light meson to the remaining mesons) become dominated by virtualities of $O(m_b)$ and can be calculated perturbatively using the combined HQET/LEET and hard-scattering approaches; these contributions are absorbed into the hard-scattering kernels (the counterpart of Wilson coefficients in the hard-scattering approach, see Sec. 2.1). What remains are factorised four-quark $[\mathcal{O}_j^{\text{fact}}(\mu)]$ and/or six-quark $[Q_j^{\text{fact}}(\mu)]$ operators that contain long-distance effects originating from soft and collinear gluons with virtualities between Λ_{QCD} and $m_b \Lambda_{\text{QCD}}$. The matrix elements of these operators fall in the three categories of process-independent non-perturbative inputs we are already familiar with: form factors, decay constants and LCDAs.

As in the construction of the WEH, this reduction in complexity (i.e., going from local four-quark operators to “factorised” operators) is exact up to corrections suppressed by inverse powers of the heavy scale, now set by m_b .

4.3.1 QCDf at work for purely hadronic decays

QCDf holds in the scenario in which the heavy quark of a heavy meson decays weakly into a lighter quark in such way that two mesons are formed in the final state: one composed by the quark resulting from the decay and the spectator quark (*recoil meson*), and another built by the two light quarks created at the weak vertex (*emission meson*) as shown in Fig. 4.2. The lowest-order contribution to this process can be seen in Fig. 4.3.

If the quark resulting from the decay is heavy ($H \rightarrow H_1 L_2$), the physical picture of the process is rather simple. Being heavy, it will have approximately the same velocity as the initial decaying quark and will hadronise into a meson by picking up the spectator quark that was already moving at that velocity. Meanwhile, the two light quarks created at the weak vertex will be very energetic. Therefore, if they have to form a light meson there are two possibilities: either they appear directly in a colour-singlet configuration and are very collinear (in this case, according to the colour transparency argument, the pair of colour-coupled quarks will leave the

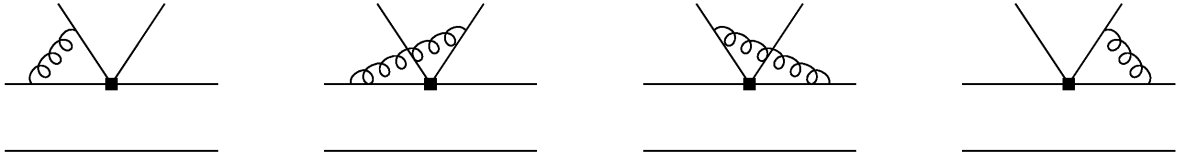
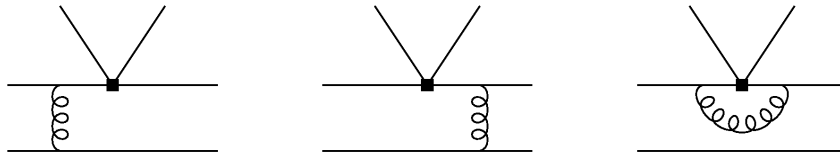


Figure 4.4: Topologies corresponding to hard-vertex corrections [30].

Figure 4.5: Form factor corrections at next-to-leading $O(\alpha_s)$ [30].

interaction region without interacting with the soft degrees of freedom that are forming the heavy meson and will hadronise with a probability given by the LCDA of $L_2 - \Phi_{L_2}(u)$, which depends on the momentum fraction of each quark) or they exchange a hard gluon with the initial or the final heavy quark to be put in the collinear colour-singlet state required for the hadronisation to occur (Fig. 4.4). The latter situation will result in a perturbatively calculable contribution of $O(\alpha_s)$ to the hard-scattering kernel (the *hard-vertex correction* introduced in Sec. 3.1.4) [30] and constitutes a source of strong interaction phases. Soft-gluon exchanges between the initial and the final heavy quark or between either of these and the spectator quark are also possible to all orders in α_s (see, for instance, the two leftmost diagrams in Fig. 4.5) and are contained in the heavy-to-heavy form factor.

The process is less straightforward if both mesons are light ($H \rightarrow L_1 L_2$). In this case, one of the light mesons will contain the slow spectator quark and the final quark resulting from the decay which, due to its small mass, will be very energetic. This highly asymmetrical configuration will only lead to a collinear colourless pair that can hadronize into a meson if a gluon is exchanged with one of the quarks. This gluon can come from two sources. If it is a soft gluon connecting the initial and the final states of the weakly decaying quark, another $O(\alpha_s)$ correction will contribute to the heavy-to-light form factor (last diagram in Fig. 4.5). But if it is a hard gluon that connects one of the two quarks of the emitted light meson with the spectator quark, it will give rise to an $O(\alpha_s)$ correction to the form factor entering through the hard-scattering kernel: it is the *hard spectator scattering* described in Sec. 3.1.4 (see Fig. 4.6). Since hard-vertex corrections and hard-spectator scattering are possible topologies involving a hard-gluon exchange, both kinds of contributions must be taken into account in $H \rightarrow L_1 L_2$; moreover, as these corrections violate the naïve factorisation approach they are commonly known as "non-factorisable", although they can be factorised out and computed in the QCdf framework [30].

There are other corrections to the decay amplitude that must be accounted for. The weak

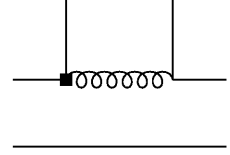
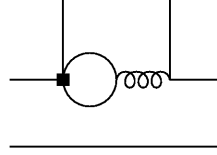
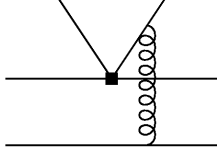
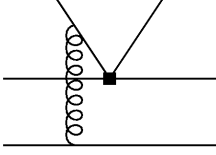


Figure 4.6: Hard-spectator scattering diagrams [30].

Figure 4.7: Penguin diagrams [30].

vertex can contain a penguin diagram or a chromomagnetic dipole operator as shown in Fig. 4.7. They also contribute to the hard-scattering kernel at $O(\alpha_s)$ [30] and constitute another source of perturbative strong phases⁵ [73], being generated by the Bander-Silverman-Soni (BSS) mechanism [79].

Graphical representation of $H \rightarrow H_1 L_2$ and $H \rightarrow L_1 L_2$ decays can be found, respectively, in Fig. 4.8 and Fig. 4.9. They show that, up to power corrections of $O(\Lambda/m_b)$, the factorisation formulae for the transition matrix element of an operator \mathcal{O}_i in the weak effective Hamiltonian are given by

$$\langle H_1 L_2 | \mathcal{O}_i | H \rangle = \sum_j F_j^{H \rightarrow H_1}(m_2^2) \int_0^1 du T_{ij}^I(u) \Phi_{L_1}(u), \quad (4.14)$$

$$\begin{aligned} \langle L_1 L_2 | \mathcal{O}_i | H \rangle &= \sum_j F_j^{H \rightarrow L_1}(m_2^2) \int_0^1 du T_{ij}^I(u) \Phi_{L_2}(u) \\ &+ \sum_k F_k^{H \rightarrow L_2}(m_1^2) \int_0^1 dv T_{ik}^I(v) \Phi_{L_1}(v) \\ &+ \int_0^1 d\xi du dv T_i^{II}(\xi, u, v) \Phi_H(\xi) \Phi_{L_1}(v) \Phi_{L_2}(u), \end{aligned} \quad (4.15)$$

where $F_j^{H \rightarrow M}$ denotes a $H \rightarrow M$ form factors, Φ_M is the LCDA corresponding to the quark-antiquark Fock state of the final state meson M , and $T_{ij}^I(u)$, $T_{ik}^I(v)$ and $T_i^{II}(\xi, u, v)$ are the hard-scattering kernels. Type "I" labels the hard vertex corrections in Fig. 4.4 whereas type "II" designs the hard spectator contributions in Fig. 4.6.

There is yet another whole kind of contributions to the decay amplitude that we have missed to include in Eqs. (4.14)–(4.15). These are the *weak annihilation diagrams* shown in Fig. 4.10.

⁵Strong phases are complex parameters that, in the SM, arise from *rescattering*, a contribution due to a possible final state interaction with on-shell intermediate states mediated by gluonic exchange. This kind of phase is therefore CP-conserving.

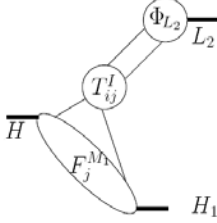


Figure 4.8: $H \rightarrow H_1 L_2$ [42].

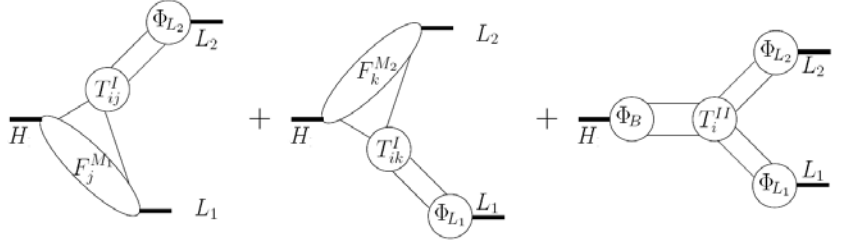


Figure 4.9: Grafical representation of $H \rightarrow L_1 L_2$ [42].

They represent the possible annihilation of both quarks in the heavy meson to form a set of very energetic final state partons. These partons can rearrange themselves into either a heavy and a light final-state meson or into two light final-state mesons. Although it has been stated that these diagrams can be safely neglected at leading order in Λ_{QCD}/m_b [30], there are some situations in which they might become enhanced enough by other factors to spoil the Λ_{QCD}/m_b suppression and give sizeable contributions [75].

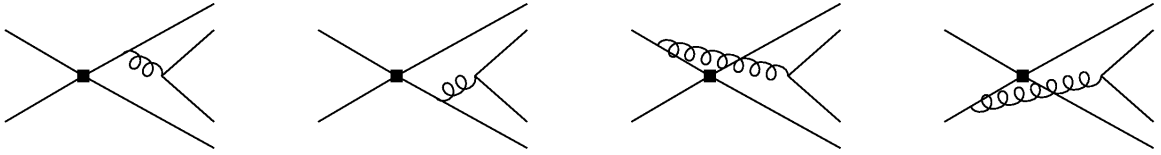


Figure 4.10: Weak annihilation diagrams [30].

4.4 Interaction scales

To understand which terms are leading and which become suppressed in the QCdf framework at leading order in Λ_{QCD}/m_b and at a given order in α_s , it is very important to establish the typical order of energies at which gluons interact with quarks inside the mesons or during the decay and hadronisation processes.

To keep a heavy meson bound, gluons must be exchanged dynamically between valence quarks. As the heavy quark has almost all the meson rest mass, the typical momentum of the light quark and soft gluons is $q^2|_{\text{soft}} \sim (\Lambda_{\text{QCD}})^2$. On the other hand, when a heavy quark decays it can create hard collinear gluons, which are expected to have a momentum of the same order as the heavy quark mass $q^2|_{\text{hard collinear}} \sim (m_b)^2$. In-between lies a gluon exchanged by a very massive or energetic quark and a slow-moving light valence quark, such as a hard-spectator scattering gluon, that is assumed to have a momentum of order $q^2|_{\text{hard-soft}} \sim m_b \Lambda_{\text{QCD}}$.

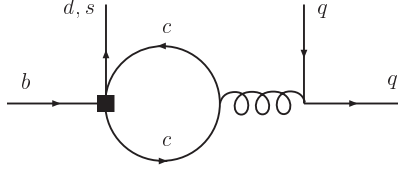


Figure 4.11: Penguin diagram with a charm-quark loop contributing to $B \rightarrow L_1 L_2$ decays [80].

4.5 Strong points and shortcomings of QCD factorisation

QCdf provides a model-independent basis for the analysis of weak decays of heavy mesons in powers and logarithms of Λ_{QCD}/m_b . At leading power in Λ_{QCD}/m_b but to all orders in α_s , the decay amplitudes assume factorised forms similar to those in Eqs. (4.14)–(4.15). Having such a formalism is of great importance, since it furnishes a well defined limit of QCD in which these processes admit a rigorous theoretical description [78], enabling the analysis at $O(\alpha_s)$ of many observables designed for the study of CP violation and NP searches.

The most important success of QCdf is that, beyond LO in α_s , there is a complete cancellation of scale and scheme dependences between the Wilson coefficients and the corresponding hadronic matrix elements in the WEH. Therefore, a general formula similar to Eq. (4.12) for the amplitudes can be written as

$$C_i(\mu) \langle \mathcal{O}_i \rangle + C_j(\mu) \langle \mathcal{O}_j \rangle = a_i^{\text{eff}} \langle \mathcal{O}_i \rangle_F + a_j^{\text{eff}}(\mu) \langle \mathcal{O}'_j \rangle_F, \quad (4.16)$$

where a_i^{eff} and a_j^{eff} are perturbatively calculable parameters. Obviously, Eq. (4.16) is just a simplification that illustrates the general structure of the result achieved, as it neither "non-factorisable" nor weak-annihilation contributions follow this structure. Another noteworthy achievement of QCdf is the ability to recover naïve factorisation in a natural way at LO in both α_s and Λ_{QCD}/m_b , hence providing a mathematical justification for the successes and drawbacks of the naïve factorisation approach.

However, QCdf also has its own drawbacks. These can be classified in two groups: limitations inherent to the formalism and model-dependence of certain input parameters. The former are the hardest to overcome as they involve a large increase in the complexity of calculations, whereas the latter may be improved as better experimental results become available and more accurate models are constructed.

In the first group fall the lack of an all-order proof, the issue of charming penguins and the theoretical uncertainty of $O(\Lambda_{\text{QCD}}/m_b)$:

- So far a proof of QCdf has been given only at order α_s^2 for heavy-to-light meson decays [30]. To get an all-order proof in α_s (but to leading power in Λ_{QCD}/m_b) a more systematic framework based on an effective Lagrangian is needed. This framework is provided by the *Soft-Collinear Effective Theory* (SCET) [80].

- The expression "charming penguins" was coined in [81] to design the penguin diagrams that contain a charm loop (see Fig. 4.11). The validity of the usual QCDF formula, when this kind of topology contributes to a heavy meson decay, has been questioned in the literature from two different perspectives. In [82], it was concluded that the experimental values of $Br(B \rightarrow K\pi)$ could only be explained if non-perturbative Λ_{QCD}/m_b corrections to the leading operators of the WEH involving a charm loop were enhanced in the cases where the factorized amplitudes were either colour or Cabibbo suppressed. On the other hand, in [83] it was argued that, within the SCET formalism, charming penguins could contribute to $Br(B^0 \rightarrow \pi^0\pi^0)$ with long-distance (i.e. non-factorisable) effects already at LO and hence free from Λ_{QCD}/m_b suppression. In [84, 85], however, this latter claim was proven to be misleading due to a missing factor of order $(\Lambda_{\text{QCD}}/m_b)^2$ in the argumentation presented in [83], and it was concluded that the resonance contribution to the charm-penguin diagrams for $B \rightarrow L_1L_2$ decays is always parametrically suppressed in the heavy-quark limit, irrespective of whether the charm quark is treated as being heavy or light.
- All computations performed in QCDF have a theoretical uncertainty of $O(\Lambda_{\text{QCD}}/m_b)$ attached to them. As we have seen in Eqs. (1.23) and (1.47), this uncertainty arises, in the first place, when the HQET/LEET Lagrangians are expanded in powers of Λ_{QCD}/m_b and just the LO is retained. Since the HQET/LEET formalism is paramount to QCDF, this uncertainty becomes intrinsically associated to it mainly via the colour transparency idea. Therefore, to obtain a consistent power counting, any computation performed within the QCDF framework must be expanded in powers of $1/m_b$ and all terms of this series other than the leading must be neglected; this affects both the hard-scattering kernels and the meson LCDA behaviour at the endpoints [see Eqs. (2.17) and (2.21)] [30]. This approximation simplifies the computations a good deal and helps in reducing the amount of independent form factors involved in the decay, as shown in Eqs. (3.30)–(3.32). The downside is that currently there is no way to calculate these corrections suppressed by powers of Λ_{QCD}/m_b in QCDF, so one has to resort to naïve dimensional arguments to obtain a rough estimate of their size as done in [86], which is *assumed* to be not greater than $O(10\%)$ [61]. Nevertheless, a comparison between the SM plot of $A_T^{(3)}$ in Fig. 4 (left) of [45] and the same observable represented in Fig. 2 of [10], where such terms are embedded in the full QCD form factors (see Secs. 6.3 – 6.7 for a comparison between both approaches), leads to an estimate of $O(7\%)$ for Λ_{QCD}/m_b corrections which is in complete agreement with the assumption on the size of these power-suppressed corrections performed in [61, 86].

The lack of precision in the calculation of some input parameters, such as heavy-to-light form factors and B light-cone distribution amplitudes, which take different values using different theoretical approaches, lies on the second group. Hopefully, with the steadily growing availability of more powerful computers and the design and implementation of better algorithms, in a few years lattice QCD results will overtake the QCD-based analytical approaches and produce both very accurate model-independent theoretical results for these quantities.

Part II

The $\bar{B}_d^0 \rightarrow \bar{K}^{*0}(\rightarrow K\pi)\ell^+\ell^-$ decay mode
at large recoil

Chapter 5

Kinematics of a 4-body decay

This chapter will be devoted to the derivation and discussion of the kinematic relations of a generic 4-body decay, aiming at finding all possible Lorentz invariant magnitudes in terms of measurable quantities as well as computing the phase space element that arise in such decays. We have considered important to include this subject in the thesis for the sake of completeness, as a 4-body decay is a quite involved process from the kinematical point of view. The following is based, to a large extent, on the Appendix B.2 of the PhD thesis by Laurenz M. Widhalm [87] which, unfortunately, is not yet available to the community in a complete electronic form at the moment of writing these lines. However, Dr. Widhalm kindly sent me a *PostScript* version of his work in 2008, which I have kept and reproduce below with some improvements here and there. Therefore, Dr. Widhalm deserves all the credit for this chapter whereas any mistake the reader might find is exclusively mine.

5.1 Definitions

Let us denote the 4-momenta of the four particles resulting from a generic $X \rightarrow Y(\rightarrow ij)Z(\rightarrow kl)$ decay by p_i (with $i = 1, \dots, 4$) and their invariant masses by m_i . For the discussion of their kinematics, the particles will be grouped in two pairs, (i, j) and (k, l) ($i \neq j \neq k \neq l$), with invariant masses m_{ij} and m_{kl} respectively. The total momentum and invariant mass of the decaying particle (and therefore of the four particles) is p and m .

There are many reference frames that can be chosen for this kind of decays, however the most suited to our purpose of obtaining all possible combinations of Lorentz scalar products will be the *rest frame of the decaying particle*, given by

$$\vec{p} = \sum_{i=1}^4 \vec{p}_i = \vec{0}, \quad (5.1)$$

and the *rest frame of a particle pair* (or "diparticle"), defined by

$$\vec{p}_{ij} = \vec{p}_i + \vec{p}_j = \vec{0}. \quad (5.2)$$

It is also very convenient to define the momenta in each pair in terms of two 4-vectors, one of them symmetric and the other antisymmetric under the exchange of the two particles in the pair:

$$P_{ij} \equiv p_i + p_j \quad (P_{ij} = P_{ji}), \quad (5.3)$$

$$Q_{ij} \equiv p_i - p_j \quad (Q_{ij} = -Q_{ji}). \quad (5.4)$$

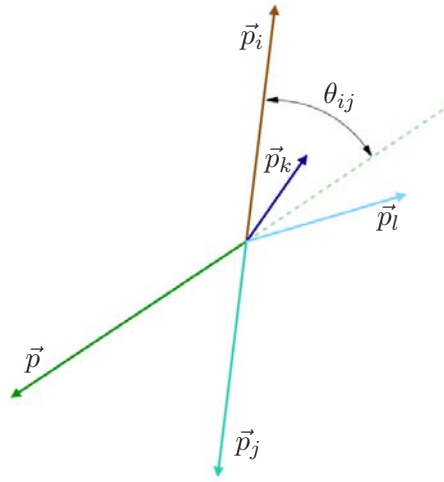


Figure 5.1: Definition of θ_{ij} . Modified from [87].

With the former definitions at hand one might realise that, when grouping the decay products in pairs, three angles arise "naturally" to describe this process. The way we define them is just a matter of taste, but once a choice has been made, consistency with these definitions is mandatory. There appears to be a tacit agreement in the literature to choose these three angles as follows:

- θ_{ij} is the angle between the forward direction of the particle i (with 3-momentum \vec{p}_i) and reversed direction of the decaying particle (defined by the 3-momentum $-\vec{p}$) in the diparticle (i, j) rest frame (see Fig. 5.1).
- θ_{kl} is the angle between the forward direction of the particle k (with 3-momentum \vec{p}_k) and reversed direction of the decaying particle (defined by the 3-momentum $-\vec{p}$) in the diparticle (k, l) rest frame.
- ϕ is the *oriented* angle between the planes defined by the diparticles (i, j) and (k, l) in the decaying particle rest frame with respect to the diparticle (i, j) 3-momentum.

Mathematical expressions for these angles can be obtained by relating them to the 3-vector parts of P [Eq. (5.3)] and Q [Eq. (5.4)]. For θ_{ij} this is straightforward. In the (i, j) rest frame Eq. (5.2) holds, so \vec{Q}_{ij} is simply given by

$$\vec{Q}_{ij} = \vec{p}_i - \vec{p}_j = 2\vec{p}_i \quad \Rightarrow \quad \vec{Q}_{ij} \parallel \vec{p}_i \quad (5.5)$$

whereas the 3-momentum of the decaying particle is

$$\vec{p} = \vec{p}_i + \vec{p}_j + \vec{p}_k + \vec{p}_l = \vec{0} + \vec{P}_{kl}. \quad (5.6)$$

Therefore,

$$\cos \theta_{ij} \equiv \frac{\vec{p}_i \cdot (-\vec{p})}{|\vec{p}_i| |-\vec{p}|} = -\frac{2\vec{p}_i \cdot \vec{p}}{2|\vec{p}_i| |\vec{p}|} = -\frac{\vec{Q}_{ij} \cdot \vec{P}_{kl}}{|\vec{Q}_{ij}| |\vec{P}_{kl}|}. \quad (5.7)$$

As Q_{ij} is antisymmetric in ij , θ_{ij} is also antisymmetric under the permutation of these indices. Also note that with the definition in Eq. (5.7), $\cos \theta_{ij}$ is unambiguous with respect to θ_{ij} in the range $[0, \pi]$.

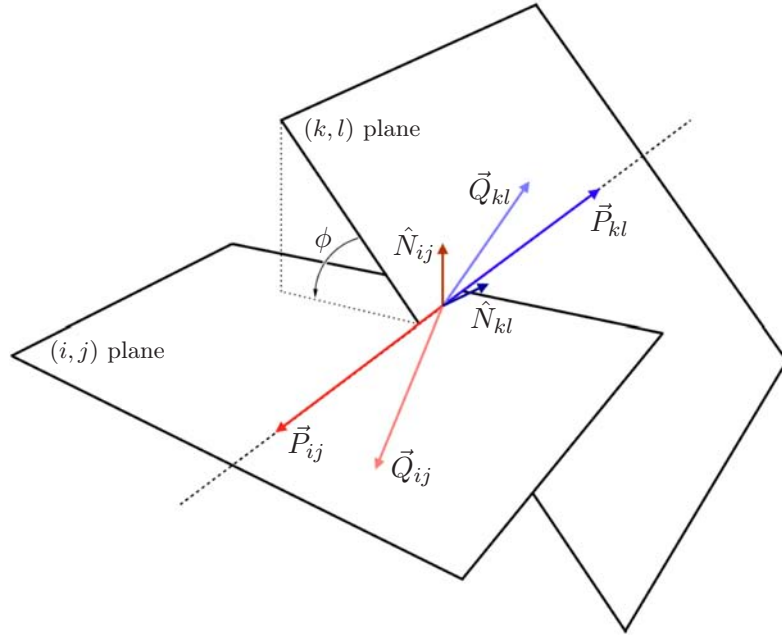


Figure 5.2: Definition of ϕ . Modified from [87].

Deriving ϕ is a bit more complicated, as it is an oriented angle. "Orientation" means that ϕ is related to one chosen direction of space. Without any orientation, ϕ would be unambiguous

only in the $[0, \frac{\pi}{2}]$ range. However, if an ordering between the two planes is introduced by using the vector product of the normal vectors to both planes (\hat{N}_{ij} and \hat{N}_{kl} in Fig. 5.2) then this range is extended unambiguously to $[0, \pi]$, as we have fixed one space dimension. The other space dimension can be set by choosing a definite direction. In our case this direction will be chosen as that of the diparticle (i, j) 3-momentum ($\vec{p}_i + \vec{p}_j = \vec{P}_{ij}$) in the reference frame of the decaying particle, where

$$\vec{P}_{ij} + \vec{P}_{kl} = \vec{p} = \vec{0}, \quad (5.8)$$

so the direction of orientation will be parallel to the line of intersection between the two planes (see Fig. 5.2). This provides a proper definition of ϕ in the whole range $[-\pi, \pi]$:

$$\cos \phi \equiv \hat{N}_{ij} \cdot \hat{N}_{kl}, \quad (5.9)$$

$$\sin \phi \equiv (\hat{N}_{ij} \times \hat{N}_{kl}) \cdot \hat{P}_{ij}, \quad (5.10)$$

with

$$\hat{P}_{ij} \equiv \frac{\vec{P}_{ij}}{|\vec{P}_{ij}|}, \quad (5.11)$$

$$\hat{N}_{ij} \equiv \frac{\vec{P}_{ij} \times \vec{Q}_{ij}}{|\vec{P}_{ij} \times \vec{Q}_{ij}|}. \quad (5.12)$$

5.2 Relations

5.2.1 General relations

The following relations are derived from the general properties of energy-momentum 4-vectors:

$$P_{ij}^2 = (p_i + p_j)^2 = m_i^2 + m_j^2 + 2p_i p_j = m_{ij}^2, \quad (5.13)$$

$$Q_{ij}^2 = (p_i - p_j)^2 = m_i^2 + m_j^2 - 2p_i p_j, \quad (5.14)$$

$$P_{ij}Q_{ij} = (p_i + p_j)(p_i - p_j) = m_i^2 - m_j^2, \quad (5.15)$$

From Eq. (5.13) we obtain

$$p_i p_j = \frac{1}{2}(m_{ij}^2 - m_i^2 - m_j^2), \quad (5.16)$$

which can be substituted into Eq. (5.14) to give

$$Q_{ij}^2 = 2(m_i^2 + m_j^2) - m_{ij}^2. \quad (5.17)$$

5.2.2 Relations in the rest frame of the decaying particle

The two main relations in the decaying particle rest frame are

$$P_{ij}^0 + P_{kl}^0 = m_{ij} + m_{kl} = m, \quad (5.18)$$

$$\vec{P}_{ij} + \vec{P}_{kl} = \vec{0}. \quad (5.19)$$

Eq. (5.13) can be rewritten for both the (i, j) and (k, l) diparticles, obtaining

$$(P_{ij}^0)^2 - m_{ij}^2 = |\vec{P}_{ij}|^2 = |\vec{P}_{kl}|^2 = (P_{kl}^0)^2 - m_{kl}^2 = (m - P_{ij}^0)^2 - m_{kl}^2, \quad (5.20)$$

where the second equality follows from Eq. (5.19) and the last from Eq. (5.18). Using the short-hand definitions

$$\bar{p} = \frac{1}{2}(m^2 - m_{ij}^2 - m_{kl}^2), \quad (5.21)$$

$$\sigma = \sqrt{\bar{p}^2 - m_{ij}^2 m_{kl}^2}, \quad (5.22)$$

we get, from the first and last equality in Eq. (5.20),

$$P_{ij}^0 = \frac{1}{2m}(m^2 + m_{ij}^2 - m_{kl}^2) \Rightarrow P_{ij}^0 = \frac{\bar{p} + m_{ij}^2}{m}. \quad (5.23)$$

On the other hand, taking the square root on both sides of $|\vec{P}_{ij}|^2 = (m - P_{ij}^0)^2 - m_{kl}^2$ from Eq. (5.20), substituting first Eq. (5.23) and then Eq. (5.21) and expanding the r.h.s. we obtain

$$|\vec{P}_{ij}| = \frac{1}{m} \sqrt{\bar{p}^2 - m_{ij}^2 m_{kl}^2} = \frac{\sigma}{m}. \quad (5.24)$$

5.2.3 Relations in the rest frame of a diparticle

The rest frame of the diparticle (i, j) is defined by the equations

$$P_{ij}'^0 = m_{ij}, \quad (5.25)$$

$$\vec{P}_{ij}' = \vec{p}_i + \vec{p}_j = \vec{0}, \quad (5.26)$$

where the "prime" denotes the kinematical variables computed in this reference frame.

Defining $p_i'^0 \equiv E_i'$ and using Eq. (5.26) in the form $|\vec{p}_i| = |\vec{p}_j|$ one can write

$$E_i'^2 = |\vec{p}_i'|^2 + m_i^2, \quad (5.27)$$

$$E_j'^2 = |\vec{p}_j'|^2 + m_j^2 = |\vec{p}_i'|^2 + m_j^2. \quad (5.28)$$

Eqs. (5.27)–(5.28), when substituted into Q_{ij}^0 , lead to

$$Q_{ij}^0 = p_i^0 - p_j^0 = E_i' - E_j' = \frac{E_i'^2 - E_j'^2}{E_i' + E_j'} = \frac{m_i^2 - m_j^2}{m_{ij}}. \quad (5.29)$$

Using the short-hand invariant quantities analogous to Eqs. (5.21)–(5.31) for this reference frame

$$\bar{p}_{ij} = \frac{1}{2}(m_{ij}^2 - m_i^2 - m_j^2), \quad (5.30)$$

$$\sigma_{ij} = \sqrt{\bar{p}_{ij}^2 - m_i^2 m_j^2}, \quad (5.31)$$

and Eq. (5.17) we obtain

$$|\vec{Q}'_{ij}| = \sqrt{(Q_{ij}^0)^2 - Q_{ij}'^2} = \sqrt{(Q_{ij}^0)^2 - Q_{ij}'^2} = \frac{2\sigma_{ij}}{m_{ij}}. \quad (5.32)$$

Employing the Gram-Schmidt orthogonalisation method, an expression for the component of \vec{Q}'_{ij} orthogonal to \vec{P}'_{kl} can also be derived for later use

$$|\vec{Q}'_{ij^\perp}| = \left| \vec{Q}'_{ij} - \frac{(\vec{Q}'_{ij} \cdot \vec{P}'_{kl})\vec{P}'_{kl}}{|\vec{P}'_{kl}|^2} \right| = |\vec{Q}'_{ij}| \left| \frac{\vec{Q}'_{ij}}{|\vec{Q}'_{ij}|} + \cos \theta_{ij} \frac{\vec{P}'_{kl}}{|\vec{P}'_{kl}|} \right| \quad (5.33)$$

$$= |\vec{Q}'_{ij}| \left| \frac{\vec{Q}'_{ij}}{|\vec{Q}'_{ij}|} - \cos^2 \theta_{ij} \frac{\vec{Q}'_{ij}}{|\vec{Q}'_{ij}|} \right| = |\vec{Q}'_{ij}| \sin \theta_{ij} = \frac{2\sigma_{ij}}{m_{ij}} \sin \theta_{ij}, \quad (5.34)$$

where Eq. (5.7) has been used in the second and third equalities. Note that this component is invariant under Lorentz transformations along \vec{P}'_{kl} and therefore has the same value in the rest frame of the decaying particle, so

$$|\vec{Q}_{ij}| = |\vec{Q}'_{ij}| = \frac{2\sigma_{ij}}{m_{ij}} \sin \theta_{ij}. \quad (5.35)$$

The energy and 3-momentum of the decaying particle in the diparticle rest frame may be obtained evaluating the invariant expression pP_{ij} in both the rest frame of the decaying particle and the rest frame of the diparticle. In the former rest frame

$$pP_{ij} = mP_{ij}^0 \quad (5.36)$$

whereas in the latter

$$pP_{ij} = p^0 m_{ij}, \quad (5.37)$$

so, combining Eqs. (5.36)–(5.37) and using Eq. (5.23), one arrives to

$$p'^0 = \frac{\bar{p} + m_{ij}^2}{m_{ij}}. \quad (5.38)$$

Using Eq. (5.38) and energy conservation, the expression of P_{ij} in the (i, j) rest frame can also be obtained:

$$P'_{kl} = p'^0 - P'_{ij} = \frac{\bar{p}}{m_{ij}}, \quad (5.39)$$

$$|\vec{P}'_{kl}| = \sqrt{(P'_{kl})^2 - P'^2_{kl}} = \sqrt{\left(\frac{\bar{p}}{m_{ij}}\right)^2 - m_{kl}^2} = \frac{\sigma}{m_{ij}}. \quad (5.40)$$

These equations can be used to evaluate the invariant expression $P_{ij}P_{kl}$ in the rest frame of the diparticle system

$$P_{jk}P_{kl} = P'_{ij}P'_{kl} - \vec{P}'_{ij} \cdot \vec{P}'_{kl} = m_{ij} \frac{\bar{p}}{m_{ij}} - 0 = \bar{p}. \quad (5.41)$$

5.2.4 Relations involving θ_{ij}

The invariant $Q_{ij}P_{ij}$ in the rest frame of the diparticle (i, j) can be evaluated using the definition of θ_{ij} in Eq. (5.7):

$$Q_{ij}P_{kl} = Q'_{ij}P'_{kl} - \vec{Q}'_{ij} \cdot \vec{P}'_{kl} = Q'_{ij}P'_{kl} + |\vec{Q}'_{ij}||\vec{P}'_{kl}| \cos \theta_{ij}. \quad (5.42)$$

Inserting Eqs. (5.29), (5.32), (5.39) and (5.40) into Eq. (5.42) the following relationship can be deduced

$$Q_{ij}P_{kl} = \frac{m_i^2 - m_j^2}{m_{ij}^2} \bar{p} + \frac{2}{m_{ij}^2} \sigma \sigma_{ij} \cos \theta_{ij}, \quad (5.43)$$

and adding Eq. (5.15) one gets

$$Q_{ij}p = Q_{ij}(P_{ij} + P_{kl}) = \frac{(m_i^2 - m_j^2)(\bar{p} + m_{ij}^2)}{m_{ij}^2} + \frac{2}{m_{ij}^2} \sigma \sigma_{ij} \cos \theta_{ij} \quad (5.44)$$

which, when evaluated in the decaying particle rest frame (characterised by $p^\mu = (m, \vec{0})$), gives

$$Q_{ij}^0 = \frac{1}{m m_{ij}} [(m_i^2 - m_j^2)(\bar{p} + m_{ij}^2) + 2\sigma \sigma_{ij} \cos \theta_{ij}]. \quad (5.45)$$

5.2.5 Relations involving ϕ

We first consider $\cos \phi$. Substituting Eqs. (5.11)–(5.12) into Eq. (5.9) one finds

$$\cos \phi = \frac{\vec{P}_{ij} \times \vec{Q}_{ij}}{|\vec{P}_{ij} \times \vec{Q}_{ij}|} \cdot \frac{\vec{P}_{kl} \times \vec{Q}_{kl}}{|\vec{P}_{kl} \times \vec{Q}_{kl}|} = \frac{(\vec{P}_{ij} \cdot \vec{P}_{kl})(\vec{Q}_{ij} \cdot \vec{Q}_{kl}) - (\vec{P}_{ij} \cdot \vec{Q}_{kl})(\vec{P}_{kl} \cdot \vec{Q}_{ij})}{|\vec{P}_{ij} \times \vec{Q}_{ij}| |\vec{P}_{kl} \times \vec{Q}_{kl}|}, \quad (5.46)$$

where the Levi-Civita tensor property

$$\epsilon_{abc}\epsilon_{ade} = (\delta_b^d\delta_c^e - \delta_b^e\delta_c^d) \quad (5.47)$$

has been used in the second equality. Every single product will be evaluated in the rest frame of the decaying particle, so that:

- $|\vec{P}_{ij} \times \vec{Q}_{ij}|$

It may be calculated easily using Eqs. (5.24) and (5.35):

$$|\vec{P}_{ij} \times \vec{Q}_{ij}| = |\vec{P}_{ij}| |\vec{Q}_{ij}^\perp| = \frac{2\sigma\sigma_{ij}}{m m_{ij}} \sin \theta_{ij}. \quad (5.48)$$

- $\vec{P}_{ij} \cdot \vec{P}_{kl}$

In the rest frame of the decaying particle Eq. (5.19) is fulfilled and, using Eq. (5.24) it is straightforward to obtain

$$\vec{P}_{ij} \cdot \vec{P}_{kl} = -\vec{P}_{ij}^2 = -\frac{\sigma^2}{m^2}. \quad (5.49)$$

- $\vec{P}_{ij} \cdot \vec{Q}_{kl}$

The definition of \bar{p} in Eq. (5.21) can be rewritten as $m^2 = m_{ij}^2 + m_{kl}^2 + 2\bar{p}$, which may be used to express

$$(\bar{p} + m_{ij}^2)(\bar{p} + m_{kl}^2) - m^2\bar{p} = -\sigma^2, \quad (5.50)$$

$$\bar{p} + m_{ij}^2 - m^2 = -\bar{p} - m_{kl}^2. \quad (5.51)$$

These two relations, together with Eqs. (5.18), (5.43) and (5.45) allow to obtain

$$\vec{P}_{ij} \cdot \vec{Q}_{kl} = P_{ij}^0 Q_{kl}^0 - P_{ij} Q_{kl} = -\frac{\sigma}{m^2 m_{kl}^2} [\sigma(m_k^2 - m_l^2) + 2\sigma_{kl}(\bar{p} + m_{kl}^2) \cos \theta_{kl}]. \quad (5.52)$$

- $\vec{Q}_{ij} \cdot \vec{Q}_{kl}$

From Eq. (5.45) the expression

$$\begin{aligned} Q_{ij}^0 Q_{kl}^0 &= \frac{1}{m^2 m_{ij}^2 m_{kl}^2} [(m_i^2 - m_j^2)(m_k^2 - m_l^2)(\bar{p} + m_{ij}^2)(\bar{p} + m_{kl}^2) \\ &\quad + 2\sigma\sigma_{ij}(m_k^2 - m_l^2)(\bar{p} + m_{kl}^2) \cos \theta_{ij} + 2\sigma\sigma_{kl}(m_i^2 - m_j^2)(\bar{p} + m_{ij}^2) \cos \theta_{kl} \\ &\quad + 4\sigma^2\sigma_{ij}\sigma_{kl} \cos \theta_{ij} \cos \theta_{kl}] \\ &\equiv \frac{Q_{ijkl}}{m^2 m_{ij}^2 m_{kl}^2}, \end{aligned} \quad (5.53)$$

and since

$$\vec{Q}_{ij} \cdot \vec{Q}_{kl} = Q_{ij}^0 Q_{kl}^0 - Q_{ij} Q_{kl} = \frac{Q_{ijkl}}{m^2 m_{ij}^2 m_{kl}^2} - Q_{ij} Q_{kl}, \quad (5.54)$$

inserting all terms in Eq. (5.9), using Eq. (5.51) and solving for $Q_{ij} Q_{kl}$ we deduce

$$\begin{aligned} Q_{ij} Q_{kl} &= \frac{1}{m_{ij}^2 m_{kl}^2} [(m_i^2 - m_j^2)(m_k^2 - m_l^2) \bar{p} + 2\sigma_{ij}(m_k^2 - m_l^2) \cos \theta_{ij} \\ &\quad + 2\sigma_{kl}(m_i^2 - m_j^2) \cos \theta_{kl} + 4\sigma_{ij}\sigma_{kl} \bar{p} \cos \theta_{ij} \cos \theta_{kl} \\ &\quad + 4\sigma_{ij}\sigma_{kl} m_{ij} m_{kl} \sin \theta_{ij} \sin \theta_{kl} \cos \phi]. \end{aligned} \quad (5.55)$$

Finally, we need to find the contribution proportional to $\sin \phi$. A visual inspection of Eqs. (5.9)–(5.10) is enough to reveal that, while $\cos \phi$ is invariant under parity transformations, $\sin \phi$ is not, so $\sin \phi$ turns out to be a pseudoscalar magnitude. As the only pseudoscalar expression that can be written using the 4-vectors P and Q as building blocks involves the four-dimensional Levi-Civita tensor, then $\sin \phi$ must be proportional to

$$\epsilon_{\alpha\beta\gamma\delta} P_{ij}^\alpha Q_{ij}^\beta P_{kl}^\gamma Q_{kl}^\delta. \quad (5.56)$$

The evaluation of Eq. (5.56) in the rest frame of the decaying particle requires the use of Eqs. (5.18)–(5.19) as well as the antisymmetry property of the Levi-Civita tensor combined with the symmetry of the product $P_{ij} P_{kl}$ under index exchange, giving as a result

$$\epsilon_{\alpha\beta\gamma\delta} P_{ij}^\alpha Q_{ij}^\beta P_{kl}^\gamma Q_{kl}^\delta = m \vec{P}_{ij} \cdot (\vec{Q}_{ij} \times \vec{Q}_{kl}). \quad (5.57)$$

On the other hand, substituting Eqs. (5.11)–(5.12) into Eq. (5.10), employing the property Eq. (5.47) and the symmetry (antisymmetry) of $P_{ij} P_{kl}$ (Levi-Civita tensor of 4 indices) under index exchange, one can evaluate $\sin \phi$ in terms of \vec{P}_{ij} and \vec{Q}_{ij} as¹

$$\begin{aligned} \sin \phi &= \left(\frac{\vec{P}_{ij} \times \vec{Q}_{ij}}{|\vec{P}_{ij} \times \vec{Q}_{ij}|} \times \frac{\vec{P}_{kl} \times \vec{Q}_{kl}}{|\vec{P}_{kl} \times \vec{Q}_{kl}|} \right) \cdot \frac{\vec{P}_{ij}}{|\vec{P}_{ij}|} \\ &= -\frac{|\vec{P}_{ij}|}{|\vec{P}_{ij} \times \vec{Q}_{ij}| |\vec{P}_{kl} \times \vec{Q}_{kl}|} \vec{P}_{ij} \cdot (\vec{Q}_{ij} \times \vec{Q}_{kl}). \end{aligned} \quad (5.58)$$

Finally, combining Eqs. (5.57)–(5.58) and using Eq. (5.24) and Eq. (5.35), the pseudoscalar magnitude of Eq. (5.56) can be expressed in terms of familiar kinematical variables as

$$\epsilon_{\alpha\beta\gamma\delta} P_{ij}^\alpha Q_{ij}^\beta P_{kl}^\gamma Q_{kl}^\delta = -\frac{4\sigma_{ij}\sigma_{kl}}{m_{ij} m_{kl}} \sin \theta_{ij} \sin \theta_{kl} \sin \phi. \quad (5.59)$$

¹There is a typo in Eq. (A.2) of [10], as $\sin \phi$ cannot be a vector.

5.2.6 Summary of Lorentz invariant scalar products of P and Q

All possible Lorentz-invariant combinations of the 4-vectors P and Q found previously are collected here systematically:

$$P_{ij}P_{ij} = m_{ij}^2, \quad (5.60)$$

$$P_{ij}Q_{ij} = m_i^2 - m_j^2 \quad (5.61)$$

$$P_{jk}P_{kl} = \bar{p} \quad (5.62)$$

$$P_{ij}Q_{kl} = \frac{m_k^2 - m_l^2}{m_{kl}^2} \bar{p} + \frac{2}{m_{kl}^2} \sigma \sigma_{kl} \cos \theta_{kl}, \quad (5.63)$$

$$Q_{ij}Q_{ij} = 2(m_i^2 + m_j^2) - m_{ij}^2, \quad (5.64)$$

$$Q_{ij}Q_{kl} = \frac{1}{m_{ij}^2 m_{kl}^2} [(m_i^2 - m_j^2)(m_k^2 - m_l^2) \bar{p} + 2\sigma \sigma_{ij} (m_k^2 - m_l^2) \cos \theta_{ij}] \quad (5.65)$$

$$+ 2\sigma \sigma_{kl} (m_i^2 - m_j^2) \cos \theta_{kl} + 4\sigma_{ij} \sigma_{kl} \bar{p} \cos \theta_{ij} \cos \theta_{kl} \quad (5.66)$$

$$+ 4\sigma_{ij} \sigma_{kl} m_{ij} m_{kl} \sin \theta_{ij} \sin \theta_{kl} \cos \phi], \quad (5.67)$$

$$\epsilon_{\alpha\beta\gamma\delta} P_{ij}^\alpha Q_{ij}^\beta P_{kl}^\gamma Q_{kl}^\delta = -\frac{4\sigma \sigma_{ij} \sigma_{kl}}{m_{ij} m_{kl}} \sin \theta_{ij} \sin \theta_{kl} \sin \phi, \quad (5.68)$$

with the definitions

$$\bar{p} = \frac{1}{2}(m^2 - m_{ij}^2 - m_{kl}^2), \quad (5.69)$$

$$\sigma = \sqrt{\bar{p}^2 - m_{ij}^2 m_{kl}^2}, \quad (5.70)$$

$$\bar{p}_{ij} = \frac{1}{2}(m_{ij}^2 - m_i^2 - m_j^2), \quad (5.71)$$

$$\sigma_{ij} = \sqrt{\bar{p}_{ij}^2 - m_i^2 m_j^2}. \quad (5.72)$$

5.3 Phase space integration

When computing the decay amplitude of a four-body decay process one will have to deal with a phase space integral of the kind

$$F \equiv \int \frac{d^3 \vec{p}_i}{(2\pi)^3 2E_i} \int \frac{d^3 \vec{p}_j}{(2\pi)^3 2E_j} \int \frac{d^3 \vec{p}_k}{(2\pi)^3 2E_k} \int \frac{d^3 \vec{p}_l}{(2\pi)^3 2E_l} (2\pi)^4 \delta^4(p_i + p_j + p_k + p_l - p) f \quad (5.73)$$

where $f \equiv f(m_{ij}, m_{kl}, \theta_{ij}, \theta_{kl}, \phi)$ to keep the notation of the previous section, although it is always possible to reparametrise the dependences in f^2 .

If two δ function integrals like $\delta^4(p_i + p_j - P_{ij})$ are inserted in Eq. (5.73), then it can be split in two symmetric parts corresponding to the particle pairs (i, j) and (k, l) :

$$F = \frac{1}{2^4(2\pi)^8} \int d^4 P_{ij} \int d^4 P_{kl} \delta^4(P_{ij} + P_{kl} - p) \int_{ij} \int_{kl} f, \quad (5.74)$$

with

$$\int_{ij} \equiv \int \frac{d^3 \vec{p}_i}{E_i} \frac{d^3 \vec{p}_j}{E_j} \delta^4(p_i + p_j - P_{ij}). \quad (5.75)$$

As this expression is Lorentz-invariant, it can be evaluated in any reference frame. We choose the diparticle rest frame (characterised by $P_{ij}^0 = m_{ij}$ and $\vec{P}_{ij} = \vec{0}$) to calculate it. The spatial part of the δ function allows the integration in \vec{p}_j (which can be performed always, independently of the function f), obtaining

$$\int_{ij} = \int \frac{d^3 \vec{p}_i}{E_i E_j} \delta(E_i + E_j - m_{ij}) = \int \frac{|\vec{p}_i|^2 d|\vec{p}_i| d(\cos \hat{\theta}) d\hat{\phi}_{ij}}{E_i E_j} \delta(E_i + E_j - m_{ij}) \quad (5.76)$$

where now $p_j = (E_j, \vec{p}_j) = (\sqrt{|\vec{p}_i|^2 + m_j^2}, -\vec{p}_i)$ due to the constraint $\vec{p}_i + \vec{p}_j = \vec{0}$.

It is always possible to choose the spherical coordinates used to write the last equality such that $\hat{\theta} = \theta_{ij}$ but then, in general, $\hat{\phi}_{ij}$ will not coincide with the Cabibbo angle ϕ . Since the argument of the last δ function depends on the integration variable \vec{p}_i , to evaluate the integral it is convenient to perform the following change of variables:

$$X \equiv E_i + E_j = \sqrt{|\vec{p}_i|^2 + m_i^2} + \sqrt{|\vec{p}_i|^2 + m_j^2}, \quad (5.77)$$

$$dX = \frac{X \vec{p}_i d\vec{p}_i}{E_i E_j}. \quad (5.78)$$

Inserting Eqs. (5.77)–(5.78) into Eq. (5.76) one finds

$$\int_{ij} = \frac{p_i}{m_{ij}} \int d(\cos \theta_{ij}) d\hat{\phi} = \frac{\sigma_{ij}}{m_{ij}} \int d(\cos \theta_{ij}) d\hat{\phi}_{ij}, \quad (5.79)$$

where the rightmost term has been deduced by substituting Eq. (5.32), as in the diparticle rest frame the relation $2\sigma_{ij}/m_{ij} = |\vec{Q}_{ij}| = |\vec{p}_i - \vec{p}_j| = 2|\vec{p}_i|$ is fulfilled.

As a last step one can perform the integration in $d\hat{\phi}_{ij}$. Since f depends only on the relative angle between the (i, j) and (k, l) planes, this integration turns out to be independent of f and gives just a factor 2π :

$$\int_{ij} = \frac{2\pi \sigma_{ij}}{m_{ij}^2} \int d(\cos \theta_{ij}). \quad (5.80)$$

²These are the so-called *Cabibbo variables* as they were first proposed in [88].

Now one can study the remaining integral

$$\int d^4 P_{ij} \int d^4 P_{kl} \delta^4(P_{ij} + P_{kl} - p) \quad (5.81)$$

The transformation $m_{ij}^2 = (P_{ij}^0)^2 - |\vec{P}_{ij}|^2$ can be used to split and rewrite conveniently the 4-dimensional differential element as follows:

$$d^4 P_{ij} = d^0 P_{ij} d^3 \vec{P}_{ij} \Rightarrow d^0 P_{ij} = dP_{ij}^0 = d \left(\sqrt{m_{ij}^2 + |\vec{P}_{ij}|^2} \right) = \frac{m_{ij} dm_{ij}}{P_{ij}^0}, \quad (5.82)$$

so that Eq. (5.81) can be rewritten as

$$\int m_{ij} dm_{ij} \int m_{kl} dm_{kl} \int \frac{d^3 \vec{P}_{ij}}{P_{ij}^0} \int \frac{d^3 \vec{P}_{kl}}{P_{kl}^0} \delta^4(P_{ij} + P_{kl} - p), \quad (5.83)$$

which is formally equivalent to Eq. (5.75), leading to

$$\int m_{ij} dm_{ij} \int m_{kl} dm_{kl} \frac{\sigma}{m^2} \int d(\cos \bar{\theta}) d\bar{\phi}, \quad (5.84)$$

where the last term is the version of Eq. (5.80) corresponding to the rest frame of the decaying particle. The spherical coordinates can now be chosen such that $\bar{\phi}$ becomes the corresponding Cabibbo variable ϕ , so the integration in this variable cannot be performed independently of f . However, f is indeed independent of $\bar{\theta}$ and the integration in this variable can be performed straightforwardly giving a factor 2. Therefore

$$\int m_{ij} dm_{ij} \int m_{kl} dm_{kl} \frac{2\sigma}{m^2} \int d\phi. \quad (5.85)$$

Using

$$m_{ij} dm_{ij} = \frac{1}{2} dm_{ij}^2 \quad (5.86)$$

and putting all pieces together the final result is achieved

$$F = \frac{1}{2^5 (2\pi)^6 m^2} \int dm_{ij}^2 dm_{kl}^2 d(\cos \theta_{ij}) d(\cos \theta_{kl}) d\phi w(m_{ij}, m_{kl}) f(m_{ij}, m_{kl}, \theta_{ij}, \theta_{kl}, \phi), \quad (5.87)$$

being $w(m_{ij}, m_{kl})$ the phase space weight, defined as

$$w(m_{ij}, m_{kl}) \equiv \frac{\sigma \sigma_{ij} \sigma_{kl}}{m_{ij}^2 m_{kl}^2}. \quad (5.88)$$

The power counting in the prefactor of Eq. (5.87) is easy to understand. The $1/m^2$ comes from Eq. (5.84). A factor $1/2^4$ was already present in Eq. (5.74) but both m_{ij}^2 and m_{kl}^2 carry a

factor $1/2$ each (see Eq. (5.86)) while a factor 2 comes from Eq. (5.85), rendering the final $1/2^5$. Something similar happens with the $1/(2\pi)^6$ factor: Eq. (5.74) contained already a $1/(2\pi)^8$ but the integration over $\hat{\phi}_{ij}$ and $\hat{\phi}_{kl}$ contributes with a 2π factor from each angle.

An important remark concerning these angular integrations is in order here. The integration over $\hat{\phi}_{ij}$, $\hat{\phi}_{kl}$ and $\bar{\theta}$ being independent of f is just a manifestation of the isotropy of space-time in physics: the choice of the spatial orientation of an arbitrary coordinate system should always be free and the physics deduced from it should remain the same, independently of the orientation chosen.

Chapter 6

Dynamics

The aim of this chapter is to assemble, piece by piece, all the knowledge collected along the previous chapters into a coherent framework. This framework will allow to obtain an analytic expression for the differential decay amplitude of the exclusive process $\bar{B}^0 \rightarrow (\bar{K}^{*0}\gamma^*) \rightarrow K^-\pi^+\ell^+\ell^-$ (and also for its CP-conjugate mode $B^0 \rightarrow (K^{*0}\gamma^*) \rightarrow K^+\pi^-\ell^+\ell^-$) in both the SM and in presence of some kinds of NP scenarios that might be fulfilled in Nature. Since QCDf will be employed to obtain the corrections to naïve factorisation in this computation, the accuracy of the resulting expressions will be limited to LO in Λ_{QCD}/m_b and NLO in α_s . We will discuss the benefits and limitations of such an approach comparing it with the proposal in [10].

6.1 The weak effective $b \rightarrow s \ell^+ \ell^-$ Hamiltonian

The WEH for $b \rightarrow s \ell^+ \ell^-$ decays is given by [89, 90, 91, 92, 77, 10]

$$\mathcal{H}_{\text{eff}} = -\frac{4G_F}{\sqrt{2}} \left(\lambda_t^{(s)} \mathcal{H}_{\text{eff}}^{(t)} + \lambda_u^{(s)} \mathcal{H}_{\text{eff}}^{(u)} \right) + \text{h.c.} = -\frac{4G_F}{\sqrt{2}} \lambda_t^{(s)} \left(\mathcal{H}_{\text{eff}}^{(t)} + \hat{\lambda}_u^{(s)} \mathcal{H}_{\text{eff}}^{(u)} \right) + \text{h.c.}, \quad (6.1)$$

with $\lambda_q^{(s)} = V_{qs}^* V_{qb}$ and $\hat{\lambda}_u^{(s)} \equiv \lambda_u^{(s)} / \lambda_t^{(s)}$. A term with $\lambda_c^{(s)} = V_{cs}^* V_{cb}$ should also appear in Eq. (6.1), however throughout this work we will assume that the CKM matrix is unitary even in presence of NP, so the equality $\lambda_u^{(s)} + \lambda_c^{(s)} + \lambda_t^{(s)} = 0$ holds and $\lambda_c^{(s)}$ can be expressed in terms of $\lambda_u^{(s)}$ and $\lambda_t^{(s)}$. The two independent components of the WEH in Eq. (6.1) are given by [92, 77, 10]

$$\begin{aligned} \mathcal{H}_{\text{eff}}^{(t)} = & C_1(\mu) \mathcal{O}_1^c + C_2(\mu) \mathcal{O}_2^c + \sum_{i=3}^6 C_i(\mu) \mathcal{O}_i + \sum_{i=7}^{10} [C_i(\mu) \mathcal{O}_i + C'_i(\mu) \mathcal{O}'_i] \\ & + \sum_{i=S,PS} [C_i(\mu) \mathcal{O}_i + C'_i(\mu) \mathcal{O}'_i] + \sum_{i=T,PT} C_i(\mu) \mathcal{O}_i, \end{aligned} \quad (6.2)$$

$$\mathcal{H}_{\text{eff}}^{(u)} = C_1(\mu) (\mathcal{O}_1^c - \mathcal{O}_1^u) + C_2(\mu) (\mathcal{O}_2^c - \mathcal{O}_2^u). \quad (6.3)$$

Since

$$\lambda_u^{(s)} = A\lambda^4(\rho + i\eta), \quad (6.4)$$

$$\lambda_t^{(s)} = A\lambda^2 \left[-1 + \lambda^2 \left(\frac{1}{2} - \rho - i\eta \right) \right] + O(\lambda^6), \quad (6.5)$$

in the Branco and Lavoura improved Wolfenstein parametrisation of the CKM matrix [93], it is clear that $\mathcal{H}_{\text{eff}}^{(u)}$ is doubly suppressed by the small parameter λ with respect to $\mathcal{H}_{\text{eff}}^{(t)}$ and therefore is usually neglected [47, 92, 32]. However, this term proves to be sensitive to complex phases and becomes important when dealing with CP-violation¹, so it will be incorporated to our analysis later on.

6.1.1 Standard Model contributions

The SM effective operators \mathcal{O}_i (with $i = 1, \dots, 10$) contributing to Eqs. (6.2)–(6.3) originate from the diagrams in Fig. 6.1 and are given by

$$\mathcal{O}_1^u = (\bar{s}\gamma_\mu T^a P_L u) (\bar{u}\gamma^\mu T^a P_L b), \quad (6.6)$$

$$\mathcal{O}_2^u = (\bar{s}\gamma_\mu P_L u) (\bar{u}\gamma^\mu P_L u), \quad (6.7)$$

$$\mathcal{O}_1^c = (\bar{s}\gamma_\mu T^a P_L c) (\bar{c}\gamma^\mu T^a P_L b), \quad (6.8)$$

$$\mathcal{O}_2^c = (\bar{s}\gamma_\mu P_L c) (\bar{c}\gamma^\mu P_L b), \quad (6.9)$$

$$\mathcal{O}_3 = (\bar{s}\gamma_\mu P_L b) \sum_q (\bar{q}\gamma^\mu q), \quad (6.10)$$

$$\mathcal{O}_4 = (\bar{s}\gamma_\mu T^a P_L b) \sum_q (\bar{q}\gamma^\mu T^a q), \quad (6.11)$$

$$\mathcal{O}_5 = (\bar{s}\gamma_\mu \gamma_\nu \gamma_\rho P_L b) \sum_q (\bar{q}\gamma^\mu \gamma^\nu \gamma^\rho q), \quad (6.12)$$

$$\mathcal{O}_6 = (\bar{s}\gamma_\mu \gamma_\nu \gamma_\rho T^a P_L b) \sum_q (\bar{q}\gamma^\mu \gamma^\nu \gamma^\rho T^a q), \quad (6.13)$$

$$\mathcal{O}_7 = \frac{e}{16\pi^2} \bar{s} \sigma^{\mu\nu} (m_b P_R + m_s P_L) b F^{\mu\nu}, \quad (6.14)$$

$$\mathcal{O}_8 = \frac{g_s}{16\pi^2} \bar{s} T^a \sigma^{\mu\nu} (m_b P_R + m_s P_L) b G_{\mu\nu}^a, \quad (6.15)$$

¹For an enlightening insight on the fundamentals of CP violation see the third chapter of [7], whereas an exhaustive study of this phenomenon and its physical implications may be found in [94].

$C_1(\mu_b)$	$C_2(\mu_b)$	$C_3(\mu_b)$	$C_4(\mu_b)$	$C_5(\mu_b)$	$C_6(\mu_b)$	$C_7^{\text{eff}}(\mu_b)$	$C_8^{\text{eff}}(\mu_b)$	$C_9(\mu_b)$	$C_{10}(\mu_b)$
-0.2632	1.0111	-0.0055	-0.0806	0.0004	0.0009	-0.2923	-0.1663	4.0749	-4.3085

Table 6.1: NNLO Wilson coefficients in the Standard Model at the scale $\mu_b=4.8$ GeV.

$$\mathcal{O}_9 = \frac{e^2}{16\pi^2} (\bar{s}\gamma_\mu P_L b) (\bar{\ell}\gamma^\mu \ell) , \quad (6.16)$$

$$\mathcal{O}_{10} = \frac{e^2}{16\pi^2} (\bar{s}\gamma_\mu P_L b) (\bar{\ell}\gamma^\mu \gamma_5 \ell) . \quad (6.17)$$

where the colour indices have been omitted, a labels the $\text{SU}(3)_c$ generators, $g_s = \sqrt{4\pi\alpha_s}$ is the strong coupling constant, q are all active quark flavours in the effective theory (in our case $q = u, d, s, c, b$) and $P_{L,R} = (1 \mp \gamma_5)/2$. The operator basis in Eqs. (6.6)–(6.17) contains all possible dimension six gauge invariant operators that have the correct quantum numbers to contribute to $b \rightarrow s \ell^+ \ell^-$, are compatible with the electroweak symmetries and cannot be transformed into each other applying the equations of motion [42]. This operator basis, named as CMM after its authors (see [95, 96, 97]), is commonly used in the literature as it exhibits several advantages over the one in [92]: aside from displaying no Dirac traces containing γ_5 (which are problematic in dimensional regularisation), it has a more natural colour structure and is also obtained easier when computing the topologies in Fig. 6.1.

The determination of the Wilson coefficients in the SM was carried out in [99] following the discussion in [100, 9]. References [101, 102, 103, 104] were also followed to include QED corrections through the five additional operators

$$\mathcal{O}_{3Q} = (\bar{s}\gamma_\mu P_L b) \sum_q Q_q (\bar{q}\gamma^\mu q) , \quad (6.18)$$

$$\mathcal{O}_{4Q} = (\bar{s}\gamma_\mu T^a P_L b) \sum_q Q_q (\bar{q}\gamma^\mu T^a q) , \quad (6.19)$$

$$\mathcal{O}_{5Q} = (\bar{s}\gamma_\mu \gamma_\nu \gamma_\rho P_L b) \sum_q Q_q (\bar{q}\gamma^\mu \gamma^\nu \gamma^\rho q) , \quad (6.20)$$

$$\mathcal{O}_{6Q} = (\bar{s}\gamma_\mu \gamma_\nu \gamma_\rho T^a P_L b) \sum_q Q_q (\bar{q}\gamma^\mu \gamma^\nu \gamma^\rho T^a q) , \quad (6.21)$$

$$\mathcal{O}_b = \frac{1}{12} [(\bar{s}\gamma_\mu \gamma_\nu \gamma_\rho P_L b) (\bar{b}\gamma^\mu \gamma^\nu \gamma^\rho b) - 4(\bar{s}\gamma_\mu P_L b) (\bar{b}\gamma^\mu b)] , \quad (6.22)$$

where Q_q are the electric charges of the corresponding quarks ($+2/3$ or $-1/3$). The matching was performed at the high scale $\mu_0 = 2M_W$ and the Wilson coefficients were run down to the low

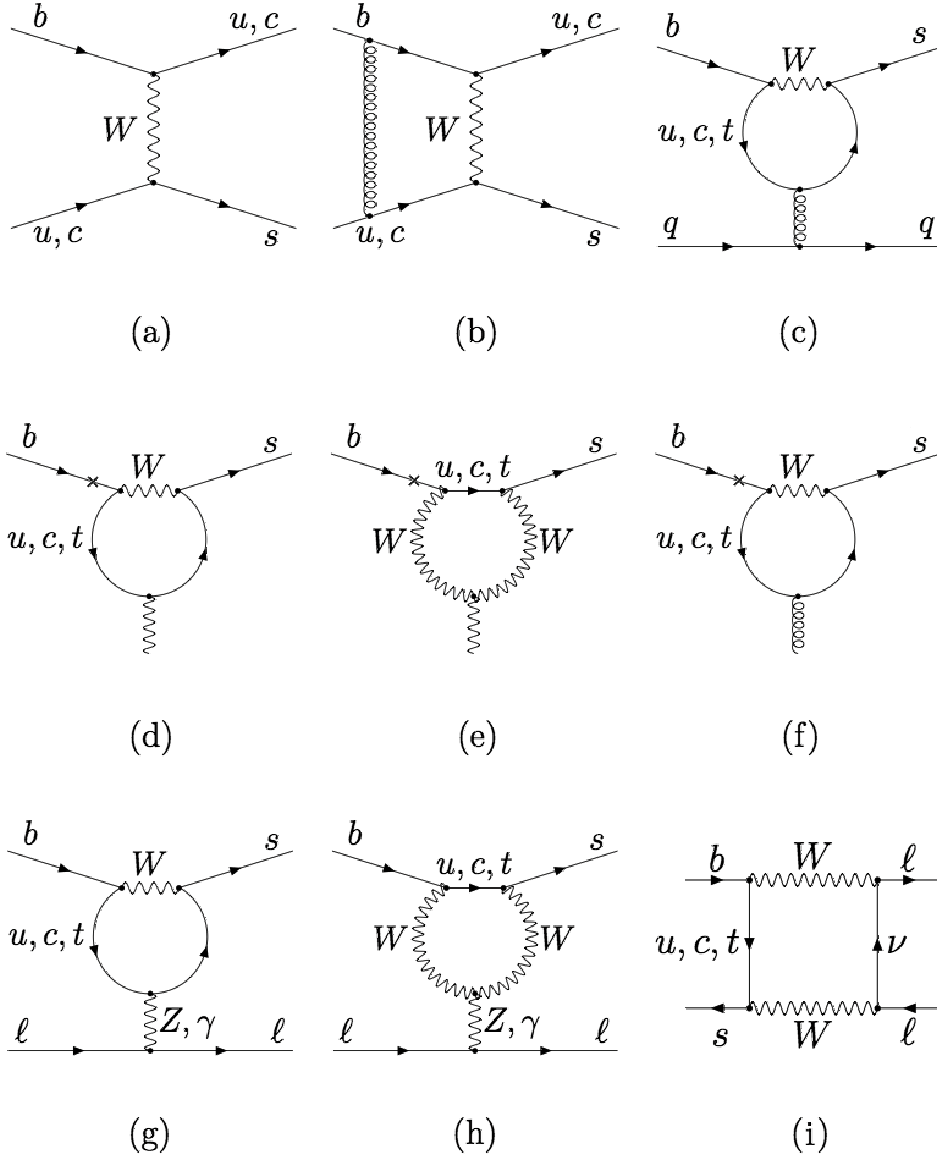


Figure 6.1: Feynman diagrams in the full theory from which the operators (6.6)-(6.17) originate. (a) is the *current-current* diagram that corresponds to operators \mathcal{O}_1 and \mathcal{O}_2 ; (b) is one of the several QCD corrections that can put \mathcal{O}_1 in a colour-allowed configuration. (c) are *QCD penguin* diagrams associated to operators $\mathcal{O}_3 - \mathcal{O}_6$. (d) and (e) depict the two *electromagnetic photon penguin* diagrams related to \mathcal{O}_7 . (f) is the *chromomagnetic gluon penguin* diagram related to \mathcal{O}_8 . (g), (h) and (i) are the *semi-leptonic penguin* and *box* diagrams associated to \mathcal{O}_9 and \mathcal{O}_{10} . Modified from [98].

scale $\mu_b = 4.8$ GeV. This introduced a mixing among all operators carrying the same quantum numbers: the weak effective $b \rightarrow s \ell^+ \ell^-$ Hamiltonian operators in Eqs. (6.8)–(6.17) and also the QED operators in Eqs. (6.18)–(6.22). The SM Wilson coefficients were obtained at NNLO accuracy at $\mu_b = 4.8$ GeV. They are given in table 6.1, where the definitions [95]

$$C_7^{\text{eff}} \equiv C_7 - \frac{1}{3} C_3 - \frac{4}{9} C_4 - \frac{20}{3} C_5 - \frac{80}{9} C_6, \quad (6.23)$$

$$C_8^{\text{eff}} \equiv C_8 + C_3 - \frac{1}{6} C_4 + 20 C_5 - \frac{10}{3} C_6 \quad (6.24)$$

have been used, as C_7 and C_8 always appear in these particular combinations with other C_i in matrix elements. It is also appropriate to define here the "effective" (i.e. basis- and scheme-independent) Wilson coefficient C_9^{eff} as

$$C_9^{\text{eff}} = C_9 + Y(q^2). \quad (6.25)$$

where q^2 is the invariant mass squared of the lepton pair $\ell^+ \ell^-$. The reason for using C_9^{eff} instead of C_9 is the following: when the RGEs are used to evolve the $b \rightarrow s \ell^+ \ell^-$ effective Hamiltonian from the high scale μ_0 to the low scale μ_b , there appears a large logarithm in C_9 which turns out to be of $O(1/\alpha_s)$, so one needs to go at NLL order in the α_s expansion to find the combination of terms necessary to cancel this logarithm and obtain a "version" of C_9 which is of $O(1)$. This combination of terms is given by the function $Y(q^2)$, which reads [89, 32]

$$\begin{aligned} Y^{(t)}(q^2) = & h(q^2, m_c) \left(\frac{4}{3} C_1 + C_2 + 6 C_3 + 60 C_5 \right) \\ & - \frac{1}{2} h(q^2, m_b) \left(7 C_3 + \frac{4}{3} C_4 + 76 C_5 + \frac{64}{3} C_6 \right) \\ & - \frac{1}{2} h(q^2, 0) \left(C_3 + \frac{4}{3} C_4 + 16 C_5 + \frac{64}{3} C_6 \right) \\ & + \frac{4}{3} C_3 + \frac{64}{9} C_5 + \frac{64}{27} C_6. \end{aligned} \quad (6.26)$$

where, in a slight abuse of notation it has been assumed $m_u \approx 0$, and [77]

$$Y^{(u)}(q^2) = \left(\frac{4}{3} C_1 + C_2 \right) [h(q^2, m_c) - h(q^2, 0)]. \quad (6.27)$$

The function $h(q^2, m_q)$ in Eq. (6.26) is given by

$$h(q^2, m_q) = -\frac{4}{9} \left[\ln \left(\frac{m_q^2}{\mu^2} \right) - \frac{2}{3} - z \right] - \frac{4}{9} (2+z) \sqrt{|z-1|} \begin{cases} \arctan \frac{1}{\sqrt{z-1}} & z > 1 \\ \ln \frac{1+\sqrt{1-z}}{\sqrt{z}} - \frac{i\pi}{2} & z \leq 1 \end{cases} \quad (6.28)$$

with $z = 4m_q^2/q^2$ and

$$h(q^2, 0) = \frac{8}{27} - \frac{4}{9} \ln\left(\frac{q^2}{\mu^2}\right) + \frac{4}{9}i\pi. \quad (6.29)$$

The first term in $h(q^2, m_q)$ represents the leading μ -dependence in the matrix elements which cancels the μ -dependence present in the leading logarithm in C_9 . The μ -dependence present in the coefficients of the other operators can only be cancelled by going to still higher order in the renormalization group improved perturbation theory. To this end the matrix elements of four-quark operators must be evaluated beyond the two-loop level [89]

As shown in Eqs. (6.28)–(6.29), $Y(q^2)$ contains absorptive parts that will also be present in the Wilson coefficient C_9^{eff} by definition. One of these imaginary terms arises as $m_q \rightarrow 0$ (i.e. is generated by light quark contributions below the $c\bar{c}$ threshold) while the other is due to $c\bar{c}$, as it appears only when $q^2 > 4m_c^2$. Since having strong phases is a prerequisite for CP-violation, this is an important remark. The Wilson coefficients C_7^{eff} and C_{10} , on the other hand, do not contain any strong phase [92].

6.1.2 New physics contributions

The WEH in Eq. (6.2) contains other operators aside from those included in Eqs. (6.6)–(6.17). These are all the conceivable dimension-six new operators that could arise if there were new physics processes at work beyond the SM, namely:

- the operators *with opposite chirality*, also known as *chirally-flipped operators* or *right-handed currents*

$$\mathcal{O}'_7 = \frac{e}{16\pi^2} \bar{s} \sigma^{\mu\nu} (m_b P_L + m_s P_R) b F^{\mu\nu}, \quad (6.30)$$

$$\mathcal{O}'_8 = \frac{g_s}{16\pi^2} \bar{s} T^a \sigma^{\mu\nu} (m_b P_L + m_s P_R) b G_{\mu\nu}^a, \quad (6.31)$$

$$\mathcal{O}'_9 = \frac{e^2}{16\pi^2} (\bar{s} \gamma_\mu P_L b) (\bar{\ell} \gamma^\mu \ell), \quad (6.32)$$

$$\mathcal{O}'_{10} = \frac{e^2}{16\pi^2} (\bar{s} \gamma_\mu P_L b) (\bar{\ell} \gamma^\mu \gamma_5 \ell); \quad (6.33)$$

- the *scalar* and *pseudoscalar* operators with their corresponding chirally-flipped counterparts, which may be written as [10]

$$\mathcal{O}_S = \frac{e^2}{16\pi^2} m_b (\bar{s} P_R b) (\bar{\ell} \ell), \quad \mathcal{O}'_S = \frac{e^2}{16\pi^2} m_b (\bar{s} P_L b) (\bar{\ell} \ell), \quad (6.34)$$

$$\mathcal{O}_{PS} = \frac{e^2}{16\pi^2} m_b (\bar{s} P_R b) (\bar{\ell} \gamma_5 \ell), \quad \mathcal{O}'_{PS} = \frac{e^2}{16\pi^2} m_b (\bar{s} P_L b) (\bar{\ell} \gamma_5 \ell); \quad (6.35)$$

- and the *tensor* and *pseudotensor* operators [105]

$$\mathcal{O}_T = \frac{e^2}{16\pi^2} (\bar{s} \sigma_{\mu\nu} b) (\bar{\ell} \sigma^{\mu\nu} \ell), \quad (6.36)$$

$$\mathcal{O}_{PT} = i \frac{e^2}{16\pi^2} \epsilon^{\mu\nu\rho\sigma} (\bar{s} \sigma_{\mu\nu} b) (\bar{\ell} \sigma_{\rho\sigma} \ell). \quad (6.37)$$

The reason that motivates the inclusion of only these effective operators, omitting the chirally-flipped $\mathcal{O}'_1 - \mathcal{O}'_6$ is the following: an RGE analysis shows that the numerical values of the Wilson coefficients associated to the matrix elements of QCD penguin operators $\mathcal{O}_3 - \mathcal{O}_6$ computed at the scale μ_b are essentially determined by the value of $C_2(M_W)$, the Wilson coefficient corresponding to tree-level operator \mathcal{O}_2 calculated at the electroweak scale. Therefore, to have large deviations from the SM predictions in the coefficients $C_3(\mu_b) - C_6(\mu_b)$, a large NP contribution to $C_2(M_W)$, associated to the colour-allowed operator \mathcal{O}_2 (and also to $C_1(M_W)$, associated to the colour-suppressed \mathcal{O}_1) would be needed. These large contributions would affect the theoretical branching ratios for two-body purely hadronic B decays. As these processes do not show big departures from the SM predictions computed within improved factorisation approaches, one does not expect that either $C_3(\mu_b) - C_6(\mu_b)$ or $C_1(\mu_b) - C_2(\mu_b)$ receive any sizeable NP effect.

Given that if there is NP it must occur at scales higher than the matching scale $\mu_0 = 2M_W$, the corresponding effects would be of very short range and therefore should be included in the Wilson coefficients, so

$$C_i(\mu_b) = C_i^{\text{SM}}(\mu_b) + \delta C_i(\mu_b) \quad (6.38)$$

would be the actual Wilson coefficient at the low scale $\mu \simeq m_b$ for the operators already present in the SM. The quantity $\delta C_i(\mu_b)$ accounts for the deviation of the "measured" value $C_i(\mu_b)$ of the Wilson coefficient² from the value computed in the SM ($C_i^{\text{SM}}(\mu)$). Hence, for the Wilson coefficients that are sensitive to NP effects in $b \rightarrow s \ell^+ \ell^-$ processes (C_i with $i = 7, \dots, 10$) we will write

$$\delta C_i(\mu_b) = C_i(\mu_b) - C_i^{\text{SM}}(\mu_b) = |\delta C_i| e^{i\phi_i}, \quad (6.39)$$

whereas the Wilson coefficients associated to purely NP operators (C_j with $j = 7', \dots, 10', S, S', PS, PS', T, PT$) will read simply

$$\delta C_j(\mu_b) = C_j(\mu_b) = |\delta C_j| e^{i\phi_j} \quad (6.40)$$

if the m_s/m_b suppressed chirally-flipped SM contributions are neglected. Both ϕ_i and ϕ_j are weak phases. These phases receive this name because they come from complex parameters which are only present in the weak sector (through Yukawa couplings) in the SM but, in a generalised Lagrangian containing both the SM and NP contributions, they might appear in other sectors too.

²More properly stated, there is actually a range of values allowed for each Wilson coefficient. This range is found using the constraints imposed by all the observables measured where the coefficient studied plays a role.

6.2 The $\bar{B}_d^0 \rightarrow \bar{K}^{*0}(\rightarrow K\pi)\ell^+\ell^-$ matrix element

6.2.1 Building the matrix element

The matrix element of the effective Hamiltonian in Eqs. (6.1)–(6.3) for the decay mode $\bar{B}_d^0 \rightarrow \bar{K}^{*0}(\rightarrow K\pi)\ell^+\ell^-$ and its CP-conjugated process may be written, at LO in α_s and in naïve factorisation, as [89, 90, 92] as

$$\begin{aligned} \mathcal{M} = & \frac{G_F \alpha}{\sqrt{2}\pi} \lambda_t^{(s)} \left\{ \left[\langle K\pi | \bar{s} \gamma^\mu (C_9^{\text{eff}} P_L + C_9^{\text{eff}'} P_R) b | \bar{B} \rangle \right. \right. \\ & - \frac{2m_b}{q^2} \langle K\pi | \bar{s} i \sigma^{\mu\nu} q_\nu \left[\left(C_7^{\text{eff}} + \frac{m_s}{m_b} C_7^{\text{eff}'} \right) P_R + \left(\frac{m_s}{m_b} C_7^{\text{eff}'} + C_7^{\text{eff}} \right) P_L \right] b | \bar{B} \rangle \left. \langle \ell^+ \ell^- | \bar{\ell} \gamma_\mu \ell | 0 \rangle \right. \\ & + \langle K\pi | \bar{s} \gamma^\mu (C_{10} P_L + C_{10}' P_R) b | \bar{B} \rangle \langle \ell^+ \ell^- | \bar{\ell} \gamma_\mu \gamma_5 \ell | 0 \rangle \\ & + \langle K\pi | \bar{s} (C_S P_R + C_S' P_L) b | \bar{B} \rangle \langle \ell^+ \ell^- | \bar{\ell} \ell | 0 \rangle + \langle K\pi | \bar{s} (C_{PS} P_R + C_{PS}' P_L) b | \bar{B} \rangle \langle \ell^+ \ell^- | \bar{\ell} \gamma_5 \ell | 0 \rangle \\ & \left. \left. + C_T \langle K\pi | \bar{s} \sigma_{\mu\lambda} b | \bar{B} \rangle \langle \ell^+ \ell^- | \bar{\ell} \sigma^{\mu\lambda} \ell | 0 \rangle + i C_{PT} \epsilon^{\mu\lambda\rho\sigma} \langle K\pi | \bar{s} \sigma_{\mu\lambda} b | \bar{B} \rangle \langle \ell^+ \ell^- | \bar{\ell} \sigma_{\rho\sigma} \ell | 0 \rangle \right\}, \quad (6.41) \end{aligned}$$

where the terms coming from $\mathcal{H}_{\text{eff}}^{(u)}$ [Eq. (6.3)] have not been included in the matrix element for the moment in order to lighten the notation.

Two remarks are in order here. On the one hand, the effective operator does not appear in Eq. (6.41) because it is only important in $b \rightarrow sq\bar{q}$ processes at LO; in $b \rightarrow s\ell^+\ell^-$, \mathcal{O}_8 will only enter at $O(\alpha_s)$, contributing to hard vertex and hard scattering topologies (see Figs. 6.7–6.8). On the other hand, the only piece that differs considerably from the effective operators in Eqs. (6.8)–(6.17) and Eqs. (6.30)–(6.37) is the one containing C_7^{eff} and $C_7^{\text{eff}'}$, but it can be deduced straightforwardly: let us consider for simplicity just the m_b term from Eq. (6.14) then, substituting the electromagnetic tensor $F^{\mu\nu} = \partial^\mu A^\nu - \partial^\nu A^\mu$ written in the momentum space one finds

$$\langle K\pi | \mathcal{O}_7 | \bar{B} \rangle = \langle K\pi | \frac{e}{16\pi^2} m_b (\bar{s} \sigma^{\mu\nu} P_R) b \left[-iq^\mu \tilde{A}^\nu + iq^\nu \tilde{A}^\mu \right] | \bar{B} \rangle, \quad (6.42)$$

and using the Lorenz condition $\partial_\nu A^\nu = 0$ on the Maxwell equation of motion $\partial_\nu F^{\nu\mu} = j^\mu$ the relation $\square A^\mu = j^\mu$ is found. In the momentum space and for the electromagnetic current this relation reads $-q^2 \tilde{A}^\mu = e \bar{\ell} \gamma^\mu \ell$. This expression may be further rearranged into $q^\nu \tilde{A}^\mu = -e \frac{q^\nu}{q^2} \bar{\ell} \gamma^\mu \ell$ and substituted into Eq. (6.42) to obtain

$$\langle K\pi | \mathcal{O}_7 | \bar{B} \rangle = \langle K\pi | \frac{e}{16\pi^2} m_b (\bar{s} \sigma^{\mu\nu} P_R) b \left[ie \frac{q^\nu}{q^2} \bar{\ell} \gamma^\mu \ell - ie \frac{q^\mu}{q^2} \bar{\ell} \gamma^\nu \ell \right] | \bar{B} \rangle, \quad (6.43)$$

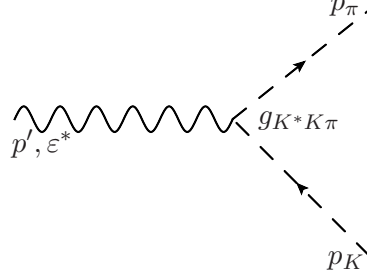


Figure 6.2: Feynman diagram representing the coupling of K^{*0} with momentum $p' = p_{K^*}$ and polarisation ε^* to a π with momentum p_π and \bar{K} with momentum p_K .

and using the antisymmetry of $\sigma^{\mu\nu}$ one finally arrives to

$$\langle K\pi | \mathcal{O}_7 | \bar{B} \rangle = \langle K\pi | \frac{e}{16\pi^2} m_b (\bar{s} \sigma^{\mu\nu} P_R) b \left[-2ie \frac{q^\nu}{q^2} \bar{\ell} \gamma^\mu \ell \right] | \bar{B} \rangle. \quad (6.44)$$

Reshuffling terms in Eq. (6.44) the piece that contains C_7^{eff} and $C_7^{\text{eff}'}$ in Eq. (6.41) is found.

6.2.2 The resonant decay

The $\bar{K}^{*0} \rightarrow K^- \pi^+$ piece

Each term of the matrix elements in Eq. (6.41) would have the same structure than the matrix elements in Eqs. (3.8), (3.9), (3.12) and (3.14) respectively if it were not for the final state, which instead of being a vector meson (a \bar{K}^{*0} in our case) is a two-particle state constituted by a K and a π . Hence, a way to express the $B \rightarrow K\pi$ matrix elements in terms of the matrix elements that define the $B \rightarrow V$ the form factors discussed in Sec. 3.1.1 must be found. This is possible if one assumes that, as a consequence of the \bar{B}_d^0 decay, the \bar{K}^{*0} is formed as an on-shell particle (i.e. a resonance) that finally decays into the $K^- \pi^+$ pair, so the process to study is the one depicted by Fig. 6.2.

The Feynman diagram in Fig. 6.2 is described by the effective Hamiltonian (i.e, the Feynman rule) [106]

$$\mathcal{H}_{\text{eff}} = g_{K^*K\pi} (p_\pi - p_K) \cdot \varepsilon^*, \quad (6.45)$$

where $g_{K^*K\pi}$ is the effective coupling between the decaying particle (K^{*0}) and the products of this decay (π, K). Eq. (6.45) can be used to obtain the squared and polarisation-averaged matrix

element

$$\begin{aligned} \overline{|\mathcal{M}|^2} &= g_{K^*K\pi}^2 (p_\pi - p_K)_\mu (p_\pi - p_K)_\nu \frac{1}{3} \sum_{\lambda=-1,0,+1} \varepsilon^{*\mu}(\lambda) \varepsilon^\nu(\lambda) \\ &= \frac{1}{3} g_{K^*K\pi}^2 (p_\pi - p_K)_\mu (p_\pi - p_K)_\nu \left(-g^{\mu\nu} + \frac{p_{K^*}^\mu p_{K^*}^\nu}{p_{K^*}^2} \right), \end{aligned} \quad (6.46)$$

with the factor 1/3 stemming from the average of the three polarisations of the K^{*0} . Contracting all indices in Eq. (6.46) and using Eq. (5.16) it may be found

$$\overline{|\mathcal{M}|^2} = \frac{1}{3} \frac{g_{K^*K\pi}^2}{m_{K^*}^2} \lambda(p_{K^*}^2, m_K^2, m_\pi^2), \quad (6.47)$$

being

$$\lambda(a, b, c) = a^2 + b^2 + c^2 - 2(ab + bc + ac) \quad (6.48)$$

the usual triangle function.

On the other hand, the differential decay amplitude of a two-body decay is given by (see Eq. (39.17) of [1])

$$d\Gamma_{K^*} = \frac{1}{32\pi^2} \overline{|\mathcal{M}|^2} \frac{|\vec{p}_f|}{m_{K^*}^2} d\Omega \quad (6.49)$$

where, according to see Eq. (39.16) of [1]

$$|\vec{p}_f| \equiv |\vec{p}_K| = |\vec{p}_\pi| = \frac{1}{2m_{K^*}} \lambda^{1/2}(p_{K^*}^2, m_K^2, m_\pi^2). \quad (6.50)$$

Therefore, substituting Eq. (6.47) and Eq. (6.47) into Eq. (6.49) one finds

$$d\Gamma_{K^*} = \frac{1}{3 \cdot 64\pi^2} \frac{g_{K^*K\pi}^2}{m_{K^*}^5} \lambda^{3/2}(p_{K^*}^2, m_K^2, m_\pi^2) d\Omega, \quad (6.51)$$

which can be trivially integrated along the solid angle to render

$$\Gamma_{K^*} = \frac{1}{48\pi} \frac{g_{K^*K\pi}^2}{m_{K^*}^5} \lambda^{3/2}(p_{K^*}^2, m_K^2, m_\pi^2) = \frac{g_{K^*K\pi}^2}{48\pi} m_{K^*} \beta^3, \quad (6.52)$$

with β defined as in [91], $\beta \equiv \lambda^{1/2}(p_{K^*}^2, m_K^2, m_\pi^2)/p_{K^*}^2$. Substituting all meson masses and the K^{*0} decay amplitude one obtains $g_{K^*K\pi}^2 = (29.87 \pm 0.49)$.

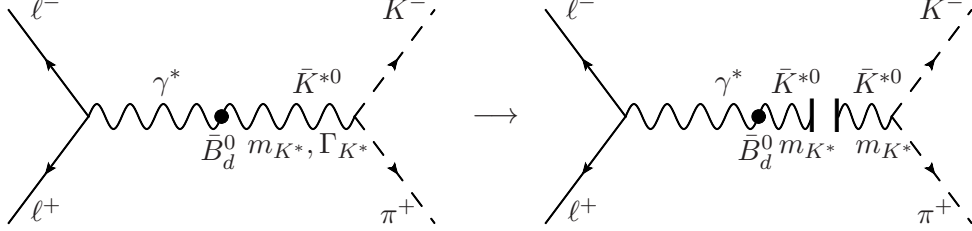


Figure 6.3: Schematic representation of the narrow-width approximation for the $\bar{B}_d^0 \rightarrow \bar{K}^{*0}\gamma^* \rightarrow (K^-\pi^+)(\ell^+\ell^-)$ decay mode.

The narrow-width approximation

The \bar{K}^{*0} is on-shell in the actual decay, with a certain mass-square distribution characterised by the Breit-Wigner formula

$$|D_{K^*}(p_{K^*})|^2 = \frac{1}{(p_{K^*}^2 - m_{K^*}^2)^2 + (m_{K^*}\Gamma_{K^*})^2} \quad (6.53)$$

which results from squaring the K^{*0} propagator D_{K^*} (see Fig. 6.3 left). An on-shell K^{*0} will acquire any four-momentum squared ranging from $p_{K^*2}^{\min} = (m_K + m_\pi)^2$ to $p_{K^*2}^{\max} = (m_B - m_{\gamma^*})^2$ (where obviously $m_{\gamma^*} = 0$) and therefore, the integral of Eq. (6.53) between these two limits will give the value of the $p_{K^*}^2$ associated to the decay mode studied:

$$\int_{p_{K^*2}^{\min}}^{p_{K^*2}^{\max}} \frac{dp_{K^*}^2}{(p_{K^*}^2 - m_{K^*}^2)^2 + (m_{K^*}\Gamma_{K^*})^2}. \quad (6.54)$$

With the change of variables

$$p_{K^*}^2 = m_{K^*}\Gamma_{K^*} \tan \theta + m_{K^*}^2, \quad (6.55)$$

Eq. (6.54) is transformed into

$$\int_{\theta^{\min}}^{\theta^{\max}} \frac{d\theta}{m_{K^*}\Gamma_{K^*}}. \quad (6.56)$$

If the assumption $\Gamma_{K^*} \ll m_{K^*}$ is made, then $(m_K + m_\pi) - \Gamma_{K^*} \ll m_{K^*} \ll m_B - \Gamma_{K^*}$ will also hold and hence the integration limits in Eq. (6.56) can be approximated by

$$\begin{aligned} \theta^{\min} &= \arctan \left[\frac{(m_K + m_\pi)^2 - m_{K^*}^2}{m_{K^*}\Gamma_{K^*}} \right] \rightarrow -\pi, \\ \theta^{\max} &= \arctan \left[\frac{m_B^2 - m_{K^*}^2}{m_{K^*}\Gamma_{K^*}} \right] \rightarrow 0, \end{aligned}$$

resulting in

$$\int_{\theta=-\pi}^{\theta=0} \frac{d\theta}{m_{K^*}\Gamma_{K^*}} = \frac{\pi}{m_{K^*}\Gamma_{K^*}}. \quad (6.57)$$

This is known as the *narrow-width approximation* and from a physical point of view it amounts to splitting the squared propagator with mass m_{K^*} and decay amplitude Γ_{K^*} to obtain a real K^{*0} that decays into a K and a π , as shown schematically in Fig. 6.3 at right. In the literature it is usually written as

$$|D_{K^*}(p_{K^*})|^2 = \frac{1}{(p_{K^*}^2 - m_{K^*}^2)^2 + (m_{K^*}\Gamma_{K^*})^2} = \frac{\pi}{m_{K^*}\Gamma_{K^*}} \delta(p_{K^*}^2 - m_{K^*}^2) + O(\Gamma_{K^*}/m_{K^*}), \quad (6.58)$$

where $O(\Gamma_{K^*}/m_{K^*})$ is the error associated to this approximation [107, 108], with $\Gamma_{K^*}/m_{K^*} = (54.36 \pm 0.25) \cdot 10^{-3}$ [1]. Incidentally, $\Lambda_{\text{QCD}}^{\overline{\text{MS}}}/m_b^{\overline{\text{MS}}} = (50.8_{-2.0}^{+5.0}) \cdot 10^{-3}$ [1, 109], so both error estimates turn out to be of the same order of magnitude. However, the main term in the series expansion has a very different magnitude: while in the Λ_{QCD}/m_b expansion the leading term is of $O(1)$, in Eq. (6.58) the factor $\pi/(m_{K^*}\Gamma_{K^*}) = (72.0 \pm 1.9)$, so $O(\Gamma_{K^*}/m_{K^*})$ accounts for less than a 1% correction to the main term and can be safely neglected. Hence,

$$|D_{K^*}(p_{K^*})|^2 \approx \frac{\pi}{m_{K^*}\Gamma_{K^*}} \delta(p_{K^*}^2 - m_{K^*}^2). \quad (6.59)$$

If one now defines $\tilde{D}_{K^*}(p_{K^*}^2) \equiv g_{K^*K\pi} D_{K^*}(p_{K^*}^2)$, using Eq. (6.59) it can be written

$$|\tilde{D}_{K^*}(p_{K^*})|^2 \approx g_{K^*K\pi}^2 \frac{\pi}{m_{K^*}\Gamma_{K^*}} \delta(p_{K^*}^2 - m_{K^*}^2) = \frac{48\pi^2}{m_{K^*}\beta^3} \delta(p_{K^*}^2 - m_{K^*}^2). \quad (6.60)$$

where Eq. (6.52) has been used to obtain the last equality. This is the expression that can be found in [106, 10].

Relating the $\bar{B} \rightarrow \bar{K}\pi$ and $\bar{B} \rightarrow \bar{K}^*$ matrix elements

According to [91], the matrix elements corresponding to the $\bar{B} \rightarrow \bar{K}\pi$ transition may be expressed

$$\langle \bar{K}(p_K)\pi(p_\pi) | J_{(\mu\lambda)} | \bar{B}(p) \rangle = -g_{K^*K\pi} \frac{g^{\nu\mu} - p_{K^*}^\nu p_{K^*}^\mu / m_{K^*}^2}{p_{K^*}^2 - m_{K^*}^2 + im_{K^*}\Gamma_{K^*}} (p_\pi - p_K)_\mu A_{\nu(\mu\lambda)}, \quad (6.61)$$

being $J_{(\mu\lambda)}$ the current responsible for the transition and K^* a true propagator which, combined with the $K^* \rightarrow K\pi$ coupling, allows us to define.

$$\tilde{D}_{K^*}(p_{K^*}^2) \equiv -\frac{g_{K^*K\pi}}{p_{K^*}^2 - m_{K^*}^2 + im_{K^*}\Gamma_{K^*}} = -g_{K^*K\pi} D_{K^*}(p_{K^*}^2), \quad (6.62)$$

providing a simple explanation for the physical motivation behind Eq. (6.60). Defining

$$W^\nu \equiv \left(g^{\nu\mu} - \frac{p_{K^*}^\nu p_{K^*}^\mu}{m_{K^*}^2} \right) (p_\pi - p_K)_\mu = Q_{\pi K}^\nu - \frac{m_\pi^2 - m_K^2}{p_{K^*}^2} P_{\pi K}^\nu, \quad (6.63)$$

where both $p_{K^*}^\mu = (p_\pi + p_K)^\mu$ and the notation introduced in Sec. 5 have been used to obtain the r.h.s. of the equality, one recovers Eq. (3.6) from [10]:

$$\langle \bar{K}(p_K)\pi(p_\pi) | J_{(\mu\lambda)} | \bar{B}(p) \rangle = -\tilde{D}_{K^*}(p_{K^*}^2)W^\nu A_{\nu(\mu\lambda)}. \quad (6.64)$$

On the other hand, noting that $A_{\nu(\mu\lambda)}$ is the current (tensor) that accounts for the matrix elements that define the $\bar{B} \rightarrow \bar{K}^*$ form factors in Eqs. (3.8) and (3.9) (with the exception of the \bar{K}^{*0} polarisation vector), the general form of a $\bar{B} \rightarrow \bar{K}^*$ transition reads

$$\langle \bar{K}^*(p_{K^*}) | J_{\nu(\mu\lambda)} | \bar{B}(p) \rangle = \varepsilon_{K^*}^{*\nu} A_{\nu(\mu\lambda)}, \quad (6.65)$$

so there is yet another way to obtain the $\bar{B} \rightarrow K\pi$ transition: calculate the differential decay amplitude in the usual way (squaring the matrix element, summing over spins *and summing also* over the K^* polarisations) and then multiply the result by the experimental value of $\mathcal{B}(K^{*0} \rightarrow K\pi)$. This method has the advantage of providing an empiric result for this source of uncertainty when the full decay distribution is computed without having to rely on the narrow-width approximation.

6.3 The $\bar{B} \rightarrow \bar{K}^*$ form factors

Once established how to transform the $\bar{B} \rightarrow K\pi$ matrix elements in Eq. (6.41) into the Eqs. (3.8), (3.9), (3.12) and (3.14) that define the seven independent $B \rightarrow K^*$ form factors [$V(q^2)$, $A_0(q^2)$, $A_1(q^2)$, $A_2(q^2)$, $T_1(q^2)$, $T_2(q^2)$ and $T_3(q^2)$] it is time to show the results obtained by two different teams of experts in the field.

In [37] these form factors were calculated from *light-meson LCSRs* (see Sec. 3.1.2) including $O(\alpha_s)$ corrections to twist-2 and twist-3 contributions and LO twist-4 corrections, and the $B \rightarrow K^*$ form factors were parametrised by the following equations (Eqs. (59-61) in [37]):

$$F^{V,A_0,T_1}(q^2) = \frac{r_1}{1 - q^2/m_R^2} + \frac{r_2}{1 - q^2/m_{\text{fit}}^2}, \quad (6.66)$$

$$F^{A_2,\tilde{T}_3}(q^2) = \frac{r_1}{1 - q^2/m_{\text{fit}}^2} + \frac{r_2}{(1 - q^2/m_{\text{fit}}^2)^2}, \quad (6.67)$$

$$F^{A_1,T_2}(q^2) = \frac{r_2}{1 - q^2/m_{\text{fit}}^2}, \quad (6.68)$$

where $F(q^2)$ is a generic label for any of the $B \rightarrow K^*$ form factors while the superscripts illustrate to which form factors should be applied each fitting formula. One comment is in order here: $T_3(q^2)$ is given by the combination of $T_2(q^2)$ and $\tilde{T}_3(q^2)$ (Eq. (8) in [37]) as

$$T_3(q^2) = \frac{m_B^2 - m_V^2}{q^2} \left(\tilde{T}_3(q^2) - T_2(q^2) \right). \quad (6.69)$$

which obviously diverges as $q^2 \rightarrow 0$. This precludes the obtention of reliable values for $T_3(q^2)$ in the region $q^2 < 1$ when Eqs. (6.67)–(6.67) are substituted into Eq. (6.69). The parameters fitted in Eqs. (6.66)–(6.68) are collected in Tab. 6.2 at the left of the double line while, at the right of the double line, the $B \rightarrow K^*$ form factors at $q^2 = 0$ used in [10] are shown

	$F(0)$	$\Delta(0)$	r_1	m_R	r_2	m_{fit}^2	$F(0)$	$\Delta(0)$
V	0.411	0.045	0.923	5.32	-0.511	49.40	0.311	0.037
A_0	0.374	0.043	1.364	5.28	-0.990	36.78	0.333	0.033
A_1	0.292	0.036	–	–	0.290	40.38	0.233	0.038
A_2	0.259	0.035	-0.084	–	0.342	52.00	0.190	0.039
T_1	0.333	0.037	0.823	5.32	-0.491	46.31	0.268	0.045
T_2	0.333	0.037	–	–	0.333	41.41	0.268	0.045
\tilde{T}_3	0.333	0.037	-0.036	–	0.368	48.10	–	–
T_3	–	–	–	–	–	–	0.162	0.023

Table 6.2: Left of double line: $B \rightarrow K^*$ form factors and fit parameters from [37]. Columns 2 – 4 give the results for $q^2 = 0$ including the total error $\Delta(0)$, computed adding in quadrature Δ_{tot} and Δ_{a_1} (see caption of Tab. 7 in [37]). The remaining columns give the fit parameters. Input parameters for the corresponding LCSRs are collected in the left column of Tab. 6.3.

Right of double line: $B \rightarrow K^*$ form factors at $q^2 = 0$ quoted from [10]. Input parameters for the LCSRs that allow the calculation of these form factors can be found at the r.h.s of Tab. 6.3.

When inspecting Tab. 6.2 one readily realises how much the central values of the $B \rightarrow K^*$ form factors at $q^2 = 0$ changed from [37] to [10]. This is specially true for $V(0)$ (which lowered a sizeable 32 %, far beyond the error bars), $A_2(0)$ (which decreased a 36 %, just within the error limits), and $T_{1,2}(0)$. While the reason of the difference in $T_1(0)$ between these two works was explained in [10]³, no explanation was given regarding the sizeable differences in $V(0)$ and $A_2(0)$. Moreover, neither updated fit data nor analytical fit curves or expressions for "the correlations between form factors which follow from the light-cone sum rules (*sic*)"⁴ were provided in [10], only the central curves for the form factors shown in Fig. 6.4, which range from $1 \leq q^2 \leq 10 \text{ GeV}^2$. Besides, it should also be noted here that in [112], published more than a year later than [10],

³The LCSR corresponding to this form factor leads to a too value large when compared with the experiment (as $T_1(0)$ is readily calculable from the $\mathcal{B}(B \rightarrow K^* \gamma)$), so instead of using the theoretical form factor the $T_1(0)^{\text{exp}} = 0.268$ was chosen which, in turn, demanded to *fix* $f_B = 0.186$ to reproduce this experimental value. Therefore, to compute all $F(0)$ in [10], $f_B = 0.186$ was used instead of the value quoted in Tab. 6.3 at right and the uncertainty associated to this decay amplitude was neglected.

⁴Although the benefits from these correlations have been widely publicised in [110, 111], to our knowledge, their expressions have never been published either numerically or analytically. In App. B of [10] the authors showed they were capable of recovering the relationships in [31] from the full QCD form factors deduced using LCSRs, but one must remember that the relations in [31] were deduced using the factorisation formula, i.e. they have unknown $O(\Lambda_{\text{QCD}}/m_b)$ corrections attached to them.

the form factors at $q^2 = 0$ (Tab. 6.2 left) and the parametrisations in Eqs. (6.66)–(6.68) from [37] were used instead of those in [10].

μ_b (GeV)	4.8	4.8
μ_h (GeV)	2.2	2.2
m_b (GeV)	4.80 ± 0.05 (pole)	4.20 ± 0.04 (MS)
m_s^{MS} (MeV)	100 ± 20	–
$a_1^{\parallel}(K^*)(\mu)$	0.10 ± 0.07 (1 GeV)	0.03 ± 0.03 (2 GeV)
$a_1^{\perp}(K^*)(\mu)$	0.10 ± 0.07 (1 GeV)	0.03 ± 0.03 (2 GeV)
$a_2^{\parallel}(K^*)(\mu)$	0.09 ± 0.05 (1 GeV)	0.08 ± 0.06 (2 GeV)
$a_2^{\perp}(K^*)(\mu)$	0.13 ± 0.08 (1 GeV)	0.08 ± 0.06 (2 GeV)
$f_{K^*}^{\parallel}$ (MeV)	217 ± 5	220 ± 5
$f_{K^*}^{\perp}(\mu_h)$ (MeV)	156 ± 8	163 ± 8
f_{B_d} (MeV)	208 ± 20	200 ± 25
$\lambda_B(\mu_h)$ (GeV)	–	0.51 ± 0.12
s_0 (GeV ²)	34.5 ± 2.5	35 ± 2
M^2 (GeV ²)	parametrisation	8 ± 2

Table 6.3: Input parameters for the LCSRs calculated in [37] (left of the double line) and in [10] (right of the double line). The Borel parameter M^2 was obtained in [37] according to the parametrisation described above Eq. (47). The running of the Gegenbauer coefficients may be computed using Eqs. (23-25) in [37].

As a final remark, we should add that in [37, 10] only the form factor uncertainties at $q^2 = 0$ are provided. Since these uncertainties lay in the range 11 – 14 %, one is forced to *assume* that they are of $O(15\%)$ in the whole q^2 range, as done in [113, 114].

On the other hand, the *B-meson LCSR* technique used in [35] (see Sec. 3.1.2) was used to provide a parametrisation in q^2 (with $0 \leq q^2 \leq 12$ GeV²) for *all* seven independent $B \rightarrow K^*$ form factors [115] (i.e., including $T_3(q^2)$). This parametrisation also enables the calculation of the error bands associated to each form factor along the full range of applicability. It is given by the following equations:

$$F(q^2) = \frac{F(0)}{1 - q^2/m_{B_s(JP)}^2} \left\{ 1 + b_1 \left(z(q^2, t_0) - z(0, t_0) + \frac{1}{2} [z(q^2, t_0)^2 - z(0, t_0)^2] \right) \right\}, \quad (6.70)$$

where

$$z(q^2, \tau_0) = \frac{\sqrt{\tau_+ - q^2} - \sqrt{\tau_+ - \tau_0}}{\sqrt{\tau_+ - q^2} + \sqrt{\tau_+ - \tau_0}} \quad (6.71)$$

and

$$\tau_+ = (m_B + m_{K^*})^2, \quad \tau_- = (m_B - m_{K^*})^2, \quad \tau_0 = \tau_+ - \sqrt{\tau_+ - \tau_-} \sqrt{\tau_+}. \quad (6.72)$$

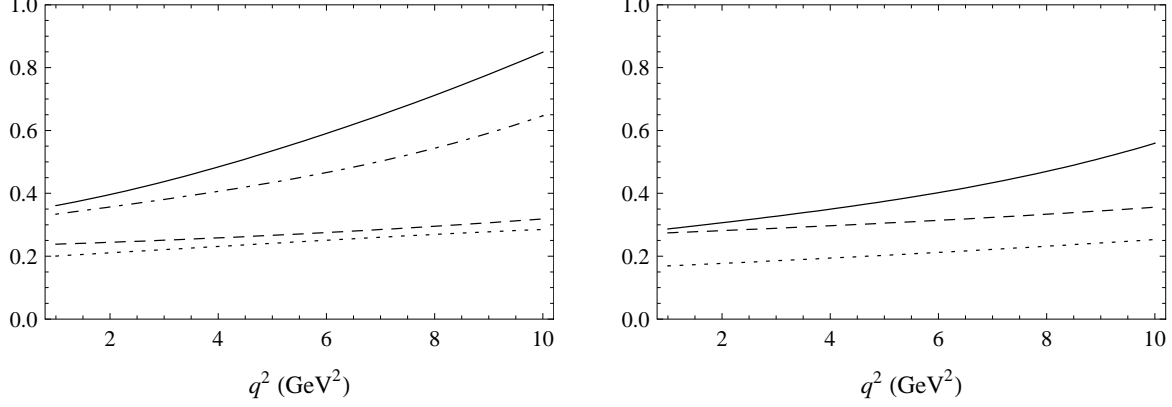


Figure 6.4: Form factors from LCSRs for central values of input parameters. Left: Solid curve: A_0 , long dashes: A_1 , short dashes: A_2 , dot-dashed curve: V . Right: Solid curve: T_1 , long dashes: T_2 , short dashes: T_3 . Reproduced from [10].

The masses of the B_s states correspond to $\bar{s}b$ resonances with appropriate J^P . They are given by $m_{B_s(0^-)} = 5.366$ GeV, $m_{B_s^*(1^-)} = 5.412$ GeV and $m_{B_s^*(1^+)} = 5.829$ GeV [1]. The fit parameters can be retrieved from Tab. 6.4 while the input parameters used in [35, 115] are collected in Tab. 6.5.

Form factor	$F(0)$	b_1^i	$B_s(J^P)$
V	$0.36^{+0.23}_{-0.12}$	$-4.8^{+0.8}_{-0.4}$	$B_s^*(1^-)$
A_1	$0.25^{+0.16}_{-0.10}$	$0.34^{+0.86}_{-0.80}$	$B_s(1^+)$
A_2	$0.23^{+0.19}_{-0.10}$	$-0.85^{+2.88}_{-1.35}$	$B_s(1^+)$
A_0	$0.29^{+0.10}_{-0.07}$	$-18.2^{+1.3}_{-3.0}$	$B_s(0^-)$
T_1	$0.31^{+0.18}_{-0.10}$	$-4.6^{+0.81}_{-0.41}$	$B_s^*(1^-)$
T_2	$0.31^{+0.18}_{-0.10}$	$-3.2^{+2.1}_{-2.2}$	$B_s(1^+)$
T_3	$0.22^{+0.17}_{-0.10}$	$-10.3^{+2.5}_{-3.1}$	$B_s(1^+)$

Table 6.4: The fit parameters of $B \rightarrow K^*$ form factors from B -meson LCSR. Reproduced from [115].

If one compares the plots in Fig. 6.5, the most striking feature is the difference in the error bands, being the ones computed according to [115] twice or even three times larger than the ones estimated for the parametrisation in [37]. This will obviously have an impact on the hadronic errors calculated for any observable not protected from form factor uncertainties at LO in α_s

$m_s(1 \text{ GeV})$ (MeV)	130 ± 10
$f_{K^*}^{\parallel}$ (MeV)	217 ± 5
f_{B_d} (MeV)	180 ± 30
λ_B (1GeV)	0.46 ± 0.11
$s_0^{K^*}$ (GeV^2)	1.7
M^2 (GeV^2)	1.0 ± 0.5

Table 6.5: Input parameters for the LCSRs calculated in [35, 115].

that one may build to explore possible NP signals in the $\bar{B}_d^0 \rightarrow \bar{K}^{*0}(\rightarrow K\pi)\ell^+\ell^-$ or in its CP -conjugated mode (like the branching ratio \mathcal{B} , A_{FB} , F_L or the S_i and A_i of [10]). However, as in the process of looking for NP one has to make sure that there is just a negligible probability that the signal observed might correspond to a fluctuation from the SM prediction, we feel justified being on the conservative side in this point and using the parametrisation in [115] to obtain the $B \rightarrow K^*$ form factors.

As a final remark we should add that there is yet another paper that computes the $B \rightarrow K^*$ form factors [116]. In this work, whenever possible, results from LCSRs and from QCD in the lattice are used to calculate the *helicity amplitudes* (certain combinations of form factors with kinematical variables) as a series expansion. The coefficients of this expansion are further constrained by dispersive bounds, exploiting the crossing symmetry between the physical B -meson decay and the pair-production of heavy and light mesons by the considered decay current. A numerical fit is finally performed to helicity amplitudes. We have not used this fit in our works so far, although it might be interesting to compare its predictions with the results in [115]. Interestingly, in Appendix E of this paper, published almost two years later than [10], the covariance matrices corresponding to $B \rightarrow K^*$ helicity amplitudes are given. These covariance matrices, however, were computed by fitting the LCSR data to form factor parametrisations in terms of the aforementioned series expansion, and therefore cannot be used within the formalism employed in [37] or in [10].

6.4 The transversity amplitudes

6.4.1 The origin of the transversity amplitudes

To introduce the transversity amplitudes Sec. (3.2) of [10] will be followed, as it is good summary of the subject, but addressing some minor issues.

We consider just the "first step" of the decay, with $\bar{B}_d^0 \rightarrow \bar{K}^{*0}V^*$, where the \bar{K}^{*0} is on-shell and the virtual boson V^* is either a γ^* or a Z^0 that will decay later on into a $\ell^+\ell^-$ pair. To fix ideas, let us assume that hadronic transition is governed by a SM-like vector/axial-vector current

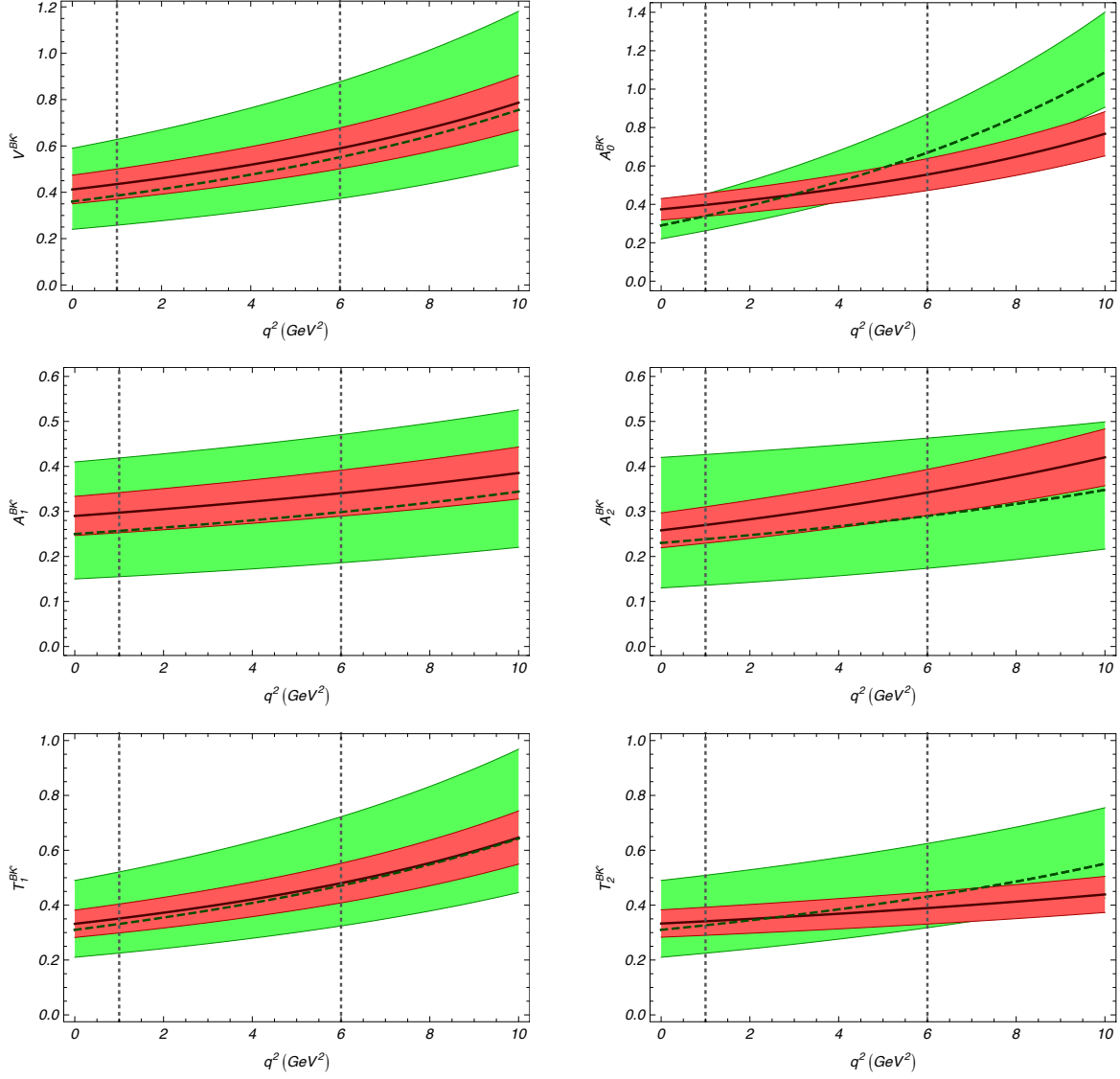


Figure 6.5: Comparison between the $B \rightarrow K^*$ form factors computed following the parametrisation given in [37] (in red, with the central value shown as a solid curve) and in [115] (in green, with the central value indicated by a dashed curve). As we will see in Sec. 6.6, the kinematical region of interest for $\bar{B}_d \rightarrow \bar{K}^{*0} \ell^+ \ell^-$ will be $1 \text{ GeV}^2 \leq q^2 \leq 6 \text{ GeV}^2$ (see Sec. 6.6.2), which corresponds to the area between the two vertical grey dotted lines.

like the one schematised by

$$\langle \bar{K}^*(p_K) | J_\mu | \bar{B}(p) \rangle = \varepsilon_{K^*}^\nu A_{\nu\mu}, \quad (6.73)$$

so the amplitude for this process can be written as

$$\mathcal{M}_{(m,n)}(B \rightarrow K^*V^*) = \varepsilon_{K^*}^{*\nu}(m) A_{\nu\mu} \varepsilon_{V^*}^{*\mu}(n) \quad (6.74)$$

where $A_{\mu\nu}$ is the tensor associated to the hadronic current, $\varepsilon_{V^*}^\mu$ is the polarisation vector of the virtual gauge boson and $\varepsilon_{K^*}^\nu$ is the K^* polarisation vector.

On the one hand, the V^* polarisation vector is off shell, so it has three spin 1 components orthogonal to the momentum q^μ transferred to V^* during the B meson decay, i.e. $\varepsilon_{V^*}^\mu(n) q_\mu = 0$ for $n = \pm, 0$, and one spin 0 time-like component $\varepsilon_{V^*}^\mu(n) = q^\mu / \sqrt{q^2}$ with $n = t$. These four polarisation vectors form an orthonormal and complete set: an helicity basis. In the B meson rest frame, the four basis vectors may be written as [106, 117]

$$\varepsilon_{V^*}^\mu(\pm) = (0, 1, \mp i, 0) / \sqrt{2}, \quad (6.75)$$

$$\varepsilon_{V^*}^\mu(0) = (-q_z, 0, 0, -q_0) / \sqrt{q^2}, \quad (6.76)$$

$$\varepsilon_{V^*}^\mu(t) = (q_0, 0, 0, q_z) / \sqrt{q^2}, \quad (6.77)$$

and the four-momentum of the gauge boson as $q^\mu = (q_0, 0, 0, q_z)$. Eqs. (6.75)–(6.77) satisfy the orthonormality [Eq. (6.78)] and completeness [Eq. (6.79)] relations

$$\varepsilon_{V^*}^{*\mu}(n) \varepsilon_{V^* \mu}(n') = g_{nn'}, \quad (6.78)$$

$$\sum_{n,n'} \varepsilon_{V^*}^{*\mu}(n) \varepsilon_{V^*}^\nu(n') g_{nn'} = g^{\mu\nu}, \quad (6.79)$$

with $n, n' = \pm, 0, t$ and $g_{nn'} \equiv \text{diag}(+, -, -, -)$.

On the other hand, the K^* is on shell, so it only has the three polarisation states that are orthogonal to the four-momentum $p_{K^*}^\mu = (p_{K^*,0}, 0, 0, p_{K^*,z})$ transferred to K^* during the B meson decay⁵. These three polarisation states read, in the B meson rest frame

$$\varepsilon_{K^*}^\mu(\pm) = (0, 1, \pm i, 0) / \sqrt{2}, \quad (6.80)$$

$$\varepsilon_{K^*}^\mu(0) = (k_z, 0, 0, k_0) / m_{K^*}, \quad (6.81)$$

and satisfy the relations

$$\varepsilon_{K^*}^{*\mu}(m) \varepsilon_{K^* \mu}(m') = -\delta_{mm'}, \quad (6.82)$$

$$\sum_{m,m'} \varepsilon_{K^*}^{*\mu}(m) \varepsilon_{K^*}^\nu(m') \delta_{mm'} = -g^{\mu\nu} + \frac{p_{K^*}^\mu p_{K^*}^\nu}{m_{K^*}^2}. \quad (6.83)$$

⁵As the whole process is studied on the B meson rest frame, then the relation $q_z = -p_{K^*,z}$ must be fulfilled.

The K^* helicity amplitudes can now be projected out from the hadronic tensor $A_{\nu\mu}$ by contracting it with the explicit polarisation vectors in Eq. (6.74), obtaining [117]

$$H(\pm) = \varepsilon_{K^*}^{*\nu}(\pm) \varepsilon_{V^*}^{*\mu}(\pm) A_{\nu\mu}, \quad (6.84)$$

$$H(0) = \varepsilon_{K^*}^{*\nu}(0) \varepsilon_{V^*}^{*\mu}(0) A_{\nu\mu}, \quad (6.85)$$

Eqs. (6.84)–(6.85) may be hence written using the short-hand notation of [10] as

$$H_m = \mathcal{M}_{(m,m)}(B \rightarrow K^*V^*), \quad m = 0, +, -. \quad (6.86)$$

Alternatively, one can also work with the *transversity amplitudes* defined in [8] as

$$A_{\perp,\parallel} \equiv (H_{+1} \mp H_{-1})/\sqrt{2}, \quad A_0 \equiv H_0. \quad (6.87)$$

This change of basis from K^* helicity amplitudes to transversity amplitudes is important, as in the $B \rightarrow K^*V^*$ decay (with V^* an off-shell gauge boson) there is yet another contribution resulting from the contraction of $A_{\nu\mu}$ with the polarisation vectors in Eq. (6.74), which has been called A_t

$$A_t = \varepsilon_{K^*}^{*\nu}(0) \varepsilon_{V^*}^{*\mu}(t) A_{\nu\mu}, \quad (6.88)$$

which, in the notation of [10] reads,

$$A_t = \mathcal{M}_{(0,t)}(B \rightarrow K^*V^*), \quad (6.89)$$

This transversity amplitude does not have a correspondence within the K^* on-shell helicity basis and therefore cannot be called "helicity" as noted in [10].

If one now considers that V^* decays into a lepton-antilepton pair through a vector/axial-vector current, then the amplitude will be

$$\mathcal{M}(B \rightarrow K^*V^*(\rightarrow \mu^+\mu^-))(m) \propto \varepsilon_{K^*}^{*\nu}(m) A_{\nu\mu} \sum_{n,n'} \varepsilon_{V^*}^{*\mu}(n) \varepsilon_{V^*}^\lambda(n') g_{nn'} (\bar{\ell} \gamma_\lambda P_{L,R} \ell). \quad (6.90)$$

where the proportionality arises from the $V^* \rightarrow \ell^+\ell^-$ coupling, omitted for simplicity.

The amplitude in Eq. (6.90) can now be expressed in terms of six transversity amplitudes, namely $A_{\perp,\parallel,0}^L$ and $A_{\perp,\parallel,0}^R$ (where L and R label the chirality of the leptonic current) and also the seventh transversity amplitude A_t , which does not display separate components for the leptonic current as $\varepsilon^\mu(t) = q^\mu/\sqrt{q^2}$ and, from current conservation one obtains

$$q^\mu (\bar{\ell} \gamma_\mu \ell) = 0, \quad (6.91)$$

$$q^\mu (\bar{\ell} \gamma_\mu \gamma_5 \ell) = 2im_\mu (\bar{\ell} \gamma_5 \ell). \quad (6.92)$$

Hence, the timelike component of V^* can only couple to an axial-vector current and, in addition, Eq. (6.92) also shows that A_t must vanish in the limit of massless leptons, as stated in [8].

We have just shown that the seven transversity amplitudes characterise completely the sequential decay $B \rightarrow K^*(\rightarrow K\pi)V^*(\rightarrow \ell^+\ell^-)$ in the case of vector/axial-vector currents, i.e. those corresponding to the SM effective operators $\mathcal{O}_7, \mathcal{O}_9, \mathcal{O}_{10}$ and their chirally-flipped counterparts $\mathcal{O}'_7, \mathcal{O}'_9, \mathcal{O}'_{10}$ [see Eq. (6.41)].

If there is NP entering the $b \rightarrow s \ell^+\ell^-$ effective Hamiltonian through pseudoscalar operators, then the combination $C_{PS} - C'_{PS}$ corresponding to $\mathcal{O}_{PS} - \mathcal{O}'_{PS}$ ⁶ will also be absorbed into the transversity amplitude A_t , because it couples to axial-vector currents in the same way as the time-like component of V^* does. This can be checked straightforwardly just by inspecting Eq. (6.41) and Eqs. (6.91)–(6.92). However, this reasoning cannot be transferred to the scalar operators \mathcal{O}_S and \mathcal{O}'_S , so their inclusion in the decay $\bar{B}_d \rightarrow \bar{K}^{*0}(\rightarrow K\pi)\ell^+\ell^-$ requires another transversity amplitude called A_S in [10].

Solving the decay amplitude with the inclusion of scalar and pseudoscalar contributions is already quite involved, even with the help of the *Mathematica*TM package *FeynCalc* [118]. In our papers [45, 46, 99, 119, 120] we concentrated on the study of $\bar{B}_d \rightarrow \bar{K}^{*0}\ell^+\ell^-$ with possible NP contributions stemming from the aforementioned chirally-flipped and scalar/pseudoscalar operators, which amounts to setting $C_T = 0$ and $C_{PT} = 0$ in Eq. (6.41). The most general analysis of this decay mode, however, demands the inclusion of tensor and pseudotensor NP effective operators. This analysis was performed in [121], where the authors claimed that six additional transversity amplitudes are needed to account for all possible dimension 6 operators of \mathcal{H}_{eff} , but in [119] we used symmetry arguments to claim that these new transversity amplitudes can always be reabsorbed into appropriate redefinitions of $A_{\perp,\parallel,0}^{(L,R)}$ and A_S .

Therefore, the amplitude of the decay $\bar{B}_d^0 \rightarrow \bar{K}^{*0}(\rightarrow K\pi)\ell^+\ell^-$ will be decomposed, in naïve factorisation and neglecting the m_s/m_b terms that appear in Eq. (6.41), into the seven transversity amplitudes

$$A_{\perp}^{L,R} = \sqrt{2} \lambda^{1/2} \left\{ \left[(C_9^{\text{eff}} + C_9^{\text{eff}'}) \mp (C_{10} + C'_{10}) \right] \frac{V(q^2)}{m_B + m_{K^*}} + \frac{2m_b}{q^2} (C_7^{\text{eff}} + C_7^{\text{eff}'}) T_1(q^2) \right\}, \quad (6.93)$$

$$A_{\parallel}^{L,R} = -\sqrt{2} (m_B^2 - m_{K^*}^2) \left\{ \left[(C_9^{\text{eff}} - C_9^{\text{eff}'}) \mp (C_{10} - C'_{10}) \right] \frac{A_1(q^2)}{m_B - m_{K^*}} + \frac{2m_b}{q^2} (C_7^{\text{eff}} - C_7^{\text{eff}'}) T_2(q^2) \right\}, \quad (6.94)$$

⁶These Wilson coefficients and effective operators are designed just $C_P^{(\prime)}$ and $\mathcal{O}_P^{(\prime)}$ respectively in [10].

$$\begin{aligned}
A_0^{L,R} = & -\frac{1}{2m_{K^*}\sqrt{q^2}} \left\{ \left[(C_9^{\text{eff}} - C_9^{\text{eff}'}) \mp (C_{10} - C'_{10}) \right] \right. \\
& \times \left[(m_B^2 - m_{K^*}^2 - q^2)(m_B + m_{K^*})A_1(q^2) - \lambda \frac{A_2(q^2)}{m_B + m_{K^*}} \right] \\
& \left. + 2m_b (C_7^{\text{eff}} - C_7^{\text{eff}'}) \left[(m_B^2 + 3m_{K^*}^2 - q^2)T_2(q^2) - \frac{\lambda}{m_B^2 - m_{K^*}^2} T_3(q^2) \right] \right\}, \quad (6.95)
\end{aligned}$$

$$A_t = \frac{1}{\sqrt{q^2}} \lambda^{1/2} \left[2(C_{10} - C'_{10}) + \frac{q^2}{m_\mu} (C_{PS} - C'_{PS}) \right] A_0(q^2), \quad (6.96)$$

$$A_S = -2\lambda^{1/2} (C_S - C'_S) A_0(q^2), \quad (6.97)$$

where $\lambda = \lambda(m_B^2, m_{K^*}^2, q^2)$ using the definition in Eq. (6.48).

The transversity amplitudes in Eqs. (6.93)–(6.97) are not physical observables for two reasons. In the first place, $A_\perp^{L,R}$, $A_\parallel^{L,R}$ and $A_0^{L,R}$ contain the Wilson coefficient C_9^{eff} which, as shown in Eqs. (6.25)–(6.29) and explained in the text under them, is a complex magnitude, so that these transversity amplitudes are unphysical objects. Besides, neither A_t nor A_S have a correspondence in the helicity basis of the on-shell K^* and therefore they cannot be physical entities either. Nevertheless, in [45, 46, 119] we showed that the differential distribution of the decay amplitude remains invariant under certain transformations performed in the space of transversity amplitudes which we called "symmetries" and that, using them, any combination of transversity amplitudes that is physically observable may be found.

6.4.2 Transversity amplitudes at large recoil

As stated in [8], the transversity amplitudes in naïve factorisation collected in Eqs. (6.93)–(6.97) acquire a simple form in the heavy quark ($m_b \rightarrow \infty$) and large energy ($E_{K^*} \rightarrow \infty$) limits. Using the relationships among form factors at large recoil in Eqs. (3.31)–(3.32) it can be obtained, at LO in α_s and Λ_{QCD}/m_b :

$$A_\perp^{L,R} \simeq \sqrt{2}m_B(1 - \hat{s}) \left[(C_9^{\text{eff}} + C_9^{\text{eff}'}) \mp (C_{10} + C'_{10}) + \frac{2\hat{m}_b}{\hat{s}} (C_7^{\text{eff}} + C_7^{\text{eff}'}) \right] \xi_\perp(E_{K^*}), \quad (6.98)$$

$$A_\parallel^{L,R} \simeq -\sqrt{2}m_B(1 - \hat{s}) \left[(C_9^{\text{eff}} - C_9^{\text{eff}'}) \mp (C_{10} - C'_{10}) + \frac{2\hat{m}_b}{\hat{s}} (C_7^{\text{eff}} - C_7^{\text{eff}'}) \right] \xi_\perp(E_{K^*}), \quad (6.99)$$

$$A_0^{L,R} \simeq -\frac{m_B}{2\hat{m}_{K^*}\sqrt{\hat{s}}} (1 - \hat{s})^2 \left[(C_9^{\text{eff}} - C_9^{\text{eff}'}) \mp (C_{10} - C'_{10}) + 2\hat{m}_b (C_7^{\text{eff}} - C_7^{\text{eff}'}) \right] \xi_\parallel(E_{K^*}), \quad (6.100)$$

$$A_t \simeq \frac{m_B}{2\hat{m}_{K^*}\sqrt{\hat{s}}}(1-\hat{s})^2 \left[2(C_{10} - C'_{10}) + \frac{q^2}{m_\mu}(C_{PS} - C'_{PS}) \right] \xi_{\parallel}(E_{K^*}), \quad (6.101)$$

$$A_S \simeq -\frac{m_B^2}{\hat{m}_{K^*}}(1-\hat{s})^2 (C_S - C'_S) \xi_{\parallel}(E_{K^*}). \quad (6.102)$$

where the definitions $\hat{s} = q^2/m_B^2$ and $\hat{m}_{K^*} = m_{K^*}/m_B$ have been used. It is important to note that, in these limits, *every* transversity amplitudes is functions of just one soft form factor: either $\xi_{\perp}(E_{K^*})$ in the case of $A_{\perp}^{L,R}$ and $A_{\parallel}^{L,R}$, or $\xi_{\parallel}(E_{K^*})$ in the case of $A_0^{L,R}$, A_t and A_S .

Given that Eqs. (3.31)–(3.32), were derived from Eqs. (3.26)–(3.29), and $O(m_V^2/m_B^2)$ terms were neglected there to be consistent with the expansion in powers of $1/m_b$, these same terms of $O(\hat{m}_{K^*}^2)$ have also been dropped here to obtain Eqs. (6.98)–(6.102). Note also that in Eq. (6.101) the final-state leptons have been considered to be μ as, in this case, the present bounds to $(C_{PS} - C'_{PS})$ imposed by the $\mathcal{B}(B_s \rightarrow \mu^+\mu^-)$ (see Tab. 4 of [119]), cannot to enhance the $O(\hat{m}_{K^*}^2)$ term sufficiently to prevent it being safely neglected in the $1 \leq q^2 \leq 6 \text{ GeV}^2$ range. However, if the final state leptons were electrons, the bounds from $\mathcal{B}(B_s \rightarrow e^+e^-)$ are less constraining at the moment of writing these lines [1] and the large factor q^2/m_e might enhance $(C_{PS} - C'_{PS})$ to prevent Eq. (6.101) from being accurate enough to be used without adding of the terms that have been dropped.

Special features of transversity amplitudes at large recoil

Looking at Eqs. (6.98)–(6.99) one can easily see that in the SM, i.e. without chirally-flipped currents stemming from \mathcal{O}'_7 , \mathcal{O}'_9 and \mathcal{O}'_{10} , one has $A_{\perp} = -A_{\parallel}$ in the large recoil limit ($m_b, E_{K^*} \rightarrow \infty$). As explained in [8], this is due to the left-handed nature of weak interactions in the SM: if $m_b \rightarrow \infty$ then one can assume that $m_s \rightarrow 0$, so the s quark resulting from the $b \rightarrow s$ transition will be produced with helicity $h = -1/2$ and, being massless, will not be affected by strong interactions [122]. Therefore, the s quark will combine with a light quark to form a K^* meson with $H = -1, 0$ but never $+1$ so that, at the quark level $H(+)=0$ and hence, using Eq. (6.87), one obtains $A_{\perp} = -A_{\parallel}$. At the hadron level this relation will be approximate and read $A_{\perp} \approx -A_{\parallel}$.

6.5 The full angular decay distribution

6.5.1 How to obtain it

As explained in–Sec. 6.4.1, solving completely the decay, i.e. obtaining the differential decay amplitude as a function of angles, transversity amplitudes and invariants only, although conceptually simple, constitutes a very involved task from the computational point of view. And this complexity increases steeply as more operators of the effective Hamiltonian are considered. Here

the basic steps to obtain the differential decay distribution will be sketched to give a flavour of how to proceed.

- (1) Choose which tag in Sec. 5 (i, j, k, l) will label each of the final-state particle resulting from the four-body decay (π, K, ℓ^+, ℓ^-). Our election is the same as in [10]:

General	$B \rightarrow K\pi\ell^+\ell^-$
(i, j)	(π, K)
(k, l)	(ℓ^+, ℓ^-)
m_{ij}	m_{K^*}
m_{kl}	$\sqrt{q^2}$
θ_{ij}	θ_K ⁷
θ_{kl}	θ_ℓ ⁸
ϕ	ϕ
σ_{ij}^2	$m_{K^*}^4 \beta^2 / 4$
σ_{kl}^2	$q^4 \beta_\mu^2 / 4$
σ^2	$\lambda / 4$
\vec{p}	$p_{K^*} \cdot q$

Table 6.6: Translation table between the variables of the general four-body decay $X \rightarrow Y(\rightarrow ij)Z(\rightarrow kl)$ discussed in Sec. 5 and the decay $B \rightarrow K^*(\rightarrow K\pi)\ell^+\ell^-$. β and λ were defined under Eq. (6.52) and Eq. (6.102) respectively while the definition of β_μ will be given in Sec. 6.5.2.

With m_{ij} fixed to m_{K^*} , the $\bar{B}_d \rightarrow \bar{K}^{*0}\ell^+\ell^-$ decay mode has an allowed kinematical range given by

$$(2m_\ell)^2 \leq q^2 \leq (m_B - m_{K^*})^2 \quad (6.103)$$

⁷It might be a bit surprising to call this angle θ_K , but it is the name it has received traditionally in the literature [8, 45, 46, 119] and there is no possible confusion. According to Sec. 5.1, $\theta_{\pi K}$ is the angle between the forward direction of the π (with 3-momentum \vec{p}_π) and reversed direction of the decaying particle (defined by the 3-momentum $-\vec{p}_B$) in the diparticle $(\pi, K) = K^*$ rest frame. Therefore, the angle between the forward direction of the K (with 3-momentum \vec{p}_K) and the forward direction of the decaying particle (defined by the 3-momentum \vec{p}_B) in the K^* rest frame will be exactly the same angle.

Something similar could be said for θ_ℓ , as in the literature is usually defined as the angle between the ℓ^- and the direction of flight of the decaying particle in the dilepton (ℓ^+, ℓ^-) rest frame. But this angle is the same as the one existing between the forward direction of the ℓ^+ (with 3-momentum \vec{p}_{ℓ^+}) and reversed direction of the decaying particle in the dilepton rest frame, as defined in Sec. 5.

(2) Invert Eqs. (5.3)–(5.4) to obtain

$$p_\pi = \frac{P_{\pi K} + Q_{\pi K}}{2}, \quad p_{\ell^+} = \frac{P_{\ell^+\ell^-} + Q_{\ell^+\ell^-}}{2}, \quad (6.104)$$

$$p_K = \frac{P_{\pi K} + Q_{\pi K}}{2}, \quad p_{\ell^-} = \frac{P_{\ell^+\ell^-} - Q_{\ell^+\ell^-}}{2}, \quad (6.105)$$

where $P_{\pi K} = p_{K^*}$, $P_{\ell^+\ell^-} = q$ and the relation $p \equiv p_B = p_{K^*} + q \equiv P_{\pi K} + P_{\ell^+\ell^-}$ is always fulfilled.

(3) Use Eqs. (6.104)–(6.105) and the general relation beneath them to write every four-moment in terms of the appropriate P and Q .

(4) Write all hadronic tensor structures of the $A_{\nu(\mu\lambda)}$ type, namely

$$A_{\nu\mu}^{C_9^{\text{eff}}, C_{10}} = -i\tilde{A}\epsilon_{\nu\mu\rho\sigma}P_{\pi K}^\rho P_{\ell^+\ell^-}^\sigma - \tilde{B}g_{\nu\mu} + \tilde{C}P_{\ell^+\ell^-, \nu}(2P_{\pi K} + P_{\ell^+\ell^-})_\mu - \tilde{D}P_{\ell^+\ell^-, \nu}P_{\ell^+\ell^-, \mu}, \quad (6.106)$$

$$A_{\nu\mu}^{C_9^{\text{eff}'}, C_{10}'} = -i\tilde{A}\epsilon_{\nu\mu\rho\sigma}P_{\pi K}^\rho P_{\ell^+\ell^-}^\sigma + \tilde{B}g_{\nu\mu} - \tilde{C}P_{\ell^+\ell^-, \nu}(2P_{\pi K} + P_{\ell^+\ell^-})_\mu + \tilde{D}P_{\ell^+\ell^-, \nu}P_{\ell^+\ell^-, \mu}, \quad (6.107)$$

$$A_{\nu\mu}^{C_7^{\text{eff}(\nu)}, R} = i\tilde{E}\epsilon_{\nu\mu\rho\sigma}P_{\pi K}^\rho P_{\ell^+\ell^-}^\sigma - \tilde{F}g_{\nu\mu} + \tilde{G}P_{\ell^+\ell^-, \nu}(2P_{\pi K} + P_{\ell^+\ell^-})_\mu - \tilde{H}P_{\ell^+\ell^-, \nu}P_{\ell^+\ell^-, \mu}, \quad (6.108)$$

$$A_{\nu\mu}^{C_7^{\text{eff}(\nu)}, L} = i\tilde{E}\epsilon_{\nu\mu\rho\sigma}P_{\pi K}^\rho P_{\ell^+\ell^-}^\sigma + \tilde{F}g_{\nu\mu} - \tilde{G}P_{\ell^+\ell^-, \nu}(2P_{\pi K} + P_{\ell^+\ell^-})_\mu + \tilde{H}P_{\ell^+\ell^-, \nu}P_{\ell^+\ell^-, \mu}, \quad (6.109)$$

$$A_\nu^{C_S, C_{PS}} = -\tilde{I}P_{\ell^+\ell^-, \nu}, \quad (6.110)$$

$$A_\nu^{C_S', C_{PS}'} = \tilde{I}P_{\ell^+\ell^-, \nu}, \quad (6.111)$$

$$A_{\nu\mu\lambda}^{C_T, C_{PT}} = -\tilde{J}\epsilon_{\nu\mu\lambda\beta}(2P_{\pi K} + P_{\ell^+\ell^-})^\beta + \tilde{K}\epsilon_{\nu\mu\lambda\beta}P_{\ell^+\ell^-}^\beta - \tilde{L}P_{\ell^+\ell^-, \nu}\epsilon_{\mu\lambda\alpha\beta}P_{\pi K}^\alpha P_{\ell^+\ell^-}^\beta, \quad (6.112)$$

where the coefficients $\tilde{A}, \tilde{B}, \tilde{C}, \tilde{D}$ can be identified directly from Eq. (3.8), $\tilde{E}, \tilde{F}, \tilde{G}, \tilde{H}$ from Eq. (3.9), \tilde{I} from Eq. (3.12) and $\tilde{J}, \tilde{K}, \tilde{L}$ from Eq. (3.14). Insert the Wilson coefficient indicated as a superindex as a multiplying factor into each tilded coefficient.

(5) If one chooses to use the narrow-width approximation, contract W^ν in Eq. (6.63) with all $A_{\nu(\mu\lambda)}$ tensors.

(6) Multiply the matrix element in Eq. (6.41) by its complex conjugate and sum and average over spins of the final state leptons (and K^* polarisations if step (5) was skipped).

- (7) Use Eqs. (6.104)–(6.105) at right to convert lepton four-momenta into the appropriate dilepton four-momenta.
- (8) Contract all indices ([106] and [117] are the best references for this step.)
- (9) Use the relations in Eqs. (5.60)–(5.72) to express all diparticle four-momenta products as functions of kinematical variables: masses (m_B, m_{K^*}), the dilepton mass squared q^2 and the three angles θ_K, θ_ℓ and ϕ .
- (10) Group the overall factors into a single term. Multiply this term by Eq. (6.60) if the narrow-width approximation was used or by the $\mathcal{B}(K^{*0} \rightarrow K\pi)$ if step (5) was skipped.
- (11) At this point the differential decay amplitude is a sum of a discrete number of trigonometric combinations of the angles θ_K, θ_ℓ and ϕ (12 in the case of a decay with SM-like and scalar operators), each of them multiplied by a prefactor called *angular coefficient* and usually designed by I_i or J_i (with $i = 1s, 1c, 2s, 2c, 3, 4, 5, 6s, 6c, 7, 8, 9$).
- (12) Identify the amplitudes as repeated structures inside the angular coefficients. This is the most difficult step and one might need to resort to the method described in Sec. 6.4.1 to single them out.
- (13) Substitute the appropriate combinations of transversity amplitudes into the angular coefficients and these into the differential decay distribution and make sure that everything works nicely checking that you have neither more nor less terms than you should.

6.5.2 The full angular decay distribution for $\bar{B}_d^0 \rightarrow \bar{K}^{*0}(\rightarrow K^-\pi^+)\ell^+\ell^-$ and its CP -conjugate process

Following the steps enumerated in the previous section one obtains the full angular decay distribution for $\bar{B}_d^0 \rightarrow \bar{K}^{*0}(\rightarrow K^-\pi^+)\ell^+\ell^-$ [91, 8, 10]:

$$\frac{d^4\Gamma}{dq^2 d\cos\theta_\ell d\cos\theta_K d\phi} = N J(q^2, \theta_\ell, \theta_K, \phi), \quad (6.113)$$

where

$$\begin{aligned} J(q^2, \theta_\ell, \theta_K, \phi) = & J_{1s} \sin^2 \theta_K + J_{1c} \cos^2 \theta_K + (J_{2s} \sin^2 \theta_K + J_{2c} \cos^2 \theta_K) \cos 2\theta_\ell \\ & + J_3 \sin^2 \theta_K \sin^2 \theta_\ell \cos 2\phi + J_4 \sin 2\theta_K \sin 2\theta_\ell \cos \phi \\ & + J_5 \sin 2\theta_K \sin \theta_\ell \cos \phi \\ & + (J_{6s} \sin^2 \theta_K + J_{6c} \cos^2 \theta_K) \cos \theta_\ell + J_7 \sin 2\theta_K \sin \theta_\ell \sin \phi \\ & + J_8 \sin 2\theta_K \sin 2\theta_\ell \sin \phi + J_9 \sin^2 \theta_K \sin^2 \theta_\ell \sin 2\phi. \end{aligned} \quad (6.114)$$

and

$$N \equiv \frac{3 \alpha_{\text{em}}^2 G_F^2 |\lambda_t^{(s)}|^2 \lambda^{1/2} q^2 \beta_\ell}{2^{15} \pi^6 m_B^3} \mathcal{B}(K^{*0} \rightarrow K\pi), \quad (6.115)$$

with

$$\beta_\ell = \sqrt{1 - \frac{4m_\ell^2}{q^2}}. \quad (6.116)$$

The corresponding expression for the CP-conjugated mode $B^0 \rightarrow K^{*0}(\rightarrow K^+\pi^-)\ell^+\ell^-$ is

$$\frac{d^4\bar{\Gamma}}{dq^2 d\cos\theta_l d\cos\theta_K d\phi} = N \bar{J}(q^2, \theta_\ell, \theta_K, \phi). \quad (6.117)$$

The function $\bar{J}(q^2, \theta_\ell, \theta_K, \phi)$ can be obtained from Eq. (6.114) through the replacements [91]

$$J_{1s,1c,2s,2c,3,4,7} \longrightarrow \bar{J}_{1s,1c,2s,2c,3,4,7}, \quad J_{5,6s,6c,8,9} \longrightarrow -\bar{J}_{5,6s,6c,8,9}, \quad (6.118)$$

where \bar{J}_i equals J_i with all weak phases conjugated. As noted in [10], the minus sign in Eq. (6.118) is a result of the convention, common among theoretical physicists [91, 8], that while the angle θ_K designs the angle between the forward direction of the kaon (regardless of it is a K^- or a K^+) and the forward direction of the B in the K^* reference frame (see footnote 7 in Tab. 6.6), the angle θ_ℓ is determined by ℓ^+ following the convention of Sec. 5.1 and Tab. 6.6 in both CP modes. The CP transformation reverses the momenta and conjugates the electric charge of all particles involved in the decay. Then, due to the antisymmetric nature of \vec{Q}_{kl} (the notation has been adapted according to Tab. 6.6, so $k \equiv \ell^+$ and $l \equiv \ell^-$) CP will flip the sign of Eq. (5.7), which amounts to changing $\theta_\ell \rightarrow \pi - \theta_\ell$ in Eq. (6.114). On the other hand, CP will also flip the sign of Eq. (5.46) while leaving Eq. (5.58) invariant, so $\phi \rightarrow \pi - \phi$ if ϕ were an angle defined between 0 and 2π , but as explained under Fig. 5.2, ϕ is an oriented angle defined in the $[-\pi, \pi]$ range and therefore $\phi \rightarrow -\phi$ under CP .

6.5.3 The angular coefficients

The angular coefficients J_i are functions of q^2 that are commonly expressed in terms of K^* transversity amplitudes. Using the eight transversity amplitudes defined in Eqs. (6.98)–(6.102),

the angular coefficients can be written as

$$J_{1s} = \frac{(2 + \beta_\ell^2)}{4} \left[|A_\perp^L|^2 + |A_\parallel^L|^2 + (L \rightarrow R) \right] + \frac{4m_\ell^2}{q^2} \text{Re} \left(A_\perp^L A_\perp^{R*} + A_\parallel^L A_\parallel^{R*} \right), \quad (6.119)$$

$$J_{1c} = |A_0^L|^2 + |A_0^R|^2 + \frac{4m_\ell^2}{q^2} \left[|A_t|^2 + 2\text{Re}(A_0^L A_0^{R*}) \right] + \beta_\ell^2 |A_S|^2, \quad (6.120)$$

$$J_{2s} = \frac{\beta_\ell^2}{4} \left[|A_\perp^L|^2 + |A_\parallel^L|^2 + (L \rightarrow R) \right], \quad (6.121)$$

$$J_{2c} = -\beta_\ell^2 \left[|A_0^L|^2 + (L \rightarrow R) \right], \quad (6.122)$$

$$J_3 = \frac{1}{2} \beta_\ell^2 \left[|A_\perp^L|^2 - |A_\parallel^L|^2 + (L \rightarrow R) \right], \quad (6.123)$$

$$J_4 = \frac{1}{\sqrt{2}} \beta_\ell^2 \left[\text{Re}(A_0^L A_\parallel^{L*}) + (L \rightarrow R) \right], \quad (6.124)$$

$$J_5 = \sqrt{2} \beta_\ell \left[\text{Re}(A_0^L A_\perp^{L*}) - (L \rightarrow R) - \frac{m_\ell}{\sqrt{q^2}} \text{Re}(A_\parallel^L A_S^* + A_\parallel^R A_S^*) \right], \quad (6.125)$$

$$J_{6s} = 2\beta_\ell \left[\text{Re}(A_\parallel^L A_\perp^{L*}) - (L \rightarrow R) \right], \quad (6.126)$$

$$J_{6c} = 4\beta_\ell \frac{m_\ell}{\sqrt{q^2}} \text{Re} \left[A_0^L A_S^* + (L \rightarrow R) \right], \quad (6.127)$$

$$J_7 = \sqrt{2} \beta_\ell \left[\text{Im}(A_0^L A_\parallel^{L*}) - (L \rightarrow R) + \frac{m_\ell}{\sqrt{q^2}} \text{Im}(A_\perp^L A_S^* + A_\perp^R A_S^*) \right], \quad (6.128)$$

$$J_8 = \frac{1}{\sqrt{2}} \beta_\ell^2 \left[\text{Im}(A_0^L A_\perp^{L*}) + (L \rightarrow R) \right], \quad (6.129)$$

$$J_9 = \beta_\ell^2 \left[\text{Im}(A_\parallel^{L*} A_\perp^L) + (L \rightarrow R) \right]. \quad (6.130)$$

Some important remarks must be done here:

- The angular coefficients J_i are all physical observables and, although it has been claimed that they are *theoretically clean* [10], it can be argued that they might be neither the *cleanest* nor the more sensitive observables one might build [45, 46, 114, 123, 124, 119, 120].

- In the limit of massless leptons the relations $J_{1s} = 3J_{2s}$ and $J_{1c} = -J_{2c}$ hold. But this is just the tip of the iceberg, as there a rich variety of symmetries (understood as transformations among the transversity amplitudes that leave invariant the coefficients of the angular distribution) that, together with the number of transversity amplitudes, determine the number of degrees of freedom available from the angular analysis [45, 46, 119].
- The coefficient J_{6c} , obtained in [10] for the first time, vanishes in the limit of massless leptons or if there are no NP contributions stemming from dimension six scalar operators.

6.6 The $O(\alpha_s)$ corrections from QCD factorisation

6.6.1 Motivation and general aspects

The $b \rightarrow s$ transition that occurs in the $\bar{B}_d^0 \rightarrow \bar{K}^{*0} \ell^+ \ell^-$ exclusive process is an example of a heavy-to-light weak decay. QCD factorisation provides a framework to compute $O(\alpha_s)$ corrections systematically for these kind of processes at LO in Λ_{QCD}/m_b , as summarised in Sec. 4.3 for purely hadronic decays. For radiative decays of the type $\bar{B} \rightarrow \bar{K}^* \gamma^{(*)}$, QCdf is also capable to deal with both factorisable strong contributions (i.e. radiative corrections to the form factors) and non-factorisable effects, which stem from electromagnetic corrections to the matrix elements of purely hadronic operators in \mathcal{H}_{eff} [32, 76, 77]. The aim of this section is to collect and summarise the information needed to include these $O(\alpha_s)$ corrections computed in QCdf into the transversity amplitudes, but the interested reader should be able to find all relevant details in [98] (in German).

The $\bar{B} \rightarrow \bar{K}^* \gamma^{(*)}$ transition amplitude in the SM, neglecting CKM-suppressed and m_s/m_b terms, is given in Eq.(6) of [32]. We have modified it just to look like Eq. (3.9), obtaining

$$\begin{aligned} \langle \gamma^*(q, \mu) \bar{K}^*(p', \varepsilon^*) | \mathcal{H}_{\text{eff}}^{(t)} | \bar{B}(p) \rangle &= \frac{e}{4\pi^2} (-2m_b) \varepsilon^{*\nu} \left\{ i \epsilon_{\nu\mu\rho\sigma} p'^{\rho} q^{\sigma} \mathcal{T}_1^{(t)}(q^2) \right. \\ &+ \frac{1}{2} \left[((m_B^2 - m_V^2) g_{\nu\mu} - q_{\nu}(2p' + q)_{\mu}) \mathcal{T}_2^{(t)}(q^2) \right. \\ &\left. \left. + q_{\nu} \left(q_{\mu} - \frac{q^2}{m_B^2 - m_V^2} (2p' + q)_{\mu} \right) \mathcal{T}_3^{(t)}(q^2) \right] \right\}, \quad (6.131) \end{aligned}$$

where the changes performed have been the following: the addition of a factor 4 in the numerator to account for the different definition of the effective operators in Eqs. (6.8)–(6.17) with respect to Eqs. (3)–(4) in [32] and the removal of the prefactor that already appears in Eq. (6.1) in front of $\mathcal{H}_{\text{eff}}^{(t)}$, the substitution of the electromagnetic coupling g_{em} by $-e$ (with e defined as $e \equiv |e|$ the charge of the electron), the use of moment conservation $p = p' + q$ to express all terms in Eq. (6.131) in function of p' and q , the substitution $\kappa = 1$ (see Sec. 3.1.1) and the reshuffling

of some terms and indices using the properties of the Levi-Civita tensor. " (t) " labels the non CKM-suppressed terms in the $b \rightarrow s\ell^+\ell^-$ effective Hamiltonian in Eq. (6.2).

Since heavy-to-light meson decays are characterised by only two universal soft form factors, i.e. $\xi_\perp(E_{K^*})$ and $\xi_\parallel(E_{K^*})$ in this case, writing the matrix element ruling the $\bar{B} \rightarrow \bar{K}^*\gamma^{(*)}$ decay in terms of $\mathcal{T}_i^{(t)}$ (with $i = 1, 2, 3$) is not the best solution if one wants to emulate Eq. (3.33) and find a schematic formula to represent the QCdf corrections entering each $\mathcal{T}_i^{(t)}$. Therefore, adopting the notation of [31] the following useful relations may be found at leading logarithmic order:

$$\mathcal{T}_1^{(t)}(q^2) \equiv \mathcal{T}_\perp^{(t)}(q^2) = \xi_\perp(q^2) \left[C_7^{\text{eff}} \delta_1 + \frac{q^2}{2m_b m_B} Y(q^2) \right], \quad (6.132)$$

$$\mathcal{T}_2^{(t)}(q^2) = \frac{2E_{K^*}}{m_B} \mathcal{T}_\perp^{(t)}(q^2), \quad (6.133)$$

$$\mathcal{T}_3^{(t)}(q^2) - \frac{m_B}{2E_{K^*}} \mathcal{T}_2^{(t)}(q^2) \equiv \mathcal{T}_\parallel^{(t)}(q^2) = -\xi_\parallel(q^2) \left[C_7^{\text{eff}} \delta_2 + \frac{m_B}{2m_b} Y(q^2) \delta_3 \right], \quad (6.134)$$

where the factors δ_i (with $i = 1, 2$) are defined such that they include the $O(\alpha_s)$ corrections ($\delta_i = 1 + O(\alpha_s)$), and the appearance of only two independent structures is a consequence of the chirality of weak interactions in the SM and of helicity conservation, so it holds also after including next-to-leading order corrections in α_s [31, 122].

So far we have been talking about $\mathcal{T}_\perp^{(t)}(q^2)$ and $\mathcal{T}_\parallel^{(t)}(q^2)$ without actually giving a meaning to them: these are decay-amplitude related non-perturbative functions which contain all contributions calculable in QCdf (i.e. factorisable and non-factorisable) stemming from the operators in the $b \rightarrow s\ell^+\ell^-$ that can contribute to the decay amplitude only through the coupling of a γ^* , which then decays into a lepton-antilepton pair (this is, all operators in Eqs. (6.8)–(6.15)). The factorisation formula for these "amplitudes" resembles Eq. (3.33):

$$\mathcal{T}_a^{(t)}(q^2) \equiv \mathcal{C}_a^{(t)} \xi_a + \Phi_B \otimes T_a^{(t)} \otimes \Phi_{K^*}, \quad (6.135)$$

with $a = \perp, \parallel$. Therefore, each $\mathcal{T}_a^{(t)}$ can now be written as a sum of universal soft form factors weighted by the hard-vertex corrections $\mathcal{C}_a^{(t)}$ (not to be confused with Wilson coefficients) and the convolution of a hard-scattering kernel $T_a^{(t)}$ with the LCDAs of the \bar{B} meson (Φ_B) and the \bar{K}^* meson (Φ_{K^*}). Given that the terms $\mathcal{C}_a^{(t)}$ and $T_a^{(t)}$ are calculable in perturbation theory [77]

$$\mathcal{C}_a^{(t)} = \mathcal{C}_a^{(0,t)} + \frac{\alpha_s C_F}{4\pi} \mathcal{C}_a^{(1,t)} + \dots, \quad (6.136)$$

$$T_{a,\pm}^{(t)}(u, \omega) = T_{a,\pm}^{(0,t)}(u, \omega) + \frac{\alpha_s C_F}{4\pi} T_{a,\pm}^{(1,t)}(u, \omega) + \dots, \quad (6.137)$$

(with C_F defined under Eq. (6.150)) but ξ_a and Φ are obtained using the combined HQET/LEET formalism (as explained in Sec. 4.5), this expression holds to all orders in α_s but just to leading order in Λ_{QCD}/m_b .

6.6.2 Assumptions and range of applicability of QCDF to the $\bar{B}_d^0 \rightarrow \bar{K}^{*0} \ell^+ \ell^-$ decay mode

In QCDF one assumes that, in the $\bar{B}_d^0 \rightarrow \bar{K}^{*0} \ell^+ \ell^-$ exclusive process, the \bar{B} meson decays into $\bar{K}^* \gamma^*$ (see Eq. (6.131)) which in turn decay into $K^- \pi^+$ and $\ell^+ \ell^-$, respectively. Therefore, the possibility of the vector gauge boson being a Z^0 , which could also decay into a lepton-antilepton pair, is neglected as the large Z^0 mass (over 90 GeV) causes this contribution to be very suppressed.

On the other hand, as we have seen, QCDF demands the heavy quark limit of the incoming heavy meson and the large energy limit of the recoiling light meson to be used together. Here "large energy" of the K^* means $E_{K^*} \sim O(m_B/2)$. Hence, if we require $E_{K^*} > 2.15$ GeV then, using Eq. (3.23) we obtain $q^2 < 6$ GeV², which is well below the $c\bar{c}$ production threshold $4m_c^2 \simeq 7$ GeV². Besides, the parallel component of the hard scattering kernel develops a logarithmic singularity as $q^2 \rightarrow 0$, which is of no consequence because this component is suppressed by a power of q^2 in relation to the transverse component in this limit. However, it implies that this parallel component is not perturbatively calculable unless $q^2 \sim m_b \Lambda_{\text{QCD}} \simeq 1$ GeV² [32], which should not be a surprise since, in the $0 < q^2 < 1$ GeV² region, there could be unknown resonance contributions from light mesons and the perturbative treatment characteristic of QCDF must break down there. Therefore, to summarise, there is a *lower limit* ($q_{\text{min}}^2 = 1$ GeV²) and also an *upper limit* ($q_{\text{max}}^2 = 6$ GeV²) to the range of applicability of QCDF to the decay mode $\bar{B}_d^0 \rightarrow \bar{K}^{*0} \ell^+ \ell^-$, so that the large dilepton invariant mass range kinematically accessible

$$(2m_\ell)^2 \leq q^2 \leq (m_B - m_{K^*})^2 \quad (6.138)$$

shrinks to just

$$1 \text{ GeV}^2 \leq q^2 \leq 6 \text{ GeV}^2 \quad (6.139)$$

and this has an important physical implication: within QCDF, the final state leptons in the $\bar{B}_d^0 \rightarrow \bar{K}^{*0} \ell^+ \ell^-$ decay mode can be either e or μ , but not τ : large- q^2 region [114, 123] should be used to deal with τ in the final state.

As a final remark we should state that one must keep a well defined criterion about the order of magnitude of the terms that can be neglected. Hence, if when computing Eqs. (3.26)–(3.29) (those that allowed relating the seven independent form factors to either ξ_\perp or ξ_\parallel , see Eqs. (3.31)–(3.32)) the terms of $O(m_V^2/m_B^2)$ were dropped at LO in $1/m_b$, then one must consistently get rid of these same terms in the equation for E_{K^*} [Eq. (3.23)]

$$E_{K^*} \simeq \frac{m_B}{2} \left(1 - \frac{q^2}{m_B^2} \right) \quad (6.140)$$

and in the transition matrix elements [Eq. (6.131)], once substituted Eqs. (6.132)–(6.134)

$$\begin{aligned}
\langle \gamma^*(q, \mu) \bar{K}^*(p', \varepsilon^*) | \mathcal{H}_{\text{eff}}^{(t)} | \bar{B}(p) \rangle &= \frac{e}{4\pi^2} (-2m_b) \varepsilon^{*\nu} \left\{ i \epsilon_{\nu\mu\rho\sigma} p'^{\rho} q^{\sigma} \mathcal{T}_{\perp}^{(t)}(q^2) \right. \\
&\quad + [E_{K^*} m_B g_{\nu\mu} - q_{\nu} p'_{\mu}] \mathcal{T}_{\perp}^{(t)}(q^2) \\
&\quad \left. + \frac{1}{2} q_{\nu} \left[q_{\mu} - \frac{q^2}{m_B^2} (2p' + q)_{\mu} \right] \mathcal{T}_{\parallel}^{(t)}(q^2) \right\}. \quad (6.141)
\end{aligned}$$

For the same reason, the m_s/m_b terms in Eq. (6.41) and everywhere else can be safely neglected, as $m_{K^*}^2/m_B^2 \simeq 0.029$ and $m_s^{\overline{\text{MS}}}/m_b^{\overline{\text{MS}}} = 0.0210 \pm 0.0061$ [99], so $m_s/m_b \sim O(m_{K^*}^2/m_B^2)$.

6.6.3 Diagrams contributing to CKM-allowed terms

Diagrams contributing to leading order in α_s

The diagrams at $O(\alpha_s^0)$ corresponding to a $b \rightarrow s \ell^+ \ell^-$ decay can be found in Fig. 6.6. (a) contains the quark or W loop related to the effective operator \mathcal{O}_7 shown in Fig. 6.1(c,d). (b) has an explicit quark loop that may be created either joining the c and \bar{c} final-state quarks in Fig. 6.1(a) for \mathcal{O}_1 and \mathcal{O}_2 , or the lower two quarks in Fig. 6.1(b) for \mathcal{O}_{3-6} . On the other hand, the diagrams in (c) can be obtained from the direct *weak annihilation* of the b quark with the spectator quark \bar{d} operators in the case of \mathcal{O}_1 and \mathcal{O}_2 or taking the generic quark q line at the bottom of Fig. 6.1(b) as d quark for \mathcal{O}_{3-6} .

Diagrams (a) and (b) contribute to the soft form factors $\xi_{\parallel}(E_{K^*})$ and $\xi_{\perp}(E_{K^*})$. The four diagrams in (c) contribute at different powers in the $1/m_b$ expansion, but the one in which the virtual photon is emitted by the spectator quark in the B meson is not suppressed at leading order in Λ_{QCD}/m_b [32], so a hard-scattering amplitude $T_a^{(t)}$ will appear already at leading order in α_s . Since the \bar{K}^{*0} recoils with a large energy, and using the convention that it moves along the minus light-cone direction, the only hard-scattering kernel different from 0 will be the one depending only on the minus component of the spectator quark momentum $T_{\parallel,-}^{(0,t)}$ [see Eq. (6.147) and also Eq. (6.146)].

Diagrams contributing to next-to-leading order in α_s

Fig. 6.7 shows the *hard-vertex diagrams* that renormalise the $b \rightarrow s$ current: since the spectator quark is connected to the hard process represented by these diagrams only through soft interactions, they will be part of the $B \rightarrow K^*$ form factors at next-to-leading order and hence their contribution will be proportional to the soft form factors ξ_a , with the hard process pictured providing an $O(\alpha_s)$ correction to the factor $\mathcal{C}_a^{(t)}$ in Eq. (6.135). In (a) appears the chromomagnetic gluon penguin diagram in Fig. 6.1(e), corresponding to the weak effective operator \mathcal{O}_8 . There

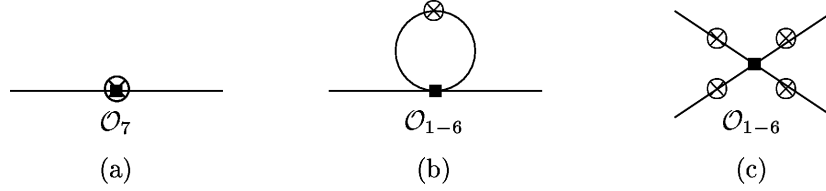


Figure 6.6: Leading order contributions in α_s and Λ_{QCD}/m_b to $\langle \gamma^* \bar{K}^* | H_{\text{eff}} | \bar{B} \rangle$. The circled cross marks the possible insertions of a virtual photon line. The spectator quark line has been omitted for simplicity in (a) and (b), which are factorisable contributions. The weak annihilation diagram in (c) in which γ^* is emitted by the spectator quark constitutes a non-factorisable LO contribution [32].

are two symmetric diagrams because the gluon emitted may couple to the b or to the s quark. (b) and (c) are just QCD radiative corrections of the (b) diagram in Fig. 6.6.

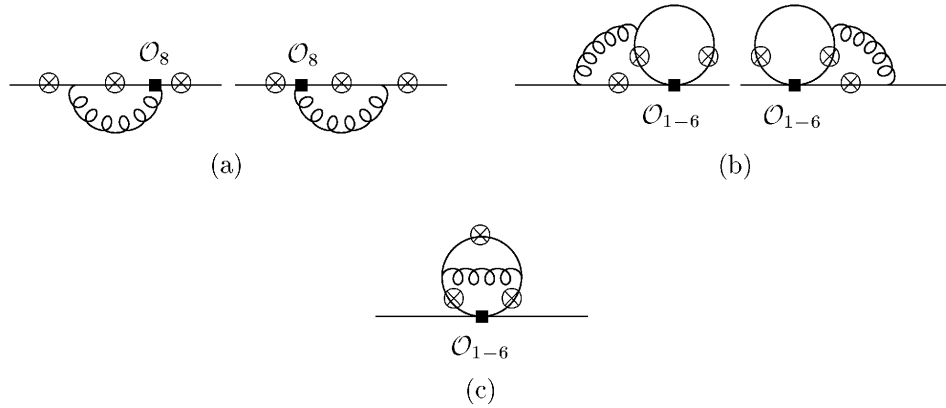


Figure 6.7: Hard-vertex factorisable contributions to the $B \rightarrow K^*$ form factor part of $\langle \gamma^* \bar{K}^* | H_{\text{eff}} | \bar{B} \rangle$. The spectator quark line has been omitted for simplicity [32].

The *hard-spectator scattering* contributions are displayed in Fig. 6.8. The high-momentum gluon radiated by the quark loop of \mathcal{O}_8 shown in (a) can reach the spectator quark \bar{d} , which has a momentum of order Λ_{QCD} , and put both final-state quarks (s and \bar{d}) in a nearly even momentum configuration that favours hadronisation. Diagram (b) is just a radiative correction to diagram (b) in Fig. 6.6, describing the spectator quark absorption of a hard gluon emitted from the quark-antiquark pair created by \mathcal{O}_{1-6} .

QCD radiative corrections to the *weak annihilation* diagram in Fig. 6.6(c) that contributes to LO in both α_s and Λ_{QCD}/m_b are shown in Fig. 6.9. However, for $b \rightarrow s$ transitions, these topologies are very suppressed for several reasons: the smallness of Wilson coefficients C_{3-6} attached to QCD penguin operators, the fact that they appear at NLO in α_s , which is small at

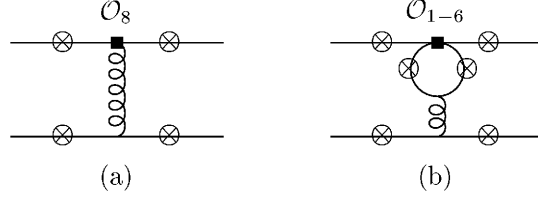


Figure 6.8: Hard-spectator scattering non-factorisable diagrams of $\langle \ell^+ \ell^- \bar{K}^* | H_{\text{eff}} | \bar{B} \rangle$ [32].

$\mu \sim m_b$, and the observation that, for small q^2 , the longitudinal contribution to the decay rate is suppressed by a factor $\sqrt{q^2}$ relative to the transverse contribution⁸, and we have restricted our calculus precisely to the kinematic region in which q^2 is small. Moreover, in [10] is reasoned that the $O(\alpha_s \Lambda_{\text{QCD}}/m_b)$ topologies with end-point divergencies in the convolution integral that could *a priori* be large due to soft-gluon effects, are similar to some contributions that occur in LCSRs and are described by three-particle DAs of the type $\langle 0 | \bar{q} G s | \bar{K}^* \rangle$, which turn out to be numerically small. Therefore these diagrams may be safely neglected when computing $\mathcal{T}_{\parallel, \perp}(q^2)$ [32].

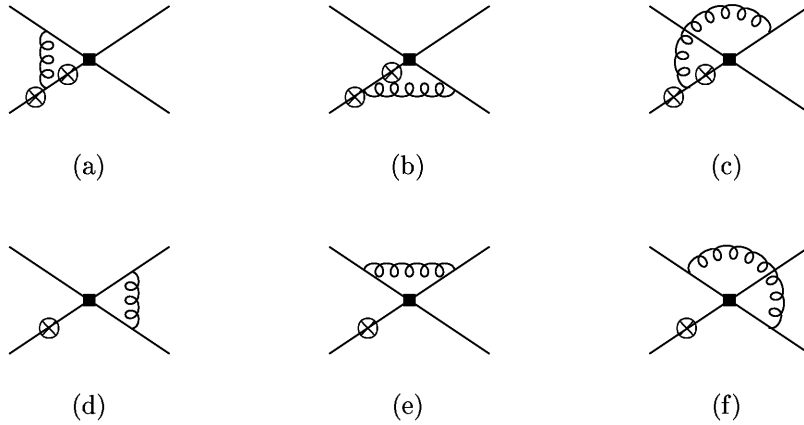


Figure 6.9: Vertex corrections to the relevant weak annihilation diagram in Fig. 6.6(c) [32].

6.6.4 The non-perturbative amplitudes $\mathcal{T}_{\parallel}^{(i)}(q^2)$ and $\mathcal{T}_{\perp}^{(i)}(q^2)$

The inclusion of CKM-suppressed terms

So far we have only dealt with contributions to the $b \rightarrow s \ell^+ \ell^-$ WEH in Eq. (6.1) that had the large $\lambda_t^{(s)}$ as a prefactor, neglecting those suppressed by the small $\hat{\lambda}_u^{(s)} = \lambda_u^{(s)}/\lambda_t^{(s)}$ term.

⁸A good place to observe this suppression already at $O(\alpha_s^0)$ is looking at Eqs. (6.98)–(6.100) in Sec. 6.4.2.

However, as stated under Eq. (6.5), $\lambda_u^{(s)}$ constitutes a source of weak phases in the Standard Model, so it is important to take into account when dealing with CP -violation. Fortunately, in [77] these CKM-suppressed terms were studied and put on the same footing as the "(t)" terms, obtaining an unified formulation. Therefore, one just needs to substitute $(t) \rightarrow (u)$ in Eqs. (6.141), (6.131), (6.135) and (6.136), (6.137) and to obtain the general expression for matrix elements and factorisation formula for the "(u)" terms. Henceforward, the $i = u, t$ index will be used to account for both kinds of contributions.

Unfortunately, changing (t) into (u) is not so easy from the practical point of view, as many functions in the formulae below require either a redefinition, as in the case of $Y^{(u)}(q^2)$, or are simply 0. All these changes are collected in appendices A.1 and A.2 of [77] and also in [125]. Unless necessary, they will not be repeated here.

Leading order

At leading order $\mathcal{T}_\perp^{(i)}(q^2)$ and $\mathcal{T}_\parallel^{(i)}$ are given by

$$\begin{aligned} \mathcal{T}_\perp^{(i)}(q^2) &= \mathcal{C}_\perp^{(0,i)} \xi_\perp(q^2) \\ &+ \frac{\pi^2}{N_c} \frac{f_B f_{K^*,\perp}(\mu_h)}{m_B} \sum_\pm \int_0^\infty \frac{d\omega}{\omega} \Phi_{B,\pm}(\omega) \int_0^1 du \Phi_{K^*,\perp}(u) T_{\perp,\pm}^{(0,i)}(u, \omega), \end{aligned} \quad (6.142)$$

$$\begin{aligned} \mathcal{T}_\parallel^{(i)}(q^2) &= \mathcal{C}_\parallel^{(0,i)} \xi_\parallel(q^2) \\ &+ \frac{\pi^2}{N_c} \frac{f_B f_{K^*,\parallel} m_{K^*}}{m_B E_{K^*}} \sum_\pm \int_0^\infty \frac{d\omega}{\omega} \Phi_{B,\pm}(\omega) \int_0^1 du \Phi_{K^*,\parallel}(u) T_{\parallel,\pm}^{(0,i)}(u, \omega), \end{aligned} \quad (6.143)$$

where N_c is the number of colours, ω (u) is the momentum fraction of the quark b (s) in the meson \bar{B} (\bar{K}^*) LCDA (see Sec. 2.2.3).

The first addend in Eqs. (6.143)–(6.142) is the form factor part stemming from the diagrams in Fig. 6.6(a,b). The $\mathcal{C}_a^{(0,i)}$ coefficients in front of $\xi_{\perp,\parallel}(q^2)$ read

$$\mathcal{C}_\perp^{(0,t)} = - \left[C_7^{\text{eff}} + \frac{m_B}{2m_b} Y^{(t)}(q^2) \right], \quad \mathcal{C}_\perp^{(0,u)} = - \frac{m_B}{2m_b} Y^{(u)}(q^2), \quad (6.144)$$

$$\mathcal{C}_\parallel^{(0,t)} = C_7^{\text{eff}} + \frac{q^2}{2m_b m_B} Y^{(t)}(q^2), \quad \mathcal{C}_\parallel^{(0,u)} = \frac{q^2}{2m_b m_B} Y^{(u)}(q^2). \quad (6.145)$$

The second addend corresponds to the hard-scattering contribution due the non-suppressed LO diagram in Fig. 6.6(c) so the hard amplitudes $T_a^{(i)}$ in Eqs. (6.142)–(6.143) are given by

$$T_{\parallel,+}^{(0,i)} = T_{\perp,+}^{(0,i)} = T_{\perp,-}^{(0,i)} = T_{\parallel,-}^{(0,u)} = 0, \quad (6.146)$$

$$T_{\parallel,-}^{(0,t)} = -e_d \frac{m_B \omega}{m_B \omega - q^2 - i\varepsilon} \frac{4m_B}{m_b} \left(C_3 + \frac{4}{3} C_4 + 16C_5 + \frac{64}{3} C_6 \right). \quad (6.147)$$

where e_q is the electric charge of the spectator quark [32], so $e_q = 1/3$ in the $\bar{B}_d^0 \rightarrow \bar{K}^{*0} \ell^+ \ell^-$ decay mode, where the spectator quark is a \bar{d} , whereas $e_q = -1/3$ in its CP -conjugated channel. It is worthwhile to point out that, since the Wilson coefficients C_3 - C_6 associated to the gluon-penguin diagrams have small values (see Tab. 6.1), the only non-zero hard-scattering contribution $T_{\parallel,-}^{(0,t)}$ will be very suppressed in comparison with the form factor at LO in α_s .

Next-to-leading order

At next-to-leading order, the expressions of $\mathcal{T}_\perp(q^2)$ and $\mathcal{T}_\parallel(q^2)$ read

$$\begin{aligned} \mathcal{T}_\perp(q^2) &= \left(\mathcal{C}_\perp^{(0,i)} + \frac{\alpha_s C_F}{4\pi} \mathcal{C}_\perp^{(1,i)} \right) \xi_\perp(q^2) \\ &+ \frac{\pi^2}{N_c} \frac{f_B f_{K^*,\perp}(\mu_h)}{m_B} \sum_{\pm} \int_0^\infty \frac{d\omega}{\omega} \Phi_{B,\pm}(\omega) \int_0^1 du \Phi_{K^*,\pm}(u) \left[T_{\perp,\pm}^{(0,i)}(u, \omega) + \frac{\alpha_s C_F}{4\pi} T_{\perp,\pm}^{(1,i)}(u, \omega) \right], \end{aligned} \quad (6.148)$$

$$\begin{aligned} \mathcal{T}_\parallel(q^2) &= \left(\mathcal{C}_\parallel^{(0,i)} + \frac{\alpha_s C_F}{4\pi} \mathcal{C}_\parallel^{(1,i)} \right) \xi_\parallel(q^2) \\ &+ \frac{\pi^2}{N_c} \frac{f_B f_{K^*,\parallel} m_{K^*}}{m_B E_{K^*}} \sum_{\pm} \int_0^\infty \frac{d\omega}{\omega} \Phi_{B,\pm}(\omega) \int_0^1 du \Phi_{K^*,\parallel}(u) \left[T_{\parallel,\pm}^{(0,i)}(u, \omega) + \frac{\alpha_s C_F}{4\pi} T_{\parallel,\pm}^{(1,i)}(u, \omega) \right], \end{aligned} \quad (6.149)$$

with $C_F \equiv (N_c^2 - 1) / 2N_c = 4/3$. $\mathcal{C}_{\parallel,\pm}^{(1,i)}$ and $T_{\parallel,\pm}^{(1,i)}(u, \omega)$ are complicated functions that can be found in [32, 77]. However, the important feature is that they can be split in two parts:

$$\mathcal{C}_{a,\pm}^{(1,i)} = \mathcal{C}_{a,\pm}^{(f,i)} + \mathcal{C}_{a,\pm}^{(\text{nf},i)}, \quad (6.150)$$

$$T_{a,\pm}^{(1,i)}(u, \omega) = T_{a,\pm}^{(f,i)}(u, \omega) + T_{a,\pm}^{(\text{nf},i)}(u, \omega), \quad (6.151)$$

where "f" stands for *factorisable* and "nf" for *non-factorisable*.

The factorisable contributions in Eqs. (6.150)–(6.151) are the $O(\alpha_s)$ corrections to the LO $\mathcal{C}_a^{(0,i)}$ and $T_{a,\pm}^{(0,i)}(u, \omega)$ terms in Eqs. (6.142)–(6.143). They arise from expressing the full QCD form factors in terms of ξ_a , so they are related to the α_s -correction to the δ_i in Eqs. (6.132)–(6.134). These terms stem from the hard-vertex topologies in Fig. 6.7 and enter both terms in Eqs. (6.150)–(6.149). The perpendicular factorisable contributions are given by [32, 77]

$$\mathcal{C}_\perp^{(f,t)} = C_7^{\text{eff}} [\ln(m_b^2/\mu^2) - L + \Delta M], \quad \mathcal{C}_\perp^{(f,u)} = 0, \quad (6.152)$$

$$T_{\perp,+}^{(f,t)}(u, \omega) = C_7^{\text{eff}} \frac{2m_B}{(1-u)E_{K^*}}, \quad T_{\perp,-}^{(f,t)} = T_{\parallel,-}^{(f,t)} = T_{a,\pm}^{(f,u)} = 0, \quad (6.153)$$

with [32]

$$L \equiv -\frac{m_b^2 - q^2}{q^2} \ln \left(1 - \frac{q^2}{m_b^2} \right), \quad (6.154)$$

and [77]

$$\Delta M = 3 \ln \frac{m_b^2}{\mu^2} - 4 \left(1 - \frac{\mu_h}{m_b} \right) \quad (6.155)$$

when $m_{b,PS}$ is used. The parallel terms, on the other hand, depend on which QCD form factors have been chosen to define the soft form factor $\xi_{\parallel}(q^2)$ (see Sec. 6.6.7).

The non-factorisable terms, on the other hand, account for the diagrams that constitute a source of new NLO strong-interaction contributions to the decay amplitude, i.e. those that are not just perturbative corrections to previously computed topologies. These are the hard-scattering diagrams in Fig. 6.8 and maybe some of the vertex corrections to weak annihilation Fig. 6.9 that, for some reason, could be enhanced and contribute at LO in Λ_{QCD}/m_b (but these have been neglected by physical and numerical arguments as explained just above Fig. 6.9). These hard-spectator scattering processes enter then as new contributions to the second term of Eqs. (6.150)–(6.149) as follows:

- The hard amplitudes $T_a^{(\text{nf},t)}$ were obtained in [32] by computing the matrix elements of the four-quark operators in Fig. 6.8(a,b). The result was projected on meson LCDAs and the LO term in Λ_{QCD}/m_b was kept and expanded in powers of the spectator quark momentum. Only the terms arising from the gluon propagator connecting with the spectator line or from the spectator quark propagator when it emits a γ^* were compatible with power counting, contributing to Eqs. (23) – (26) in [32]. On the other hand, the non-factorisable hard-scattering amplitudes $T_{a,\pm}^{(1,u)}$ are given in appendix A.2 of [77].
- The $\mathcal{C}_a^{(\text{nf},t)}$ contributions collected in Eqs. (37) – (38) of [32] require the calculation two loop diagrams with several different mass scales. Since most of these were not yet computed when [32] was published, only the diagrams involving \mathcal{O}_1 , \mathcal{O}_2 and \mathcal{O}_8 (those that correspond to the larger Wilson coefficients at the $\mu = m_b$ scale) were included in the formulae of [32]. Therefore, the operators involving QCD penguins were neglected, which should be a good approximation given to the smallness of C_{3-6} (see Tab. 6.1). A very important remark must be done here regarding $\mathcal{C}_a^{(\text{nf},u)}$: the prescription $F_{1,2}^{(7,9)} \rightarrow F_{1,2}^{(7,9)} + F_{1,2,u}^{(7,9)}$ in [77] is wrong and should read $F_{1,2}^{(7,9)} \rightarrow F_{1,2}^{(7,9)} - F_{1,2,u}^{(7,9)}$ instead. This is due to an overall minus sign difference between Eq. (16) of [126] (used in [32]) and Eq. (16) of [125] (used in [77]).

Eqs. (6.149)–(6.150) can be rewritten using the numerical value of C_F , Eq. (6.147) and the

definitions^{9, 10}

$$\lambda_{B,+}^{-1} \equiv \int_0^\infty \frac{d\omega}{\omega} \Phi_{B,+}(\omega), \quad \lambda_{B,-}^{-1} \equiv \int_0^\infty d\omega \frac{m_B}{m_B \omega - q^2 - i\epsilon} \Phi_{B,-}(\omega), \quad (6.156)$$

$$\kappa_a \equiv \frac{\pi^2 f_B f_{K^*,a}}{N_c m_B}, \quad (6.157)$$

$$\hat{T}_{\parallel,-}^{(0;\text{nf},i)}(u) \equiv \frac{m_B \omega - q^2 - i\epsilon}{m_B \omega} T_{\parallel,-}^{(0;\text{nf},i)}(u, \omega), \quad (6.158)$$

obtaining the simplified general expressions for $i = t, u$:

$$\mathcal{T}_\perp^{(i)}(q^2) = \mathcal{C}_\perp^{(0,i)} \xi_\perp(q^2) + \frac{\alpha_s}{3\pi} \left[\mathcal{C}_\perp^{(1,i)} \xi_\perp(q^2) + \kappa_\perp(\mu_h) \lambda_{B,+}^{-1} \int_0^1 du \Phi_{K^*,\perp}(u) \left(T_{\perp,+}^{(f,i)}(u) + T_{\perp,+}^{(\text{nf},i)}(u) \right) \right] \quad (6.159)$$

and

$$\begin{aligned} \mathcal{T}_\parallel^{(i)}(q^2) = & \left(\mathcal{C}_\parallel^{(0,i)} \xi_\parallel(q^2) + \kappa_\parallel \frac{m_{K^*}}{E_{K^*}} \lambda_{B,-}^{-1}(q^2) \int_0^1 du \Phi_{K^*,\parallel}(u) \hat{T}_{\parallel,-}^{(0,i)}(u) \right) \\ & + \frac{\alpha_s}{3\pi} \left\{ \mathcal{C}_\parallel^{(1,i)} \xi_\parallel(q^2) + \kappa_\parallel \frac{m_{K^*}}{E_{K^*}} \left[\lambda_{B,+}^{-1} \int_0^1 du \Phi_{K^*,\parallel}(u) \left(T_{\parallel,+}^{(f,i)}(u) + T_{\parallel,+}^{(\text{nf},i)}(u) \right) \right. \right. \\ & \left. \left. + \lambda_{B,-}^{-1}(q^2) \int_0^1 du \Phi_{K^*,\parallel}(u) \hat{T}_{\parallel,-}^{(\text{nf},i)}(u) \right] \right\}. \quad (6.160) \end{aligned}$$

Eqs. (6.159)–(6.159) generalise Eqs. (4.7)–(4.8) of [8], as they also account for the CKM-suppressed "(u)" terms of the $b \rightarrow s\ell^+\ell^-$ WEH and do not depend on the parametrisation of $\xi_{\perp,\parallel}(q^2)$ given in Eq. (47) of [32]. The separation between LO and NLO corrections is also clearly manifested in them. Note that all the terms in Eqs. (6.159)–(6.159) do appear for the "(t)" part of the WEH but some of them will become 0 when dealing with its "(u)" part (for instance, $T_{a,\pm}^{(f,i)} = 0$).

One final important remark must be done here: in this analysis, the Wilson coefficients must be evaluated at the scale μ_b (as the running of four-quark operators ends at this scale) as well as

⁹Note that the notation of the B meson LCDAs does not coincide with Eqs. (2.18)–(2.19). The reason for this discrepancy is twofold: in the first place, formulae in Sec. 2.2.3 were given in terms of the spectator quark momentum fraction, while here ω represents its full momentum. Besides, in Sec. 2.2.3 it was assumed that the spectator quark transverse momentum could be neglected, whereas in the general case this approximation is not justified and the light-cone matrix element should be decomposed according to Eq. (101) in [31]. Therefore, Φ_{B_1} equals $\Phi_{B,+}$ (and hence λ_B^{-1} in Eq. (2.20) is equivalent to λ_B^{-1} in Eq. (6.156) as stated in [32]), but Φ_{B_2} does not correspond to $\Phi_{B,-}$. $\lambda_{B,-}^{-1}(q^2)$ is modeled according to Eq. (54) of [32]. The interested reader should refer first to [127] and afterwards to [31] and [35] for a complete B meson matrix element calculation in the light-cone.

¹⁰In fact, $T_{\parallel,-}^{(0,i)}(u, \omega)$ and $T_{\parallel,-}^{(\text{nf},i)}(u, \omega)$ are the only hard amplitudes T that depend on ω [32, 77].

the strong coupling constant multiplying the hard-vertex functions $C_a^{(i)}$ at NLO, but α_s should be evaluated at $\mu_h \simeq (m_b \Lambda_{\text{QCD}})^{1/2}$ when it appears in front of the $T_{a,\pm}^{(1,i)}$ amplitudes, as the gluons exchanged in hard-scattering processes are assumed to possess virtualities of $O(m_b \Lambda_{\text{QCD}})$ (as explained in Sec. 4.4).

6.6.5 The inclusion of power-suppressed corrections to $\mathcal{T}_{\perp,\parallel}^{(i)}(q^2)$

In [32] the authors were concerned about the possibility of power-suppressed corrections to $\mathcal{T}_{\perp}^{(t)}(q^2)$ (i.e. those of $O(1)$ in an α_s expansion but of $O(\Lambda_{\text{QCD}}/m_b)$) that they were neglecting might be enhanced and become numerically important, so they were computed in [77] and labeled $\Delta\mathcal{T}_{\perp}^{(i)}$.

Weak annihilation

The power-suppressed contributions to weak-annihilation terms at order α_s^0 are given by [77]

$$\begin{aligned} \Delta\mathcal{T}_{\perp}^{(t)}\Big|_{\text{ann}} &= -e_q \frac{4\kappa_{\perp}(\mu_h)}{m_b} \left(C_3 + \frac{4}{3}(C_4 + 3C_5 + 4C_6) \right) \int_0^1 du \frac{\Phi_{K^*,\perp}(u)}{(1-u) + u\hat{s}} \\ &\quad + e_q \frac{2\kappa_{\parallel}}{m_b} \frac{m_{K^*}}{(1-\hat{s})\lambda_{B,+}} \left(C_3 + \frac{4}{3}(C_4 + 12C_5 + 16C_6) \right), \end{aligned} \quad (6.161)$$

$$\Delta\mathcal{T}_{\perp}^{(u)}\Big|_{\text{ann}} = 0 \quad (6.162)$$

where, as before, $\hat{s} = q^2/m_B^2$.

Hard spectator scattering

As the hard-spectator scattering contribution appears for the first time at $O(\alpha_s)$, the corresponding power suppressed contribution calculated in [77] will be of $O(\alpha_s \Lambda_{\text{QCD}}/m_b)$

$$\begin{aligned} \Delta\mathcal{T}_{\perp}^{(t)}\Big|_{\text{hss}} &= e_q \frac{\alpha_s}{3\pi} \frac{1}{m_b} \left\{ 12 C_8^{\text{eff}} \frac{m_b}{m_B} \kappa_{\perp}(\mu_h) X_{\perp}(\hat{s}) \right. \\ &\quad + 8 \kappa_{\perp}(\mu_h) \int_0^1 du \frac{\Phi_{K^*,\perp}(u)}{(1-u) + u\hat{s}} F_{K^*}^{(t)} [(1-u)m_B^2 + uq^2] \\ &\quad \left. - \frac{4m_{K^*} \kappa_{\parallel}}{(1-\hat{s})\lambda_{B,+}} \int_0^1 du \int_0^u dv \frac{\Phi_{K^*,\parallel}(v)}{1-v} F_{K^*}^{(t)} [(1-u)m_B^2 + uq^2] \right\}, \end{aligned} \quad (6.163)$$

where [128]

$$X_{\perp}(\hat{s}) = \frac{1}{3} \left[\int_0^1 du \frac{\Phi_{K^*,\perp}(u)}{1-u+u\hat{s}} + \int_0^1 du \frac{\Phi_{K^*,\perp}(u)}{(1-u+u\hat{s})^2} \right], \quad (6.164)$$

and the quark-loop function is given by

$$F_{K^*}^{(t)}(x) = \frac{3}{4} \left[h(x, m_c) \left(-\frac{1}{6}C_1 + C_2 + C_4 + 10C_6 \right) + h(x, m_b) \left(C_3 + \frac{5}{6}C_4 + 16C_5 + \frac{22}{3}C_6 \right) + h(x, 0) \left(C_3 + \frac{17}{6}C_4 + 16C_5 + \frac{82}{3}C_6 \right) - \frac{8}{27} \left(-\frac{15}{2}C_4 + 12C_5 - 32C_6 \right) \right]. \quad (6.165)$$

For $q^2 = 0$, the integral $X_{\perp}(\hat{s})$ suffers from a logarithmic endpoint singularity as $u \rightarrow 1$, but since our region of interest is $1 \text{ GeV}^2 \leq q^2 \leq 6 \text{ GeV}^2$ this has no consequences to $\bar{B}_d \rightarrow \bar{K}^{*0} \ell^+ \ell^-$.

The corresponding expression for $\Delta \mathcal{T}_{\perp}^{(u)} \Big|_{\text{hss}}$ reads [77]

$$\Delta \mathcal{T}_{\perp}^{(u)} \Big|_{\text{hss}} = e_q \frac{\alpha_s}{3\pi} \frac{1}{m_b} \left\{ 8 \kappa_{\perp}(\mu_h) \int_0^1 du \frac{\Phi_{K^*,\perp}(u)}{(1-u) + u\hat{s}} F_{K^*}^{(u)} [(1-u)m_B^2 + uq^2] - \frac{4m_{K^*} \kappa_{\parallel}}{(1-\hat{s}) \lambda_{B,+}} \int_0^1 du \int_0^u dv \frac{\Phi_{K^*,\parallel}(v)}{1-v} F_{K^*}^{(u)} [(1-u)m_B^2 + uq^2] \right\}, \quad (6.166)$$

with

$$F_{K^*}^{(u)}(s) = \frac{3}{4} \left(C_2 - \frac{1}{6}C_1 \right) [h(s, m_c) - h(s, 0)]. \quad (6.167)$$

6.6.6 Final expressions for $\mathcal{T}_{\perp,\parallel}^{(i)}(q^2)$ including power-suppressed corrections

For $\mathcal{T}_{\perp}^{(i)}(q^2)$

Collecting Eqs. (6.159), (6.161), (6.162) as well as (6.163) and (6.166) one arrives to:

$$\mathcal{T}_{\perp}^{(t),\text{full}} = \mathcal{T}_{\perp}^{(t)} + \Delta \mathcal{T}_{\perp}^{(t)} \Big|_{\text{ann}} + \Delta \mathcal{T}_{\perp}^{(t)} \Big|_{\text{hss}}, \quad (6.168)$$

$$\mathcal{T}_{\perp}^{(u),\text{full}} = \mathcal{T}_{\perp}^{(u)} + \Delta \mathcal{T}_{\perp}^{(u)} \Big|_{\text{hss}}, \quad (6.169)$$

which, according to the structure of the $b \rightarrow s \ell^+ \ell^+$ WEH in Eq. (6.1) can be further combined to obtain

$$\mathcal{T}_{\perp}^{(t),\text{full}} + \hat{\lambda}_u^{(s)} \mathcal{T}_{\perp}^{(u),\text{full}}. \quad (6.170)$$

For $\mathcal{T}_{\parallel}^{(i)}(q^2)$

As there are no power-suppressed terms contributing to $\mathcal{T}_{\parallel}^{(i)}(q^2)$ we can combine them directly into

$$\mathcal{T}_{\perp}^{(t)} + \hat{\lambda}_u^{(s)} \mathcal{T}_{\perp}^{(u)}. \quad (6.171)$$

6.6.7 Final considerations

Implications of choosing a soft form factor definition

When it comes to form factors, a renormalisation convention must be chosen by defining some relations that will hold to all others in perturbation theory, i.e. they will not receive any $O(\alpha_s)$ correction [31]. These conventions changed from [31, 32] to [77] and nowadays most groups are using the latter convention [10, 113, 99, 114, 123, 119]. However, since the $O(\alpha_s)$ corrections to the full form factors calculated within the combined HQET/LEET formalism rely on this choice, this also affects the layout of some functions in Eq. (6.135). In particular

- choosing [31, 32]

$$\left. \begin{aligned} \xi_{\perp}(q^2) &\equiv \frac{m_B}{m_B+m_{K^*}} V(q^2) \\ \xi_{\parallel}(q^2) &\equiv \frac{m_{K^*}}{E_{K^*}} A_0 \end{aligned} \right\} \Rightarrow \begin{cases} C_{\parallel}^{(f,t)} = -C_7^{\text{eff}} \left(4 \ln \frac{m_b^2}{\mu^2} - 6 - 4L \right) + \frac{m_B}{m_b} Y^{(t)}(q^2) (1-L) , \\ T_{\parallel,+}^{(f,t)}(u, \omega) = \left[C_7^{\text{eff}} + \frac{q^2}{2m_b m_B} Y^{(t)}(q^2) \right] \frac{2m_B^2}{(1-u)E_{K^*}^2} , \end{cases}$$

- whereas choosing [77]

$$\left. \begin{aligned} \xi_{\perp}(q^2) &\equiv \frac{m_B}{m_B+m_{K^*}} V(q^2) \\ \xi_{\parallel}(q^2) &\equiv \frac{m_B+m_{K^*}}{2E_{K^*}} A_1(q^2) - \frac{m_B-m_{K^*}}{m_B} A_2(q^2) \end{aligned} \right\} \Rightarrow \begin{cases} C_{\parallel}^{(f,t)} = -C_7^{\text{eff}} \left(\ln \frac{m_b^2}{\mu^2} + 2L + \Delta M \right) , \\ T_{\parallel,+}^{(f,t)}(u, \omega) = C_7^{\text{eff}} \frac{4m_B}{(1-u)E_{K^*}} , \end{cases}$$

The b quark mass

In [32] there is a trading of the m_b mass from one scheme to the other. This might result a bit awkward to the reader used to the "standard" $\overline{\text{MS}}$ scheme, so we will try to review briefly and motivate what are the b quark masses used in [32] and the reasons that motivate going from one to the other.

The bare mass m_0 by itself cannot be observed. To calculate observable quantities at a scale $\mu \ll M_0$ it is convenient to relate m_0 to some mass parameter relevant to the scale μ , so that after integrating out momentum scales above μ we are left with $m(\mu)$, which is the parameter that enters the effective Hamiltonian. The free quark propagator then reads

$$G(p) = \frac{1}{m_b(\mu) - \not{p}} \quad (6.172)$$

which obviously has a pole at $p^2 = m_b^2(\mu)$ and therefore describes a particle with mass $m_b^2(\mu)$. However, when one accounts for gluon exchanges at $O(\alpha_s)$ the pole moves to $p^2 \simeq [m_b(\mu) + (4\alpha_s/3)\mu]^2$ so now the particle has a mass $m_b^{(1)} \simeq m_b(\mu) + (4\alpha_s/3)\mu$, and so on so forth as one considers higher orders in perturbation theory. Therefore, the "pole" mass m_b^{pole} , which is

of paramount importance to HQET (upon which relies the QCdf framework), is a theoretical construction that is well defined only up to the order considered in perturbation theory. The problems arise in the long distance (i.e. non-perturbative) regime: as the distance R from a static source of colour grows, the energy stored in the chromodynamic field that must be added to the bare mass of the heavy particle to determine the "physical" mass (bare mass + QCD corrections) decays as $1/R$ but grows exponentially with α_s due to confinement. The definition of "pole" mass amounts to setting $R \rightarrow \infty$, but this is not possible as colour interaction becomes non-perturbative already at $R_0 \sim 1/\Lambda_{\text{QCD}}$. Therefore, when the m_b^{pole} is used one must account for non-perturbative effects that can make the Wilson coefficients ill-defined theoretically and poorly convergent numerically [129].

To solve this problem it is clear that $m_b(\mu)$ should be used everywhere instead of m_b^{pole} [130], but then a renormalisation scheme is needed to avoid any ambiguity in the numerical value of $m_b(\mu)$. The most popular one is the $\overline{\text{MS}}$ scheme and the masses calculated within this scheme are sometimes designed $\hat{m}_b(\mu)$. $\overline{\text{MS}}$ masses are not parameters in the effective Hamiltonian, but rather a certain combination of parameters which results very convenient in calculations that use dimensional regularisation. In the b quark $\hat{m}_b(\mu)$ is related to the perturbative pole mass by [32]

$$\hat{m}_b(\mu) = m_b^{\text{pole}} \left[1 + \frac{\alpha_s C_F}{4\pi} \left(3 \ln \frac{m_b^2}{\mu^2} - 4 \right) + O(\alpha_s^2) \right], \quad (6.173)$$

but, as we can see, it becomes rather meaningless at $\mu \ll m_b$ as the logarithm starts to diverge. For this reason, $\hat{m}_b(\mu)$ is not appropriate in HQET (and hence neither in QCdf), where the possibility to evolving down to scale $\mu \simeq (m_b \Lambda_{\text{QCD}})^{1/2}$ or lower is crucial. Therefore, another scheme is needed.

In [131] the *potential subtraction* (PS) scheme was introduced. After observing that the heavy quark potential in the momentum space was better behaved than in coordinate space, and knowing that the long distance contribution of $O(\Lambda_{\text{QCD}} r)$ to the potential in coordinate space enters only through the Fourier transform, this Fourier transform was restricted to $|\vec{q}| > \mu_h$ for some scale μ_h satisfying $\Lambda_{\text{QCD}} < \mu_h < m_b v$ (where v is the b quark velocity). This defined a subtracted potential from which large perturbative corrections were eliminated and, using the Schrödinger equation one could obtain a residual mass term $\delta m(\mu_h)$, so that a *potential-subtracted* quark mass $m_{b,\text{PS}} = m_b^{\text{pole}} - \delta m(\mu_h)$ could be defined. The crucial observation was that this $\delta m(\mu_h)$ cancelled the leading long-distance sensitivity of m_b^{pole} to all orders in perturbation theory. This is the reason of using $m_{b,\text{PS}}$ in [32, 77]. The relation between $m_{b,\text{PS}}$ and $\overline{m}_b \equiv \hat{m}_b(\hat{m}_b)$ was found to be (Eq. (25) in [131])

$$m_{b,\text{PS}} = \overline{m}_b \left[1 + \frac{4\alpha_s(\overline{m}_b)}{3\pi} \left(1 - \frac{\mu_h}{\overline{m}_b} \right) + O(\alpha_s^2) \right], \quad (6.174)$$

while the relation between $m_{b,\text{PS}}$ and m_b^{pole} at $O(\alpha_s)$ is even simpler

$$m_{b,\text{PS}} \simeq m_b^{\text{pole}} - \frac{4\alpha_s(\mu)}{3\pi} \mu_h. \quad (6.175)$$

Unless stated otherwise, m_b is to be understood as $m_{b,PS}$ everywhere in this section.

Cancellation of scale- and scheme-dependence in $\mathcal{T}_{\perp,\parallel}(q^2)$

It has been stated that both $C_{\parallel,\perp}$ and $T_{\parallel,\perp,\pm}(u,\omega)$ depend on m_b and m_c the quark masses and on the renormalization scale μ . Then, the non-perturbative amplitudes $\mathcal{T}_{\parallel}(q^2)$ and $\mathcal{T}_{\perp}(q^2)$ constructed with should not be physical quantities unless the photon is on-shell, i.e. for $B \rightarrow K^*\gamma$. However, it can be proved that this scheme- and scale-dependence cancels almost completely, up to next-to-leading order in α_s , when $\mathcal{T}_{\parallel}(q^2)$ and $\mathcal{T}_{\perp}(q^2)$ are multiplied by m_b . The uncanceled $O(\alpha_s)$ terms are those proportional only to the small Wilson coefficients of the QCD penguin operators and weak annihilation topologies that were previously neglected [32].

6.7 Including the $O(\alpha_s)$ corrections from QCDf into the transversity amplitudes

Inspecting the formulae on the previous section one readily realises that the only Wilson coefficient included in these equations that also appears as a "free" coefficient in the matrix element of the $\bar{B}_d \rightarrow \bar{K}^{*0}\ell^+\ell^-$ decay in the SM (this is, setting $C_S^{(l)}$, $C_{PS}^{(l)}$, C_T , $C_{PT} = 0$ in Eq. (6.41)) is C_7^{eff} . In particular, it can be shown with just a bit of algebra, that when the function $Y^{(t)}(q^2)$ is taken away from C_9^{eff} and moved next to C_7^{eff} , then one can perform the replacements [8, 9]¹¹

$$C_9^{\text{eff}} \rightarrow C_9, \quad (C_7^{\text{eff}} + C_7^{\text{eff}'})T_i \rightarrow \mathcal{T}_{i,P}^{(t)} \quad \text{and} \quad (C_7^{\text{eff}} - C_7^{\text{eff}'})T_i \rightarrow \mathcal{T}_{i,M}^{(t)} \quad (i = 1, 2, 3) \quad (6.176)$$

and, following Eqs. (6.132)–(6.134), perform the substitutions

$$\mathcal{T}_1^{(t)} = \mathcal{T}_{\perp}^{(t)}, \quad \mathcal{T}_2^{(t)} = \frac{2E_{K^*}}{m_B}\mathcal{T}_{\perp}^{(t)}, \quad \mathcal{T}_3^{(t)} = \mathcal{T}_{\perp}^{(t)} + \mathcal{T}_{\parallel}^{(t)}. \quad (6.177)$$

The process followed to include the CKM-suppressed terms "u" is even simpler, as these terms does not depend on any explicit Wilson coefficient in Eq. (6.41) and can be embedded directly into the matrix element of Eq. (6.41).

Finally, when all these changes have been properly implemented, Eqs. (6.170)–(6.171) may be substituted into the transversity amplitudes in Eqs. (6.93)–(6.97) to obtain

$$A_{\perp}^{L,R} = \sqrt{2}\lambda^{1/2} \left\{ \left[(C_9^{\text{eff}} + C_9^{\text{eff}'}) \mp (C_{10} + C_{10}') \right] \frac{V(q^2)}{m_B + m_{K^*}} + \frac{2m_b}{q^2} \left(\mathcal{T}_{\perp,P}^{(t), \text{full}} + \hat{\lambda}_u^{(s)} \mathcal{T}_{\perp}^{(u), \text{full}} \right) \right\}, \quad (6.178)$$

¹¹There is no formal problem in embedding $C_7^{\text{eff}'}$ into the definition of the \mathcal{T}_i 's as the Wilson coefficients contain the short distance effects with virtualities above $\mu = m_b$, whereas QCDf deals with the perturbative and non-perturbative long distance effects contained in the matrix elements of the WEH operators. As \mathcal{O}_7 and \mathcal{O}_7' matrix elements are indeed related (up to chiralities leading to relative signs), they involve the same kind of hadronic effects, and these can be computed within the QCDF framework.

$$A_{\parallel}^{L,R} = -\sqrt{2} (m_B^2 - m_{K^*}^2) \left\{ \left[(C_9^{\text{eff}} - C_9^{\text{eff}'}) \mp (C_{10} - C'_{10}) \right] \frac{A_1(q^2)}{m_B - m_{K^*}} + \frac{2m_b}{q^2} \left[\frac{2E_{K^*}}{m_B} \left(\mathcal{T}_{\perp,M}^{(t),\text{full}} + \hat{\lambda}_u^{(s)} \mathcal{T}_{\perp}^{(u),\text{full}} \right) \right] \right\}, \quad (6.179)$$

$$A_0^{L,R} = -\frac{1}{2m_{K^*}\sqrt{q^2}} \left\{ \left[(C_9^{\text{eff}} - C_9^{\text{eff}'}) \mp (C_{10} - C'_{10}) \right] \times \left[(m_B^2 - m_{K^*}^2 - q^2)(m_B + m_{K^*})A_1(q^2) - \lambda \frac{A_2(q^2)}{m_B + m_{K^*}} \right] + 2m_b \left[\left((m_B^2 + 3m_{K^*}^2 - q^2) \frac{2E_{K^*}}{m_B} - \frac{\lambda}{m_B^2 - m_{K^*}^2} \right) \left(\mathcal{T}_{\perp,M}^{(t),\text{full}} + \hat{\lambda}_u^{(s)} \mathcal{T}_{\perp}^{(u),\text{full}} \right) - \frac{\lambda}{m_B^2 - m_{K^*}^2} \left(\mathcal{T}_{\parallel,M}^{(t)} + \hat{\lambda}_u^{(s)} \mathcal{T}_{\parallel}^{(u)} \right) \right] \right\}, \quad (6.180)$$

$$A_t = \frac{1}{\sqrt{q^2}} \lambda^{1/2} \left[2(C_{10} - C'_{10}) + \frac{q^2}{m_{\mu}} (C_{PS} - C'_{PS}) \right] A_0(q^2), \quad (6.181)$$

$$A_S = -2\lambda^{1/2} (C_S - C'_S) A_0(q^2). \quad (6.182)$$

Eqs. (6.178)–(6.182) should be the final step if it not were for the fact that they contain $O(m_{K^*}^2/m_B^2)$ terms, which should be neglected to have a formalism fully consistent with QCDf. Fortunately, these transversity amplitudes can be simplified straightforwardly into

$$A_{\perp}^{L,R} \simeq \sqrt{2} (m_B^2 - q^2) \left\{ \left[(C_9^{\text{eff}} + C_9^{\text{eff}'}) \mp (C_{10} + C'_{10}) \right] \frac{V(q^2)}{m_B} + \frac{2m_b}{q^2} \left(\mathcal{T}_{\perp,P}^{(t),\text{full}} + \hat{\lambda}_u^{(s)} \mathcal{T}_{\perp}^{(u),\text{full}} \right) \right\}, \quad (6.183)$$

$$A_{\parallel}^{L,R} \simeq -\sqrt{2} \left\{ \left[(C_9^{\text{eff}} - C_9^{\text{eff}'}) \mp (C_{10} - C'_{10}) \right] (m_B + m_{K^*}) A_1(q^2) + \frac{2m_b}{q^2} \left[(m_B^2 - q^2) \left(\mathcal{T}_{\perp,M}^{(t),\text{full}} + \hat{\lambda}_u^{(s)} \mathcal{T}_{\perp}^{(u),\text{full}} \right) \right] \right\}, \quad (6.184)$$

$$A_0^{L,R} \simeq -\frac{m_B^2 - q^2}{2\sqrt{q^2}} \left\{ \left[(C_9^{\text{eff}} - C_9^{\text{eff}'}) \mp (C_{10} - C'_{10}) \right] \left[\left(1 + \frac{m_B}{m_{K^*}} \right) A_1(q^2) - \frac{m_B}{m_{K^*}} \left(1 - \frac{q^2}{m_B^2} \right) A_2(q^2) \right] - \frac{2m_b}{m_{K^*}} \left(1 - \frac{q^2}{m_B^2} \right) \left(\mathcal{T}_{\parallel,M}^{(t)} + \hat{\lambda}_u^{(s)} \mathcal{T}_{\parallel}^{(u)} \right) \right\}, \quad (6.185)$$

$$A_t \simeq \frac{1}{\sqrt{q^2}} (m_B^2 - q^2) \left[2(C_{10} - C'_{10}) + \frac{q^2}{m_\mu} (C_{PS} - C'_{PS}) \right] A_0(q^2), \quad (6.186)$$

$$A_S \simeq -2(m_B^2 - q^2)(C_S - C'_S) A_0(q^2), \quad (6.187)$$

Arrived to this point the inclusion of next-to-leading corrections into the transversity amplitudes is almost done but not yet completely. The form factors appearing explicitly in Eqs. (6.183)–(6.187) should also be expressed as linear combinations of $\xi_\perp(q^2)$ and $\xi_\parallel(q^2)$ and include $O(\alpha_s)$ corrections to them in order to achieve consistency with the QCDf framework used so far. Using the definitions [31]

$$V(q^2) \equiv \frac{m_B + m_{K^*}}{m_B} \xi_\perp(q^2), \quad A_0(q^2) \equiv \frac{E_{K^*}}{m_{K^*}} \xi_\parallel(q^2), \quad (6.188)$$

one obtains, from Eqs. (32)–(33) and Eqs. (59)–(60) in [31]:

$$A_1(q^2) = \frac{2E_{K^*}}{m_B + m_{K^*}} \xi_\perp(q^2), \quad (6.189)$$

$$A_2(q^2) = \frac{m_B}{m_B - m_{K^*}} (\xi_\perp(q^2) - \xi_\parallel(q^2)) \quad (6.190)$$

$$+ \frac{\alpha_s}{3\pi} \frac{2m_B}{m_B - m_{K^*}} \left[(1 - L) \xi_\parallel(q^2) + \frac{m_{K^*} m_B (m_B - 2E_{K^*})}{E_{K^*}^2} \kappa_\parallel \lambda_{B,+}^{-1} \int_0^1 du \frac{\Phi_{K^*,\parallel}(u)}{1 - u} \right].$$

where L was defined in Eq. (6.154) and the leading and next-to-leading order α_s contributions have been collected separately.

6.7.1 Comparison with other approaches

We have used the method described in this chapter to build observables that could explore the possible presence of NP in the $\bar{B}_d \rightarrow \bar{K}^{*0} \ell^+ \ell^-$ decay mode [45, 46, 99, 119] (see a short review of all these works in the Epilogue). Our point of view is that, as in the combined HQET/LEET formalism at LO *all* transversity amplitudes can be related to just the two universal form factors $\xi_\perp(q^2)$ and $\xi_\parallel(q^2)$ (see Eqs. (6.98)–(6.102)), constructing these observables as quotients where this soft form factor dependence cancels at LO would make them quite insensitive to the form factors calculated from LCSR and all their drawbacks (see Sec. 6.3). The price to pay, however is having $O(\Lambda_{\text{QCD}}/m_b)$ corrections, allegedly small but of unknown size, arising from the combined HQET/LEET used to build the QCDf framework. Therefore these unknown $O(\Lambda_{\text{QCD}}/m_b)$ had to be included into our analysis in the most conservative way we can figure out, to make sure that if a non-SM-like signal is detected it is not due to spurious fluctuations from the SM predictions.

In [10] the approach was radically different: they relied completely in the LCSR calculation of $B \rightarrow K^*$ QCD full form factors described in Sec. 6.3 with some unspecified but small errors

attached to them¹² to obtain CP -conserving and CP -violating observables. Neither the LO topologies in Fig. 6.6(a,b) nor the factorisable hard-vertex corrections contributing to \mathcal{C}_a and T_a were taken into account in [10], as these terms only arise when expressing the seven independent QCD form factors as functions of $\xi_{\perp}(q^2)$ and $\xi_{\parallel}(q^2)$. Hence, these contributions were redundant there and were discarded. However, there are some corrections that could not be obtained from LCSRs and the authors had to resort to QCdf: these are the LO WA contribution $T_{\parallel,-}^{(0,t)}(u, \omega)$ which, as we have seen, is leading in both α_s and Λ_{QCD}/m_b and was kept, and the corresponding power-suppressed correction in Eq. (6.161) that was neglected. Besides, the non-factorisable contributions stemming from hard-spectator scattering phenomena in Fig. 6.8(a,b) had to be introduced in [10] too. However, it is not completely clear to the author if the power-suppressed corrections of Eqs. (6.163)–(6.166) were taken into account in [10]. This can be a somewhat tricky point as all weak annihilation and non-factorisable contributions depend on the charge of the spectator quark e_q . This quark has different signs in $\bar{B}_d \rightarrow \bar{K}^{*0} \ell^+ \ell^-$ and its CP -conjugated process, so it might have a large impact when one tries to construct observables sensitive to CP -violation, as these terms do not cancel but contribute twice. The observable itself, on the other hand, tends to be very small in the SM, since the only source of strong phases are the functions $h(q^2, m_q)$ in $Y^{(u,t)}(q^2)$ and the weak phases come from the CKM-suppressed element $\hat{\lambda}_u$.

In conclusion, we find the proposal in [10] very interesting from a theoretical point of view but we feel that, apart from the non-calculable $O(\Lambda_{\text{QCD}}/m_b)$ corrections that also enter their analysis through the two aforementioned QCdf contributions, the observables in [10] will be only really trustworthy when reliable lattice calculations of the full $B \rightarrow K^*$ form factors are published. Meanwhile, with the current lack of consensus regarding the errors associated to these form factors when computed using LCSRs (see Fig. 6.5), we feel we are being on the safe side using the complete QCdf machinery in the way explained above on observables with a much reduced sensitivity to soft form factors.

¹²This can be inferred from the narrow error bands in the SM observables plotted in Fig. 2 of [10]. Note that those error bands included not only the correlated errors between form factors which follow from the LCSRs, but also from all other sources of hadronic uncertainty (for instance from varying the renormalisation scale in the narrow $4.0 \text{ GeV} \leq \mu \leq 5.6 \text{ GeV}$ range).

Part III

Epilogue and conclusions

Chapter 7

Epilogue

7.1 Forerunners of this thesis

The exclusive decay mode $\bar{B}_d^0 \rightarrow \bar{K}^{*0}(\rightarrow K\pi)\ell^+\ell^-$ was suggested as an interesting testing ground for the Standard Model and its possible extensions a long time ago. Many of the relevant references have already been cited along the previous chapters of this work. It was not until the birth of QCDF that perturbative $O(\alpha_s)$ corrections could be included within a generalised factorisation approach, but as this framework relied heavily on the combined HQET/LEET approaches, only the $O(1)$ term in the Λ_{QCD}/m_b expansion could be included. As we have seen, the papers by Beneke and Feldmann [31, 32, 77] paved the way towards the possibility of building observables sensitive to certain types of NP in this decay channel.

The milestone in this process was [8]. In this work, QCDF was put at work and a number of new observables were proposed to study this decay mode. These were written in terms of the transversity amplitudes and they could be plotted including, for the first time, both factorisable and non-factorisable NLO strong interaction corrections. One of these observables (called $A_{\text{T}}^{(2)}$) was particularly well behaved, being almost 0 in the SM for a long dilepton invariant mass square range, and also very sensitive to possible right-handed currents contributing through the chirally-flipped effective operator \mathcal{O}'_7 . In [9] it was shown that, in the context of certain supersymmetric models with non-minimal flavour violation in the down-squark sector, the Wilson coefficient C'_7 corresponding to this operator could acquire relatively large values, leading to NP curves that could be easily distinguished from the SM curve (including error bands). Moreover, $A_{\text{T}}^{(2)}$, was independent of soft-form factors at LO in the large recoil limit, since it was built as a quotient and this dependence cancelled between numerator and denominator. The drawback, of course, was that the unknown $O(\Lambda_{\text{QCD}}/m_b)$ corrections, inherent to the QCDF calculations used to calculate the transversity amplitudes were present too, and they had to be accounted for somehow. In [9] they were estimated to give an extra 10% contribution above and below the central value of each transversity amplitude, i.e. $A_i = (1 \pm 0.1)A_i^{\text{central}}$ (with $i = \perp, \parallel$ as

only massless leptons were considered there). It was also assumed that this contribution was the same for L and R components because they had the same analytical structure (up to signs due to different chiralities).

7.2 Overview of the papers published

When I enrolled in the Master/PhD program we pursued the study of $\bar{B}_d^0 \rightarrow \bar{K}^{*0}(\rightarrow K\pi)\ell^+\ell^-$ in [45], aiming to build new observables that shared the same features of $A_T^{(2)}$, namely: being as free as possible from form factor-related hadronic uncertainties, i.e. they had to be quotients that could cancel the soft-form factor dependency at LO¹ in α_s , and display also good sensitivity to the NP right-handed currents induced by \mathcal{O}'_7 in [9], which were used as benchmark curves. Two new form factor independent (FFI) observables ($A_T^{(3)}$ and $A_T^{(4)}$) were built to explore the transversity amplitude A_0 , to which $A_T^{(2)}$ was not sensitive by construction. Also F_L (the longitudinal polarisation fraction of the \bar{K}^{*0}) and A_{FB} (the leptonic forward-backward asymmetry) were plotted from theoretical data with their corresponding error bars, which were wider as there is no cancellation of soft form factors at LO in them (so they will be called generically FFD). The differential decay distribution (DDD), already computed in [91, 8], was given as well as explicit equations for the uniaxial distributions in terms of these observables. On the other hand, we had to make sure that the proposed observables could really be extracted from the differential decay distribution, as it turned out that one of the observables proposed in [8] ($A_T^{(1)}$), although having the desired features explained just above, could not be measured experimentally. Three symmetries of the DDD² were identified, which allowed to understand why $A_T^{(1)}$ could not be observed and also contributed to the experimental part of the paper. There, our experimental colleagues from LHCb used these symmetries to get rid of some superfluous transversity amplitudes and parametrised the remaining ones by means of a 2nd order polynomial fit ansatz. With the number of free parameters reduced in this way, a toy Monte Carlo approach was performed to estimate the statistical uncertainty of the full set of observables at integrated luminosities of 10 fb^{-1} and 100 fb^{-1} (which could be reached if LHCb is upgraded in the future). These preliminary studies showed remarkable separations of possible NP scenarios between the experimental error band and the SM prediction, foreseeing high sensitivity to this kind of NP.

In [46] we concentrated on four different aspects of the $\bar{B}_d^0 \rightarrow \bar{K}^{*0}(\rightarrow K\pi)\mu^+\mu^-$ decay mode. On one side, the seed of DDD symmetries that was sown in [45] grew to a fruitful formalism that allowed us to count how many symmetries should be present in different scenarios, combining

¹The weak annihilation term $T_{\parallel,-}^{(0,t)}$ that also appears at LO is proportional to a linear combination of the small Wilson coefficients C_{3-6} at the $\mu \simeq m_b$ scale, so its contribution can be safely neglected in the heavy quark and large energy limits.

²When we refer to a symmetry of the DDD we are referring to an invariance of the DDD under a transformation in the space of the transversity amplitudes.

massive and massless leptons with the presence or absence of the new scalar contribution found in [10]. This could be done just by counting how many angular coefficients J_i had the angular distribution, how many transversity amplitudes appeared in them and how many dependencies were present between the J_i . The number of dependencies was obtained from the infinitesimal symmetries, which were built by taking the gradient of each J_i with respect to the spin amplitudes and then identifying the vector orthogonal to the hyperplane spanned by the set of gradient vectors. From the infinitesimal symmetry we had to identify the corresponding continuous symmetry, which enabled us to rewrite the transversity amplitudes transformed by these symmetries in terms of the angular coefficients. The consequence of this method was twofold: on the one hand it had an experimental impact improving the fit convergence and stability, while on the other hand allowed to build any observable as a combination of the transversity amplitudes (even though this combination might not appear explicitly in the angular observables J_i) and then check if this combination was allowed by the symmetries. A method to estimate statistically the $O(\Lambda_{\text{QCD}}/m_b)$ corrections was proposed in [46], as we felt that the magnitude of these contributions could be being overestimated by just adding them linearly to each amplitude; this method was adopted and used henceforward. We also examined the possibility of building FFI CP -violating observables that could be measured at LHCb, but the statistical uncertainty found using the toy Monte Carlo model developed earlier showed that, unless the CP -violating phases approached $\pm\pi/2$, LHCb could not resolve this kind of observables from a SM signal. Moreover, we showed the advantage of building FFI CP -violating observables in comparison to other observables proposed in [10] unprotected from form factor cancellation. Finally, we illustrated with several examples how the CP -conserving observables could separate different benchmark scenarios of NP and how powerful was the use of the large recoil expressions for the transversity amplitudes in Eqs. (6.98)–(6.102) to reproduce and explain the features characteristic of each of them.

In [46] we used the bounds in Figs. 2 and 3 of [114] to extract $\delta C_i^{(\prime)}$ values from regions permitted by several observables. This enabled us to draw the CP -conserving and CP -violating NP curves for the observables studied in a model independent way with some confidence. However, we felt that these bounds were not restrictive enough. Besides, the Wilson coefficients we were using were already quite outdated and required an update. As we were aware of a couple of works also aimed at constraining the values allowed for the Wilson coefficients [132, 133, 112], we decided to pursue this objective with a larger set of observables. Our objective in [99] was to distinguish excluded and allowed regions in the real Wilson coefficient parameter space (we did not allow complex Wilson coefficients in this work), in a systematic manner and using a well defined theoretical approach. Three scenarios were defined: in scenario A the main NP contributions were due to \mathcal{O}_7 and \mathcal{O}'_7 , in scenario B NP could also affect the SM operators \mathcal{O}_9 and \mathcal{O}_{10} , while scenario C could receive NP contributions from all the previous operators and also from \mathcal{O}'_9 and \mathcal{O}'_{10} . We also distinguished three classes of observables: those sensitive only to \mathcal{O}_7 and \mathcal{O}'_7 (class I, formed by $\mathcal{B}(\bar{B} \rightarrow X_s \gamma)$, $S_{K^* \gamma}$ and $A_I(B \rightarrow X_s \gamma)$), observables sensitive not only to \mathcal{O}_7 and \mathcal{O}'_7 but also to the semileptonic operators \mathcal{O}_9 and \mathcal{O}_{10} and their chirally-flipped counterparts

(\mathcal{O}'_9 and \mathcal{O}'_{10}) (class II, constituted by $A_T^{(2)}$), and observables sensitive to all the former effective operators and also to scalar and tensor contributions (class III, made up by $\mathcal{B}(\bar{B} \rightarrow X_s \mu^+ \mu^-)$ and the integrated versions of the already introduced A_{FB} and F_L). Restrictions to δC_{10} and $\delta C'_{10}$ were also imposed using the $\mathcal{B}(B_s \rightarrow \mu^+ \mu^-)$ bound at that time. Semi-analytic expressions for all these observables were given, including the SM central value with errors and all NP contributions to each observable parametrised in terms of the corresponding Wilson coefficients $\delta C'_i$. The theoretical calculations used to obtain the semi-analytical expression for each observable were summarised in the appendices. Observable classes allowed us to compute the allowed regions in the $\delta C_7 - \delta C'_7$, $\delta C_9 - \delta C_{10}$ and $\delta C'_9 - \delta C'_{10}$ planes we had chosen for that purpose, and this was performed for every scenario at both 1σ and 2σ . It should be pointed out here that the last experimental results presented at Moriond 2012 demanded a complete update of the figures in this paper and the conclusions deduced from them. This was one of the motivations behind the preprint of our latest paper released on July 2012 [120].

In [119] we deepened in the study of the DDD of the channel $\bar{B}_d^0 \rightarrow \bar{K}^{*0}(\rightarrow K\pi)\mu^+\mu^-$. From the number of continuous transformations that left the angular coefficients J_i invariant (deduced from the infinitesimal symmetries) and the number of transversity amplitudes, one could easily deduce the number of independent experimental observables that could be extracted from the angular analysis. As these observables constitute a complete set (i.e., each observable contains unique information about the DDD and any other observable one might figure out can be expressed as a combination of them), we called this set a *basis*. We found out that an optimal basis needs the maximum number possible of FFI observables but also some FFD observables and examined several scenarios. In the massless leptons case, 8 observables were needed, 6 of which were of the FFI type. We selected them with the idea of maximising their sensitivity to NP, so not only observables designed by ourselves were included, but also some proposed by other teams dealing with the same subject [114, 124]. When massive leptons were introduced, two new FFI observables were also needed, which were called M_1 and M_2 . Moreover, the possibility of NP contributions stemming from scalar and pseudoscalar operators was considered so two more FFI observables were required in this case (S_1 and S_2), which should obviously vanish if there were no such type of NP operators. We also expressed the observable basis as a function of the angular coefficients J_i and provided expressions for each uniaxial distribution in the three scenarios discussed (massless leptons, massive leptons and massive leptons with scalars). The sensitivity of each observable in the basis was explored using benchmark combinations of Wilson coefficients allowed by the analysis performed in [99] and by the latest bound from $\mathcal{B}(\bar{B} \rightarrow X_s \mu^+ \mu^-)$ aired in Moriond 2012 [134]. For the relevant observables, the position of their zeroes was given both analytically, using the large recoil expressions in appendix B, and numerically (from our calculations at NLO in QCDf). Finally, in appendix A, an update of the DDD symmetries was given following a bottom-up approach (i.e., going from the massless leptons approximation to the general situation in which massive leptons and scalar operators contributions were included). In this section, the original notation in [46] was changed first to

two-dimensional vectors made up of transversity amplitudes components to make the massive case easier to understand. Afterwards it was generalised to the four-dimensional vectors needed to obtain the symmetries in the extremely involved scenario with scalars.

Chapter 8

Conclusions and Outlook

It would not be fair to say that the $\bar{B}_d^0 \rightarrow \bar{K}^{*0}(\rightarrow K\pi)\mu^+\mu^-$ is the *golden channel* for the research of physics beyond the Standard Model as there are a lot of interesting rare decay modes of the D and B mesons where to look for NP, but the truth is that, over the last few years, this process has been attracting a growing attention onto it, mainly due to the large amount of information that can be collected from its full angular analysis and the possibility of tailor-making any observable one can imagine with maximal sensitivity to a particular kind of NP. Since [45], a lot of interesting papers have been published, each one tackling one or several aspects of this decay. The subsequent works by Bobeth *et al.* [114, 123], extending the analysis to the large dilepton mass or *low recoil* region (where QCDF cannot be used to compute NLO corrections) and Khodjamirian *et al.* [115], however, was a sign that the theoretical study of this decay mode was far from being complete.

The former were very welcome by the experimental community as, using the observables proposed in [45] and building new ones protected from soft form factors at LO, Bobeth *et al.* looked at a region never explored before with these kind of observables, and saved the experimentalists from having to throw large amounts of useful data. The weak point in [114, 123] was the lack of a formalism equivalent to QCDF that could account for $O(\alpha_s)$ and other kinds of corrections, but the recent release of [135] will amend this, providing a better control over hadronic uncertainties in the high- q^2 region. The latter paper, on the other hand, raised doubts about the commonly accepted opinion that below the $c\bar{c}$ threshold of $q^2 \ll 4m_c^2$ the effect of virtual charm loops is small enough to neglect it, and only near the $J/\Psi(1S)$ becomes important. Unfortunately, the results in [115] were not intended¹ to be implemented into the analysis at large recoil presented along this thesis, as the ΔC_9 presented in Table 2 are correlated and in [115] it was not attempted to quantify the correlations between the theoretical uncertainties of \mathcal{M}_i (with $i = 1, 2, 3$). Moreover, besides the soft gluon emission from the charm loop, which is likely to affect in a similar way part of the low recoil region that lies near the $\Psi(2S)$ resonance, there

¹From private correspondence with A. Khodjamirian.

are several nonlocal effects for $\bar{B}_d \rightarrow \bar{K}^{*0} \ell^+ \ell^-$ caused by four-quark, quark-penguin and \mathcal{O}_8 operators that might also affect the precision of the observables SM curves and their associated error bands [136, 137]. Finally, in [121, 138], tensor contributions arising from possible dimension six NP operators in the effective Hamiltonian were introduced and the combined effects of right-handed currents, scalar and tensor operators could be explored for the first time. Therefore, the message to keep in mind is that, even though the $\bar{B}_d^0 \rightarrow \bar{K}^{*0}(\rightarrow K\pi)\mu^+\mu^-$ decay mode is self-tagging and, although rare, it can be detected easily when produced experimentally, exclusive decay modes are always very difficult to control from a theoretical point of view. In particular, they involve many non-perturbative effects that might be very difficult to deal with and calculate and many theoreticians are struggling to keep these uncertainties under control [139, 140] or, at least, estimate them in a conservative way. We believe this is the only way of making sure that, if in the near future a signal deviating from the SM prediction is detected, this signal will probably correspond to NP.

On the other hand, many observables related to these decay mode are being measured nowadays. In addition to the "classic" FFD $\mathcal{B}(\bar{B}_d \rightarrow \bar{K}^{*0} \ell^+ \ell^-)$, A_{FB} and F_L [141, 142, 143], there is recent experimental data on some of the the new FFD observables proposed in [10] (see [2]) and also of the FFI observables $A_{\text{T}}^{(2)} \equiv P_1$ and $A_{\text{T}}^{(\text{im})} \equiv P_3$ [141]². All these experimental measurements, combined with the data from other inclusive and exclusive $b \rightarrow s$ channels and their corresponding theoretical predictions, allow for model-independent studies intended to constrain the effective short-distance couplings (i.e., the Wilson coefficients), which are known with precision in the SM and constitute the main objects of interest due to their sensitivity to NP contributions beyond the electroweak scale. Some interesting works in this direction have been published lately: the first one by ourselves [99] using a purely theoretical approach, whereas the latest approaches tend to perform fits using statistical tools, either from a frequentist [110, 111, 120] or from a bayesian point of view [144]. Performing this kind of statistical analysis might be the best option, as the results obtained in this way might be easier to interpret by the whole particle physics community: theoreticians and experimentalists.

At the moment of writing these lines (06/28/2012), the CERN call for a press conference scheduled on July the 4th about the status of Higgs searches has aroused particle physicists. Almost everybody expects a confirmation of the evidence (if not a discovery) of a Higgs-like boson with $m_H \simeq 125$ GeV. Now the question will be to which of the many theoretical models available this Higgs boson belongs to. Here, direct particle searches at the TeV scale might need to be complemented by the indirect searches performed in B and D decays to unravel the behaviour of Nature at this energy scale.

² P_3 may be obtained indirectly from the data on A_{im} and F_L , while $A_{\text{T}}^{(\text{re})} \equiv P_2$ can be accessed in the same fashion from A_{FB} and F_L . This may be deduced straightforwardly from Eqs.(22) – (23) in [119]

Bibliography

- [1] J. Beringer *et al.*, Phys. Rev. D **86** (2012) 010001.
- [2] T. Blake and N. Serra, LHCb-ANA-2011-089.
- [3] G. Buchalla, A. J. Buras and M. E. Lautenbacher, Rev. Mod. Phys. **68** (1996) 1125 [hep-ph/9512380].
- [4] M. Neubert, hep-ph/0512222.
- [5] A. Pich, hep-ph/9806303.
- [6] C. P. Burgess, Ann. Rev. Nucl. Part. Sci. **57** (2007) 329 [hep-th/0701053].
- [7] J. Virto, arXiv:0712.3367 [hep-ph].
- [8] F. Kruger and J. Matias, Phys. Rev. D **71** (2005) 094009 [hep-ph/0502060].
- [9] E. Lunghi and J. Matias, JHEP **0704** (2007) 058 [hep-ph/0612166].
- [10] W. Altmannshofer, P. Ball, A. Bharucha, A. J. Buras, D. M. Straub and M. Wick, JHEP **0901** (2009) 019 [arXiv:0811.1214 [hep-ph]].
- [11] M. Neubert, Phys. Rept. **245** (1994) 259 [hep-ph/9306320].
- [12] T. Mannel. *Effective Field Theories In Flavour Physics*. Springer Tracts in Modern Physics, n. 203. Springer, 2004.
- [13] G. Buchalla, hep-ph/0202092.
- [14] M. Neubert, hep-ph/0001334.
- [15] J. Charles, A. Le Yaouanc, L. Oliver, O. Pene and J. C. Raynal, Phys. Rev. D **60** (1999) 014001 [hep-ph/9812358].
- [16] H. Na, C. J. Monahan, C. T. H. Davies, R. Horgan, G. P. Lepage and J. Shigemitsu, Phys. Rev. D **86** (2012) 034506 [arXiv:1202.4914 [hep-lat]].

-
- [17] Z. Liu, S. Meinel, A. Hart, R. R. Horgan, E. H. Muller and M. Wingate, PoS LAT **2009** (2009) 242 [arXiv:0911.2370 [hep-lat]].
- [18] M. Della Morte, PoS ICHEP **2010** (2010) 364 [arXiv:1011.5974 [hep-lat]].
- [19] Z. Liu, S. Meinel, A. Hart, R. R. Horgan, E. H. Muller and M. Wingate, arXiv:1101.2726 [hep-ph].
- [20] G. P. Lepage and S. J. Brodsky, Phys. Rev. Lett. **43** (1979) 545 [Erratum-ibid. **43** (1979) 1625].
- [21] G. P. Lepage and S. J. Brodsky, Phys. Lett. B **87** (1979) 359.
- [22] G. P. Lepage and S. J. Brodsky, Phys. Rev. D **22** (1980) 2157.
- [23] D. Mueller, Phys. Rev. D **51** (1995) 3855 [hep-ph/9411338].
- [24] K. Passek-Kumericki, Springer Proc. Phys. **98** (2005) 399 [hep-ph/0407122].
- [25] M. E. Peskin and D. V. Schroeder. *An Introduction To Quantum Field Theory*. Frontiers in Physics. Westview Press, 1995.
- [26] S. J. Brodsky, In *Shifman, M. (ed.): At the frontier of particle physics*, vol. 2 1343-1444.
- [27] T. Gousset and B. Pire, In *Montauk 1994, Pulsed RF sources for linear colliders* 114-121.
- [28] V. M. Braun, In *Rostock 1997, Progress in heavy quark physics* 105-118 [hep-ph/9801222].
- [29] P. Colangelo and A. Khodjamirian, In *Shifman, M. (ed.): At the frontier of particle physics*, vol. 3 1495-1576 [hep-ph/0010175].
- [30] M. Beneke, G. Buchalla, M. Neubert and C. T. Sachrajda, Nucl. Phys. B **591** (2000) 313 [hep-ph/0006124].
- [31] M. Beneke and T. Feldmann, Nucl. Phys. B **592** (2001) 3 [hep-ph/0008255].
- [32] M. Beneke, T. Feldmann and D. Seidel, Nucl. Phys. B **612** (2001) 25 [hep-ph/0106067].
- [33] M. A. Shifman, A. I. Vainshtein and V. I. Zakharov, Nucl. Phys. B **147** (1979) 448.
- [34] E. de Rafael, hep-ph/9802448.
- [35] A. Khodjamirian, T. Mannel and N. Offen, Phys. Rev. D **75** (2007) 054013 [hep-ph/0611193].
- [36] B. V. Geshkenbein and M. S. Marinov, Sov. J. Nucl. Phys. **30** (1979) 726 [Yad. Fiz. **30** (1979) 1400].

-
- [37] P. Ball and R. Zwicky, Phys. Rev. D **71** (2005) 014029 [hep-ph/0412079].
- [38] I. I. Balitsky, V. M. Braun and A. V. Kolesnichenko, Nucl. Phys. B **312** (1989) 509.
- [39] V. M. Braun and I. E. Filyanov, Z. Phys. C **44** (1989) 157 [Sov. J. Nucl. Phys. **50** (1989) 511] [Yad. Fiz. **50** (1989) 818].
- [40] V. L. Chernyak and I. R. Zhitnitsky, Nucl. Phys. B **345** (1990) 137.
- [41] A. Khodjamirian, Eur. Phys. J. C **6** (1999) 477 [hep-ph/9712451].
- [42] S. W. Bosch, hep-ph/0208203.
- [43] P. Ball and R. Zwicky, Phys. Rev. D **71** (2005) 014015 [hep-ph/0406232].
- [44] P. Ball and V. M. Braun, Phys. Rev. D **58** (1998) 094016 [hep-ph/9805422].
- [45] U. Egede, T. Hurth, J. Matias, M. Ramon and W. Reece, JHEP **0811** (2008) 032 [arXiv:0807.2589 [hep-ph]].
- [46] U. Egede, T. Hurth, J. Matias, M. Ramon and W. Reece, JHEP **1010** (2010) 056 [arXiv:1005.0571 [hep-ph]].
- [47] A. Ali, P. Ball, L. T. Handoko and G. Hiller, Phys. Rev. D **61** (2000) 074024. [hep-ph/9910221].
- [48] M. Neubert and V. Rieckert, Nucl. Phys. B **382** (1992) 97.
- [49] N. Isgur and M. B. Wise, Phys. Lett. B **232** (1989) 113.
- [50] M. Neubert and B. Stech, Adv. Ser. Direct. High Energy Phys. **15** (1998) 294. [hep-ph/9705292].
- [51] I. Shipsey, Nat. Phys. **4** (2008) 06, 438.
- [52] G. Colangelo, S. Durr, A. Juttner, L. Lellouch, H. Leutwyler, V. Lubicz, S. Necco and C. T. Sachrajda *et al.*, Eur. Phys. J. C **71** (2011) 1695 [arXiv:1011.4408 [hep-lat]].
- [53] E. Gamiz *et al.* [HPQCD Collaboration], Phys. Rev. D **80** (2009) 014503 [arXiv:0902.1815 [hep-lat]].
- [54] A. Bazavov *et al.* [Fermilab Lattice and MILC Collaboration], Phys. Rev. D **85** (2012) 114506 [arXiv:1112.3051 [hep-lat]].
- [55] G. Bell, arXiv:0705.3133 [hep-ph].
- [56] M. Bauer, B. Stech and M. Wirbel, Z. Phys. C **34** (1987) 103.

- [57] M. J. Dugan and B. Grinstein, *Phys. Lett. B* **255** (1991) 583.
- [58] A. Datta and D. London, *Int. J. Mod. Phys. A* **19** (2004) 2505 [hep-ph/0303159].
- [59] A. J. Buras, J. M. Gerard and R. Ruckl, *Nucl. Phys. B* **268** (1986) 16.
- [60] J. D. Bjorken, *Nucl. Phys. Proc. Suppl.* **11** (1989) 325.
- [61] M. Neubert, *AIP Conf. Proc.* **602** (2001) 168 [*AIP Conf. Proc.* **618** (2002) 217] [hep-ph/0110093].
- [62] A. J. Buras and L. Silvestrini, *Nucl. Phys. B* **548** (1999) 293 [hep-ph/9806278].
- [63] H. -Y. Cheng, *Phys. Lett. B* **335** (1994) 428 [hep-ph/9406262].
- [64] A. Ali and C. Greub, *Phys. Rev. D* **57** (1998) 2996 [hep-ph/9707251].
- [65] H. -Y. Cheng and B. Tseng, *Phys. Rev. D* **58** (1998) 094005 [hep-ph/9803457].
- [66] A. Ali, G. Kramer and C. -D. Lu, *Phys. Rev. D* **58** (1998) 094009 [hep-ph/9804363].
- [67] J. Botts and G. F. Sterman, *Nucl. Phys. B* **325** (1989) 62.
- [68] H. -n. Li and G. F. Sterman, *Nucl. Phys. B* **381** (1992) 129.
- [69] C. -H. V. Chang and H. -n. Li, *Phys. Rev. D* **55** (1997) 5577 [hep-ph/9607214].
- [70] T. -W. Yeh and H. -n. Li, *Phys. Rev. D* **56** (1997) 1615 [hep-ph/9701233].
- [71] H. -Y. Cheng, H. -n. Li and K. -C. Yang, *Phys. Rev. D* **60** (1999) 094005 [hep-ph/9902239].
- [72] S. Descotes-Genon and C. T. Sachrajda, *Nucl. Phys. B* **625** (2002) 239 [hep-ph/0109260].
- [73] M. Beneke, G. Buchalla, M. Neubert and C. T. Sachrajda, *Phys. Rev. Lett.* **83** (1999) 1914 [hep-ph/9905312].
- [74] M. Beneke, G. Buchalla, M. Neubert and C. T. Sachrajda, *Nucl. Phys. B* **606** (2001) 245 [hep-ph/0104110].
- [75] M. Beneke and M. Neubert, *Nucl. Phys. B* **675** (2003) 333 [hep-ph/0308039].
- [76] S. W. Bosch and G. Buchalla, *Nucl. Phys. B* **621** (2002) 459 [hep-ph/0106081].
- [77] M. Beneke, T. .Feldmann and D. Seidel, *Eur. Phys. J. C* **41** (2005) 173 [hep-ph/0412400].
- [78] M. Neubert, *Nucl. Phys. Proc. Suppl.* **99B** (2001) 113 [hep-ph/0011064].
- [79] M. Bander, D. Silverman and A. Soni, *Phys. Rev. Lett.* **43** (1979) 242.

- [80] C. W. Bauer, D. Pirjol and I. W. Stewart, Phys. Rev. Lett. **87** (2001) 201806 [hep-ph/0107002].
- [81] M. Ciuchini, E. Franco, G. Martinelli and L. Silvestrini, Nucl. Phys. B **501** (1997) 271 [hep-ph/9703353].
- [82] M. Ciuchini, E. Franco, G. Martinelli, M. Pierini and L. Silvestrini, Phys. Lett. B **515** (2001) 33 [hep-ph/0104126].
- [83] C. W. Bauer, D. Pirjol, I. Z. Rothstein and I. W. Stewart, Phys. Rev. D **70** (2004) 054015 [hep-ph/0401188].
- [84] M. Beneke, G. Buchalla, M. Neubert and C. T. Sachrajda, Phys. Rev. D **72** (2005) 098501 [hep-ph/0411171].
- [85] M. Beneke, G. Buchalla, M. Neubert and C. T. Sachrajda, Eur. Phys. J. C **61** (2009) 439 [arXiv:0902.4446 [hep-ph]].
- [86] B. Grinstein, Y. Grossman, Z. Ligeti and D. Pirjol, Phys. Rev. D **71** (2005) 011504 [hep-ph/0412019].
- [87] L. M. Widhalm. *Studie des seltenen Zerfalls $K_L^0 \rightarrow \pi^0 \pi^\pm e^\mp \nu_e$ (Ke_4) am CERN Experiment NA48*. PhD. thesis. TU Wien, 2005.
- [88] N. Cabibbo and A. Maksymowicz, Phys. Rev. **137** (1965) B438 [Erratum-ibid. **168** (1968) 1926].
- [89] A. J. Buras and M. Munz, Phys. Rev. D **52** (1995) 186 [hep-ph/9501281].
- [90] M. Misiak, Nucl. Phys. B **393** (1993) 23 [Erratum-ibid. B **439** (1995) 461].
- [91] F. Kruger, L. M. Sehgal, N. Sinha and R. Sinha, Phys. Rev. D **61** (2000) 114028 [Erratum-ibid. D **63** (2001) 019901] [hep-ph/9907386].
- [92] F. Kruger and E. Lunghi, Phys. Rev. D **63** (2001) 014013 [hep-ph/0008210].
- [93] G. C. Branco and L. Lavoura, Phys. Rev. D **38** (1988) 2295.
- [94] G. C. Branco, L. Lavoura and J. P. Silva. *CP Violation*. International Series of Monographs on Physics. Clarendon Press, 1999.
- [95] K. G. Chetyrkin, M. Misiak and M. Munz, Phys. Lett. B **400** (1997) 206 [Erratum-ibid. B **425** (1998) 414] [hep-ph/9612313].
- [96] K. G. Chetyrkin, M. Misiak and M. Munz, Nucl. Phys. B **520** (1998) 279 [hep-ph/9711280].

- [97] C. Bobeth, M. Misiak and J. Urban, Nucl. Phys. B **574** (2000) 291 [hep-ph/9910220].
- [98] D. Seidel. *Exklusive radiative und elektroschwache $b \rightarrow s$ und $b \rightarrow d$ Zerfälle in nächst-führender Ordnung*. PhD thesis. RWTH Aachen, 2001.
- [99] S. Descotes-Genon, D. Ghosh, J. Matias and M. Ramon, JHEP **1106** (2011) 099 [arXiv:1104.3342 [hep-ph]].
- [100] M. Misiak, H. M. Asatrian, K. Bieri, M. Czakon, A. Czarnecki, T. Ewerth, A. Ferroglia and P. Gambino *et al.*, Phys. Rev. Lett. **98** (2007) 022002 [hep-ph/0609232].
- [101] T. Huber, E. Lunghi, M. Misiak and D. Wyler, Nucl. Phys. B **740** (2006) 105 [hep-ph/0512066].
- [102] P. Gambino, M. Gorbahn and U. Haisch, Nucl. Phys. B **673** (2003) 238 [hep-ph/0306079].
- [103] M. Gorbahn and U. Haisch, Nucl. Phys. B **713** (2005) 291 [hep-ph/0411071].
- [104] C. Bobeth, P. Gambino, M. Gorbahn and U. Haisch, JHEP **0404** (2004) 071 [hep-ph/0312090].
- [105] S. Fukae, C. S. Kim, T. Morozumi and T. Yoshikawa, Phys. Rev. D **59** (1999) 074013 [hep-ph/9807254].
- [106] C. S. Kim, Y. G. Kim, C. -D. Lu and T. Morozumi, Phys. Rev. D **62** (2000) 034013 [hep-ph/0001151].
- [107] N. Kauer, Phys. Lett. B **649** (2007) 413 [hep-ph/0703077].
- [108] C. F. Uhlemann and N. Kauer, Nucl. Phys. B **814** (2009) 195 [arXiv:0807.4112 [hep-ph]].
- [109] S. J. Brodsky and X. -G. Wu, Phys. Rev. D **85** (2012) 034038 [arXiv:1111.6175 [hep-ph]].
- [110] W. Altmannshofer, P. Paradisi and D. M. Straub, JHEP **1204** (2012) 008 [arXiv:1111.1257 [hep-ph]].
- [111] W. Altmannshofer and D. M. Straub, JHEP **1208** (2012) 121 [arXiv:1206.0273 [hep-ph]].
- [112] A. Bharucha and W. Reece, Eur. Phys. J. C **69** (2010) 623 [arXiv:1002.4310 [hep-ph]].
- [113] C. Bobeth, G. Hiller and G. Piranishvili, JHEP **0807** (2008) 106 [arXiv:0805.2525 [hep-ph]].
- [114] C. Bobeth, G. Hiller and D. van Dyk, JHEP **1007** (2010) 098 [arXiv:1006.5013 [hep-ph]].
- [115] A. Khodjamirian, T. Mannel, A. A. Pivovarov and Y. -M. Wang, JHEP **1009** (2010) 089 [arXiv:1006.4945 [hep-ph]].

-
- [116] A. Bharucha, T. Feldmann and M. Wick, JHEP **1009** (2010) 090 [arXiv:1004.3249 [hep-ph]].
- [117] A. Faessler, T. Gutsche, M. A. Ivanov, J. G. Korner and V. E. Lyubovitskij, Eur. Phys. J. direct C **4** (2002) 18 [hep-ph/0205287].
- [118] R. Mertig, M. Bohm and A. Denner, Comput. Phys. Commun. **64** (1991) 345.
- [119] J. Matias, F. Mescia, M. Ramon and J. Virto, JHEP **1204** (2012) 104 [arXiv:1202.4266 [hep-ph]].
- [120] S. Descotes-Genon, J. Matias, M. Ramon and J. Virto, arXiv:1207.2753 [hep-ph].
- [121] A. K. Alok, A. Datta, A. Dighe, M. Duraisamy, D. Ghosh and D. London, JHEP **1111** (2011) 121 [arXiv:1008.2367 [hep-ph]].
- [122] G. Burdman and G. Hiller, Phys. Rev. D **63** (2001) 113008 [hep-ph/0011266].
- [123] C. Bobeth, G. Hiller and D. van Dyk, JHEP **1107** (2011) 067 [arXiv:1105.0376 [hep-ph]].
- [124] D. Becirevic and E. Schneider, Nucl. Phys. B **854** (2012) 321 [arXiv:1106.3283 [hep-ph]].
- [125] D. Seidel, Phys. Rev. D **70** (2004) 094038 [hep-ph/0403185].
- [126] H. H. Asatrian, H. M. Asatrian, C. Greub and M. Walker, Phys. Lett. B **507** (2001) 162 [hep-ph/0103087].
- [127] A. G. Grozin and M. Neubert, Phys. Rev. D **55** (1997) 272 [hep-ph/9607366].
- [128] T. Feldmann and J. Matias, JHEP **0301** (2003) 074 [hep-ph/0212158].
- [129] N. Uraltsev, In *Varenna 1997, Heavy flavour physics* 329-409 [hep-ph/9804275].
- [130] I. I. Y. Bigi, M. A. Shifman, N. G. Uraltsev and A. I. Vainshtein, Phys. Rev. D **50** (1994) 2234 [hep-ph/9402360].
- [131] M. Beneke, Phys. Lett. B **434** (1998) 115 [hep-ph/9804241].
- [132] P. Gambino, U. Haisch and M. Misiak, Phys. Rev. Lett. **94** (2005) 061803 [hep-ph/0410155].
- [133] T. Hurth, G. Isidori, J. F. Kamenik and F. Mescia, Nucl. Phys. B **808** (2009) 326 [arXiv:0807.5039 [hep-ph]].
- [134] R. Aaij *et al.* [LHCb Collaboration], Phys. Rev. Lett. **108** (2012) 231801 [arXiv:1203.4493 [hep-ex]].

-
- [135] M. Beylich, G. Buchalla and T. Feldmann, *Eur. Phys. J. C* **71** (2011) 1635 [arXiv:1101.5118 [hep-ph]].
- [136] A. Y. .Korchin and V. A. Kovalchuk, *Phys. Rev. D* **82** (2010) 034013 [arXiv:1004.3647 [hep-ph]].
- [137] A. Y. .Korchin, V. A. Kovalchuk and V. A. Kovalchuk, *Eur. Phys. J. C* **72** (2012) 2155 [arXiv:1205.3683 [hep-ph]].
- [138] A. K. Alok, A. Datta, A. Dighe, M. Duraisamy, D. Ghosh and D. London, *JHEP* **1111** (2011) 122 [arXiv:1103.5344 [hep-ph]].
- [139] D. Das and R. Sinha, arXiv:1202.5105 [hep-ph].
- [140] D. Das and R. Sinha, arXiv:1205.1438 [hep-ph].
- [141] T. Aaltonen *et al.* [CDF Collaboration], *Phys. Rev. Lett.* **108** (2012) 081807 [arXiv:1108.0695 [hep-ex]].
- [142] R. Aaij *et al.* [LHCb Collaboration], *Phys. Rev. Lett.* **108** (2012) 181806 [arXiv:1112.3515 [hep-ex]].
- [143] V. Poireau [BaBar Collaboration], arXiv:1205.2201 [hep-ex].
- [144] F. Beaujean, C. Bobeth, D. van Dyk and C. Wacker, *JHEP* **1208** (2012) 030 [arXiv:1205.1838 [hep-ph]].

Acknowledgements

I would like to thank everybody who helped, not only this thesis into being, but also providing humane support during these years.

In the first place I would like to express my most sincere gratitude to my thesis advisor, Joaquim Matias. He is the most brilliant and hard-worker scientist I have ever known. His never-ending capacity of having new ideas, his stubbornness to get results from them and his ability to relate different kinds of concepts while keeping all of them in his mind at the same time just keeps me amazed. I must also acknowledge his worries about the possibility of me having a heart stroke during my talks, about my future and his efforts to contribute to my job-finding task. But the most important thing he taught me is related to my way of dealing with life: that other people demands or priorities should never go against one's own feelings or before one's own priorities, that one is not silly for being just slower than others and that empathy is one of the best virtues in the human being.

I am also extremely grateful to Javier Virto, for his deep understanding of Physics, for so many enlightening talks in just a few months, for his incomparable sense of humor and for having housed me in Rome and introducing his friends to me; I am sure he stands just at the beginning of a fruitful career in particle physics. I wish to express my deepest gratitude to Federico Mescia for so many afternoons at UB, for his patience explaining the concepts I was having difficulties with and for the talks about life during coffee breaks. I am also deeply in debt to Diptimoy Ghosh for his encouraging words, to Sébastien Descotes-Genon for his fine irony and for his advice on quark masses (I understood this issue reading the reference you gave, thanks!), to Tobias Hurth for his incredible capacity of pushing forward his ideas with conviction and enroll us into our second paper, to Will Reece for his patience teaching me how to compute the A_{QCD}/m_b using Phyton and to Ulrik Egede for his remarkable physics intuition. It has been a pleasure to work with all of them. I also acknowledge the correspondence exchanged with Alexander Khodjamiriand and Thorsten Feldmann, who kindly answered my questions about their works.

It has been a pleasure for me working all these years with a group of such brilliant and

cheerful young people, both from Theoretical Physics and from IFAE. They have been the ones with whom I shared most hours of the day for a long period of time and became part of my family, as I could actually barely see mine. Our paths split here by now but I hope to meet all of them at some point or another in the future. An enormous "thank you" to Joan Antoni Cabrer without whom my daily work would have been unbearable. Thank you for helping me with LaTeX, Mathematica and for listening to me and always giving me good advices when I was low. The same goes for Marc Montull with the plus of the strong bond created by our simultaneous metamorphosis into "monkeys" occurred while sitting in front of our respective computers. Thanks to Julia Stasińska for helping me improve my spoken English during the Renfe journeys and for here ironical sense of humor. My gratitude to Martí Cuquet for so many questions answered about LaTeX and Mathematica and for his combative and nonconformist spirit and also to Yonatan Calderón for his continuous encouragement and joking while teaching at the Thermodynamics lab. I must thank specially Carles Rodó too, my office mate for one year, for making me consider for the first time Veterinary Medicine as a possibility for expanding my career and skills. I also thank Jordi Nadal and Chiara Conidi for being always so cheerful, Clara Peset for the interesting and well-timed after-lunch scatological conversations, Javi Serra for paying attention to them and preventing himself from feeling too sick and Sebastian Krug for his kindness and sense of humor. I keep also a very nice memory of the experiences lived together with Oriol Domenech and Lluís Galbany, which I do actually miss considerably. And also with the rest of the people who already departed: Alvisé, Juanjo, Diogo, Volker, Ermano, Felix, Pere, Nikos,...

Many thanks to all my former students from whom I have learned a lot. I hope that they have also learnt something from me. Thanks to Joan Elias for making me teaching Theoretical Physics an "unbearable" experience. I foresee you will be one of the best theoretical particle physicists from UAB in many years: I have never seen so much talent gathered in a single mind. I wish to express also my gratefulness to all those students with whom I became friends: Cristina Sans for sharing so many talks about life and for those incredibly delicious muffins, Hernan Pino and Vanessa Pastor for their cheerfulness, sympathy and the formulae+cats tea cup, Maria Cabello for sharing that lunch time with me and keeping in contact during all these years, Gerard Ariño for his sense of humor and, of course, to Silvia Pérez for your kindness, your capacity of listening, your love for animals and your empathy.

My recognition to the people from Veterinary Medicine for withstanding the strange man-in-the-butane-orange-coat: Vanessa Bentanachs (I know that if you are not the first one here you'll put "Bamby eyes"), Elisa Ruiz (for having let me help you and the friendship that arose afterwards. I also know you do not mind being the second here), Dolors Pi (Dolors... you are doing great), Núria Puigdelívol and Aina Sanz (you lent me so many class notes... and I passed so many exams with them...), Nelly Nájjar (thank you for that Ismael Serrano concert), Alba Maldonado, Laia Toneu, Patricia Torrico, Alba and Gemma Pérez and so many other classmates.

I also thank Marta Vila for having awoken feelings that were so deeply buried inside me that I did not know if they were there anymore. You were the turning point I needed in my life.

A special "thank you" to Isabel Elduque for listening me and giving me insight during so many past and future conversation times.

A huge hug and "thank you" to my two dearest friends Àngels Puig and Sandra Cabot for always being there. My best wishes and encouragement to the vital projects you are just starting. I'm also extremely grateful to Àngels for proofreading this text.

And last but not least to my "former" family, in special to my mother and sister for their unconditional support of any kind and also to Eva, my current family, the one I chose to share that turning point with, for coping with my nervousness and misfortunes and overcoming, lovingly and together, the past tough times and the better ones yet to come.

Part IV

Published papers

New observables in the decay mode $\bar{B}_d \rightarrow \bar{K}^{*0} \ell^+ \ell^-$

Ulrik Egede,^a Tobias Hurth,^b Joaquim Matias,^c Marc Ramon^c and Will Reece^a

^a*Physics Department, Imperial College London,
London SW7 2AZ, U.K.*

^b*Dept. of Physics, Theory Division, CERN,
CH-1211 Geneva 23, Switzerland**

^c*Departament de Física & IFAE, Universitat Autònoma de Barcelona,
E-08193 Bellaterra (Barcelona), Spain*

*E-mail: U.Egede@imperial.ac.uk, Tobias.Hurth@cern.ch, matias@ifae.es,
mramon@ifae.es, w.reece06@imperial.ac.uk*

ABSTRACT: We discuss the large set of observables available from the angular distributions of the decay $\bar{B}_d \rightarrow \bar{K}^{*0} \ell^+ \ell^-$. We present a NLO analysis of all observables based on the QCD factorization approach in the low-dilepton mass region and an estimate of Λ/m_b corrections. Moreover, we discuss their sensitivity to new physics. We explore the experimental sensitivities at LHCb (10 fb^{-1}) and SuperLHCb (100 fb^{-1}) based on a full-angular fit method and explore the sensitivity to right handed currents. We also show that the previously discussed transversity amplitude $A_T^{(1)}$ cannot be measured at the LHCb experiment or at future B factory experiments as it requires a measurement of the spin of the final state particles.

KEYWORDS: Rare Decays, B-Physics.

*Also SLAC, Stanford University, Stanford, CA 94309, U.S.A.

Contents

1. Introduction	1
2. Differential decay distribution	2
3. K^* spin amplitudes	3
4. Theoretically clean observables	6
4.1 General criteria	6
4.2 Observables	7
4.3 The problem with $A_T^{(1)}$	8
5. Method to calculate experimental sensitivity	9
5.1 $\bar{B}_d \rightarrow \bar{K}^{*0} \ell^+ \ell^-$ decay model	9
5.2 Full angular fit	10
5.3 Comparisons with fits to projections	11
6. Phenomenological analysis	12
6.1 Preliminaries	13
6.2 Results	14
7. Summary	21
A. Kinematics	22
B. Theoretical framework	23
C. NLO corrections to the spin amplitudes	24

1. Introduction

A major aim of particle physics in the LHC era is the discovery of new degrees of freedom at the TeV energy scale which might contribute to our understanding of the origin of electroweak symmetry breaking. Rare B and kaon decays (for reviews see [1–3]) representing loop-induced processes are highly sensitive probes for new degrees of freedom beyond the Standard Model (SM) and will be used when making indirect searches for these unknown effects. It is well-known that the indirect constraints on new physics (NP) from the present flavour data indicate a NP scale much higher than the electroweak scale when such new effects are naturally parameterised by higher-dimensional operators. Thus, if there is NP at the electroweak scale, then its flavour structure has to be highly non-trivial and the

experimental measurement of flavour-violating couplings is mandatory. This ‘flavour problem’, namely why flavour-changing neutral currents are suppressed, has to be solved by any NP scenario at the electroweak scale.

In this article we discuss theoretical and experimental preparations for an indirect NP search using the rare decay $\bar{B}_d \rightarrow \bar{K}^{*0} \mu^+ \mu^-$. This exclusive decay was first observed at Belle [4]. It offers a rich phenomenology of various kinematical distributions beyond the measurement of the branching ratio. Some experimental analyses of those angular distributions are already presented by the B factories [5–9] but only the large increase in statistics at LHCb [10–12] for $\bar{B}_d \rightarrow \bar{K}^{*0} \mu^+ \mu^-$ will make much higher precision measurements possible. There are also great opportunities at the future (Super-) B factories in this respect [13–16]. A careful choice of observables needs to be made to take full advantage of this exclusive decay as only in certain ratios such as CP and forward-backward asymmetries, the hadronic uncertainties cancel out in specific observables making such ratios the only observables that are sensitive to NP. In this respect the by now standard theoretical tools like QCD factorization (QCDF) [17] and its quantum field theoretical formulation, soft-collinear effective theory (SCET), are crucial. They imply form factor relations which simplify the theoretical structure of various kinematical distributions such that at least at the leading order (LO) level any hadronic uncertainties cancel out. A well-known example of this is the zero-crossing of the forward-backward asymmetry.

We construct new observables of this kind in the $\bar{B}_d \rightarrow \bar{K}^{*0} \mu^+ \mu^-$ decay which have very small theoretical uncertainties and good experimental resolution. Moreover, it is possible to design the new observables for a specific kind of NP operator within the model independent analysis using the effective field theory approach.

Previously proposed angular distributions and CP violating observables in $\bar{B}_d \rightarrow \bar{K}^{*0} \mu^+ \mu^-$ are reviewed in ref. [18, 15], and more recently QCDF analyses of such angular distributions [19, 20] and CP violating observables [21] were presented.

The paper is organised as follows: in section 2 we recall the differential decay distribution in the $\bar{B}_d \rightarrow \bar{K}^{*0} \mu^+ \mu^-$ decay; in section 3 we recall the basic theoretical formulae which are crucial for our construction of new observables; in section 4 we discuss the basic properties and symmetries of potential observables and propose a new set of observables which are sensitive to new right-handed currents and we also discuss the previously proposed quantity $A_T^{(1)}$; in section 5 we explain our method to calculate the experimental sensitivity obtainable with the statistics of LHCb to new and old observables; and finally in section 6 we present our phenomenological analysis, in particular we analyse the theoretical and experimental sensitivity to NP. We also comment very briefly on recent $BABAR$ measurements of certain angular distributions. In appendices we make angular definitions explicit, provide the theoretical framework for the derivation of the spin amplitudes, and present the theoretical NLO expressions.

2. Differential decay distribution

The decay $\bar{B}_d \rightarrow \bar{K}^{*0} \ell^+ \ell^-$ with $\bar{K}^{*0} \rightarrow K^- \pi^+$ on the mass shell, is completely described by four independent kinematic variables, the lepton-pair invariant mass squared, q^2 , and

the three angles θ_l, θ_K, ϕ . Summing over the spins of the final particles, the differential decay distribution of $\bar{B}_d \rightarrow \bar{K}^{*0} \ell^+ \ell^-$ can be written as

$$\frac{d^4\Gamma_{\bar{B}_d}}{dq^2 d\theta_l d\theta_K d\phi} = \frac{9}{32\pi} I(q^2, \theta_l, \theta_K, \phi) \sin\theta_l \sin\theta_K, \quad (2.1)$$

with the physical region of phase space $4m_l^2 \leq q^2 \leq (m_B - m_{K^*})^2$ and

$$I = I_1 + I_2 \cos 2\theta_l + I_3 \sin^2 \theta_l \cos 2\phi + I_4 \sin 2\theta_l \cos \phi + I_5 \sin \theta_l \cos \phi + I_6 \cos \theta_l + I_7 \sin \theta_l \sin \phi + I_8 \sin 2\theta_l \sin \phi + I_9 \sin^2 \theta_l \sin 2\phi. \quad (2.2)$$

The I_i depend on products of the seven complex K^* spin amplitudes, $A_{\perp L/R}, A_{\parallel L/R}, A_{0L/R}, A_t$ (see next section) with each of these a function of q^2 . A_t is related to the time-like component of the virtual K^* , which does not contribute in the case of massless leptons and can be neglected if the lepton mass is small in comparison to the mass of the lepton pair. We will consider this case in our present analysis. For $m_l = 0$, one finds [22–25]:

$$I_1 = \frac{3}{4} (|A_{\perp L}|^2 + |A_{\parallel L}|^2 + (L \rightarrow R)) \sin^2 \theta_K + (|A_{0L}|^2 + |A_{0R}|^2) \cos^2 \theta_K \equiv a \sin^2 \theta_K + b \cos^2 \theta_K, \quad (2.3a)$$

$$I_2 = \frac{1}{4} (|A_{\perp L}|^2 + |A_{\parallel L}|^2) \sin^2 \theta_K - |A_{0L}|^2 \cos^2 \theta_K + (L \rightarrow R) \equiv c \sin^2 \theta_K + d \cos^2 \theta_K, \quad (2.3b)$$

$$I_3 = \frac{1}{2} [(|A_{\perp L}|^2 - |A_{\parallel L}|^2) \sin^2 \theta_K + (L \rightarrow R)] \equiv e \sin^2 \theta_K, \quad (2.3c)$$

$$I_4 = \frac{1}{\sqrt{2}} [\text{Re}(A_{0L} A_{\parallel L}^*) \sin 2\theta_K + (L \rightarrow R)] \equiv f \sin 2\theta_K, \quad (2.3d)$$

$$I_5 = \sqrt{2} [\text{Re}(A_{0L} A_{\perp L}^*) \sin 2\theta_K - (L \rightarrow R)] \equiv g \sin 2\theta_K, \quad (2.3e)$$

$$I_6 = 2 [\text{Re}(A_{\parallel L} A_{\perp L}^*) \sin^2 \theta_K - (L \rightarrow R)] \equiv h \sin^2 \theta_K, \quad (2.3f)$$

$$I_7 = \sqrt{2} [\text{Im}(A_{0L} A_{\parallel L}^*) \sin 2\theta_K - (L \rightarrow R)] \equiv j \sin 2\theta_K, \quad (2.3g)$$

$$I_8 = \frac{1}{\sqrt{2}} [\text{Im}(A_{0L} A_{\perp L}^*) \sin 2\theta_K + (L \rightarrow R)] \equiv k \sin 2\theta_K, \quad (2.3h)$$

$$I_9 = [\text{Im}(A_{\parallel L}^* A_{\perp L}) \sin^2 \theta_K + (L \rightarrow R)] \equiv m \sin^2 \theta_K. \quad (2.3i)$$

The exact equations presented here depend on the definition of the angles which we for this reason have made explicit in appendix A.

From comparing the amplitude terms in eq. (2.3), we see that $a = 3c$ and $b = -d$ thus leaving nine independent parameters which can be fixed experimentally in a full angular fit. Assuming massless leptons in the theory we have on the other hand 12 parameters from the six complex \bar{K}^{*0} spin amplitudes, $A_{\perp L/R}, A_{\parallel L/R}, A_{0L/R}$. See section 4 for an analysis of the apparent mismatch between the 9 and 12 parameters.

3. K^* spin amplitudes

The six complex K^* spin amplitudes under the assumption of massless leptons are related

to the well-known helicity amplitudes (used for example in [23, 24, 26]) through

$$A_{\perp,\parallel} = (H_{+1} \mp H_{-1})/\sqrt{2}, \quad A_0 = H_0. \quad (3.1)$$

The amplitudes describe the $B \rightarrow K\pi$ transition and can be parameterised in terms of the seven $B \rightarrow K^*$ form factors by means of a narrow-width approximation. They also depend on the short-distance Wilson coefficients C_i corresponding to the various operators of the effective electroweak Hamiltonian. The precise definitions of the form factors and of the effective operators are given in appendix B. One obtains [19]

$$A_{\perp L,R} = N\sqrt{2}\lambda^{1/2} \left[(\mathcal{C}_9^{(\text{eff})} \mp \mathcal{C}_{10}) \frac{V(s)}{m_B + m_{K^*}} + \frac{2m_b}{q^2} (\mathcal{C}_7^{(\text{eff})} + \mathcal{C}'_7^{(\text{eff})}) T_1(q^2) \right], \quad (3.2)$$

$$A_{\parallel L,R} = -N\sqrt{2}(m_B^2 - m_{K^*}^2) \left[(\mathcal{C}_9^{(\text{eff})} \mp \mathcal{C}_{10}) \frac{A_1(q^2)}{m_B - m_{K^*}} + \frac{2m_b}{q^2} (\mathcal{C}_7^{(\text{eff})} - \mathcal{C}'_7^{(\text{eff})}) T_2(q^2) \right], \quad (3.3)$$

$$\begin{aligned} A_{0L,R} = & -\frac{N}{2m_{K^*}\sqrt{q^2}} \times \\ & \times \left[(\mathcal{C}_9^{(\text{eff})} \mp \mathcal{C}_{10}) \left\{ (m_B^2 - m_{K^*}^2 - q^2)(m_B + m_{K^*})A_1(q^2) - \right. \right. \\ & \left. \left. -\lambda \frac{A_2(q^2)}{m_B + m_{K^*}} \right\} + \right. \\ & \left. + 2m_b(\mathcal{C}_7^{(\text{eff})} - \mathcal{C}'_7^{(\text{eff})}) \left\{ (m_B^2 + 3m_{K^*}^2 - q^2)T_2(q^2) - \right. \right. \\ & \left. \left. -\frac{\lambda}{m_B^2 - m_{K^*}^2} T_3(q^2) \right\} \right], \quad (3.4) \end{aligned}$$

where

$$\lambda = m_B^4 + m_{K^*}^4 + q^4 - 2(m_B^2 m_{K^*}^2 + m_{K^*}^2 q^2 + m_B^2 q^2) \quad (3.5)$$

and

$$N = \sqrt{\frac{G_F^2 \alpha^2}{3 \cdot 2^{10} \pi^5 m_B^3} |V_{tb} V_{ts}^*|^2 q^2 \lambda^{1/2} \sqrt{1 - \frac{4m_l^2}{q^2}}}. \quad (3.6)$$

The crucial theoretical input we use in our analysis is the observation that in the limit where the initial hadron is heavy and the final meson has a large energy [27] the hadronic form factors can be expanded in the small ratios Λ_{QCD}/m_b and Λ_{QCD}/E , where E is the energy of the light meson. Neglecting corrections of order $1/m_b$ and α_s , the seven a priori independent $B \rightarrow K^*$ form factors reduce to two universal form factors ξ_{\perp} and ξ_{\parallel} [27, 28]. These relations can be strictly derived within the QCDf and SCET approach and are given in the appendix. Using those simplifications the spin amplitudes at leading order in $1/m_b$ and α_s have a very simple form:

$$A_{\perp L,R} = \sqrt{2} N m_B (1 - \hat{s}) \left[(\mathcal{C}_9^{(\text{eff})} \mp \mathcal{C}_{10}) + \frac{2\hat{m}_b}{\hat{s}} (\mathcal{C}_7^{(\text{eff})} + \mathcal{C}'_7^{(\text{eff})}) \right] \xi_{\perp}(E_{K^*}), \quad (3.7)$$

$$A_{\parallel L,R} = -\sqrt{2} N m_B (1 - \hat{s}) \left[(\mathcal{C}_9^{(\text{eff})} \mp \mathcal{C}_{10}) + \frac{2\hat{m}_b}{\hat{s}} (\mathcal{C}_7^{(\text{eff})} - \mathcal{C}'_7^{(\text{eff})}) \right] \xi_{\parallel}(E_{K^*}), \quad (3.8)$$

$$A_{0L,R} = -\frac{Nm_B}{2\hat{m}_{K^*}\sqrt{\hat{s}}}(1-\hat{s})^2 \left[(\mathcal{C}_9^{(\text{eff})} \mp \mathcal{C}_{10}) + 2\hat{m}_b(\mathcal{C}_7^{(\text{eff})} - \mathcal{C}'_7^{(\text{eff})}) \right] \xi_{\parallel}(E_{K^*}), \quad (3.9)$$

with $\hat{s} = q^2/m_B^2$, $\hat{m}_i = m_i/m_B$. Here we neglected terms of $O(\hat{m}_{K^*}^2)$.

Some remarks are in order:

- The theoretical simplifications are restricted to the kinematic region in which the energy of the K^* is of the order of the heavy quark mass, i.e. $q^2 \ll m_B^2$. Moreover, the influences of very light resonances below 1 GeV^2 question the QCD factorization results in that region. Thus, we will confine our analysis of all observables to the dilepton mass in the range, $1 \text{ GeV}^2 \leq q^2 \leq 6 \text{ GeV}^2$.
- Within the SM, we recover the naive quark-model prediction of $A_{\perp} = -A_{\parallel}$ [29, 30] in the $m_B \rightarrow \infty$ and $E_{K^*} \rightarrow \infty$ limit (equivalently $\hat{m}_{K^*}^2 \rightarrow 0$). In this case, the s quark is produced in helicity $-1/2$ by weak interactions in the limit $m_s \rightarrow 0$, which is not affected by strong interactions in the massless case [31]. Thus, the strange quark combines with a light quark to form a K^* with helicity either -1 or 0 but not $+1$. Consequently, the SM predicts at quark level $H_{+1} = 0$, and hence $A_{\perp} = -A_{\parallel}$ [cf. eq. (3.1)], which is revealed as $|H_{-1}| \gg |H_{+1}|$ (or $A_{\perp} \approx -A_{\parallel}$) at the hadron level.
- As noted in ref. [19], the contributions of the chirality-flipped operators $\mathcal{O}'_{9,10} = \mathcal{O}_{9,10}(P_L \rightarrow P_R)$ can be included in the above amplitudes by the replacements $\mathcal{C}_{9,10}^{(\text{eff})} \rightarrow \mathcal{C}_{9,10}^{(\text{eff})} + \mathcal{C}'_{9,10}^{(\text{eff})}$ in eq. (3.7), $\mathcal{C}_{9,10}^{(\text{eff})} \rightarrow \mathcal{C}_{9,10}^{(\text{eff})} - \mathcal{C}'_{9,10}^{(\text{eff})}$ in eqs. (3.8) and (3.9). However, they play a sub-dominant role in our NP analysis presented here.
- The symmetry breaking corrections of order α_s can be calculated in the QCDf/SCET approach. Those NLO corrections are included in our numerical analysis following ref. [17]. The corresponding formulae for the case $\mathcal{C}'_7^{(\text{eff})} \neq 0$ are given in appendix C.
- In general we have no means to calculate Λ/m_b corrections to the QCDf amplitudes so they are treated as unknown corrections. This leads to a large uncertainty of theoretical predictions based on the QCDf/SCET approach. However, in specific examples one can combine QCDf/SCET results with calculations based on the QCD sum rule approach in order to estimate the leading power corrections.

To take into account the present situation, we introduce a set of extra parameters, one for each spin amplitude, to explore what the effect of a possible Λ/m_b correction could be:

$$A_{\perp,\parallel,0} = A_{\perp,\parallel,0}^0 (1 + c_{\perp,\parallel,0}) \quad (3.10)$$

where the ‘0’ superscript stands for the QCD NLO Factorization amplitude and $c_{\perp,\parallel,0}$ are taken to vary in a range $\pm 10\%$ which corresponds to a naive dimensional estimate. For each observable we look at, each of the amplitudes were varied in turn leaving the others at their central value. All the variations were then added in quadrature. Furthermore, we also give our final predictions taking into account further improvements on the power corrections and varying the independent parameters in a less conservative range of $\pm 5\%$.

4. Theoretically clean observables

4.1 General criteria

We recall again that 2 of the 11 measurable distribution functions a, b, \dots, m of the differential decay distribution in the limit $m_\ell^2 \ll q^2$, defined in eq. (2.3), include redundant information due to the relations $a = 3c$ and $b = -d$. So in principle there are 9 independent observables. However, the dependence of those functions on the six complex theoretical spin amplitudes, $A_{\perp L/R}$, $A_{\parallel L/R}$ and $A_{0L/R}$, is special. By inspection one finds that the distribution functions are *invariant* under the following three independent symmetry transformations of the spin amplitudes: global phase transformation of the L -amplitudes

$$A'_{\perp L} = e^{i\phi_L} A_{\perp L}, \quad A'_{\parallel L} = e^{i\phi_L} A_{\parallel L}, \quad A'_{0L} = e^{i\phi_L} A_{0L}, \quad (4.1)$$

global phase transformation of the R -amplitudes

$$A'_{\perp R} = e^{i\phi_R} A_{\perp R}, \quad A'_{\parallel R} = e^{i\phi_R} A_{\parallel R}, \quad A'_{0R} = e^{i\phi_R} A_{0R}, \quad (4.2)$$

and a continuous $L \leftrightarrow R$ rotation

$$A'_{\perp L} = +\cos\theta A_{\perp L} - \sin\theta A_{\perp R}^* \quad (4.3a)$$

$$A'_{\perp R} = +\sin\theta A_{\perp L} + \cos\theta A_{\perp R}^* \quad (4.3b)$$

$$A'_{0L} = +\cos\theta A_{0L} - \sin\theta A_{0R}^* \quad (4.3c)$$

$$A'_{0R} = +\sin\theta A_{0L} + \cos\theta A_{0R}^* \quad (4.3d)$$

$$A'_{\parallel L} = +\cos\theta A_{\parallel L} + \sin\theta A_{\parallel R}^* \quad (4.3e)$$

$$A'_{\parallel R} = -\sin\theta A_{\parallel L} + \cos\theta A_{\parallel R}^*. \quad (4.3f)$$

Normally, there is the freedom to pick a single global phase, but as L and R amplitudes do not interfere here, two phases can be chosen arbitrarily as reflected in the first two transformations. The third symmetry reflects that an average is made over the spin amplitudes to obtain the angular distribution. So it is clear that only 9 out of the 12 parameters arising from the 6 complex amplitudes are independent which fits exactly with the 9 independent measurable distribution functions.

A consequence of the three symmetries is that any observable based on the differential decay distribution has also to be invariant under the same symmetry transformations.

Besides the mandatory criterion above there are further criteria required for an interesting observable:

Simplicity: A simple functional dependence on the 9 independent measurable distribution functions; at best it should depend only from one or two in the numerator and denominator of an asymmetry.

Cleanliness: At leading order in Λ/m_b and in α_s the observable should be independent of any form factor, at best for all q^2 . Also the influence of symmetry-breaking corrections at order α_s and at order Λ/m_b should be minimal.

Sensitivity: The sensitivity to the $C_7^{(\text{eff})}$ Wilson coefficient representing NP with another chirality than in the SM should be maximal.

Precision: The experimental precision obtainable should be good enough to distinguish different NP models.

In the limit where the \bar{K}^{*0} meson has a large energy, only two independent form factors occur in $A_{0L/R}$ and in $A_{\perp L/R}$ and $A_{\parallel L/R}$. Clearly, any ratio of two of the nine measurable distribution functions proportional to the same form factor fulfil the criterion of symmetry, simplicity, and theoretical cleanliness up to Λ/m_b and α_s corrections. However, the third criterion, a sensitivity to a special kind of NP and the subsequent requirement of experimental precision, singles out particular combinations. In this paper we focus on new right-handed currents. Other NP sensitivities may single out other observables as will be analysed in a forthcoming paper [32].

4.2 Observables

There are some proposals for theoretical clean observables already in the literature which we should briefly discuss in view of the above criteria:

- The forward backward asymmetry is the most popular quantity in the $\bar{B}_d \rightarrow \bar{K}^{*0} \mu^+ \mu^-$ decay [33]. In terms of the \bar{K}^{*0} spin amplitudes it can be written as [17, 34]

$$A_{\text{FB}} = \frac{3 \operatorname{Re}(A_{\parallel L} A_{\perp L}^*) - \operatorname{Re}(A_{\parallel R} A_{\perp R}^*)}{2 \left(|A_0|^2 + |A_{\parallel}|^2 + |A_{\perp}|^2 \right)} \quad (4.4)$$

where

$$A_i A_j^* \equiv A_{iL}(q^2) A_{jL}^*(q^2) + A_{iR}(q^2) A_{jR}^*(q^2) \quad (i, j = 0, \parallel, \perp). \quad (4.5)$$

While the criteria of symmetry and simplicity are fulfilled, the form factors cancel out only at the specific value of q^2 where $A_{\text{FB}} = 0$. Thus the measurement provide only a single clean number, the zero crossing point, rather than a theoretically clean distribution.

- The fractions of the \bar{K}^{*0} polarisation

$$F_L(q^2) = \frac{|A_0|^2}{|A_0|^2 + |A_{\parallel}|^2 + |A_{\perp}|^2}, \quad (4.6)$$

$$F_T(q^2) = 1 - F_L(q^2) = \frac{|A_{\perp}|^2 + |A_{\parallel}|^2}{|A_0|^2 + |A_{\parallel}|^2 + |A_{\perp}|^2}, \quad (4.7)$$

and the K^* polarisation parameter

$$\alpha_{K^*}(q^2) = \frac{2F_L}{F_T} - 1 = \frac{2|A_0|^2}{|A_{\parallel}|^2 + |A_{\perp}|^2} - 1. \quad (4.8)$$

All fulfil the criteria of symmetry and simplicity, but the form factors do not cancel in the LO approximation; thus, suffering from larger hadronic uncertainties. The fraction of the \bar{K}^* polarisation can be measured from the angular projections alone and the first experimental measurements of F_L with limited accuracy are available [8, 9].

- Defining the helicity distributions $\Gamma_{\pm} = |H_{\pm 1}^L|^2 + |H_{\pm 1}^R|^2$ one can construct [23]

$$A_T^{(1)} = \frac{\Gamma_- - \Gamma_+}{\Gamma_- + \Gamma_+} = \frac{-2\text{Re}(A_{\parallel} A_{\perp}^*)}{|A_{\perp}|^2 + |A_{\parallel}|^2}. \quad (4.9)$$

It has been shown [19, 20] that this quantity has adequate cleanliness and is very sensitive to right-handed currents, making an ideal observable if just these two criteria were sufficient. However, the quantity $A_T^{(1)}$ does not fulfil the most important criterion of symmetry. The important consequences out of this observation are briefly discussed in the next subsection.

- The other transversity amplitude, first proposed in [19], is defined as

$$A_T^{(2)} = \frac{|A_{\perp}|^2 - |A_{\parallel}|^2}{|A_{\perp}|^2 + |A_{\parallel}|^2}. \quad (4.10)$$

It obviously fulfils all three criteria of symmetry, simplicity and theoretical cleanliness. It is also rather sensitivity to $\mathcal{C}_7^{(\text{eff})}$ as one can see by inspection of the LO formulae of the \bar{K}^{*0} amplitudes in eqs. (3.7)–(3.9); in this approximation it is directly proportional to $\mathcal{C}_7^{(\text{eff})}$, thus vanishes in the SM.

By inspection of the formulae of the K^* spin amplitudes in terms of the Wilson coefficients and the SCET form factors at the LO approximation, eqs. (3.7)–(3.9), one is led to some new observables which fulfil the first three criteria *and* have an enhanced sensitivity to $\mathcal{C}_7^{(\text{eff})}$. They are defined as

$$A_T^{(3)} = \frac{|A_{0L} A_{\parallel L}^* - A_{0R}^* A_{\parallel R}|}{\sqrt{|A_0|^2 |A_{\perp}|^2}}, \quad (4.11)$$

and

$$A_T^{(4)} = \frac{|A_{0L} A_{\perp L}^* - A_{0R}^* A_{\perp R}|}{|A_{0L}^* A_{\parallel L} + A_{0R} A_{\parallel R}^*|}, \quad (4.12)$$

One could also consider the real and imaginary parts of $A_T^{(3)}$.

There are no further independent quantities which fulfil the criteria we have set out. However, when we will consider NP sensitivities beyond $\mathcal{C}_7^{(\text{eff})}$ further observables may be singled out [32].

4.3 The problem with $A_T^{(1)}$

Contrary to the case of $A_T^{(i)}$ with $i = 2, 3, 4$, it is not possible to extract $A_T^{(1)}$ from the full angular distribution. This is a direct consequence of the fact that the quantity $A_T^{(1)}$ is not invariant under the symmetry (4.3) of the distribution function (2.1) which represent the complete set of observables in the case spins of the final states are summed up. Let us elaborate further on this surprising observation; it seems practically not possible to measure the helicity of the final states on a *event-by-event* basis. At the forthcoming LHCb experiment for example one only measures the charge, the three-momentum of the final

state particles and its nature through different types of particle identification. So one has the four-momentum for each particle and its charge. The situation does not look different for the present B factories and their future upgrades. While the e^+e^- environment is much simpler there is still no practical way to measure the spin of the muons on an *event-by-event* basis. We should emphasise that this is a practical and not a conceptual problem; in a *gedanken* experiment where the helicity of the individual final state leptons are measured, it would indeed be possible to measure $A_T^{(1)}$. So while $A_T^{(1)}$ is in principle a good observable, we cannot see any way it can be measured at either LHC***b*** or at a Super- B factory with electrons or muons in the final state.

5. Method to calculate experimental sensitivity

In this section we explain how to investigate the sensitivity to the angular observables presented in section 4 using a toy Monte Carlo model. We estimate the statistical uncertainty on all observables with statistics corresponding to 5 years of nominal running at LHC***b*** (10 fb^{-1}) and comment on the experimental prospects for a measurement at the end of an upgrade to LHC***b*** (100 fb^{-1}). For the estimates here we are only considering the final state with muons.

5.1 $\bar{B}_d \rightarrow \bar{K}^{*0} \ell^+ \ell^-$ decay model

The angles θ_l , θ_K and ϕ , as well as the q^2 of the lepton pair can be measured with small uncertainty and no experimental resolution effects need to be considered. A toy Monte Carlo model of the decay was created using eq. (2.1) as a probability density function (PDF) normalised to the width,

$$\int_{q_{\min}^2}^{q_{\max}^2} \frac{d\Gamma}{dq^2} dq^2. \tag{5.1}$$

It is parameterised in terms of the real and imaginary parts of the spin amplitudes where each of these amplitudes is q^2 dependent. A simple approach, where the data is divided into regions of q^2 and the spin amplitudes determined within these, will not work; the coefficients in front of the different angular components as seen in eq. (2.1) depend in a non-linear way on the spin amplitudes meaning that the angular distribution after integration over a bin in q^2 cannot be expressed in terms of eq. (2.1) with some q^2 -averaged spin amplitudes. Instead an approach is used where the q^2 dependence of each of the spin amplitudes is parameterised as a function of q^2 .

A special choice of the symmetry transformations described in section 4 can be used to reduce the number of parameters. Here we use the first two symmetry transformations eqs. (4.1) and (4.2) to get rid of the two phases in A_{0R} and A_{0L} . Then the third transformation eq. (4.3) is used with $\theta = \arctan(-A_{0R}/A_{0L})$ leading to A_{0L} being real and $A_{0R} = 0$ thus disappearing completely from the parametrisation. At a given value of q^2 we are thus left with 9 parameters corresponding to the real and imaginary components of $A_{\parallel L,R}$ and $A_{\perp L,R}$ and the real component of A_{0L} . We now parameterise each of these spin amplitudes as a 2nd order polynomial. Through the polynomial ansatz we are introducing a weak model dependence; we checked that the error introduced by this was significantly

smaller than the corresponding experimental errors across the squared dimuon mass range $1 \text{ GeV}^2 < q^2 < 6 \text{ GeV}^2$. To describe the full q^2 and angular dependence of the decay we thus need 27 parameters. As a final step we recognise that an absolute measurement of the total width is difficult to obtain in a hadronic environment such as LHC**b** and fix the value of A_{0L} to 1 at a reference value of q^2 thus reducing the number of free parameters to 26. This last step has no influence on the experimental determination of any of the observables discussed in this paper as they are all formed as ratios where the total width cancels out. While no longer sensitive to the absolute width we are still sensitive to the shape of the differential width as a function of q^2 .

We follow the resolution, yield and background numbers in [10] to construct a model that includes a realistic level of background. The signal is assumed to have a Gaussian distribution in m_B with a width of 14 MeV in a window of $m_B \pm 50$ MeV and a Breit-Wigner in $m_{K\pi}$ with width 48 MeV in a window of $m_{K^*0} \pm 100$ MeV. A simplified background model is included; it is flat in all angles, effectively treating all background as combinatorial, but follows the q^2 distribution of the signal. Acceptance and CP violation effects are neglected allowing us to treat $\bar{B}_d \rightarrow \bar{K}^{*0} \mu^+ \mu^-$ and its charge conjugate simultaneously. We do not include any contributions from non-resonant $\bar{B}_d \rightarrow K^- \pi^+ \mu^+ \mu^-$.

Using the toy Monte Carlo model, a dataset for the observables θ_l , θ_K , ϕ and q^2 can be generated with the calculated values of the spin amplitudes as input without making use of the polynomial ansatz. Physics beyond the SM can be included in a straightforward way by providing the relevant spin amplitudes. Using the yield and background estimates from [10] and assuming a flat efficiency for the signal as a function of q^2 we use on average 4032 signal events and 1168 background events in the q^2 interval from $4m_\mu^2$ to 9 GeV^2 in a dataset of 2 fb^{-1} . These are scaled linearly in order to obtain 10 fb^{-1} and 100 fb^{-1} yield estimates. For each dataset we generate, the signal and background numbers are varied according to Poisson statistics.

The purpose of the toy Monte Carlo model is to enable us to illustrate the methodology of this approach and be able to make precise statements on the relative performance of a full angular fit compared to just looking at projections. Accurate estimates of the resolution in each parameter will only be possible with a complete detector simulation and with a complete understanding of the actual detector performance following the first data.

5.2 Full angular fit

With the model above we can generate an ensemble of experiments corresponding to a given integrated luminosity. In each of these experiments we can use a general minimiser to find the spin value parametrisation that best corresponds to the data. Each fit has in total 27 parameters; 26 from the signal described above and a single parameter to describe the level of the simplified background model. From the ensemble of experiments, estimates of the experimental uncertainties can be made and any biases introduced can be studied. For each dataset, the extracted spin amplitude components were used to calculate the value of each angular observable as a function of q^2 . In total we created an ensemble of 1000 experiments and will thus at a given value of q^2 get 1000 different determinations of a given observable. By looking at the point where 33% and 47.5% of results lie within either side

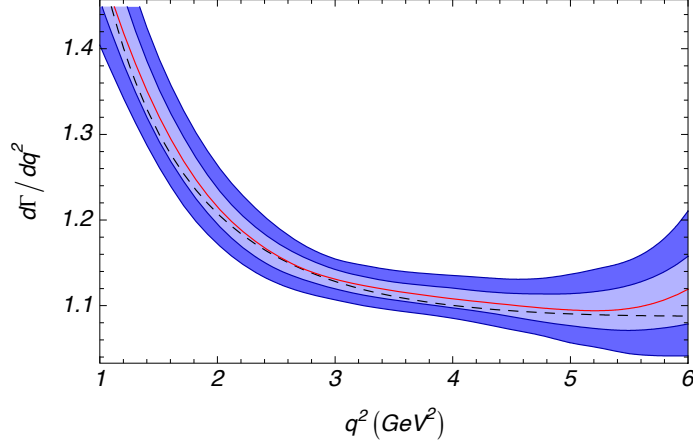


Figure 1: The experimental sensitivity to $\frac{d\Gamma}{dq^2}$ with the SM as input. The inner and outer bands correspond to 1σ and 2σ experimental errors with statistics corresponding to a 10 fb^{-1} dataset from LHC**b**. The black dashed line is the theoretical input and the red solid line the central value of the ensemble experiments.

of the median of the results we can form asymmetric 1σ and 2σ errors. Connecting these at different q^2 values gives us 1σ and 2σ bands for the experimental errors on the observable. An illustration of the method in figure 1 shows the experimental sensitivity to the width distribution relative to the normalisation point which was arbitrarily chosen as 3.5 GeV^2 . The inner and outer bands correspond to 1σ and 2σ experimental errors with statistics corresponding to a 10 fb^{-1} dataset from LHC**b**. The dashed line is the theoretical input and the red line the central value of the ensemble experiments. The difference between these two lines is caused by limitations imposed by the second order polynomial assumption. As it is well inside the 1σ band this is not problem.

The experimental sensitivity to the observables introduced in section 4.2 will be presented in section 6 within the phenomenological analysis to allow for an easy comparison of experimental and theoretical errors.

5.3 Comparisons with fits to projections

The full angular fit gives access to angular observables not accessible in other ways. However, A_{FB} , $A_T^{(2)}$, F_L and A_{im}^1 can be extracted from distributions in just a single angle after integration over the other 2 in eq. (2.1):

$$\frac{d\Gamma'}{d\phi} = \frac{\Gamma'}{2\pi} \left(1 + \frac{1}{2}(1 - F_L)A_T^{(2)} \cos 2\phi + A_{\text{im}} \sin 2\phi \right), \quad (5.2a)$$

$$\frac{d\Gamma'}{d\theta_l} = \Gamma' \left(\frac{3}{4}F_L \sin^2 \theta_l + \frac{3}{8}(1 - F_L)(1 + \cos^2 \theta_l) + A_{\text{FB}} \cos \theta_l \right) \sin \theta_l, \quad (5.2b)$$

$$\frac{d\Gamma'}{d\theta_K} = \frac{3\Gamma'}{4} \sin \theta_K (2F_L \cos^2 \theta_K + (1 - F_L) \sin^2 \theta_K), \quad (5.2c)$$

¹ A_{im} is defined as $A_{\text{im}} = \frac{\text{Im}(A_{\perp L}A_{\parallel L}^*) + \text{Im}(A_{\perp R}A_{\parallel R}^*)}{|A_0|^2 + |A_{\perp}|^2 + |A_{\parallel}|^2}$ and is included for completeness here. It is not of importance for the measurement of right handed currents.

where $\Gamma' = b + 4c$. This method was investigated for *LHCb* in [12]. The observables appear linearly in the expressions so the fits can be performed on data binned in q^2 . The value extracted from these fits is then a $\frac{d\Gamma}{dq^2}$ weighted average of each parameter.

The full angular model described in section 5.2 was used to generate data sets which were then fit simultaneously using the distributions in eq. (5.2). The treatment of background and the $m_{B,K\pi}$ distributions were the same as in the full angular model. For a direct comparison between this method and the full angular fit, the q^2 dependent values of the observables were averaged using a weighted mean,

$$A_T^{(i)} = \frac{\int_{q_{\min}^2}^{q_{\max}^2} \frac{d\Gamma}{dq^2} A_T^{(i)}(q^2)}{\int_{q_{\min}^2}^{q_{\max}^2} \frac{d\Gamma}{dq^2}}. \quad (5.3)$$

The central values produced for the full angular approach in this case show some small biases due to the breakdown of the polynomial ansatz at the edges of the q^2 distribution, however this is still well below the statistical error expected with 10 fb^{-1} of data from *LHCb*. The power of the full angular fit is striking for $A_T^{(2)}$ where the resolution is above a factor 2 better compared to fitting the projections. This can easily be understood in terms of the $(1 - F_L)$ factor in eq. (5.2a), where F_L is large in the SM.

For all the observables where a comparison can be made, we see that the full angular fit provides improvements in the resolution of between 15% and 60%.

In the full angular fit we can calculate the position of the zero crossing for the forward-backward asymmetry, q_0^2 . We illustrate the distribution of results obtained from the ensemble of datasets in figure 2 where a resolution, assuming the SM as input, of 0.17 GeV^2 is obtained. Alternatively we can perform the simpler task of binning the data in 1 GeV^2 bins and then in each bin perform simultaneous fits to the three angular projections. The value of A_{FB} is extracted by performing a straight line fit in the range $2 - 6 \text{ GeV}^2$ to the A_{FB} values found in each q^2 bin. This gives us, with exactly the same assumptions for how background and acceptance are treated, a resolution of 0.24 GeV^2 . So also in this case we see an improvement of 30% in the statistical power by performing a full angular fit.

The comparisons made here demonstrate that there is significant advantage in performing the full angular fit once the data sets are large enough. Using the simplified model described here it is possible to use this approach even with a smaller 2 fb^{-1} data set. In reality, detector effects not accounted for such as angular acceptance will complicate the process and a proper full angular analysis may not be possible with data sets this small. However, we have shown that with the signal and background statistics at *LHCb* a full angular analysis is possible once the detector effects have been properly understood.

6. Phenomenological analysis

In this section we present our phenomenological analysis of the old and new observables in the SM and in extensions of the SM with new right-handed currents. The latter can be done in a model independent way by introducing the chiral partners of the SM Wilson

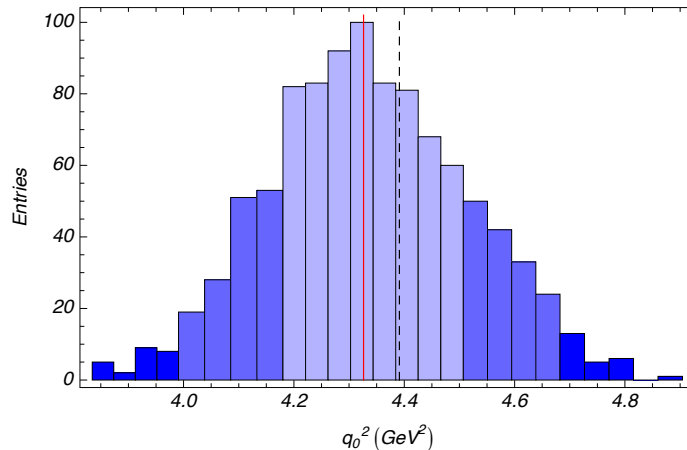


Figure 2: The distribution in the determination of the zero crossing of A_{FB} from an ensemble of datasets created from the toy Monte Carlo model with statistics corresponding to 10 fb^{-1} at LHCb. The edge of the inner (light blue) and middle (medium blue) regions correspond to 1σ and 2σ experimental errors. The solid (red) line is the median of the fitted values and the dashed (black) line is the input value from the SM theory predictions. From the figure we see a resolution of 0.17 GeV^2 .

coefficients $C_7^{(\text{eff})}$, $C_9^{(\text{eff})}$, and C_{10} .² This general new-physics scenario can be realized for example via gluino-mediated FCNC in the general R-parity conserving MSSM.

6.1 Preliminaries

Our analysis is based on the numerical input as summarized in table 1. Regarding the form factor value we follow ref. [35] and use the value fixed by experimental data. Moreover, we introduce four representative benchmark points of supersymmetry with non-minimal flavour violation in the down squark sector which were already used in ref. [20]. The most important flavour diagonal parameters are fixed as follows: $\tan\beta = 5$, $\mu = M_1 = M_2 = M_{H^+} = m_{\tilde{u}_R} = 1 \text{ TeV}$. Note that we choose a low value for $\tan\beta$; this shows that we do not need to rely on a large- $\tan\beta$ to see an effect, and ensures automatic fulfilment of the constraint coming from $B_s \rightarrow \mu^+ \mu^-$. Furthermore, we make the assumption that all the entries in $m_{u,LR}^2$ and $m_{d,LR}^2$ vanish, with the exception of the one that corresponds to $(\delta_{LR}^d)_{32}$. The remaining parameters of the four benchmark points correspond to two different scenarios and are fixed as follows:³

- Scenario A: $m_{\tilde{g}} = 1 \text{ TeV}$ and $m_{\tilde{d}} \in [200, 1000] \text{ GeV}$. The only non-zero mass insertion is varied between $-0.1 \leq (\delta_{LR}^d)_{32} \leq 0.1$. For all parameter sets the compatibility with other B physics constraints, the electroweak constraints, constraints from particle searches, and also with the vacuum stability bounds is verified [20]. The curves denoted by (a) and (b) correspond respectively to $m_{\tilde{g}}/m_{\tilde{d}} = 2.5$, $(\delta_{LR}^d)_{32} = 0.016$

²We note here that the impact of $C_9^{(\text{eff})}$ and C_{10} and their chiral partners is rather small compared with $C_7^{(\text{eff})}$ in the low- q^2 region, due to the $2 \hat{m}_b/\hat{s}$ factor in the matrix element and the experimental constraints from the inclusive decay $B \rightarrow X_s \ell^+ \ell^-$.

³We follow here the conventions of ref. [36]

m_B	$5.27950 \pm 0.00033 \text{ GeV}$	λ	0.2262 ± 0.0014
m_K	$0.896 \pm 0.040 \text{ GeV}$	A	0.815 ± 0.013
M_W	$80.403 \pm 0.029 \text{ GeV}$	$\bar{\rho}$	0.235 ± 0.031
M_Z	$91.1876 \pm 0.0021 \text{ GeV}$	$\bar{\eta}$	0.349 ± 0.020
$\hat{m}_t(\hat{m}_t)$	$167 \pm 5 \text{ GeV}$	$A_{\text{QCD}}^{(n_f=5)}$	$220 \pm 40 \text{ MeV}$
$m_{b,\text{PS}}(2 \text{ GeV})$	$4.6 \pm 0.1 \text{ GeV}$	$\alpha_s(M_Z)$	0.1176 ± 0.0002
m_c	$1.5 \pm 0.2 \text{ GeV}$	α_{em}	$1/137$
f_B	$200 \pm 30 \text{ MeV}$	$a_1(K^*)_{\perp, \parallel}$	0.10 ± 0.07
$f_{K^*, \perp}$	$175 \pm 25 \text{ MeV}$	$a_2(K^*)_{\perp}$	0.13 ± 0.08
$f_{K^*, \parallel}$	$217 \pm 5 \text{ MeV}$	$a_2(K^*)_{\parallel}$	0.09 ± 0.05
$m_B \xi_{K^*, \parallel}(0)/(2m_{K^*})$	0.47 ± 0.09	$\lambda_{B,+}(1.5\text{GeV})$	$0.485 \pm 0.115 \text{ GeV}$
$\xi_{K^*, \perp}(0)$	0.26 ± 0.02		

Table 1: Summary of input parameters and estimated uncertainties.

and $m_{\tilde{g}}/m_{\tilde{d}} = 4$, $(\delta_{LR}^d)_{32} = 0.036$. We will refer to this case as the large-gluino and positive mass insertion scenario. In terms of the effective Wilson coefficients at m_b , model (a) corresponds to $(\mathcal{C}_7^{(\text{eff})}, \mathcal{C}'_7^{(\text{eff})}) = (-0.32, 0.16)$ and (b) to $(-0.32, 0.24)$. This should be compared to the SM value of $(\mathcal{C}_7^{(\text{eff})}, \mathcal{C}'_7^{(\text{eff})}) = (-0.31, 0.00)$.

- Scenario B: $m_{\tilde{d}} = 1 \text{ TeV}$ and $m_{\tilde{g}} \in [200, 800] \text{ GeV}$. The mass insertion is varied in the same range as Scenario A. The curves denoted by (c) and (d) correspond respectively to $m_{\tilde{g}}/m_{\tilde{d}} = 0.7$, $(\delta_{LR}^d)_{32} = -0.004$ and $m_{\tilde{g}}/m_{\tilde{d}} = 0.6$, $(\delta_{LR}^d)_{32} = -0.006$. We will refer to this case as the low-gluino mass (although large squark mass would be more appropriate) and negative mass insertion scenario. In this case the corresponding effective Wilson coefficients are $(\mathcal{C}_7^{(\text{eff})}, \mathcal{C}'_7^{(\text{eff})}) = (-0.32, -0.08)$ for (c) and $(-0.32, -0.13)$ for (d).

Notice that we have changed curve (c) with respect to ref. [20] reducing its corresponding mass insertion to avoid any conflict with vacuum stability or colour breaking constraints [37].

Finally, we emphasize again that the validity of our theoretical predictions is restricted to the kinematic region in which the energy of the K^* is of the order of the heavy quark mass. So we restrict our analysis to the low- q^2 region from 1 GeV^2 to 6 GeV^2 . In the region below 1 GeV^2 the QCDf/SCET results are questioned by the presence of very light resonances.

6.2 Results

We present our results on the observables $A_T^{(2)}$, $A_T^{(3)}$, $A_T^{(4)}$, A_{FB} and F_L in the figures 3–7 (for definitions see section 4). For all the observables we plot the theoretical sensitivity on the left hand side of each figure.

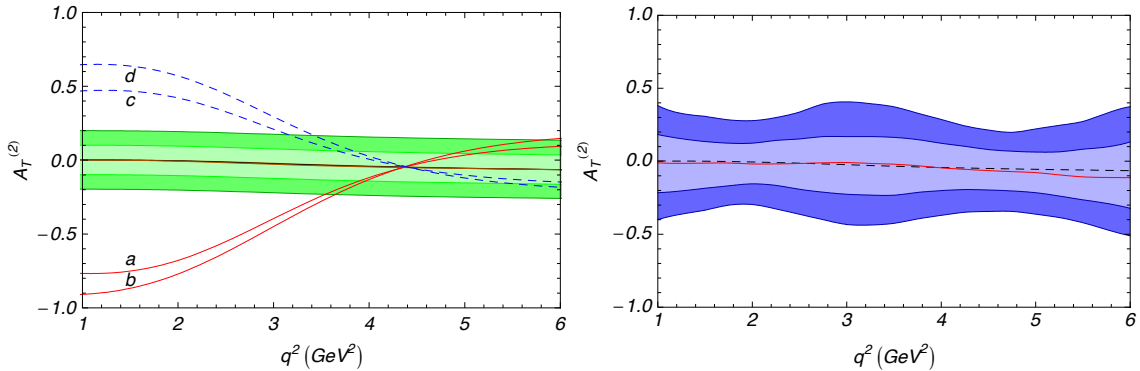


Figure 3: For $A_T^{(2)}$ we compare the theoretical errors (left) with the experimental errors (right) as a function of the squared dimuon mass. For the theory, the narrow inner dark (orange) bands correspond to the NLO result for the SM including all uncertainties (except for Λ/m_b) as explained in the text. Light grey (green) bands include the estimated Λ/m_b uncertainty at a $\pm 5\%$ level and the external dark grey (green) bands correspond to a $\pm 10\%$ correction for each spin amplitude. The curves labelled (a)–(d) correspond to different SUSY scenarios as explained in the text. For the experimental aspects the inner and outer bands correspond to 1σ and 2σ statistical errors with a yield corresponding to a 10 fb^{-1} dataset from LHC**b**.

- The thin dark line is the central NLO result for the SM and the narrow inner dark (orange) band that surrounds it corresponds to the NLO SM uncertainties due to both input parameters and perturbative scale dependence. Light grey (green) bands are the estimated $\Lambda/m_b \pm 5\%$ corrections for each spin amplitude (as given in eq. (3.10)) while darker grey (green) ones are the more conservative $\Lambda/m_b \pm 10\%$ corrections. The curves labelled (a)–(d) correspond to the four different benchmark points in the MSSM introduced above.
- The experimental sensitivity for a dataset corresponding to 10 fb^{-1} of LHC**b** data is given in each figure on the right hand side. Here the solid (red) line shows the median extracted from the fit to the ensemble of data and the dashed (black) line shows the theoretical input distribution. The inner and outer bands correspond to 1σ and 2σ experimental errors.

Let us start with some concrete observations on the new observables $A_T^{(3)}$ and $A_T^{(4)}$. They offer sensitivity to the longitudinal spin amplitude $A_{0L,R}$ in a controlled way compared to the old observables F_L and α_K^* : the dependence on both the parallel and perpendicular soft form factors $\xi_{\parallel}(0)$ and $\xi_{\perp}(0)$ cancels at LO. A residual of this dependence may appear at NLO, but as shown in figures 4 and 5, it is basically negligible. It is also remarkable that for $A_T^{(3)}$ and $A_T^{(4)}$ at low q^2 the impact of this uncertainty is less important than the uncertainties due to input parameters and scale dependence.

The peaking structure in $A_T^{(4)}$ as a function of q^2 for the benchmark MSSM points is due to the different way $\mathcal{C}'_7^{(\text{eff})}$ enters numerator and denominator; the numerator has a positive slope in the region of the peak, while the denominator has a minimum at the same

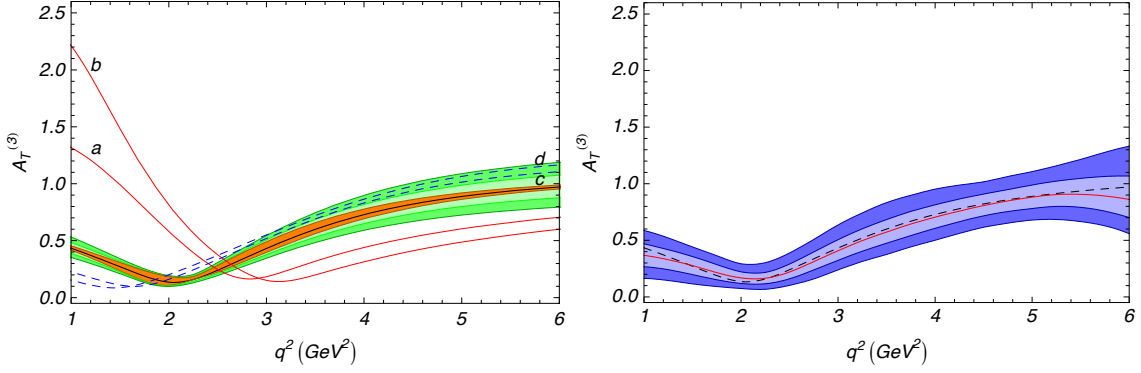


Figure 4: For the new observable $A_T^{(3)}$ we compare the theoretical errors (left) with the experimental errors (right). See the caption of figure 3 for details.

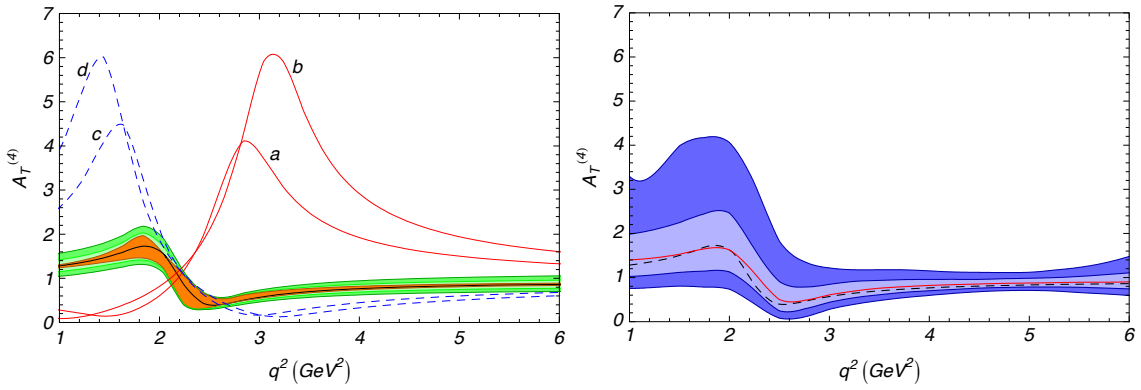


Figure 5: For the new observable $A_T^{(4)}$ we compare the theoretical errors (left) with the experimental errors (right). See the caption of figure 3 for details.

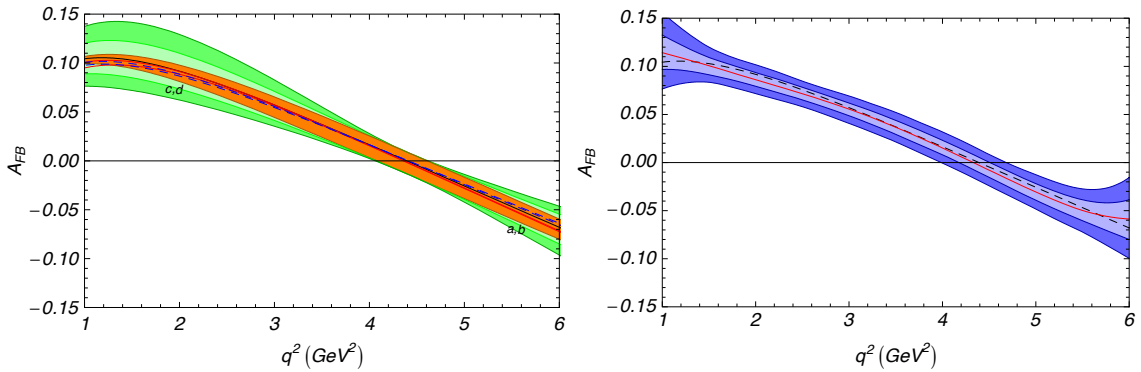


Figure 6: For A_{FB} we compare the theoretical errors (left) with the experimental errors (right). See the caption of figure 3 for details.

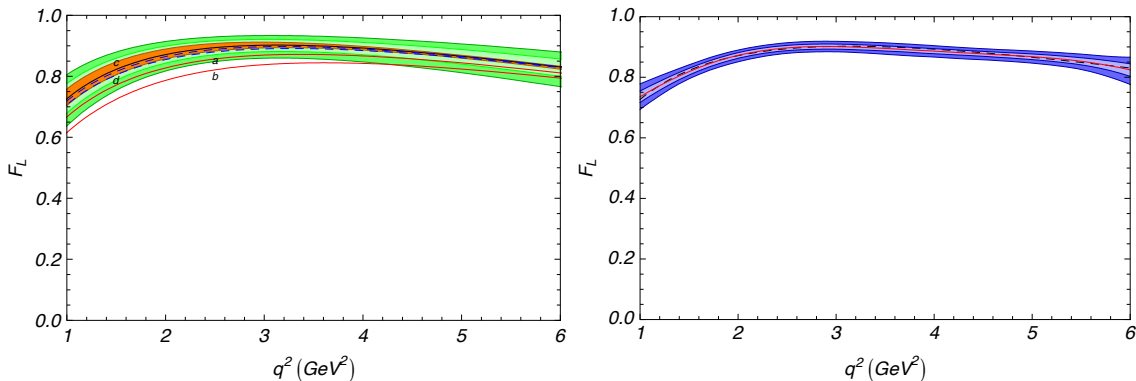


Figure 7: For F_L we compare the theoretical errors (left) with the experimental errors (right). See the caption of figure 3 for details.

point. If one uses the simplified L0 expressions from eqs. (3.7)–(3.9) the denominator is exactly zero, generating an infinity at the point of the peak; however, once NLO QCD is included the zero in the denominator is lifted and the result is a curve with a peak instead.

The new observables $A_T^{(3)}$ and $A_T^{(4)}$ also present a different sensitivity to $\mathcal{C}'_7^{(\text{eff})}$ via their dependence on $A_{0L,R}$ compared with $A_T^{(2)}$. This may allow for a particularly interesting cross check of the sensitivity to this chirality flipped operator \mathcal{O}'_7 ; for instance, new contributions coming from tensor scalars and pseudo-scalars will behave differently among the set of observables.

Another remarkable point that comes clear when comparing the set of clean observables $A_T^{(2)}$, $A_T^{(3)}$ and $A_T^{(4)}$ versus the old observables like F_L concerns the potential discovery of NP, in particular of new right-handed currents. The new observables share the nice feature of $A_T^{(2)}$ that there are large deviations from the SM curve from the ones of the four supersymmetric benchmark points. In case of $A_T^{(2)}$ this is caused by the balance between the competing contributions of order $1/q^2$ and $1/q^4$ originating from the photon pole in the numerator and denominator of $A_T^{(2)}$, providing a strong sensitivity to $\mathcal{C}'_7^{(\text{eff})}$. This sensitivity is near maximal around the 1 GeV^2 region precisely inside the theoretically well controlled area. A large deviation from the SM for $A_T^{(2)}$, $A_T^{(3)}$ or $A_T^{(4)}$ can thus show the presence of right-handed currents in a way that is not possible with F_L or A_{FB} . In the latter cases the deviations from the SM prediction of the same four representative curves are marginal.

In the experimental plots we find a good agreement between the central values extracted from the fits and the theoretical input. Any deviations seen are small compared to the statistical uncertainties, however the weakness of the polynomial parametrisation, particularly at the extremes of the q^2 range, can be seen. For much larger data sets this could be addressed by increasing the order of the polynomials used. The experimental resolution for F_L is very good but with the small deviations from the SM expected this is not helpful in the discovery of new right-handed currents. Comparing the theoretical and experimental figures for the other observables it can be seen that in particular $A_T^{(3)}$ show great promise to distinguish between NP models.

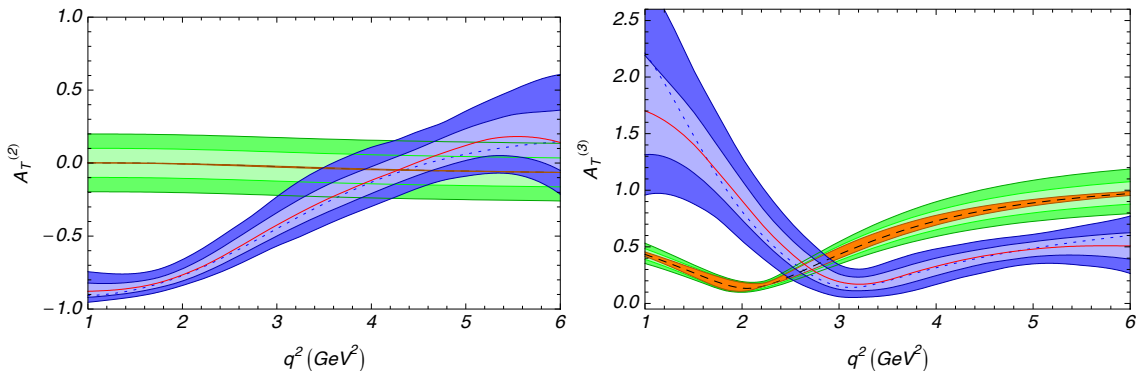


Figure 8: The experimental errors (blue, on top) assuming SUSY scenario (b) with large-gluino mass and positive mass insertion, is compared to the theoretical errors (green, below) assuming the SM. To the left for $A_T^{(2)}$ and the right for $A_T^{(3)}$.

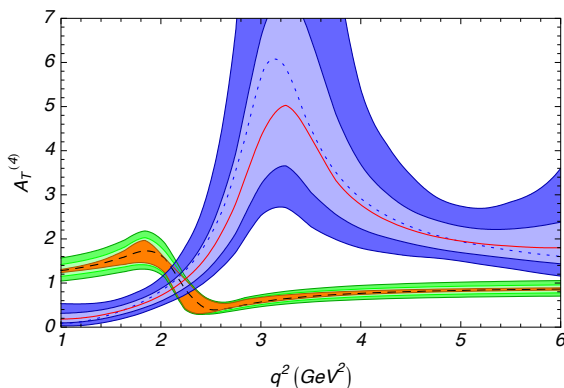


Figure 9: The experimental errors (blue, on top) assuming SUSY scenario (b) with large-gluino mass and positive mass insertion, is compared to the theoretical errors (green, below) assuming the SM. Here the observable $A_T^{(4)}$ is considered.

To further explore the power of the observables we can imagine that nature corresponds to SUSY scenario (b). We create an ensemble of datasets from the toy Monte Carlo model assuming model (b) as input and compare the results to the SM prediction including the theoretical errors to get a feeling for how significantly different from the SM prediction the results are. The results of this are presented in figures 8–10: It can be seen that $A_T^{(2)}$, $A_T^{(3)}$ and $A_T^{(4)}$ all show a remarkable separation between the experimental error band and the SM prediction thus providing high sensitivity to NP. For the SUSY scenario (b) chosen here, the deviation for A_{FB} and F_L on the other hand is minor.

As mentioned in the introduction, the B factories can already access some of the angular observables using the projection-fit method described in section 5. For example, recently the *BABAR* collaboration announced the first measurement of the longitudinal polarisation in the low q^2 region as an average over the bin $q^2 \in [4m_\mu^2, 6.25 \text{ GeV}^2]$ [8] (see figure 11):

$$F_L(q^2 \in [4m_\mu^2, 6.25 \text{ GeV}^2]) = 0.35 \pm 0.16_{\text{stat}} \pm 0.04_{\text{syst}}. \quad (6.1)$$

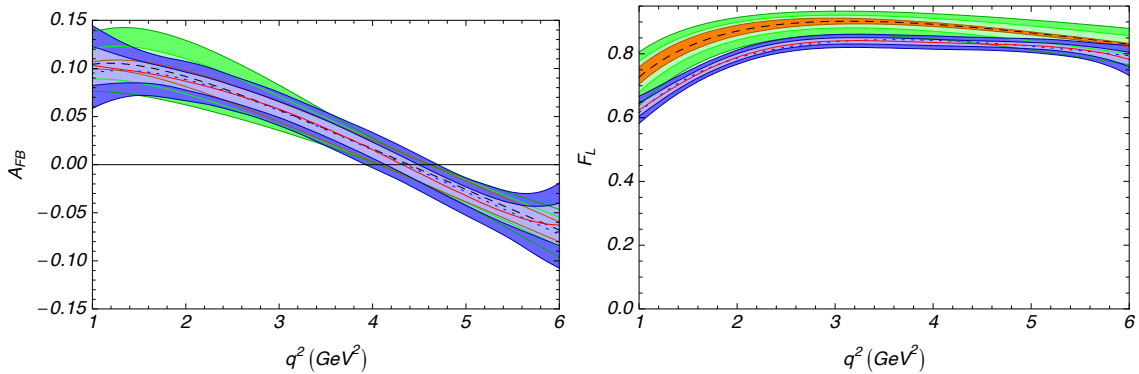


Figure 10: The experimental errors (blue, on top) assuming SUSY scenario (b) with large-gluino mass and positive mass insertion, is compared to the theoretical errors (green, below) assuming the SM. To the left for A_{FB} and the right for F_L .

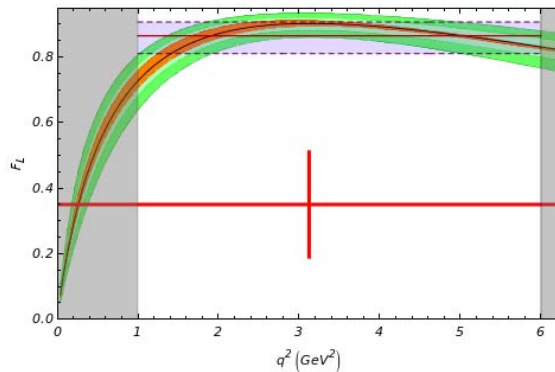


Figure 11: Weighted SM average over the bin $q^2 \in [1 \text{ GeV}^2, 6 \text{ GeV}^2]$ and recent *BABAR* measurement using the extended bin $q^2 \in [4m_\mu^2, 6.25 \text{ GeV}^2]$ (shown in grey).

However, as mentioned before, the spectrum below 1 GeV^2 is theoretically problematic; moreover the rate and also the polarisation F_L are changing dramatically around 1 GeV^2 . Therefore, we strongly recommend to use the standard bin from 1 GeV^2 to 6 GeV^2 . For future comparison we give here the theoretical average, weighted over the rate, using the bin, $q^2 \in [1 \text{ GeV}^2, 6 \text{ GeV}^2]$, based on our results:

$$F_L(q^2 \in [1 \text{ GeV}^2, 6 \text{ GeV}^2]) = 0.86 \pm 0.05. \quad (6.2)$$

and refer to figure 7 for the future experimental sensitivity of the LHC*b* experiment. In figure 11 we see the theoretical q^2 distribution of F_L with the rate average overlaid.

Rather than using the benchmark supersymmetry points for the illustration of the power of the observables, one can also look at it from a model independent point of view. For this we have taken four illustrative points from figure 2 in [21] which are all allowed given the constraints from present measurements of $b \rightarrow s$ transitions. In figure 12 the effect can be seen on $A_T^{(2)}$, $A_T^{(3)}$ and $A_T^{(4)}$. It is clear that the combination of all observables will act as a way to reduce the allowed regions for a model independent analysis.

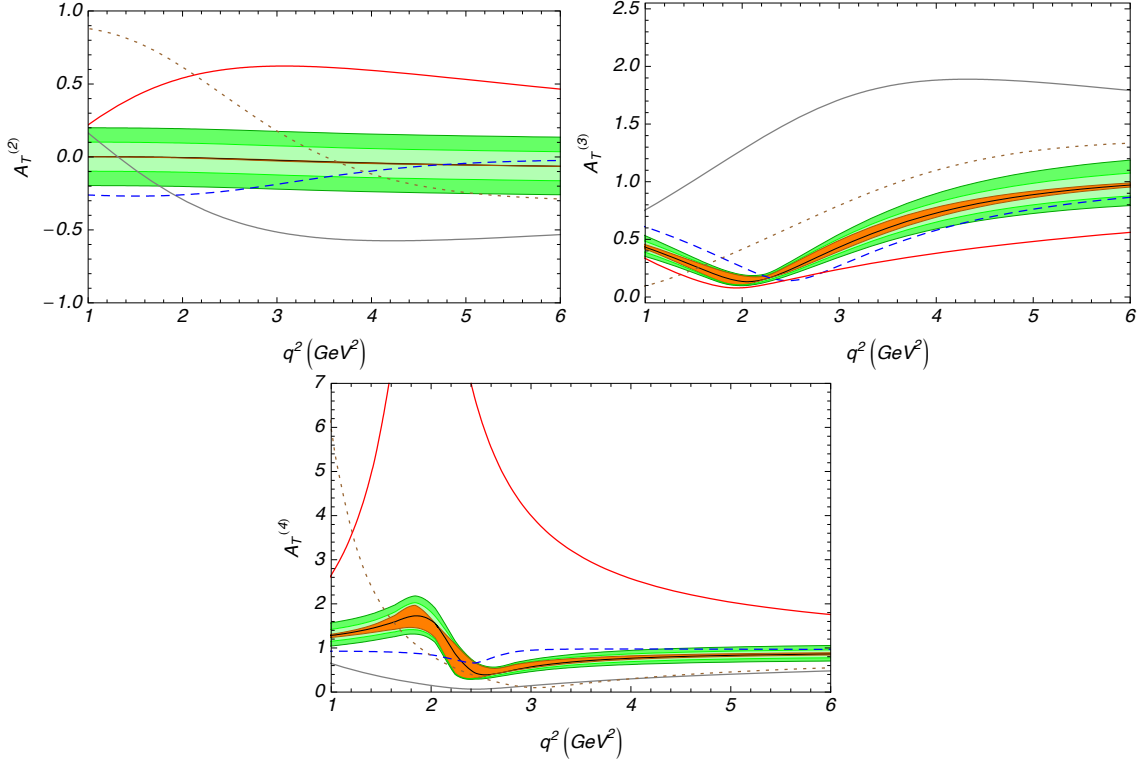


Figure 12: The distribution of $A_T^{(2)}$, $A_T^{(3)}$ and $A_T^{(4)}$ for four allowed combinations of $\mathcal{C}_7^{(\text{eff})}$ and $\mathcal{C}'_7^{(\text{eff})}$ following the model independent analysis of [21]. The bands correspond to the SM and the theoretical uncertainty as described in figure 3. The solid heavy (red) line corresponds to $(\mathcal{C}_7^{(\text{eff})}, \mathcal{C}'_7^{(\text{eff})}) = (0.04, 0.31)$, the solid light (grey) line $(-0.03, -0.32)$, the dashed (blue) line $(-0.35, 0.05)$, and the dotted (brown) line $(-0.24, -0.19)$. Combining measurements in all three asymmetries will provide clear distinction between the different allowed regions.

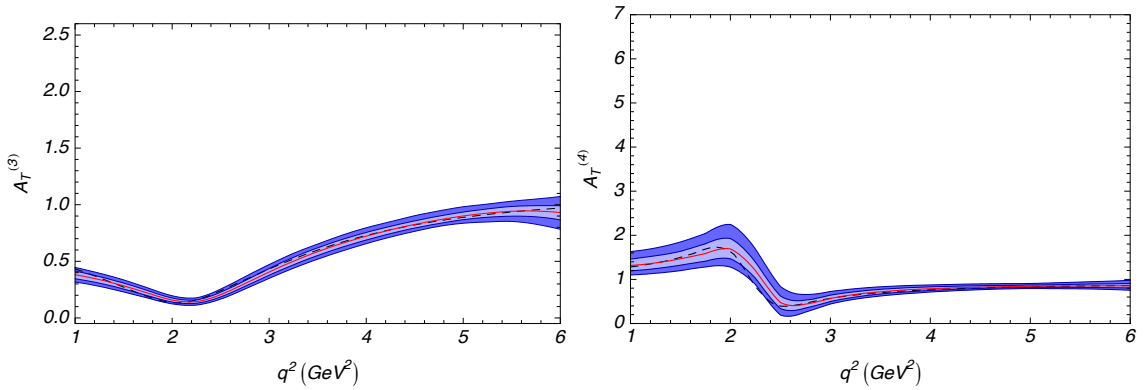


Figure 13: The experimental errors in $A_T^{(3)}$ (right) and $A_T^{(4)}$ left assuming the SM for statistics equivalent to 100 fb^{-1} at the end of an upgrade to LHCb.

Finally we might ask what happens if we consider the situation with 100 fb^{-1} of experimental data corresponding to the full dataset from an upgrade to LHCb. We assume the

same performance of the experiment so simply scale the statistics by a factor 10 compared to the 10fb^{-1} study. The experimental errors are shown in figure 13 and are in general just a factor $\sqrt{10}$ smaller as expected. Comparing to figures 4 and 5 it can be seen that the Λ/m_b uncertainties will dominate unless progress is made on the theoretical side.

7. Summary

We have constructed two new observables $A_T^{(3)}$ and $A_T^{(4)}$ out of the K^* spin amplitudes of the $\bar{B}_d \rightarrow \bar{K}^{*0} \mu^+ \mu^-$ decay, that fulfil the criteria of being theoretically clean and can be experimentally extracted from the angular distribution of this decay with good precision. We have shown how to design the new observables for a specific kind of NP operator within the model independent analysis using the effective field theory approach.

We have presented a complete calculation of all observables in QCD factorization and have made the impact of unknown Λ/m_b corrections to the various observables explicit. Subsequently, we demonstrated the high sensitivity of $A_T^{(2)}$, $A_T^{(3)}$ and $A_T^{(4)}$ to right handed currents. Clearly theoretical progress on the Λ/m_b corrections would enhance that sensitivity significantly and would be desirable in view of an upgrade of the LHC**b** experiment.

The new observables $A_T^{(3)}$ and $A_T^{(4)}$ exhibit the important property of presenting a direct sensitivity to the longitudinal spin amplitude, while reducing at maximum the sensitivity to the poorly known longitudinal soft form factors within the whole low dilepton mass spectrum. Previously defined F_L or A_{FB} does not exhibit this behaviour. This same idea was behind the construction of $A_T^{(2)}$ using the transverse amplitudes.

The combination of the three observables offer a full view of the sensitivity to NP of the three spin amplitudes with a good control of hadronic uncertainties.

Using a toy Monte Carlo approach we have estimated the statistical uncertainty of all observables for statistics corresponding to LHC**b** and also for Super-LHC**b**. The model performs a fit to the full angular and q^2 distribution. $A_T^{(3)}$ and $A_T^{(4)}$ require a full angular fit and for $A_T^{(2)}$ we have demonstrated that the resolution improves by more than a factor 2 compared to extracting $A_T^{(2)}$ from angular projection. The experimental errors are such that measuring these new observables will be a powerful way to detect the presence of right handed currents. For the well known measurement of the zero point of the forward-backward asymmetry we see an improvement of 30% in the resolution from a full angular fit compared to fitting the angular projections.

Finally we have shown that the previously discussed angular distribution $A_T^{(1)}$ cannot be measured at either LHC**b** or at a Super-*B* factory.

Acknowledgments

We thank Martin Beneke for detailed discussions on the forward-backward asymmetry. JM acknowledges financial support from FPA2005-02211, 2005-SGR-00994 and the RyC programme, MR from the Universitat Autònoma de Barcelona, and UE and WR from the Science and Technology Facilities Council (STFC).

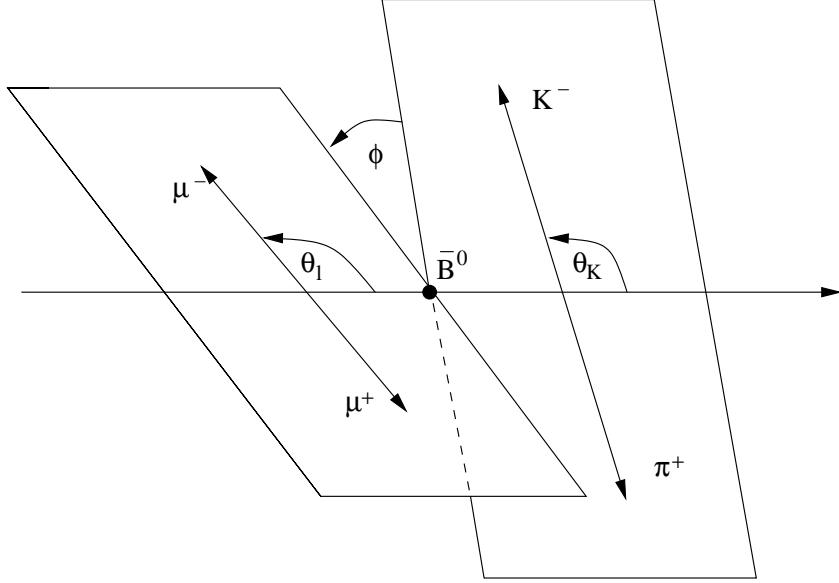


Figure 14: Definition of kinematic variables in the decay $\bar{B}_d \rightarrow \bar{K}^{*0} \mu^+ \mu^-$: The z -axis is the direction in which the B meson flies in the rest frame of the $\mu^+ \mu^-$. θ_l is the angle between the μ^- and the z -axis in the $\mu^+ \mu^-$ rest frame, θ_K is the angle between the K^- and the z -axis in the \bar{K}^* rest frame, and ϕ is the angle between the normals to the $\mu^+ \mu^-$ and $K\pi$ decay planes in the B rest frame.

A. Kinematics

Assuming the K^* to be on the mass shell, the decay $\bar{B}^0 \rightarrow \bar{K}^{*0} (\rightarrow K^- \pi^+) \ell^+ \ell^-$ is completely described by four independent kinematic variables; namely, the lepton-pair invariant mass, q^2 , and the three angles θ_l , θ_{K^*} , ϕ as illustrated in figure 14. The sign of the angles for the \bar{B}_d decay shows great variation in the literature. Therefore we present here the most explicit definition of our conventions. Here \mathbf{p} denote three momentum vectors in the \bar{B}_d rest frame, \mathbf{q} the same in the di-muon rest frame, and \mathbf{r} in the \bar{K}^{*0} rest frame, the z -axis is defined as the direction of the \bar{K}^{*0} in the \bar{B}_d rest frame. Three unit vectors are given in the following way: the first one is in the direction of the z -axis where the θ angles are measured with respect to, and the other two are perpendicular to the di-muon and \bar{K}^{*0} decay planes.

$$\mathbf{e}_z = \frac{\mathbf{p}_{K^-} + \mathbf{p}_{\pi^+}}{|\mathbf{p}_{K^-} + \mathbf{p}_{\pi^+}|}, \quad \mathbf{e}_l = \frac{\mathbf{p}_{\mu^-} \times \mathbf{p}_{\mu^+}}{|\mathbf{p}_{\mu^-} \times \mathbf{p}_{\mu^+}|}, \quad \mathbf{e}_K = \frac{\mathbf{p}_{K^-} \times \mathbf{p}_{\pi^+}}{|\mathbf{p}_{K^-} \times \mathbf{p}_{\pi^+}|}. \quad (\text{A.1})$$

It follows for the \bar{B}_d

$$\cos \theta_l = \frac{\mathbf{q}_{\mu^-} \cdot \mathbf{e}_z}{|\mathbf{q}_{\mu^-}|}, \quad \cos \theta_K = \frac{\mathbf{r}_{K^-} \cdot \mathbf{e}_z}{|\mathbf{r}_{K^-}|} \quad (\text{A.2})$$

and

$$\sin \phi = (\mathbf{e}_l \times \mathbf{e}_K) \cdot \mathbf{e}_z, \quad \cos \phi = \mathbf{e}_K \cdot \mathbf{e}_l. \quad (\text{A.3})$$

The angles are defined in the intervals

$$-1 \leq \cos \theta_l \leq 1, \quad -1 \leq \cos \theta_K \leq 1, \quad -\pi \leq \phi < \pi, \quad (\text{A.4})$$

where in particular it should be noted that the ϕ angle is signed.

In words, for the \bar{B}_d the angle θ_l is measured as the angle between the μ^- and the z -axis in the dimuon rest frame. As the \bar{B}_d flies in the direction of the z -axis in the dimuon rest frame this is equivalent to measuring θ_l as the angle between the muon and the \bar{B}_d in the di-muon rest frame. The angle θ_K is measured as the angle between the kaon and the z -axis measured in the \bar{K}^{*0} rest frame. Finally ϕ is the angle between the normals to the planes defined by the $K\pi$ system and the $\mu^+\mu^-$ system in the rest frame of the \bar{B}_d meson.

B. Theoretical framework

The coefficient functions I_i in the differential decay rate are given in terms of the K^* spin amplitudes (see eq. (2.3)) discussed in section 3. The theoretical expressions of those spin amplitudes can be derived using the following standard steps:

- The effective Hamiltonian describing the quark transition $b \rightarrow s\ell^+\ell^-$ is given by

$$\mathcal{H}_{\text{eff}} = -\frac{4G_F}{\sqrt{2}}V_{tb}V_{ts}^* \sum_{i=1}^{10} [C_i(\mu)\mathcal{O}_i(\mu) + C'_i(\mu)\mathcal{O}'_i(\mu)], \quad (\text{B.1})$$

where in addition to the SM operators we have also added the chirally flipped partners. In what follows, the same conventions are used as in [19]. In the NP analysis, we will focus on the the chirally flipped \mathcal{O}'_7 operator in addition to the most important SM operators \mathcal{O}_7 , \mathcal{O}_9 , and \mathcal{O}_{10} :

$$\mathcal{O}_7 = \frac{e}{16\pi^2}m_b(\bar{s}\sigma_{\mu\nu}P_R b)F^{\mu\nu}, \quad \mathcal{O}'_7 = \frac{e}{16\pi^2}m_b(\bar{s}\sigma_{\mu\nu}P_L b)F^{\mu\nu}, \quad (\text{B.2})$$

$$\mathcal{O}_9 = \frac{e^2}{16\pi^2}(\bar{s}\gamma_\mu P_L b)(\bar{\ell}\gamma^\mu \ell), \quad \mathcal{O}_{10} = \frac{e^2}{16\pi^2}(\bar{s}\gamma_\mu P_L b)(\bar{\ell}\gamma^\mu \gamma_5 \ell), \quad (\text{B.3})$$

where $P_{L,R} = (1 \mp \gamma_5)/2$ and $m_b \equiv m_b(\mu)$ is the running mass in the $\overline{\text{MS}}$ scheme.

- The hadronic part of the matrix element describing the $B \rightarrow K\pi$ transition can be parameterised in terms of $B \rightarrow K^*$ form factors by means of a narrow-width approximation (see for example [22]). The relevant form factors are defined as:

$$\begin{aligned} \langle K^*(p_{K^*}) | \bar{s}\gamma_\mu P_{L,R} b | B(p) \rangle &= i\epsilon_{\mu\nu\alpha\beta} \epsilon^{\nu*} p^\alpha q^\beta \frac{V(q^2)}{m_B + m_{K^*}} \mp \\ &\mp \frac{1}{2} \left\{ \epsilon_\mu^*(m_B + m_{K^*}) A_1(q^2) - (\epsilon^* \cdot q)(2p - q)_\mu \frac{A_2(q^2)}{m_B + m_{K^*}} - \right. \\ &\quad \left. - \frac{2m_{K^*}}{q^2} (\epsilon^* \cdot q) [A_3(q^2) - A_0(q^2)] q_\mu \right\}, \end{aligned} \quad (\text{B.4})$$

where

$$A_3(q^2) = \frac{m_B + m_{K^*}}{2m_{K^*}} A_1(q^2) - \frac{m_B - m_{K^*}}{2m_{K^*}} A_2(q^2), \quad (\text{B.5})$$

and

$$\langle K^*(p_{K^*}) | \bar{s}i\sigma_{\mu\nu} q^\nu P_{R,L} b | B(p) \rangle = -i\epsilon_{\mu\nu\alpha\beta} \epsilon^{\nu*} p^\alpha q^\beta T_1(q^2) \pm$$

$$\pm \frac{1}{2} \left\{ [\epsilon_\mu^*(m_B^2 - m_{K^*}^2) - (\epsilon^* \cdot q)(2p - q)_\mu] T_2(q^2) + (\epsilon^* \cdot q) \left[q_\mu - \frac{q^2}{m_B^2 - m_{K^*}^2} (2p - q)_\mu \right] T_3(q^2) \right\}. \quad (\text{B.6})$$

In the above, $q = p_{l^+} + p_{l^-}$ and ϵ^μ is the K^* polarisation vector.

- In the heavy-quark and large-energy limit the seven a priori independent $B \rightarrow K^*$ form factors in eqs. (B.4) and (B.6) reduce to two universal form factors ξ_\perp and ξ_\parallel in the leading order [27, 28]:⁴

$$A_1(q^2) = \frac{2E_{K^*}}{m_B + m_{K^*}} \xi_\perp(E_{K^*}), \quad (\text{B.7a})$$

$$A_2(q^2) = \frac{m_B}{m_B - m_{K^*}} [\xi_\perp(E_{K^*}) - \xi_\parallel(E_{K^*})], \quad (\text{B.7b})$$

$$A_0(q^2) = \frac{E_{K^*}}{m_{K^*}} \xi_\parallel(E_{K^*}), \quad (\text{B.7c})$$

$$V(q^2) = \frac{m_B + m_{K^*}}{m_B} \xi_\perp(E_{K^*}), \quad (\text{B.7d})$$

$$T_1(q^2) = \xi_\perp(E_{K^*}), \quad (\text{B.7e})$$

$$T_2(q^2) = \frac{2E_{K^*}}{m_B} \xi_\perp(E_{K^*}), \quad (\text{B.7f})$$

$$T_3(q^2) = \xi_\perp(E_{K^*}) - \xi_\parallel(E_{K^*}). \quad (\text{B.7g})$$

Here, E_{K^*} is the energy of the final vector meson in the B rest frame,

$$E_{K^*} \simeq \frac{m_B}{2} \left(1 - \frac{q^2}{m_B^2} \right). \quad (\text{B.8})$$

These relations, valid in the low- q^2 region, allow to simplify the spin amplitudes to obtain eqs. (3.7)–(3.9) which are crucial for the construction of our new observables. They are violated by symmetry breaking corrections of order α_s and $1/m_b$.

C. NLO corrections to the spin amplitudes

The NLO corrections to the form factors at order α_s are given in ref. [17]. In the presence of right-handed currents ($\mathcal{C}_7^{(\text{eff})} \neq 0$), the spin amplitudes read [19, 20]

$$A_{\perp L,R} = N\sqrt{2} \lambda^{1/2} \left[(\mathcal{C}_9 \mp \mathcal{C}_{10}) \frac{V(q^2)}{m_B + m_{K^*}} + \frac{2m_b}{q^2} \mathcal{T}_{\perp \text{NLO}}^+(q^2) \right], \quad (\text{C.1})$$

$$A_{\parallel L,R} = -N\sqrt{2} (m_B^2 - m_{K^*}^2) \left[(\mathcal{C}_9 \mp \mathcal{C}_{10}) \frac{A_1(q^2)}{m_B - m_{K^*}} + \frac{4m_b E_{K^*}}{m_B \cdot s} \mathcal{T}_{\perp \text{NLO}}^-(q^2) \right], \quad (\text{C.2})$$

$$A_{0L,R} = -\frac{N}{2m_{K^*} q} \times \left[(\mathcal{C}_9 \mp \mathcal{C}_{10}) \left\{ (m_B^2 - m_{K^*}^2 - q^2)(m_B + m_{K^*}) A_1(q^2) - \lambda \frac{A_2(q^2)}{m_B + m_{K^*}} \right\} \right]$$

⁴Following ref. [28], the longitudinal form factor ξ_\parallel is related to that of ref. [27] by $\xi_\parallel = (m_{K^*}/E_{K^*})\zeta_\parallel$.

$$2m_b \left\{ (m_B^2 + 3m_{K^*}^2 - q^2) \frac{2E_{K^*}}{m_B} \mathcal{T}_{\perp\text{NLO}}^-(q^2) - \frac{\lambda}{m_B^2 - m_{K^*}^2} \left(\mathcal{T}_{\perp\text{NLO}}^-(q^2) + \mathcal{T}_{\parallel\text{NLO}}^-(q^2) \right) \right\}, \quad (\text{C.3})$$

where λ is defined in eq. (3.5) and the form factor relations for $V(q^2)$, $A_0(q^2)$ and $A_1(q^2)$ are as in eq. (3.7). $A_2(q^2)$ is given by

$$A_2(q^2) = \frac{m_B}{m_B - m_{K^*}} [\xi_{\perp}(q^2) - \xi_{\parallel}(q^2) (1 + C)], \quad (\text{C.4})$$

with C the $\mathcal{O}(\alpha_s)$ correction to the form factor A_2 computed in [28, 17, 35]:

$$C = \frac{\alpha_s}{3\pi} \left[(2 - 2L) + 8 \frac{m_{K^*}}{E_{K^*}} \frac{m_B(m_B - 2E_{K^*})}{4E_{K^*}^2} \kappa_{\parallel}(q^2) \lambda_{B,+}^{-1} \int_0^1 du \frac{\Phi_{K^*,\parallel}(u)}{1-u} \right] \quad (\text{C.5})$$

with $\Phi_{K^*,\parallel}(u)$ being the longitudinal light-cone distribution amplitude of the vector meson \bar{K}^{*0} . Moreover, we have

$$\mathcal{T}_{\perp\text{NLO}}^{\pm} = \xi_{\perp}(q^2) \left\{ C_{\perp}^{(0,\pm)} + \frac{\alpha_s}{3\pi} \left[C_{\perp}^{(1,\pm)} + \kappa_{\perp}(q^2) \lambda_{B,+}^{-1} \int_0^1 du \Phi_{K^*,\perp}(u) \left[T_{\perp,+}^{(f\pm)}(u) + T_{\perp,+}^{(\text{nf})}(u) \right] \right] \right\}$$

and

$$\begin{aligned} \mathcal{T}_{\parallel\text{NLO}}^{\pm} = \xi_{\parallel}(q^2) \left\{ C_{\parallel}^{(0,\pm)} + \kappa_{\parallel}(q^2) \frac{m_{K^*}^*}{E_{K^*}} \lambda_{B,-}^{-1}(q^2) \int_0^1 du \Phi_{K^*,\parallel}(u) \hat{T}_{\parallel,-}^{(0)}(u) + \right. \\ \left. + \frac{\alpha_s}{3\pi} \left[C_{\parallel}^{(1,\pm)} + \kappa_{\parallel}(q^2) \frac{m_{K^*}^*}{E_{K^*}} \left(\lambda_{B,+}^{-1} \int_0^1 du \Phi_{K^*,\parallel}(u) \left[T_{\parallel,+}^{(f\pm)}(u) + T_{\parallel,+}^{(\text{nf})}(u) \right] + \right. \right. \right. \\ \left. \left. + \lambda_{B,-}^{-1}(q^2) \int_0^1 du \Phi_{K^*,\parallel}(u) \hat{T}_{\parallel,-}^{(\text{nf})}(u) \right) \right] \right\}, \quad (\text{C.6}) \end{aligned}$$

where $\kappa_z \equiv \pi^2 f_B f_{K^*,z}(\mu) / (N_c m_B \xi_z(q^2))$ (with $z = \perp, \parallel$). $\lambda_{B,+}^{-1}$ and $\lambda_{B,-}^{-1}(q^2)$ are the two \bar{B}_d meson light-cone distribution amplitude moments defined in [17]; they are given by

$$\lambda_{B,+}^{-1} = \int_0^{\infty} d\omega \frac{\Phi_{B,+}(\omega)}{\omega}, \quad (\text{C.7a})$$

$$\lambda_{B,-}^{-1}(q^2) = \int_0^{\infty} d\omega \frac{\Phi_{B,-}(\omega)}{\omega - q^2/m_B - i\epsilon}. \quad (\text{C.7b})$$

In all cases the symbol $+$ stands for the substitution of $\mathcal{C}_7^{(\text{eff})} \rightarrow \mathcal{C}_7^{(\text{eff})} + \mathcal{C}_7^{\prime(\text{eff})}$ and $-$ for $\mathcal{C}_7^{(\text{eff})} \rightarrow \mathcal{C}_7^{(\text{eff})} - \mathcal{C}_7^{\prime(\text{eff})}$, wherever $\mathcal{C}_7^{(\text{eff})}$ appears. For instance, in the definition of

$$C_z^{(1,\pm)} = C_z^{(f\pm)} + C_z^{(\text{nf})} \quad (\text{C.8})$$

with $z = \perp, \parallel$, the factorizable correction reads [28, 17]

$$C_{\perp}^{(f\pm)} = \left(C_7^{\text{eff}} \pm C_7^{\text{eff}'} \right) \left(4 \ln \frac{m_b^2}{\mu^2} - 4 - L \right), \quad (\text{C.9})$$

$$C_{\parallel}^{(f\pm)} = - \left(C_7^{\text{eff}} \pm C_7^{\text{eff}'} \right) \left(4 \ln \frac{m_b^2}{\mu^2} - 6 + 4L \right) + \frac{m_B}{2m_b} Y(q^2) (2 - 2L) \quad (\text{C.10})$$

with

$$L \equiv - \frac{m_b^2 - q^2}{q^2} \ln \left(1 - \frac{q^2}{m_b^2} \right). \quad (\text{C.11})$$

while the non-factorizable contribution $C_z^{(\text{nf})}$ is common to both. In the definition of the hard scattering functions with $T_{z,\pm}^{(1\pm)} = T_{z,\pm}^{(f\pm)} + T_{z,\pm}^{(\text{nf})}$, the factorizable correction reads [28, 17]:

$$T_{\perp,+}^{(f\pm)}(u, \omega) = \left(C_7^{\text{eff}} \pm C_7^{\text{eff}'} \right) \frac{2 m_B}{\bar{u} E_{K^*}}, \quad (\text{C.12})$$

$$T_{\parallel,+}^{(f\pm)}(u, \omega) = \left[\left(C_7^{\text{eff}} \pm C_7^{\text{eff}'} \right) + \frac{q^2}{2 m_b m_B} Y(q^2) \right] \frac{2 m_B^2}{(1-u) E_{K^*}^2}, \quad (\text{C.13})$$

$$T_{\perp,-}^{(f)}(u, \omega) = T_{\parallel,-}^{(f)}(u, \omega) = 0. \quad (\text{C.14})$$

Again the non-factorizable part is common to both cases, because it does not receive contributions from \mathcal{O}_7 . For the definition of the function $Y(q^2)$ and for the non-factorizable contributions we refer the reader to [28, 17].

References

- [1] M. Artuso et al., *B, D and K decays*, arXiv:0801.1833.
- [2] T. Hurth, *Present status of inclusive rare B decays*, *Rev. Mod. Phys.* **75** (2003) 1159 [hep-ph/0212304].
- [3] T. Hurth, *Status of SM calculations of $b \rightarrow s$ transitions*, *Int. J. Mod. Phys. A* **22** (2007) 1781 [hep-ph/0703226].
- [4] BELLE collaboration, A. Ishikawa et al., *Observation of the electroweak penguin decay $B \rightarrow K^* \ell^+ \ell^-$* , *Phys. Rev. Lett.* **91** (2003) 261601 [hep-ex/0308044].
- [5] BABAR collaboration, B. Aubert et al., *Evidence for the rare decay $B \rightarrow K^* \ell^+ \ell^-$ and measurement of the $B \rightarrow K \ell^+ \ell^-$ branching fraction*, *Phys. Rev. Lett.* **91** (2003) 221802 [hep-ex/0308042].
- [6] A. Ishikawa et al., *Measurement of forward-backward asymmetry and Wilson coefficients in $B \rightarrow K^* \ell^+ \ell^-$* , *Phys. Rev. Lett.* **96** (2006) 251801 [hep-ex/0603018].
- [7] BABAR collaboration, B. Aubert et al., *Measurements of branching fractions, rate asymmetries and angular distributions in the rare decays $B \rightarrow K \ell^+ \ell^-$ and $B \rightarrow K^* \ell^+ \ell^-$* , *Phys. Rev. D* **73** (2006) 092001 [hep-ex/0604007].
- [8] BABAR collaboration, B. Aubert et al., *Angular distributions in the decays $B \rightarrow K^* \ell^+ \ell^-$* , arXiv:0804.4412.
- [9] THE BELLE collaboration, I. Adachi, *Measurement of the differential branching fraction and forward-backward asymmetry for $B \rightarrow K^* \ell^+ \ell^-$* , arXiv:0810.0335.
- [10] J. Dickens, V. Gibson, C. Lazzeroni and M. Patel, *Selection of the decay $B \rightarrow K^* \ell^+ \ell^-$ at LHCb*, CERN-LHCB-2007-038.

- [11] J. Dickens, V. Gibson, C. Lazzeroni and M. Patel, *A study of the sensitivity to the forward-backward asymmetry in $B_d \rightarrow K^* \mu^+ \mu^-$ decays at LHCb*, CERN-LHCB-2007-039.
- [12] U. Egede, *Angular correlations in the $\bar{B}_d \rightarrow \bar{K}^{*0} \mu^+ \mu^-$ decay*, CERN-LHCB-2007-057.
- [13] T. Browder et al., *On the physics case of a super flavour factory*, *JHEP* **02** (2008) 110 [[arXiv:0710.3799](#)].
- [14] M. Bona et al., *SuperB: a high-LuMINOSity asymmetric e^+e^- super flavor factory. Conceptual design report*, [arXiv:0709.0451](#).
- [15] J.L. Hewett et al., *The discovery potential of a super B factory. Proceedings, SLAC Workshops, Stanford, U.S.A., 2003*, [hep-ph/0503261](#).
- [16] SUPERKEKB PHYSICS WORKING GROUP collaboration, A.G. Akeroyd et al., *Physics at super B factory*, [hep-ex/0406071](#).
- [17] M. Beneke, T. Feldmann and D. Seidel, *Systematic approach to exclusive $B \rightarrow V \ell^+ \ell^-$, $V \gamma$ decays*, *Nucl. Phys. B* **612** (2001) 25 [[hep-ph/0106067](#)].
- [18] C.-H. Chen and C.Q. Geng, *Analysis of $B \rightarrow K^* \ell^+ \ell^-$ decays at large recoil*, *Nucl. Phys. B* **636** (2002) 338 [[hep-ph/0203003](#)].
- [19] F. Krüger and J. Matias, *Probing new physics via the transverse amplitudes of $B^0 \rightarrow K^{*0}(\rightarrow K^- \pi^+) \ell^+ \ell^-$ at large recoil*, *Phys. Rev. D* **71** (2005) 094009 [[hep-ph/0502060](#)]; J. Matias, *The angular distribution of $B^0 \rightarrow K^{*0}(\rightarrow K^- \pi^+) \ell^+ \ell^-$ at large recoil in and beyond the SM*, *PoS(HEP2005)281* [[hep-ph/0511274](#)].
- [20] E. Lunghi and J. Matias, *Huge right-handed current effects in $B \rightarrow K^*(K\pi) \ell^+ \ell^-$ in supersymmetry*, *JHEP* **04** (2007) 058 [[hep-ph/0612166](#)].
- [21] C. Bobeth, G. Hiller and G. Piranishvili, *CP Asymmetries in $\bar{B} \rightarrow \bar{K}^*(\rightarrow \bar{K}\pi) \ell^+ \ell^-$ and untagged $\bar{B}_s, B_s \rightarrow \phi(\rightarrow K^+ K^-) \ell^+ \ell^-$ decays at NLO*, *JHEP* **07** (2008) 106 [[arXiv:0805.2525](#)].
- [22] F. Krüger, L.M. Sehgal, N. Sinha and R. Sinha, *Angular distribution and CP asymmetries in the decays $\bar{B} \rightarrow K^- \pi^+ e^- e^+$ and $\bar{B} \rightarrow \pi^- \pi^+ e^- e^+$* , *Phys. Rev. D* **61** (2000) 114028 [*Erratum ibid.* **D 63** (2001) 019901] [[hep-ph/9907386](#)];
- [23] D. Melikhov, N. Nikitin and S. Simula, *Probing right-handed currents in $B \rightarrow K^* \ell^+ \ell^-$ transitions*, *Phys. Lett. B* **442** (1998) 381 [[hep-ph/9807464](#)].
- [24] C.S. Kim, Y.G. Kim, C.-D. Lü and T. Morozumi, *Azimuthal angle distribution in $B \rightarrow K^*(\rightarrow K\pi) \ell^+ \ell^-$ at low invariant $m(\ell^+ \ell^-)$ region*, *Phys. Rev. D* **62** (2000) 034013 [[hep-ph/0001151](#)]; C.S. Kim, Y.G. Kim and C.-D. Lü, *Possible supersymmetric effects on angular distributions in $B \rightarrow K^*(\rightarrow K\pi) \ell^+ \ell^-$ decays*, *Phys. Rev. D* **64** (2001) 094014 [[hep-ph/0102168](#)].
- [25] A. Faessler, T. Gutsche, M.A. Ivanov, J.G. Körner and V.E. Lyubovitskij, *The exclusive rare decays $B \rightarrow K(K^*) \bar{\ell} \ell$ and $B_c \rightarrow D(D^*) \bar{\ell} \ell$ in a relativistic quark model*, *Eur. Phys. J. Direct. C* **4** (2002) 18 [[hep-ph/0205287](#)].
- [26] A. Ali and A.S. Safir, *Helicity analysis of the decays $B \rightarrow K^* \ell^+ \ell^-$ and $B \rightarrow \rho \nu_\ell$ in the large energy effective theory*, *Eur. Phys. J. C* **25** (2002) 583 [[hep-ph/0205254](#)].

- [27] J. Charles, A. Le Yaouanc, L. Oliver, O. Pene and J.C. Raynal, *Heavy-to-light form factors in the heavy mass to large energy limit of QCD*, *Phys. Rev. D* **60** (1999) 014001 [[hep-ph/9812358](#)]; *Heavy-to-light form factors in the final hadron large energy limit: covariant quark model approach*, *Phys. Lett. B* **451** (1999) 187 [[hep-ph/9901378](#)]; M.J. Dugan and B. Grinstein, *QCD basis for factorization in decays of heavy mesons*, *Phys. Lett. B* **255** (1991) 583.
- [28] M. Beneke and T. Feldmann, *Symmetry-breaking corrections to heavy-to-light B meson form factors at large recoil*, *Nucl. Phys. B* **592** (2001) 3 [[hep-ph/0008255](#)].
- [29] B. Stech, *Form-factor relations for heavy to light transitions*, *Phys. Lett. B* **354** (1995) 447 [[hep-ph/9502378](#)]; J.M. Soares, *Form factor relations for heavy-to-heavy and heavy-to-light meson transitions*, *Phys. Rev. D* **54** (1996) 6837 [[hep-ph/9607284](#)]; *Form factor relations for pseudoscalar to vector meson transitions*, [hep-ph/9810402](#).
- [30] J.M. Soares, *Form factor relations for heavy-to-light meson transitions: tests of the quark model predictions*, [hep-ph/9810421](#).
- [31] G. Burdman and G. Hiller, *Semileptonic form-factors from $B \rightarrow K^* \gamma$ decays in the large energy limit*, *Phys. Rev. D* **63** (2001) 113008 [[hep-ph/0011266](#)].
- [32] U. Egede, T. Hurth, J. Matias, M. Ramon and W. Reece, in preparation.
- [33] A. Ali, T. Mannel and T. Morozumi, *Forward backward asymmetry of dilepton angular distribution in the decay $b \rightarrow s \ell^+ \ell^-$* , *Phys. Lett. B* **273** (1991) 505.
- [34] T. Feldmann and J. Matias, *Forward-backward and isospin asymmetry for $B \rightarrow K^* \ell^+ \ell^-$ decay in the standard model and in supersymmetry*, *JHEP* **01** (2003) 074 [[hep-ph/0212158](#)].
- [35] M. Beneke, T. Feldmann and D. Seidel, *Exclusive radiative and electroweak $b \rightarrow d$ and $b \rightarrow s$ penguin decays at NLO*, *Eur. Phys. J. C* **41** (2005) 173 [[hep-ph/0412400](#)].
- [36] J. Foster, K.-I. Okumura and L. Roszkowski, *Probing the flavour structure of supersymmetry breaking with rare B-processes: a beyond leading order analysis*, *JHEP* **08** (2005) 094 [[hep-ph/0506146](#)].
- [37] J.A. Casas and S. Dimopoulos, *Stability bounds on flavor-violating trilinear soft terms in the MSSM*, *Phys. Lett. B* **387** (1996) 107 [[hep-ph/9606237](#)].

Erratum

- Eq. (4.3) should read

$$\begin{aligned}
 A'_{\perp L} &= +\cos\theta A_{\perp L} + \sin\theta A_{\perp R}^* \\
 A'_{\perp R} &= -\sin\theta A_{\perp L} + \cos\theta A_{\perp R} \\
 A'_{0L} &= +\cos\theta A_{0L} - \sin\theta A_{0R}^* \\
 A'_{0R} &= +\sin\theta A_{0L} + \cos\theta A_{0R} \\
 A'_{\parallel L} &= +\cos\theta A_{\parallel L} - \sin\theta A_{\parallel R}^* \\
 A'_{\parallel R} &= +\sin\theta A_{\parallel L} + \cos\theta A_{\parallel R}.
 \end{aligned}$$

- Eq. (4.11) changes to

$$A_T^{(3)} = \frac{|A_{0L}A_{\parallel L}^* + A_{0R}^*A_{\parallel R}|}{\sqrt{|A_0|^2|A_{\perp}|^2}}.$$

- Eq. (C.4) should read

$$A_2(q^2) = \frac{m_B}{m_B - m_{K^*}} [\xi_{\perp}(q^2) - \xi_{\parallel}(q^2)(1 - C)].$$

These corrections are purely typographical errors in the original publication. All analyses, plots and conclusions are unchanged.

JHEP11(2008)032

On the new physics reach of the decay mode

$$\bar{B}_d \rightarrow \bar{K}^{*0} \ell^+ \ell^-$$

Ulrik Egede,^a Tobias Hurth,^b Joaquim Matias,^c Marc Ramon^c and Will Reece^{a,d}

^aImperial College London,
London SW7 2AZ, United Kingdom

^bInstitute for Physics, Johannes Gutenberg-University,
D-55099 Mainz, Germany

^cUniversitat Autònoma de Barcelona,
08193 Bellaterra, Barcelona, Spain

^dCERN, Dept. of Physics,
CH-1211 Geneva 23, Switzerland

E-mail: u.egede@imperial.ac.uk, tobias.hurth@cern.ch, matias@ifae.es,
mramon@ifae.es, will.reece@cern.ch

ABSTRACT: We present a complete method to construct QCD-protected observables based on the exclusive 4-body B -meson decay $\bar{B}_d \rightarrow \bar{K}^{*0} \ell^+ \ell^-$ in the low dilepton mass region. The core of the method is the requirement that the constructed quantities should fulfil the symmetries of the angular distribution. We have identified all symmetries of the angular distribution in the limit of massless leptons and explore: a new non-trivial relation between the coefficients of the angular distribution, the possibility to fully solve the system for the K^* amplitudes, and the construction of non-trivial observables.

We also present a phenomenological analysis of the new physics sensitivity of angular observables in the decay based on QCD factorisation. We further analyse the CP -conserving observables, $A_T^{(2)}$, $A_T^{(3)}$ and $A_T^{(4)}$. They are practically free of theoretical uncertainties due to the soft form factors for the full range of dilepton masses rather than just at a single point as for A_{FB} . They also have a higher sensitivity to specific new physics scenarios compared to observables such as A_{FB} . Moreover, we critically examine the new physics reach of CP -violating observables via a complete error analysis due to scale dependences, form factors and Λ_{QCD}/m_b corrections. We have developed an ensemble method to evaluate the error on observables from Λ_{QCD}/m_b corrections. Finally, we explore the experimental prospects of CP -violating observables and find that they are rather limited. Indeed, the CP -conserving (averaged) observables $A_T^{(i)}$ (with $i = 2, 3, 4$) will offer a better sensitivity to large CP phases and may be more suitable for experimental analysis.

KEYWORDS: Rare Decays, B-Physics, Beyond Standard Model, CP violation

ARXIV EPRINT: [1005.0571](https://arxiv.org/abs/1005.0571)

Contents

1	Introduction	2
2	Theoretical framework	4
2.1	Differential decay distribution	4
2.2	QCdf/SCET framework	6
2.3	Estimating Λ_{QCD}/m_b corrections	8
3	Symmetries and observables	9
3.1	Infinitesimal symmetries	10
3.2	Explicit form of symmetries	11
3.3	Relationship between coefficients in differential distribution	11
3.4	Experimental issues	13
3.5	Constructing observables	13
3.6	More general cases	14
4	Experimental sensitivities	15
4.1	Experimental analysis	16
4.1.1	Generation	17
4.1.2	Observable sensitivities	17
4.1.3	CP asymmetries	17
4.2	The polynomial ansatz re-examined	17
4.3	Fit quality	19
4.4	Discussion	20
5	Analysis of CP-violating observables	20
5.1	Preliminaries	21
5.2	Phenomenological analysis	22
6	Analysis of CP-conserving observables	27
6.1	Leading-order expressions of $A_{\text{T}}^{(2)}$	27
6.2	Leading-order expressions of $A_{\text{T}}^{(5)}$	29
6.3	Analysis of $A_{\text{T}}^{(3)}$ and $A_{\text{T}}^{(4)}$	31
7	Conclusion	31
A	Kinematics	32
B	Theoretical input parameters and uncertainties	34

1 Introduction

The LHC era is just beginning. Flavour physics will play an important complementary role to direct searches for the theory that lies beyond the standard model (SM). One central strategy in this period is to construct observables that are mostly sensitive to specific types of new physics (NP), in such a way that a deviation could immediately provide information on the type of NP required: isospin breaking NP, presence of right-handed currents, scalars, etc. It is essential to work in a bottom up approach in the direction of constructing a decision tree that help us to discern which features the NP model must incorporate and then try to match them into a group of models.

Few decays are able to provide such a wealth of information with different observables as $\bar{B}_d \rightarrow \bar{K}^{*0} \ell^+ \ell^-$, ranging from forward-backward asymmetries (A_{FB}) and isospin asymmetries to a large number of angular observables. Each of these observables can provide information on the different types of NP mentioned above. First published results from BELLE [1] and BABAR [2] based on $O(100)$ decays already demonstrate their feasibility.

In the early years of LHC running one will be restricted to those observables that may be extracted from the angular distribution using relatively simple analyses. A study of those observables relevant for the first few fb^{-1} may be found in [3]. However, once enough statistics have been accumulated to perform a full angular analysis based on the full 4-body decay distribution of the $\bar{B}_d \rightarrow \bar{K}^{*0} \ell^+ \ell^-$, one has the freedom to design observables with reduced theoretical uncertainties and specific NP sensitivity.

In [4], it was proposed to construct observables that maximise the sensitivity to contributions driven by the electro-magnetic dipole operator \mathcal{O}'_7 , while, at the same time, minimising the dependence on the poorly known soft form factors. This led to the construction of the observable $A_{\text{T}}^{(2)}$, based on the parallel and perpendicular spin amplitudes of the K^{*0} . The basic idea behind the construction of the observable was inspired by the zero point of A_{FB} when calculated as a function of the dilepton mass squared, q^2 . The zero point has attracted a lot of attention because of its cleanliness; only at that point one gets a complete cancellation at LO of the form factor dependence and its precise position may provide information on the fundamental theory that lies beyond the SM. For $A_{\text{T}}^{(2)}$ the soft form factor dependence cancels at LO, not only at one point, but in the full q^2 region thus providing much more experimental information. Moreover, the angular observable is highly sensitive to new right-handed currents driven by the operator \mathcal{O}'_7 [5], to which A_{FB} is blind.

Looking for the complete set of angular observables sensitive to right-handed currents, one is guided to the construction of the so-called $A_{\text{T}}^{(3)}$ and $A_{\text{T}}^{(4)}$ which include longitudinal spin amplitudes [6]. The observables $A_{\text{T}}^{(i)}$ (with $i = 2, 3, 4$) use the K^{*0} spin amplitudes as the fundamental building block. This provides more freedom to disentangle the information on specific Wilson coefficients than just restricting oneself to use the coefficients of the angular distribution as it was recently done in [7]. For instance, $A_{\text{T}}^{(2)}$, being directly proportional to \mathcal{C}'_7 enhances its sensitivity to the type of NP entering this coefficient. Moreover, using each coefficient of the angular distribution instead of selected ratios of them induces a larger sensitivity to the soft form factors.

The spin amplitudes are not directly observable quantities; to ensure that a quantity

constructed out of the spin amplitudes can be observed, it is necessary that it fulfils the same symmetries as the angular distribution. This observation has the important consequence [6] that $A_T^{(1)}$ (first proposed in [8]) cannot be extracted from the angular distribution because it does not respect all its symmetries. Only a measurement of definite helicity distributions would allow it, but that is beyond any particle physics experiment that can currently be imagined [6].

To identify all the symmetries of the angular distribution is one of the main results of this paper. We discuss the counting of all the symmetries of the distribution in different scenarios, with and without scalars and with and without mass terms. We explain the general method of infinitesimal transformations that allow us to identify all the symmetries, and we develop here in full detail the explicit form of the four symmetries in the massless case with no scalars. As an important cross check of this result, we solve explicitly the set of spin amplitudes in terms of the coefficients of the distribution, making use of three out of the four symmetries. Two important consequences of this analysis are: in solving the system one naturally encounters an extra freedom to fix one of the variables, and there is a non-trivial constraint between the coefficients of the angular distribution considered before as free parameters. It is remarkable that this unexpected constraint is valid for any decay that has this same structure.

Finally, we provide an illustrative example of the use of the method of designing observables with an observable called $A_T^{(5)}$ that mixes simultaneously left/right and perpendicular/parallel spin amplitudes in a specific way that none of the coefficients of the angular distribution exhibits, opening different sensitivities to Wilson coefficients.

In the second part of the paper we present a phenomenological analysis of the various angular observables based on a QCD factorisation (QCdf) calculation to NLO precision. Recently, a very detailed analysis of angular quantities of the decay $\bar{B}_d \rightarrow \bar{K}^{*0} \mu^+ \mu^-$ in various NP scenarios [7] and also an analysis of the NP sensitivities of angular CP asymmetries [9] were presented. In contrast to the former work [7], we do not assume that the main part of the A_{QCD}/m_b corrections are inside the QCD form factors, but use the soft form factors and develop a new ensemble method for treating these unknown corrections in a systematic way. The main differences to the latter analysis of CP violating observables is the redefinition of the CP asymmetries in order to eliminate the soft form factor dependence at LO and the inclusion of the A_{QCD}/m_b corrections into the error budget, which turn out to be significant in the presence of new weak phases.

In [6] the experimental preparations for an indirect NP search using these angular observables were worked out, showing that a full angular analysis of the decay $\bar{B}_d \rightarrow \bar{K}^{*0} \mu^+ \mu^-$ at the LHCb experiment offers great opportunities. We re-evaluate this analysis in light of the fourth symmetry for the angular distribution and conclude that it has no effect on the estimated experimental errors as all observables are indeed invariant under this symmetry. We extend the experimental sensitivity study to CP -violating observables and show that even with an upgraded LHCb there is no real sensitivity to CP -violating NP phases in \mathcal{C}_9 and \mathcal{C}_{10} .

The paper is organised as follows: section 2 briefly recall the differential distribution in $\bar{B}_d \rightarrow \bar{K}^{*0} \ell^+ \ell^-$ and the theoretical framework of QCdf and soft-collinear effective

theory (SCET), section 3 extends and completes our previous discussion about symmetries in the angular distribution, its experimental consequences are discussed in section 4, and we perform a phenomenological analysis of the CP -violating and CP -conserving observables in sections 5 and 6 respectively.

2 Theoretical framework

The separation of NP effects and hadronic uncertainties is the key issue when using flavour observables in a NP search. Our analysis is based on QCDf and SCET and critically examines the NP reach of those observables via a detailed error analysis including the impact of the unknown Λ_{QCD}/m_b corrections. In order to make the paper self contained, we briefly recall the various theoretical ingredients of our analysis.

2.1 Differential decay distribution

The decay $\bar{B}_d \rightarrow \bar{K}^{*0} \ell^+ \ell^-$, with $\bar{K}^{*0} \rightarrow K^- \pi^+$ on the mass shell, is completely described by four independent kinematic variables, the lepton-pair invariant mass squared, q^2 , and the three angles θ_l, θ_K, ϕ . Summing over the spins of the final state particles, the differential decay distribution of $\bar{B}_d \rightarrow \bar{K}^{*0} \ell^+ \ell^-$ can be written as

$$\frac{d^4\Gamma}{dq^2 d\cos\theta_l d\cos\theta_K d\phi} = \frac{9}{32\pi} J(q^2, \theta_l, \theta_K, \phi), \quad (2.1)$$

The dependence on the three angles can be made more explicit:

$$\begin{aligned} J(q^2, \theta_l, \theta_K, \phi) = & \\ & = J_{1s} \sin^2 \theta_K + J_{1c} \cos^2 \theta_K + (J_{2s} \sin^2 \theta_K + J_{2c} \cos^2 \theta_K) \cos 2\theta_l + J_3 \sin^2 \theta_K \sin^2 \theta_l \cos 2\phi \\ & + J_4 \sin 2\theta_K \sin 2\theta_l \cos \phi + J_5 \sin 2\theta_K \sin \theta_l \cos \phi + (J_{6s} \sin^2 \theta_K + J_{6c} \cos^2 \theta_K) \cos \theta_l \\ & + J_7 \sin 2\theta_K \sin \theta_l \sin \phi + J_8 \sin 2\theta_K \sin 2\theta_l \sin \phi + J_9 \sin^2 \theta_K \sin^2 \theta_l \sin 2\phi. \end{aligned} \quad (2.2)$$

As the signs of the expression depend on the exact definition of the angles, we have made their definition explicit in appendix A.

The J_i depend on products of the six complex K^* spin amplitudes, $A_{\parallel}^{L,R}$, $A_{\perp}^{L,R}$ and $A_0^{L,R}$ in the case of the SM with massless leptons. Each of these is a function of q^2 . The amplitudes are just linear combinations of the well-known helicity amplitudes describing the $B \rightarrow K\pi$ transition:

$$A_{\perp,\parallel} = (H_{+1} \mp H_{-1})/\sqrt{2}, \quad A_0 = H_0. \quad (2.3)$$

Two generalisations will be made from the massless case within our analysis: if the leptons are considered massive the additional amplitude A_t has to be introduced. And if we allow for scalar operators, there is a new amplitude A_S . Both can be introduced independently

of the other. For the J_i we find the following expressions (see also [4, 10–12]):¹

$$J_{1s} \equiv a = \frac{(2 + \beta_\ell^2)}{4} \left[|A_\perp^L|^2 + |A_\parallel^L|^2 + (L \rightarrow R) \right] + \frac{4m_\ell^2}{q^2} \text{Re} \left(A_\perp^L A_\perp^{R*} + A_\parallel^L A_\parallel^{R*} \right), \quad (2.4a)$$

$$J_{1c} \equiv b = |A_0^L|^2 + |A_0^R|^2 + \frac{4m_\ell^2}{q^2} \left[|A_t|^2 + 2\text{Re}(A_0^L A_0^{R*}) \right] + \beta_\ell^2 |A_S|^2, \quad (2.4b)$$

$$J_{2s} \equiv c = \frac{\beta_\ell^2}{4} \left[|A_\perp^L|^2 + |A_\parallel^L|^2 + (L \rightarrow R) \right], \quad (2.4c)$$

$$J_{2c} \equiv d = -\beta_\ell^2 \left[|A_0^L|^2 + (L \rightarrow R) \right], \quad (2.4d)$$

$$J_3 \equiv e = \frac{1}{2} \beta_\ell^2 \left[|A_\perp^L|^2 - |A_\parallel^L|^2 + (L \rightarrow R) \right], \quad (2.4e)$$

$$J_4 \equiv f = \frac{1}{\sqrt{2}} \beta_\ell^2 \left[\text{Re}(A_0^L A_\parallel^{L*}) + (L \rightarrow R) \right], \quad (2.4f)$$

$$J_5 \equiv g = \sqrt{2} \beta_\ell \left[\text{Re}(A_0^L A_\perp^{L*}) - (L \rightarrow R) - \frac{m_\ell}{\sqrt{q^2}} \text{Re}(A_\parallel^L A_S^* + A_\parallel^R A_S^*) \right], \quad (2.4g)$$

$$J_{6s} \equiv h = 2\beta_\ell \left[\text{Re}(A_\parallel^L A_\perp^{L*}) - (L \rightarrow R) \right], \quad (2.4h)$$

$$J_{6c} \equiv h^* = 4\beta_\ell \frac{m_\ell}{\sqrt{q^2}} \text{Re} \left[A_0^L A_S^* + (L \rightarrow R) \right], \quad (2.4i)$$

$$J_7 \equiv j = \sqrt{2} \beta_\ell \left[\text{Im}(A_0^L A_\parallel^{L*}) - (L \rightarrow R) + \frac{m_\ell}{\sqrt{q^2}} \text{Im}(A_\perp^L A_S^* + A_\perp^R A_S^*) \right], \quad (2.4j)$$

$$J_8 \equiv k = \frac{1}{\sqrt{2}} \beta_\ell^2 \left[\text{Im}(A_0^L A_\perp^{L*}) + (L \rightarrow R) \right], \quad (2.4k)$$

$$J_9 \equiv m = \beta_\ell^2 \left[\text{Im}(A_\parallel^{L*} A_\perp^L) + (L \rightarrow R) \right], \quad (2.4l)$$

with

$$\beta_\ell = \sqrt{1 - \frac{4m_\ell^2}{q^2}}. \quad (2.5)$$

The notations with the letters a - m has been included to make the comparison to [6] easier. Note that $J_{6c} = 0$ in the massless case.

The amplitudes themselves can be parametrised in terms of the seven $B \rightarrow K^*$ form factors by means of a narrow-width approximation. They also depend on the short-distance Wilson coefficients \mathcal{C}_i corresponding to the various operators of the effective electroweak Hamiltonian. The precise definitions of the form factors and of the effective operators are given in [6]. Assuming only the three most important SM operators for this decay mode, namely \mathcal{O}_7 , \mathcal{O}_9 , and \mathcal{O}_{10} , and the chirally flipped ones, being numerically relevant, we

¹The generalizations to the case which includes scalar operators was recently presented in [7].

have²

$$A_{\perp}^{L,R} = N\sqrt{2}\lambda^{1/2} \left[\left\{ (\mathcal{C}_9^{(\text{eff})} + \mathcal{C}'_9^{(\text{eff})}) \mp (\mathcal{C}_{10}^{(\text{eff})} + \mathcal{C}'_{10}^{(\text{eff})}) \right\} \frac{V(q^2)}{m_B + m_{K^*}} + \frac{2m_b}{q^2} (\mathcal{C}_7^{(\text{eff})} + \mathcal{C}'_7^{(\text{eff})}) T_1(q^2) \right], \quad (2.6a)$$

$$A_{\parallel}^{L,R} = -N\sqrt{2}(m_B^2 - m_{K^*}^2) \left[\left\{ (\mathcal{C}_9^{(\text{eff})} - \mathcal{C}'_9^{(\text{eff})}) \mp (\mathcal{C}_{10}^{(\text{eff})} - \mathcal{C}'_{10}^{(\text{eff})}) \right\} \frac{A_1(q^2)}{m_B - m_{K^*}} + \frac{2m_b}{q^2} (\mathcal{C}_7^{(\text{eff})} - \mathcal{C}'_7^{(\text{eff})}) T_2(q^2) \right], \quad (2.6b)$$

$$A_0^{L,R} = -\frac{N}{2m_{K^*}\sqrt{q^2}} \left[\left\{ (\mathcal{C}_9^{(\text{eff})} - \mathcal{C}'_9^{(\text{eff})}) \mp (\mathcal{C}_{10}^{(\text{eff})} - \mathcal{C}'_{10}^{(\text{eff})}) \right\} \times \left\{ (m_B^2 - m_{K^*}^2 - q^2)(m_B + m_{K^*})A_1(q^2) - \frac{\lambda A_2(q^2)}{m_B + m_{K^*}} \right\} + 2m_b(\mathcal{C}_7^{(\text{eff})} - \mathcal{C}'_7^{(\text{eff})}) \left\{ (m_B^2 + 3m_{K^*}^2 - q^2)T_2(q^2) - \frac{\lambda}{m_B^2 - m_{K^*}^2} T_3(q^2) \right\} \right], \quad (2.6c)$$

$$A_t = N\lambda^{1/2}/\sqrt{q^2} \left\{ 2(\mathcal{C}_{10}^{(\text{eff})} - \mathcal{C}'_{10}^{(\text{eff})}) \right\} A_0(q^2), \quad (2.6d)$$

where the \mathcal{C}_i denote the corresponding Wilson coefficients and

$$\lambda = m_B^4 + m_{K^*}^4 + q^4 - 2(m_B^2 m_{K^*}^2 + m_{K^*}^2 q^2 + m_B^2 q^2), \quad (2.7)$$

$$N = \sqrt{\frac{G_F^2 \alpha^2}{3 \cdot 2^{10} \pi^5 m_B^3} |V_{tb} V_{ts}^*|^2 q^2 \lambda^{1/2} \sqrt{1 - \frac{4m_b^2}{q^2}}}. \quad (2.8)$$

Finally we note that, if one additionally considers scalar operators then A_t is modified by the new Wilson coefficients and an additional amplitude, A_S , proportional to the form factor $A_0(q^2)$, is introduced.

2.2 QCDf/SCET framework

The *up-to-date* predictions of exclusive modes are based on QCDf and its quantum field theoretical formulation, soft-collinear effective theory (SCET) [13, 14]. The crucial theoretical observation is that in the limit where the initial hadron is heavy and the final meson has a large energy [15] the hadronic form factors can be expanded in the small ratios Λ_{QCD}/m_b and Λ_{QCD}/E , where E is the energy of the meson that picks up the s quark from the B_d decay. Neglecting corrections of order $1/m_b$ and α_s , the seven a-priori independent $B \rightarrow K^*$ form factors reduce to two universal form factors ξ_{\perp} and ξ_{\parallel} [15, 16]. These relations can be strictly derived within the QCDf and SCET approach and lead to a simple factorisation formulae for the $B \rightarrow K^*$ form factors

$$F_i(q^2) \equiv H_i \xi + \Phi_B \otimes T_i \otimes \Phi_{K^*} + O(\Lambda_{\text{QCD}}/m_b). \quad (2.9)$$

²Following common convention, we use the effective Wilson coefficients of these operators which include contributions from four-quark operators as well.

There is also a similar factorisation formula for the decay amplitudes. The rationale of such formulae is that the hard vertex renormalisations (H_i) and the hard scattering kernels (T_i) are quantities that can be computed perturbatively so they can be separated from the non-perturbative functions that go with them; i.e. the light-cone wave functions (Φ_i) which are process-independent and the soft form factors (ξ) which enter in several different $B \rightarrow K^*$ processes.

In general we have no means to calculate Λ_{QCD}/m_b corrections to the QCdf amplitudes so they are treated as unknown corrections, with the method used for this described in the following section. This, in general, leads to a large uncertainty of theoretical predictions based on the QCdf/SCET which we will explore systematically and make manifest in our phenomenological analysis.

We do not follow here the approach of [7] where the full QCD form factors are used in the QCdf formulae. There it is *assumed* that the main part of the Λ_{QCD}/m_b corrections are inside the QCD form factors, and additional Λ_{QCD}/m_b corrections are just neglected. Clearly some of the Λ_{QCD}/m_b corrections could be moved into the full QCD form factors. However, there is no robust quantitative estimate of the additional corrections and, thus, it is not allowed to neglect those unknown corrections, especially in view of the expected smallness of new physics effects.

We follow here another strategy. We construct observables in which the soft form factor dependence cancels out at leading order. Then the influence of the soft form factors to the physics is almost eliminated from the phenomenological analysis in a controlled way. On the other hand we make the uncertainty due to Λ_{QCD}/m_b corrections manifest in our analysis. It is not expected that there are as large as 20 – 30% as in the $B \rightarrow \pi\pi$ decay as argued below. The inclusion of the 5 – 10% errors due to the Λ_{QCD}/m_b corrections in our analysis is exploratory of its impact on our observables, even at the risk to be too conservative. Obviously, it is this issue which calls for improvement in view of the new physics reach of these modes.

The theoretical simplifications of the QCdf/SCET approach are restricted to the kinematic region in which the energy of the K^* is of the order of the heavy quark mass, i.e. $q^2 \ll m_B^2$. Moreover, the influences of very light resonances below 1 GeV^2 question the QCdf results in that region. In addition, the longitudinal amplitude in the QCdf/SCET approach generates a logarithmic divergence in the limit $q^2 \rightarrow 0$ indicating problems in the theoretical description below 1 GeV^2 [13]. Thus, we will confine our analysis of all observables to the dilepton mass in the range, $1 \text{ GeV}^2 \leq q^2 \leq 6 \text{ GeV}^2$.

Using the discussed simplifications, the K^* spin amplitudes at leading order in $1/m_b$ and α_s have a very simple form:

$$A_{\perp}^{L,R} = \sqrt{2} N m_B (1 - \hat{s}) \left[(\mathcal{C}_9^{(\text{eff})} + \mathcal{C}'_9^{(\text{eff})}) \mp (\mathcal{C}_{10} + \mathcal{C}'_{10}) + \frac{2\hat{m}_b}{\hat{s}} (\mathcal{C}_7^{(\text{eff})} + \mathcal{C}'_7^{(\text{eff})}) \right] \xi_{\perp}(E_{K^*}), \quad (2.10a)$$

$$A_{\parallel}^{L,R} = -\sqrt{2} N m_B (1 - \hat{s}) \left[(\mathcal{C}_9^{(\text{eff})} - \mathcal{C}'_9^{(\text{eff})}) \mp (\mathcal{C}_{10} - \mathcal{C}'_{10}) + \frac{2\hat{m}_b}{\hat{s}} (\mathcal{C}_7^{(\text{eff})} - \mathcal{C}'_7^{(\text{eff})}) \right] \xi_{\perp}(E_{K^*}), \quad (2.10b)$$

$$A_0^{L,R} = -\frac{N m_B}{2\hat{m}_{K^*} \sqrt{\hat{s}}} (1 - \hat{s})^2 [(\mathcal{C}_9^{(\text{eff})} - \mathcal{C}'_9^{(\text{eff})}) \mp (\mathcal{C}_{10} - \mathcal{C}'_{10}) + 2\hat{m}_b (\mathcal{C}_7^{(\text{eff})} - \mathcal{C}'_7^{(\text{eff})})] \xi_{\parallel}(E_{K^*}), \quad (2.10c)$$

$$A_t = \frac{N m_B}{\hat{m}_{K^*} \sqrt{\hat{s}}} (1 - \hat{s})^2 [\mathcal{C}_{10} - \mathcal{C}'_{10}] \xi_{\parallel}(E_{K^*}), \quad (2.10d)$$

with $\hat{s} = q^2/m_B^2$, $\hat{m}_i = m_i/m_B$. Here we neglected terms of $O(\hat{m}_{K^*}^2)$. The scalar spin amplitude A_S is also proportional to $\xi_{\parallel}(E_{K^*})$ in this limit.

The symmetry breaking corrections of order α_s can be calculated in the QCDf/SCET approach. Those NLO corrections are included in our numerical analysis following [13, 14]. They are presented in the appendix of [6].

2.3 Estimating A_{QCD}/m_b corrections

Our observables have reduced theoretical uncertainties due to the cancellation of the soft form factors. However, the relations used to make these cancellations are only valid at LO in the A_{QCD}/m_b expansion, and corrections to higher orders are unknown. For these theoretically clean observables to be useful, the impact of these corrections on the observables must be robustly bounded. If NP is to be discovered in $\bar{B}_d \rightarrow \bar{K}^{*0} \ell^+ \ell^-$, it must be possible to demonstrate that any effect seen is indeed NP and not just the effect of an unknown SM correction.

To evaluate the effect of the A_{QCD}/m_b corrections, we parametrise each of the K^{*0} spin-amplitudes with some unknown linear correction,

$$A'_i = A_i(1 + C_i e^{i\theta_i}), \tag{2.11}$$

where C_i is the relative amplitude and θ_i the relative strong phase. If we vary C_i and θ_i within their allowed ranges, an estimate for the theoretical uncertainty due to these unknown parameters can be found. In order to make this parametrisation generic, however, extra terms must be introduced. In principle the effective Hamiltonian which controls the decay has three terms,

$$\mathcal{H}_{\text{eff}} = \mathcal{H}_{\text{eff}}^{(u)\text{SM}} + \mathcal{H}_{\text{eff}}^{(t)\text{SM}} + \mathcal{H}_{\text{eff}}^{(t)\text{NP}}. \tag{2.12}$$

The first term is very small as it is suppressed by the factor $\lambda_u = V_{\text{ub}} V_{\text{us}}^*/V_{\text{tb}} V_{\text{ts}}^*$ but is responsible for all the SM CP -violation in the decay; the second term is responsible for the decay in the SM; and the third adds possible NP contributions. A fourth possible term $\mathcal{H}_{\text{eff}}^{(u)\text{NP}}$ generically does not contribute to the model independent amplitudes and is neglected. Each of these contributions is generated by different sets of diagrams and may have different values of C_i and θ_i .

Each amplitude must be modified to include the three sub-amplitudes with their corrections:

$$\begin{aligned} A' = & \left[(A_{\text{SM}}(\lambda_u \neq 0) - A_{\text{SM}}(\lambda_u = 0)) \times (1 + C_1 e^{i\theta_1}) \right] + \\ & \left[A_{\text{SM}}(\lambda_u = 0) \times (1 + C_2 e^{i\theta_2}) \right] + \\ & \left[(A_{\text{Full}}(\lambda_u \neq 0) - A_{\text{SM}}(\lambda_u \neq 0)) \times (1 + C_3 e^{i\theta_3}) \right]. \end{aligned} \tag{2.13}$$

It is assumed that only a single NP operator is active so as not to introduce extra terms. In this formalism, the SM CP -violating, SM CP -conserving, and NP parts of the amplitude are then allowed to have independent A_{QCD}/m_b corrections and strong phases.

An estimate of the theoretical uncertainty arising from the unknown A_{QCD}/m_b corrections and strong phases can now be made using a randomly selected ensemble. For each

member of the ensemble, values of C_{1-3} and θ_{1-3} are chosen in the ranges $C_i \in [-0.1, 0.1]$ or $C_i \in [-0.05, 0.05]$ and $\theta_i \in [-\pi, \pi]$ from a random uniform distribution. This is done for the seven amplitudes, $A_t, A_0^{L,R}, A_{\parallel}^{L,R}, A_{\perp}^{L,R}$, to provide a complete description of the decay. It is assumed that the corrections and phases are not functions of q^2 , although in practise they may actually be. Any unknown correlations are also ignored. While these effects could lead to an underestimate of the theoretical envelope, it is thought that this method allows for a conservative estimate of the theoretical uncertainties to be made.

To estimate the contribution to the theoretical uncertainties from Λ_{QCD}/m_b corrections for a particular observable, each element in the ensemble was used to calculate the value of that observable at a fixed value of q^2 . A one σ error is evaluated as the interval that contains 66% of the values around the median. This is done for both $C_i \in [-0.05, 0.05]$ and $C_i \in [-0.1, 0.1]$ to illustrate the effects of five and ten percent corrections. By repeating this process for different values of q^2 , bands can be built up. No assumption of Gaussian statistics has been made; the bands illustrate the probable range for the true value of each observable, given the current central value. The method allows for the probability that a given experimental result is due to an unknown SM correction to be found.

The choice $|C_i| < 10\%$ is based on a simple dimensional estimate. We emphasize here that there is no strict argument available to bound the Λ_{QCD}/m_b corrections this way. But we can state that the chiral enhancement of Λ_{QCD}/m_b corrections in the case of hadronic B decays does not happen in the case of the semileptonic decay mode with a *vector* final state.

The process described here avoids any assumptions about correlations between the corrections and is thus statistically more rigorous than what was done in [6], where corrections to amplitudes were considered one by one and then added in quadrature. The Λ_{QCD}/m_b bands it produces are reduced when compared to those of [6]. It also allows us to investigate the effect of the Λ_{QCD}/m_b corrections for CP -violating observables.

3 Symmetries and observables

The experimental degrees of freedom determined by the J_i terms and the theoretical degrees of freedom determined by the spin amplitudes A_j have to match. There are two effects to consider for this: different values of the A_j can give rise to the same differential distribution eq. (2.1) and thus cannot be distinguished; and in some cases the experimental coefficients are not independent, meaning that not all arbitrary values of the J_i are possible. The first effect we call a continuous symmetry transformation. For the degrees of freedom to match we have

$$n_c - n_d = 2n_A - n_s, \tag{3.1}$$

where n_c is the number of coefficients in the differential distribution (the number of J_i), n_d the number of dependencies between the different coefficients, n_A the number of spin amplitudes (the A_j , each is complex and hence has two degrees of freedom), and n_s the number of continuous symmetries.

We considered this situation in our previous paper [6] for the case of massless leptons and return to it again here. It is easy to see that in the massless limit, $J_{1s} = 3J_{2s}$ and

$J_{1c} = -J_{2c}$. What is not so obvious is that J_9 can be expressed in terms of the other 8 remaining coefficients. Going back to eq. (3.1) it can be seen that the massless case in fact must have 4 symmetries and not 3 as we claimed in the previous paper.

Below we first outline how the symmetries and dependencies can be identified before we move onto their explicit form and the interpretation.

3.1 Infinitesimal symmetries

By an infinitesimal symmetry is meant one where the theoretical spin amplitudes A_j are changed in an infinitesimal way leaving the J_i coefficients in eq. (2.4) unchanged. The infinitesimal symmetries will define a system of coupled ordinary differential equations that, if solved, are the global symmetries we look for. There is no guarantee that these symmetries will allow for the continuous transformation between two arbitrary sets of amplitudes which have the identical angular distribution; there could in principle be several disjoint regions separated by divergences.

If we, in this example, look at massless leptons and ignore the scalar amplitude, we define the coefficients of the spin amplitudes as a vector \vec{A} with 12 components

$$\vec{A} = \left(\text{Re}(A_{\perp}^L), \text{Im}(A_{\perp}^L), \text{Re}(A_{\parallel}^L), \text{Im}(A_{\parallel}^L), \text{Re}(A_0^L), \text{Im}(A_0^L), \right. \\ \left. \text{Re}(A_{\perp}^R), \text{Im}(A_{\perp}^R), \text{Re}(A_{\parallel}^R), \text{Im}(A_{\parallel}^R), \text{Re}(A_0^R), \text{Im}(A_0^R) \right) \quad (3.2)$$

corresponding to the real and imaginary parts of the amplitudes. For each of the coefficients J_i we can find the derivative with respect to the spin amplitudes. As an example

$$\vec{\nabla}(J_{1c}) = (0, 0, 0, 0, 2\text{Re}(A_0^L), 2\text{Im}(A_0^L), 0, 0, 0, 0, 2\text{Re}(A_0^R), 2\text{Im}(A_0^R)) . \quad (3.3)$$

There will be eleven such gradient vectors in the massless case, as $J_{6c} = 0$.

Now, any infinitesimal transformation can be written on the form

$$\vec{A}' = \vec{A} + \delta\vec{s}. \quad (3.4)$$

For the infinitesimal transformation to leave the coefficients unchanged, the vector $\delta\vec{s}$ has to be perpendicular to the hyperplane spanned by the set of gradient vectors. Or in other words $\delta\vec{s}$ represents a symmetry *if, and only if*

$$\forall i \in J_i : \vec{\nabla}_i \perp \delta\vec{s}. \quad (3.5)$$

Looking back at eq. (3.1) we have, for the massless case, $n_c = 11$. If the J_i were all independent the gradient vectors would span an 11 dimensional hyperplane. In fact, it turns out, that they only span 8 dimensions,³ which shows that there are three dependencies between the J_i 's, giving $n_d = 3$. As we have $n_A = 6$ from the amplitudes we see from eq. (3.1) that we have $n_s = 4$ corresponding to 4 symmetries. For the dependencies, only the first two $J_{1s} = 3J_{2s}$ and $J_{1c} = -J_{2c}$ are trivial; the third one we derive in the next section.

³Any program able to handle symbolic algebra will be able to show this.

3.2 Explicit form of symmetries

It is helpful for the discussion to make the following definitions.

$$n_1 = (A_{\parallel}^L, A_{\parallel}^{R*}), \quad (3.6a)$$

$$n_2 = (A_{\perp}^L, -A_{\perp}^{R*}), \quad (3.6b)$$

$$n_3 = (A_0^L, A_0^{R*}), \quad (3.6c)$$

or in terms of helicity amplitudes

$$m_1 = \frac{1}{\sqrt{2}}(n_1 + n_2) = (H_{+1}^L, H_{-1}^{R*}), \quad (3.7a)$$

$$m_2 = \frac{1}{\sqrt{2}}(n_1 - n_2) = (H_{-1}^L, H_{+1}^{R*}), \quad (3.7b)$$

$$m_3 = n_3 = (H_0^L, H_0^{R*}). \quad (3.7c)$$

In fact, all the information of the angular distribution is encoded in the moduli of the three n_i vectors and their relative complex scalar products:

$$|n_1|^2 = \frac{2}{3}J_{1s} - J_3, \quad |n_2|^2 = \frac{2}{3}J_{1s} + J_3, \quad |n_3|^2 = J_{1c}, \quad (3.8)$$

$$n_1 \cdot n_2 = \frac{J_{6s}}{2} - iJ_9, \quad n_1 \cdot n_3 = \sqrt{2}J_4 - i\frac{J_7}{\sqrt{2}}, \quad n_2 \cdot n_3 = \frac{J_5}{\sqrt{2}} - i\sqrt{2}J_8, \quad (3.9)$$

where n_i being a complex vector implies that the scalar product is $n_i \cdot n_j = \sum_k n_{ik} n_{jk}^*$. The coefficients J_{2s} and J_{2c} are absent because they are obviously redundant.

The differential distribution is invariant under the following four independent symmetry transformations of the amplitudes

$$n_i' = \begin{bmatrix} e^{i\phi_L} & 0 \\ 0 & e^{-i\phi_R} \end{bmatrix} \begin{bmatrix} \cos\theta & -\sin\theta \\ \sin\theta & \cos\theta \end{bmatrix} \begin{bmatrix} \cosh i\tilde{\theta} & -\sinh i\tilde{\theta} \\ -\sinh i\tilde{\theta} & \cosh i\tilde{\theta} \end{bmatrix} n_i, \quad (3.10)$$

where ϕ_L , ϕ_R , θ and $\tilde{\theta}$ can be varied independently. Identical transformations can be carried out on the m_i . Normally, there is the freedom to pick a single global phase, but as L and R amplitudes do not interfere here, two phases can be chosen arbitrarily as reflected in the first transformation matrix.

The interpretation of the third and fourth symmetry is that they transform a helicity $+1$ final state with a left handed current into a helicity -1 state with a right handed current. As we experimentally cannot measure the simultaneous change of helicity and handedness of the current, these transformations turn into symmetries for the differential decay rate.

3.3 Relationship between coefficients in differential distribution

As was mentioned earlier, we have identified an extra dependency among the coefficients in the massless case. Here we outline how it can be derived.

If we use the two global phase symmetry transformations we can rotate the vector n_1 to make it real (A_{\parallel}^L and A_{\parallel}^R become real).⁴ We can then choose the angle θ of the third symmetry to make $A_{\parallel}^L = 0$. Notice that we have not made use of the fourth symmetry. The implications of this fourth symmetry will become manifest when solving the system. With these choices

$$n_1 = (0, A_{\parallel}^R), \quad (3.11)$$

where A_{\parallel}^R is a positive real parameter. Using three of eqs. (3.8)–(3.9) together with the symmetries, one can determine four of the spin amplitudes (their moduli and phases):

$$A_{\parallel}^L = 0, \quad (3.12a)$$

$$A_{\parallel}^R = \sqrt{|n_1|^2} = \sqrt{\frac{2}{3}J_{1s} - J_3}, \quad (3.12b)$$

$$A_{\perp}^R = -\frac{n_1 \cdot n_2}{\sqrt{|n_1|^2}} = -\frac{(J_{6s} - 2iJ_9)}{2\sqrt{\frac{2}{3}J_{1s} - J_3}}, \quad (3.12c)$$

$$A_0^R = \frac{n_1 \cdot n_3}{\sqrt{|n_1|^2}} = \frac{2J_4 - iJ_7}{\sqrt{\frac{4}{3}J_{1s} - 2J_3}}. \quad (3.12d)$$

The remaining three equations from eqs. (3.8)–(3.9) determine, on one side, the moduli of A_{\perp}^L and A_0^L :

$$|A_{\perp}^L|^2 = |n_2|^2 - \frac{|(n_1 \cdot n_2)|^2}{|n_1|^2} = \frac{\frac{4}{9}J_{1s}^2 - J_3^2 - \frac{1}{4}J_{6s}^2 - J_9^2}{\frac{2}{3}J_{1s} - J_3}, \quad (3.13a)$$

$$|A_0^L|^2 = |n_3|^2 - \frac{|(n_1 \cdot n_3)|^2}{|n_1|^2} = \frac{J_{1c}(\frac{2}{3}J_{1s} - J_3) - 2J_4^2 - \frac{1}{2}J_7^2}{\frac{2}{3}J_{1s} - J_3}, \quad (3.13b)$$

and on the other, the phase difference corresponding to the previous two amplitudes:

$$\begin{aligned} e^{i(\phi_{\perp}^L - \phi_0^L)} &= \frac{(n_2 \cdot n_3)|n_1|^2 - (n_2 \cdot n_1)(n_1 \cdot n_3)}{[(|n_1|^2|n_2|^2 - |(n_2 \cdot n_1)|^2)(|n_1|^2|n_3|^2 - |(n_3 \cdot n_1)|^2)]^{1/2}} \\ &= \frac{J_5(\frac{2}{3}J_{1s} - J_3) - J_4J_{6s} - J_7J_9 - i(\frac{4}{3}J_{1s}J_8 - 2J_3J_8 + 2J_4J_9 - \frac{1}{2}J_{6s}J_7)}{[2(\frac{4}{9}J_{1s}^2 - J_3^2 - \frac{1}{4}J_{6s}^2 - J_9^2)(J_{1c}(\frac{2}{3}J_{1s} - J_3) - 2J_4^2 - \frac{1}{2}J_7^2)]^{1/2}}. \end{aligned} \quad (3.14)$$

Here is where the fourth symmetry becomes manifest. On one side, this equation tells us that you have the freedom to choose one of the two phases ϕ_{\perp}^L or ϕ_0^L to zero. On the other side, given that the l.h.s. of the previous equation is a pure phase, the modulus of the r.h.s. should be one. This implies the following important non-trivial relationship between the coefficients of the distribution

$$\begin{aligned} J_{1c} &= 6 \frac{(2J_{1s} + 3J_3)(4J_4^2 + J_7^2) + (2J_{1s} - 3J_3)(J_5^2 + 4J_8^2)}{16J_1^2 - 9(4J_3^2 + J_6^2 + 4J_9^2)} \\ &\quad - 36 \frac{J_{6s}(J_4J_5 + J_7J_8) + J_9(J_5J_7 - 4J_4J_8)}{16J_{1s}^2 - 9(4J_3^2 + J_6^2 + 4J_9^2)}. \end{aligned} \quad (3.15)$$

⁴Indeed the system can also be solved using only one of the two global symmetries and keep A_{\parallel}^R complex.

It is important to remark that this equation can be very easily generalised to the massless case with scalars by using the relations $J_{1s} = 3J_{2s}$ and $J_{1c} = -J_{2c}$ in the previous equation. Also the massive case with no scalars can be included by introducing the β factors inside the J_i coefficients. There is no such equation in the massive case with scalars due the fact that the number of coefficients of the experimental distribution is identical to the number of theoretical amplitudes and symmetries (see table 1).

3.4 Experimental issues

The symmetries discussed above can be used to fix the spin-amplitude components by choosing specific values of the relevant rotation angles. We give an explicit example of this for the case where the lepton mass is neglected. We choose to make the following constraint:

$$\text{Re}(A_{\parallel}^L) = \text{Im}(A_{\parallel}^L) = \text{Im}(A_{\parallel}^R) = \text{Im}(A_{\perp}^L) = 0. \quad (3.16)$$

This can be achieved by first performing the last transformation, shown in Eq. (3.10), with the value of $\tilde{\theta}$ given by:

$$\sin \tilde{\theta} = \sqrt{\frac{z-1}{2z}}, \quad \cos \tilde{\theta} = \sqrt{\frac{z+1}{2z}}, \quad (3.17)$$

where

$$z = \sqrt{1 + 4 \left[\frac{\text{Re}(A_{\parallel}^L)\text{Im}(A_{\parallel}^R) + \text{Re}(A_{\parallel}^R)\text{Im}(A_{\parallel}^L)}{\text{Re}(A_{\parallel}^R)^2 + \text{Im}(A_{\parallel}^R)^2 - \text{Re}(A_{\parallel}^L)^2 - \text{Im}(A_{\parallel}^L)^2} \right]^2}. \quad (3.18)$$

Next, the third rotation angle, θ , is used again in Eq. (3.10):

$$\tan \theta = \frac{\sqrt{1+z} \text{Re}(A_{\parallel}^L) - \sqrt{z-1} \text{Im}(A_{\parallel}^R)}{\sqrt{1+z} \text{Re}(A_{\parallel}^R) + \sqrt{z-1} \text{Im}(A_{\parallel}^L)}. \quad (3.19)$$

The L -fields are phase shifted by ϕ_L :

$$\tan \phi_L = -\frac{\cos \tilde{\theta} [\cos \theta \text{Im}(A_{\perp}^L) - \sin \theta \text{Im}(A_{\perp}^R)] + \sin \tilde{\theta} [\cos \theta \text{Re}(A_{\perp}^R) + \sin \theta \text{Re}(A_{\perp}^L)]}{\sin \tilde{\theta} [\cos \theta \text{Im}(A_{\perp}^R) - \sin \theta \text{Im}(A_{\perp}^L)] + \cos \tilde{\theta} [\cos \theta \text{Re}(A_{\perp}^L) + \sin \theta \text{Re}(A_{\perp}^R)]}, \quad (3.20)$$

and finally the last R -field transformation can be performed by substituting ($\perp \rightarrow \parallel$) and ($L \leftrightarrow R$) into the previous expression:

$$\tan \phi_R = -\frac{\cos \tilde{\theta} [\cos \theta \text{Im}(A_{\parallel}^R) - \sin \theta \text{Im}(A_{\parallel}^L)] + \sin \tilde{\theta} [\cos \theta \text{Re}(A_{\parallel}^L) + \sin \theta \text{Re}(A_{\parallel}^R)]}{\sin \tilde{\theta} [\cos \theta \text{Im}(A_{\parallel}^L) - \sin \theta \text{Im}(A_{\parallel}^R)] + \cos \tilde{\theta} [\cos \theta \text{Re}(A_{\parallel}^R) + \sin \theta \text{Re}(A_{\parallel}^L)]}. \quad (3.21)$$

3.5 Constructing observables

In [4, 6], as well as here, we use the spin amplitudes to construct our observables. There are two main advantages of this approach, one is experimental and the other is theoretical. On the experimental side, we have found that fitting directly the angular coefficients J_i , without taking into account the relations between them, leads to fit instabilities. These

relations, coming from the underlying K^{*0} spin amplitudes, can be found in section 3.3. The theoretical argument has to do with our aim at constructing observables that fulfil certain criteria, namely maximal sensitivity to a specific NP operator, like new right-handed currents, and minimal sensitivity to poorly known form factors. Given that our main tools are directly the spin amplitudes it is a straight-forward exercise to design observables with a specific NP sensitivity and small hadronic uncertainties. We also have more freedom to construct observables than just using each coefficient of the distribution as an observable. As the spin amplitudes can be extracted directly in the full-angular analysis, there is no penalty on the final experimental uncertainty from using a non-trivial functional form to make the observable.

The symmetries of the angular distribution play a crucial role in our approach. Once a quantity has been designed, it is a necessary condition for being an observable based on the angular distribution that it respects all the symmetries of this distribution. For example in [6], we have explicitly shown that a previously discussed transversity amplitude $A_T^{(1)}$ does not fulfil all the symmetries of the angular distribution. This implies that this quantity cannot be measured at the LHCb experiment or at future super- B factory experiments; a measurement of the spins of the final-state particles would be required for that.

Let us finally discuss a new CP -conserving observable that we call $A_T^{(5)}$. It is defined as:

$$A_T^{(5)} = \frac{|A_\perp^L A_\parallel^{R*} + A_\perp^{R*} A_\parallel^L|}{|A_\perp^L|^2 + |A_\perp^R|^2 + |A_\parallel^L|^2 + |A_\parallel^R|^2}. \quad (3.22)$$

It probes the transverse spin amplitudes A_\perp and A_\parallel in a different way than $A_T^{(2)}$. Direct inspection of eq. (2.4) shows that there is no single angular coefficient mixing L with R and \perp with \parallel simultaneously in the way $A_T^{(5)}$ does.

It is a simple exercise to check that this observable fulfils the four symmetries described in eq. (3.10). Once this invariance is fulfilled⁵ one is allowed to use the explicit solution in the massless case provided in the previous subsection eqs. (3.8)–(3.9):

$$A_T^{(5)} \Big|_{m_\ell=0} = \frac{\sqrt{16J_1^{s2} - 9J_6^{s2} - 36(J_3^2 + J_9^2)}}{8J_1^s}. \quad (3.23)$$

A discussion on the properties and sensitivities of this observable is presented in section 6.

3.6 More general cases

The discussion of the differential symmetries from section 3.1 can be generalised to the cases where the leptons are no longer considered massless and where a scalar amplitude is included:

Massless leptons with scalars The inclusion of the scalar amplitude A_S , gives us seven amplitudes. The four explicit symmetries in eq. (3.10) are still valid and we have in addition

$$A_S' = e^{i\phi_S} A_S, \quad (3.24)$$

expressing that the phase of A_S cannot be determined.

⁵Notice that the quantity $A_T^{(1)}$ could also be written in terms of the J_i using the explicit solution, but this is not allowed since $A_T^{(1)}$ is not invariant [6].

Case	Coefficients	Dependencies	Amplitudes	Symmetries
$m_\ell = 0, A_S = 0$	11	3	6	4
$m_\ell = 0$	11	2	7	5
$m_\ell > 0, A_S = 0$	11	1	7	4
$m_\ell > 0$	12	0	8	4

Table 1. The dependencies between the coefficients in the differential distribution and the symmetries between the amplitudes in several special cases.

Massive leptons without scalars We have the seven amplitudes $A_{\perp}^{L,R}$, $A_{\parallel}^{L,R}$, $A_0^{L,R}$ and A_t in this case and still eleven coefficients. As a fact of elementary quantum mechanics we still have a global phase transformation corresponding to $\phi_L = \phi_R$, but the other two symmetries from the massless case are no longer valid. There is a new symmetry concerning the phase of A_t given as:

$$A'_t = e^{i\phi_t} A_t. \tag{3.25}$$

This leaves us with two symmetries where only the differential form is known.

Massive leptons with scalars We now have all eight amplitudes and, with the inclusion of J_{6c} , we have twelve coefficients. The global phase transformation, $\phi_L = \phi_R$, and the phase transformation of A_t in eq. (3.25) are still valid. In this case, there is no dependency between any of the coefficients, leaving us with two symmetries where only the differential form is known.

So while we in some cases only know the differential form of the symmetries, we are still able to test if observables respect the symmetries (see section 3.5) and we can also determine the optimal set of amplitudes to fit for in an experimental fit (see section 3.4). In table 1 we summarise the full knowledge about the symmetries.

4 Experimental sensitivities

In [6], a fitting technique was investigated that allowed the extraction of the K^{*0} spin amplitudes from the full angular distribution in the massless lepton limit. Eq. (2.1) can be interpreted as a probability density function (PDF) and normalised numerically. We parametrise it in terms of six complex K^{*0} spin amplitudes, which are functions of q^2 only. In the limit of infinite experimental data, and for a fixed value of q^2 , these amplitudes can be found by fitting the relative contribution of each angular coefficient as a function of the three decay angles. As discussed in section 3, the symmetries of the distribution can then be used to reduce the number of unknowns; if we consider the real and imaginary amplitude components separately, the twelve parameters can be reduced to eight using the symmetry constraints. A further spin-amplitude component may be removed by noting that Eq. (2.1) is only sensitive to relative normalisations. This leaves seven free parameters at each point in q^2 . However, in [6], only three, out of four, symmetry constraints were considered

meaning that, in principle, the fits presented were under-constrained. The implications of this will be investigated in this section.

Despite the large increases in $\bar{B}_d \rightarrow \bar{K}^{*0} \mu^+ \mu^-$ statistics expected at LHC**b**, the number of signal events available will still be too small for a fixed q^2 approach to be taken. Instead, the spin-amplitude components are parametrised as second-order polynomials in the region $q^2 \in [1, 6] \text{ GeV}^2$. These are normalised relative to the value of $\text{Re}(A_0^L)$ at a fixed value, X_0 , of q^2 . Rather than fitting directly for the amplitudes, we aim to extract the coefficients of these polynomials. This introduces a number of model biases: the underlying spin amplitudes are assumed to be smoothly varying in the q^2 window considered. As noted in [6], this was verified for a number of NP models. There is also an implicit assumption that the q^2 -dependent shape of the spin amplitudes is invariant under the symmetries of the angular distribution. Neglecting background parameters, the q^2 -dependent fit has $((12 - 4) \times 3) - 1 = 23$ free parameters to be extracted, or 26 in [6]. These will be labelled the four- and three-symmetry fits respectively.

The three-symmetry fit although, in principle, under-constrained is able to converge due to the polynomial parametrisation employed. By requiring that three of the spin amplitude components vanish for all values of q^2 , we have used our freedom to choose values of ϕ_L , ϕ_R , and θ from eq. (3.10) at each point in q^2 ; the value of $\tilde{\theta}$ is still free to vary. However, the PDF, Eq. (2.1), is invariant under changes of $\tilde{\theta}$; hence, the negative log-likelihood (NLL) used during minimisation should not be sensitive to its value. The q^2 dependent shape of each amplitude component is manifestly not invariant under changes in $\tilde{\theta}$ — the rotation it implies mixes the imaginary parts of the left- and right-handed amplitudes. The polynomial parametrisation of the spin-amplitude components requires that each amplitude must be smoothly varying. The fit then selects the value of $\tilde{\theta}$ for each signal event which produces the most polynomial-like distribution, as this will have the smallest NLL. The general minimising algorithm employed is then able to find a genuine minimum and converge properly; the imposition of the polynomial ansatz allowed the under-constrained fit of [6] to converge properly. As the experimental observables are invariant under all four symmetries, their q^2 dependent distributions can be found correctly; there are no significant biases seen in the central values extracted compared to the input distribution. Small biases *are* seen in the individual spin-amplitude components; with hindsight, correlations between these components were induced by the presence of the fourth symmetry.

4.1 Experimental analysis

The discussion above explains why the three-symmetry fit is able to converge successfully, and suggests that there should be no change in the experimental uncertainties found when the extra symmetry constraint is added. It is important to demonstrate that this is the case. As before, the experimental sensitivity to different observables can be estimated using a toy Monte Carlo (MC) approach and used to compare the three- and four-symmetry fits.

4.1.1 Generation

An ensemble of data sets for $\bar{B}_d \rightarrow \bar{K}^{*0} \mu^+ \mu^-$ can be generated; each data set contains the Poisson-fluctuated number of signal and background events expected after LHCb has collected 10 fb^{-1} of integrated luminosity. Estimates of the signal and background yields were taken from [17, 18] and scaled linearly. The signal distribution was generated using the K^{*0} spin amplitudes discussed in section 2 as input. The contribution from terms including the muon mass were included. No assumption of polynomial variation of the amplitudes was used in the generation. The signal is assumed to have a Gaussian distribution in m_B with a width of 14 MeV in a window of $m_B \pm 50$ MeV and a Breit-Wigner in $m_{K\pi}$ with width 48 MeV in a window of $m_{K^{*0}} \pm 100$ MeV. A simplified background model is included; it is flat in all decay angles, effectively treating all background as combinatorial, but follows the q^2 distribution of the signal. Detector acceptance effects as described in [17] are not taken into account. When considering CP -conserving quantities, the B and \bar{B} samples are simply considered together. We do not include any contributions from non-resonant $\bar{B}_d \rightarrow K^- \pi^+ \mu^+ \mu^-$.

4.1.2 Observable sensitivities

The ensemble of simulated data sets can then be used to estimate the experimental uncertainties expected for a given integrated luminosity at LHCb. For each data set, the full angular fit was performed to find the most likely value for each of the free parameters for that data set. For the three-symmetry fit there were 27 free parameters; 26 for the signal distribution and one to describe the level of background seen. For the four-symmetry fit, only 24 parameters were required. In total we created an ensemble of 1200 experiments and will, thus, at a given value of q^2 , get 1200 different determinations of each observable. By looking at the point where 33% and 47.5% of results lie within either side of the median of the results we can form asymmetric 1σ and 2σ errors. Connecting these at different q^2 values gives us 1σ and 2σ bands for the experimental errors on the observable.

4.1.3 CP asymmetries

The sensitivity to various CP asymmetries was also considered. In this case, separate B and \bar{B} samples were generated and fit independently. Each sample had on average half the number of signal and background events as those described in section 4.1.1. The results of a B and a \bar{B} fit could then be combined by re-normalising the B amplitudes found, so that the extracted value of $\text{Re}(A_0^L)$ at X_0 was the same in both samples. This gives sensitivity to CP asymmetries relative to this point. By considering many B and \bar{B} samples together, estimates of the experimental sensitivity to the CP asymmetries could then be found. In a real measurement, a more sophisticated approach would be taken which considered the two samples simultaneously; however, our simplified approach gives a reasonable first estimate of the experimental sensitivities obtainable and allow comparison with theoretical requirements.

4.2 The polynomial ansatz re-examined

A key assumption of the fitting approach taken in [6] is that the spin-amplitude components are smoothly varying functions in the range $q^2 \in [1, 6] \text{ GeV}^2$. It was found that

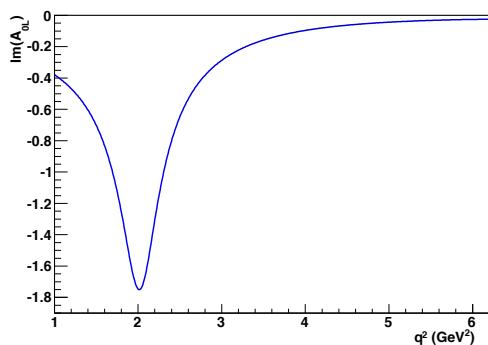


Figure 1. The q^2 dependence of $\text{Im}(A_0^L)$ after using the four symmetries of the full-angular distribution to fix $\text{Im}(A_{\parallel}^L)$, $\text{Im}(A_{\parallel}^R)$, $\text{Re}(A_{\parallel}^L)$, and $\text{Im}(A_{\perp}^L)$ to zero.

when all four symmetries of the massless angular distribution are taken into account, this assumption *no longer holds*; indeed the shape of the spin-amplitude components is not invariant under the four symmetries and their shape can be distorted so they are no longer well described by second-order polynomials. Other parameterization choices are likely to be equally vulnerable to these problems unless they are explicitly invariant under all symmetries of the angular distribution. Consider the three-symmetry case at a fixed q^2 value: in [6], A_0^R is removed by setting $\theta = \arctan(-A_0^R/A_0^L)$ once their phases have been rotated away. This can be understood by substituting the trigonometric identities,

$$\sin(\arctan(\theta)) = \frac{\theta}{\sqrt{1+\theta^2}}, \quad \cos(\arctan(\theta)) = \frac{1}{\sqrt{1+\theta^2}}, \quad (4.1)$$

into eq. (3.10). This introduces a $[1 + (A_0^R/A_0^L)^2]^{-\frac{1}{2}}$ term into each non-zero amplitude component, which will not be well behaved as $A_0^L \rightarrow 0$. For the three-symmetry fit, these problems can be avoided by taking $\text{Re}(A_0^L)$ as the reference amplitude component, forcing it to be relatively large at X_0 . However, to include the fourth symmetry constraint, a more complicated form must be used in order to set four amplitude components simultaneously. A different value of each of the four rotation angles is required for every point in q^2 due to the changing spin amplitudes. There is no guarantee that a set of rotation angles can be found such that the unfixed spin-amplitude components resemble smoothly varying polynomials for all q^2 . The q^2 dependence of the SM input amplitude $\text{Re}(A_0^L)$ is shown in figure 1 once the four symmetries have been applied to fix $\text{Im}(A_{\parallel}^L)$, $\text{Im}(A_{\parallel}^R)$, $\text{Re}(A_{\parallel}^L)$, and $\text{Im}(A_{\perp}^L)$ to zero, as required for in the next section. This particular feature is caused by $\text{Re}(A_{\parallel}^L) \rightarrow 0$ at $q^2 \approx 2 \text{ GeV}^2$; other rotation choices lead to similar features. The distribution can no longer be well described by a second-order polynomial. It may be possible to find a choice of rotation parameters that preserve the polynomial features of the input spin-amplitude components, however, there are no guarantee that a particular choice would work when faced with experimental data. Indeed, an incorrect choice will lead to biases in the case where the parametrisation is a poor match for the underlying amplitudes. A more generic solution is required and could form the basis for further investigations.

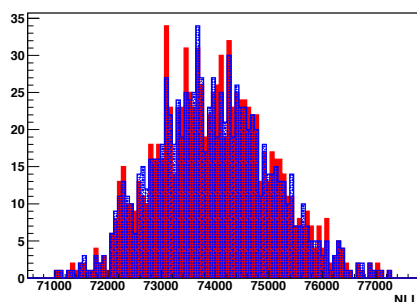


Figure 2. The negative log-likelihood factor for the three-symmetry (blue hatched) and four-symmetry (red solid) ensembles of fits to 10 fb^{-1} toy data sets of LHC***b*** data, assuming the SM and with $q^2 \in [2.5, 6] \text{ GeV}^2$.

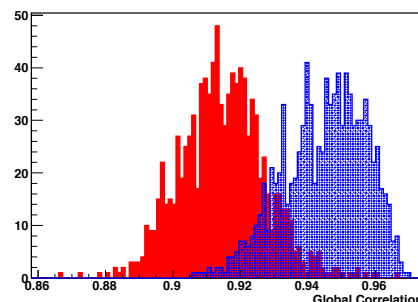


Figure 3. The global correlation factor for the three-symmetry and four-symmetry ensembles of fits to 10 fb^{-1} toy data sets of LHC***b*** data, assuming the SM and with $q^2 \in [2.5, 6] \text{ GeV}^2$. The colour scheme is the same as in figure 2.

4.3 Fit quality

The effect of adding the fourth symmetry constraint was tested, by comparing ensembles of three- and four-symmetry fits. The two ensembles were generated with the same random seed values so that the ensemble of input data sets was the same for the two approaches. The fixed spin-amplitude components were chosen to be $\text{Im}(A_{\parallel}^L)$, $\text{Im}(A_{\parallel}^R)$, $\text{Re}(A_{\parallel}^L)$, and in the case of the four-symmetry fit also $\text{Im}(A_{\perp}^L)$. The amplitudes were still normalised relative to $\text{Re}(A_{\parallel}^L)$ at $X_0 = 3.5 \text{ GeV}^2$, however the fits were performed in the range $q^2 \in [2.5, 6] \text{ GeV}^2$ to avoid the non-polynomial features seen in the spin-amplitude components, such as shown in figure 1.

The sensitivities found for the angular observables are poorer than those presented in [6], due to the decreased signal statistics in the reduced q^2 window, however, it is interesting to compare the performance of the two fitting methods. A histogram of the NLL of each fit is shown in figure 2. The ensemble of three-symmetry fits (hatched) and four-symmetry fits (solid) can be seen. The ensemble of input data sets is slightly different in each case due to a small number of failed computing jobs, but the output distributions look very similar. This shows that the depth of the minima found is approximately the same for the three- and four-symmetry fits. We can also introduce a global correlation factor G_C , which is the unsigned mean of the individual global correlation coefficients calculated from the full covariance matrix. It takes values in the range $G_C \in [0, 1]$, where zero shows all variables as completely uncorrelated, and one shows total fit correlation. It can be seen in figure 3 that the mean correlation of the fit is reduced once the fourth symmetry is taken into account. There are less outliers at very low G_C and the distribution appears more Gaussian, indicating an increase in fit stability has been achieved. The convergence of the fit starting from arbitrary initial parameters has also much improved.

Figure 4 shows the estimated experimental sensitivities found for the theoretically clean observable $A_{\Gamma}^{(3)}$ in the range $q^2 \in [2.5, 6] \text{ GeV}^2$, with and without the fourth symmetry

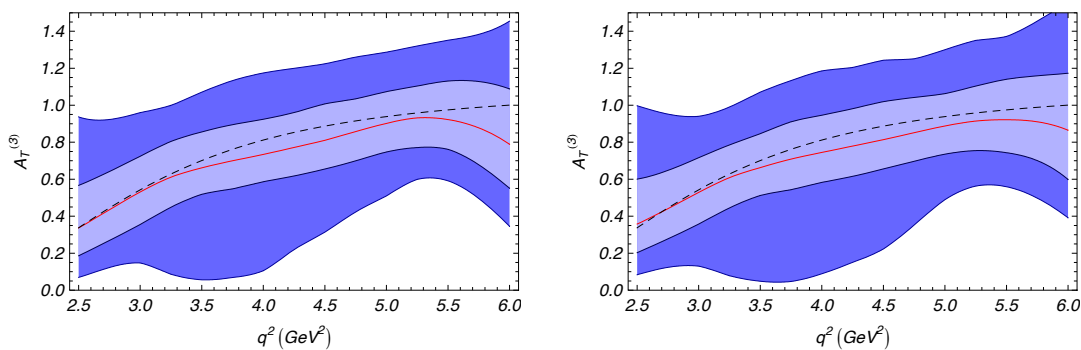


Figure 4. One and two σ contours of estimated experimental sensitivity to the theoretically clean observable $A_T^{(3)}$ with full-angular fit to 10 fb^{-1} of LHCb data assuming the SM. The results of the three-symmetry fit are shown on the left, and the four-symmetry fit on the right. The fits were performed in the range $q^2 \in [2.5, 6] \text{ GeV}^2$.

constraint. The fits are for 10 fb^{-1} of LHCb integrated luminosity assuming the SM. As might be expected from figure 2, there is little difference in the estimated experimental resolutions seen. The same conclusion is reached when inspecting other observables.

4.4 Discussion

The discovery of a fourth symmetry in the massless leptons limit of the full-angular distribution of $\bar{B}_d \rightarrow \bar{K}^{*0} \mu^+ \mu^-$ requires that the experimental analysis proposed in [6] be re-evaluated. The previous analysis used three of the four available symmetry constraints to perform a fit, that was, in principle, under-constrained, by parametrising the real and imaginary parts of the K^{*0} spin amplitudes as second-order polynomials. The invariance of the observables under all four symmetries, and the freedom to take arbitrary values of the $\tilde{\theta}$ rotation angle, allowed the fits to converge and produce correct output, but introduced a subtle parametrisation bias. As the observables are *by definition* invariant to all the symmetries, the estimated experimental sensitivities are the same for the two methods. This has been demonstrated in this section. However, the need for the development of a new fitting method, so that the full experimental statistics available in $q^2 \in [1, 6] \text{ GeV}^2$ can be used, is now clear. The sensitivities found will be similar to those estimated in Ref. [6] and in this paper for the CP asymmetries, but with improved fit stability.

5 Analysis of CP -violating observables

In [10, 19], it was shown that eight CP -violating observables can be constructed by combining the differential decay rates of $d\Gamma(\bar{B}_d \rightarrow \bar{K}^{*0} \ell^+ \ell^-)$ and $d\bar{\Gamma}(B_d \rightarrow K^{*0} \ell^+ \ell^-)$. In this section we analyse the theoretical and experimental uncertainties of those observables in order to judge the NP sensitivity of such CP -violating observables.

5.1 Preliminaries

The corresponding decay rate for the CP -conjugated decay mode $B_d \rightarrow K^{*0} \ell^+ \ell^-$ is given by

$$\frac{d^4 \bar{\Gamma}}{dq^2 d \cos \theta_l d \cos \theta_K d \phi} = \frac{9}{32\pi} \bar{J}(q^2, \theta_l, \theta_K, \phi). \quad (5.1)$$

As shown in [10], the corresponding functions $\bar{J}_i(q^2, \theta_l, \theta_K, \phi)$ are connected to functions J_i in the following way:

$$J_{1,2,3,4,7} \rightarrow \bar{J}_{1,2,3,4,7}, \quad J_{5,6,8,9} \rightarrow -\bar{J}_{5,6,8,9}, \quad (5.2)$$

where \bar{J}_i equals J_i with all weak phases conjugated.

Besides the CP asymmetry in the dilepton mass distribution, there are several CP -violating observables in the angular distribution. The latter are sensitive to CP -violating effects as differences between the angular coefficient functions, $J_i - \bar{J}_i$. As was discussed in [10, 19], and more recently in [9], those CP asymmetries are all very small in the SM; they originate from the small CP -violating imaginary part of $\lambda_u = (V_{ub}V_{us}^*)/(V_{tb}V_{ts}^*)$. This weak phase present in the Wilson coefficient $\mathcal{C}_9^{(\text{eff})}$ is doubly-Cabibbo suppressed and further suppressed by the ratio of the Wilson coefficients $(3\mathcal{C}_1 + \mathcal{C}_2)/\mathcal{C}_9 \approx 0.085$.

Moreover, it is important to note [9, 19] that the CP asymmetries corresponding to $J_{7,8,9}$ are odd under the transformation $\phi \rightarrow -\phi$ and thus, these asymmetries are T-odd (T transformation reverses all particle momenta and particle spins) while the other angular CP asymmetries are T-even. T-odd CP asymmetries are favoured because they involve the combination $\cos(\delta\theta) \sin(\delta\phi_W)$ of the strong and weak phase differences [9, 19], thus, they are still large in spite of small strong phases as predicted for example within the QCDF/SCET approach. In contrast, T-even CP asymmetries involve the combination to $\sin(\delta\theta) \cos(\delta\phi_W)$ [9, 19].⁶

Another remark is that the CP asymmetries related to $J_{5,6,8,9}$ can be extracted from $(d\Gamma + d\bar{\Gamma})$ due to the property eq. (5.2), and thus can be determined for an untagged equal mixture of B and \bar{B}_d mesons. This is important for the decay modes $B_d^0 \rightarrow K^{*0}(\rightarrow K^0 \pi^0) \ell^+ \ell^-$ and $B_s \rightarrow \phi(\rightarrow K^+ K^-) \ell^+ \ell^-$ but it is less relevant for the self-tagging mode $B_d \rightarrow K^{*0}(\rightarrow K^+ \pi^-) \ell^+ \ell^-$.

Recently, a QCdf/SCET analysis of the angular CP -violating observables, based on the NLO results in [13, 14], was presented for the first time [9]. The NLO corrections are shown to be sizable. The crucial impact of the NLO analysis is that the scale dependence gets reduced to the 10% level for most of the CP asymmetries. However, for some of them, which essentially start with a nontrivial NLO contribution, there is a significantly larger scale dependence. The q^2 -integrated SM predictions are all shown to be below the 10^{-2} level due to the small weak phase as mentioned above. The uncertainties due to the form factors, the scale dependence, and the uncertainty due to CKM parameters are identified as the main sources of SM errors [9].

⁶We note here that this specific behaviour of T-odd and T-even observables was shown in many examples of T-odd CP asymmetries (see [20] and references therein) but a general proof of this statement is still missing to our knowledge.

5.2 Phenomenological analysis

The NP sensitivity of CP -violating observables in the mode $\bar{B}_d \rightarrow \bar{K}^{*0} \ell^+ \ell^-$ was discussed in a model-independent way [9] and also in various popular concrete NP models [7]. It was found that the NP contributions to the phases of the Wilson coefficients \mathcal{C}_7 , \mathcal{C}_9 , and \mathcal{C}_{10} and of their chiral counterparts drastically enhance such CP -violating observables, while presently most of those phases are very weakly constrained. It was claimed that these observables offer clean signals of NP contributions.

However, the NP reach of such observables can only be judged with a *complete* analysis of the theoretical and experimental uncertainties. To the very detailed analyses in [7, 9] we add the following points:

- We redefine the various CP asymmetries following the general method presented in our previous paper [6]: an appropriate normalisation of the CP asymmetries almost eliminates any uncertainties due to the soft form factors which is one of the major sources of errors in the SM prediction.
- We explore the effect of the possible Λ_{QCD}/m_b corrections and make the uncertainty due to those unknown Λ_{QCD}/m_b corrections manifest in our analysis within the SM and NP scenarios.
- We investigate the experimental sensitivity of the angular CP asymmetries using a toy Monte Carlo model and estimate the statistical uncertainty of the observables with statistics corresponding to five years of nominal running at LHCb (10 fb^{-1}) using a full angular fit method.

We discuss these issues by example of the two angular asymmetries corresponding to the angular coefficient functions J_{6s} and J_8 ;

$$A_{6s} = \frac{J_{6s} - \bar{J}_{6s}}{d(\Gamma + \bar{\Gamma})/dq^2}, \quad A_8 = \frac{J_8 - \bar{J}_8}{d(\Gamma + \bar{\Gamma})/dq^2}. \quad (5.3)$$

Within the SM the first CP asymmetry related to J_{6s} turns out to be the well-known forward-backward CP asymmetry which was proposed in [21, 22].

As a first step we redefine the two CP observables. We make sure that the form factor dependence cancels out at the LO level by using an appropriate normalisation:

$$A_{6s}^{V2s} = \frac{J_{6s} - \bar{J}_{6s}}{J_{2s} + \bar{J}_{2s}}, \quad A_8^V = \frac{J_8 - \bar{J}_8}{J_8 + \bar{J}_8}. \quad (5.4)$$

The J_i are bilinear in the K^* spin amplitudes, so it is clear from the LO formulae eq. (2.6) that, following the strategy of [6], any form factor dependence at this order cancels out in both observables. We note that J_{2s} has the same form factor dependence as J_{6s} but has larger absolute values over the dilepton mass spectrum that stabilises the quantity. In figure 5 the uncertainty due to the form factor dependence is estimated in a conservative way (see appendix B) for A_{6s} defined in eq. (5.3) and for A_{6s}^V defined in eq. (5.4). Comparing the plots, one sees that with the appropriate normalisation, this main source of hadronic

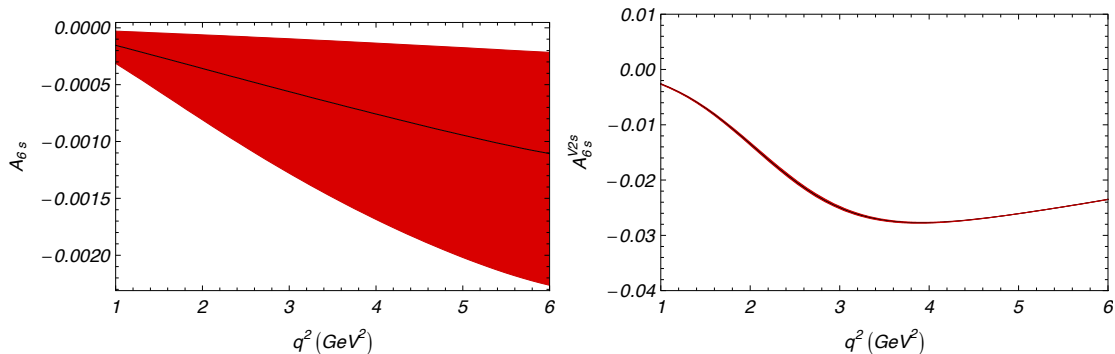


Figure 5. SM prediction of the CP -violating observables A_{6s} (left) and A_{6s}^{V2s} (right) as function of the squared lepton mass with uncertainty due to the soft form factors only. Notice the difference in scale and the difference in relative error in the two figures.

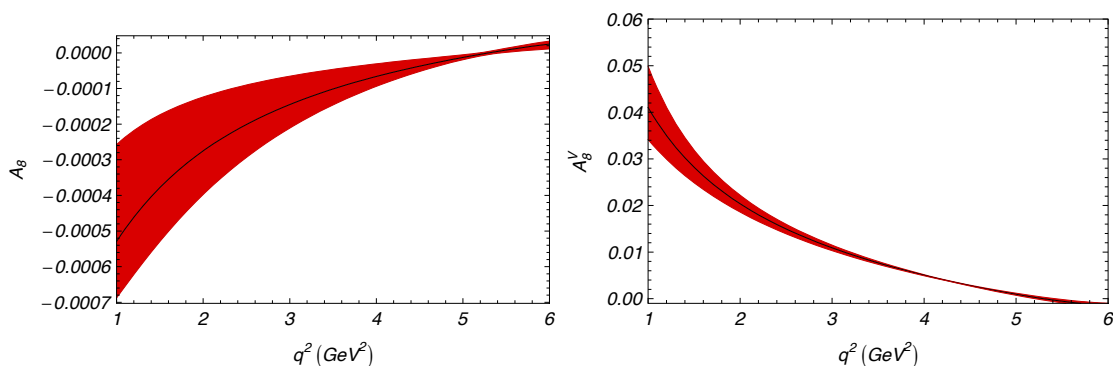


Figure 6. SM prediction of the CP -violating observables A_8 (left) and A_8^V (right) with uncertainty due to the soft form factors only. Notice the difference in scale of the two figures.

uncertainties gets almost eliminated. The leftover uncertainty enters through the form factor dependence of the NLO contribution. Figure 6 shows the analogous results for the observable A_8^V .

In the second step we make the possible Λ_{QCD}/m_b corrections manifest in our final results by using the procedure described in section 2.3. It turns out that in spite of this very conservative ansatz for the possible power corrections, we neglect for example any kind of correlations between such corrections in the various spin amplitudes; the impact of those corrections is smaller than the SM uncertainty in case of the two observables A_{6s}^V and A_8^V . In the left plot of figure 7 the SM error is given, including uncertainties due to the scale dependence and input parameters and the spurious error due to the form factors. In the right plot the estimated power corrections are given, which in case of the CP -violating observable A_{6s}^V are significantly smaller than the combined uncertainty due to scale and input parameters. Figure 8 shows the same feature for the CP -violating observable A_8^V . This result is in contrast to the one for CP -averaged angular observables discussed in [6], where the estimated power corrections always represent the dominant error. The reason for this specific feature is the smallness of the weak phase in the SM. Thus, one expects

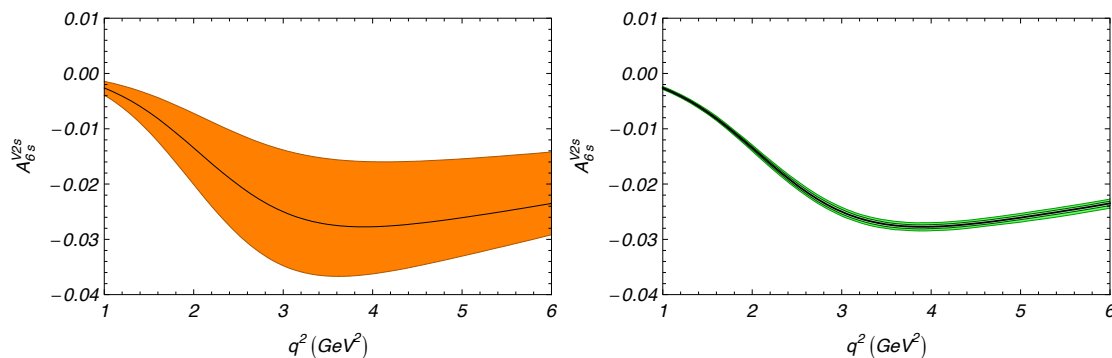


Figure 7. SM uncertainty in A_{6s}^{V2s} (left) and estimate of uncertainty due to Λ_{QCD}/m_b corrections with $C_{1,2} = 10\%$ (right).

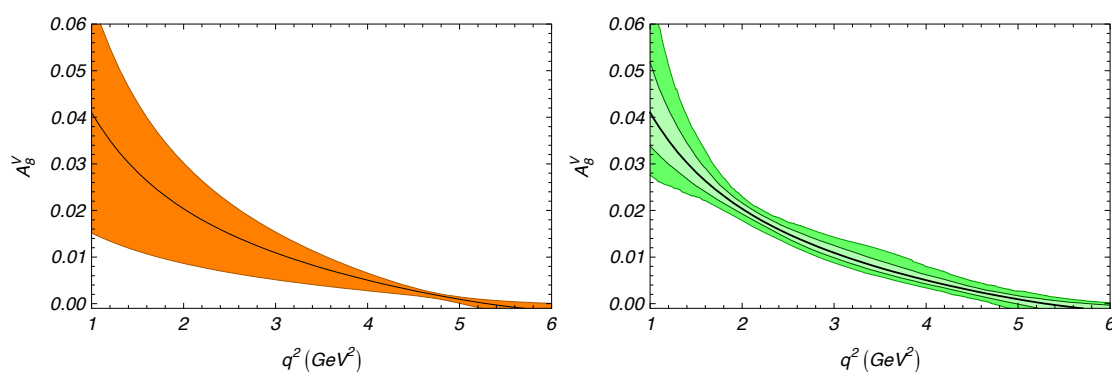


Figure 8. SM uncertainty in A_8^V (left) and estimate of uncertainty due to Λ_{QCD}/m_b corrections (right, light grey (green) corresponds to $C_{1,2} = 5\%$, dark grey (green) to $C_{1,2} = 10\%$).

that the impact of power corrections will be significantly larger when NP scenarios with new CP phases are considered (see below).

In the third step we consider various NP scenarios. Here we follow the model-independent constraints derived in [9] assuming only one NP Wilson coefficient being nonzero. We consider three different NP benchmarks scenarios of this kind:

1. $|\mathcal{C}_9^{\text{NP}}| = 2$ and $\phi_9^{\text{NP}} = \frac{\pi}{8}, \frac{\pi}{2}, \pi$ (Red);
2. $|\mathcal{C}_{10}^{\text{NP}}| = 1.5$ and $\phi_{10}^{\text{NP}} = \frac{\pi}{8}, \frac{\pi}{2}, \pi$ (Grey);
3. $|\mathcal{C}'_{10}| = 3$ and $\phi'_{10} = \frac{\pi}{8}, \frac{\pi}{2}, \pi$ (Blue);

where the colours refer to the ones used in the following figures. The absolute values of the Wilson coefficients are chosen in such a way that the model-independent analysis, assuming *one* nontrivial NP Wilson coefficient acting at a time, does not give any bound on the corresponding NP phase.

Figure 9 shows our two observables in the three scenarios with the phase value $\frac{\pi}{8}$: the CP -violating observable A_{6s}^V might separate a NP scenario (2), while the central values of scenarios (1) and (3) are very close to the SM. Moreover observable A_8^V seems to be suited to separate scenarios (1) and (3) from the SM.

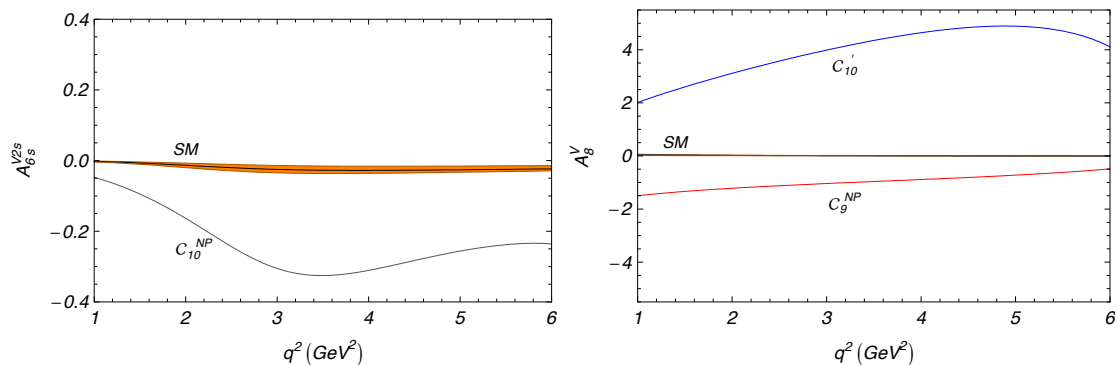


Figure 9. NP scenarios, assuming one nontrivial NP Wilson coefficient at a time, next to SM prediction for A_{6s}^{V2s} (left) and A_8^V (right), for concrete values see text.

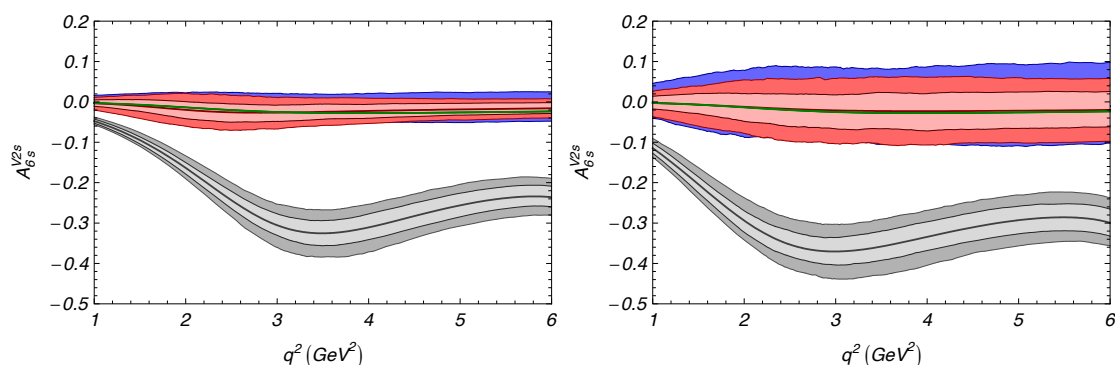


Figure 10. A_{6s}^{V2s} : Estimate of uncertainty due to Λ_{QCD}/m_b corrections within NP scenarios as in previous figure with phases $\phi_i = \frac{\pi}{8}$ (left) and $\phi_i = \frac{\pi}{2}$ (right).

However, to judge the NP reach we need a complete error analysis within the three NP scenarios. As shown in section 2.3 we now work with three weak sub-amplitudes in which possible power corrections are varied independently. The plots in figures 10 and 11 show that the possible Λ_{QCD}/m_b corrections have a much larger impact on our two observables in the NP scenarios than in the SM and become the dominating theoretical uncertainty. We also get significantly larger possible Λ_{QCD}/m_b corrections when changing the value of the new weak phase from $\frac{\pi}{8}$ to $\frac{\pi}{2}$. Regarding even larger phase values, we note here that the NP effects drastically decrease again when phase values around π are chosen as expected. Nevertheless, in view of the theoretical Λ_{QCD}/m_b uncertainties only, the two CP -violating observables could discriminate some specific NP scenarios with new CP phase of order $\frac{\pi}{8}$ or $\frac{\pi}{2}$ from the SM; in case of A_{6s}^{V2s} NP scenario 2, in case of A_8^V NP scenario 3 and possibly 1.

One should also consider the additional theoretical uncertainties due to scale dependence, input parameters and soft form factor dependencies within the NP scenarios. Those additional theoretical uncertainties are sizable and of the same order as the ones due to Λ_{QCD}/m_b corrections: they are shown in the left plots in figures 12 and 13 as orange bands overlaying the *total* errors bars including also the Λ_{QCD}/m_b corrections.

As the last step, we analyse the experimental sensitivity of the angular CP asymmetries

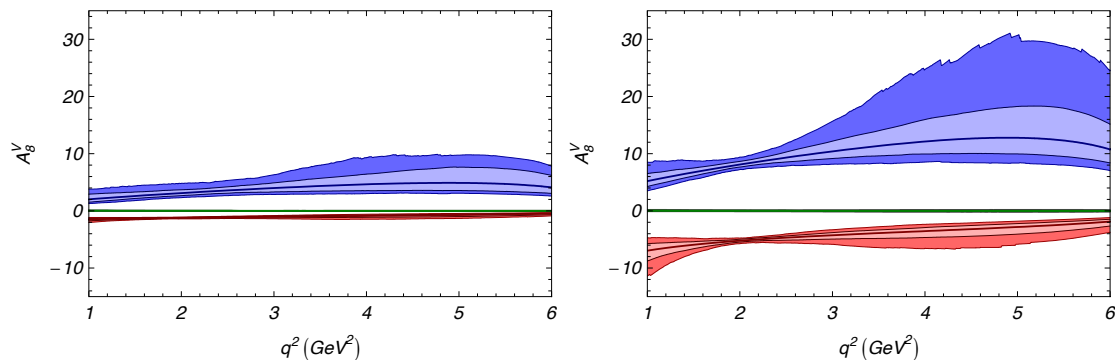


Figure 11. A_8^V : Estimate of uncertainty due to Λ_{QCD}/m_b corrections within NP scenarios as in previous figure with phases $\phi_i = \frac{\pi}{8}$ (left) and $\phi_i = \frac{\pi}{2}$ (right).

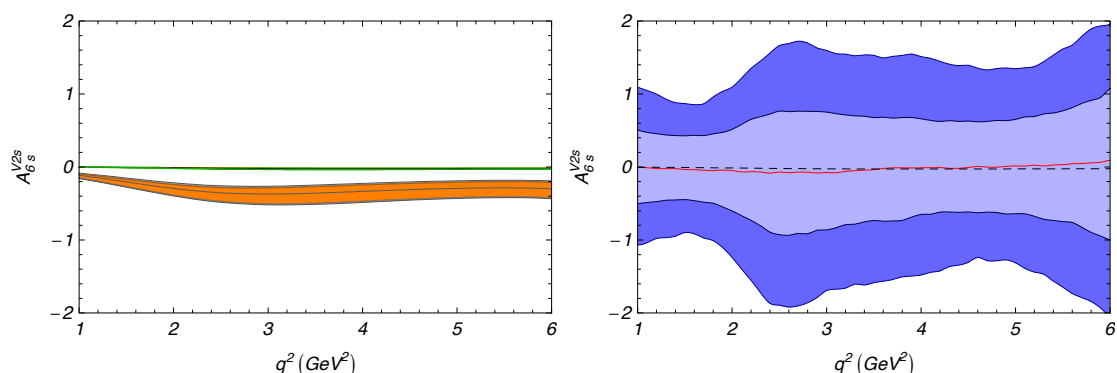


Figure 12. A_{6s}^{V2s} : Estimate of uncertainty due to Λ_{QCD}/m_b corrections (grey bands) in NP scenario 2, $|C_{10}^{\text{NP}}| = 1.5$ and $\phi_{10}^{\text{NP}} = \frac{\pi}{2}$ with the other theoretical uncertainties overlaid (orange bands) and in SM (left) and experimental uncertainty (right).

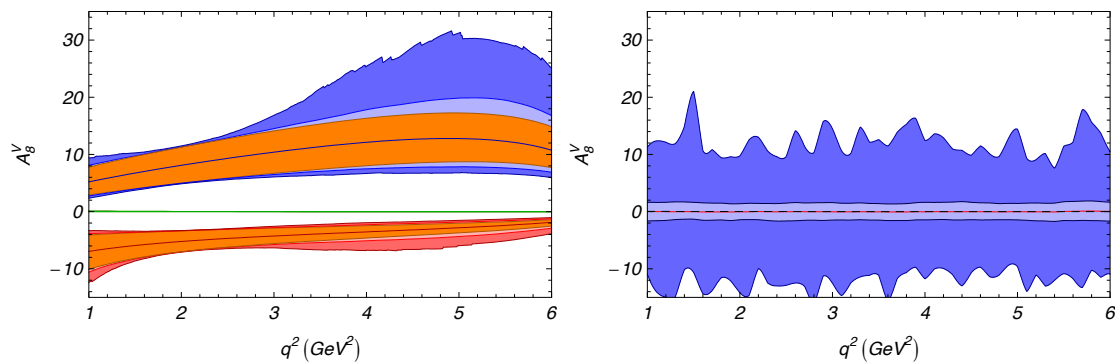


Figure 13. A_8^V : Estimate of uncertainty due to Λ_{QCD}/m_b corrections in NP scenarios 1 ($|C_9^{\text{NP}}| = 2$, $\phi_9^{\text{NP}} = \frac{\pi}{2}$, red bands) and 3 ($|C'_{10}| = 3$, $\phi'_{10} = \frac{\pi}{2}$, blue bands) with the other theoretical uncertainties overlaid (orange bands) and in SM (left) and experimental uncertainty (right).

using a toy Monte Carlo model. The right plots in figures 12 and 13 show the estimates of the statistical uncertainty of A_{6s}^V and A_8^V with statistics corresponding to five years of nominal running at LHCb (10 fb^{-1}). The inner and outer bands correspond to 1σ and 2σ

statistical errors. The plots show that all the NP benchmarks are within the 1σ range of the expected experimental error in case of the observable A_{6s}^V , and within the 2σ range of the experimental error in case of the observable A_8^V . We emphasise that from the experimental point of view the normalisation is not important when calculating the overall significance because the overall error is dominated by the error on the numerator. So the experimental error of the observables A_{6s} and A_8 defined in eq. (5.3) using the traditional normalisation will be similarly large to the one of our new observables A_{6s}^V and A_8^V defined in eq. (5.4).

Our final conclusion is that the possibility to disentangle different NP scenarios for the CP -violating observables remains rather difficult. For the rare decay $\bar{B}_d \rightarrow \bar{K}^{*0} \ell^+ \ell^-$, LHCb has no real sensitivity for NP phases up to values of $\frac{\pi}{2}$ (and neither up to values of π) in the Wilson coefficients $\mathcal{C}_9, \mathcal{C}_{10}$ and their chiral counterparts. Even Super-LHCb with 100 fb^{-1} integrated luminosity does not improve the situation significantly. This is in contrast to the CP -conserving observables presented in [6] and further discussed in the next chapter which, both from the theoretical and experimental point of view, are very promising.

6 Analysis of CP -conserving observables

The CP -conserving observables can be analysed at LO in the large recoil limit using the heavy-quark and large- E_{K^*} expressions for the spin amplitudes, as first proposed in [4]. One of the advantages of this approach is that we obtain analytic expressions of these observables in a very simple way. These expressions can be used to study the behaviour of the observables without having to rely on numerical computations, since the most relevant features arise already at LO. The main goal of this section is to perform this type of analysis on the $A_T^{(i)}$ observables.

6.1 Leading-order expressions of $A_T^{(2)}$

The asymmetry $A_T^{(2)}$, first proposed in [4] is given by

$$A_T^{(2)} = \frac{|A_\perp|^2 - |A_\parallel|^2}{|A_\perp|^2 + |A_\parallel|^2}, \quad (6.1)$$

where $|A_i|^2 = |A_i^L|^2 + |A_i^R|^2$. It has a simple form, free from $\xi_\perp(0)$ form factor dependencies, in the heavy-quark ($m_B \rightarrow \infty$) and large \bar{K}^{*0} energy ($E_{K^*} \rightarrow \infty$) limits:⁷

$$A_T^{(2)} = \frac{2 \left[\text{Re} \left(\mathcal{C}'_{10} \mathcal{C}_{10}^* \right) + F^2 \text{Re} \left(\mathcal{C}'_7 \mathcal{C}_7^* \right) + F \text{Re} \left(\mathcal{C}'_7 \mathcal{C}_9^* \right) \right]}{|\mathcal{C}_{10}|^2 + |\mathcal{C}'_{10}|^2 + F^2 (|\mathcal{C}_7|^2 + |\mathcal{C}'_7|^2) + |\mathcal{C}_9|^2 + 2F \text{Re} \left(\mathcal{C}_7 \mathcal{C}_9^* \right)}, \quad (6.2)$$

where $F \equiv 2m_b m_B / q^2$. The Wilson coefficients can take the most general form:

$$\mathcal{C}_i = \mathcal{C}_i^{\text{SM}} + |\mathcal{C}_i^{\text{NP}}| e^{i\phi_i^{\text{NP}}}, \quad \mathcal{C}'_i = |\mathcal{C}'_i| e^{i\phi'_i}, \quad i = 7, 9, 10. \quad (6.3)$$

We will neglect henceforward both the tiny SM weak phase ϕ_9^{SM} , that arises from the CKM elements ratio $\lambda_u = (V_{ub} V_{us}^*) / (V_{tb} V_{ts}^*)$, and the SM strong phase θ_9^{SM} , smaller than 1° in the low dilepton mass region $1 \text{ GeV}^2 \leq q^2 \leq 6 \text{ GeV}^2$ [22].

⁷Notice that along this section we will drop the superscript ‘‘eff’’ that \mathcal{C}_7 and \mathcal{C}_9 should bear in order to simplify the notation.

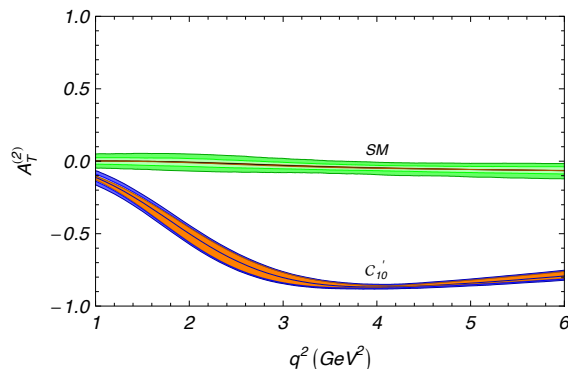


Figure 14. $A_T^{(2)}$ in the SM (green) and with NP in $C'_{10} = 3e^{i\frac{\pi}{8}}$ (blue), this value is allowed by the model independent analysis of [9]. The inner line corresponds to the central value of each curve. The dark orange bands surrounding it are the NLO results including all uncertainties (except for A_{QCD}/m_b) as explained in the text. Internal light green/blue bands (barely visible) include the estimated A_{QCD}/m_b uncertainty at a $\pm 5\%$ level and the external dark green/blue bands correspond to a $\pm 10\%$ correction for each spin amplitude.

Obviously, the observable $A_T^{(2)}$ vanishes in the heavy-quark and large \bar{K}^{*0} energy limits at LO when all the Wilson coefficients are taken to be SM-like. This result can be understood rather easily. The left-handed structure of weak interactions in the SM guarantees that, in these limits, the s quark created in the $b \rightarrow s$ transition will have helicity $h(s) = -1/2$ in the massless limit ($m_s \rightarrow 0$) [23]. This s quark will combine with the spectator quark \bar{d} of the \bar{B}_d to form the \bar{K}^{*0} meson with $h(\bar{K}^{*0}) = -1$ or 0 (but not $+1$), therefore $H_+ = 0$ at quark level in the SM. Using eq. (2.3), this translates into $A_\perp = -A_\parallel$ at the quark level, which corresponds to $A_\perp \simeq -A_\parallel$ at the hadron level [24–26].

The NP dependence of $A_T^{(2)}$ can be studied in a model independent way by switching on one Wilson coefficient each time and keeping all the others at their SM values. A simple inspection of eq. (6.2) shows that only the chirally flipped operators \mathcal{O}'_7 and \mathcal{O}'_{10} give a non-zero expression for $A_T^{(2)}$ in our approximation:

$$A_T^{(2)} \Big|_{7'} = \frac{2F(F\mathcal{C}_7^{\text{SM}} + \mathcal{C}_9^{\text{SM}})|\mathcal{C}'_7|\cos(\phi'_7)}{(\mathcal{C}_{10}^{\text{SM}})^2 + F^2|\mathcal{C}'_7|^2 + (F\mathcal{C}_7^{\text{SM}} + \mathcal{C}_9^{\text{SM}})^2}, \quad (6.4)$$

and

$$A_T^{(2)} \Big|_{10'} = \frac{2\mathcal{C}_{10}^{\text{SM}}|\mathcal{C}'_{10}|\cos(\phi'_{10})}{(\mathcal{C}_{10}^{\text{SM}})^2 + |\mathcal{C}'_{10}|^2 + (F\mathcal{C}_7^{\text{SM}} + \mathcal{C}_9^{\text{SM}})^2}. \quad (6.5)$$

Equations. (6.5) and (6.4) show that $A_T^{(2)}$ is sensitive to both the modulus and the sign of the Wilson coefficients \mathcal{C}'_7 and \mathcal{C}'_{10} . When NP enters only \mathcal{C}'_{10} , the fact that $\mathcal{C}_{10} < 0$ in the SM makes the observable negative unless $\frac{\pi}{2} < |\phi'_{10}| < \pi$, enabling us to distinguish the sign of this weak phase (figure 14). Likewise, if NP appears in \mathcal{C}'_7 , $A_T^{(2)}$ will display a zero in the dilepton mass spectrum when $F\mathcal{C}_7^{\text{SM}} + \mathcal{C}_9^{\text{SM}} = 0$, which will coincide exactly with the zero of the observable A_{FB} at LO [13]. As the zero is independent of \mathcal{C}'_7 , all curves with $\mathcal{C}_7^{\text{SM}}$ should exhibit it at $q^2 \sim 4 \text{ GeV}^2$, but if there is also a NP contribution to \mathcal{C}_7 , the zero

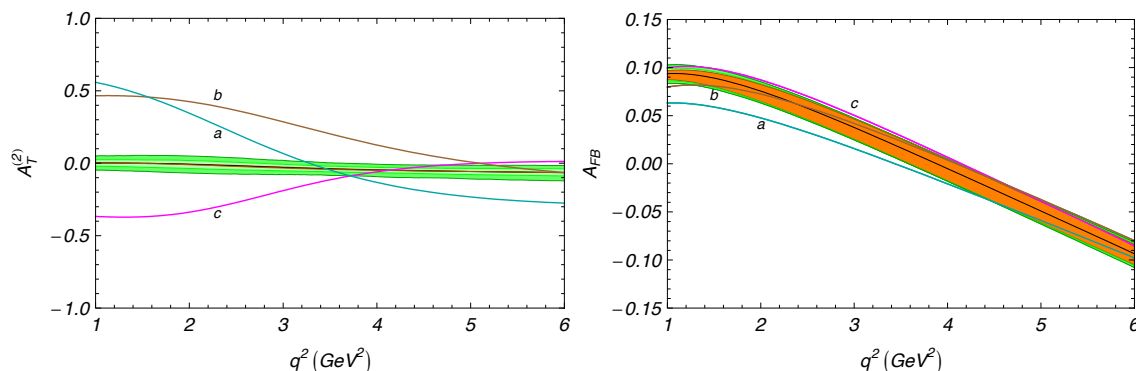


Figure 15. Observables $A_T^{(2)}$ and A_{FB} with NP curves for three allowed combinations of \mathcal{C}_7 and \mathcal{C}'_7 following the model independent analysis of [9]. The bands correspond to the SM and the theoretical uncertainty as described in figure 14. The cyan line (shown with the label *a*) corresponds to $(\mathcal{C}_7^{\text{NP}}, \mathcal{C}'_7) = (0.26e^{-i\frac{7\pi}{16}}, 0.2e^{i\pi})$, the brown line *b* to $(0.07e^{i\frac{3\pi}{5}}, 0.3e^{i\frac{3\pi}{5}})$ and the magenta line *c* to $(0.03e^{i\pi}, 0.07)$.

will be shifted either to higher or lower values of q^2 . In case of a sign flip affecting \mathcal{C}_7 , $A_T^{(2)}$ would not have a zero at any value of q^2 , exactly as for A_{FB} (see [27] for a recent discussion of different mechanisms to achieve this). In fact, should NP enter both \mathcal{O}_7 and \mathcal{O}'_7 simultaneously, eq. (6.2) would imply

$$A_T^{(2)} \Big|_{7', 7^{\text{NP}}} \propto 2F \left[(F\mathcal{C}_7^{\text{SM}} + \mathcal{C}_9^{\text{SM}}) |\mathcal{C}'_7| \cos(\phi'_7) + F |\mathcal{C}'_7| |\mathcal{C}_7^{\text{NP}}| \cos(\phi'_7 - \phi_7^{\text{NP}}) \right] \quad (6.6)$$

while

$$A_{FB} \Big|_{7', 7^{\text{NP}}} \propto F\mathcal{C}_7^{\text{SM}} + \mathcal{C}_9^{\text{SM}} + F |\mathcal{C}_7^{\text{NP}}| \cos(\phi_7^{\text{NP}}). \quad (6.7)$$

The comparison of eq. (6.6) with eq. (6.7) can be used to explain the improved sensitivity of $A_T^{(2)}$ to certain types of NP versus that of A_{FB} . The numerator of $A_T^{(2)}$ exhibits sensitivity to the weak phases ϕ_7^{NP} and ϕ'_7 , having an interference term enhanced by the large factor F ($8 \lesssim F \lesssim 48$ in the dilepton mass region studied), while A_{FB} is only sensitive to ϕ_7^{NP} . Thus, a wider departure from the SM behaviour is to be expected in $A_T^{(2)}$ when NP enters the operators \mathcal{O}_7 and \mathcal{O}'_7 . This is shown in figure 15 using three different scenarios, described in the caption of figure 15, compatible with present experimental and theoretical constraints. Therefore, we emphasise that $A_T^{(2)}$ must be regarded as an improved version of A_{FB} once the full-angular analysis becomes possible.

6.2 Leading-order expressions of $A_T^{(5)}$

In the SM, we get in the heavy-quark and large- E_{K^*} limits at LO:

$$A_T^{(5)} \Big|_{\text{SM}} = \frac{|-(\mathcal{C}_{10}^{\text{SM}})^2 + (F\mathcal{C}_7^{\text{SM}} + \mathcal{C}_9^{\text{SM}})^2|}{2[(\mathcal{C}_{10}^{\text{SM}})^2 + (F\mathcal{C}_7^{\text{SM}} + \mathcal{C}_9^{\text{SM}})^2]}, \quad (6.8)$$

which sets the “wave-like” behaviour of $A_T^{(5)}$. At low q^2 , eq. (6.8) can be used to check that $A_T^{(5)} \Big|_{\text{SM}}^{1 \text{ GeV}^2} \simeq 0.4$. On the other hand, at the zero-point of $A_T^{(2)}$ and A_{FB} , $A_T^{(5)}$ exhibits an absolute maximum of magnitude $A_T^{(5)} \Big|_{\text{SM}}^{4 \text{ GeV}^2} \simeq 0.5$.

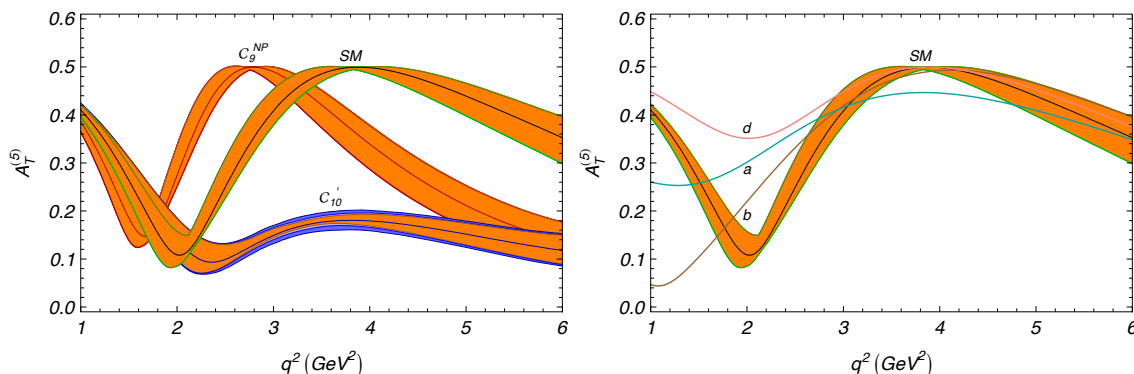


Figure 16. $A_T^{(5)}$ in the SM and with NP in $C'_{10} = 3e^{i\frac{\pi}{8}}$ and $C_9^{NP} = 2e^{i\frac{\pi}{8}}$ (left) and in both C_7 and C'_7 Wilson coefficients (right). The cyan line (a) corresponds to $(C_7^{NP}, C'_7) = (0.26e^{-i\frac{7\pi}{16}}, 0.2e^{i\pi})$, the brown line (b) to $(0.07e^{i\frac{3\pi}{5}}, 0.3e^{i\frac{3\pi}{5}})$ and the pink line (d) to $(0.18e^{-i\frac{\pi}{2}}, 0)$. The bands symbolise the theoretical uncertainty as described in figure 14.

Any inclusion of NP in the Wilson coefficients C_7 , C_9 and C_{10} will give rise to the appearance of an extra term in the numerator (with respect to eq. (6.8)) that will shift the observable along the y -axis.

$$A_T^{(5)}\Big|_{7NP}^{\pi/2} = \frac{\sqrt{[-(C_{10}^{\text{SM}})^2 + F^2|C_7^{\text{NP}}|^2 + (FC_7^{\text{SM}} + C_9^{\text{SM}})^2]^2 + 4[FC_{10}^{\text{SM}}|C_7^{\text{NP}}|^2]}}{2[(C_{10}^{\text{SM}})^2 + F^2|C_7^{\text{NP}}|^2 + (FC_7^{\text{SM}} + C_9^{\text{SM}})^2]}, \quad (6.9a)$$

$$A_T^{(5)}\Big|_{9NP}^{\pi/2} = \frac{\sqrt{[-(C_{10}^{\text{SM}})^2 + |C_9^{\text{NP}}|^2 + (FC_7^{\text{SM}} + C_9^{\text{SM}})^2]^2 + 4[C_{10}^{\text{SM}}|C_9^{\text{NP}}|^2]}}{2[(C_{10}^{\text{SM}})^2 + |C_9^{\text{NP}}|^2 + (FC_7^{\text{SM}} + C_9^{\text{SM}})^2]}, \quad (6.9b)$$

$$A_T^{(5)}\Big|_{10NP}^{\pi/2} = \frac{\sqrt{[-(C_{10}^{\text{SM}})^2 - |C_{10}^{\text{NP}}|^2 + (FC_7^{\text{SM}} + C_9^{\text{SM}})^2]^2 + 4[|C_{10}^{\text{NP}}|(FC_7^{\text{SM}} + C_9^{\text{SM}})]^2}}{2[(C_{10}^{\text{SM}})^2 + |C_{10}^{\text{NP}}|^2 + (FC_7^{\text{SM}} + C_9^{\text{SM}})^2]}. \quad (6.9c)$$

In eq. (6.9) we have chosen for simplicity the weak phase $\phi_i^{\text{NP}} = \pi/2$ for $i = 7, 9, 10$, but they turn out to be dominated by the SM contribution unless the NP Wilson coefficients are very large. However, if the weak phases associated to NP Wilson coefficients are different from $\pi/2$, the $A_T^{(5)}$ curve will get shifted either to the left or to the right, depending on the value of the angle, as shown in figure 16.

NP might also enter via the chirally flipped \mathcal{O}'_7 and \mathcal{O}'_{10} . The corresponding LO expressions of $A_T^{(5)}$ in the heavy-quark and high- E_{K^*} limits read

$$A_T^{(5)}\Big|_{7'} = \frac{|-(C_{10}^{\text{SM}})^2 + (FC_7^{\text{SM}} + C_9^{\text{SM}})^2 - F^2|C_7'|^2|}{2[(C_{10}^{\text{SM}})^2 + (FC_7^{\text{SM}} + C_9^{\text{SM}})^2 + F^2|C_7'|^2]} \quad (6.10)$$

and

$$A_T^{(5)}\Big|_{10'} = \frac{|-(C_{10}^{\text{SM}})^2 + |C'_{10}|^2 + (FC_7^{\text{SM}} + C_9^{\text{SM}})^2|}{2[(C_{10}^{\text{SM}})^2 + |C'_{10}|^2 + (FC_7^{\text{SM}} + C_9^{\text{SM}})^2]}. \quad (6.11)$$

Equations (6.10) and (6.11) are both free from NP weak-phase dependence. $A_T^{(5)}$ evaluated at the q^2 value of the A_{FB} zero-point can be computed easily using eq. (6.11), obtaining

$$A_T^{(5)}|_{q_0^2} = \frac{1}{2} \frac{|-(C_{10}^{SM})^2 + |C'_{10}|^2|}{(C_{10}^{SM})^2 + |C'_{10}|^2}, \quad (6.12)$$

where the choice $C'_{10} = 0$ enables us to recover the SM prediction $A_T^{(5)}|_{SM}^{4\text{GeV}^2} = 0.5$. In figure 16 (left) it can be seen that for $|C'_{10}| = 3$ the departure of the NP curve obtained from the SM behaviour is indeed large.

6.3 Analysis of $A_T^{(3)}$ and $A_T^{(4)}$

The observables $A_T^{(3)}$ and $A_T^{(4)}$ were first introduced in [6] to test the longitudinal spin amplitude A_0 in a controlled way:

$$A_T^{(3)} = \frac{|A_{0L}A_{\parallel L}^* + A_{0R}^*A_{\parallel R}|}{\sqrt{|A_0|^2|A_{\perp}|^2}}, \quad A_T^{(4)} = \frac{|A_{0L}A_{\perp L}^* - A_{0R}^*A_{\perp R}|}{|A_{0L}A_{\parallel L}^* + A_{0R}^*A_{\parallel R}|}. \quad (6.13)$$

Unfortunately, the simultaneous appearance of A_{\perp} , A_{\parallel} and A_0 inside square roots turns the heavy-quark and large-energy limits into rather awkward expressions, not really useful to explain the behaviour of these observables at a glance. Therefore, we only outline their general properties. Equation (6.13) shows that $A_T^{(3)}$ and $A_T^{(4)}$ play a complementary role, as the numerator of $A_T^{(3)}$ and the denominator of $A_T^{(4)}$ are the same. Thus, when a minimum appears in one of them, a maximum is expected in the other observable and the other way around. This is indeed what can be observed in figure 17. For the values of the Wilson coefficients chosen, NP entering C'_{10} can easily be distinguished from the SM curve, displaying a maximum at around 3.5-4 GeV² (exactly in the energy region where $A_T^{(4)}$ is showing a minimum), while C_{10}^{NP} can only be clearly identified using $A_T^{(4)}$. Something similar happens with NP entering C_7^{SM} and C'_7 : the model-independent values chosen for these Wilson coefficients do not give rise to clear NP signals from $A_T^{(3)}$, but they can be easily told apart using $A_T^{(4)}$. In those situations where the origin of the NP curve can not be clearly established using a single observable (for instance, the c curve in the $A_T^{(4)}$ plot of figure 17 is very similar to the C_{10}^{NP} curve), the combined use of $A_T^{(2)}$, $A_T^{(3)}$, $A_T^{(4)}$, $A_T^{(5)}$ and maybe A_{FB} enables us to identify which Wilson coefficient(s) has a contribution from NP.

7 Conclusion

In this paper we have presented how the decay $\bar{B}_d \rightarrow \bar{K}^{*0} \ell^+ \ell^-$ can provide detailed knowledge of NP effects in the flavour sector. We developed a method for constructing observables with specific sensitivity to some types of NP while, at the same time, keeping theoretical errors from form factors under control. A method based on infinitesimal symmetries was presented which allows in a generic way to identify if an arbitrary combination of spin amplitudes is an observable of the angular distribution. For the case of massless leptons we identified the explicit form of all four symmetries present. We showed the possible impact of the unknown Λ_{QCD}/m_b corrections on the NP sensitivity of the various angular

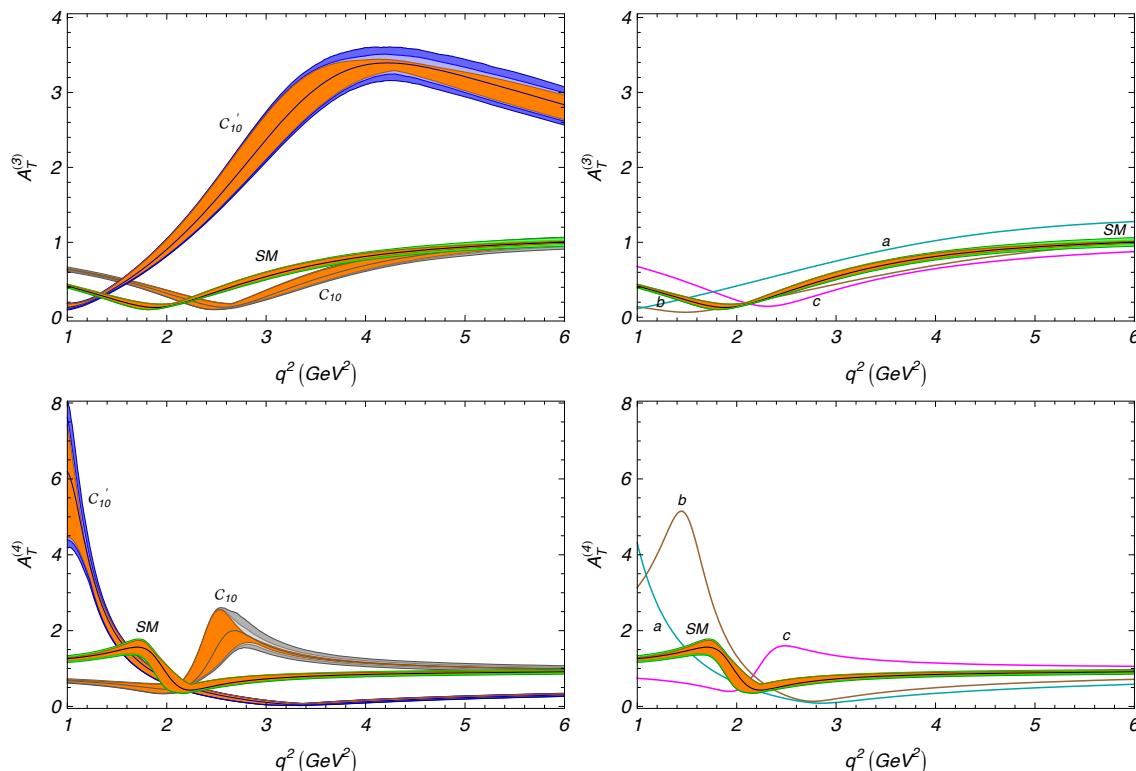


Figure 17. $A_T^{(3)}$ and $A_T^{(4)}$ in the SM and with NP in and $C_{10}^{\text{NP}} = 1.5e^{i\frac{\pi}{8}}$ and $C'_{10} = 3e^{i\frac{\pi}{8}}$ (left) and in both C_7 and C'_7 Wilson coefficients (right). The cyan line (curve *a*) corresponds to $(C_7^{\text{NP}}, C'_7) = (0.26e^{-i\frac{7\pi}{10}}, 0.2e^{i\pi})$, the brown line (curve *b*) to $(0.07e^{i\frac{3\pi}{5}}, 0.3e^{i\frac{3\pi}{5}})$ and the magenta line (curve *c*) to $(0.03e^{i\pi}, 0.07)$. The bands symbolise the theoretical uncertainty as described in figure 14.

observables in a systematic way using an ensemble method. Experimental sensitivity to the observables was evaluated for datasets corresponding to 10fb^{-1} of data at LHC*b*. Using these tools, we did a phenomenological analysis for both *CP*-conserving and *CP*-violating observables. The conclusion from this is that the *CP*-violating observables have very poor experimental sensitivity while the *CP*-conserving observables $A_T^{(i)}$ (with $i = 2, 3, 4$) are very powerful for finding NP, including situations with large weak phases.

Acknowledgments

JM acknowledges financial support from FPA2005-02211, 2005-SGR-00994, MR from the Universitat Autònoma de Barcelona, UE and WR from the Science and Technology Facilities Council (STFC), and TH from the European network Heptools. TH thanks the CERN theory group for its hospitality during his visits to CERN.

A Kinematics

Assuming the \bar{K}^{*0} to be on the mass shell, the decay $\bar{B}_d \rightarrow \bar{K}^{*0}\ell^+\ell^-$ is completely described by four independent kinematic variables; namely, the square of the lepton-pair

invariant mass, q^2 , and the three angles θ_l , θ_K and ϕ . The sign of the angles for the \bar{B}_d decay shows great variation in the literature. Therefore we present here an explicit definition of our conventions and point out where the same or different definitions have been used.

First we consider the $\bar{B}_d \rightarrow \bar{K}^{*0} \ell^+ \ell^-$ decay. The angle θ_l is the angle between the μ^+ momentum in the rest frame of the dimuon and the direction of the dimuon in the rest frame of the \bar{B}_d . The θ_K angle is in a similar way the angle between the K^- momentum in the \bar{K}^{*0} rest frame and the direction of the \bar{K}^{*0} in the rest frame of the \bar{B}_d .

Let us for $\bar{B}_d \rightarrow \bar{K}^{*0} \ell^+ \ell^-$ define the momentum vectors

$$\vec{P}_{\ell^+ \ell^-} = \vec{p}_{\ell^+} + \vec{p}_{\ell^-}, \quad (\text{A.1})$$

$$\vec{Q}_{\ell^+ \ell^-} = \vec{p}_{\ell^+} - \vec{p}_{\ell^-}, \quad (\text{A.2})$$

$$\vec{P}_{K^- \pi^+} = \vec{p}_{K^-} + \vec{p}_{\pi^+}, \quad (\text{A.3})$$

$$\vec{Q}_{K^- \pi^+} = \vec{p}_{K^-} - \vec{p}_{\pi^+}. \quad (\text{A.4})$$

In the dimuon rest frame, we have that the ℓ^+ momentum is parallel to $\vec{Q}_{\ell^+ \ell^-}$ and also that $\vec{P}_{K^- \pi^+}$ points in the opposite direction of the dimuon in the \bar{B}_d rest frame. Thus we can compute the θ_l angle as

$$\cos \theta_l = - \frac{\vec{Q}_{\ell^+ \ell^-}^{\ell\ell} \cdot \vec{P}_{K^- \pi^+}^{\ell\ell}}{|\vec{Q}_{\ell^+ \ell^-}^{\ell\ell}| |\vec{P}_{K^- \pi^+}^{\ell\ell}|}, \quad (\text{A.5})$$

where the superscript is used to indicate the frame. In a similar way we have in the \bar{K}^{*0} rest frame

$$\cos \theta_K = - \frac{\vec{Q}_{K^- \pi^+}^{K^*} \cdot \vec{P}_{\ell^+ \ell^-}^{K^*}}{|\vec{Q}_{K^- \pi^+}^{K^*}| |\vec{P}_{\ell^+ \ell^-}^{K^*}|}. \quad (\text{A.6})$$

Finally, if we go to the rest frame of the \bar{B}_d , we have ϕ as the signed angle between the planes defined by the two muons and the \bar{K}^{*0} decay products respectively. Vectors perpendicular to the decay planes are

$$\vec{N}_{\ell^+ \ell^-} = \vec{P}_{\ell^+ \ell^-}^B \times \vec{Q}_{\ell^+ \ell^-}^B, \quad \vec{N}_{K^- \pi^+} = \vec{P}_{K^- \pi^+}^B \times \vec{Q}_{K^- \pi^+}^B, \quad (\text{A.7})$$

which lets us define ϕ from

$$\cos \phi = - \frac{\vec{N}_{\ell^+ \ell^-} \cdot \vec{N}_{K^- \pi^+}}{|\vec{N}_{\ell^+ \ell^-}| |\vec{N}_{K^- \pi^+}|}, \quad \sin \phi = \left(\frac{\vec{N}_{\ell^+ \ell^-} \times \vec{N}_{K^- \pi^+}}{|\vec{N}_{\ell^+ \ell^-}| |\vec{N}_{K^- \pi^+}|} \right) \cdot \frac{\vec{P}_{\ell^+ \ell^-}^B}{|\vec{P}_{\ell^+ \ell^-}^B|}. \quad (\text{A.8})$$

The angles are defined in the intervals

$$-1 \leq \cos \theta_l \leq 1, \quad -1 \leq \cos \theta_K \leq 1, \quad -\pi \leq \phi < \pi. \quad (\text{A.9})$$

The definition given here is identical to [6] but is different to [7]. However, the two definitions result in the same signs for all the coefficients J_i in eq. (2.4).

Now for the $B_d \rightarrow K^{*0} \ell^+ \ell^-$ decay the θ_l angle is still specified with respect to the ℓ^+ while for θ_K the angle is for the K^+ . This is equivalent to what is done in [7]. As the θ_l angle does not change the sign of the lepton, we have

$$\bar{J}_{1,2,3,4,7} = J_{1,2,3,4,7}, \quad \bar{J}_{5,6,8,9} = -J_{5,6,8,9}. \quad (\text{A.10})$$

m_B [29]	5279.50 ± 0.30 MeV	λ [29]	0.226 ± 0.001
m_K [29]	896.00 ± 0.25 MeV	A [29]	0.814 ± 0.022
M_W [29]	80.398 ± 0.025 GeV	$\bar{\rho}$ [29]	0.135 ± 0.031
M_Z [29]	91.1876 ± 0.0021 GeV	$\bar{\eta}$ [29]	0.349 ± 0.017
$\hat{m}_t(\hat{m}_t)$ [13]	167 ± 5 GeV	$\Lambda_{\text{QCD}}^{(n_f=5)}$ [29]	220 ± 40 MeV
$\hat{m}_b(\hat{m}_b)$ [30]	4.20 ± 0.04 GeV	$\alpha_s(M_Z)$ [29]	0.1176 ± 0.0002
$\hat{m}_c(\hat{m}_c)$ [31]	1.26 ± 0.02 GeV	α_{em} [29]	$1/137$
f_B [32]	200 ± 25 MeV	$a_{1,K^*}^{\perp,\parallel}(2 \text{ GeV})$ [33]	0.03 ± 0.03
$f_{K^*}^{\perp}(2 \text{ GeV})$ [33]	163 ± 8 MeV	$a_{2,K^*}^{\perp,\parallel}(2 \text{ GeV})$ [33]	0.08 ± 0.06
$f_{K^*}^{\parallel}(2 \text{ GeV})$ [33]	220 ± 5 MeV		
$m_B \xi_{\parallel}(0)/(2m_{K^*})$ [14]	0.47 ± 0.09	$\lambda_{B,+}(\mu_h)$ [34]	0.51 ± 0.12 GeV
$\xi_{\perp}(0)$ [7]	0.266 ± 0.032	μ_h [7]	2.2 GeV

Table 2. Summary of input parameters and estimated uncertainties.

in the full-angular distribution in the absence of CP violation.

For the experimental papers [1, 2], a definition has been adopted where all angular distributions have been plotted for the $B_d \rightarrow K^{*0} \ell^+ \ell^-$ decay, with the $\bar{B}_d \rightarrow \bar{K}^{*0} \ell^+ \ell^-$ events overlaid assuming CP conservation. In practise this means that $\bar{B}_d \rightarrow \bar{K}^{*0} \ell^+ \ell^-$ events have the sign of $\cos \theta_l$ reversed before plotting. When experiments progress to measuring the ϕ angle as well, special care needs to be taken to get the definitions correct.

B Theoretical input parameters and uncertainties

To compute the soft form factor error bands in figures 5 and 6 in a conservative fashion, we have used, as input data, the values of $\xi_{\parallel}(0)$ and $\xi_{\perp}(0)$ shown in table 2. One can notice that the $\xi_{\perp}(0)$ value has been taken from [7], as it is compatible to $\xi_{\perp}(0) = 0.26$ used in [14], while for $\xi_{\parallel}(0)$ we have kept the value from [14] to allow for a wider uncertainty range.

The q^2 -dependence of the form factors V , A_1 and A_2 has been parametrised according to [28]

$$F(q^2) = \frac{F(0)}{1 - a_F q^2/m_B^2 + b_F q^4/m_B^4}, \quad (\text{B.1})$$

where $F(0)$, a_F and b_F are the fit parameters shown in table 3 of [28]. Substituting the outcomes of eq. (B.1) into [14]

$$\begin{aligned} \xi_{\perp}(q^2) &= \frac{m_B}{m_B + m_{K^*}} V(q^2), \\ \xi_{\parallel}(q^2) &= \frac{m_B + m_{K^*}}{2E_{K^*}} A_1(q^2) - \frac{m_B - m_{K^*}}{m_B} A_2(q^2), \end{aligned} \quad (\text{B.2})$$

we can obtain both the central value and the associated uncertainty curves for $\xi_{\parallel}(q^2)$ and $\xi_{\perp}(q^2)$ in the 1-6 GeV² range. These are used to get the fitting parameters A , B , C and D

of

$$\begin{aligned}\xi_{\perp}(q^2) &= \xi_{\perp}(0) \left(\frac{1}{A - B(q^2/m_B^2)} \right)^2, \\ \xi_{\parallel}(q^2) &= \xi_{\parallel}(0) \left(\frac{1}{C - D(q^2/m_B^2)} \right)^3,\end{aligned}\tag{B.3}$$

where $A, C \simeq 1$ within a per mille precision. This parametrisation follows closely eq. (47) in [13] and allows us to explore the impact of $\xi_{\perp}(0)$ and $\xi_{\parallel}(0)$ (with their corresponding uncertainties) to the CP -violating and CP -conserving observables studied throughout this paper.

The next step is to compute the amplitudes, keeping one soft form factor fixed at the central value and varying the other in the range allowed by its uncertainty. From them, the observables can be obtained in a straightforward way and the errors added in quadrature.

To generate the theoretical error bands not due to Λ/m_b corrections (plotted as the inner orange strips in the plots of sections 5 and 6) we have used the criteria of Beneke et al. in [13] and added the following uncertainties in quadrature: the renormalisation scale uncertainty has been found by varying μ between 2.3 and 9.2 GeV (where μ is the scale at which the Wilson Coefficients, α_s and the $\overline{\text{MS}}$ masses are evaluated), the uncertainty in the ratio m_c/m_b by varying this quantity between 0.29 and 0.31, and the other parametric uncertainties have been collected into the factor [6]

$$\kappa(q^2) = \frac{\pi^2 f_B f_{K^*,z}(\mu)}{N_c m_B \xi_z(q^2)} \quad \text{with } z = \perp, \parallel \tag{B.4}$$

that determines the relative magnitude of the hard-scattering versus the form factor term [13], which is uncertain by about $\pm 35\%$. In our numerical analysis we have used the values of the Wilson coefficients in table 1 of ref. [13].

Open Access. This article is distributed under the terms of the Creative Commons Attribution Noncommercial License which permits any noncommercial use, distribution, and reproduction in any medium, provided the original author(s) and source are credited.

References

- [1] BELLE collaboration, J.T. Wei et al., *Measurement of the Differential Branching Fraction and Forward-Backward Asymmetry for $B \rightarrow K^{(*)}\ell^+\ell^-$* , *Phys. Rev. Lett.* **103** (2009) 171801 [[arXiv:0904.0770](#)] [[SPIRES](#)].
- [2] BABAR collaboration, B. Aubert et al., *Measurements of branching fractions, rate asymmetries and angular distributions in the rare decays $B \rightarrow K\ell^+\ell^-$ and $B \rightarrow K^*\ell^+\ell^-$* , *Phys. Rev. D* **73** (2006) 092001 [[hep-ex/0604007](#)] [[SPIRES](#)].
- [3] A. Bharucha and W. Reece, *Constraining new physics with $B \rightarrow K^*\mu^+\mu^-$ in the early LHC era*, [arXiv:1002.4310](#) [[SPIRES](#)].
- [4] F. Krüger and J. Matias, *Probing new physics via the transverse amplitudes of $B^0 \rightarrow K^{*0}(\rightarrow K^-\pi^+)\ell^+\ell^-$ at large recoil*, *Phys. Rev. D* **71** (2005) 094009 [[hep-ph/0502060](#)] [[SPIRES](#)].

- [5] E. Lunghi and J. Matias, *Huge right-handed current effects in $B \rightarrow K^*(\rightarrow K\pi)\ell^+\ell^-$ in supersymmetry*, *JHEP* **04** (2007) 058 [[hep-ph/0612166](#)] [[SPIRES](#)].
- [6] U. Egede, T. Hurth, J. Matias, M. Ramon and W. Reece, *New observables in the decay mode $\bar{B}_d \rightarrow \bar{K}^{*0}\ell^+\ell^-$* , *JHEP* **11** (2008) 032 [[arXiv:0807.2589](#)] [[SPIRES](#)].
- [7] W. Altmannshofer et al., *Symmetries and Asymmetries of $B \rightarrow K^*\mu^+\mu^-$ Decays in the Standard Model and Beyond*, *JHEP* **01** (2009) 019 [[arXiv:0811.1214](#)] [[SPIRES](#)].
- [8] D. Melikhov, N. Nikitin and S. Simula, *Probing right-handed currents in $B \rightarrow K^*\ell^+\ell^-$ transitions*, *Phys. Lett. B* **442** (1998) 381 [[hep-ph/9807464](#)] [[SPIRES](#)].
- [9] C. Bobeth, G. Hiller and G. Piranishvili, *CP Asymmetries in $\bar{B} \rightarrow \bar{K}^*(\rightarrow \bar{K}\pi)\bar{\ell}\ell$ and Untagged $\bar{B}_s, B_s \rightarrow \phi(\rightarrow K^+K^-)\bar{\ell}\ell$ Decays at NLO*, *JHEP* **07** (2008) 106 [[arXiv:0805.2525](#)] [[SPIRES](#)].
- [10] F. Krüger, L.M. Sehgal, N. Sinha and R. Sinha, *Angular distribution and CP asymmetries in the decays $\bar{B}_d \rightarrow K^-\pi^+e^-e^+$ and $\bar{B}_d \rightarrow \pi^-\pi^+e^-e^+$* , *Phys. Rev. D* **61** (2000) 114028 [[hep-ph/9907386](#)] [[SPIRES](#)].
- [11] C.S. Kim, Y.G. Kim, C.-D. Lu and T. Morozumi, *Azimuthal angle distribution in $B \rightarrow K^*(\rightarrow K\pi)\ell^+\ell^-$ at low invariant $m(\ell^+\ell^-)$ region*, *Phys. Rev. D* **62** (2000) 034013 [[hep-ph/0001151](#)] [[SPIRES](#)].
- [12] A. Faessler, T. Gutsche, M.A. Ivanov, J.G. Korner and V.E. Lyubovitskij, *The Exclusive rare decays $B \rightarrow K(K^*)\bar{\ell}\ell$ and $B_c \rightarrow D(D^*)\bar{\ell}\ell$ in a relativistic quark model*, *Eur. Phys. J. direct C* **4** (2002) 18 [[hep-ph/0205287](#)] [[SPIRES](#)].
- [13] M. Beneke, T. Feldmann and D. Seidel, *Systematic approach to exclusive $B \rightarrow V\ell^+\ell^-$, $V\gamma$ decays*, *Nucl. Phys. B* **612** (2001) 25 [[hep-ph/0106067](#)] [[SPIRES](#)].
- [14] M. Beneke, T. Feldmann and D. Seidel, *Exclusive radiative and electroweak $b \rightarrow d$ and $b \rightarrow s$ penguin decays at NLO*, *Eur. Phys. J. C* **41** (2005) 173 [[hep-ph/0412400](#)] [[SPIRES](#)].
- [15] J. Charles, A. Le Yaouanc, L. Oliver, O. Pene and J.C. Raynal, *Heavy-to-light form factors in the heavy mass to large energy limit of QCD*, *Phys. Rev. D* **60** (1999) 014001 [[hep-ph/9812358](#)] [[SPIRES](#)].
- [16] M. Beneke and T. Feldmann, *Symmetry-breaking corrections to heavy-to-light B meson form factors at large recoil*, *Nucl. Phys. B* **592** (2001) 3 [[hep-ph/0008255](#)] [[SPIRES](#)].
- [17] THE LHCb collaboration, et al., *Roadmap for selected key measurements of LHCb*, [arXiv:0912.4179](#) [[SPIRES](#)].
- [18] M. Patel and H. Skottowe, *A Fisher discriminant selection for $B_d \rightarrow K^{*0}\mu^+\mu^-$ at LHCb*, Tech. Rep. [LHCb-2009-009](#), CERN Geneva (2010).
- [19] J.L. Hewett, (Ed.) et al., *The Discovery potential of a Super B Factory. Proceedings, SLAC Workshops, Stanford, USA, 2003*, [hep-ph/0503261](#) [[SPIRES](#)].
- [20] G. Valencia, *Constructing CP odd observables*, [hep-ph/9411441](#) [[SPIRES](#)].
- [21] G. Buchalla, G. Hiller and G. Isidori, *Phenomenology of nonstandard Z couplings in exclusive semileptonic $b \rightarrow s$ transitions*, *Phys. Rev. D* **63** (2000) 014015 [[hep-ph/0006136](#)] [[SPIRES](#)].
- [22] F. Krüger and E. Lunghi, *Looking for novel CP-violating effects in $\bar{B} \rightarrow K^*\ell^+\ell^-$* , *Phys. Rev. D* **63** (2001) 014013 [[hep-ph/0008210](#)] [[SPIRES](#)].

- [23] G. Burdman and G. Hiller, *Semileptonic form-factors from $B \rightarrow K^* \gamma$ decays in the large energy limit*, *Phys. Rev. D* **63** (2001) 113008 [[hep-ph/0011266](#)] [[SPIRES](#)].
- [24] B. Stech, *Form-factor relations for heavy to light transitions*, *Phys. Lett. B* **354** (1995) 447 [[hep-ph/9502378](#)] [[SPIRES](#)].
- [25] J.M. Soares, *Form factor relations for heavy-to-heavy and heavy-to-light meson transitions*, *Phys. Rev. D* **54** (1996) 6837 [[hep-ph/9607284](#)] [[SPIRES](#)].
- [26] J.M. Soares, *Form factor relations for heavy-to-light meson transitions: Tests of the quark model predictions*, [hep-ph/9810421](#) [[SPIRES](#)].
- [27] A.K. Alok et al., *New-physics contributions to the forward-backward asymmetry in $B \rightarrow K^* \mu^+ \mu^-$* , *JHEP* **02** (2010) 053 [[arXiv:0912.1382](#)] [[SPIRES](#)].
- [28] P. Ball and V.M. Braun, *Exclusive semileptonic and rare B meson decays in QCD*, *Phys. Rev. D* **58** (1998) 094016 [[hep-ph/9805422](#)] [[SPIRES](#)].
- [29] PARTICLE DATA GROUP collaboration, C. Amsler et al., *Review of particle physics*, *Phys. Lett. B* **667** (2008) 1 [[SPIRES](#)].
- [30] O. Buchmuller and H. Flacher, *Fits to moment measurements from $B \rightarrow X_c \ell \nu$ and $B \rightarrow X_s \gamma$ decays using heavy quark expansions in the kinetic scheme*, *Phys. Rev. D* **73** (2006) 073008 [[hep-ph/0507253](#)] [[SPIRES](#)].
- [31] K. Zyablyuk, *Gluon condensate and c -quark mass in pseudoscalar sum rules at 3-loop order*, *JHEP* **01** (2003) 081 [[hep-ph/0210103](#)] [[SPIRES](#)].
- [32] T. Onogi, *Heavy flavor physics from lattice QCD*, [PoS\(LAT2006\)017](#) [[hep-lat/0610115](#)] [[SPIRES](#)].
- [33] P. Ball, V.M. Braun and A. Lenz, *Twist-4 Distribution Amplitudes of the K^* and ϕ Mesons in QCD*, *JHEP* **08** (2007) 090 [[arXiv:0707.1201](#)] [[SPIRES](#)].
- [34] P. Ball and R. Zwicky, *$|V_{td}/V_{ts}|$ from $B \rightarrow V \gamma$* , *JHEP* **04** (2006) 046 [[hep-ph/0603232](#)] [[SPIRES](#)].

Exploring new physics in the C_7 - $C_{7'}$ plane

Sébastien Descotes-Genon,^a Diptimoy Ghosh,^b Joaquim Matias^c and Marc Ramon^c

^aLaboratoire de Physique Théorique, CNRS/Univ. Paris-Sud 11 (UMR 8627)
91405 Orsay Cedex, France

^bTata Institute of Fundamental Research, Homi Bhabha Road,
Mumbai 400005, India

^cUniversitat Autònoma de Barcelona,
08193 Bellaterra, Barcelona, Spain

E-mail: descotes@th.u-psud.fr, diptimoyghosh@theory.tifr.res.in,
matias@ifae.es, mramon@ifae.es

ABSTRACT: The Wilson coefficient C_7 governing the radiative electromagnetic decays of B meson has been calculated to a very high accuracy in the Standard Model, but experimental bounds on either the magnitude or the sign of C_7 are often model-dependent. In the present paper, we attempt at constraining both the magnitude and sign of C_7 using a systematic approach. We consider already measured observables like the branching ratios of $B \rightarrow X_s \mu^+ \mu^-$ and $B \rightarrow X_s \gamma$, the isospin and CP asymmetries in $B \rightarrow K^* \gamma$, as well as A_{FB} and F_L in $B \rightarrow K^* \ell^+ \ell^-$. We also discuss the transverse observable $A_T^{(2)}$ which, once measured, may help to disentangle some of the scenarios considered. We explore the constraints on C_7, C_9, C_{10} as well as their chirality-flipped counterparts. Within our framework, we find that we need to extend the constraints up to 1.6σ to allow for the “flipped-sign solution” of C_7 . The SM solution for C_7 exhibits a very mild tension if New Physics is allowed in dipole operators only. We provide semi-numerical expressions for all these observables as functions of the relevant Wilson coefficients at the low scale.

KEYWORDS: B-Physics, Rare Decays

ARXIV EPRINT: [1104.3342](https://arxiv.org/abs/1104.3342)

Contents

1	Introduction	1
2	Operators, method and observables	5
2.1	$b \rightarrow s$ effective Hamiltonian	5
2.2	Method	7
2.3	Class-I observables	8
2.4	Class II	11
2.5	Class III	14
2.6	$\mathcal{B}(B_s \rightarrow \mu^+ \mu^-)$	20
3	Results	21
3.1	$(C_7, C_{7'})$ plane	21
3.2	Scenario A	23
3.3	Scenario B	24
3.4	Scenario C	25
3.5	2σ constraints	26
3.6	Generalization to extended frameworks	27
4	Discussion and outlook	32
A	Inputs	35
B	Extension to chirally-flipped operators	35
B.1	$B \rightarrow X_s \gamma$	35
B.2	$B \rightarrow K^* \gamma$ isospin asymmetry	36
B.3	$S_{K^* \gamma}$	37
B.4	$B \rightarrow X_s \ell^+ \ell^-$	40
B.5	$\bar{B} \rightarrow \bar{K}^{*0} \ell^+ \ell^-$ observables	41
B.5.1	General considerations	41
B.5.2	Soft form factors	42
B.5.3	The differential decay distribution and uniangular projections	44
B.5.4	$\bar{B}_d \rightarrow K^{*0} \ell^+ \ell^-$ observables at leading order in the large-recoil limit	45

1 Introduction

In the last decade, one of the main avenues to search for New Physics signals in B and K decays has consisted in overdetermining the parameters of the Cabibbo-Kobayashi-Maskawa matrix (which encodes charged weak transitions in the Standard Model (SM)) and

its representation as a unitarity triangle embedding CP-violation. The resulting picture has shown a very good overall agreement of all the constraints, apart from some discrepancies (direct CP asymmetries difference between $B^- \rightarrow K^- \pi^0$ and $\bar{B}^0 \rightarrow K^- \pi^+$, $B \rightarrow \tau \nu$ versus $\sin 2\beta$, B_s meson mixing from $J/\Psi \phi$ channel, and the dimuon asymmetry), which are still under experimental scrutiny but may be understood in terms of New Physics contributions [1–5].

In the meanwhile, a long list of rare B decays has been determined at present with high theoretical and experimental accuracy. A tool of choice for these analysis is the effective Hamiltonian describing flavour transitions, allowing an elegant separation between long-distance operators \mathcal{O}_i (leading to contributions governed by strong and electromagnetic SM interactions) and short-distance Wilson coefficients C_i (summing up all the details of the fundamental theory lying beyond the SM at higher energies). Once expressed in this language, the analysis of rare B decays corresponds to constraining the allowed range of Wilson coefficients (WC), taking into account several observables. One must be careful that New Physics (NP) can not only change the value of the SM Wilson coefficients, but also introduce new operators with a Dirac structure that is different from the SM ones. We hope that overconstraining these Wilson coefficients will push them into regions incompatible with the Standard Model, providing hints of the structure of the underlying theory responsible for these New Physics effects (right-handed currents, scalar or tensor contributions, etc.).

This program turns out to be quite challenging as many observables depend not on a single WC but a combination of many of them. Hence the constraint on a particular WC depends very much on the assumptions made on the type of New Physics present and its impact on different WCs. Many model-independent analyses with the aim of avoiding fine tuning assume that only the Wilson coefficient analysed receives a contribution from New Physics (all the other ones being set to their SM values). The limits of such an approach are quite obvious, and the conclusions that can be extracted are rather limited, specially when the framework is not clearly defined. As an illustration, it was proposed sometime ago to consider a NP contribution to the WC of the electromagnetic operator \mathcal{O}_7 approximately twice as large as the SM one but of the opposite sign, so that the prediction for $\mathcal{B}(B \rightarrow X_s \gamma)$ would be similar to that of the Standard Model, which was in good agreement with the current experimental value. This solution attracted some interest recently, as it could explain the Belle measurements [6] for the exclusive decay $B \rightarrow K^* \ell^+ \ell^-$ suggesting that the forward-backward asymmetry did not exhibit any zero at low energies. In ref. [7], this so-called “flipped-sign solution” was shown to be at odds with the prediction of $\mathcal{B}(B \rightarrow X_s \ell^+ \ell^-)$. More generally, this question can be answered only once we fix the values of the other operators that can contribute to the observables: the conclusions may change if NP is allowed to contribute also to the semileptonic operators $O_{9,10}$, or if relevant operators with a non-SM structure are included. Other solutions to this forward-backward asymmetry issue were also discussed in ref. [8].

Fortunately, the rich phenomenology of B decays together with the increasingly large amount of data from B factories and hadron machines open new perspectives to deal with larger sets of operators. In this article, we propose to focus on the two Wilson coefficients

associated with the electromagnetic operator \mathcal{O}_7 and its chirally-flipped counterpart $\mathcal{O}_{7'}$ as tools to search for New Physics in a systematic approach. Our goal is that these coefficients play here a similar role to the $\bar{\rho}$ and $\bar{\eta}$ parameters in the studies of the unitarity triangle. C_7 and $C_{7'}$ do not exhaust all the information that can be obtained concerning New Physics, exactly as $\bar{\rho}$ and $\bar{\eta}$ are not sufficient to describe the full structure of the CKM matrix, but they provide an interesting summary of the situation and a good starting point to investigate NP contributions with other structures.

We will focus on the allowed regions for this pair of Wilson coefficients under different scenarios defined later on and corresponding to letting more and more Wilson coefficients receive New Physics contributions. Each scenario will be more general than the previous one. The basic idea is that different choices of NP scenarios may in principle lead to different solutions or allowed regions for each Wilson coefficient in agreement with all present constraints. The non-overlapping regions may be distinguished thanks to additional observables, yet to be measured, providing a criterion to distinguish between the different NP scenarios.

We will consider seven observables in our analysis. Six of them are believed to exhibit a limited sensitivity to hadronic uncertainties:¹

1. for inclusive decays, the branching ratios $\mathcal{B}(B \rightarrow X_s \gamma)$ and $\mathcal{B}(B \rightarrow X_s \ell^+ \ell^-)$,
2. for $B \rightarrow K^* \ell^+ \ell^-$, the polarization fraction F_L , the forward-backward asymmetry A_{FB} and the transverse asymmetry $A_{\text{T}}^{(2)}$.
3. for $B \rightarrow K^* \gamma$, the exclusive CP asymmetry $S_{K^* \gamma}$. This observable is not in the same footing of robustness as the previous observables, however its main theoretical uncertainties are reasonably under control.

The list could be extended to include other future and theoretically clean observables like $A_{\text{T}}^{(i)}$ ($i = 3, 4, 5$) proposed in ref. [9]. However for the sake of simplicity we will not include them in this paper. All of the observables above are measured with different levels of accuracy except for $A_{\text{T}}^{(2)}$, which will be measured in the near future and can be used as an efficient probe to constrain the dipole operators in a different way from current observables. The seventh observable in our analysis, not included in this list, is the isospin asymmetry $A_I(B \rightarrow K^* \gamma)$. Even though it is strongly sensitive to hadronic uncertainties, we include this asymmetry because of its discriminating power in our discussion of NP solutions.

Our New Physics *framework* is defined by considering that NP enters in \mathcal{O}_i with $i = 7, 9, 10$ (electromagnetic and semileptonic operators), together with the chirally-flipped operators $\mathcal{O}_{i'}$ with $i = 7, 9, 10$. The precise definition and conventions for all those operators is presented in section 2. We will split² this framework in three different scenarios

¹Notice that even though we analysed the branching ratios for $\mathcal{B}(B \rightarrow K^* \gamma)$ and $\mathcal{B}(B \rightarrow K^* \ell^+ \ell^-)$ we decided not to include them in the list, mainly due to the presence of significant hadronic uncertainties in form factors (see figure 15).

²This splitting is not unique and different choices are possible. The only condition is to start from a restrictive NP scenario, where only dipole operators are affected by NP, and end up with the most general scenario.

corresponding to switching on NP step by step, starting from dipole operators and finishing with the full set of operators in the framework:

- Scenario A. In this scenario the main New Physics contributions affect the electromagnetic dipole operators $\mathcal{O}_7, \mathcal{O}_{7'}$.
- Scenario B. Here New Physics affects not only $\mathcal{O}_7, \mathcal{O}_{7'}$, but also the SM-like semileptonic operators \mathcal{O}_9 and \mathcal{O}_{10} .
- Scenario C. This is the most general case in the framework we have defined, where all operators $\mathcal{O}_{7,9,10}$ and $\mathcal{O}_{7',9',10'}$ can receive NP contributions.

This will allow us to have a better control, once confronted with data, on the impact of enlarging, step by step, the set of operators, as well as providing information on the effects from right-handed currents [10–17]. Our guideline in splitting the framework in scenarios will be to try to find in a systematic way the minimal set of operators compatible with data inside a framework (and extend it if necessary). Once this is done, a future step would be to find which theories can contribute to the selected operators.

We will assume that NP enters only these operators, and that their Wilson coefficients are real. If no solution compatible with all constraints is found at the end of our analysis, within our defined framework, the next step will consist in generalizing the framework to other operators (like scalars, tensors, the chromomagnetic operator³ or further chirally-flipped operators). The generalization is systematic and straightforward and will be presented elsewhere, but some details will be given here. We classify our observables in three *categories*:

1. Class-I observables mainly sensitive to \mathcal{O}_7 and $\mathcal{O}_{7'}$, but not to $\mathcal{O}_{i=9,10,9',10'}$.
2. Class-II observables exclusively sensitive to \mathcal{O}_7 and $\mathcal{O}_{7'}$, to semileptonic operators (\mathcal{O}_9 and \mathcal{O}_{10}) and their chiral counterparts $\mathcal{O}_{9'}, \mathcal{O}_{10'}$. Only these operators intervene, even within more general frameworks than the one considered here.
3. Class-III observables that are also sensitive to all the previous operators \mathcal{O}_i with $i = 7 \dots 10'$, and in addition have the potential of exhibiting a sensitivity to NP contributions from other operators like scalars, tensors, chromomagnetic operator. . .⁴ including all the previous operators \mathcal{O}_i with $i = 7, 7', 9, 9', 10, 10'$ but also scalar, tensor, chromomagnetic, etc., operators.

³This generalization may be particularly interesting because it would affect most of the observables described here, and only weak bounds on this operator are available till now.

⁴There is an important distinction in our way of treating Class-I observables with respect to the other classes: the definition of Class-I observables involves only their sensitivity to dipole operators and their lack of contributions from semileptonic operators. Other potential sensitivities beyond the defined framework are not relevant at this stage. This is essential to be able to define primary regions in a systematic way for each framework. On the contrary, we prefer to split Class II from Class III, to identify more easily the observables that will change if new sources beyond the framework are included.

Notice that, strictly speaking, within our defined framework, Class-II and Class-III observables coincide. However, having in mind a systematic forthcoming generalization of this work we need to split them as a function of their potential NP sensitivity beyond our present framework. We will also discuss how this classification would change if we extend the framework to include additional Dirac structures. It would basically require to re-classify some observables (mostly in Class I) and introduce more Class II subdivisions (even if not required here, one could also add intermediate stages between Class II and Class III at will).

In this paper we will illustrate the method on the practical example of determining the sign of C_7 , already discussed in ref. [7], using a subset of our observables.⁵ We will focus not only on the restrictive “flipped-sign” solution, but allow also for deviations in the modulus of C_7 . As it is well known, the sign of C_7 has an important impact on observables like the forward-backward asymmetry (A_{FB}) in the rare exclusive semileptonic decay $B \rightarrow K^* \mu^+ \mu^-$, that is at present slightly at odds with the SM prediction.

In section 2, we present in detail the operators entering our framework and the observables of interest, with their current experimental accuracy as well as numerical expressions for the implementation of their theoretical determination. In section 3, we discuss the three different scenarios and combine the present constraints for each of those scenarios to look for different solutions or allowed regions in the WC planes. In section 4, we summarize the elements learned concerning the sign of C_7 and the values of the WCs. Most technical details concerning the inputs and the computation of the observables are collected in the appendices.

2 Operators, method and observables

2.1 $b \rightarrow s$ effective Hamiltonian

We consider the effective Hamiltonian for radiative $b \rightarrow s$ transitions [19, 20]

$$\mathcal{H}_{\text{eff}} = -\frac{4G_F}{\sqrt{2}} \left(\lambda_t^{(s)} \mathcal{H}_{\text{eff}}^{(t)} + \lambda_u^{(s)} \mathcal{H}_{\text{eff}}^{(u)} \right) + \text{h.c.}, \tag{2.1}$$

with the CKM matrix combinations $\lambda_q^{(s)} = V_{qb} V_{qs}^*$, and

$$\begin{aligned} \mathcal{H}_{\text{eff}}^{(t)} &= C_1 \mathcal{O}_1^c + C_2 \mathcal{O}_2^c + \sum_{i=3}^6 C_i \mathcal{O}_i + \sum_{i=7}^{10} (C_i \mathcal{O}_i + C_{i'} \mathcal{O}_{i'}), \\ \mathcal{H}_{\text{eff}}^{(u)} &= C_1 (\mathcal{O}_1^c - \mathcal{O}_1^u) + C_2 (\mathcal{O}_2^c - \mathcal{O}_2^u). \end{aligned} \tag{2.2}$$

$C_{i(\nu)} \equiv C_{i(\nu)}(\mu_b)$ and $\mathcal{O}_{i(\nu)} \equiv \mathcal{O}_{i(\nu)}(\mu_b)$ are the Wilson coefficients and the local effective operators respectively. The contribution of $\mathcal{H}_{\text{eff}}^{(u)}$ is usually dropped for being doubly Cabibbo-suppressed with respect to that of $\mathcal{H}_{\text{eff}}^{(t)}$, but we will keep it for the observables of interest. In

⁵An interesting analysis was also presented in ref. [18], considering another subset of our observables but adding NP to one Wilson coefficient at a time. See section 4 for further details.

$C_1(\mu_b)$	$C_2(\mu_b)$	$C_3(\mu_b)$	$C_4(\mu_b)$	$C_5(\mu_b)$	$C_6(\mu_b)$	$C_7^{\text{eff}}(\mu_b)$	$C_8^{\text{eff}}(\mu_b)$	$C_9(\mu_b)$	$C_{10}(\mu_b)$
-0.2632	1.0111	-0.0055	-0.0806	0.0004	0.0009	-0.2923	-0.1663	4.0749	-4.3085

Table 1: NNLO Wilson coefficients in the Standard Model at the scale $\mu_b=4.8$ GeV, obtained from the inputs in table 2. For the computation of the observables, we considered a variation of μ_b from half to twice its value.

eq. (2.1) we use the same operator basis as ref. [21]. We focus our attention on the operators

$$\begin{aligned}
 \mathcal{O}_7 &= \frac{e}{16\pi^2} m_b (\bar{s} \sigma_{\mu\nu} P_R b) F^{\mu\nu}, & \mathcal{O}_{7'} &= \frac{e}{16\pi^2} m_b (\bar{s} \sigma_{\mu\nu} P_L b) F^{\mu\nu}, \\
 \mathcal{O}_9 &= \frac{e^2}{16\pi^2} (\bar{s} \gamma_\mu P_L b) (\bar{\ell} \gamma^\mu \ell), & \mathcal{O}_{9'} &= \frac{e^2}{16\pi^2} (\bar{s} \gamma_\mu P_R b) (\bar{\ell} \gamma^\mu \ell), \\
 \mathcal{O}_{10} &= \frac{e^2}{16\pi^2} (\bar{s} \gamma_\mu P_L b) (\bar{\ell} \gamma^\mu \gamma_5 \ell), & \mathcal{O}_{10'} &= \frac{e^2}{16\pi^2} (\bar{s} \gamma_\mu P_R b) (\bar{\ell} \gamma^\mu \gamma_5 \ell),
 \end{aligned} \tag{2.3}$$

where $P_{L,R} = (1 \mp \gamma_5)/2$ and $m_b \equiv m_b(\mu_b)$ denotes the running b quark mass in the $\overline{\text{MS}}$ scheme. The primed operators, with flipped chirality with respect to the unprimed ones, are either highly suppressed or vanish in the SM. Hence,

$$C_{7'}^{\text{SM}} = \frac{m_s}{m_b} C_7^{\text{SM}}, \quad C_{9',10'}^{\text{SM}} = 0 \tag{2.4}$$

In the following, we will assume that only the Wilson coefficients of the operators in eq. (2.3) are potentially affected by NP according to our framework.

The determination of the Wilson coefficients in the Standard Model follows the discussion in refs. [19, 20] to perform the matching at the high scale μ_0 (potentially affected by short-distance NP) and the running of the Wilson coefficients from the high-scale down to μ_b , leading to SM Wilson coefficients at NNLO accuracy. The error budget of the observables includes a variation of μ_b from twice to half its central value (we take $\mu_b = 4.8$ GeV). We have also checked that the variation of the high scale μ_0 yields only a tiny uncertainty on the observables. We follow refs. [22–25] and include QED corrections through five additional operators ($\mathcal{O}_{3,4,5,6Q}$ and \mathcal{O}_b) mixing with the ones displayed in eq. (2.1). The values of the Wilson coefficients at the low-scale $\mu_b = 4.8$ GeV are given in table 1, where the definitions [26]

$$\begin{aligned}
 C_7^{\text{eff}} &\equiv C_7 - \frac{1}{3} C_3 - \frac{4}{9} C_4 - \frac{20}{3} C_5 - \frac{80}{9} C_6, \\
 C_8^{\text{eff}} &\equiv C_8 + C_3 - \frac{1}{6} C_4 + 20 C_5 - \frac{10}{3} C_6
 \end{aligned}$$

have been used, since C_7 and C_8 always appear in these particular combinations with other C_i in matrix elements.

In tables 1 and 2 we present the most important inputs used in our observables including the values of the Wilson coefficients in the SM.

$\mu_b = 4.8 \text{ GeV}$	$\mu_0 = 2M_W$	[19]
$m_B = 5.27950 \text{ GeV}$	$m_{K^*} = 0.89594 \text{ GeV}$	[27]
$m_{B_s} = 5.3663 \text{ GeV}$	$m_\mu = 0.105658367 \text{ GeV}$	[27]
$\sin^2 \theta_W = 0.2313$		[27]
$M_W = 80.399 \pm 0.023 \text{ GeV}$	$M_Z = 91.1876 \text{ GeV}$	[27]
$\alpha_{em}(M_Z) = 1/128.940$	$\alpha_s(M_Z) = 0.1184 \pm 0.0007$	[27]
$m_t^{\text{pole}} = 173.3 \pm 1.1 \text{ GeV}$	$m_b^{1S} = 4.68 \pm 0.03 \text{ GeV}$	[28]
$m_c^{\overline{MS}}(m_c) = 1.27 \pm 0.09 \text{ GeV}$	$m_s^{\overline{MS}}(2 \text{ GeV}) = 0.101 \pm 0.029 \text{ GeV}$	[27]
$\lambda_{CKM} = 0.22543 \pm 0.0008$	$A_{CKM} = 0.805 \pm 0.020$	[29]
$\bar{\rho} = 0.144 \pm 0.025$	$\bar{\eta} = 0.342 \pm 0.016$	[29]
$\mathcal{B}(B \rightarrow X_c e \bar{\nu}) = 0.1061 \pm 0.00017$	$C = 0.58 \pm 0.016$	[19]
$\lambda_2 = 0.12 \text{ GeV}^2$		[19]
$\Lambda_h = 0.5 \text{ GeV}$	$f_B = 0.200 \pm 0.025 \text{ GeV}$	[31]
$f_{K^*, } = 0.220 \pm 0.005 \text{ GeV}$	$f_{K^*,\perp}(2 \text{ GeV}) = 0.163 \pm 0.008 \text{ GeV}$	[30]
$\xi_\perp(0) = 0.31_{-0.10}^{+0.20}$	$\xi_{ }(0) = 0.10 \pm 0.03$	[64]
$a_{1, ,\perp}(2 \text{ GeV}) = 0.03 \pm 0.03$	$a_{2, ,\perp}(2 \text{ GeV}) = 0.08 \pm 0.06$	[30]
$\lambda_B(\mu_h) = 0.51 \pm 0.12 \text{ GeV}$		[30]
$f_{B_s} = 0.2358 \pm 0.0089 \text{ GeV}$	$\tau_{B_s} = 1.472 \pm 0.026 \text{ ps}$	[29]

Table 2: Input parameters, based on refs. [19, 27–31].

2.2 Method

We start by describing in full detail how the method applies to our previously defined framework (New Physics allowed only in electromagnetic dipole, semileptonic operators, with SM and flipped-chirality structures). We will proceed in the following way:

1. We start by classifying observables in three classes, as already mentioned: Class-I observables sensitive only to \mathcal{O}_7 and $\mathcal{O}_{7'}$ contributions, Class-II observables exclusively sensitive to the full set of operators that we consider may be affected by New Physics ($\mathcal{O}_7, \mathcal{O}_9, \mathcal{O}_{10}$ as well as their flipped chirality counterparts) and Class-III observables, not only sensitive to all these operators, but also to further new operators (scalars, tensors, etc).
2. We define a reference frame of allowed regions using observables sensitive to NP only through a pair of Wilson coefficients, in our case $C_7, C_{7'}$. These reference regions, that we will call *primary regions*, are determined by Class-I observables, and are the maximally allowed regions inside our defined framework. They can only shrink when new observables are added. In principle, one could define a different reference frame, where NP enters only in C_7 , but this can be inferred directly from the projection of our reference region along the C_7 axis. We are in Scenario A.
3. We add a larger set of observables with sensitivity to larger sets of operators (Class II and Class III), but still inside Scenario A. Those new observables when restricted to the $(C_7, C_{7'})$ plane may cut further the primary regions, defining a smaller allowed region inside the primary ones.

4. In order to expand again these allowed regions (with the maximal area always defined as the primary regions), we will now move to Scenario B and C, allowing new contributions for the extra coefficients, in our case, C_9 , C_{10} and the flipped-chirality ones.

The same procedure should be repeated if other structures are included defining an extended framework. A discussion can be found in section 3.6.

We will list the observables of interest for our analysis, providing in each case a semi-numerical expression for the observables with their central values and their uncertainties in the Standard Model, as well as their dependence on the deviation $\delta C_i = C_i - C_i^{\text{SM}}$ at the low scale μ_b . This treatment assumes that the analysis of uncertainties performed in the SM is not significantly affected by the presence of NP.

In many places along this paper we will refer to the correlation between pairs of WCs, sometimes denoted as (C_i, C_j) or $(\delta C_i, \delta C_j)$. The relation between both is linear $C_i(\mu_b) = C_i^{\text{SM}}(\mu_b) + \delta C_i$. In all cases we will plot only the correlation between $(\delta C_i, \delta C_j)$.

2.3 Class-I observables

Class-I observables receive contributions from \mathcal{O}_7 , $\mathcal{O}_{7'}$ but not from the semileptonic operators $\mathcal{O}_{9,10}$ or $\mathcal{O}_{9',10'}$. Three observables considered here fall into this category: the branching ratio of the inclusive radiative decay $B \rightarrow X_s \gamma$, as well as the isospin asymmetry (A_I) and the CP-asymmetry ($S_{K^* \gamma}$) of the exclusive decay $B \rightarrow K^* \gamma$.

- $\mathcal{B}(\bar{B} \rightarrow X_s \gamma)$ is one of the cleanest observables in B physics from the theoretical point of view. Apart from contributions to the chromomagnetic operator, it is only sensitive to electromagnetic dipole operators, without pollution from other New Physics contributions. The currently available experimental world average is [32]:

$$\mathcal{B}(\bar{B} \rightarrow X_s \gamma)_{E_\gamma > 1.6 \text{ GeV}} = (3.55 \pm 0.24 \pm 0.09) \times 10^{-4} \quad (2.5)$$

The following formula updates the expression in ref. [20], using ref. [34], based on the NNLO SM results of [19, 35, 36] (more details can be found in appendix B).

$$\begin{aligned} \mathcal{B}(\bar{B} \rightarrow X_s \gamma)_{E_\gamma > 1.6 \text{ GeV}} = & \left[a_{(0,0)} \pm \delta_a + a_{(7,7)} [(\delta C_7)^2 + (\delta C_{7'})^2] + \right. \\ & \left. + a_{(0,7)} \delta C_7 + a_{(0,7')} \delta C_{7'} \right] \cdot 10^{-4} \end{aligned}$$

where the scale of the NP contributions to the Wilson coefficients $\delta C_i(\mu_b)$ (with $i = 7, 7'$) is taken at $\mu_b = 4.8 \text{ GeV}$. The coefficients a_i are collected in table 3, from which one can extract the SM prediction, in good agreement with the experimental measurements:

$$\mathcal{B}(\bar{B} \rightarrow X_s \gamma)_{E_\gamma > 1.6 \text{ GeV}}^{\text{SM}} = (3.15 \pm 0.23) \cdot 10^{-4} \quad (2.6)$$

- $A_I(B \rightarrow K^* \gamma)$: The measurement of the isospin asymmetry (A_I) in $B \rightarrow K^* \gamma$ was reported by BaBar and Belle, with a slightly larger neutral decay rate and hence a positive A_I .

$$A_I \equiv \frac{\Gamma(\bar{B}^0 \rightarrow \bar{K}^{*0} \gamma) - \Gamma(B^- \rightarrow K^{*-} \gamma)}{\Gamma(\bar{B}^0 \rightarrow \bar{K}^{*0} \gamma) + \Gamma(B^- \rightarrow K^{*-} \gamma)} = \left(I \cdot R^{+/0} \tau^+ / \tau_0 - 1 \right) / 2 \quad (2.7)$$

$a_{(0,0)} = 3.15$	$\delta_a = 0.23$	$a_{(0,7)} = -14.81$	$a_{(7,7)} = 16.68$	$a_{(0,7')} = -0.23$
--------------------	-------------------	----------------------	---------------------	----------------------

Table 3: Coefficients describing the dependence of $\mathcal{B}(B \rightarrow X_s \gamma)$ on C_7 and $C_{7'}$.

where the two isospin-breaking ratios are $I = \mathcal{B}(\bar{B}^0 \rightarrow \bar{K}^{*0} \gamma) / \mathcal{B}(B^- \rightarrow K^{*-} \gamma)$ and $R^{+/0} = \Gamma(\Upsilon(4s) \rightarrow B^+ B^-) / \Gamma(\Upsilon(4s) \rightarrow B^0 \bar{B}^0)$.

The recent update of BaBar collaboration [37] with a five times larger sample than their previous result has moved substantially A_I in the positive direction ($A_I = 0.066 \pm 0.021 \pm 0.022$), being now consistent with zero at more than 2σ , while previously the consistency was below 1σ . The older result from the Belle collaboration [38]: $A_I = 0.012 \pm 0.044 \pm 0.026$ requires an update to determine whether it follows the same trend as BaBar. The average of these two measurements according to the Heavy Flavor Averaging Group is [32]:

$$A_I^{\text{exp}}(B \rightarrow K^* \gamma) = 0.052 \pm 0.026. \tag{2.8}$$

In the Standard Model, A_I vanishes in naïve factorisation, and it gets contribution only from non-factorizable graphs where a photon is radiated from the spectator quark. This quantity was first calculated in the SM within the QCD Factorisation (QCDF) framework in ref. [31] and confirmed in ref. [39], with a result $9.3_{-3.2}^{+3.8} \%$ [39]. Later on, it was reevaluated adding some (Cabibbo-suppressed) annihilation contributions but changing the factorisation scale from around 2 GeV to near 4.8 GeV, due to the fact that, below this scale, the four-quark operators factorise, so that the gluon exchange responsible for the running of these operators does not probe small scales and thus does not induce running below μ_b [40].

This observable is dominated by $1/m_b$ corrections inducing important hadronic uncertainties, but we include it because of its particular sensitivity to C_7 and $C_{7'}$ which will prove very important in our discussions. The corresponding numerical expression is:

$$A_I(B \rightarrow K^* \gamma) = c \times \frac{\sum_k d_k (\delta C_7)^k}{\sum_{k,l} e_{(k,l)} (\delta C_7)^k (\delta C_{7'})^l} \pm \delta c. \tag{2.9}$$

where the non-zero coefficients are collected in table 4, out of which one extracts the SM prediction:

$$A_I(B \rightarrow K^* \gamma)^{\text{SM}} = 0.041 \pm 0.025 \tag{2.10}$$

once again in good agreement with the experimental value.

- $S_{K^* \gamma}$: The radiative decay $b \rightarrow s \gamma$ constitutes a major probe of both the flavour structure of the SM and NP. In the SM, the left-handed structure of the weak interactions makes the emitted photon mainly left-handed in b decays and right-handed in \bar{b} decays, as can be seen from the structure of the (dominant) electromagnetic dipole operator $\bar{s}_{L(R)} \sigma_{\mu\nu} b_{R(L)}$. The needed helicity flip of one of the external quarks results

$c = 4.11\%$	$\delta c = 2.52\%$
$d_0 = 1$	$d_1 = -2.51757$
$e_{(0,0)} = 1$	$e_{(1,0)} = -5.0165$
$e_{(0,1)} = -0.0919061$	$e_{(2,0)} = 6.30856$
$e_{(0,2)} = 7.49847$	

Table 4: Coefficients describing the dependence of $A_I(B \rightarrow K^*\gamma)$ on C_7 and $C_{7'}$.

into a factor m_b for $b_R \rightarrow s_L\gamma_L$ and a factor m_s for $b_L \rightarrow s_R\gamma_R$. Therefore, at LO in the SM, the emission of right-handed photons is suppressed by a factor m_s/m_b . This suppression can be overridden in a large number of NP scenarios where the helicity flip occurs on an internal line, which may cause appearance of a factor much larger than m_s/m_b .

The photon helicity is difficult to probe directly, but can be accessed indirectly using the time-dependent CP asymmetry in $B^0 \rightarrow K^{*0}\gamma$:

$$A_{\text{CP}} = \frac{\Gamma(\bar{B}^0(t) \rightarrow \bar{K}^{*0}\gamma) - \Gamma(B^0(t) \rightarrow K^{*0}\gamma)}{\Gamma(\bar{B}^0(t) \rightarrow \bar{K}^{*0}\gamma) + \Gamma(B^0(t) \rightarrow K^{*0}\gamma)} = S_{K^*\gamma} \sin(\Delta m_B t) - C_{K^*\gamma} \cos(\Delta m_B t), \quad (2.11)$$

where K^{*0} and \bar{K}^{*0} are observed through their decay into the CP eigenstate $K_S\pi^0$ and B^0 mixing is assumed to be SM-like.⁶ The helicity suppression of right-handed photons make A_{CP} dominated by B -meson mixing in the SM, irrespective of hadronic uncertainties. Since NP can relieve this suppression, eq. (2.11) is a good candidate for null-tests of the SM [41–44]. In the present article, we will focus on $S_{K^*\gamma}$ in eq. (2.11), as it involves the interference of photons with different polarisation and provide interesting constraints on $C_{7'}$ (see appendix B.3 for further details).

The experimental results available from the B factories for $S_{K^*\gamma}$ are the following:

$$S_{K^*\gamma}^{\text{exp}} = \begin{cases} -0.32_{-0.33}^{+0.36} (\text{stat.}) \pm 0.05 (\text{syst.}) & \text{Belle [45]} \quad (535 \cdot 10^6 \text{ } B\bar{B} \text{ pairs}), \\ -0.03 \pm 0.29 (\text{stat.}) \pm 0.03 (\text{syst.}) & \text{BaBar [46]} \quad (467 \cdot 10^6 \text{ } B\bar{B} \text{ pairs}), \end{cases}$$

with the HFAG average [32]

$$S_{K^*\gamma}^{\text{exp}} = -0.16 \pm 0.22. \quad (2.12)$$

A numerical expression for this observable with our inputs is:

$$S_{K^*\gamma} = f \begin{matrix} +\delta_f^u \\ -\delta_f^d \end{matrix} + \frac{\sum_{k,l} g_{(k,l)} (\delta C_7)^k (\delta C_{7'})^l}{\sum_{k,l} h_{(k,l)} (\delta C_7)^k (\delta C_{7'})^l}, \quad (2.13)$$

⁶This assumption is compatible with the latest measurements of the CP-violating parameter $|p/q| = 1.0024 \pm 0.0023$ [32] derived from the data gathered at B factories only.

$f = -0.0297336$	$\delta_f^u = 0.0089893$ $\delta_f^d = 0.0089767$
$g_{(0,1)} = +152.774$	$h_{(0,0)} = +39.9999$
$g_{(1,0)} = -3.17764$	$h_{(0,1)} = -4.51218$
$g_{(1,1)} = -415.441$	$h_{(1,0)} = -214.866$
$g_{(0,2)} = +8.63917$	$h_{(0,2)} = +290.553$
$g_{(2,0)} = +8.63917$	$h_{(2,0)} = +290.553$

Table 5: Coefficients describing the dependence of $S_{K^*\gamma}$ on C_7 and $C_{7'}$.

where f corresponds to the SM central value and δ_f^u, δ_f^d the corresponding error bars. The non-vanishing g and h coefficients can be found in table 5. One can see that the SM prediction is:

$$S_{K^*\gamma}^{\text{SM}} = -0.03 \pm 0.01 \tag{2.14}$$

2.4 Class II

In this set, we find some of the observables constructed out of the coefficients of the angular distribution of $B \rightarrow K^*(\rightarrow K\pi)\ell^+\ell^-$ for which the hadronic uncertainties due to form factors cancel largely, and which are only dependent on some of the spin amplitudes involved in this decay. The observables called $A_{\text{T}}^{(i)}$ (with $i = 2, 3, 4, 5$) fall inside this category.

- $A_{\text{T}}^{(2)}$: This is the only observable which has not been measured yet and is included in our analysis though. Its unique sensitivity to $\mathcal{O}_{7',g',10'}$ (shown in [9, 21, 47]) and the very limited hadronic uncertainties attached to it makes it into a very appealing observable to distinguish between different NP scenarios.

Its definition in terms of spin amplitudes is [21]:

$$A_{\text{T}}^{(2)}(q^2) = \frac{|A_{\perp}|^2 - |A_{\parallel}|^2}{|A_{\perp}|^2 + |A_{\parallel}|^2}, \tag{2.15}$$

where A_{\perp} and A_{\parallel} are the corresponding spin amplitudes of the K^* and q^2 (or s in the following) is the lepton-pair invariant mass squared. This asymmetry avoids one of the main sources of uncertainty for observables based on the $B \rightarrow K^*\ell^+\ell^-$ decay, namely the soft form factors ξ_{\perp} and ξ_{\parallel} [48]. $A_{\text{T}}^{(2)}$ is constructed to cancel its dependence on $\xi_{\perp}(q^2)$ exactly at LO and displays only a very mild sensitivity on it at NLO in QCDF. Its extraction from the uniangular distributions is described in appendix B.5.3.⁷

⁷The other asymmetries $A_{\text{T}}^{(i)}$ (with $i = 2, 3, 4, 5$) require the determination of the full distribution ($A_{\text{T}}^{(5)}$

	1	s	s^2	s^3	s^4	s^5	s^6
dim	1	GeV ⁻²	GeV ⁻⁴	GeV ⁻⁶	GeV ⁻⁸	GeV ⁻¹⁰	GeV ⁻¹²
$F_{(0,0)}$	+12904.2	-17256.7	+10543.8	-3519.19	+667.247	-67.3536	+2.78209
$G_{(0,0)}$	+402941	-533447	+329442	-111219	+21408.6	-2184.57	+91.6832
P_1	-.0398044	+.271220	-.205904	+.072199	-.0119735	+8.56923 · 10 ⁻⁴	-1.74034 · 10 ⁻⁵
P_2	-.0398265	+.0779803	-.106152	+.0549163	-.0132171	+1.50452 · 10 ⁻³	-6.58489 · 10 ⁻⁵

Table 6: Coefficients of the polynomial functions $F_{(0,0)}$ and $G_{(0,0)}$ entering SM prediction of $A_T^{(2)}$ and those of the polynomials P_1 and P_2 corresponding to the associated upper and lower error bands respectively. The second row in this table and the following ones indicates the dimension of the coefficients in each column.

$A_T^{(2)}$ has been computed in QCDF at NLO using our inputs in table 2, the soft form factors described in appendix B.5.2 and an estimate of Λ/m_b suppressed corrections of order 10%. A detailed discussion of its sensitivity to some of the operators in our framework can be found in ref. [9].

After computing this asymmetry with our inputs, we have fitted the results to a simple parametrisation of the following form

$$A_T^{(2)}(q^2) = A_T^{(2), CV}(q^2) \frac{+\delta_u(q^2)}{-\delta_d(q^2)} \quad (2.16)$$

with the central value

$$A_T^{(2), CV}(q^2) = \frac{\sum_{i=0,7,7',9,9',10,10'} \sum_{j=i,\dots,10'} F_{(i,j)}(q^2) \delta C_i \delta C_j}{\sum_{i=0,7,7',9,9',10,10'} \sum_{j=i,\dots,10'} G_{(i,j)}(q^2) \delta C_i \delta C_j} \quad (2.17)$$

where we have introduced the definition $\delta C_0 \equiv 1$ to write down the constant and linear terms in the same way as the quadratic ones. The errors on the asymmetry are given with respect to the SM central value $F_{(0,0)}/G_{(0,0)}$:

$$\delta_u(q^2) \equiv P_1(q^2) - \frac{F_{(0,0)}(q^2)}{G_{(0,0)}(q^2)}, \quad (2.18)$$

$$\delta_d(q^2) \equiv \frac{F_{(0,0)}(q^2)}{G_{(0,0)}(q^2)} - P_2(q^2). \quad (2.19)$$

All the above functions of $q^2 = s$ have been fitted to polynomials in this variable. The coefficients corresponding to the functions $F_{(0,0)}$, $G_{(0,0)}$, P_1 and P_2 are given in table 6 and that of $F_{(i,j)}$ and $G_{(i,j)}$ in tables 7 and 8 respectively. All these coefficients are dimensionful (but can be easily turned into dimensionless quantities once F, G

is particularly sensitive to $\mathcal{O}_{10'}$, whereas $A_T^{(3,4)}$ probe the longitudinal spin amplitude).

(i, j)	1	s	s^2	s^3	s^4	s^5	s^6
dim	1	GeV ⁻²	GeV ⁻⁴	GeV ⁻⁶	GeV ⁻⁸	GeV ⁻¹⁰	GeV ⁻¹²
(0, 7)	-35566.4	+46009.2	-27457.0	+9232.04	-1776.93	+181.164	-7.59797
(0, 7')	-2260921	+2797565	-1657496	+557358	-106615	+10798.0	-448.880
(0, 9)	-495.374	+80.4698	+25.6073	-1.54246	-1.27554	+0.20500	-0.0141835
(0, 9')	-17643.1	+2256.36	+1655.96	-634.239	+148.767	-18.4135	+0.947823
(0, 10)	+2.27472	-99.4500	-11.2441	+3.95594	+0.138949	+0.00447390	-0.000140794
(0, 10')	+104.982	-4549.99	-73.8320	+2.77725	+0.370546	-0.0131493	+0.00113558
(7, 7)	-3487.35	-591.758	+157.560	-57.9418	+11.0662	-1.12697	+0.0470920
(7, 7')	+6381006	-7188264	+4269996	-1437676	+275442	-27951.3	+1164.94
(7, 9)	+504.942	+22.2744	-52.3132	+7.14332	-1.60871	+0.161286	-0.00668765
(7, 9')	+46001.8	+4619.49	-2289.01	+755.115	-145.752	+14.8194	-0.618975
(9, 9)	-0.263978	+11.5410	+1.30486	-0.459081	-0.0161249	-0.000519191	+0.0000163389
(9, 9')	-24.3660	+1056.04	+17.1362	-0.644594	-0.0860028	+0.00305192	-0.000263564

Table 7: Coefficients of the polynomial functions $F_{(i,j)}$ entering $A_T^{(2)}$.

(i, j)	1	s	s^2	s^3	s^4	s^5	s^6
dim	1	GeV ⁻²	GeV ⁻⁴	GeV ⁻⁶	GeV ⁻⁸	GeV ⁻¹⁰	GeV ⁻¹²
(7, 7)	+3190503	-3594132	+2134998	-718838	+137721	-13975.7	+582.471
(7, 7')	-6974.70	-1183.52	+315.119	-115.884	+22.1324	-2.25393	+0.0941840
(9, 9)	-12.1830	+528.020	+8.56811	-0.322297	-0.0430014	+0.00152596	-0.000131782
(9, 9')	-0.527956	+23.0821	+2.60973	-0.918163	-0.0322497	-0.00103838	+0.0000326779

Table 8: Coefficients of the polynomial functions $G_{(i,j)}$ entering $A_T^{(2)}$.

are expressed as a function of $\tilde{s} \equiv s/m_B^2$) with the dimension indicated in the second row of table 6.⁸

⁸As an example of how to read those tables, we provide here the function $F_{(0,0)}(s)$:

$$\begin{aligned}
 F_{(0,0)}(s) = & + 12904.2 - 17256.7 \text{ GeV}^{-2} \times s + 10543.8 \text{ GeV}^{-4} \times s^2 - 3519.19 \text{ GeV}^{-6} \times s^3 \\
 & + 667.247 \text{ GeV}^{-8} \times s^4 - 67.3536 \text{ GeV}^{-10} \times s^5 + 2.78209 \text{ GeV}^{-12} \times s^6.
 \end{aligned}$$

All entries of the matrices F and G should be taken to be zero, except for those provided in tables 6, 7 and 8 and those related to them through the following equations

$$\begin{aligned} F_{(7',7')} &= F_{(7,7)}, & F_{(7',9')} &= F_{(7,9)}, & F_{(10,10')} &= F_{(9,9')}, \\ F_{(7',9)} &= F_{(7,9')} & \text{and} & & F_{(9',9')} &= F_{(10',10')} = F_{(10,10)} = F_{(9,9)}. \end{aligned} \quad (2.20)$$

Most of these symmetries, and the following ones between different $F_{(i,j)}$ ($G_{(i,j)}$) elements, are easily understood once the large recoil limit of the spin amplitudes is inserted into the definition of the observable [21] (see appendix B.5.4 for details). Similarly for the $G_{(i,j)}$ functions we have

$$\begin{aligned} G_{(7',9)} &= G_{(7,9')}, & G_{(10,10')} &= G_{(9,9')}, \\ G_{(7',7')} &= G_{(7,7)}, & G_{(7',9')} &= G_{(7,9)} \text{ and } G_{(9',9')} = G_{(10',10')} = G_{(10,10)} = G_{(9,9)}, \end{aligned} \quad (2.21)$$

together with the relations between the $G_{(i,j)}$ and $F_{(i,j)}$ functions:

$$\begin{aligned} G_{(0,7')} &= F_{(0,7)}, & G_{(7,9')} &= F_{(7,9)}, & G_{(0,9')} &= F_{(0,9)}, & G_{(0,10')} &= F_{(0,10)}, \\ G_{(0,7)} &= F_{(0,7')}, & G_{(7,9)} &= F_{(7,9')}, & G_{(0,9)} &= F_{(0,9')}, & G_{(0,10)} &= F_{(0,10')}. \end{aligned} \quad (2.22)$$

In conclusion, the total number of non-zero entries of the matrices $F_{(i,j)}$ and $G_{(i,j)}$ entering eq. (2.17) is 20 for each matrix.⁹

As stated earlier, there is no current measurement of this asymmetry, but we will present in section 3 the predicted $A_{\text{T}}^{(2)}$ value for each of the allowed regions in our different scenarios.

2.5 Class III

Here we consider observables affected by \mathcal{O}_7 , $\mathcal{O}_{7'}$, $\mathcal{O}_{9,10}$, $\mathcal{O}_{9',10'}$, and in principle other kinds of NP operators such as scalars or tensors. The most important observable in this category is $\mathcal{B}(B \rightarrow X_s \ell^+ \ell^-)$ due to its limited sensitivity to non-perturbative physics. In the same category fall also other observables defined through the angular distribution of $B \rightarrow K^*(\rightarrow K\pi)\ell^+ \ell^-$, in particular the forward-backward asymmetry A_{FB} and the longitudinal polarisation fraction F_{L} .

- $\mathcal{B}(B \rightarrow X_s \mu^+ \mu^-)$ will be used only in the low- q^2 region (from 1 GeV² to 6 GeV²) as the theoretical prediction in the high- q^2 (above 14.4 GeV²) region suffers from further theoretical uncertainties [49–52]. In the low- q^2 region, the branching ratio is measured to be [52]:

$$\mathcal{B}(\bar{B} \rightarrow X_s \mu^+ \mu^-)_{\text{low-}q^2} = \begin{cases} (1.49 \pm 0.50^{+0.41}_{-0.32}) \times 10^{-6} & (\text{Belle}), \\ (1.8 \pm 0.7 \pm 0.5) \times 10^{-6} & (\text{BaBar}), \\ (1.60 \pm 0.50) \times 10^{-6} & (\text{Average}). \end{cases} \quad (2.23)$$

⁹For instance, the 20 non-zero elements for the matrix $F_{(i,j)}$ correspond to the values of

$$(i, j) = \{(0, 0), (0, 7), (0, 7'), (0, 9), (0, 9'), (0, 10), (0, 10'), (7, 7), (7, 7'), (7, 9), (7, 9'), (9, 9), (9, 9'), (7', 7'), (7', 9'), (7', 9), (9', 9'), (10, 10), (10, 10'), (10', 10')\}.$$

$b_{(0,0)} = 15.86 \quad \delta_b = 1.51$		
$b_{(0,7)} = -0.517$	$b_{(0,9)} = 2.663$	$b_{(0,10)} = -4.679$
$b_{(0,7')} = -0.680$	$b_{(0,9')} = -0.049$	$b_{(0,10')} = 0.061$
$b_{(7,7)} = b_{(7',7')} = 27.776$	$b_{(9,9)} = b_{(9',9')} = 0.534$	$b_{(10,10)} = b_{(10',10')} = 0.543$
$b_{(7,7')} = -0.399$	$b_{(9,9')} = -0.014$	$b_{(10,10')} = -0.014$
$b_{(7,9)} = b_{(7',9')} = 4.920$	$b_{(7,9')} = b_{(7',9)} = -0.113$	

Table 9: Coefficients describing the dependence of $\mathcal{B}(B \rightarrow X_s \mu^+ \mu^-)$ on $C_{7,9,10}$ and $C_{7',9',10'}$.

The SM prediction for $\mathcal{B}(\bar{B} \rightarrow X_s \mu^+ \mu^-)$ is $(1.59 \pm 0.11) \times 10^{-6}$ [52]. With our inputs and including m_s -suppressed terms (see appendix B.4 for more details), we obtain the corresponding expression for the integrated branching ratio at the scale $\mu_b = 4.8 \text{ GeV}$ in the low- q^2 region (from 1 to 6 GeV^2):

$$\mathcal{B}(B \rightarrow X_s \mu^+ \mu^-) = 10^{-7} \times \left[\sum_{i,j=0,7,7',9,9',10,10'} b_{(i,j)} \delta C_i \delta C_j \pm \delta_b \right] \quad (2.24)$$

The values of the non-vanishing coefficients b are listed in table 9.

- $A_{\text{FB}}(q^2)$. The forward-backward asymmetry in $\bar{B}_d \rightarrow \bar{K}^{*0} \ell^+ \ell^-$ is defined by:

$$A_{\text{FB}}(q^2) = \frac{1}{d\Gamma/dq^2} \left(\int_0^1 d(\cos\theta_l) \frac{d^2\Gamma}{dq^2 d\cos\theta_l} - \int_{-1}^0 d(\cos\theta_l) \frac{d^2\Gamma}{dq^2 d\cos\theta_l} \right). \quad (2.25)$$

with θ_l the angle between the positively charged lepton in dimuon rest frame and the direction of the dilepton in the \bar{B}_d rest frame. This asymmetry can also be written in terms of spin amplitudes [47] inside our framework as¹⁰

$$A_{\text{FB}}(q^2) = -\frac{3}{2} \beta_\mu \frac{1}{d\Gamma/dq^2} [\text{Re}(A_{\parallel L} A_{\perp L}^*) - \text{Re}(A_{\parallel R} A_{\perp R}^*)]. \quad (2.26)$$

(See appendix B.5 for definitions). The overall minus sign with respect to eq. (4.4) in ref. [47] stems from the definition of $A_{\text{FB}}(q^2)$ in eq. (2.25) chosen to match the plots in refs. [6, 53]. The expression of $d\Gamma/dq^2$ in terms of K^* spin amplitudes (including the muon mass terms) can be found in eq. (B.42). The QCDF framework at NLO is well suited to compute A_{FB} , just as we did previously with $A_{\text{T}}^{(2)}$, including an estimate of Λ/m_b corrections. However, unlike $A_{\text{T}}^{(2)}$, A_{FB} can receive not only contributions from the operators $\mathcal{O}_i, \mathcal{O}'_i$ with $i = 7, 9, 10$ but also from scalar and tensor operators [8, 54]. Another important difference between $A_{\text{T}}^{(2)}$ and A_{FB} is that A_{FB} is not protected at

¹⁰Notice that while eq. (2.25) is valid in general, eq. (2.26) is valid only within our framework, which means that one should add extra amplitudes in eq. (2.26) when scalar operators are included.

	1	s	s^2	s^3	s^4	s^5	s^6
dim	1	GeV ⁻²	GeV ⁻⁴	GeV ⁻⁶	GeV ⁻⁸	GeV ⁻¹⁰	GeV ⁻¹²
$H_{(0,0)}$	+35333.6	-311396	+119428	-30281.3	+8546.83	-1169.16	+65.2322
$I_{(0,0)}$	+773134	-72762.1	+280788	-88514.3	+24423.2	-3375.38	+188.8567
P_3	+118304	-602706	+410711	-125244	+0214497	$-1.98680 \cdot 10^{-3}$	$+7.74701 \cdot 10^{-5}$
P_4	+302083	-1.13742	+847601	-299722	+0580893	$-5.87352 \cdot 10^{-3}$	$+2.41917 \cdot 10^{-4}$

Table 10: Coefficients of the polynomial functions $H_{(0,0)}$ and $I_{(0,0)}$ entering SM prediction of A_{FB} and those of the polynomials P_3 and P_4 corresponding to the associated upper and lower error bands respectively.

LO from soft form factor uncertainties contrary to $A_T^{(2)}$. Besides, $A_T^{(2)}$ exhibits the same remarkable features as A_{FB} like, for instance, the presence or absence of a zero (in the presence of right-handed currents) [9, 55, 56]. A_{FB} has been under scrutiny lately, as a consequence of the Belle measurement suggesting that, contrary to SM prediction, it might not display a zero in the low- q^2 region, triggering many proposals to explain this behaviour [8, 54].

We define the integrated forward-backward asymmetry in the low- q^2 region to agree with the experimental determination:

$$\tilde{A}_{FB} = \frac{\int_{1\text{GeV}^2}^{6\text{GeV}^2} \frac{d\Gamma}{dq^2} A_{FB}(q^2) dq^2}{\int_{1\text{GeV}^2}^{6\text{GeV}^2} \frac{d\Gamma}{dq^2}}, \quad (2.27)$$

while the average of the measured values by Belle [6] and CDF collaborations [53] is

$$\tilde{A}_{FB}^{\text{exp}} = 0.33_{-0.24}^{+0.22}. \quad (2.28)$$

We can provide a semi-numerical expression for this observable in a similar way to $A_T^{(2)}$. Starting from the unintegrated asymmetry

$$A_{FB}(q^2) = A_{FB}^{\text{CV}}(q^2)_{-\delta_d(q^2)}^{+\delta_u(q^2)}, \quad (2.29)$$

where the central value (CV) is

$$A_{FB}^{\text{CV}}(q^2) = \frac{\sum_{i=0,7,7',9,9',10,10'} \sum_{j=i,\dots,10'} H_{(i,j)}(q^2) \delta C_i \delta C_j}{\sum_{i=0,7,7',9,9',10,10'} \sum_{j=i,\dots,10'} I_{(i,j)}(q^2) \delta C_i \delta C_j} \quad (2.30)$$

(using again $\delta C_0 = 1$) and the uncertainties are given with respect to the SM central value curve ($H_{(0,0)}/I_{(0,0)}$):

$$\delta_u(q^2) \equiv P_3(q^2) - \frac{H_{(0,0)}(q^2)}{I_{(0,0)}(q^2)}, \quad (2.31)$$

$$\delta_d(q^2) \equiv \frac{H_{(0,0)}(q^2)}{I_{(0,0)}(q^2)} - P_4(q^2). \quad (2.32)$$

(i, j)	1	s	s^2	s^3	s^4	s^5	s^6
dim	1	GeV ⁻²	GeV ⁻⁴	GeV ⁻⁶	GeV ⁻⁸	GeV ⁻¹⁰	GeV ⁻¹²
(0, 7)	-28429.0	+636004	+11547.1	-654.500	-35.5189	-0.448945	-0.0797274
(0, 7')	+309.261	-6889.37	-1839.42	+195.417	+6.25264	+0.200244	-0.0220619
(0, 9)	-5.09654	-595.133	+13614.3	+237.012	-13.3497	-0.0975163	-0.0602829
(0, 10)	-8200.84	+72274.3	-27719.1	+7028.21	-1983.70	+271.360	-15.1402
(0, 10')	-50.4373	-146.677	-31.1282	+62.7360	-22.6837	+3.00773	-0.162833
(7, 10)	+6598.30	-147615	-2680.06	+151.908	+8.24386	+0.104199	+0.0185045
(7, 10')	+71.7787	-1599.01	-426.925	+45.3559	+1.45122	+0.0464761	-0.00512052
(9, 10)	+1.18289	+138.129	-3159.85	-55.0098	+3.09843	+0.0226333	+0.0139915

Table 11: Coefficients of the polynomial functions $H_{(i,j)}$ entering A_{FB} .

After integrating over the low- q^2 experimental kinematic range ($1 \leq q^2 \leq 6 \text{ GeV}^2$), following eq. (2.27) we obtain

$$\tilde{A}_{\text{FB}} = \tilde{A}_{\text{FB}}^{\text{CV}} \begin{matrix} +\tilde{\delta}_u \\ -\tilde{\delta}_d \end{matrix}, \quad (2.33)$$

where the central value can be split into SM and NP contributions:

$$\tilde{A}_{\text{FB}}^{\text{CV}} = \tilde{A}_{\text{FB}}^{\text{SM}} + \tilde{A}_{\text{FB}}^{\text{NP}}, \quad (2.34)$$

with

$$\tilde{A}_{\text{FB}}^{\text{SM}} = \frac{\int_{1\text{GeV}^2}^{6\text{GeV}^2} H_{(0,0)}(q^2) dq^2}{\int_{1\text{GeV}^2}^{6\text{GeV}^2} I_{(0,0)}(q^2) dq^2}, \quad (2.35)$$

$$\tilde{A}_{\text{FB}}^{\text{NP}} = \frac{\int_{1\text{GeV}^2}^{6\text{GeV}^2} \sum_{i=0,7,7',9,9',10,10'} \sum_{j=i,\dots,10'} H_{(i,j)}(q^2) \delta C_i \delta C_j dq^2}{\int_{1\text{GeV}^2}^{6\text{GeV}^2} \sum_{i=0,7,7',9,9',10,10'} \sum_{j=i,\dots,10'} I_{(i,j)}(q^2) \delta C_i \delta C_j dq^2} - \tilde{A}_{\text{FB}}^{\text{SM}}, \quad (2.36)$$

and the uncertainties are defined, according to eq. (2.32), as

$$\tilde{\delta}_u = \frac{\int_{1\text{GeV}^2}^{6\text{GeV}^2} I_{(0,0)}(q^2) P_3(q^2) - H_{(0,0)}(q^2) dq^2}{\int_{1\text{GeV}^2}^{6\text{GeV}^2} I_{(0,0)}(q^2) dq^2}, \quad (2.37)$$

$$\tilde{\delta}_d = \frac{\int_{1\text{GeV}^2}^{6\text{GeV}^2} H_{(0,0)}(q^2) - I_{(0,0)}(q^2) P_4(q^2) dq^2}{\int_{1\text{GeV}^2}^{6\text{GeV}^2} I_{(0,0)}(q^2) dq^2}. \quad (2.38)$$

The coefficients of the polynomials $H_{(0,0)}$, $I_{(0,0)}$, P_3 and P_4 can be found in table 10 and those of $H_{(i,j)}$ and $I_{(i,j)}$ are in tables 11 and 12 respectively.

(i, j)	1	s	s^2	s^3	s^4	s^5	s^6
dim	1	GeV ⁻²	GeV ⁻⁴	GeV ⁻⁶	GeV ⁻⁸	GeV ⁻¹⁰	GeV ⁻¹²
(0, 7)	-3468590	+813560	+227870	-94496.6	+25300.8	-3459.65	+192.642
(0, 7')	-85589.1	-122670	-69994.6	+28153.7	-7862.34	+1093.91	-61.8971
(0, 9)	+20442.1	-22730.3	+69374.6	-22297.5	+6185.70	-856.470	+48.1719
(0, 9')	-12916.9	-74730.4	-32300.8	+13192.5	-3605.75	+501.316	-28.4231
(0, 10)	+261.790	-121102	-25790.2	-176.716	+45.8313	-0.759850	+0.113787
(0, 10')	-273.106	+122339	+7232.91	-179.752	-13.9840	+1.84675	-0.0526165
(7, 7)	+4577553	+174071	-20355.8	+6184.18	-1315.63	+135.290	-5.76932
(7, 7')	+329.213	-145167	-9858.44	-33.5940	+28.1525	-1.45144	+0.0810919
(7, 9)	-567.508	+254709	+6889.36	-155.447	-43.8097	+2.35024	-0.130858
(7, 9')	+125.219	-55064.8	-3710.40	-58.9805	+9.25472	-0.632663	+0.0321131
(9, 9)	-34.1907	+14218.8	+2996.38	+20.4260	-5.33164	+0.0886881	-0.0132486
(9, 9')	+64.3379	-28435.7	-1680.38	+41.4648	+3.23993	-0.429103	+0.0122379
(10, 10)	-30.3804	+14053.7	+2992.92	+20.5077	-5.31866	+0.0881797	-0.0132048
(10, 10')	+63.3872	-28394.6	-1678.74	+41.7200	+3.24565	-0.428626	+0.0122122

Table 12: Coefficients of the polynomials functions $I_{(i,j)}$ entering A_{FB} .

All components of the matrices H and I are taken to be zero (as it was done for $A_{\text{T}}^{(2)}$) except for those provided in these tables and those related to them via the equations

$$H_{(7',10')} = -H_{(7,10)}, \quad H_{(9',10')} = -H_{(9,10)} \quad \text{and} \quad H_{(7',10)} = -H_{(7,10')}. \quad (2.39)$$

and

$$\begin{aligned} I_{(7',9')} &= I_{(7,9)}, & I_{(7',9)} &= I_{(7,9')}, \\ I_{(7',7')} &= I_{(7,7)}, & I_{(9',9')} &= I_{(9,9)} \quad \text{and} \quad I_{(10',10')} &= I_{(10,10)}, \end{aligned} \quad (2.40)$$

which leaves finally 12 $H_{(i,j)}$ and 20 $I_{(i,j)}$ non-zero functions entering eq. (2.30)–(2.38).

Using eqs. (2.35), (2.37), (2.38) and table 10 we get the following prediction for the integrated forward-backward asymmetry ($\tilde{A}_{\text{FB}}^{\text{SM}}$) in the SM:

$$\tilde{A}_{\text{FB}}^{\text{SM}} = 0.0218_{-0.0277}^{+0.0280}. \quad (2.41)$$

	1	s	s^2	s^3	s^4	s^5	s^6
dim	1	GeV ⁻²	GeV ⁻⁴	GeV ⁻⁶	GeV ⁻⁸	GeV ⁻¹⁰	GeV ⁻¹²
$J_{(0,0)}$	+42950.7	+326107	+137315	-54729.1	+14915.6	-2078.06	+117.102
$I_{(0,0)}$	+773134	-72762.1	+280788	-88514.3	+24423.2	-3375.38	+188.857
P_5	-.0792139	+.952685	-.395205	+.0821238	-.00911051	+4.67994 · 10 ⁻⁴	-6.09404 · 10 ⁻⁶
P_6	-.133068	+.720264	-.154064	-.0186277	+.0121348	-1.77815 · 10 ⁻³	+8.87194 · 10 ⁻⁵

Table 13: Coefficients of the polynomial functions $J_{(0,0)}$ and $I_{(0,0)}$ entering SM prediction of F_L and those of the polynomials P_5 and P_6 corresponding to the associated upper and lower error bands respectively.

- F_L : The longitudinal polarization fraction of the K^* in the exclusive $B \rightarrow K^* \ell^+ \ell^-$ decay is defined in terms of the spin amplitudes as

$$F_L = \frac{|A_0|^2}{\frac{d\Gamma}{dq^2}}. \quad (2.42)$$

in absence of scalar and tensor operators [54], with $d\Gamma/dq^2$ given by eq. (B.42). F_L can also be computed in QCDF and, as before, an estimate of Λ/m_b corrections has been added to the other sources of uncertainty of this observable.

The integrated version of this observable in the low- q^2 region can be defined as in eq. (2.27)

$$\tilde{F}_L = \frac{\int_{1\text{GeV}^2}^{6\text{GeV}^2} \frac{d\Gamma}{dq^2} F_L(q^2) dq^2}{\int_{1\text{GeV}^2}^{6\text{GeV}^2} \frac{d\Gamma}{dq^2}}, \quad (2.43)$$

and the average of the data measured by Belle [6] and CDF collaborations [53] from this observable yields

$$\tilde{F}_L^{\text{exp}} = 0.60_{-0.19}^{+0.18}. \quad (2.44)$$

The analysis of A_{FB} and \tilde{A}_{FB} performed in eqs. (2.29)–(2.38) can be repeated, step by step, for F_L and \tilde{F}_L with the substitutions $H_{(0,0)} \rightarrow J_{(0,0)}$, $H_{(i,j)} \rightarrow J_{(i,j)}$, $P_3 \rightarrow P_5$, $P_4 \rightarrow P_6$ and, obviously, $A_{\text{FB}} \rightarrow F_L$, $\tilde{A}_{\text{FB}} \rightarrow \tilde{F}_L$. Table 13 contains the coefficients of $J_{(0,0)}$, $I_{(0,0)}$ (for completeness), P_5 and P_6 , while the different non-zero $J_{(i,j)}$ are either shown in table 14 or given by

$$\begin{aligned} J_{(7',7')} &= J_{(7,7)}, & J_{(7',9')} &= -J_{(7,9')} = -J_{(7',9)} = J_{(7,9)}, \\ J_{(9',9')} &= J_{(10',10')} = J_{(10,10)} = J_{(9,9)}, & J_{(10,10')} &= J_{(9,9')}, \\ J_{(0,7')} &= -J_{(0,7)}, & J_{(0,9')} &= -J_{(0,9)}, & J_{(0,10')} &= -J_{(0,10)}, \\ J_{(7,7')} &= -2J_{(7,7)}, & \text{and } J_{(9,9')} &= -2J_{(9,9)}, \end{aligned} \quad (2.45)$$

rendering 20 entries $J_{(i,j)}$ different from zero entering F_L .

(i, j)	1	s	s^2	s^3	s^4	s^5	s^6
dim	1	GeV ⁻²	GeV ⁻⁴	GeV ⁻⁶	GeV ⁻⁸	GeV ⁻¹⁰	GeV ⁻¹²
(0, 7)	+21257.2	+146631	+65353.0	-26003.8	+7140.37	-997.823	+56.4467
(0, 9)	+10438.4	+73176.5	+32041.6	-12776.8	+3503.48	-489.692	+27.7109
(0, 10)	+2821.90	-122131	-7771.38	+178.016	+20.9504	-0.329242	+0.0223758
(7, 7)	-1326.63	+57405.1	+3778.94	-61.4705	-9.92262	+0.105597	-0.01443264
(7, 9)	-1318.24	+57047.6	+3692.75	-72.1696	-9.82836	+0.128021	-0.0122690
(9, 9)	-327.478	+14173.1	+901.859	-20.6586	-2.43126	+0.0382081	-0.00259668

Table 14: Coefficients of the polynomial functions $J_{(i,j)}$ entering F_L .

Therefore, the value of the integrated polarization fraction (\tilde{F}_L) in the SM can be computed theoretically using our inputs to get

$$\tilde{F}_L^{\text{SM}} = 0.732_{-0.031}^{+0.021}. \tag{2.46}$$

2.6 $\mathcal{B}(B_s \rightarrow \mu^+ \mu^-)$

The branching ratio of $\bar{B}_s^0 \rightarrow \mu^+ \mu^-$ in presence of only NP axial operators (relevant to this analysis) is given, at leading order, by [8, 30, 57]

$$\mathcal{B}(\bar{B}_s \rightarrow \mu^+ \mu^-)|_{\text{axial}} = \frac{G_F^2 \alpha^2}{16\pi^3} f_{B_s}^2 m_{B_s} \tau_{B_s} |V_{tb} V_{ts}^*|^2 m_\mu^2 \sqrt{1 - \frac{4m_\mu^2}{m_{B_s}^2}} |C_{10} - C_{10'}|^2 \tag{2.47}$$

Using the inputs in table 1 and 2 we get the SM prediction

$$\mathcal{B}(\bar{B}_s \rightarrow \mu^+ \mu^-)^{\text{SM}} = (3.44 \pm 0.32) \cdot 10^{-9}, \tag{2.48}$$

which is one order of magnitude smaller than the most recent experimental averaged upper bound, obtained at the 90% confidence level in ref. [32]:¹¹

$$\mathcal{B}(\bar{B}_s \rightarrow \mu^+ \mu^-)^{\text{exp}} < 3.2 \cdot 10^{-8}. \tag{2.49}$$

Eq. (2.47) can be used to compute a semi-numerical expression for this observable that will impose constrains in the $(\delta C_{10}, \delta C_{10'})$ plane (see figure 1),

$$\mathcal{B}(\bar{B}_s \rightarrow \mu^+ \mu^-) = 1.8525 \cdot 10^{-10} [| -4.3085 + \delta C_{10} - \delta C_{10'} |^2 \pm 1.7274]. \tag{2.50}$$

We have employed eq. (2.50) to check that the values of δC_{10} and $\delta C_{10'}$ used in Scenarios B and C (see below) were compatible with the constraints coming from $\mathcal{B}(\bar{B}_s \rightarrow \mu^+ \mu^-)$. Since the experimental upper bound is still much larger than the SM prediction, no further cuts in the parameter space of Wilson coefficients have been found.

¹¹The LHCb Collaboration has just released a paper [33] where the upper limit on the branching ratio is set to $\mathcal{B}(\bar{B}_s \rightarrow \mu^+ \mu^-) < 5.6 \cdot 10^{-8}$ at 95% confidence level for an integrated luminosity of 37 pb⁻¹. Since this upper bound is larger than the one obtained by the CDF collaboration [32] we are not using it in this work.

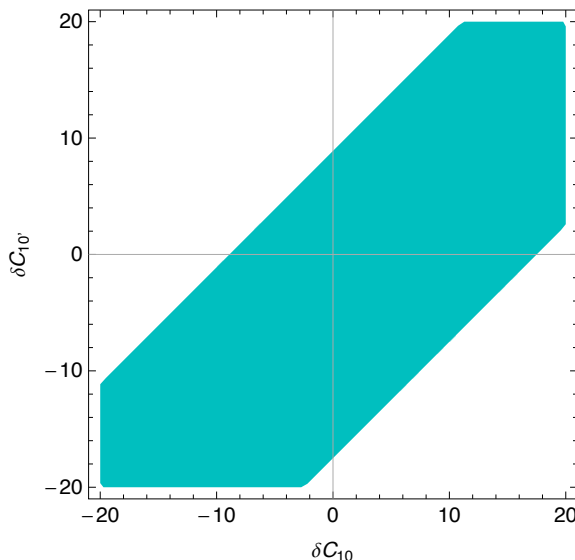


Figure 1: Constraint imposed by $\mathcal{B}(\bar{B}_s \rightarrow \mu^+ \mu^-)$ to the values of the Wilson coefficients in the $(\delta C_{10}, \delta C_{10'})$ plane.

3 Results

In this section we obtain the allowed regions systematically from all the observables discussed previously. Since we aim first at illustrating how much our conclusions vary depending on the precise framework adopted to analyse the data, we will not adopt a sophisticated statistical approach (see refs. [57, 58] for examples of such approaches in similar contexts), and we will stick to a scanning approach, combining the 1σ theoretical and experimental ranges for each observable linearly to draw the corresponding constraint. For instance, if an observable \hat{X}_i has been measured experimentally $X_i \pm \delta X_i$ and has the theoretical prediction $Y_i(\delta C_j) \pm \delta Y_i$, we draw the projection of the region corresponding to the constraint $|X_i - Y_i| \leq (\delta X_i + \delta Y_i)$.

3.1 $(C_7, C_{7'})$ plane

As discussed in the introduction, we focus first on the $C_7, C_{7'}$ plane, which will be the starting point of our discussion. Therefore, we consider the three Class-I observables which only depend on the electromagnetic operators $C_7, C_{7'}$, leading to figure 2. If one considers only $\mathcal{B}(B \rightarrow X_s \gamma)$ (ring in figure 2) and $S_{K^* \gamma}$ (cross in figure 2), four regions remain allowed: the SM one sitting around the origin, the “flipped-sign” solution [7] discussed in the introduction around $(\delta C_7, \delta C_{7'}) = (0.9, 0)$, and two non SM-like solutions with $\delta C_7 \simeq 0.35$ and $\delta C_{7'}$ around ± 0.5 . The flipped-signed solution does not correspond exactly to $C_7^{\text{eff}} \rightarrow -C_7^{\text{eff}}$ (and $C_{7'} \simeq 0$), due to interference terms between the electromagnetic operator and the four-quark operators in the observables considered here. The discriminating power of the isospin asymmetry in $B \rightarrow K^* \gamma$ is quite obvious at this stage, as it discards this flipped-sign solution at 1σ without requiring further assumptions concerning

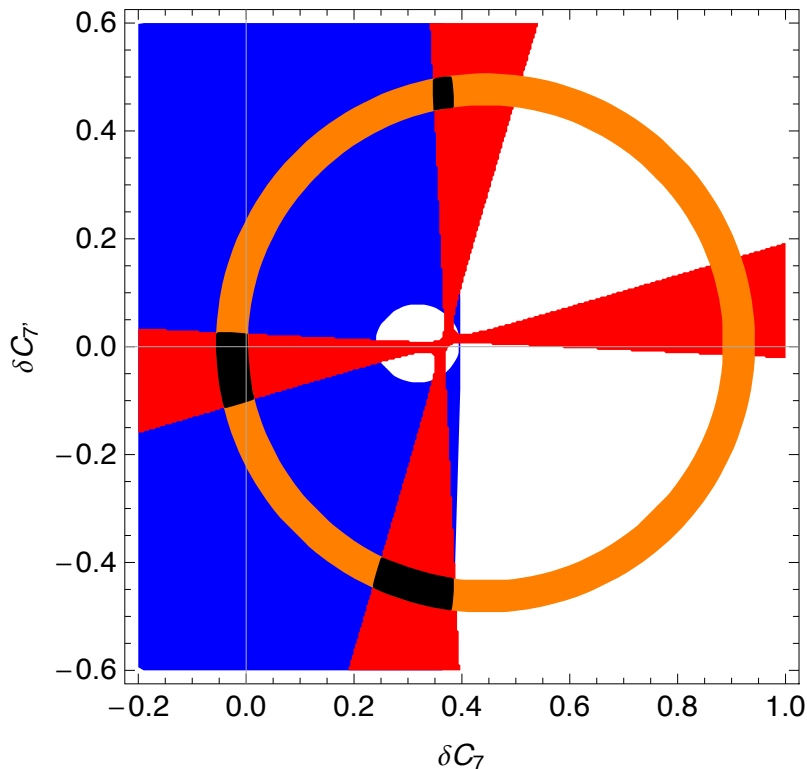


Figure 2: Class I observables at 1σ : A_I (solid blue region with a white disk), $\mathcal{B}(B \rightarrow X_s \gamma)$ (orange ring) and $S_{K^* \gamma}$ (red cross). The three disconnected regions allowed by the intersection of these three observables are depicted in black. The SM value is given by the crossing of light gray lines at $(\delta C_7, \delta C_{7'}) = (0, 0)$ point. All plots of Wilson coefficients are taken at $\mu_b = 4.8 \text{ GeV}$.

NP for other operators. To recover this solution one needs to enlarge both theoretical and experimental uncertainties up to 1.59σ . In our analysis, we disfavour this solution, working at 1σ , on the sole basis of Class-I operators, contrary to ref. [7, 18] which needed Class-III quantities [$\mathcal{B}(B \rightarrow X_s \ell^+ \ell^-)$] and thus obtained conclusions with more restrictive assumptions concerning the manifestations of NP.

We will use the three identified black regions in figure 2 as the reference or primary regions:

- the region around $(\delta C_7, \delta C_{7'}) = (0, 0)$, referred to as the “Central” or SM-like solution;
- the upper region around $(\delta C_7, \delta C_{7'}) = (0.35, 0.45)$, referred to as the “Upper” region;
- the lower region around $(\delta C_7, \delta C_{7'}) = (0.30, -0.45)$, referred to as the “Lower” region.

The last two regions will be commonly called non SM-like solutions in the following. These regions constitute the starting point to study the impact of Class-II and Class-III observables under the three different scenarios (A, B and C) presented in the introduction, each more general than the previous one.

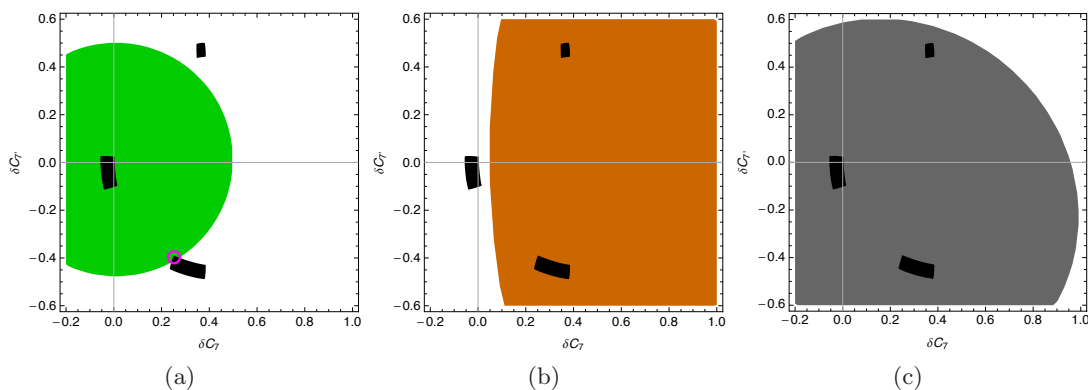


Figure 3: Constraint from Class-III observables $\mathcal{B}(B \rightarrow X_s \mu^+ \mu^-)$ (left), \tilde{A}_{FB} (middle) and \tilde{F}_L at 1σ in the $(\delta C_7, \delta C_{7'})$ plane in Scenario A together with the three (black) regions allowed by Class-I observables. The magenta circle centered at $(0.25, -0.40)$ on the first plot indicates the tiny allowed region in this Scenario A.

It is important to remark that the two non SM-like primary regions of figure 2 contain an interesting subset of solutions for C_7 with a flipped sign with respect to the SM. These solutions are characterised by a small modulus of C_7 and the addition of a larger contribution from $C_{7'}$ to get agreement with data.

3.2 Scenario A

Let us start with Scenario A. If we consider the Class-III observables $\mathcal{B}(B \rightarrow X_s \mu^+ \mu^-)$, \tilde{A}_{FB} and \tilde{F}_L for $B \rightarrow K^* \mu^+ \mu^-$ in the low- q^2 region, we obtain the constraints shown in figures 3a, 3b and 3c respectively. One observes that the three observables favour different regions of the $(C_7, C_{7'})$ plane: the inclusive decay favours the SM region and a very small subregion inside one of the non-SM like solutions, whereas (as expected) the forward-backward asymmetry would favour the flipped sign-solution (had it not disappeared due to the isospin asymmetry) but also the two non-SM like solutions. The longitudinal polarisation would agree with all the regions (cutting only a very small part of the flipped-sign solution region).

We see that Scenario A yields somewhat contradictory information from the various observables concerning which region in the $(C_7, C_{7'})$ plane should be preferred. There is actually only a very small region in perfect agreement with all the observables measured (Class I and Class III), around $\delta C_7 \simeq 0.25, \delta C_{7'} \simeq -0.40$ highlighted with a magenta circle in figure 3a, corresponding to the intersection of the lower black region with the $\mathcal{B}(B \rightarrow X_s \mu^+ \mu^-)$ constraint. It makes therefore sense to extend the set of operators potentially affected by NP and to consider Scenario B, including also New Physics in C_9 and C_{10} . Before leaving Scenario A, it is very interesting to compute the values for the (Class-II) observable $A_T^{(2)}$ that is not yet measured, and turn it into a prediction. Figure 4 illustrates the prediction for this observable as a function of q^2 for the small set of points allowed by Scenario A. This leads to a very precise prediction for the variation

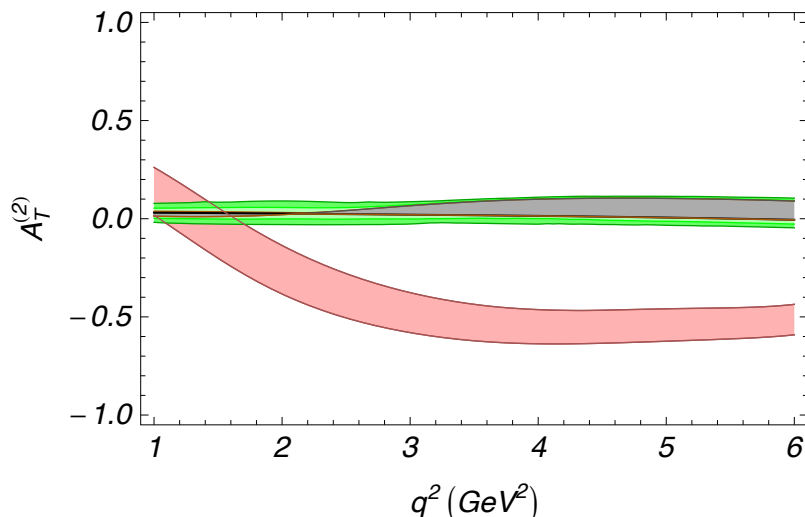


Figure 4: Prediction for $A_T^{(2)}$ under Scenario A (lower pink band), including error bars for all the allowed New Physics curves. The band around zero corresponds to the SM prediction.

of $A_T^{(2)}$ (including error bars) with q^2 . Notice that all the curves included in this region exhibit a zero in a range between 1 to 1.6 GeV^2 which is controlled, at LO, by the same equation that fixes the position of the zero of A_{FB} [55, 56]. Given the small value of $C_7^{\text{eff}}(\mu_b) \simeq -0.29 + 0.25 = -0.04$, the position of this zero is shifted to the left with respect to the SM. Finally, another important prediction of this scenario is that $A_T^{(2)}(q^2)$ would clearly prefer negative values, due to the negative value of $C_{7'} \simeq -0.4$. Therefore, a measured value for $A_T^{(2)}$ different from the narrow prediction given here would be enough to rule out this scenario. On the contrary, a measurement consistent with this prediction would make Scenario A the most plausible one (compared to the other scenarios), and furthermore, would signal clearly the presence of right-handed currents in radiative decays.

3.3 Scenario B

In case of Scenario B, the regions permitted by the Class-III observables $\mathcal{B}(B \rightarrow X_s \mu^+ \mu^-)$, \tilde{A}_{FB} and \tilde{F}_L in figures 3a, 3b, 3c become extended to the whole plane, and thus are not constraining anymore either C_7 or $C_{7'}$. In this scenario, the three primary (black) regions in figure 2 allowed by the Class-I observables are compatible with all the Class-III observables considered and become the allowed region for C_7 and $C_{7'}$ in this scenario. This obviously does not mean that the observables of class III mentioned above do not provide any constraint on NP, just that these constraints are not visible in this particular subspace of NP parameters. As emphasized in the introduction, the $(C_7, C_{7'})$ plane is a summary that does not provide the full information on NP. It is thus interesting to turn to the (C_9, C_{10}) plane. Figures 5a, 5b and 5c are obtained taking the values of the (now) permitted three primary (black) regions in figure 2 for $(C_7, C_{7'})$ and determining the values of C_9 and C_{10} that are then allowed for $\mathcal{B}(B \rightarrow X_s \mu^+ \mu^-)$, \tilde{A}_{FB} and \tilde{F}_L , respectively.

It is quite interesting to notice that the region excluded by \tilde{F}_L is very close to the central region excluded by $\mathcal{B}(B \rightarrow X_s \mu^+ \mu^-)$. This is more striking once all constraints from the three observables are overlapped in one single figure 6, where only two regions (shown in black) are allowed by all constraints. The nature of these two areas can be understood by in the following way:

- SM region: the region centered at the origin corresponds to deviations from SM values for (C_9, C_{10}) keeping the same sign for these coefficients as in SM;
- flipped-values region or non-SM region: this solution contains a subregion with opposite sign values for C_9 and C_{10} with respect to the SM ones.

The existence of these two regions can be understood from the fact that most of the observables have an approximate symmetry consisting in changing the sign of C_9, C_{10} altogether, as long as C_7 or $C_{7'}$ remain small (see, for instance, the large recoil expression for A_{FB} in eq. (B.47) of appendix B.5.4 with $C_{9'} = C_{10'} = 0$). We checked that each of the three primary (black) regions in the $(C_7, C_{7'})$ plane yield Class-III constraints in the (C_9, C_{10}) plane that cover the two regions in figure 6 almost entirely. It implies that the two regions in (C_9, C_{10}) plane exist independently of the precise values for C_7 and $C_{7'}$, as long as any of the latter remain small and have a limited impact on the leptonic observables. In our framework, this smallness is indeed ensured by the constraints in $(C_7, C_{7'})$ plane coming from $\mathcal{B}(\bar{B} \rightarrow X_s \gamma)$.

It is interesting to provide predictions for the (still not measured) asymmetry $A_T^{(2)}$, using as inputs the WCs associated to the three black regions allowed in $(C_7, C_{7'})$ plane, together with the corresponding set of values in the (C_9, C_{10}) plane (two black regions). This is shown in figure 7. We can see there that the large allowed areas for (C_9, C_{10}) lead to wide bands in $A_T^{(2)}(q^2)$. The Upper non-SM like $(C_7, C_{7'})$ region associated to the SM-like (C_9, C_{10}) area gives a clear prediction for the sign of $A_T^{(2)}$, which is just opposite to the one preferred by Scenario A. Also the Central (SM-like) $(C_7, C_{7'})$ region associated to the non SM-like (C_9, C_{10}) area (figure 7a) and the Lower $(C_7, C_{7'})$ region associated to the SM-like (C_9, C_{10}) area (figure 7f) yield constraints on $A_T^{(2)}$, though less stringent than those in figure 7e.

In conclusion, in this scenario the upper region of $(C_7, C_{7'})$ with the corresponding SM-like region for (C_9, C_{10}) could be discriminated clearly only if the sign of $A_T^{(2)}$ would turn out to be negative, as predicted by Scenario A. Besides, high- q^2 measurements, not included in the present analysis, could shrink the allowed (C_9, C_{10}) region and thus reduce the range of possibilities for $A_T^{(2)}$ in this scenario.

3.4 Scenario C

Finally, we could imagine that the previous constraints did not overlap as nicely as in figure 6. We would then turn to Scenario C, allowing for chirally-flipped semileptonic operators. For $(\delta C_7, \delta C_{7'})$, we take all the model-independent allowed values from the three regions of figure 2. Among all the constraints considered previously from Class-III observables, only $\mathcal{B}(B \rightarrow X_s \mu^+ \mu^-)$ still provides a constraint on the semileptonic (primed

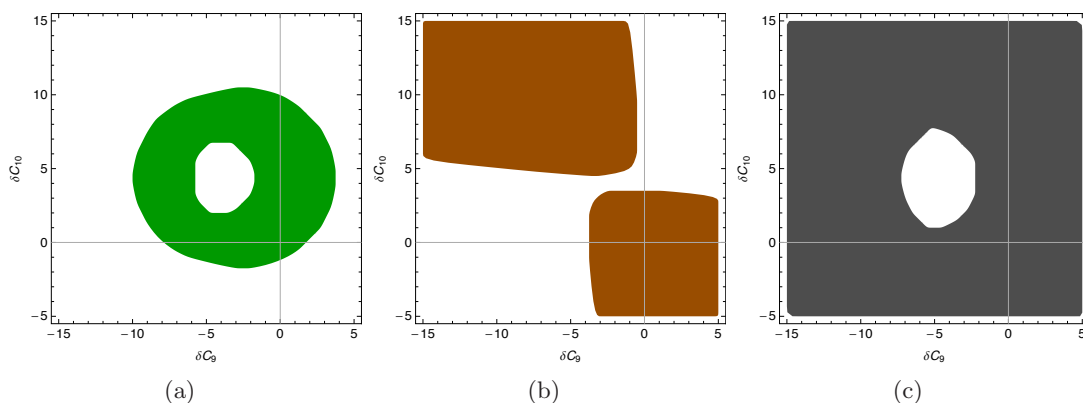


Figure 5: Constraint from Class-III observables $\mathcal{B}(B \rightarrow X_s \mu^+ \mu^-)$ (left), \tilde{A}_{FB} (middle) and \tilde{F}_L (right) at 1σ in the $(\delta C_9, \delta C_{10})$ plane in Scenario B. The region shown is compatible with the constraints on δC_7 and $\delta C_{7'}$ imposed by Class-I observables.

and unprimed) Wilson coefficients. Indeed, when NP contributions in $C_{9'}$ and $C_{10'}$ are also considered, the empty region in the middle of figure 5a gets filled up but the minimum and maximum values of δC_9 and δC_{10} allowed do not change perceptibly, as can be seen in figure 8a. In figure 8b we show the allowed region in the $(\delta C_{9'}, \delta C_{10'})$ plane in the same scenario. It is not very surprising to obtain such oval shapes in the various planes of interest, since it corresponds to the projections of the quadratic (elliptic) constraint given by eq. (2.24). In conclusion in Scenario C, the allowed region for $(\delta C_7, \delta C_{7'})$ is given by the three black regions in figure 2, and the corresponding ones for the planes $(\delta C_9, \delta C_{10})$ and $(\delta C_{9'}, \delta C_{10'})$ are given by figures 8a and 8b respectively.

We have not given the predictions for $A_T^{(2)}$ under this scenario, as the extra freedom provided by $C_{9'}$ and $C_{10'}$ is likely to fill the whole parameter space available.

3.5 2σ constraints

When the uncertainty in both theoretical and experimental results is increased to 2σ , the regions allowed in the $(\delta C_7, \delta C_{7'})$ plane are enlarged, as $\mathcal{B}(B \rightarrow X_s \gamma)$, $S_{K^* \gamma}$ and A_I yield larger overlapping regions. More importantly, the whole region corresponding to the “flipped-sign” solution is no longer excluded by Class I observables (see figure 9a). We have followed the procedure explained before and used the resulting four disconnected regions to explore the behaviour of Class-II and Class-III observables under scenarios A, B and C.

In Scenario A, $\mathcal{B}(B \rightarrow X_s \mu^+ \mu^-)$ excludes the whole “flipped-sign” solution region, a sizeable portion of the upper region and small part of the lower one, as shown in figure 9b, whereas neither \tilde{A}_{FB} nor \tilde{F}_L provide further constraints, since they fill the whole of the $(\delta C_7, \delta C_{7'})$ area explored.

Next we move to Scenario B and include possible NP contributions to $(\delta C_9, \delta C_{10})$, as depicted in figures 10a and 10b. The region allowed by $\mathcal{B}(B \rightarrow X_s \mu^+ \mu^-)$ becomes enlarged

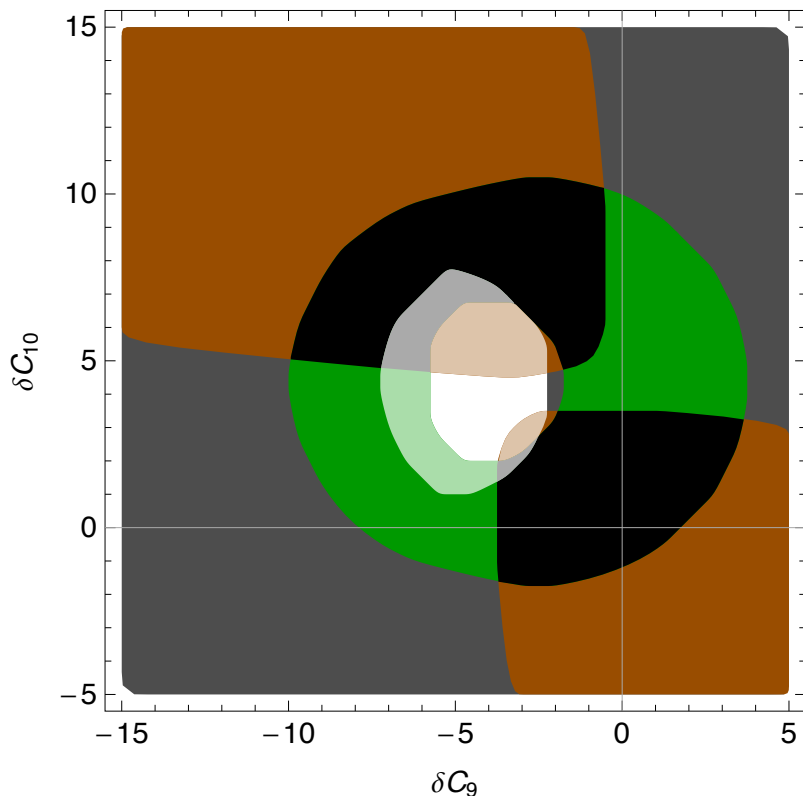


Figure 6: Overlap of the constraints from Class-III observables $\mathcal{B}(B \rightarrow X_s \mu^+ \mu^-)$ (green ring), A_{FB} (upper and lower “hyperbolic-like” brown regions; see figure 5b) and F_L (dark gray area with a central inlet) at 1σ in the $(\delta C_9, \delta C_{10})$ plane in Scenario B. The constraints imposed by their intersection are shown as two black regions.

by about a 40% with respect to the 1σ plot and the central region, previously forbidden, becomes filled altogether. In this scenario, \tilde{A}_{FB} does not provide extra constraints but \tilde{F}_L maintains an excluded central zone, although much reduced in area. Figure 11 shows (in black) the regions allowed by the overlapping of these two observables. Moreover, the “flipped sign solution” for the $(\delta C_7, \delta C_{7'})$ plane is now allowed under this scenario and the following one.

We come finally to Scenario C. Besides $(\delta C_9, \delta C_{10})$, we must also allow for NP in the Wilson coefficients $C_{9'}$ and $C_{10'}$, while $(\delta C_7, \delta C_{7'})$ remain confined to the four black regions of figure 9a. $\mathcal{B}(B \rightarrow X_s \mu^+ \mu^-)$ is again the only observable that imposes constraints in the Wilson coefficients related to \mathcal{O}_i and $\mathcal{O}_{i'}$ (with $i = 9, 10$) as shown in figures 12a and 12b.

3.6 Generalization to extended frameworks

Let us assume, for instance, that we want also to include contributions from scalar operators (like those defined in [8]). Consequently the scenarios will also be enlarged: Scenario A ($\mathcal{O}_7, \mathcal{O}_{7'}$), B ($\mathcal{O}_7, \mathcal{O}_{7'}, \mathcal{O}_9, \mathcal{O}_{10}$), C ($\mathcal{O}_7, \mathcal{O}_{7'}$, scalars), D ($\mathcal{O}_7, \mathcal{O}_{7'}, \mathcal{O}_9, \mathcal{O}_{10}, \mathcal{O}_{9'}, \mathcal{O}_{10'}$), E

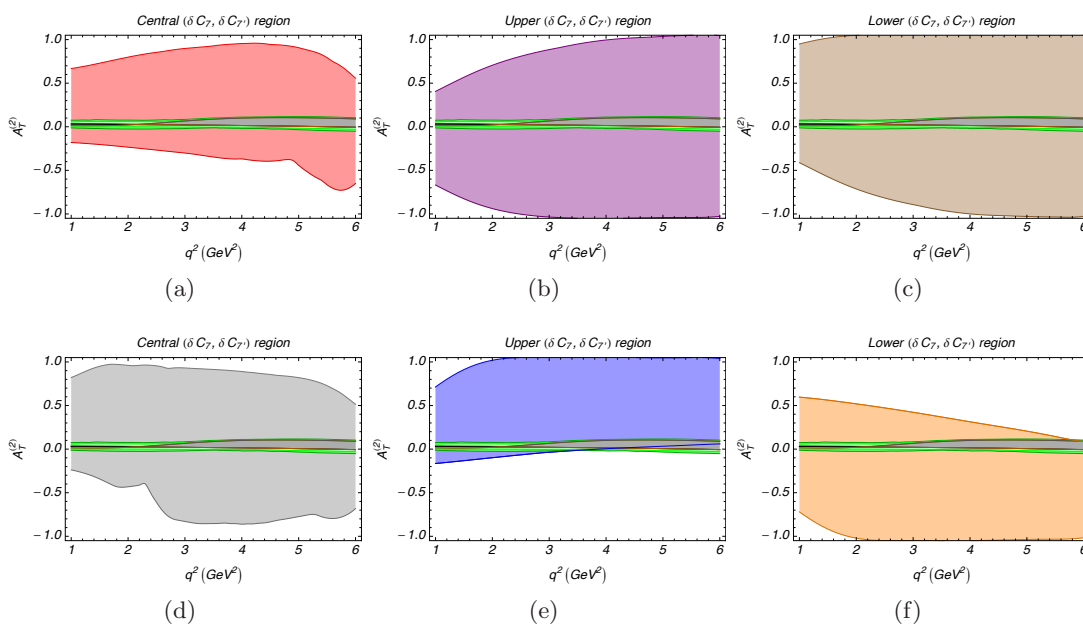


Figure 7: Prediction for $A_T^{(2)}(q^2)$ corresponding to the “flipped-values” region in (C_9, C_{10}) plane (first row of plots) and the SM-like region in (C_9, C_{10}) plane (second row) in figure 6. Each column corresponds to SM-like Central region (left), non SM-like Upper region (center), non SM-like Lower region (right) for the $(C_7, C_{7'})$ plane allowed regions in figure 2.

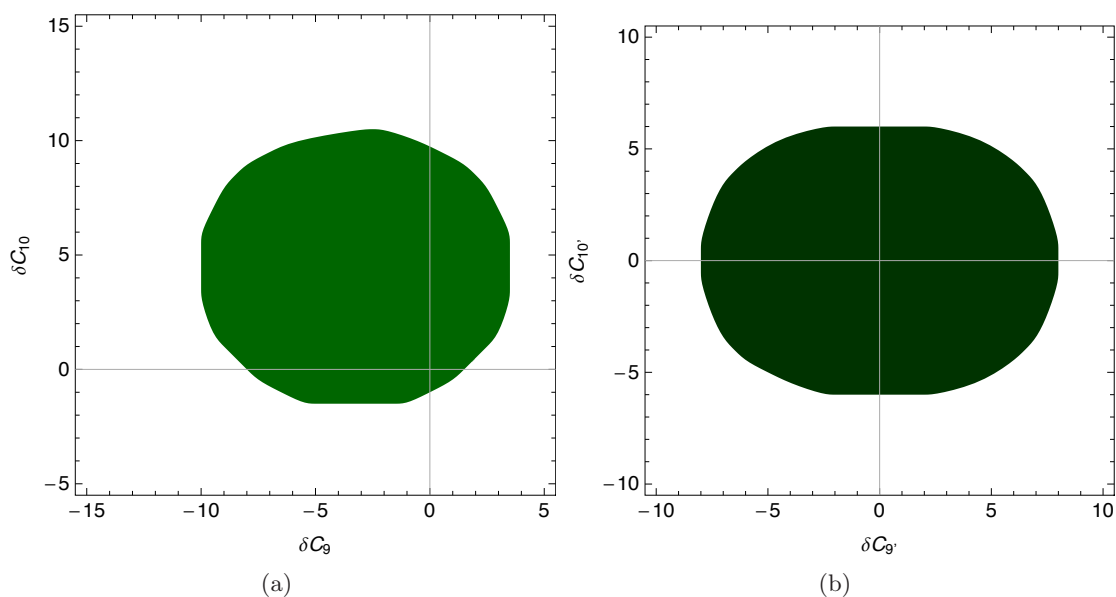


Figure 8: Constraints from Class-III observable $\mathcal{B}(B \rightarrow X_s \mu^+ \mu^-)$ at 1σ in the $(\delta C_9, \delta C_{10})$ and $(\delta C_{9'}, \delta C_{10'})$ planes in Scenario C. The regions shown are compatible with the constraints on δC_7 and $\delta C_{7'}$ imposed by Class-I observables.

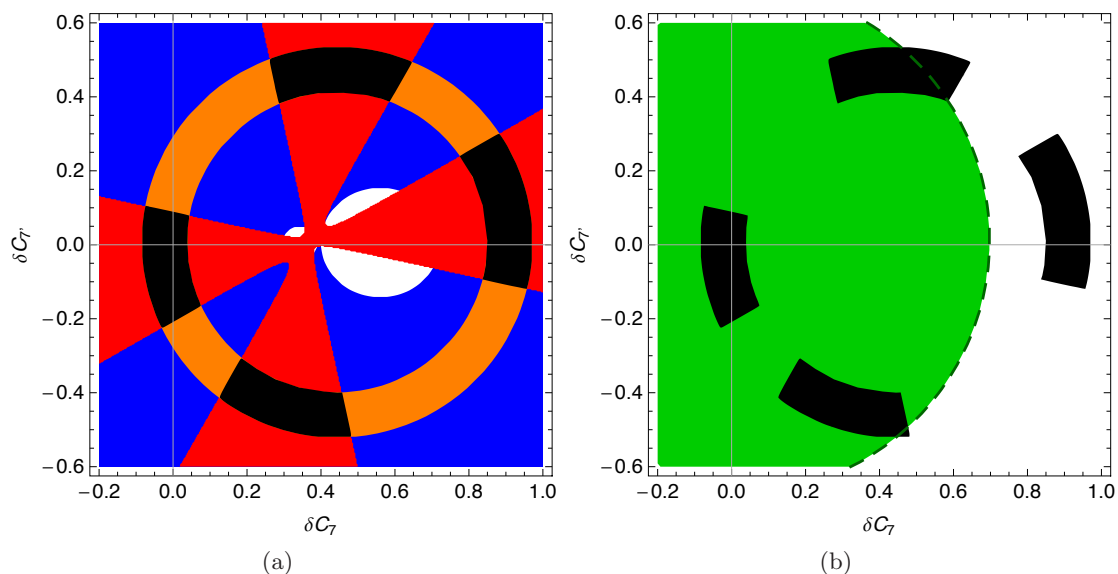


Figure 9: On the left, 2σ constraint from Class-I observables: A_I (background solid blue region with two white disks -partially hidden-), $\mathcal{B}(B \rightarrow X_s \gamma)$ (orange ring) and $S_{K^* \gamma}$ (red cross). The three disconnected regions allowed by the intersection of these three observables are depicted in black. On the right, 2σ constraint from Class-III observable $\mathcal{B}(B \rightarrow X_s \mu^+ \mu^-)$. The SM value is given by the crossing of light gray lines at $(\delta C_7, \delta C_{7'}) = (0, 0)$ point.

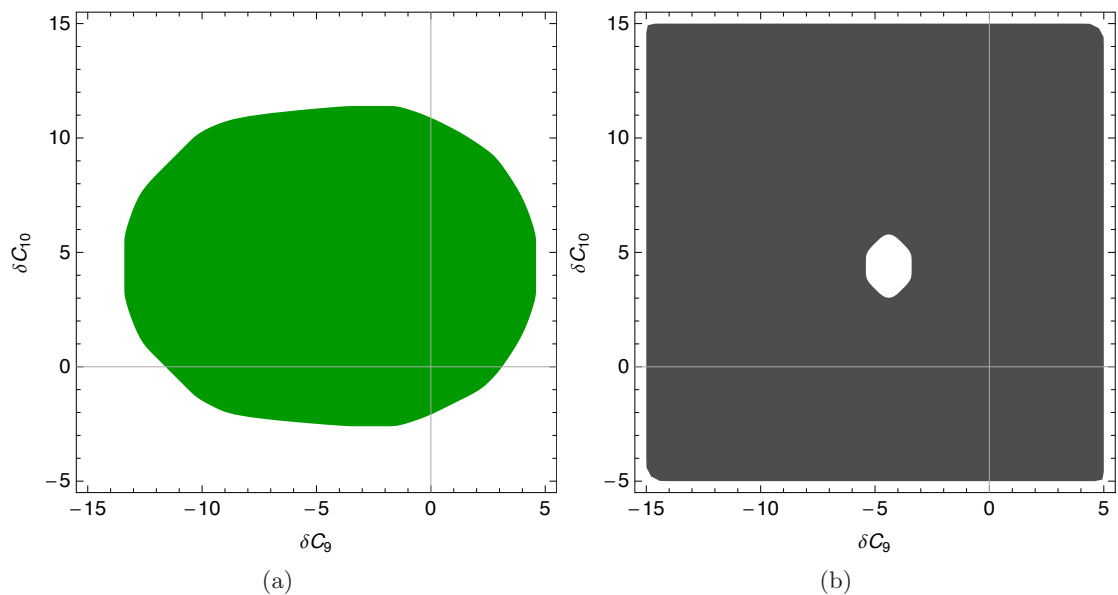


Figure 10: Constraints from Class-III observables $\mathcal{B}(B \rightarrow X_s \mu^+ \mu^-)$ (left) and \tilde{F}_L (right) at 2σ in the $(\delta C_9, \delta C_{10})$ plane in Scenario B.

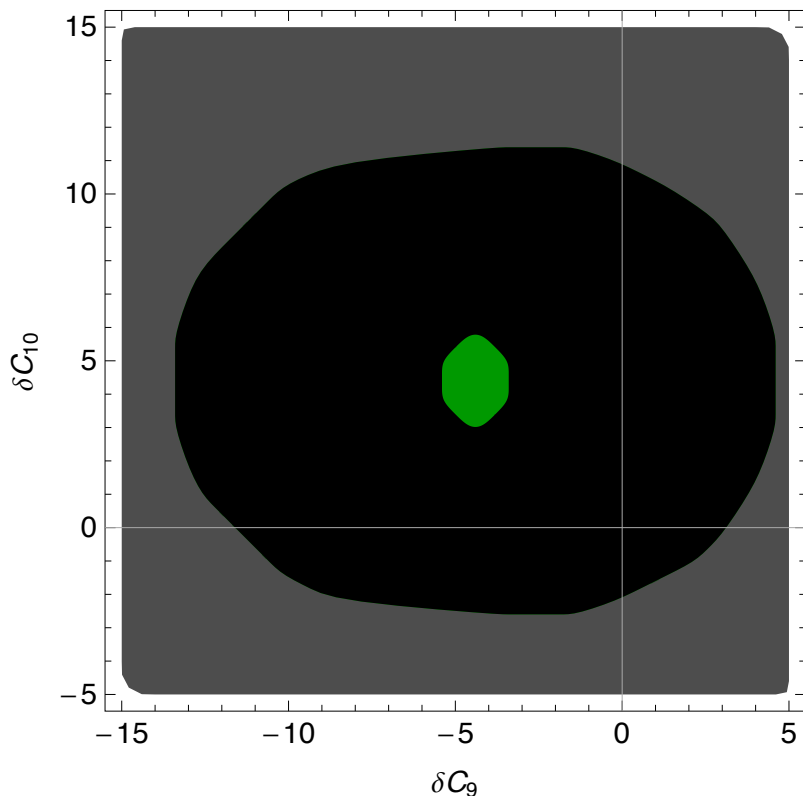


Figure 11: Overlap of the constraints from Class-III observables $\mathcal{B}(B \rightarrow X_s \mu^+ \mu^-)$ and \tilde{F}_L at 2σ in the $(\delta C_9, \delta C_{10})$ plane in Scenario B. The constraints imposed by their intersection are shown as a black region.

$(\mathcal{O}_7, \mathcal{O}_{7'}, \mathcal{O}_9, \mathcal{O}_{10}, \text{scalars}), F$ (all operators). We would then proceed again along the same steps as before, up to certain changes:

1. We classify again the observables according to this new framework. This may move some observable from Class-I to higher classes, because they have sensitivity to scalars, like the $K^* \gamma$ observables A_I or $S_{K^* \gamma}$. Only $\mathcal{B}(\bar{B} \rightarrow X_s \gamma)$ will remain.
2. We determine the new reference region for C_7 and $C_{7'}$ defined by the (now reduced) set of Class-I observables. The new primary regions will be larger than in the previous framework because some observables are not included in the new Class-I.
3. At this stage, and working in Scenario A, it is interesting to define two types of Class-II observables, Class-IIa, only sensitive to dipole, semileptonic and chirally flipped (our observables in Class II of the previous framework will be here) and Class-IIb, only sensitive to dipole operator (and its chirally flipped counterpart) and scalars. These observables may shrink the new reference regions, leading to allowed regions of different shapes for Class-IIa and Class-IIb. If we add now Class-III observables with sensitivity to the whole list of operators in the framework, this will generate a further cut on the primary region. If the same set of observables as in the previous

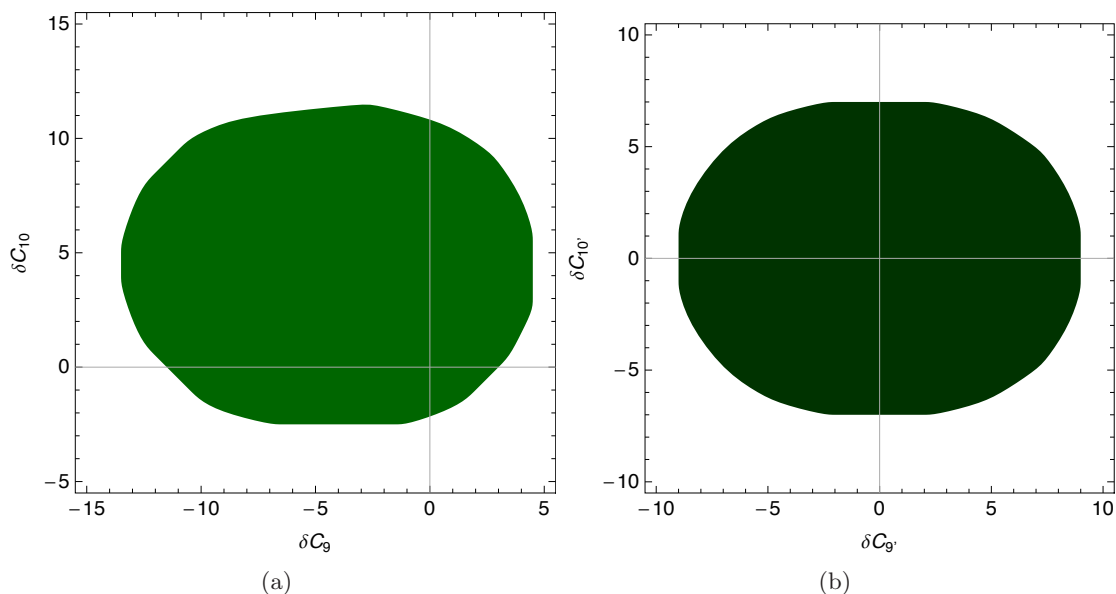


Figure 12: Constraints from Class-III observable $\mathcal{B}(B \rightarrow X_s \mu^+ \mu^-)$ at 2σ in the $(\delta C_9, \delta C_{10})$ and $(\delta C_{9'}, \delta C_{10'})$ planes in Scenario C. The regions shown are compatible with the constraints on δC_7 and $\delta C_{7'}$ imposed by Class-I observables.

framework has been included it is clear that, even if re-classified, the allowed region under Scenario A will be exactly the same as in the previous framework, even if the primary regions are different.

4. The main differences arise when dealing with the rest of scenarios. We should repeat the same analysis under Scenario B till F. It is clear that Scenario B and Scenario C, for instance, may select different subregions inside the primary regions, and that Scenario D will enlarge the region for Scenario B, and the same will happen between scenarios E and C. Finally Scenario F will cover all previous ones, defining the largest allowed subregion inside the primary regions. This region may be larger than in the previous framework (since more freedom in the value of the WC already studied is provided by the introduction of scalar contributions).
5. This systematic procedure that subdivides the primary regions in different subregions may help to disentangle the importance of each set of operators: dipole, semileptonic, chirally flipped, scalar, when confronting theory with data. In particular, certain observables like $A_T^{(2)}$ and its generalization, may discriminate between the different subregions.

This procedure can be generalized to other frameworks following the same steps. Defining intermediate steps between the dipole-only case and the full-fledged scenario for the introduction of New Physics helps in understanding the importance of the NP contribution for each observable. In the present paper, we have restricted ourselves to the framework where NP arises in dipole, semileptonic operators and their chirally-flipped partners.

4 Discussion and outlook

We have exploited the $(\delta C_7, \delta C_{7'})$ plane as a starting point to investigate the pattern of NP in the Wilson coefficients for radiative $\Delta B = 1$ transitions. We have defined several classes of observables to help us in this task, selecting only observables with a good theoretical control over hadronic uncertainties (or a significant discriminating power for our NP scenarios) and providing numerical expressions for these quantities as functions of $\delta C_{7,7',9,9',10,10'}$. We defined reference regions for $(\delta C_7, \delta C_{7'})$ from Class-I observables, then studied several scenarios of NP involving chirality-flipped operators with the help of Class-II and Class-III observables.

As far as the theory and experimental errors of the measured observables remain inside the 1σ range we can draw the following conclusions. Scenario A, where only $(C_7, C_{7'})$ receive large NP contributions, is a predictive scenario. Class-I observables provide three different regions (one corresponding to the SM case, two other ones with almost vanishing C_7 values and large $C_{7'}$ value). Once Class-III observables are included only a very small subregion (inside one of the two non-SM like regions) is allowed if we keep all the constraints at 1σ . Consequently, only those theories that can provide values for $(C_7, C_{7'}) \simeq (C_7^{\text{SM}} + 0.25, -0.4)$ are compatible (within 1σ) with current (Class-I and Class-III) data, due to the interplay between the inclusive decay $B \rightarrow X_s \mu^+ \mu^-$ and the forward-backward asymmetry \tilde{A}_{FB} . Notice that the SM is not one of such theories. This motivated us to enlarge the set of operators where NP contributions can be sizeable, leading to constraints on the semileptonic operators. Scenario B constitutes the first extension, allowing for NP in $C_{7,7',9,10}$. In this case, the previous constraints from Class-III observables are transferred from the $(\delta C_7, \delta C_{7'})$ plane to the $(\delta C_9, \delta C_{10})$ one. There are two distinctive regions allowed, corresponding to the SM solution, but also to a flipped-value configuration, where C_9 and C_{10} have some values opposite to the SM. It is interesting to notice that $\mathcal{B}(B \rightarrow X_s \mu^+ \mu^-)$ and \tilde{F}_L exclude almost the same central area in the $(\delta C_9, \delta C_{10})$ plane. Scenario C (with NP in $C_{7,7',9,9',10,10'}$) would be an interesting extension if the previous experimental constraints shift in the future, or if the measurement of the (Class-II) asymmetry $A_T^{(2)}$ shows a discrepancy with the pattern of Wilson coefficients exhibited in Scenario B, once more data and constraints have been added. The (Class-I) constraints on $(C_7, C_{7'})$ remain unchanged with respect to Scenario B, whereas Class-III observables provide only limited constraints on the largest set of Wilson coefficients considered. Currently, only $B \rightarrow X_s \mu^+ \mu^-$ provides constraints on $C_{9,9',10,10'}$.

We have also indicated how the (Class-II) asymmetry $A_T^{(2)}$ gives a very precise prediction for Scenario A, that can be used either to confirm it or to rule it out. It may also help, depending on its sign, to discriminate among the allowed regions in Scenario B. $A_T^{(2)}$ exhibits a strong sensitivity to the allowed regions for (C_9, C_{10}) ; further cuts in these regions using high- q^2 measurements, will improve the predictive power of $A_T^{(2)}$ in this scenario. Under Scenario C, there is too much freedom with all WC switched on to be able to cut on precise regions as it happens for most of the other observables.

We also have shown that Class-I observables alone allow us to dismiss the flipped-sign solution at 1.59σ , even in a NP scenario much more general than in ref. [7], allowing for

NP in dipole and semileptonic operators, but also in their chirally-flipped counterparts. We achieved this by trading the Class-III observable $\mathcal{B}(B \rightarrow X_s \mu^+ \mu^-)$ (considered in ref. [7], and sensitive to many NP contributions apart from those in the dipole ones) for the Class-I isospin asymmetry in $B \rightarrow K^* \gamma$ (even though the theoretical control on hadronic uncertainties is less satisfying for this observable).

A summary of the maximum and minimum values of the WC analyzed in the different scenarios is provided in table 15.¹²

In ref. [18], an analysis of various NP contributions was considered, allowing either for New Physics in $(C_7, C_{7'})$ (both of them being real), or C_{10} (considered as potentially complex). In particular, our findings concerning Scenario A (NP only in C_7 and $C_{7'}$) are in agreement with figure 2 in ref. [18] concerning $S_{K^* \gamma}$, as well as the fact that the flipped-sign solution is excluded (even though the conclusion is based on different observables). However, the other scenarios discussed in [18] considered NP entering in one Wilson coefficient at a time, and thus provide only a particular section of the parameter space of Wilson coefficients. Another related study was performed in ref. [59], where $B \rightarrow K^* \ell^+ \ell^-$ at large and low recoil (which was not considered here) was combined with $B \rightarrow X_s \ell^+ \ell^-$ to study the (C_9, C_{10}) plane, considering $C_7 = \pm C_7^{\text{SM}}$. This led to two regions in (C_9, C_{10}) similar to the ones obtained in our case, however smaller partly due to the additional constraints put on C_7 (and $C_{7'}$) in this reference.

In ref. [57], a global analysis of $\Delta B = 1$ observables was performed in a minimal flavour violating framework that included the possibility of sizable scalar contributions (but no chirally flipped operators). The combination of the various observables was performed using a Bayesian statistical approach. Even though the inputs and the underlying assumptions concerning the structure of NP are different (scalar versus chirality-flipped operators), we observe some common features. Two different regions for (C_7, C_9, C_{10}) are allowed, corresponding approximately to a change of sign for the Wilson coefficients (figure 1 in ref. [57]). Once NP is allowed for (C_9, C_{10}) (Scenario B), there is a ring-like constraint from $\mathcal{B}(B \rightarrow X_s \ell^+ \ell^-)$ in the (C_9, C_{10}) plane, with only two regions surviving once the forward-backward asymmetry \tilde{A}_{FB} is included (figure 4 in ref. [57]). This is in basic agreement with our own plots, even though we should highlight that the non-SM region in the (C_9, C_{10}) plane corresponds to different allowed values for the electromagnetic operators: in ref. [57], this region corresponds to the SM and the “flipped-sign” solution ($C_7 \simeq -C_7^{\text{SM}}$, $C_{7'} \simeq 0$) disfavoured by $B \rightarrow X_s \mu^+ \mu^-$ in their framework, whereas our region corresponds to the SM solution and to the flipped-value regions where $C_7 \simeq 0$ and $|C_{7'}| \simeq |C_7^{\text{SM}}|$.

Our approach could be extended to other, more involved, scenarios of New Physics, including contributions to the chromomagnetic, scalar and/or tensors operators as explained in detail in Sec 3.6, allowing us to assess the impact of each observable in a controlled way. Such a task is left for future work.

¹²For the internal 4-d and 6-d correlations involving 4 WCs (Scenario B) and 6 WCs (Scenario C) we can provide a datafile with the correlated points upon request.

	$\delta C_7(\mu_b)$	$\delta C_{7'}(\mu_b)$	$\delta C_9(\mu_b)$	$\delta C_{10}(\mu_b)$	$\delta C_{9'}(\mu_b)$	$\delta C_{10'}(\mu_b)$
Overlap of the 1σ constraints						
Sc. A	[0.244, 0.274]	[-0.417, -0.39]	0	0	0	0
Sc. B	[0.346, 0.385]	[0.435, 0.501]	[-9.75, -0.5]	[4.75, 10.5]	0	0
	[-0.056, 0.016]	[-0.114, 0.027]	[-3.75, 3.5]	[-1.75, 3.5]		
	[0.235, 0.385]	[-0.489, -0.39]				
Sc. C	[0.346, 0.385]	[0.435, 0.501]	[-10, 3.5]	[-1.5, 10.5]	[-8, 8]	[-6, 6]
	[-0.056, 0.016]	[-0.114, 0.027]				
	[0.235, 0.385]	[-0.489, -0.39]				
Overlap of the 2σ constraints						
Sc. A	[0.262, 0.586]	[0.381, 0.531]	0	0	0	0
	[-0.083, 0.076]	[-0.225, 0.105]				
	[0.124, 0.475]	[-0.519, -0.306]				
Sc. B	[0.262, 0.646]	[0.381, 0.534]	[-13.4, 4.5]	[-2.5, 11.4]	0	0
	[-0.083, 0.076]	[-0.225, 0.105]				
	[0.775, 0.97]	[-0.12, 0.3]				
	[0.124, 0.481]	[-0.519, -0.306]				
Sc. C	[0.262, 0.646]	[0.381, 0.534]	[-13.5, 4.6]	[-2.6, 11.5]	[-9, 9]	[-7, 7]
	[-0.083, 0.076]	[-0.225, 0.105]				
	[0.775, 0.97]	[-0.12, 0.3]				
	[0.124, 0.481]	[-0.519, -0.306]				

Table 15: Summary table of the maximum and minimum Wilson coefficients values allowed by the three different scenarios within our framework. The table is organized in three independent blocks corresponding to the pairs $(\delta C_7, \delta C_{7'})$, $(\delta C_9, \delta C_{9'})$ and $(\delta C_{10}, \delta C_{10'})$ respectively. Notice that the correlations between different WCs are more complex than those summarised in this table. In order to recover the exact 2d-correlations, one should look at figure 3a (Scenario A), figures 1, 6 (Scenario B) and figures 1, 6, 8a, 8b (Scenario C) at 1σ , and at figure 9b (Scenario A), figures 9a, 11 (Scenario B) and figures 9a, 11, 12a, 12b (Scenario C) at 2σ .

Acknowledgments

The authors would like to thank A. Dighe, T. Feldmann, U. Haisch, J. Kamenik, E. Lunghi and M. Misiak for fruitful exchanges. SDG would like to thank UAB where part of this work was completed under project 2009PIV00066. DG would like to thank specially A. Dighe for encouragement. JM thanks the Tata Institute for Fundamental Research for their hospitality. JM acknowledges financial support from FPA2008-01430, SGR2009-00894. MR also thanks A. Khodjamirian, R. Miquel, Ll. Galbany and P. Martí for enlightening discussions. MR work has been supported by Universitat Autònoma de Barcelona.

A Inputs

We have followed the discussion in refs. [22–25, 35] concerning the matching and the running of the Wilson coefficients from the high scale $\mu_0 = 2M_W$ down to the low scale $\mu_b = 4.8$ GeV. We were able to reproduce at the 1% level the tables 3, 4 and 5 in ref. [22] (apart from $C_7^{(11)}, C_9^{(22)}, C_{10}^{(22)}$) and the table 5 in ref. [35] for the Wilson coefficients, providing a check that we control the scale dependence of the Wilson coefficients accurately. Contrary to other analyses in the literature, we have expressed the deviations from the SM Wilson coefficients at the low scale μ_b around 4.8 GeV. However, the evolution from μ_0 to μ_b can be determined as the linear combinations:

$$\begin{aligned}\delta C_7(\mu_b) &= 0.575 \times \delta C_7(\mu_0), \\ \delta C_9(\mu_b) &= 1.021 \times \delta C_9(\mu_0) + 0.008 \times \delta C_{10}(\mu_0), \\ \delta C_{10}(\mu_b) &= 0.008 \times \delta C_9(\mu_0) + 1.038 \times \delta C_{10}(\mu_0).\end{aligned}\tag{A.1}$$

Several schemes have been used to define the quark masses:

- For m_t and m_c , we used the $\overline{\text{MS}}$ scheme at the required scale (respectively μ_0 and m_c). We convert m_t^{pole} into $m_t^{\overline{\text{MS}}}$ using the conversion formulae in refs. [26, 60].
- For m_b , two different masses are needed: the mass in the 1S scheme (or an equivalent scheme with infrared subtraction) is required whenever the b -quark is close to the mass shell, whereas the pole mass is used for normalisation purposes as well as for loop computations where the b -quark is off-shell. Following ref. [22, 35], we take the value of m_b^{1S} obtained from fits to hadronic and leptonic moments of the differential branching ratio for the inclusive decay $B \rightarrow X_c \ell \nu$ [61], and we determine the pole mass using the conversion formulae in ref. [62].
- For m_s , we use the strange quark mass in the $\overline{\text{MS}}$ scheme, taken at the scale μ_b . We are aware that there is an ambiguity in the scheme and scale chosen for this mass (this ambiguity would be resolved by going to higher orders in perturbation theory, which are not included in the present analysis). We used m_s/m_b both in the $\overline{\text{MS}}$ scheme to evaluate the SM value of $C_{7'}$ (however we kept the m_b^{pole} normalisation to determine $\hat{m}_s = m_s/m_b$ needed for $B \rightarrow X_s \ell^+ \ell^-$).

The running of the quark masses in the $\overline{\text{MS}}$ is performed following ref. [22]. The strong and electromagnetic coupling constants are determined by their value at M_Z , and their running is given by the equations in ref. [22].

B Extension to chirally-flipped operators

B.1 $B \rightarrow X_s \gamma$

The branching ratio for $B \rightarrow X_s \gamma$ for a photon energy larger than $E_0 = 1.6$ GeV can be written as [35]:

$$\mathcal{B}(B \rightarrow X_s \gamma)_{E_\gamma > E_0, \text{SM}} = \mathcal{B}(B \rightarrow X_c e \bar{\nu}) \left| \frac{V_{ts}^* V_{tb}}{V_{cb}} \right|^2 \frac{6\alpha_{\text{em}}}{C_\pi} [P(E_0) + N(E_0)],\tag{B.1}$$

where

$$C = \left| \frac{V_{ub}}{V_{cb}} \right|^2 \frac{\Gamma(\bar{B} \rightarrow X_c e \bar{\nu})}{\Gamma(\bar{B} \rightarrow X_u e \bar{\nu})}, \quad (\text{B.2})$$

$$P(E_0) = \sum_{i,j=1\dots 8} C_i^{\text{eff}}(\mu) C_j^{\text{eff}*}(\mu) K_{ij}(E_0, \mu). \quad (\text{B.3})$$

Concerning $B \rightarrow X_s \gamma$, we were able to reproduce, not only the central value and uncertainty for the branching ratio, but also the results from the three different interpolation procedures and the scale dependence on μ_0 and μ_b described in ref. [35] as well as the dependence on $C_{7,8}$ at the scale μ_0 in eq. (29) of ref. [34]. The contribution from the chirally-flipped operator $\mathcal{O}_{7'}$ should have the same structure as the SM operator \mathcal{O}_7 and there are no interferences between the two contributions, leading to an additional contribution to eq. (B.1) of the form:

$$P(E_0) \rightarrow P(E_0) + (C_{7'})^2 [1 + \tilde{\alpha}_s(\mu) K_{77}^{(1)} + \tilde{\alpha}_s(\mu)^2 K_{77}^{(2)}], \quad (\text{B.4})$$

where $K_{77}^{(i)}$ are the coefficients of the perturbative expansion of the kernel $K_{77}(E_0, \mu)$.

B.2 $B \rightarrow K^* \gamma$ isospin asymmetry

Concerning the isospin asymmetry, we reproduced the central value of the isospin asymmetry quoted in ref. [31], following the formalism discussed in ref. [39]:

$$A_I[B \rightarrow K^* \gamma]_{\text{SM}} = \text{Re}[b_d^\perp(0) - b_u^\perp(0)]_{\text{SM}}, \quad (\text{B.5})$$

$$b_{q,\text{SM}}^\perp(0) = \frac{12\pi^2 f_B e_q}{m_b \mathcal{C}_7 \xi_\perp(0)} \left[\frac{f_{K^*}^\perp}{m_B} K_1^\perp(0) + \frac{f_{K^*} m_{K^*}}{6\lambda_B m_B} K_2^\perp(0) \right], \quad (\text{B.6})$$

where $\mathcal{C}_7 = C_7^{\text{eff}} + O(\alpha_s)$ includes NLO corrections to the amplitude for $B \rightarrow K^* \gamma$, computed in ref. [63]. In $K_{1,2}^\perp(0)$, we have included the Cabibbo-suppressed power corrections discussed in appendix A.3 in ref. [40] and neglected in ref. [39], performing the replacements

$$K_{1,2}^{\perp(c)} \rightarrow K_{1,2}^{\perp(c)} + \frac{\lambda_u}{\lambda_t} K_{1,2}^{\perp(c)} [F_V \rightarrow F_V^{(u)}], \quad (\text{B.7})$$

$$F_V^{(u)}(s = \bar{u}m_B^2) = \frac{3}{4} \left(C_2 - \frac{C_1}{6} \right) [h(s, m_c) - h(s, 0)], \quad (\text{B.8})$$

following the notation in ref. [39].

Unfortunately, the hard-spectator scattering involving the chromomagnetic operator \mathcal{O}_8 exhibits an endpoint divergence indicating a breakdown of QCD factorisation. We follow refs. [31, 39] to regularise the divergent integral

$$\int_0^1 du \rightarrow (1 + \rho e^{i\phi}) \int_0^{1-\Lambda_h/m_B} du, \quad (\text{B.9})$$

where ρ is assumed to be smaller than 1 for our numerical estimations, and the phase ϕ is arbitrary.

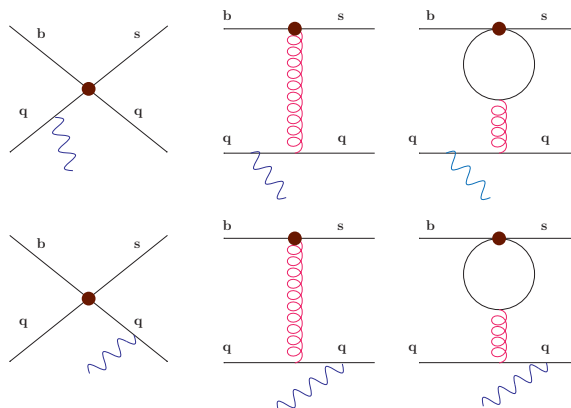


Figure 13: Annihilation topologies involving operators \mathcal{O}_{1-6} (left). Hard spectator interaction involving operator \mathcal{O}_8 (center) and \mathcal{O}_{1-6} (right).

Once we add chirality-flipped operators, $\mathcal{O}_{7'}$ will contribute to the branching ratio of $B \rightarrow K^* \gamma$. It is not difficult to check that its contribution is the same as the one from \mathcal{O}_7 , and that there are no interferences between the two contributions. We will neglect the contributions from SM operators to the amplitude for a photon of right-handed helicity. On the other hand, the flipped operators considered in the present paper do not contribute to the spectator interactions responsible for the isospin asymmetry (which are induced by the four-quark operators and the chromomagnetic operators). Therefore, the only change induced by chirality-flipped operators corresponds to modifying the normalisation, i.e., the denominator in the expression of the isospin asymmetry (at first order in isospin breaking)

$$A_I[B \rightarrow K^* \gamma] = \frac{\text{Re}[b_d^\perp(0) - b_u^\perp(0)]}{1 + |C_{7'}/C_7|^2}. \quad (\text{B.10})$$

B.3 $S_{K^* \gamma}$

We define the decay amplitudes of B_d mesons into K^* and $\gamma_{L(R)}$ as in [43]:

$$\bar{\mathcal{A}}_{L(R)} = \bar{\mathcal{A}}(\bar{B}_d^0 \rightarrow \bar{K}^{*0} \gamma_{L(R)}), \quad \mathcal{A}_{L(R)} = \mathcal{A}(B_d^0 \rightarrow K^{*0} \gamma_{L(R)}). \quad (\text{B.11})$$

With the assumptions explained under eq. (2.11) and using eqs. (B.11), the mixing induced CP-asymmetry (S) and the direct CP asymmetry (C) can be written as

$$S = \frac{2 \text{Im} [r_d (\mathcal{A}_L^* \bar{\mathcal{A}}_L + \mathcal{A}_R^* \bar{\mathcal{A}}_R)]}{|\mathcal{A}_L|^2 + |\mathcal{A}_R|^2 + |\bar{\mathcal{A}}_L|^2 + |\bar{\mathcal{A}}_R|^2}, \quad C = \frac{|\mathcal{A}_L|^2 + |\mathcal{A}_R|^2 - |\bar{\mathcal{A}}_L|^2 - |\bar{\mathcal{A}}_R|^2}{|\mathcal{A}_L|^2 + |\mathcal{A}_R|^2 + |\bar{\mathcal{A}}_L|^2 + |\bar{\mathcal{A}}_R|^2}. \quad (\text{B.12})$$

where $r_d = e^{-i\phi_d}$ and ϕ_d is the $\bar{B}_d^0 - B_d^0$ mixing angle.

In “naïve” factorisation, the decay amplitudes of eqs. (B.11) are given by

$$\bar{\mathcal{A}}_L = -\frac{4G_F}{\sqrt{2}} \left[\lambda_u^{(s)} \mathcal{C}_7^{(u)} + \lambda_t^{(s)} \mathcal{C}_7^{(t)} \right] \langle \bar{K}^* \gamma_L | \mathcal{O}_7^L | \bar{B} \rangle, \quad (\text{B.13a})$$

$$\bar{\mathcal{A}}_R = -\frac{4G_F}{\sqrt{2}} \left[\lambda_u^{(s)} \mathcal{C}_{7',\text{SM}}^{(u)} + \lambda_t^{(s)} \left(\mathcal{C}_{7',\text{SM}}^{(t)} + C_{7'}^{(t)} \right) \right] \langle \bar{K}^* \gamma_R | \mathcal{O}_7^R | \bar{B} \rangle, \quad (\text{B.13b})$$

and

$$\mathcal{A}_L = -\frac{4G_F}{\sqrt{2}} \left[(\lambda_u^{(s)})^* \mathcal{C}_{7',\text{SM}}^{(u)} + (\lambda_t^{(s)})^* \left(\mathcal{C}_{7',\text{SM}}^{(t)} + C_{7'}^{(t)} \right) \right] \langle K^* \gamma_L | (\mathcal{O}_7^R)^\dagger | B \rangle, \quad (\text{B.14a})$$

$$\mathcal{A}_R = -\frac{4G_F}{\sqrt{2}} \left[(\lambda_u^{(s)})^* \mathcal{C}_7^{(u)} + (\lambda_t^{(s)})^* \mathcal{C}_7^{(t)} \right] \langle K^* \gamma_R | (\mathcal{O}_7^L)^\dagger | B \rangle, \quad (\text{B.14b})$$

where, we have used the short-hand notation introduced in eq. (2.4)

$$\mathcal{C}_{7',\text{SM}}^{(q)} = \frac{m_s}{m_b} \mathcal{C}_{7,\text{SM}}^{(q)} \quad (\text{B.15})$$

with $q = u, t$. We have taken the notation and definitions from ref. [40]: $\mathcal{C}_7^{(q)}$ are coefficients, defined as a ratio of full form factors and soft form factors, that can be computed in QCDF ($\mathcal{C}_7^{(t)}$ is equivalent to C_7^{eff} at LO in α_s whereas $\mathcal{C}_7^{(u)}$ vanishes). Setting $\mathcal{C}_{7',\text{SM}}^{(q)} = 0$ and taking real Wilson coefficients C_7^{eff} and $C_{7'}$, the mixing-induced CP-asymmetry yields the simple tree-level expression in ref. [18, 41, 42]:

$$S_{K^*\gamma}^{(\text{LO})} = \frac{-2 |C_{7'}/C_7^{\text{eff}(0)}|}{1 + |C_{7'}/C_7^{\text{eff}(0)}|^2} \sin \left(2\beta - \arg \left(C_7^{\text{eff}(0)} C_{7'} \right) \right). \quad (\text{B.16})$$

Eq. (B.16) determines the cross-shaped plot of $S_{K^*\gamma}$ in the $(\delta C_7, \delta C_{7'})$ plane (see figure 2) to a very good degree of approximation. We checked that $S_{K^*\gamma}^{(\text{LO})}$ allows us to recover, at 2σ , the shape of figure 2 (left) in [18] using their input parameters. Notice, however, that our actual computation, used for the plots in the present article, is performed including NLO QCDF corrections.

Some comments are in order here. On the one hand, the operators $\mathcal{O}_7^{L(R)}$ are given by

$$\mathcal{O}_7^{L(R)} = \frac{e}{16\pi^2} m_b \bar{s} \sigma_{\mu\nu} \frac{1 \pm \gamma_5}{2} b F^{\mu\nu}, \quad (\text{B.17})$$

and generate the left- (right-) handed photons in the $b \rightarrow s\gamma$ decay. Following refs. [43, 44] we express the matrix elements in eqs. (B.13b) and (B.14b) in terms of the form factor $T_1^{B \rightarrow K^*}(q^2)$ as

$$\begin{aligned} \langle \bar{K}^*(p, \eta) \gamma_{L(R)}(q, e) | \mathcal{O}_7^{L(R)} | \bar{B} \rangle &= \\ &= -\frac{e}{8\pi^2} m_b T_1^{B \rightarrow K^*}(0) \left\{ \epsilon^{\mu\nu\rho\sigma} e_\mu^* \eta_\nu^* p_\rho q_\sigma \pm i [(e^* \eta^*)(pq) - (e^* p)(\eta^* q)] \right\} \\ &\equiv -\frac{e}{8\pi^2} m_b T_1^{B \rightarrow K^*}(0) S_{L(R)}, \end{aligned} \quad (\text{B.18})$$

$$\langle K^*(p, \eta) \gamma_{L(R)}(q, e) | (\mathcal{O}_7^{R(L)})^\dagger | B \rangle = -\frac{e}{8\pi^2} m_b T_1^{B \rightarrow K^*}(0) S_{L(R)}, \quad (\text{B.19})$$

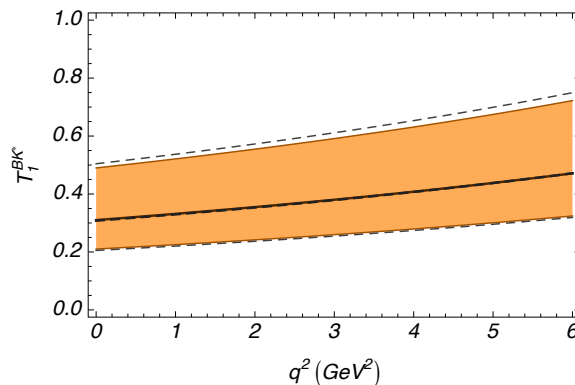


Figure 14: Form factor $T_1^{B \rightarrow K^*}(q^2)$ in the $0 - 6 \text{ GeV}^2$ energy range. The orange bands represent the full form factor with its associated errors given by the parametrisation in appendix B.4 of [64] and the gray dashed lines depict $T_1^{B \rightarrow K^*}(q^2)$ computed from $\xi_\perp(q^2)$ using the large-recoil expressions in refs. [21, 48].

where $S_{L,R}$ are the helicity amplitudes corresponding, respectively, to left- and right-handed photons and $e_\mu(\eta_\mu)$ is the polarisation four-vector of the photon (K^*).

On the other hand, since the photon emitted in the decay $b \rightarrow s\gamma$ is real, only the operators $\mathcal{O}_{1,\dots,8}$ of the weak effective Hamiltonian contribute to this process. In particular, those that build up C_7^{eff} (see eq. (2.5)) appear at $O(\alpha_s^0)$, while the rest of the operators enter the NLO QCDF corrections. Even though there is just one form factor contributing to this process, we have used the corresponding soft form factor computed by means of eq. (B.41) to be consistent with the QCDF formalism applied to both A_I and $\bar{B}_d^0 \rightarrow \bar{K}^{*0} \ell^+ \ell^-$ observables. This amounts to replacing $T_1^{B \rightarrow K^*}(0) \rightarrow \xi_\perp(0)$ in eqs. (B.19), which is indeed a very good approximation, as we can see in figure 14.

Contrary to ref. [40] we have chosen to keep the CKM-suppressed terms proportional to $\lambda_u^{(s)}$. In “naïve” factorisation, both $C_7^{(u)}$ and $C_{7',\text{SM}}^{(u)}$ vanish at LO in α_s . If NP is absent, $C_{7'}^{(t)}$ vanishes, as we have split the $C_{7',\text{SM}}^{(q)}$ helicity-suppressed γ_R terms already present in the SM (see eq. (2.4)) from the $\mathcal{O}_{7'}$ NP contribution. Therefore, including NP in the decay amplitudes can be obtained upon the following replacements in eqs. (B.13b), (B.14b):

$$C_{7'}^{(t)} \rightarrow \delta C_{7'}, \quad C_7^{(t)} \rightarrow C_{7,\text{SM}}^{(t)} + \delta C_7, \tag{B.20}$$

where, as said in the previous section, $C_7^{(q)} = C_7^{\text{eff}(q)} + O(\alpha_s)$ includes the NLO corrections to the decay amplitude $B \rightarrow K^* \gamma$ [63]. Therefore, the replacement $\xi_\perp(0) C_7^{(q)} \rightarrow \mathcal{T}_\perp^{(q)}$ [21, 40, 63] in the expressions above will be enough to account for these corrections in QCDF. Using this framework, we have computed the $O(\alpha_s)$ factorisable and non-factorisable corrections to hard-spectator scattering diagrams, as well as to those diagrams that involve a $B \rightarrow K^*$ form factor [63]. We have also included the power-suppressed weak annihilation and hard-spectator scattering contributions following [40, 65]; the latter suffer from the same kind of endpoint divergence that we find in A_I , and they have been regularised by means of eq. (B.9).

B.4 $B \rightarrow X_s \ell^+ \ell^-$

The branching ratio for $B \rightarrow X_s \ell^+ \ell^-$, normalised by $B \rightarrow X_c \ell \nu$ and integrated between 1 and 6 GeV² can be written in the following manner:

$$\frac{d\mathcal{B}(\bar{B} \rightarrow X_s \ell^+ \ell^-)_{SM}}{d\hat{s}} = \mathcal{B}(B \rightarrow X_c e \bar{\nu}) \left| \frac{V_{ts}^* V_{tb}}{V_{cb}} \right|^2 \frac{4}{C} \frac{\Phi_{\ell\ell}(\hat{s})}{\Phi_u}, \quad \hat{s} = \frac{s}{m_{b,pole}^2} \quad (\text{B.21})$$

where

$$\frac{\Phi_{\ell\ell}(\hat{s})}{\Phi_u} = \sum_{i \leq j} \text{Re} \left[C_i^{\text{eff}}(\mu) C_j^{\text{eff}*}(\mu) \left(\sum_{A,B=7,9,10} M_i^A M_j^{B*} \tilde{S}_{AB} + \Delta H_{ij} \right) \right] \quad (\text{B.22})$$

and C has already been defined in eq. (B.2).

We were able to reproduce the central value and uncertainty of $B \rightarrow X_s \ell^+ \ell^-$, but also the dependence on $C_{7,8,9,10}$ at the scale μ_0 in eq. (12) of ref. [22] (apart from the linear term in $C_7(\mu_0)$ which is very sensitive to small changes in the input parameters).

We have modified the building blocks S following ref. [66] to include m_s corrections and contributions from chirality-flipped operators in the following way.¹³

- For the functions involving only $A, B = 7, 9, 10$, we modified the functions to include m_s -suppressed contributions to the phase space and to $O(\alpha_s^0)$ part.
- For the functions involving only $A, B = 7', 9', 10'$, we took the same expression as their unprimed counterparts, profiting from the fact that the expressions are symmetric with respect to the change $\gamma_5 \rightarrow -\gamma_5$.
- For the functions involving both a SM operator and a chirally-flipped one, we took the expressions from ref. [66], which include only $O(\alpha_s^0)$ contributions (contrary to the other functions that include also $O(\alpha_s)$ and $O(1/m_b^2)$ corrections).

$$S_{77} = S_{7'7'} = N \left(1 + \frac{2\hat{m}_\ell^2}{\hat{s}} \right) \left[-4\hat{s} - 4(1 + \hat{m}_s^2) + \frac{8(1 - \hat{m}_s^2)^2}{\hat{s}} + O(\alpha_s, 1/m_b^2) \right] \quad (\text{B.23})$$

$$S_{79} = S_{7'9'} = N \left(1 + \frac{2\hat{m}_\ell^2}{\hat{s}} \right) \cdot 12[1 - \hat{m}_s^2 - \hat{s} + O(\alpha_s, 1/m_b^2)] \quad (\text{B.24})$$

$$S_{99} = S_{9'9'} = N \left[1 + 2\hat{m}_\ell^2 - 2\hat{m}_s^2 + 2\hat{m}_\ell^2 \hat{m}_s^2 + \hat{m}_s^4 + \frac{2\hat{m}_\ell^2(1 - \hat{m}_s^2)^2}{\hat{s}} + (1 - 4\hat{m}_\ell^2 + \hat{m}_s^2)\hat{s} - 2\hat{s}^2 + O(\alpha_s, 1/m_b^2) \right] \quad (\text{B.25})$$

¹³We checked and agreed with the expressions in ref. [66], taking into account the fact that this reference uses a different definition of \mathcal{O}_7 and \mathcal{O}'_7 which mixes different chiralities, contrary to ours.

$$S_{1010} = S_{10'10'} = N \left[1 - 10\hat{m}_\ell^2 - 2\hat{m}_s^2 - 10\hat{m}_\ell^2\hat{m}_s^2 + \hat{m}_s^4 + \frac{2\hat{m}_\ell^2(1 - \hat{m}_s^2)^2}{\hat{s}} + (1 + 8\hat{m}_\ell^2 + \hat{m}_s^2)\hat{s} - 2\hat{s}^2 + O(\alpha_s, 1/m_b^2) \right] \quad (\text{B.26})$$

$$S_{77'} = N \left(1 + \frac{2\hat{m}_\ell^2}{\hat{s}} \right) (-48\hat{m}_s) \quad (\text{B.27})$$

$$S_{79'} = S_{7'9} = N \left(1 + \frac{2\hat{m}_\ell^2}{\hat{s}} \right) (-12\hat{m}_s)(1 - \hat{m}_s^2 + \hat{s}) \quad (\text{B.28})$$

$$S_{99'} = N(-12\hat{m}_s)(\hat{s} + 2\hat{m}_\ell^2) \quad (\text{B.29})$$

$$S_{1010'} = N(-12\hat{m}_s)(\hat{s} - 6\hat{m}_\ell^2) \quad (\text{B.30})$$

with the phase space factor

$$N = \sqrt{1 + \hat{s}^2 + \hat{m}_s^4 - 2\hat{s} - 2\hat{m}_s^2 - 2\hat{s}\hat{m}_s^2} \sqrt{1 - \frac{4\hat{m}_\ell^2}{\hat{s}}} \quad (\text{B.31})$$

For the quantities related to matrix elements M_i^A , we have taken the expressions of ref. [22] for the unprimed operators. The situation is much simpler for chirally-flipped operators since only three of them are to be considered:

$$M_i^{7'} = \tilde{\alpha}_s \kappa \delta_{i,7'}, \quad M_i^{9'} = (1 + \tilde{\alpha}_s \kappa f_9^{\text{pen}}(\hat{s})) \delta_{i,9'}, \quad M_i^{10'} = \delta_{i,10'}. \quad (\text{B.32})$$

The uncertainty attached to the central value in table 9 includes not only the uncertainties from the variation of the difference input parameters, but also a 5% error estimated in ref. [22] as the uncertainty from non-perturbative $1/m_b$ -suppressed contributions.

B.5 $\bar{B} \rightarrow \bar{K}^{*0} \ell^+ \ell^-$ observables

B.5.1 General considerations

The differential decay amplitude of the exclusive process $\bar{B}_d \rightarrow \bar{K}^{*0} \ell^+ \ell^-$, with $\bar{K}^{*0} \rightarrow K^- \pi^+$ on the mass shell, can be characterised completely in terms of the dilepton pair invariant mass q^2 , which is embedded in the so-called *angular coefficients*, and the three independent angles θ_l , θ_K and ϕ (see section 2.1 of [9]). These angular coefficients J_i are observable quantities that depend on kinematical parameters, real combinations of the six complex \bar{K}^{*0} spin amplitudes and the seventh transverse amplitude A_t (in the presence of scalars an extra amplitude is required [30]).

Within our framework, the spin amplitudes can be expressed in terms of the seven $B \rightarrow K^*$ form factors and the Wilson coefficients C_i of the weak effective Hamiltonian, that account for the short-distance interactions. Neglecting $O(\alpha_s)$ corrections and using the effective Wilson coefficient associated to \mathcal{O}_7 (which includes the contributions from the four-quark operators $\mathcal{O}_{1\dots 8}$), as well as the numerically relevant coefficients C_9 and C_{10}

associated to \mathcal{O}_9 and \mathcal{O}_{10} respectively, we find [9]:

$$A_{\perp}^{L,R} = N\sqrt{2}\lambda^{1/2} \left[\{(C_9 + C_{9'}) \mp (C_{10} + C_{10'})\} \frac{V(q^2)}{m_B + m_{K^*}} + \frac{2m_b}{q^2}(C_7^{\text{eff}} + C_{7'}^{\text{eff}})T_1(q^2) \right], \quad (\text{B.33})$$

$$A_{\parallel}^{L,R} = -N\sqrt{2}(m_B^2 - m_{K^*}^2) \left[\{(C_9 - C_{9'}) \mp (C_{10} - C_{10'})\} \frac{A_1(q^2)}{m_B - m_{K^*}} + \frac{2m_b}{q^2}(C_7^{\text{eff}} - C_{7'}^{\text{eff}})T_2(q^2) \right], \quad (\text{B.34})$$

$$A_0^{L,R} = -\frac{N}{2m_{K^*}\sqrt{q^2}} \left[\{(C_9 - C_{9'}) \mp (C_{10} - C_{10'})\} \cdot \left\{ (m_B^2 - m_{K^*}^2 - q^2)(m_B + m_{K^*})A_1(q^2) - \frac{\lambda A_2(q^2)}{m_B + m_{K^*}} \right\} + 2m_b(C_7^{\text{eff}} - C_{7'}^{\text{eff}}) \left\{ (m_B^2 + 3m_{K^*}^2 - q^2)T_2(q^2) - \frac{\lambda}{m_B^2 - m_{K^*}^2}T_3(q^2) \right\} \right], \quad (\text{B.35})$$

$$A_t = \frac{N\lambda^{1/2}}{\sqrt{q^2}} \left[2(C_{10} - C_{10'}) \right] A_0(q^2), \quad (\text{B.36})$$

where

$$\lambda = m_B^4 + m_{K^*}^4 + q^4 - 2(m_B^2 m_{K^*}^2 + m_{K^*}^2 q^2 + m_B^2 q^2), \quad (\text{B.37})$$

$$N = \sqrt{\frac{G_F^2 \alpha^2}{3 \cdot 2^{10} \pi^5 m_B^3} |V_{tb} V_{ts}^*|^2 q^2 \lambda^{1/2} \beta_{\mu}}, \quad (\text{B.38})$$

with

$$\beta_{\mu} = \sqrt{1 - \frac{4m_{\mu}^2}{q^2}}. \quad (\text{B.39})$$

We have introduced the Wilson coefficients corresponding to the chirally flipped operators $\mathcal{O}_{7'}$, $\mathcal{O}_{9'}$ and $\mathcal{O}_{10'}$, so we consider only NP contributions stemming from the SM-like operators and their chirally-flipped partners (i.e. we assume there are neither scalar/pseudoscalar nor tensor/pseudotensor operators at work).

B.5.2 Soft form factors

Concerning the $B \rightarrow K^*$ form factors, there are seven a priori independent hadronic form factors, encoding the non-perturbative long-distance interactions, that enter the $B \rightarrow K^*$ matrix elements, namely the vector current form factor $V(q^2)$, the three axial current form factors $A_0(q^2)$, $A_1(q^2)$, $A_2(q^2)$, the tensor form factor $T_1(q^2)$ and the pseudo-tensor form factors $T_2(q^2)$ and $T_3(q^2)$ [48]. Although there are several computations of these form factors in the literature (see for instance ref. [67]), we have chosen the parametrisation in appendix B.4 of ref. [64] to remain more conservative in the estimation of the uncertainties associated to the fitting coefficients that describe them. In the limit where the decaying hadron is heavy (as in B_d) and the recoiling meson acquires a large energy (E_{K^*}), the

form factors can be expanded in the small ratios Λ_{QCD}/m_b and $\Lambda_{\text{QCD}}/E_{K^*}$. Neglecting corrections of order Λ_{QCD}/m_b and α_s , the seven $B \rightarrow K^*$ form factors reduce to just two universal “soft” form factors ξ_{\perp} and ξ_{\parallel} [48, 68].

In this limit the K^* spin amplitudes and A_t acquire very simple forms which prove to be most useful to explain the symmetries between the fitting coefficients (F, G, H, I, J and K) of $\bar{B}_d \rightarrow \bar{K}^{*0} \ell^+ \ell^-$ observables given in sections 2.4 and 2.5 [21]

$$A_{\perp}^{L,R} = \sqrt{2} N m_B (1 - \hat{s}) \left[(C_9 + C_{9'}) \mp (C_{10} + C_{10'}) + \frac{2\hat{m}_b}{\hat{s}} (C_7^{\text{eff}} + C_{7'}^{\text{eff}}) \right] \xi_{\perp}(E_{K^*}), \quad (\text{B.40a})$$

$$A_{\parallel}^{L,R} = -\sqrt{2} N m_B (1 - \hat{s}) \left[(C_9 - C_{9'}) \mp (C_{10} - C_{10'}) + \frac{2\hat{m}_b}{\hat{s}} (C_7^{\text{eff}} - C_{7'}^{\text{eff}}) \right] \xi_{\perp}(E_{K^*}), \quad (\text{B.40b})$$

$$A_0^{L,R} = -\frac{N m_B}{2\hat{m}_{K^*} \sqrt{\hat{s}}} (1 - \hat{s})^2 \left[(C_9 - C_{9'}) \mp (C_{10} - C_{10'}) + 2\hat{m}_b (C_7^{\text{eff}} - C_{7'}^{\text{eff}}) \right] \xi_{\parallel}(E_{K^*}), \quad (\text{B.40c})$$

$$A_t = \frac{N m_B}{\hat{m}_{K^*} \sqrt{\hat{s}}} (1 - \hat{s})^2 \left[C_{10} - C_{10'} \right] \xi_{\parallel}(E_{K^*}), \quad (\text{B.40d})$$

with $\hat{s} = q^2/m_B^2$ and $\hat{m}_i = m_i/m_B$.

The QCDF framework allows us to calculate the α_s corrections to form factors and decay amplitudes up to the NLO [40, 48, 63] in a systematic way but, since we have no means of computing the $1/m_b$ -suppressed corrections, we decided to estimate them consistently using an ensemble method for the K^{*0} spin amplitudes; an exhaustive discussion of all these issues can be found in sections 2.2 and 2.3 of ref. [9].

However, since QCDF uses only soft form factors and not the full form factors, we are restricted to the kinematic region in which $E_{K^*} \sim m_b$ (or equivalently, $q^2 \ll m_B$). Moreover, the longitudinal spin amplitude displays a logarithmic divergence as $q^2 \rightarrow 0$, which signals the breakdown of QCDF for energies below 1 GeV². Further cuts are provided by the light (below 1 GeV²) and J/ψ (over 6 GeV²) resonances. Thus, we have confined the analysis of $A_T^{(2)}$, A_{FB} and F_L to the dilepton mass range, $1 \text{ GeV}^2 \leq q^2 \leq 6 \text{ GeV}^2$.

We obtain the soft form factors demanded by the QCDF framework [40, 63] from the full form factors $V(q^2)$, $A_1(q^2)$ and $A_2(q^2)$ [64] using [9, 18, 40, 59]

$$\begin{aligned} \xi_{\perp}(q^2) &= \frac{m_B}{m_B + m_{K^*}} V(q^2), \\ \xi_{\parallel}(q^2) &= \frac{m_B + m_{K^*}}{2E_{K^*}} A_1(q^2) - \frac{m_B - m_{K^*}}{m_B} A_2(q^2). \end{aligned} \quad (\text{B.41})$$

Our choice of ref. [64] with sizeable error bars compared to other possible determinations is guided by our aim to be conservative in our estimation of errors. Eq. (B.41), in particular, defines the value of the soft form factors at $q^2 = 0$ from the values of the full form factors taken from ref. [64].

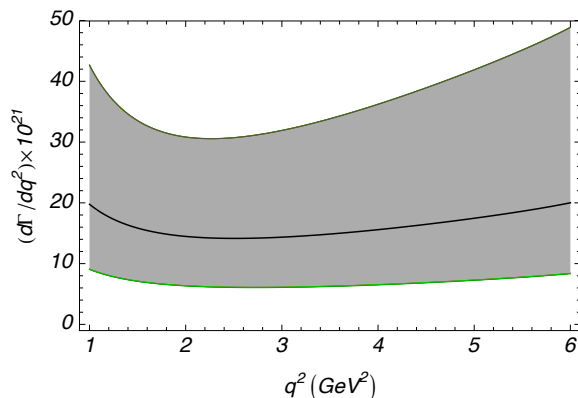


Figure 15: SM prediction for the differential decay distribution of $\bar{B}_d \rightarrow \bar{K}^{*0} \ell^+ \ell^-$ in the $1 - 6 \text{ GeV}^2$ energy range. The black line corresponds to the central value of $d\Gamma/dq^2$. The wide gray band corresponds to the uncertainties associated to $B \rightarrow K^*$ form factors (according to the parametrisation in appendix 4 of ref. [64]). Hadronic (orange) and Λ_{QCD}/m_b (green) uncertainty bands are barely visible. The central value compares well with figure 2 in ref. [30] (note that the CP-averaged differential decay distribution $d(\Gamma + \bar{\Gamma})/dq^2$ is plotted there, so their central value curve is twice ours).

B.5.3 The differential decay distribution and uniangular projections

The angular dependence of the $\bar{B}_d \rightarrow \bar{K}^{*0} \ell^+ \ell^-$ differential decay distribution can be integrated out yielding, in terms of the \bar{K}^{*0} spin amplitudes,

$$\begin{aligned} \frac{d\Gamma}{dq^2} = & \frac{1}{4} [(3 + \beta_\mu^2)(|A_\perp|^2 + |A_\parallel|^2 + |A_0|^2)] + \\ & + \frac{3m_\mu^2}{q^2} \left\{ |A_t|^2 + 2[\text{Re}(A_{\perp L} A_{\perp R}^*) + \text{Re}(A_{\parallel L} A_{\parallel R}^*) + \text{Re}(A_{0L} A_{0R}^*)] \right\} \quad (\text{B.42}) \end{aligned}$$

where we have defined $A_i A_j^* \equiv A_{iL} A_{jL}^* + A_{iR} A_{jR}^*$, with $i, j = 0, \perp, \parallel$.

The large uncertainties coming from the $B \rightarrow K^*$ form factors turn $d\Gamma/dq^2$ into a theoretically ill-controlled observable (as can be seen in figure 15). However, since it appears only in the denominator of A_{FB} and F_L , and the corresponding numerators display the same kind of uncertainties correlated to those in $d\Gamma/dq^2$, A_{FB} and F_L become much better behaved observables (see figures 16a and 16b, and refs. [9, 47] for an in-depth discussion of this issue). $A_T^{(2)}$, on the contrary, is essentially free from this problem.

As shown in refs. [9, 47], a full angular fit can be performed on $\bar{B}_d \rightarrow \bar{K}^{*0} \ell^+ \ell^+$ observables, but this will probably require more integrated luminosity than the one delivered by the end of the first run of LHC [47, 69, 70]. However, we can also integrate out two of the three angles of the K^* differential decay distribution to get three single-angle distributions,

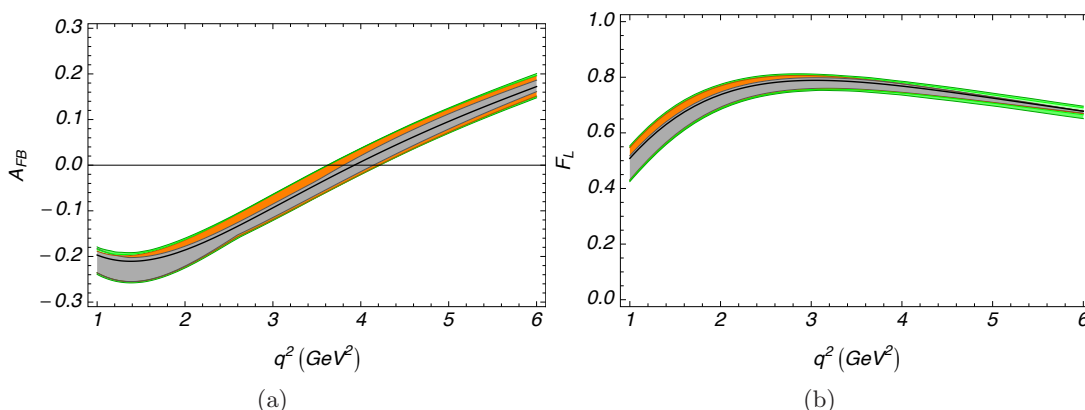


Figure 16: SM prediction for A_{FB} (left) and F_L (right) in the $1 - 6 \text{ GeV}^2$ energy range. The color scheme used for uncertainties is the same as in figure 15.

which, in the massless case¹⁴ read

$$\frac{1}{\Gamma'} \frac{d\Gamma'}{d\phi} = \frac{1}{2\pi} \left(1 + \frac{1}{2}(1 - F_L)A_T^{(2)} \cos 2\phi + A_{\text{im}} \sin 2\phi \right), \quad (\text{B.43a})$$

$$\frac{1}{\Gamma'} \frac{d\Gamma'}{d\theta_l} = \left(\frac{3}{4}F_L \sin^2 \theta_l + \frac{3}{8}(1 - F_L)(1 + \cos^2 \theta_l) + A_{\text{FB}} \cos \theta_l \right) \sin \theta_l, \quad (\text{B.43b})$$

$$\frac{1}{\Gamma'} \frac{d\Gamma'}{d\theta_K} = \frac{3}{4} \sin \theta_K (2F_L \cos^2 \theta_K + (1 - F_L) \sin^2 \theta_K), \quad (\text{B.43c})$$

where

$$\Gamma' \equiv \frac{d\Gamma}{dq^2} \quad \text{and} \quad A_{\text{im}} = \frac{\text{Im}(A_{\perp L} A_{\parallel L}^*) + \text{Im}(A_{\perp R} A_{\parallel R}^*)}{\frac{d\Gamma}{dq^2}}. \quad (\text{B.44})$$

Since A_{FB} , F_L and $A_T^{(2)}$ appear in all the expressions above, experimental data can be binned in q^2 and the corresponding fits performed on these bins. The value extracted from these fits is then a $\frac{d\Gamma}{dq^2}$ -weighted average of each parameter. Some strategies have already been devised to perform the binning in a way that allows to increase the statistics signal for some chosen observables [54, 70, 71].

B.5.4 $\bar{B}_d \rightarrow K^{*0} \ell^+ \ell^-$ observables at leading order in the large-recoil limit

This section is devoted to the analysis of the relations existing between the different fitting functions, namely eqs. (2.20), (2.21) and (2.22) for $A_T^{(2)}$, eqs. (2.39) and (2.40) for A_{FB} and eqs. (2.45) for F_L . The simple large recoil spin amplitudes in eqs. (B.40) will be used to account for the existence of these relations, allowing us to proceed as we did in section 6 of ref. [9]. The LO large-recoil expressions are sufficient to understand these symmetries, since NLO contributions do not break the pairing of the coefficients.

¹⁴Massive terms are suppressed by $m_\mu^2 \simeq 0.011 \text{ GeV}^2$ so that their impact in absence of possible large scalar/pseudoscalar or tensor/pseudotensor NP operators is negligible.

The following short-hand notation will be used

$$\begin{aligned}
 M_{\pm} &\equiv 12m_{\mu}^2 \pm q^2(3 + \beta_{\mu}^2), & F &\equiv \frac{2\hat{m}_b}{\hat{s}}, \\
 P_1 &\equiv \sqrt{2}Nm_B(1 - \hat{s}), & P_2 &\equiv \frac{1}{2\sqrt{2}\hat{m}_{K^*}\sqrt{\hat{s}}}(1 - \hat{s}),
 \end{aligned}$$

and

$$C_i \equiv C_i^{\text{SM}} + \delta C_i, \quad C_{i'} \equiv \delta C_{i'}. \quad (\text{B.45})$$

From the simplified expression of the spin amplitudes given earlier in appendix B.5.2 we obtain:

- $A_{\text{T}}^{(2)}$. Being built in terms of just A_{\perp} and A_{\parallel} , the LO behaviour of this observable can be readily understood (see ref. [9]).

$$A_{\text{T}}^{(2)} \Big|_{\text{LR}} = \frac{2[C_{10}C_{10'} + (C_9 + C_7F)(C_{9'} + C_{7'}F)]P_1^2 4\xi_{\perp}^2}{[C_{10}^2 + C_{10'}^2 + (C_9 + C_7F)^2 + (C_{9'} + C_{7'}F)^2]P_1^2 4\xi_{\perp}^2}, \quad (\text{B.46})$$

where LR stands for “large recoil”. Eq. (B.46) shows that, at LO, only the terms with primed coefficients ($\delta C_{j'}$) and cross terms like $\delta C_i \delta C_{j'}$ (with $i, j = 7, 9, 10$) might appear in the numerator of $A_{\text{T}}^{(2)}$. Neither those involving just unprimed coefficients (δC_i , with $i = 7, 9, 10$) nor products of same chirality operators ($\delta C_{i(\prime)} \delta C_{j(\prime)}$) are allowed, whereas in table 7, the latter are also present but they come from NLO corrections and are much smaller than the LO ones.¹⁵ Furthermore they are very suppressed by the corresponding NP terms in the denominator (see table 8). Since both primed and unprimed coefficients enter the full expression of $A_{\text{T}}^{(2)}$ at NLO in the same way, the relations on the first row of eqs. (2.20), (2.21) and (2.22) hold. The remaining relations can be checked trivially using eq. (B.46).

- $d\Gamma/dq^2$. The differential decay distribution appears in the denominator of both A_{FB} and F_{L} as a sum of $I_{(i,j)} \delta C_i \delta C_j$. At LO it can be expressed as

$$\begin{aligned}
 \left. \frac{d\Gamma}{dq^2} \right|_{\text{LR}} &= \frac{P_1^2}{2q^2} \left\{ M_+ \left[[(C_9 - C_{9'} + (C_7 - C_{7'})F\hat{s})^2 + (C_{10} - C_{10'})^2] P_2^2 \xi_{\parallel}^2 \right. \right. \\
 &\quad \left. \left. + [(C_9 - C_{9'} + (C_7 - C_{7'})F)^2 + 2(C_9 + C_7F)(C_{9'} + C_{7'}F)] 2\xi_{\perp}^2 \right] \right. \\
 &\quad \left. - M_- (C_{10}^2 + C_{10'}^2) 2\xi_{\perp}^2 \right\}.
 \end{aligned}$$

Although quite cumbersome, eq. (12) allows us to understand table 10, since all the coefficients there appear already at LO. In particular, we can check that the largest fitting coefficients ($I_{(0,7)}$ and $I_{(7,7)}$) are enhanced either by the square of the factor $F = (2m_b m_B)/q^2$ (which becomes very important in the low- q^2 region) or by $C_9^{\text{SM}} F$,

¹⁵The fitting coefficients of the terms forbidden at LO are at most 4% of those allowed.

whereas others are enhanced by F but suppressed by C_7^{SM} (like $I_{(0,9)}$ and $I_{(0,9')}$) and the remaining ones are not enhanced at all. Eq. (10) can be used also to verify the relations in eq. (2.40).

- A_{FB} . At LO and in the large recoil limit, the numerator of this observable has a structure given by

$$A_{\text{FB}} \Big|_{\text{LR}} = \frac{-6\beta_\mu P_1^2 [C_{10}(C_9 + C_7 F) - C_{10'}(C_{9'} + C_{7'} F)] \xi_\perp^2}{d\Gamma/dq^2}. \quad (\text{B.47})$$

All fitting coefficients in table 10 arise already at LO except for those that involve a primed coefficient, i.e. $(0, 7')$, $(0, 10')$ and $(7, 10')$. In the case of $I_{(0,7')}$, the effect of the enhancement factor F at low- q^2 explained above is particularly visible, while $I_{(7,10')}$, which also receives this enhancement, is suppressed by C_7^{SM} and $I_{(0,10')}$ is not enhanced at all.

Regarding eq. (2.39), the first and the second equalities are LO relations due to the antisymmetric behaviour of primed and unprimed coefficients in eq. (B.47), whereas the last one appears only at NLO but respects the same symmetry.

- F_L . The numerator of this F_L at LO and in the large recoil limit simplifies into

$$F_L \Big|_{\text{LR}} = \frac{2P_1^2 P_2^2 [(C_{10} - C_{10'})^2 + (C_9 - C_{9'} + (C_7 - C_{7'}) F \hat{s})^2] \xi_\parallel^2}{d\Gamma/dq^2}. \quad (\text{B.48})$$

Using eq. (B.45) we can expand the numerator of F_L into products of NP Wilson coefficients. This is enough to derive all relations in eq. (2.45) and to explain the enhancement of some fitting coefficients over others in the low- q^2 region.

Open Access. This article is distributed under the terms of the Creative Commons Attribution Noncommercial License which permits any noncommercial use, distribution, and reproduction in any medium, provided the original author(s) and source are credited.

References

- [1] A. Lenz et al., *Anatomy of new physics in $B - \bar{B}$ mixing*, *Phys. Rev. D* **83** (2011) 036004 [[arXiv:1008.1593](#)] [[SPIRES](#)].
- [2] E. Lunghi and A. Soni, *Possible evidence for the breakdown of the CKM-paradigm of CP-violation*, *Phys. Lett. B* **697** (2011) 323 [[arXiv:1010.6069](#)] [[SPIRES](#)].
- [3] UTFIT collaboration, A.J. Bevan et al., *Update of the unitarity triangle analysis*, *PoS ICHEP2010* (2010) 270 [[arXiv:1010.5089](#)] [[SPIRES](#)].
- [4] B. Bhattacharjee, A. Dighe, D. Ghosh and S. Raychaudhuri, *Do new data on $[B^+ \rightarrow \tau^+ \nu_\tau]$ decays point to an early discovery of supersymmetry at the LHC?*, *Phys. Rev. D* **83** (2011) 094026 [[arXiv:1012.1052](#)] [[SPIRES](#)].
- [5] A. Dighe, D. Ghosh, A. Kundu and S.K. Patra, *Reconciling anomalous measurements in $B_s - \bar{B}_s$ mixing: the role of CPT-conserving and CPT-violating new physics*, [[arXiv:1105.0970](#)] [[SPIRES](#)].

- [6] BELLE collaboration, J.T. Wei et al., *Measurement of the differential branching fraction and forward-backward asymmetry for $B \rightarrow K^* \ell^+ \ell^-$* , *Phys. Rev. Lett.* **103** (2009) 171801 [[arXiv:0904.0770](#)] [[SPIRES](#)].
- [7] P. Gambino, U. Haisch and M. Misiak, *Determining the sign of the $b \rightarrow s \gamma$ amplitude*, *Phys. Rev. Lett.* **94** (2005) 061803 [[hep-ph/0410155](#)] [[SPIRES](#)].
- [8] A.K. Alok et al., *New-physics contributions to the forward-backward asymmetry in $B \rightarrow K^* \mu^+ \mu^-$* , *JHEP* **02** (2010) 053 [[arXiv:0912.1382](#)] [[SPIRES](#)].
- [9] U. Egede, T. Hurth, J. Matias, M. Ramon and W. Reece, *New physics reach of the decay mode $\bar{B} \rightarrow \bar{K}^{*0} \ell^+ \ell^-$* , *JHEP* **10** (2010) 056 [[arXiv:1005.0571](#)] [[SPIRES](#)].
- [10] J.C. Pati and A. Salam, *Are there anomalous lepton-hadron interactions?*, *Phys. Rev. Lett.* **32** (1974) 1083 [[SPIRES](#)].
- [11] R.N. Mohapatra and J.C. Pati, *A natural left-right symmetry*, *Phys. Rev. D* **11** (1975) 2558 [[SPIRES](#)].
- [12] R.N. Mohapatra and J.C. Pati, *Left-right gauge symmetry and an isoconjugate model of CP-violation*, *Phys. Rev. D* **11** (1975) 566 [[SPIRES](#)].
- [13] V. Bernard, M. Oertel, E. Passemar and J. Stern, *$K_L(\mu_3)$ decay: a stringent test of right-handed quark currents*, *Phys. Lett. B* **638** (2006) 480 [[hep-ph/0603202](#)] [[SPIRES](#)].
- [14] V. Bernard, M. Oertel, E. Passemar and J. Stern, *Tests of non-standard electroweak couplings of right-handed quarks*, *JHEP* **01** (2008) 015 [[arXiv:0707.4194](#)] [[SPIRES](#)].
- [15] A. Crivellin, *Effects of right-handed charged currents on the determinations of $|V_{ub}|$ and $|V_{cb}|$* , *Phys. Rev. D* **81** (2010) 031301 [[arXiv:0907.2461](#)] [[SPIRES](#)].
- [16] A.J. Buras, K. Gemmler and G. Isidori, *Quark flavour mixing with right-handed currents: an effective theory approach*, *Nucl. Phys. B* **843** (2011) 107 [[arXiv:1007.1993](#)] [[SPIRES](#)].
- [17] A.K. Alok et al., *New physics in $b \rightarrow s \mu^+ \mu^-$: CP-violating observables*, [arXiv:1103.5344](#) [[SPIRES](#)].
- [18] C. Bobeth, G. Hiller and G. Piranishvili, *CP asymmetries in $\bar{B} \rightarrow \bar{K}^*(\rightarrow \bar{K} \pi) \bar{\ell} \ell$ and untagged $\bar{B}_s, B_s \rightarrow \phi(\rightarrow K^+ K^-) \bar{\ell} \ell$ decays at NLO*, *JHEP* **07** (2008) 106 [[arXiv:0805.2525](#)] [[SPIRES](#)].
- [19] M. Misiak et al., *The first estimate of $B(\bar{B} \rightarrow X_s \gamma)$ at $O(\alpha_s^2)$* , *Phys. Rev. Lett.* **98** (2007) 022002 [[hep-ph/0609232](#)] [[SPIRES](#)].
- [20] E. Lunghi and J. Matias, *Huge right-handed current effects in $B \rightarrow K^*(K \pi) \ell^+ \ell^-$ in supersymmetry*, *JHEP* **04** (2007) 058 [[hep-ph/0612166](#)] [[SPIRES](#)].
- [21] F. Krüger and J. Matias, *Probing new physics via the transverse amplitudes of $B_0 \rightarrow K^{*0}(\rightarrow K^- \pi^+) \ell^+ \ell^-$ at large recoil*, *Phys. Rev. D* **71** (2005) 094009 [[hep-ph/0502060](#)] [[SPIRES](#)].
- [22] T. Huber, E. Lunghi, M. Misiak and D. Wyler, *Electromagnetic logarithms in $\bar{B} \rightarrow X_s \ell^+ \ell^-$* , *Nucl. Phys. B* **740** (2006) 105 [[hep-ph/0512066](#)] [[SPIRES](#)].
- [23] P. Gambino, M. Gorbahn and U. Haisch, *Anomalous dimension matrix for radiative and rare semileptonic B decays up to three loops*, *Nucl. Phys. B* **673** (2003) 238 [[hep-ph/0306079](#)] [[SPIRES](#)].
- [24] M. Gorbahn and U. Haisch, *Effective Hamiltonian for non-leptonic $|\Delta(F)| = 1$ decays at NNLO in QCD*, *Nucl. Phys. B* **713** (2005) 291 [[hep-ph/0411071](#)] [[SPIRES](#)].

- [25] C. Bobeth, P. Gambino, M. Gorbahn and U. Haisch, *Complete NNLO QCD analysis of $\bar{B} \rightarrow X_s \ell^+ \ell^-$ and higher order electroweak effects*, *JHEP* **04** (2004) 071 [[hep-ph/0312090](#)] [[SPIRES](#)].
- [26] K.G. Chetyrkin, M. Misiak and M. Münz, *Weak radiative B-meson decay beyond leading logarithms*, *Phys. Lett. B* **400** (1997) 206 [Erratum-ibid. **B 425** (1998) 414] [[hep-ph/9612313](#)] [[SPIRES](#)].
- [27] PARTICLE DATA GROUP collaboration, K. Nakamura et al., *Review of particle physics*, *J. Phys. G* **37** (2010) 075021 [[SPIRES](#)].
- [28] J. Alcaraz, *Precision electroweak measurements and constraints on the standard model*, [arXiv:0911.2604](#) [[SPIRES](#)].
- [29] CKMFITTER GROUP collaboration, J. Charles et al., *CP violation and the CKM matrix: assessing the impact of the asymmetric B factories*, *Eur. Phys. J. C* **41** (2005) 1 [[hep-ph/0406184](#)] [[SPIRES](#)].
- [30] W. Altmannshofer et al., *Symmetries and asymmetries of $B \rightarrow K^* \mu^+ \mu^-$ decays in the standard model and beyond*, *JHEP* **01** (2009) 019 [[arXiv:0811.1214](#)] [[SPIRES](#)].
- [31] A.L. Kagan and M. Neubert, *Isospin breaking in $B \rightarrow K^* \gamma$ decays*, *Phys. Lett. B* **539** (2002) 227 [[hep-ph/0110078](#)] [[SPIRES](#)].
- [32] HEAVY FLAVOR AVERAGING GROUP collaboration, D. Asner et al., *Averages of b-hadron, c-hadron and τ -lepton properties*, [arXiv:1010.1589](#) [[SPIRES](#)].
- [33] THE LHCb collaboration, R. Aaij et al., *Search for the rare decays $B_s \rightarrow \mu\mu$ and $B_d \rightarrow \mu\mu$* , *Phys. Lett. B* **699** (2011) 330 [[arXiv:1103.2465](#)] [[SPIRES](#)].
- [34] A. Freitas and U. Haisch, *$\bar{B} \rightarrow X_s \gamma$ in two universal extra dimensions*, *Phys. Rev. D* **77** (2008) 093008 [[arXiv:0801.4346](#)] [[SPIRES](#)].
- [35] M. Misiak and M. Steinhauser, *NNLO QCD corrections to the $B \rightarrow X_s \gamma$ matrix elements using interpolation in m_c* , *Nucl. Phys. B* **764** (2007) 62 [[hep-ph/0609241](#)] [[SPIRES](#)].
- [36] M. Misiak and M. Steinhauser, *Large- m_c asymptotic behaviour of $O(\alpha_s^2)$ corrections to $B \rightarrow X_s \gamma$* , *Nucl. Phys. B* **840** (2010) 271 [[arXiv:1005.1173](#)] [[SPIRES](#)].
- [37] BABAR collaboration, B. Aubert et al., *Measurement of branching fractions and CP and isospin asymmetries in $B \rightarrow K^*(892)\gamma$ decays*, *Phys. Rev. Lett.* **103** (2009) 211802 [[arXiv:0906.2177](#)] [[SPIRES](#)].
- [38] BELLE collaboration, M. Nakao et al., *Measurement of the $B \rightarrow K^* \gamma$ branching fractions and asymmetries*, *Phys. Rev. D* **69** (2004) 112001 [[hep-ex/0402042](#)] [[SPIRES](#)].
- [39] T. Feldmann and J. Matias, *Forward-backward and isospin asymmetry for $B \rightarrow K^* \ell^+ \ell^-$ decay in the standard model and in supersymmetry*, *JHEP* **01** (2003) 074 [[hep-ph/0212158](#)] [[SPIRES](#)].
- [40] M. Beneke, T. Feldmann and D. Seidel, *Exclusive radiative and electroweak $b \rightarrow d$ and $b \rightarrow s$ penguin decays at NLO*, *Eur. Phys. J. C* **41** (2005) 173 [[hep-ph/0412400](#)] [[SPIRES](#)].
- [41] B. Grinstein, Y. Grossman, Z. Ligeti and D. Pirjol, *The photon polarization in $B \rightarrow X \gamma$ in the standard model*, *Phys. Rev. D* **71** (2005) 011504 [[hep-ph/0412019](#)] [[SPIRES](#)].
- [42] B. Grinstein and D. Pirjol, *The CP asymmetry in $B_0(t) \rightarrow K_S \pi_0 \gamma$ in the standard model*, *Phys. Rev. D* **73** (2006) 014013 [[hep-ph/0510104](#)] [[SPIRES](#)].

- [43] P. Ball and R. Zwicky, *Time-dependent CP asymmetry in $B \rightarrow K^*\gamma$ as a (quasi) null test of the standard model*, *Phys. Lett. B* **642** (2006) 478 [[hep-ph/0609037](#)] [[SPIRES](#)].
- [44] P. Ball, G.W. Jones and R. Zwicky, *$B \rightarrow V\gamma$ beyond QCD factorisation*, *Phys. Rev. D* **75** (2007) 054004 [[hep-ph/0612081](#)] [[SPIRES](#)].
- [45] BELLE collaboration, Y. Ushiroda et al., *Time-dependent CP asymmetries in $B_0 \rightarrow K_0(S)\pi_0\gamma$ transitions*, *Phys. Rev. D* **74** (2006) 111104 [[hep-ex/0608017](#)] [[SPIRES](#)].
- [46] BABAR collaboration, B. Aubert et al., *Measurement of time-dependent CP asymmetry in $B_0 \rightarrow K_0(S)\pi_0\gamma$ decays*, *Phys. Rev. D* **78** (2008) 071102 [[arXiv:0807.3103](#)] [[SPIRES](#)].
- [47] U. Egede, T. Hurth, J. Matias, M. Ramon and W. Reece, *New observables in the decay mode $\bar{B} \rightarrow \bar{K}^{*0}\ell^+\ell^-$* , *JHEP* **11** (2008) 032 [[arXiv:0807.2589](#)] [[SPIRES](#)].
- [48] M. Beneke and T. Feldmann, *Symmetry-breaking corrections to heavy-to-light B meson form factors at large recoil*, *Nucl. Phys. B* **592** (2001) 3 [[hep-ph/0008255](#)] [[SPIRES](#)].
- [49] A. Ghinculov, T. Hurth, G. Isidori and Y.P. Yao, *New NNLL QCD results on the decay $B \rightarrow X_s\ell^+\ell^-$* , *Eur. Phys. J. C* **33** (2004) s288 [[hep-ph/0310187](#)] [[SPIRES](#)].
- [50] M. Neubert, *On the inclusive determination of $|V_{ub}|$ from the lepton invariant mass spectrum*, *JHEP* **07** (2000) 022 [[hep-ph/0006068](#)] [[SPIRES](#)].
- [51] C.W. Bauer, Z. Ligeti and M.E. Luke, *Precision determination of $|V_{ub}|$ from inclusive decays*, *Phys. Rev. D* **64** (2001) 113004 [[hep-ph/0107074](#)] [[SPIRES](#)].
- [52] T. Huber, T. Hurth and E. Lunghi, *Logarithmically enhanced corrections to the decay rate and forward backward asymmetry in $\bar{B} \rightarrow X_s\ell^+\ell^-$* , *Nucl. Phys. B* **802** (2008) 40 [[arXiv:0712.3009](#)] [[SPIRES](#)].
- [53] CDF collaboration, T. Aaltonen et al., *Measurement of the forward-backward asymmetry in the $B \rightarrow K^*\mu^+\mu^-$ decay and first observation of the $B_s \rightarrow \phi\mu^+\mu^-$ decay*, *Phys. Rev. Lett.* **106** (2011) 161801 [[arXiv:1101.1028](#)] [[SPIRES](#)].
- [54] A.K. Alok et al., *New physics in $b \rightarrow s\mu^+\mu^-$: CP-conserving observables*, [arXiv:1008.2367](#) [[SPIRES](#)].
- [55] U. Egede, T. Hurth, J. Matias, M. Ramon and W. Reece, *The exclusive $B \rightarrow K^*(\rightarrow K\pi)\ell^+\ell^-$ decay: CP conserving observables*, *Acta Phys. Polon. B* **3** (2010) 151 [[arXiv:0912.1339](#)] [[SPIRES](#)].
- [56] U. Egede, T. Hurth, J. Matias, M. Ramon and W. Reece, *Symmetries in the angular distribution of exclusive semileptonic B decays*, *PoS ICHEP2010* (2010) 245 [[arXiv:1012.4603](#)] [[SPIRES](#)].
- [57] T. Hurth, G. Isidori, J.F. Kamenik and F. Mescia, *Constraints on new physics in MFV models: a model-independent analysis of $\Delta F = 1$ processes*, *Nucl. Phys. B* **808** (2009) 326 [[arXiv:0807.5039](#)] [[SPIRES](#)].
- [58] O. Deschamps et al., *The two Higgs doublet of type II facing flavour physics data*, *Phys. Rev. D* **82** (2010) 073012 [[arXiv:0907.5135](#)] [[SPIRES](#)].
- [59] C. Bobeth, G. Hiller and D. van Dyk, *The benefits of $B \rightarrow K^*\ell^+\ell^-$ decays at low recoil*, *JHEP* **07** (2010) 098 [[arXiv:1006.5013](#)] [[SPIRES](#)].
- [60] K.G. Chetyrkin, *Quark mass anomalous dimension to $O(\alpha_s^4)$* , *Phys. Lett. B* **404** (1997) 161 [[hep-ph/9703278](#)] [[SPIRES](#)].

- [61] C.W. Bauer, Z. Ligeti, M. Luke, A.V. Manohar and M. Trott, *Global analysis of inclusive B decays*, *Phys. Rev. D* **70** (2004) 094017 [[hep-ph/0408002](#)] [[SPIRES](#)].
- [62] A.H. Hoang, *Bottom quark mass from Upsilon mesons: Charm mass effects*, [hep-ph/0008102](#) [[SPIRES](#)].
- [63] M. Beneke, T. Feldmann and D. Seidel, *Systematic approach to exclusive $B \rightarrow V\ell^+\ell^-$, $V\gamma$ decays*, *Nucl. Phys. B* **612** (2001) 25 [[hep-ph/0106067](#)] [[SPIRES](#)].
- [64] A. Khodjamirian, T. Mannel, A.A. Pivovarov and Y.M. Wang, *Charm-loop effect in $B \rightarrow K^{(*)}\ell^+\ell^-$ and $B \rightarrow K^*\gamma$* , *JHEP* **09** (2010) 089 [[arXiv:1006.4945](#)] [[SPIRES](#)].
- [65] D. Seidel, *Analytic two-loop virtual corrections to $b \rightarrow d \ell^+\ell^-$* , *Phys. Rev. D* **70** (2004) 094038 [[hep-ph/0403185](#)] [[SPIRES](#)].
- [66] D. Guetta and E. Nardi, *Searching for new physics in rare $B \rightarrow \tau$ decays*, *Phys. Rev. D* **58** (1998) 012001 [[hep-ph/9707371](#)] [[SPIRES](#)].
- [67] P. Ball and R. Zwicky, *$B_{d,s} \rightarrow \rho, \omega, K^*, \phi$ decay form factors from light-cone sum rules revisited*, *Phys. Rev. D* **71** (2005) 014029 [[hep-ph/0412079](#)] [[SPIRES](#)].
- [68] J. Charles, A. Le Yaouanc, L. Oliver, O. Pene and J.C. Raynal, *Heavy-to-light form factors in the heavy mass to large energy limit of QCD*, *Phys. Rev. D* **60** (1999) 014001 [[hep-ph/9812358](#)] [[SPIRES](#)].
- [69] U. Egede, *Angular correlations in the $\bar{B}_d \rightarrow \bar{K}^{*0}\ell^+\ell^+$ decay*, CERN-LHCB-2007-057 [[SPIRES](#)].
- [70] A. Bharucha and W. Reece, *Constraining new physics with $B \rightarrow K^*\mu^+\mu^-$ in the early LHC era*, *Eur. Phys. J. C* **69** (2010) 623 [[arXiv:1002.4310](#)] [[SPIRES](#)].
- [71] E. Lunghi and A. Soni, *An improved observable for the forward-backward asymmetry in $B \rightarrow K^*\ell^+\ell^-$ and $B_s \rightarrow \phi\ell^+\ell^-$* , *JHEP* **11** (2010) 121 [[arXiv:1007.4015](#)] [[SPIRES](#)].

Complete anatomy of $\bar{B}_d \rightarrow \bar{K}^{*0}(\rightarrow K\pi)\ell^+\ell^-$ and its angular distribution

J. Matias,^a F. Mescia,^b M. Ramon^a and J. Virto^a

^a *Universitat Autònoma de Barcelona,
08193 Bellaterra, Barcelona, Spain*

^b *Departament d'Estructura i Constituents de la Matèria and
Institut de Ciències del Cosmos (ICCUB), Universitat de Barcelona,
08028 Barcelona, Spain*

E-mail: matias@ifae.es, mescia@ub.edu, mramon@ifae.es,
javier.virto@uab.cat

ABSTRACT: We present a complete and optimal set of observables for the exclusive 4-body \bar{B} meson decay $\bar{B}_d \rightarrow \bar{K}^{*0}(\rightarrow K\pi)\ell^+\ell^-$ in the low dilepton mass region, that contains a maximal number of clean observables. This basis of observables is built in a systematic way. We show that all the previously defined observables and any observable that one can construct, can be expressed as a function of this basis. This set of observables contains all the information that can be extracted from the angular distribution in the cleanest possible way. We provide explicit expressions for the full and the uniaxial distributions in terms of this basis. The conclusions presented here can be easily extended to the large- q^2 region. We study the sensitivity of the observables to right-handed currents and scalars. Finally, we present for the first time all the symmetries of the full distribution including massive terms and scalar contributions.

KEYWORDS: Rare Decays, Beyond Standard Model, B-Physics

ARXIV EPRINT: [1202.4266](https://arxiv.org/abs/1202.4266)

Contents

1	Introduction	1
2	Symmetries of the angular distribution	5
3	Observables for massless leptons	7
4	Observables in the massive case	10
5	Inclusion of scalar operators	12
6	Uniangular distributions	13
7	New physics sensitivity of the observables	14
	7.1 SM contribution and hadronic uncertainties	15
	7.2 New Physics	15
8	Summary of results	21
A	Symmetry formalism	22
	A.1 Symmetries of the massless distribution	23
	A.1.1 Solution to the massless distribution	24
	A.2 Symmetries of the massive distribution	25
	A.3 Symmetries in the presence of scalar contributions	28
B	Large recoil limit expressions	32

1 Introduction

The rare decay $\bar{B}_d \rightarrow \bar{K}^{*0}(\rightarrow K\pi)\ell^+\ell^-$ provides unique opportunities in the search for New Physics in flavor physics due to the wealth and variety of angular observables available experimentally. A total of 12 different angular coefficients characterize its angular distribution, each being a function of the invariant squared mass of the lepton pair, q^2 . Although a full angular analysis with a small q^2 binning requires a good deal of statistics, it constitutes a conceivable goal for LHCb, at least in its upgraded form.

First data on the decay rate and several angular observables are already available from BABAR, Belle, CDF and LHCb. BABAR [1] has measured the decay rate, the forward-backward asymmetry A_{FB} and the K^* longitudinal polarization fraction F_L , all integrated separately in the low and high- q^2 regions. Concerning q^2 -dependent measurements, Belle [2] has provided a measurement of the total branching ratio and A_{FB} , while CDF [3, 4] has

provided also measurements of F_L as well as the observables $A_T^{(2)}$ and A_{im} (see [5, 6]), with a measurement of the q^2 dependence in the form of 3 bins in the low- q^2 region (below the J/ψ resonance), a bin between the J/ψ and ψ' resonances, and two bins in the high- q^2 region (above the ψ'). The LHCb collaboration has also provided measurements of the branching ratio, A_{FB} and F_L based on $\sim 300 \text{ pb}^{-1}$ of data [7], while a larger data set of 1 fb^{-1} is on tape. In order to cope with limited statistics, near future plans focus on fully integrated observables, where the q^2 dependence is lost, at least within the low- and high- q^2 regions.

On the theoretical side, the interest is focused on the tayloring of observables with desired properties. These properties are: 1) a reduced hadronic uncertainty, and 2) an enhanced sensitivity to short distance contributions from New Physics (e.g. right handed currents, etc). Concerning hadronic uncertainties, the objective is to minimize the dependence on the soft form factors, which are difficult to compute and are the source of large theoretical uncertainties. This is achieved with the construction of ratios of angular observables where a complete LO cancellation of the form factors occurs. The search for observables with such desired properties has led to the formulation of a set of observables called $A_T^{(2)}$ [5], $A_T^{(3,4,5)}$ [6, 8] and $A_T^{(\text{re,im})}$ [9] at low- q^2 , and an analogous set $H_T^{(1,2,3,4,5)}$ [10] at high- q^2 . These observables have been studied in detail and they indeed exhibit a low theoretical uncertainty and a clean sensitivity to characteristic New Physics features.¹

The source of experimental input is the differential decay distribution of the 4-body final state $\bar{K}^{*0}(\rightarrow K\pi)\ell^+\ell^-$. It is described by four independent kinematic variables, which are traditionally chosen to be: the invariant squared mass q^2 of the lepton pair; the angle θ_K between the directions of flight of the kaon and the \bar{B} meson in the rest frame of the \bar{K}^{*0} ; the angle θ_l between the directions of flight of the ℓ^- and the \bar{B} meson in the dilepton rest frame; and the azimuthal angle ϕ between the two planes defined by the lepton pair and the $K\pi$ system.² In terms of these kinematic variables, the differential decay distribution can be written as

$$\begin{aligned} \frac{d^4\Gamma}{dq^2 d\cos\theta_K d\cos\theta_l d\phi} = \frac{9}{32\pi} & \left[J_{1s} \sin^2\theta_K + J_{1c} \cos^2\theta_K + (J_{2s} \sin^2\theta_K + J_{2c} \cos^2\theta_K) \cos 2\theta_l \right. \\ & + J_3 \sin^2\theta_K \sin^2\theta_l \cos 2\phi + J_4 \sin 2\theta_K \sin 2\theta_l \cos \phi + J_5 \sin 2\theta_K \sin \theta_l \cos \phi \\ & + (J_{6s} \sin^2\theta_K + J_{6c} \cos^2\theta_K) \cos \theta_l + J_7 \sin 2\theta_K \sin \theta_l \sin \phi + J_8 \sin 2\theta_K \sin 2\theta_l \sin \phi \\ & \left. + J_9 \sin^2\theta_K \sin^2\theta_l \sin 2\phi \right], \end{aligned} \tag{1.1}$$

The explicit dependence of the coefficients $J_i(q^2)$ in terms of transversity amplitudes (A_i) is given in section 2. The point to emphasize here is that only observables that respect the symmetries of this angular distribution can be obtained. These symmetries³ are transfor-

¹For a representative set of references discussing the phenomenology of this decay mode see [11–20].

²This definition of the kinematic variables coincides exactly with that of refs. [10, 21]

³Even if the term ‘symmetry’ usually denotes an invariance of the Lagrangian, in the present paper and following ref. [8], it refers to an invariance of the angular distribution under a rotation in the space of spin amplitudes.

mations among the transversity amplitudes that leave invariant the coefficients $J_i(q^2)$ of the angular distribution [8]. The number of amplitudes and the number of such symmetries determine precisely the number of degrees of freedom that are available from an angular analysis alone. This number is given by [8]

$$n_{\text{exp}} = 2n_A - n_s, \tag{1.2}$$

where n_{exp} denotes the number of experimental degrees of freedom, n_A is the number of transversity amplitudes A_j ($j = 1, \dots, n_A$) and n_s is the number of continuous transformations (or symmetries) of the A 's that leave the J 's invariant.

The number n_s of continuous symmetries can be obtained by inspection of the set of infinitesimal transformations of the A 's, by the method described in ref. [8]. In this way, one can infer the true number of independent experimental degrees of freedom n_{exp} . If the number n_J of coefficients J_i is larger than n_{exp} , then the J_i are not independent observables, and a set of $(n_J - n_{\text{exp}})$ relations must exist between them. As shown in ref. [8], there are exactly 8 independent J 's (and consequently 8 independent observables) in the case of massless leptons, and 10 considering the mass terms –not including the CP-conjugated mode–. Adding scalar contributions increases these numbers to 9 (with massless leptons) and 12 including masses. The conclusion is that there is a definite number of independent experimental observables that can be extracted from the angular analysis, and this number n_{exp} is known from symmetry arguments. From a pragmatic standpoint, the symmetry formalism can be substituted by this set of n_{exp} independent observables.⁴ This set of n_{exp} independent observables can be considered complete, in the sense that any additional observable can be expressed as a function of the observables in this set. Such a complete non-redundant set may be conveniently called a *basis*.

In this context, the natural question is what is the best choice for the observables in the basis. The answer is not different from before: these observables should satisfy the desired properties of reduced hadronic uncertainty and good sensitivity to New Physics. The observables $A_T^{(2,3,4,5)}$, $A_T^{(\text{re,im})}$, $H_T^{(1,2,3,4,5)}$ proposed in refs. [5, 6, 8–10] are excellent candidates, since they were designed to satisfy these requirements. The question is whether this set of observables contains a basis, or if other observables must be introduced.

The purpose of this paper is to give an answer to this issue and to construct, in a systematic way, an optimal basis of observables related to the angular distribution of the decay $\bar{B}_d \rightarrow \bar{K}^{*0}(\rightarrow K^+\pi^-)\ell^+\ell^-$, including lepton masses and scalar contributions (and valid in the presence of tensor operators). We do not consider in this paper the CP-conjugated mode nor the corresponding CP asymmetries. Anticipating some of the results of the paper, we shall see that:

1. The optimal basis contains two types of observables: observables with LO dependence on the soft form factors (Form Factor Dependent (FFD) observables) and observables free from this dependence at LO (Form Factor Independent (FFI) observables). The

⁴Still, we will use the symmetries at some points to furnish more formal proofs of certain aspects of the approach. Also, the symmetry formalism can be used, for instance, to obtain explicit expressions of the transversity amplitudes in terms of the coefficients J_i .

FFD observables suffer from large hadronic uncertainties due to the poorly known soft form factors. For this reason, the goal is to maximize the number of FFI observables in our basis. Examples of FFD observables are $J_i(q^2)$, F_L or A_{im} . We will choose as FFD observables for our basis the differential rate $d\Gamma/dq^2$ and the forward-backward asymmetry A_{FB} , although other choices are also possible.

2. In the case of massless leptons, the optimal basis according to the previous counting, must contain 8 independent observables: two FFD observables ($d\Gamma/dq^2$ and A_{FB}) and six clean FFI observables. Examples of FFI observables are $A_T^{(2,3,4,5)}$, $A_T^{(\text{re,im})}$ or $H_T^{(1,2,3,4,5)}$. FFI observables can be constructed in a systematic way as we will show in section 3, leading to a set of observables $P_{1,2,3,4,5,6}$, which we call *primary observables*. $P_{1,2,3,4,5}$ are directly related to all already known observables, but P_6 is new, and it is necessary for obtaining full information from the angular distribution.
3. In the massive lepton case, the basis must contain 10 observables (2 FFD and 8 FFI). Eight of those observables are $d\Gamma/dq^2$, A_{FB} and P_i with $i=1\dots 6$. The two remaining FFI observables, which vanish in the massless limit, will be called M_1 and M_2 and have never been considered before.
4. In the scalar case with massive leptons the counting of symmetries establishes the existence of 12 independent observables. The full set of observables is composed by the two FFD $d\Gamma/dq^2$ and A_{FB} together with 10 FFI $P_{1,2,3,4,5,6}$, M_1 , M_2 , S_1 and S_2 . The two new observables S_1 and S_2 vanish in the absence of scalar contributions.
5. Any conceivable FFD observable can be written as a function of $d\Gamma/dq^2$, A_{FB} , P_i, M_i and S_i , but most importantly, any conceivable theoretically clean (FFI) observable can be written as a function of the P_i , M_i and S_i alone. At the same time, each of these observables contains unique information. It is in this sense that the basis is optimal and complete.

The structure of the paper is the following. In section 2 we briefly review the symmetry formalism for the angular distribution of $\bar{B}_d \rightarrow \bar{K}^{*0}(\rightarrow K\pi)\ell^+\ell^-$. In section 3 we build the basis of observables in the massless case, and show how the full set of observables that have been considered in the literature can be recovered from this basis. We shall keep mass effects at this stage to make the generalization in section 4 most straightforward. After presenting the generalization to the massive case, and introducing the massive observables, we write the full angular distribution in terms of the observables in the basis.

In section 5 we include the effect of scalar operators, and show how the previous results are modified. In particular, we introduce two extra observables, S_1 and S_2 , that vanish in the absence of scalar contributions. In section 6 we present the most general expressions for the three uniaxial distributions in terms of the observables in the basis.

In section 7 we study the New Physics sensitivity of the proposed observables. For that purpose we study the SM contribution including NLO effects using QCD Factorization, hadronic uncertainties and an estimate of Λ/m_b corrections. We also consider how the SM expectations are modified in several NP scenarios. We analyze the position of the zeroes

of the observables as well as those NP scenarios that affect most strongly each of the observables.

In section 8 we summarize the relevant results of the paper. Finally, the core of the mathematical machinery related to the symmetry formalism, including constructive proofs of existence of the continuous symmetries has been collected in appendix A. This appendix contains the explicit form of the symmetry transformations among the amplitudes in the massless (appendix A.1), the massive (appendix A.2) and scalar case (appendix A.3). In appendix B we present the building blocks of the observables in the large recoil limit.

2 Symmetries of the angular distribution

The coefficients of the distribution given in eq. (1.1) can be written in terms of transversity amplitudes. In the massless case there are six such complex amplitudes: $A_0^{R,L}$, $A_{\parallel}^{R,L}$ and $A_{\perp}^{R,L}$. An additional complex amplitude A_t is required in the massive case, and in the presence of scalar contributions a new amplitude A_S must be included. The expressions for these coefficients read,

$$\begin{aligned}
 J_{1s} &= \frac{(2 + \beta_{\ell}^2)}{4} \left[|A_{\perp}^L|^2 + |A_{\parallel}^L|^2 + |A_{\perp}^R|^2 + |A_{\parallel}^R|^2 \right] + \frac{4m_{\ell}^2}{q^2} \text{Re} \left(A_{\perp}^L A_{\perp}^{R*} + A_{\parallel}^L A_{\parallel}^{R*} \right), \\
 J_{1c} &= |A_0^L|^2 + |A_0^R|^2 + \frac{4m_{\ell}^2}{q^2} \left[|A_t|^2 + 2\text{Re}(A_0^L A_0^{R*}) \right] + \beta_{\ell}^2 |A_S|^2, \\
 J_{2s} &= \frac{\beta_{\ell}^2}{4} \left[|A_{\perp}^L|^2 + |A_{\parallel}^L|^2 + |A_{\perp}^R|^2 + |A_{\parallel}^R|^2 \right], & J_{2c} &= -\beta_{\ell}^2 \left[|A_0^L|^2 + |A_0^R|^2 \right], \\
 J_3 &= \frac{1}{2} \beta_{\ell}^2 \left[|A_{\perp}^L|^2 - |A_{\parallel}^L|^2 + |A_{\perp}^R|^2 - |A_{\parallel}^R|^2 \right], & J_4 &= \frac{1}{\sqrt{2}} \beta_{\ell}^2 \left[\text{Re}(A_0^L A_{\parallel}^{L*} + A_0^R A_{\parallel}^{R*}) \right], \\
 J_5 &= \sqrt{2} \beta_{\ell} \left[\text{Re}(A_0^L A_{\perp}^{L*} - A_0^R A_{\perp}^{R*}) - \frac{m_{\ell}}{\sqrt{q^2}} \text{Re}(A_{\parallel}^L A_S^* + A_{\parallel}^{R*} A_S) \right], \\
 J_{6s} &= 2\beta_{\ell} \left[\text{Re}(A_{\parallel}^L A_{\perp}^{L*} - A_{\parallel}^R A_{\perp}^{R*}) \right], & J_{6c} &= 4\beta_{\ell} \frac{m_{\ell}}{\sqrt{q^2}} \text{Re}(A_0^L A_S^* + A_0^{R*} A_S), \\
 J_7 &= \sqrt{2} \beta_{\ell} \left[\text{Im}(A_0^L A_{\parallel}^{L*} - A_0^R A_{\parallel}^{R*}) + \frac{m_{\ell}}{\sqrt{q^2}} \text{Im}(A_{\perp}^L A_S^* - A_{\perp}^{R*} A_S) \right], \\
 J_8 &= \frac{1}{\sqrt{2}} \beta_{\ell}^2 \left[\text{Im}(A_0^L A_{\perp}^{L*} + A_0^R A_{\perp}^{R*}) \right], & J_9 &= \beta_{\ell}^2 \left[\text{Im}(A_{\parallel}^{L*} A_{\perp}^L + A_{\parallel}^{R*} A_{\perp}^R) \right], \quad (2.1)
 \end{aligned}$$

where the parameter β_{ℓ} is given by

$$\beta_{\ell} = \sqrt{1 - \frac{4m_{\ell}^2}{q^2}}. \quad (2.2)$$

We will distinguish between the three cases of interest: massless leptons and no scalar amplitude, massive leptons and no scalar amplitude, and massive leptons plus a scalar amplitude. We also show that tensor contributions cannot change the picture.

Massless leptons, no scalars. In this case we can put $A_S \rightarrow 0$, drop the m_ℓ^2 terms and set $\beta_\ell \rightarrow 1$. There are in total six complex transversity amplitudes: $A_0^{R,L}$, $A_{\parallel}^{R,L}$ and $A_{\perp}^{R,L}$, which add up to $2n_A = 12$ real theoretical quantities. However, an infinitesimal transformation of the distribution (see [8]) shows that there must be $n_s = 4$ continuous transformations between the $A_i^{L,R}$ that leave invariant the angular distribution. Two of them are simple phase transformations: $A_i^L \rightarrow e^{i\phi_L} A_i^L$ and $A_i^R \rightarrow e^{i\phi_R} A_i^R$, while the other two mix L and R amplitudes (see appendix A and ref. [8] for the explicit form of these transformations). According to eq. (1.2), there must be precisely $n_{\text{exp}} = 8$ independent observables. This implies, in turn, that there should be 4 relationships among the 12 coefficients $J_i(q^2)$. Three of them are straightforward: $J_{6c} = 0$, $J_{1s} = 3J_{2s}$ and $J_{1c} = -J_{2c}$, while the remaining one is more involved [8]:

$$\begin{aligned}
 J_{2c} = & -2 \frac{(2J_{2s} + J_3)(4J_4^2 + \beta_\ell^2 J_7^2) + (2J_{2s} - J_3)(\beta_\ell^2 J_5^2 + 4J_8^2)}{16J_{2s}^2 - (4J_3^2 + \beta_\ell^2 J_{6s}^2 + 4J_9^2)} \\
 & + 4 \frac{\beta_\ell^2 J_{6s}(J_4 J_5 + J_7 J_8) + J_9(\beta_\ell^2 J_5 J_7 - 4J_4 J_8)}{16J_{2s}^2 - (4J_3^2 + \beta_\ell^2 J_{6s}^2 + 4J_9^2)}, \tag{2.3}
 \end{aligned}$$

where $\beta_\ell \rightarrow 1$ should be understood in the massless case. The derivation of this expression requires the symmetry formalism and will be outlined later.

B. Massive leptons, no scalars. In this case we just set $A_S \rightarrow 0$ in eq. (2.1). Now there are seven complex transversity amplitudes, including A_t , which add up to $2n_A = 14$ real theoretical quantities. As discussed in appendix A.2, there are $n_s = 4$ continuous transformations that leave the J_i invariant (these are different from the symmetries of the massless case, since those are broken by mass effects). Two of these symmetries are phase rotations: $A_t \rightarrow e^{i\phi_t} A_t$ and $A_{0,\parallel,\perp}^{L,R} \rightarrow e^{i\phi} A_{0,\parallel,\perp}^{L,R}$, while the other two are nonlinear transformations (see appendix A.2). According to eq. (1.2), there must be precisely $n_{\text{exp}} = 10$ independent observables, which means that 2 relationships between the coefficients J_i can be found. The relationships $J_{1s} = 3J_{2s}$ and $J_{1c} = -J_{2c}$ are no longer satisfied; however, $J_{6c} = 0$ and eq. (2.3) remain exactly true in the massive case (this was the reason for keeping the factors β_ℓ explicit in eq. (2.3)). Notice that in ref. [8] the discussion was limited to the massless lepton case, so eq. (2.3) generalizes the relation in ref. [8] to the massive case.

C. Massive leptons plus scalars. In this case we deal with 8 complex transversity amplitudes, which add up to $2n_A = 16$ real theoretical variables. As demonstrated in appendix A.3 (see also ref. [8]), there are $n_s = 4$ symmetries. This means there must be exactly $n_{\text{exp}} = 12$ independent observables, which implies that all the J_i are independent, and none of the previous relations hold in this case.

D. Massive leptons, scalars and tensors. The fact that all the J_i are independent in the scalar case can be used to go a bit further in the reasoning. Imagine we wanted to include NP contributions from tensor operators. Then we would expect, at least, a new amplitude A_T modifying somehow the angular distribution [eqs. (2.1)]. However, according to eq. (1.2) and since n_{exp} is as large as it can be, for each new amplitude A_T there must

be two extra symmetries. These symmetries must disappear in the limit $A_T \rightarrow 0$, and therefore they can be used to set $A_T \rightarrow 0$. Another way to see this is the following: since the J_i are all independent in the scalar case, one can always obtain a set of $A_{\parallel,\perp,0}^{R,L'}$, A'_t , A'_S that reproduce the angular distribution in the presence of new amplitudes such as A_T . Therefore, new tensor operators can only give new contributions to existing amplitudes, meaning that the basis of observables defined in the scalar case remains unchanged in the presence of tensors.

We will now discuss in turn the relevant set of observables that one can consider in each of these three cases of interest.

3 Observables for massless leptons

Not any observable constructed from the transversity amplitudes can be obtained from the angular distribution. As a necessary and sufficient condition, such an observable must be invariant under the symmetry transformations of the transversity amplitudes A 's; we then say that the observable respects the symmetries of the angular distribution. Fortunately, there exists a systematic procedure to construct all such possible observables.

We start defining the following complex vectors [8],

$$n_{\parallel} = \begin{pmatrix} A_{\parallel}^L \\ A_{\parallel}^{R*} \end{pmatrix}, \quad n_{\perp} = \begin{pmatrix} A_{\perp}^L \\ -A_{\perp}^{R*} \end{pmatrix}, \quad n_0 = \begin{pmatrix} A_0^L \\ A_0^{R*} \end{pmatrix}. \quad (3.1)$$

With these vectors we can construct the products $|n_i|^2 = n_i^\dagger n_i$ and $n_i^\dagger n_j$,

$$\begin{aligned} |n_{\parallel}|^2 &= |A_{\parallel}^L|^2 + |A_{\parallel}^R|^2 = \frac{2J_{2s} - J_3}{\beta_\ell^2}, & n_{\perp}^\dagger n_{\parallel} &= A_{\perp}^{L*} A_{\parallel}^L - A_{\perp}^R A_{\parallel}^{R*} = \frac{\beta_\ell J_{6s} - 2iJ_9}{2\beta_\ell^2}, \\ |n_{\perp}|^2 &= |A_{\perp}^L|^2 + |A_{\perp}^R|^2 = \frac{2J_{2s} + J_3}{\beta_\ell^2}, & n_0^\dagger n_{\parallel} &= A_0^{L*} A_{\parallel}^L + A_0^R A_{\parallel}^{R*} = \frac{2J_4 - i\beta_\ell J_7}{\sqrt{2}\beta_\ell^2}, \\ |n_0|^2 &= |A_0^L|^2 + |A_0^R|^2 = -\frac{J_{2c}}{\beta_\ell^2}, & n_0^\dagger n_{\perp} &= A_0^{L*} A_{\perp}^L - A_0^R A_{\perp}^{R*} = \frac{\beta_\ell J_5 - 2iJ_8}{\sqrt{2}\beta_\ell^2}. \end{aligned} \quad (3.2)$$

These quantities automatically respect the symmetries of the angular distribution, since they can be expressed in terms of the J_i . Considering real and imaginary parts, there are 9 real quantities that encode all the information of the angular distribution, and by combining them one can construct systematically all possible allowed observables consistent with the symmetry requirements. However they are not all independent: any set of complex 2-vectors $\{n_0, n_{\parallel}, n_{\perp}\}$ satisfies

$$|(n_{\parallel}^\dagger n_{\perp})n_0|^2 - (n_{\parallel}^\dagger n_0)(n_0^\dagger n_{\perp})^2 = (|n_0|^2 |n_{\parallel}|^2 - |n_0^\dagger n_{\parallel}|^2)(|n_0|^2 |n_{\perp}|^2 - |n_0^\dagger n_{\perp}|^2). \quad (3.3)$$

Using eqs. (3.2), this relation translates precisely into the relation for the J_i given in eq. (2.3).

Now that the formalism assures the systematic construction of observables that respect the symmetries of the angular distribution, we must focus on the cancellation of hadronic

form factors. At leading order in $1/m_b$ and α_s , and at large recoil ($E_{K^*} \rightarrow \infty$), the transversity amplitudes $A_0^{L,R}$, $A_{\parallel}^{L,R}$ and $A_{\perp}^{L,R}$ can be written as:

$$\begin{aligned}
 A_{\perp}^{L,R} &= \sqrt{2}Nm_B(1 - \hat{s}) \left[(\mathcal{C}_9^{\text{eff}} + \mathcal{C}_9^{\text{eff}'}) \mp (\mathcal{C}_{10} + \mathcal{C}'_{10}) + \frac{2\hat{m}_b}{\hat{s}}(\mathcal{C}_7^{\text{eff}} + \mathcal{C}_7^{\text{eff}'}) \right] \xi_{\perp}(E_{K^*}) \\
 A_{\parallel}^{L,R} &= -\sqrt{2}Nm_B(1 - \hat{s}) \left[(\mathcal{C}_9^{\text{eff}} - \mathcal{C}_9^{\text{eff}'}) \mp (\mathcal{C}_{10} - \mathcal{C}'_{10}) + \frac{2\hat{m}_b}{\hat{s}}(\mathcal{C}_7^{\text{eff}} - \mathcal{C}_7^{\text{eff}'}) \right] \xi_{\perp}(E_{K^*}) \\
 A_0^{L,R} &= -\frac{Nm_B(1 - \hat{s})^2}{2\hat{m}_{K^*}\sqrt{\hat{s}}} \left[(\mathcal{C}_9^{\text{eff}} - \mathcal{C}_9^{\text{eff}'}) \mp (\mathcal{C}_{10} - \mathcal{C}'_{10}) + 2\hat{m}_b(\mathcal{C}_7^{\text{eff}} - \mathcal{C}_7^{\text{eff}'}) \right] \xi_{\parallel}(E_{K^*}) \quad (3.4)
 \end{aligned}$$

where $\hat{s} = q^2/m_B^2$, $\hat{m}_i = m_i/m_B$, and terms of $O(\hat{m}_{K^*}^2)$ have been neglected. The normalization is given by

$$N = V_{tb}V_{ts}^* \sqrt{\frac{\beta_{\ell} G_F^2 \alpha^2 q^2 \lambda^{1/2}}{3 \cdot 2^{10} \pi^5 m_B^3}}, \quad (3.5)$$

with $\lambda = [q^2 - (m_B + m_{K^*})^2][q^2 - (m_B - m_{K^*})^2]$. Therefore, at first order, we have $n_0 \propto \xi_{\parallel}$ and $n_{\parallel}, n_{\perp} \propto \xi_{\perp}$. This establishes a clear guideline in the construction of clean observables, as ratios of quantities in eq. (3.2) where the $\xi_{\parallel, \perp}$ cancel [Form Factor Independent (FFI) observables].

Before providing a complete list of observables constructed according to this procedure, we should note the following. There are 8 independent quantities in eq. (3.2) that constitute the building blocks of the observables. The soft form factors $\xi_{\parallel, \perp}$ can be thought of as 2 irreducible normalization factors in the products $n_i^{\dagger} n_j$, and therefore one cannot construct 8 independent combinations where the soft form factors cancel. The best one can do is to construct 6 clean observables, plus 2 observables that contain the information on the two form factors —or Form Factor Dependent (FFD) observables—.

For these two FFD observables we can choose, quite naturally, the angular-integrated differential decay rate $d\Gamma/dq^2$, and the forward-backward asymmetry A_{FB} :

$$\frac{d\Gamma}{dq^2} = \int d\cos\theta_l d\cos\theta_K d\phi \frac{d^4\Gamma}{dq^2 d\cos\theta_K d\cos\theta_l d\phi} = \frac{1}{4} (3J_{1c} + 6J_{1s} - J_{2c} - 2J_{2s}), \quad (3.6)$$

$$A_{\text{FB}} = \frac{1}{d\Gamma/dq^2} \left[\int_{-1}^0 - \int_0^1 \right] d\cos\theta_l \frac{d^2\Gamma}{dq^2 d\cos\theta_l} = -\frac{3J_{6s}}{3J_{1c} + 6J_{1s} - J_{2c} - 2J_{2s}}. \quad (3.7)$$

Notice that, while eq. (3.6) is completely general, in the last equality of eq. (3.7) we have assumed that $J_{6c} = 0$ due to the absence of scalar contributions. In the massless case, since $J_{1s} = 3J_{2s}$ and $J_{1c} = -J_{2c}$, these expressions simplify to $d\Gamma/dq^2 = J_{1c} + 4J_{2s}$ and $A_{\text{FB}} = -3J_{6s}/[4(J_{1c} + 4J_{2s})]$.

For the six (clean) FFI observables we choose the following set:

$$P_1 = \frac{|n_\perp|^2 - |n_\parallel|^2}{|n_\perp|^2 + |n_\parallel|^2} = \frac{J_3}{2J_{2s}}, \quad (3.8)$$

$$P_2 = \frac{\text{Re}(n_\perp^\dagger n_\parallel)}{|n_\parallel|^2 + |n_\perp|^2} = \beta_\ell \frac{J_{6s}}{8J_{2s}}, \quad (3.9)$$

$$P_3 = \frac{\text{Im}(n_\perp^\dagger n_\parallel)}{|n_\parallel|^2 + |n_\perp|^2} = -\frac{J_9}{4J_{2s}}, \quad (3.10)$$

$$P_4 = \frac{\text{Re}(n_0^\dagger n_\parallel)}{\sqrt{|n_\parallel|^2 |n_0|^2}} = \frac{\sqrt{2}J_4}{\sqrt{-J_{2c}(2J_{2s} - J_3)}}, \quad (3.11)$$

$$P_5 = \frac{\text{Re}(n_0^\dagger n_\perp)}{\sqrt{|n_\perp|^2 |n_0|^2}} = \frac{\beta_\ell J_5}{\sqrt{-2J_{2c}(2J_{2s} + J_3)}}, \quad (3.12)$$

$$P_6 = \frac{\text{Im}(n_0^\dagger n_\parallel)}{\sqrt{|n_\parallel|^2 |n_0|^2}} = -\frac{\beta_\ell J_7}{\sqrt{-2J_{2c}(2J_{2s} - J_3)}}, \quad (3.13)$$

although other similar ratios are possible. We have used the following criteria for choosing among the different possible FFI observables: (1) they are simple ratios of the quantities in eq. (3.2) where the form factors $\xi_{\perp,\parallel}$ cancel, (2) they take values in the range $[-1,1]$, and (3) they show good sensitivity to selected New Physics (see section 7). To summarize, the complete basis of observables in the massless case is given by:

$$O_{m_\ell=0} = \left\{ \frac{d\Gamma}{dq^2}, A_{\text{FB}}, P_1, P_2, P_3, P_4, P_5, P_6 \right\} \quad (3.14)$$

where the six P_i are clean observables.

As mentioned, all possible observables can be expressed in terms of the observables in the basis. In particular, all known observables can be related to this set. For example, the usual FFI observables can be expressed in terms of $P_{1,2,3,4,5,6}$:

$$\begin{aligned} A_T^{(2)} &= P_1, & A_T^{(5)} &= \frac{1}{2}\sqrt{1 - P_1^2 - 4P_2^2 - 4P_3^2}, \\ A_T^{(\text{re})} &= 2P_2, & A_T^{(\text{im})} &= -2P_3, \\ H_T^{(1)} &= P_4, & H_T^{(2)} &= P_5. \end{aligned} \quad (3.15)$$

Also, the relationship $(2A_T^{(5)})^2 + (A_T^{(2)})^2 + (A_T^{(\text{re})})^2 + (A_T^{(\text{im})})^2 = 1$, presented in ref. [9], follows trivially in terms of the P_i .

In the case of the observables $A_T^{(3)}$ and $A_T^{(4)}$, the corresponding expressions are more involved. They can be expressed in terms of our basis by first recovering their expression in terms of the J 's:

$$A_T^{(3)} = \sqrt{\frac{4J_4^2 + \beta_\ell^2 J_7^2}{-2J_{2c}(2J_{2s} + J_3)}}, \quad A_T^{(4)} = \sqrt{\frac{4J_8^2 + \beta_\ell^2 J_5^2}{4J_4^2 + \beta_\ell^2 J_7^2}}, \quad (3.16)$$

and substituting the J 's in terms of our basis of observables as given in eqs. (4.8)–(4.17) in the following section.

The same can be done for all the known FFD observables, which can be expressed in terms of P_i , $d\Gamma/dq^2$ and A_{FB} , for example:

$$F_T = 1 - F_L = -\frac{2\beta_\ell}{3} \frac{A_{\text{FB}}}{P_2} \quad (3.17)$$

$$A_{\text{im}} = \frac{2}{3} \frac{A_{\text{FB}} P_3}{P_2} \quad (3.18)$$

4 Observables in the massive case

All the coefficients in the massive case can be expressed in terms of the quantities of eq. (3.2), with the exception of J_{1c} and J_{1s} , which can be written as:

$$J_{1s} = \frac{2 + \beta_\ell}{4} [|n_\perp|^2 + |n_\parallel|^2] + \frac{2m_\ell^2}{q^2} [n_\parallel^T \sigma_1 n_\parallel + n_\parallel^\dagger \sigma_1 n_\parallel^* - n_\perp^T \sigma_1 n_\perp - n_\perp^\dagger \sigma_1 n_\perp^*], \quad (4.1)$$

$$J_{1c} = |n_0|^2 + \frac{2m_\ell^2}{q^2} [2|A_t|^2 + n_0^T \sigma_1 n_0 + n_0^\dagger \sigma_1 n_0^*] . \quad (4.2)$$

where σ_1 is the Pauli matrix:

$$\sigma_1 = \begin{pmatrix} 0 & 1 \\ 1 & 0 \end{pmatrix} . \quad (4.3)$$

The important point demonstrated in appendix A.2 is that in this case the symmetries, like in the massless case, can be expressed as a single unitary rotation U on $n_{0,\perp,\parallel}$. This means that all the products [eq. (3.2)] that were invariant in the massless case are still invariant under the new symmetries (so all the observables defined in section 3 are still valid), which in turn means that the new terms appearing in J_{1c} and J_{1s} :

$$\frac{4m_\ell^2}{q^2} \text{Re} \left(A_\perp^L A_\perp^{R*} + A_\parallel^L A_\parallel^{R*} \right) , \quad \frac{4m_\ell^2}{q^2} \left[|A_t|^2 + 2\text{Re}(A_0^L A_0^{R*}) \right] ,$$

must be invariant by themselves. This is a key idea in order to find the continuous symmetries (see appendix A.2), but it is also crucial to the construction of the new observables, the obvious ones being:

$$M_1 = \frac{2m_\ell^2}{q^2} \frac{1}{\beta_\ell^2} \cdot \frac{n_\parallel^T \sigma_1 n_\parallel + n_\parallel^\dagger \sigma_1 n_\parallel^* - n_\perp^T \sigma_1 n_\perp - n_\perp^\dagger \sigma_1 n_\perp^*}{|n_\parallel|^2 + |n_\perp|^2} = \frac{\beta_\ell^2 J_{1s} - (2 + \beta_\ell^2) J_{2s}}{4\beta_\ell^2 J_{2s}} , \quad (4.4)$$

$$M_2 = \frac{2m_\ell^2}{q^2} \cdot \frac{2|A_t|^2 + n_0^T \sigma_1 n_0 + n_0^\dagger \sigma_1 n_0^*}{|n_0|^2} = -\frac{\beta_\ell^2 J_{1c} + J_{2c}}{J_{2c}} . \quad (4.5)$$

We note that these observables are of the FFI type, and thus theoretically clean. This can be inferred from the large recoil limit expressions (3.4) and

$$A_t = \frac{Nm_B}{\hat{m}_{K^*} \sqrt{\hat{s}}} (1 - \hat{s})^2 \left[2(\mathcal{C}_{10} - \mathcal{C}'_{10}) + \frac{q^2}{m_\ell} (\mathcal{C}_P - \mathcal{C}'_P) \right] \xi_\parallel(E_{K^*}) . \quad (4.6)$$

Moreover, M_1 and M_2 vanish in the massless limit (from the right hand side of eqs. (4.4) and (4.5) one can see that this follows from the relationships of the massless case, $J_{1s} = 3J_{2s}$ and $J_{1c} = -J_{2c}$, that are broken for non-zero lepton masses; in fact M_1 measures the breaking of the relation $J_{1s} = 3J_{2s}$, while M_2 measures the breaking of $J_{1c} = -J_{2c}$).

From the discussion in section 2, together with the observations that M_1 and M_2 vanish for $m_\ell \rightarrow 0$, and that the observables of the massless case are still valid, one concludes that these two observables complete the basis of 10 independent observables of the massive case. This basis is:

$$O_{m_\ell \neq 0} = \left\{ \frac{d\Gamma}{dq^2}, A_{\text{FB}}, P_1, P_2, P_3, P_4, P_5, P_6, M_1, M_2 \right\}. \quad (4.7)$$

The coefficients J_i of the angular distribution are themselves observables (of the FFD type), and it is interesting to express them in terms of $d\Gamma/dq^2$, A_{FB} and P_i . The explicit expressions read:

$$J_{1s} = -\frac{2 + (1 + 4M_1)\beta_\ell^2}{6\beta_\ell} \chi \frac{d\Gamma}{dq^2}, \quad (4.8)$$

$$J_{1c} = \frac{2(1 + M_2)}{3\beta_\ell(3 + 3M_2 + \beta_\ell^2)} (6\beta_\ell + [3 + (1 + 6M_1)\beta_\ell^2] \chi) \frac{d\Gamma}{dq^2}, \quad (4.9)$$

$$J_{2s} = -\frac{\beta_\ell}{6} \chi \frac{d\Gamma}{dq^2}, \quad (4.10)$$

$$J_{2c} = -\frac{2\beta_\ell}{3(3 + 3M_2 + \beta_\ell^2)} (6\beta_\ell + [3 + (1 + 6M_1)\beta_\ell^2] \chi) \frac{d\Gamma}{dq^2}, \quad (4.11)$$

$$J_3 = -\frac{\beta_\ell P_1}{3} \chi \frac{d\Gamma}{dq^2}, \quad (4.12)$$

$$J_4 = \frac{P_4}{3} \sqrt{\frac{(P_1 - 1)\beta_\ell^2}{3 + 3M_2 + \beta_\ell^2}} (6\beta_\ell + [3 + (1 + 6M_1)\beta_\ell^2] \chi) \chi \frac{d\Gamma}{dq^2}, \quad (4.13)$$

$$J_5 = \frac{2P_5}{3} \sqrt{\frac{(-P_1 - 1)}{3 + 3M_2 + \beta_\ell^2}} (6\beta_\ell + [3 + (1 + 6M_1)\beta_\ell^2] \chi) \chi \frac{d\Gamma}{dq^2}, \quad (4.14)$$

$$J_{6s} = -\frac{4P_2}{3} \chi \frac{d\Gamma}{dq^2}, \quad (4.15)$$

$$J_7 = -\frac{2P_6}{3} \sqrt{\frac{(P_1 - 1)}{3 + 3M_2 + \beta_\ell^2}} (6\beta_\ell + [3 + (1 + 6M_1)\beta_\ell^2] \chi) \chi \frac{d\Gamma}{dq^2}, \quad (4.16)$$

$$J_9 = \frac{2\beta_\ell P_3}{3} \chi \frac{d\Gamma}{dq^2}, \quad (4.17)$$

where, in this case,

$$\chi = \frac{A_{\text{FB}}}{P_2}. \quad (4.18)$$

The observable χ is well defined because A_{FB} and P_2 share the same zeroes [see eqs. (3.7) and (3.9)]. This will change after including scalars, but also χ will change. On the other hand, since $J_{1c} > J_{2c}$ [as can be checked from eq. (2.1)], it follows that $3 + 3M_2 + \beta_\ell^2 > 0$, and no vanishing denominators can occur in eqs. (4.8)–(4.17).

Notice that J_8 is absent from this list, as it is not an independent coefficient in the absence of scalar contributions. In order to obtain its expression in terms of the observables one should write J_8 as a function of the other J_i using eq. (2.3), and then plug in the expressions (4.8)–(4.17). Alternatively, one might want to leave J_8 as a free parameter when fitting the angular distribution in terms of the observables, and then check the relationship in eq. (2.3), to look for scalar contributions (see next section).

Using the substitutions $M_1, M_2 \rightarrow 0$ and $\beta_\ell \rightarrow 1$, eqs. (4.8)–(4.17) transform into the corresponding massless case expressions.

5 Inclusion of scalar operators

In the presence of scalar operators, a new amplitude A_S appears. This makes 16 the number of real theoretical degrees of freedom (8 complex amplitudes): $2n_A = 16$. There are 4 symmetries, making $n_{\text{exp}} = 12$. This means that all the J_i are independent, which in turn implies that the relationship $J_{6c} = 0$ and eq. (2.3) do not hold any longer. This observation allows us to choose the two extra observables that are needed in the basis in the presence of scalar contributions, as the amount by which these relationships are broken. This provides two independent observables, S_1 and S_2 , that vanish in the absence of scalars. The first observable is:

$$S_1 = -\frac{\beta_\ell \sqrt{q^2} J_{6c}}{4m_\ell J_{2c}}, \quad (5.1)$$

which measures the breaking of the relation $J_{6c} = 0$. The second one is:

$$S_2 = \frac{16J_{2c}J_{2s}^2 - 4J_{2c}J_3^2 + 16J_{2s}J_4^2 + 8J_3J_4^2 + 16J_{2s}J_8^2 - 8J_3J_8^2 + 16J_4J_8J_9 - 4J_{2c}J_9^2}{J_{2c}J_{2s}^2} + \beta^2 \frac{4J_{2s}J_5^2 - 2J_3J_5^2 - 4J_4J_5J_{6s} - J_{2c}J_{6s}^2 + 4J_{2s}J_7^2 + 2J_3J_7^2 - 4J_{6s}J_7J_8 - 4J_5J_7J_9}{J_{2c}J_{2s}^2}, \quad (5.2)$$

which gives a measure of the violation of eq. (2.3). One can easily check that both observables are of the FFI type, by noting that the large recoil expression for A_S is:

$$A_S = -2 \frac{Nm_B}{\hat{m}_{K^*}} (1 - \hat{s})^2 [\mathcal{C}_S - \mathcal{C}'_S] \xi_{\parallel}(E_{K^*}). \quad (5.3)$$

While most of the results in the previous sections remain unchanged in the presence of scalars, some differences must be clarified. When $A_S \neq 0$, the observables P_5 , P_6 and M_2 get modified. In particular eqs. (3.12), (3.13) and (4.5) in terms of the vectors n_i do not hold since new terms proportional to A_S arise, and these observables must be redefined. The simplest way to generalize these observables in presence of scalars is simply to use their definition in terms of the J_i in eqs. (3.12), (3.13) and (4.5). These three observables are, together with S_1 and S_2 , the only ones sensitive to scalar contributions. With this in mind, an optimal basis of observables in the presence of scalars reads:

$$O_{m_\ell \neq 0}^{\text{scalars}} = \left\{ \frac{d\Gamma}{dq^2}, A_{\text{FB}}, P_1, P_2, P_3, P_4, P_5, P_6, M_1, M_2, S_1, S_2 \right\}. \quad (5.4)$$

In the case of A_{FB} , we keep the definition in eq. (3.7) as the angular integral, which means that now:

$$A_{\text{FB}} = -\frac{3J_{6s} + 3J_{6c}/2}{3J_{1c} + 6J_{1s} - J_{2c} - 2J_{2s}}. \quad (5.5)$$

Because of this, eqs. (4.8)–(4.17) are modified slightly. First, when $S_i \neq 0$ we have:

$$\chi = \frac{(3 + 3M_2 + \beta_\ell^2)A_{\text{FB}} + (m_\ell/\sqrt{q^2})6\beta_\ell S_1}{(3 + 3M_2 + \beta_\ell^2)P_2 - (m_\ell/\sqrt{q^2})(3 + 6\beta_\ell^2 M_1 + \beta_\ell^2)S_1} \quad (5.6)$$

in (4.8)–(4.17). Furthermore, J_{6c} is non-zero:

$$J_{6c} = \frac{8m_\ell S_1}{3\sqrt{q^2}} \frac{(6\beta_\ell^2 M_1 + \beta_\ell^2 + 3)A_{\text{FB}} + 6\beta_\ell P_2}{(3M_2 + \beta_\ell^2 + 3)P_2 - (m_\ell/\sqrt{q^2})(6\beta_\ell^2 M_1 + \beta_\ell^2 + 3)S_1} \frac{d\Gamma}{dq^2}. \quad (5.7)$$

The generalization of χ in eq. (5.6) could be expected: in the case $A_S \rightarrow 0$, the zeroes of A_{FB} and P_2 coincide, because they are both proportional to J_{6s} [see eqs. (3.7) and (3.9)], and that is the reason for which the combination A_{FB}/P_2 is well defined in eqs. (3.17), (3.18) and (4.8)–(4.17). However, turning on A_S moves the zero in A_{FB} away from that of P_2 , making A_{FB}/P_2 singular when $J_{6s} = 0$. On the other hand, the expression in eq. (5.6) is regular at every point and goes to $\chi = A_{\text{FB}}/P_2$ only in the limit $A_S \rightarrow 0$.

6 Uniangular distributions

A full angular analysis designed to extract the complete set of q^2 -dependent observables requires a good deal of statistics, and will be possible at LHCb not before an integrated luminosity $\gtrsim 10 \text{ fb}^{-1}$ has been collected. However, certain angular observables are available from partially integrated distributions, and experimental analyses have focused to this day on uniangular distributions, leading to the set of measured observables reviewed in section 1.

Starting from the full angular distribution of eq. (1.1), the three uniangular distributions can be obtained:

$$\frac{d^2\Gamma}{dq^2 d\phi} = \frac{1}{8\pi} \left[(6J_{1s} + 3J_{1c} - 2J_{2s} - J_{2c} + 4J_3 \cos 2\phi + 4J_9 \sin 2\phi) \right] \quad (6.1)$$

$$\frac{d^2\Gamma}{dq^2 d\cos\theta_\ell} = \frac{1}{8} \left[6J_{1s} + 3J_{1c} + (6J_{2s} + 3J_{2c}) \cos 2\theta_\ell + (6J_{6s} + 3J_{6c}) \cos \theta_\ell \right] \quad (6.2)$$

$$\frac{d^2\Gamma}{dq^2 d\cos\theta_K} = \frac{1}{8} \left[(9J_{1s} - 3J_{2s}) \sin^2 \theta_K + (9J_{1c} - 3J_{2c}) \cos^2 \theta_K \right] \quad (6.3)$$

Substituting the expressions (4.8)–(4.17) for the J_i coefficients, the uniangular distributions

in the presence of scalars can be written as functions of the observables as follows:

$$\frac{d^2\Gamma}{dq^2 d\phi} = \frac{1}{2\pi} \left[1 - \frac{\beta_\ell}{3} \chi P_1 \cos 2\phi + \frac{2\beta_\ell}{3} \chi P_3 \sin 2\phi \right] \frac{d\Gamma}{dq^2} \quad (6.4)$$

$$\begin{aligned} \frac{d^2\Gamma}{dq^2 d\cos\theta_\ell} = & \left[\frac{3(M_2 + 1)}{2(3M_2 + \beta_\ell^2 + 3)} - \beta_\ell \frac{4\beta_\ell^2 M_1 + M_2 + \beta_\ell^2 + 3}{8(3M_2 + \beta_\ell^2 + 3)} \chi - A_{\text{FB}} \cos\theta_\ell \right. \\ & \left. - \left(\frac{3\beta_\ell^2}{2(3M_2 + \beta_\ell^2 + 3)} + \frac{3\beta_\ell(4\beta_\ell^2 M_1 + M_2 + \beta_\ell^2 + 3)}{8(3M_2 + \beta_\ell^2 + 3)} \chi \right) \cos 2\theta_\ell \right] \frac{d\Gamma}{dq^2} \end{aligned} \quad (6.5)$$

$$\frac{d^2\Gamma}{dq^2 d\cos\theta_K} = \left[\left(\frac{3}{2} + \frac{6\beta_\ell^2 M_1 + \beta_\ell^2 + 3}{4\beta_\ell} \chi \right) \cos^2\theta_K - \frac{6\beta_\ell^2 M_1 + \beta_\ell^2 + 3}{8\beta_\ell} \chi \sin^2\theta_K \right] \frac{d\Gamma}{dq^2} \quad (6.6)$$

where χ is given by:

$$\chi = \begin{cases} \frac{A_{\text{FB}}}{P_2} & \text{if } A_S = 0, \\ \frac{(3 + 3M_2 + \beta_\ell^2)A_{\text{FB}} + (m_\ell/\sqrt{q^2})6\beta_\ell S_1}{(3 + 3M_2 + \beta_\ell^2)P_2 - (m_\ell/\sqrt{q^2})(3 + 6\beta_\ell^2 M_1 + \beta_\ell^2)S_1} & \text{if } A_S \neq 0. \end{cases} \quad (6.7)$$

Note that in the limit $m_\ell \rightarrow 0$ all scalar effects disappear. The corresponding well-known expressions for the uniangular distributions in the massless case are obtained by setting $m_\ell \rightarrow 0$, $\beta_\ell \rightarrow 1$ and $M_1, M_2 \rightarrow 0$.

7 New physics sensitivity of the observables

In this section we analyze and discuss the New Physics sensitivity of the full set of observables $O_{m_\ell \neq 0}^{\text{scalars}}$. In particular, we study the impact of New Physics contributions to the Wilson Coefficients:

$$C_i = C_i^{\text{SM}} + \delta C_i, \quad (7.1)$$

where $i = 7^{(\prime)}, 9^{(\prime)}, 10^{(\prime)}, S, P$, always taking into account the existing bounds from other processes that constrain substantially the New Physics contributions δC_i .

We consider the 10 FFI observables $P_{1,2,3,4,5,6}$, $M_{1,2}$ and $S_{1,2}$ in terms of the transversity amplitudes $A_{\parallel}^{L,R}$, $A_{\perp}^{L,R}$, A_t and A_S . These amplitudes can be written in terms of the Wilson coefficients C_i and a set of seven form factors $V(q^2)$, $A_{0,1,2}(q^2)$ and $T_{1,2,3}(q^2)$ (see for example ref. [22]). We first consider the SM contribution to the observables including NLO corrections, hadronic uncertainties and an estimate of the Λ/m_b corrections. We will see that indeed these FFI observables show reduced hadronic uncertainties.

After having the SM contribution under control, we consider NP contributions in several different scenarios, all of them compatible with current bounds from other processes, and study the possible deviations from the SM. The outcome of this analysis is shown in figures 1, 2 and tables 5, 6.

$\mathcal{C}_1(\mu_b)$	$\mathcal{C}_2(\mu_b)$	$\mathcal{C}_3(\mu_b)$	$\mathcal{C}_4(\mu_b)$	$\mathcal{C}_5(\mu_b)$	$\mathcal{C}_6(\mu_b)$	$\mathcal{C}_7^{\text{eff}}(\mu_b)$	$\mathcal{C}_8^{\text{eff}}(\mu_b)$	$\mathcal{C}_9(\mu_b)$	$\mathcal{C}_{10}(\mu_b)$
-0.2632	1.0111	-0.0055	-0.0806	0.0004	0.0009	-0.2923	-0.1663	4.0749	-4.3085

Table 1. NNLO Wilson coefficients in the Standard Model at the scale $\mu_b = 4.8 \text{ GeV}$ [28]. In the computation of the observables, we consider a variation of $\mu \in [\mu_b/2, 2\mu_b]$. The coefficients \mathcal{C}_9 and $\mathcal{C}_9^{\text{eff}}$ are related though $\mathcal{C}_9^{\text{eff}} = \mathcal{C}_9 + Y(q^2)$ (see ref. [30]).

7.1 SM contribution and hadronic uncertainties

The SM Wilson coefficients at the matching scale $\mu_0 = 2M_W$, and their running from μ_0 down to $\mu_b = 4.8 \text{ GeV}$, as well as the running of quark masses and couplings, are obtained following refs. [23–27] (see also ref. [28]). For reference we quote in table 1 the used values for the Wilson coefficients at the hadronic scale, taken from ref. [28].

Concerning the seven $B \rightarrow K^*$ form factors ($V(q^2)$, $A_{0,1,2}(q^2)$ and $T_{1,2,3}(q^2)$), their q^2 -dependence is parametrized following ref. [29], giving more conservative uncertainties than other parameterizations. Their values at $q^2 = 0$ are given in the same reference, obtained from light-cone sum rules with B distribution amplitudes. The definitions of the soft form factors $\xi_{\parallel,\perp}$ in terms of the full form factors are given in ref. [31]. All numerical inputs used in this analysis are the same as the ones tabulated in section 2.1 of ref. [28]. Maximum and minimum values for $\xi_{\parallel}(q^2)$ and $\xi_{\perp}(q^2)$ give rise to the grey regions in figures 1, 2 around the central SM value.

At this point, the rest of the hadronic uncertainties are calculated:

1. The renormalization scale μ_b is varied between 2.4 and 9.6 GeV.
2. The value of $\hat{m}_c = m_c/m_b$ is varied in the range $\hat{m}_c = 0.29 \pm 0.02$, according to the discussion in refs. [30, 32].
3. The uncertainty related to the factor that determines the relative size of the hard scattering term vs. the form factor, (see eq. (55) of ref. [30] and discussion below), is estimated at the level of a 30%.

These uncertainties are added in quadrature together with the uncertainties related to the form factors, giving rise to the orange bands in figures 1, 2, on top of the gray bands (which include only the form factor uncertainties).

As a third step, Λ/m_b contributions are estimated following the procedure in section 2.3 of ref. [8], but widening the error band to include a 68.2% of the probability (as opposed to the 66% used in that reference). This uncertainty is added in quadrature to the rest of the uncertainties computed before, giving rise to the light green bands (5% Λ/m_b correction) and the dark green bands (10% Λ/m_b correction) in figures 1, 2.

7.2 New Physics

The impact of NP on $P_{1,2,3,4,5,6}$, $M_{1,2}$ and $S_{1,2}$ is shown in figures 1, 2. According to the model-independent fit of ref. [28] (updated in ref. [33]), three sets of values for \mathcal{C}_i are chosen in order to represent the NP impact on the observables.

	Scenario A		Scenario B		Scenario C	
	A.1	A.2	B.1	B.2	C.1	C.2
$\delta\mathcal{C}_7(\mu_b)$	-0.041	0.25	-0.002	-0.002	-0.002	-0.002
$\delta\mathcal{C}'_7(\mu_b)$	-0.114	-0.414	-0.006	-0.006	-0.006	-0.006
$\delta\mathcal{C}_9(\mu_b)$	-	-	-1.25	-	-	-
$\delta\mathcal{C}'_9(\mu_b)$	-	-	-	-	-3	-
$\delta\mathcal{C}_{10}(\mu_b)$	-	-	-	3	-	-
$\delta\mathcal{C}'_{10}(\mu_b)$	-	-	-	-	-	-3.5

Table 2. Wilson Coefficients at the hadronic scale $\mu_b = 4.8 \text{ GeV}$ within Scenarios A,B,C.

Scenario A ($\mathcal{C}_7, \mathcal{C}'_7$). In this scenario, \mathcal{C}_7 and \mathcal{C}'_7 are chosen according to the allowed regions obtained in the analysis of refs. [28, 33], while the rest of the coefficients are set to their SM values. In particular, \mathcal{C}'_7 is set to values where deviations between experimental data and the SM are maximal. We choose two subscenarios: Scenario A.1 corresponds to a “SM-like” point in the $\mathcal{C}_7 - \mathcal{C}'_7$ plane belonging to the allowed connected region where the SM lives (see figure 2 of ref. [33]). Scenario A.2 corresponds to a “non SM-like” point belonging to a disconnected region, most likely to be probed in the near future by improved measurements of the branching ratio of $B \rightarrow X_s \mu^+ \mu^-$. The values of the relevant Wilson coefficients in these scenarios are summarized in the first column of table 2.

Scenario B ($\mathcal{C}_9, \mathcal{C}_{10}$). In this scenario, \mathcal{C}_7 and \mathcal{C}'_7 are fixed with small NP contributions, while \mathcal{C}_9 and \mathcal{C}_{10} take maximum allowed values compatible with the chosen \mathcal{C}_7 and \mathcal{C}'_7 . We distinguish between Scenario B.1, where only \mathcal{C}_9 receives a non-zero NP contribution, and Scenario B.2 where the NP enters only in \mathcal{C}_{10} . The values of the relevant Wilson coefficients in these scenarios are summarized in the second column of table 2.

Scenario C ($\mathcal{C}'_9, \mathcal{C}'_{10}$). In this scenario, $\mathcal{C}_7, \mathcal{C}'_7$ are fixed as in Scenario B, and $\mathcal{C}_9, \mathcal{C}_{10}$ are SM, whereas \mathcal{C}'_9 and \mathcal{C}'_{10} take the maximum allowed values compatible with the given $\mathcal{C}_7, \mathcal{C}'_7$, according to refs. [28, 33]. We again distinguish between Scenario C.1, where only \mathcal{C}'_9 receives a non-zero NP contribution, and Scenario C.2 where the NP affects only to \mathcal{C}'_{10} . The values of the relevant Wilson coefficients in these scenarios are summarized in the third column of table 2.

Observables P_3 and P_6 are mostly sensitive to imaginary components of the Wilson coefficients, since they are built out of imaginary parts of amplitude products [see eqs. (3.10) and (3.13)]. In order to test this dependence, we consider a fourth scenario with complex NP contributions to the Wilson coefficients $\mathcal{C}_{7,9,10}$ and $\mathcal{C}'_{7,9,10}$:

Scenario D (complex WC’s). In this scenario, the NP contributions $\delta\mathcal{C}_{7,9,10}^{(\prime)}$ take complex values. We consider three possibilities. In Scenarios D.1 and D.2, only $\mathcal{C}_{7,9,10}$ receive NP contributions. Scenario D.1 consists on a point inside the “SM-like” allowed region found in ref. [34], while Scenario D.2 is a point in the other “non SM-like” region of

	Scenario D.1	Scenario D.2	Scenario D.3
$\delta\mathcal{C}_7(\mu_b)$	$0.1 + 0.5 i$	$1.5 + 0.3 i$	–
$\delta\mathcal{C}_9(\mu_b)$	–1.4	$-8 + 2 i$	–
$\delta\mathcal{C}_{10}(\mu_b)$	$1 - 1.5 i$	$8 - 2 i$	–
$\delta\mathcal{C}'_7(\mu_b)$	–	–	$-0.3 - 0.1 i$
$\delta\mathcal{C}'_9(\mu_b)$	–	–	$3 + i$
$\delta\mathcal{C}'_{10}(\mu_b)$	–	–	$-0.6 + 2 i$

Table 3. Wilson Coefficients at the hadronic scale $\mu_b = 4.8 \text{ GeV}$ within Scenario D.

	Scenario S				Scenario P			
	S.1	S.2	S.3	S.4	P.1	P.2	P.3	P.4
$(\mathcal{C}_S - \mathcal{C}'_S)(\mu_b)$	0.03	0.01	–0.01	–0.03	–	–	–	–
$(\mathcal{C}_P - \mathcal{C}'_P)(\mu_b)$	–	–	–	–	0.07	0.0467	0.0233	0

Table 4. Wilson Coefficients at the scale $\mu_b = 4.8 \text{ GeV}$ within Scenarios S and P.

ref. [34]. In Scenario D.3, only $\mathcal{C}'_{7,9,10}$ are affected by NP. The values chosen for the Wilson coefficients in these scenarios are summarized in table 3.

Finally, we consider two additional scenarios with scalar and pseudoscalar New Physics contributions, to study the scalar observables $S_{1,2}$ and the pseudoscalar sensitivity of M_2 :

Scenario S ($\mathcal{C}_S - \mathcal{C}'_S$). All Wilson coefficients are SM except for $\mathcal{C}_S^{(\prime)}$. Since the amplitudes are only sensitive to the difference $\mathcal{C}_S - \mathcal{C}'_S$, we consider four different values for this difference, all compatible with the latest $B_s \rightarrow \mu^+ \mu^-$ bounds [35–37]:

$$BR(B_s \rightarrow \mu^+ \mu^-) < 4.5 \times 10^{-9} \tag{7.2}$$

at 95% confidence level. These four values constitute Scenarios S.1 to S.4 and are summarized in table 4.

Scenario P ($\mathcal{C}_P - \mathcal{C}'_P$). In this case, all Wilson coefficients are SM except for $\mathcal{C}_P^{(\prime)}$. Again, since the amplitudes are only sensitive to the difference $\mathcal{C}_P - \mathcal{C}'_P$, we consider four different values compatible with the $B_s \rightarrow \mu^+ \mu^-$ bound. These four values constitute Scenarios P.1 to P.4 and are summarized in table 4.

The set of observables can be divided in two groups: $P_{1,2,3,4,5,6}$ and M_1 , which are only sensitive to \mathcal{C}_i with $i = 7^{(\prime)}, 9^{(\prime)}, 10^{(\prime)}$ constitute the first group. In the second group we include M_2 and $S_{1,2}$, which are also sensitive to \mathcal{C}_S and \mathcal{C}_P . In principle, P_5 and P_6 contain also \mathcal{C}_S [see discussion below eq. (5.3)] but the overall sensitivity, considering the present bounds on \mathcal{C}_S , is negligible (for this reason we do not present the curves for $P_{5,6}$ in Scenario S). We will focus on the case $\ell = \mu$ in all considerations concerning lepton mass effects.

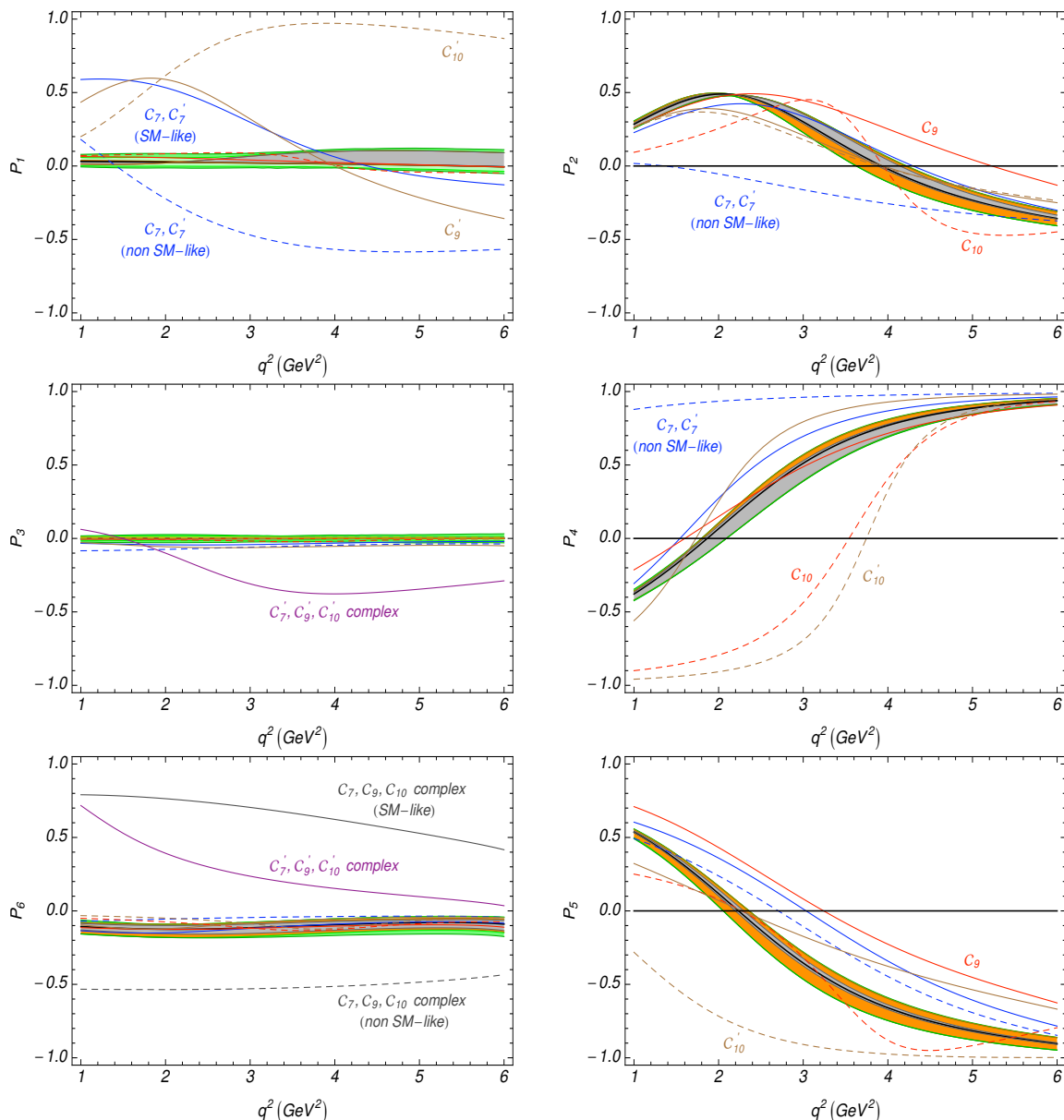


Figure 1. Observables $P_{1,2,3,4,5,6}$ in the SM at NLO, including all hadronic uncertainties (wide bands) as explained in section 7.1. The solid and dashed curves correspond to the NP scenarios exposed in the text: Scenario A.1 (blue solid), Scenario A.2 (blue dashed), Scenario B.1 (red solid), Scenario B.2 (red dashed), Scenario C.1 (brown solid) and Scenario C.2 (brown dashed). Scenarios D.1, D.2 and D.3 are explicitly indicated in P_3 and P_6 . The Wilson coefficients responsible for the largest deviations are highlighted.

Within the first group we have the observables P_1 , P_3 and P_6 , that are suppressed in the SM in all the q^2 region, but which can take sizeable non-vanishing values in specific NP scenarios, as shown in the left column of figure 1.

The rest of observables in the first group, namely P_2 , P_4 , P_5 and M_1 are non-vanishing

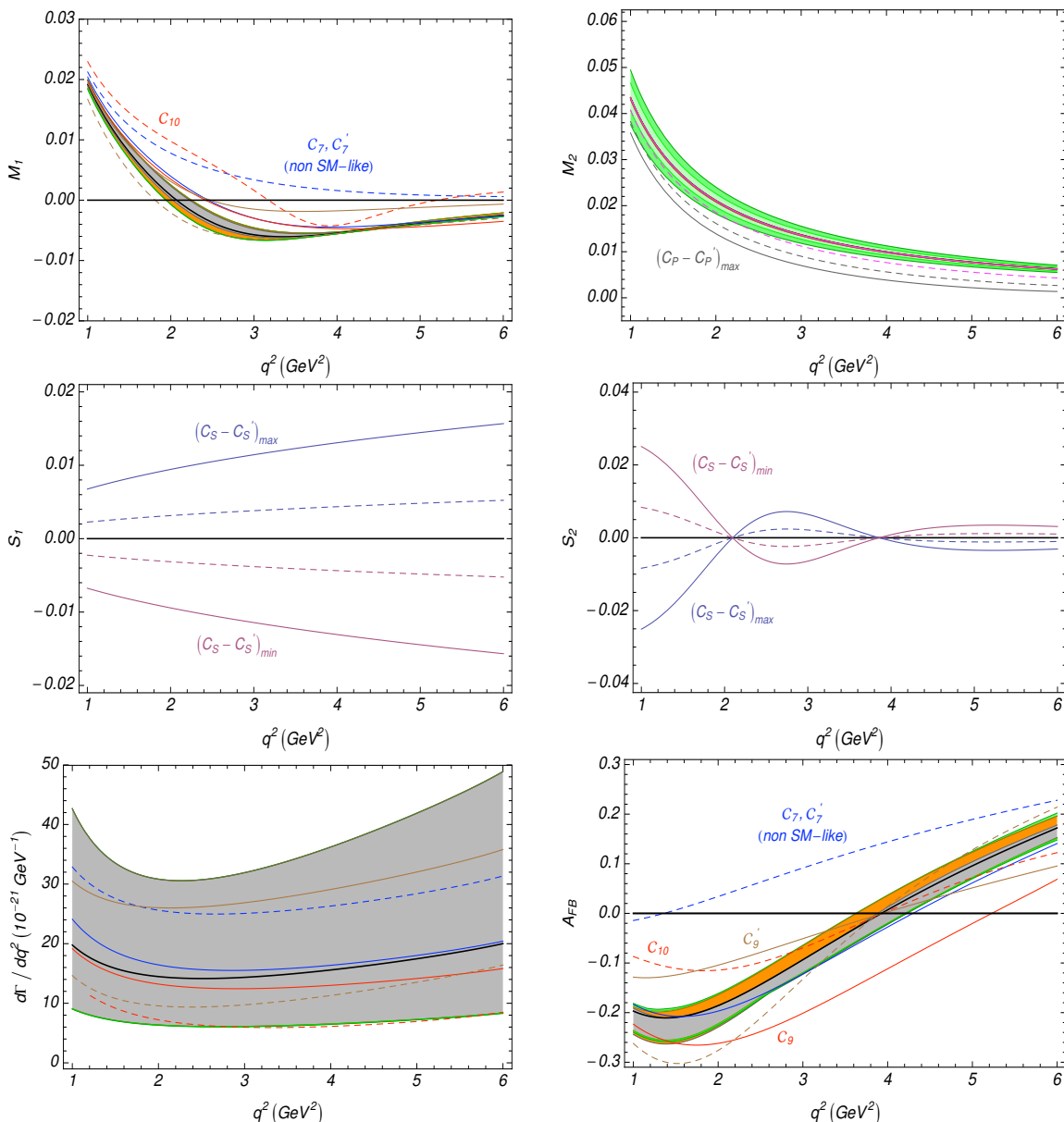


Figure 2. Observables $M_{1,2}$ (for $\ell = \mu$), $S_{1,2}$, $d\Gamma/dq^2$ and A_{FB} . The bands correspond to the SM at NLO and with all hadronic uncertainties. Notice that S_1 and S_2 are strictly zero in the SM. Dashed and solid lines in M_1 , $d\Gamma/dq^2$ and A_{FB} correspond to NP Scenarios A,B,C as in figure 1. In the case of M_2 and $S_{1,2}$, the curves correspond to: Scenario S.1 (blue solid), Scenario S.2 (blue dashed), Scenario S.3 (red dashed), Scenario S.4 (red solid), Scenario P.1 (gray solid), Scenario P.2 (gray dashed), Scenario P.3 (magenta dashed) and Scenario S.4 (magenta solid). The Wilson coefficients responsible for the largest deviations are indicated.

already in the SM and present a non-trivial q^2 -dependence. They all contain a zero at a value of q^2 within the experimentally accessible region 1-6 GeV^2 . At LO, these zeroes occur at the positions specified in the left column of table 5 (these include NLO corrections in

Obs.	q_0^{2SM} at Large Recoil		q_0^{2SM} (NLO)	q_0^{2NP}
P_2	$-\frac{2m_b m_B C_7^{\text{eff}}}{C_9^{\text{eff}}}$	3.06	3.93	5.23 [B.1]
P_4	$-\frac{2m_b m_B (m_B C_9^{\text{eff}} + 2m_b C_7^{\text{eff}}) C_7^{\text{eff}}}{2m_b C_7^{\text{eff}} C_9^{\text{eff}} + m_B (C_9^{\text{eff}^2} + C_{10}^2)}$	1.58	1.87	3.75 [C.2] 3.55 [B.2]
P_5	$-\frac{m_b m_B^2 C_7^{\text{eff}}}{m_b C_7^{\text{eff}} + m_B C_9^{\text{eff}}}$	1.64	2.23	3.25 [B.1] 3.03 [A.1]
M_1	$-\frac{2m_b m_B C_7^{\text{eff}}}{C_9^{\text{eff}} - C_{10}}$	1.61	2.07	3.15 [B.2]

Table 5. Position of the zeroes of observables $P_{2,4,5}$ and M_1 , in the SM at large recoil, at NLO, and in selected NP scenarios. In the last column, the zeroes correspond to the scenarios indicated in brackets. All values are given in GeV^2 . In the calculation of the large recoil zeroes, we use the Wilson coefficients given in table 1, and $m_b = 4.68 \text{ GeV}$. The zeroes of A_{FB} coincide exactly with those of P_2 , except in the presence of scalars.

the Wilson coefficients). At NLO, hadronic corrections shift the zeroes by amounts that can be computed in QCD factorization (see the second column in table 5). In the presence of NP, the positions of the zeroes are substantially modified (moved to lower or higher q^2 values) as can be seen in figures 1, 2. In the third column of table 5, we summarize the position of the zeroes in the most relevant NP scenarios considered above. In some NP scenarios, the zero can even disappear from the low- q^2 region. This is the case for example for P_4 in Scenario A.2, or P_5 in Scenario C.2.

As mentioned before, these zeroes cannot produce any singular behavior in the coefficients J_i . The only potential singular points are the zero of P_2 and the zero of the combination $3 + \beta_\ell + 3M_2$. However, $3 + \beta_\ell + 3M_2$ is always strictly positive, and the zero of P_2 coincides exactly with the zero of the forward-backward asymmetry, and cancels out. This is true in the absence of scalars; in general, the relevant parameter is χ , which is always well defined, as discussed in section 5.

The observables M_2 , S_1 and S_2 are affected by scalar Wilson coefficients (see figure 2) — we recall that C_S effects in P_5 and P_6 are negligible. Moreover, M_2 plays a special role since it is the only observable in $\bar{B} \rightarrow \bar{K}^* \ell \ell$ sensitive to C_P . As can be seen in figure 2, the most promising place to look for scalar effects is in the observable S_1 , when integrated in the full q^2 region. This is due to the fact that for fixed $C_S^{(\prime)}$, the curves are always positive (if $C_S > C_S'$) or negative (if $C_S < C_S'$), while in the absence of scalars S_1 is strictly zero in the full range. Integrating over q^2 has a clear experimental advantage from the point of view of statistics. However, we would need to discriminate values for the integrated observable below the level of $|\int dq^2 S_1| \sim 0.12 \text{ GeV}^2$ in order to improve the $B_s \rightarrow \mu^+ \mu^-$ bound.

In the case of M_2 , considering the fully integrated q^2 region also leads to better sensi-

Observable	Wilson Coefficients
P_1	$\mathcal{C}_7, \mathcal{C}'_7, \mathcal{C}'_9, \mathcal{C}'_{10}$
P_2	$\mathcal{C}_7, \mathcal{C}'_7$
P_3	$\text{Im}(\mathcal{C}'_7, \mathcal{C}'_9, \mathcal{C}'_{10})$
P_4	$\mathcal{C}_7, \mathcal{C}'_7, \mathcal{C}_{10}, \mathcal{C}'_{10}$
P_5	$\mathcal{C}'_{10}, [\mathcal{C}_9]$
P_6	$\text{Im}(\mathcal{C}_7^{(\prime)}, \mathcal{C}_9^{(\prime)}, \mathcal{C}_{10}^{(\prime)})$
M_1	$[\mathcal{C}_7, \mathcal{C}'_7]$
M_2	$[\mathcal{C}_P - \mathcal{C}'_P]$
S_1	$\mathcal{C}_S - \mathcal{C}'_S$
S_2	$[\mathcal{C}_S - \mathcal{C}'_S]$

Table 6. Main contributions to the observables from NP Wilson Coefficients. The listed WC's produce strong deviations from the SM (consistent with all other bounds). For those listed in brackets, the effect is milder.

tivity to $\mathcal{C}_P^{(\prime)}$, since $M_2 > 0$ for all q^2 . However, the sensitivity in this case should be better than $\Delta(\int dq^2 M_2) \sim 0.03 \text{ GeV}^2$, before the current bounds on the difference $\mathcal{C}_P - \mathcal{C}'_P$ can be probed.

Finally, for the sake of completeness, we show in the third row of figure 2 the observables $d\Gamma/dq^2$ and A_{FB} in the SM and in Scenarios A, B, C and D. It becomes manifest that these observables are affected by larger hadronic uncertainties, and show a milder sensitivity to NP effects. Although the forward-backward asymmetry seems to suffer a significant enhancement in Scenario A.2, this scenario can be much more effectively probed by the observables P_1 or P_4 .

A summary of the NP sensitivity of each observable can be found in table 6. For each observable, we list the Wilson coefficients whose NP contributions affect most strongly the values of the given observable. We also present within brackets those Wilson coefficients whose effect is moderate.

8 Summary of results

The angular distribution of the four body decay $\bar{B}_d \rightarrow \bar{K}^{*0}(\rightarrow K\pi)\ell^+\ell^-$ can be studied experimentally by doing a fit to the coefficients $J_i(q^2)$ of the distribution, defined customarily as in eq. (1.1). The contact with theory is given by the expressions of the coefficients J_i in terms of the transversity amplitudes, as shown in eq. (2.1) [where β_ℓ is defined in eq. (2.2)]. In general, these amplitudes are $A_{\parallel,\perp,0}^{L,R}$, A_t and A_S .

However, depending on the case (if the masses of the leptons are negligible, as for example if $\ell^\pm = e^\pm$, or if there are no NP contributions from scalar operators), these coefficients are not independent. In such cases, an independent fit to all the coefficients can be problematic. Moreover, since such correlations contain physical information, it is interesting not only to have them identified, but to take profit of them.

On the other hand, the coefficients J_i are not the best observables to consider from the theory point of view because they suffer from large hadronic uncertainties. This has been noticed before and many theoretically clean observables have been devised in the literature. However, not all the observables that one can construct from the transversity amplitudes can be extracted from the angular distribution if they violate some “symmetry properties”.

With the development of a formalism based on these “symmetries”, together with the above considerations, in this paper we have constructed a complete and efficient set of observables engineered to extract the maximum information from the angular distribution:

1. In the most general case, the chosen basis of observables is composed by the FFD observables $d\Gamma/dq^2$ and A_{FB} [eqs. (3.6), (5.5)], and the FFI observables $P_{1,2,3,4,5,6}$ [eqs. (3.8)–(3.13)], $M_{1,2}$ [eqs. (4.4), (4.5)] and $S_{1,2}$ [eqs. (5.1), (5.2)]. The angular distribution in terms of the observables is given by eqs. (4.8)–(4.17), with χ defined in eq. (5.6). The uniangular distributions can be found in eqs. (6.4)–(6.6).
2. The reduction to the $A_S = 0$ case is obtained by setting $S_i = 0$ and $\chi = A_{\text{FB}}/P_2$. The vanishing of S_i leads to two dependencies among the J 's: $J_{6c} = 0$ and the relationship of eq. (2.3). In fact, S_1 and S_2 measure the breaking of these relations by scalar effects.
3. The reduction to the massless case ($m_\ell = 0$) is obtained by setting $\beta_\ell \rightarrow 1$ and $M_i = 0$. This leads to two further relationships between the J 's: $J_{1s} = 3J_{2s}$ and $J_{1c} = -J_{2c}$. In fact, M_1 and M_2 measure the breaking of these relations by mass effects.

The NP sensitivity analysis shows that these observables are quite sensitive to complementary NP effects. This can be observed in figures 1, 2 and in table 6. It is almost a certainty that future analyses of LHC data by the LHCb collaboration will be putting serious constraints on NP physics by studying these observables, or else discrepancies with respect to our SM predictions will be made manifest and constitute part of the first studies of true physics beyond the Standard Model.

Acknowledgments

We would like to thank Damir Becirevic for correspondence. J.M. acknowledges financial support from FPA2011-25948, SGR2009-00894. F.M. acknowledges financial support from FPA2010-20807 and the Consolider CPAN project. J.V. is supported in part by ICREA-Academia funds and FPA2011-25948.

A Symmetry formalism

In this appendix we complete the symmetry approach to the angular distribution that was originally presented for the massless case in ref. [8]. We present two different formalisms to describe the distribution. The first formalism, constructed using unitary matrices and two-component complex vectors, will be appropriate to describe both the massless and massive

cases. However, in order to introduce the scalar contributions a more general formalism is required. This second more powerful formalism introduces, instead, orthogonal matrices and four-component vectors and is valid for all cases.

We follow here a bottom-up approach, from the simplest (massless) case to the general case (massive with scalars). We also recall the solution of the system, expressing transversity amplitudes in terms of J 's, in the massless case (see ref. [8]), while the full solution to the system in the general case will be presented elsewhere [38].

The importance of determining these symmetries is mainly twofold. On the one hand, from the experimental point of view, the symmetries allow to identify all correlations between the coefficients of the distribution that may affect the stability of the fit; but they are also helpful to determine which amplitudes can be consistently put to zero, in order to simplify the system and consequently the fit. On the other hand, they provide you with an alternative procedure to construct observables directly in terms of the transversity amplitudes: verifying that they are invariant in the first place, and afterwards, translating their expression in terms of transversity amplitudes to an expression in terms of the measured coefficients J_i of the distribution (an example of this procedure was the observable $A_T^{(5)}$ designed in [8]).

A.1 Symmetries of the massless distribution

In this section we review the symmetry formalism for the massless angular distribution, as presented originally in ref. [8].

The six complex amplitudes present in this case can be arranged into three complex vectors:

$$n_{\parallel} = \begin{pmatrix} A_{\parallel}^L \\ A_{\parallel}^{R*} \end{pmatrix}, \quad n_{\perp} = \begin{pmatrix} A_{\perp}^L \\ -A_{\perp}^{R*} \end{pmatrix}, \quad n_0 = \begin{pmatrix} A_0^L \\ A_0^{R*} \end{pmatrix}. \quad (\text{A.1})$$

All the coefficients J_i can be expressed in terms of the products $n_i^{\dagger} n_j$:

$$\begin{aligned} J_{1s} &= \frac{3}{4} (|n_{\perp}|^2 + |n_{\parallel}|^2), & J_{1c} &= |n_0|^2, & J_{2s} &= \frac{1}{4} (|n_{\perp}|^2 + |n_{\parallel}|^2), \\ J_{2c} &= -|n_0|^2, & J_3 &= \frac{1}{2} (|n_{\perp}|^2 - |n_{\parallel}|^2), & J_4 &= \frac{1}{\sqrt{2}} \text{Re}(n_0^{\dagger} n_{\parallel}), \\ J_5 &= \sqrt{2} \text{Re}(n_0^{\dagger} n_{\perp}), & J_{6s} &= 2 \text{Re}(n_{\perp}^{\dagger} n_{\parallel}), & J_7 &= -\sqrt{2} \text{Im}(n_0^{\dagger} n_{\parallel}), \\ J_8 &= -\frac{1}{\sqrt{2}} \text{Im}(n_0^{\dagger} n_{\perp}), & J_9 &= -\text{Im}(n_{\perp}^{\dagger} n_{\parallel}), & J_{6c} &= 0. \end{aligned} \quad (\text{A.2})$$

A symmetry of the angular distribution will therefore be a unitary transformation U acting in the same way on n_0 , n_{\parallel} and n_{\perp} , that is: $n_i \rightarrow U n_i$. Such a symmetry has four independent parameters, and can be written as:

$$n_i' = U n_i = \begin{bmatrix} e^{i\phi_L} & 0 \\ 0 & e^{-i\phi_R} \end{bmatrix} \begin{bmatrix} \cos \theta & -\sin \theta \\ \sin \theta & \cos \theta \end{bmatrix} \begin{bmatrix} \cosh i\tilde{\theta} & -\sinh i\tilde{\theta} \\ -\sinh i\tilde{\theta} & \cosh i\tilde{\theta} \end{bmatrix} n_i. \quad (\text{A.3})$$

Of course, other parametrizations are possible, but we prefer to keep this one to make an easy contact with the generalization to the massive case and the notation introduced in

ref. [8]. The matrix U defines the four symmetries of the massless angular distribution: two global phase transformations (ϕ_L and ϕ_R), a rotation θ among the real and imaginary components of the amplitudes independently and another rotation $\tilde{\theta}$ that mixes real and imaginary components of the transversity amplitudes.

A.1.1 Solution to the massless distribution

We can now use these symmetries to reduce the number of theoretical parameters and solve for the transversity amplitudes in terms of the coefficients J 's. It is instructive to use only three out of the four symmetries and see how the extra freedom related to the fourth symmetry arises from the equations. This extra freedom gives rise to the non-linear relation between the J 's given in eq. (2.3).

Using the symmetries we choose to fix the following amplitudes to zero: $A_{\parallel}^L = 0$ and $\text{Im}A_{\parallel}^R = 0$. We achieve this configuration easily using the rotation phases ϕ_L and ϕ_R to set the phases of A_{\parallel}^L and A_{\parallel}^R to zero. Then a rotation by an angle θ given by

$$\tan \theta = \frac{\text{Re}A_{\parallel}^L}{\text{Re}A_{\parallel}^R} \tag{A.4}$$

will also set the modulus of A_{\parallel}^L to zero.

With these simplifications, rewriting the products $n_i^\dagger n_j$ in this configuration, and taking into account eqs. (A.2), one gets immediately:

$$\begin{aligned} A_{\parallel}^L &= 0, & A_{\parallel}^R &= \sqrt{2J_{2s} - J_3}, \\ A_{\perp}^R &= -\frac{J_{6s} - 2iJ_9}{2\sqrt{2J_{2s} - J_3}}, & A_0^R &= \frac{2J_4 - iJ_7}{\sqrt{4J_{2s} - 2J_3}}. \end{aligned} \tag{A.5}$$

The remaining equations involving the last two amplitudes (A_{\perp}^L and A_0^L) lead to [8]

$$e^{i(\phi_0^L - \phi_{\perp}^L)} = \frac{2(2J_{2s} - J_3)(J_5 + 2iJ_8) - (2J_4 + iJ_7)(J_{6s} - 2iJ_9)}{\sqrt{16J_{2s}^2 - 4J_3^2 - J_{6s}^2 - 4J_9^2} \sqrt{2J_{1c}(2J_{2s} - J_3) - 4J_4^2 - J_7^2}}, \tag{A.6}$$

where ϕ_0^L and ϕ_{\perp}^L are the phases associated to the amplitudes A_0^L and A_{\perp}^L . The relation between the J_i coefficients (eq. (2.3)) arises naturally from imposing in eq. (A.6) that the modulus of this phase difference should be one. Notice also that the freedom to choose one of the two phases in eq. (A.6) to be zero is somehow related to the freedom associated to the last unused symmetry transformation $\tilde{\theta}$. The choice $\phi_{\perp}^L = 0$ fixes the last two amplitudes to

$$\begin{aligned} A_{\perp}^L &= \frac{\sqrt{16J_{2s}^2 - 4J_3^2 - J_{6s}^2 - 4J_9^2}}{2\sqrt{2J_{2s} - J_3}}, \\ A_0^L &= \frac{2(2J_{2s} - J_3)(J_5 + 2iJ_8) - (2J_4 + iJ_7)(J_{6s} - 2iJ_9)}{\sqrt{4J_{2s} - 2J_3} \sqrt{16J_{2s}^2 - 4J_3^2 - J_{6s}^2 - 4J_9^2}}. \end{aligned} \tag{A.7}$$

The solution in any other configuration can be obtained by applying the symmetry transformation in eq. (A.3). Any observable constructed from the transversity amplitudes, can be expressed in terms of the coefficients J_i using eqs. (A.5) and (A.7). The condition that the observable is invariant under the symmetries of the angular distribution, guarantees that the configuration used to derive these equations gives the same result for the observables as any other configuration, and the result is unique.

A.2 Symmetries of the massive distribution

In the massive case the balance equation between theoretical and experimental degrees of freedom [8]

$$n_{exp} \equiv n_J - n_d = 2n_A - n_S \quad (\text{A.8})$$

is fulfilled with $n_J = 12$, $n_d = 2$, $n_A = 7$ and $n_S = 4$, where n_d is the number of relationships among the J_i , as explained in section 2. When the masses are switched on to account for lepton mass corrections in $B_d \rightarrow K^{*0}(\rightarrow K\pi)\ell^+\ell^-$, all the massless symmetries described in the previous section are broken by the mass terms and have to be redefined. The four symmetries in the massive case are then:

- A common global phase transformation for both left and right components

$$n'_i = U_0(\phi)n_i = \begin{bmatrix} e^{i\phi} & 0 \\ 0 & e^{-i\phi} \end{bmatrix} n_i, \quad (\text{A.9})$$

for $i = \parallel, \perp, 0$.

- An independent new global phase transformation for the A_t amplitude: $A'_t = e^{i\phi_t} A_t$.
- Two rotations $U_1(\theta)$ and $U_2(\tilde{\theta})$ between the real and imaginary components of the transversity amplitudes $A_i^{L,R}$:

$$n'_i = U_1(\theta)n_i, \quad n'_i = U_2(\tilde{\theta})n_i,$$

($i = \perp, \parallel, 0$) with a similar structure to those in the massless case, but including some important differences to be discussed below.

In order to find the explicit form of the last two symmetries, $U_1(\theta)$ and $U_2(\tilde{\theta})$, it is helpful to analyze their infinitesimal form. This can be obtained following the approach described in ref. [8]. Let us focus on $U_1(\theta)$ and require that the infinitesimal transformation of the amplitudes is a symmetry of the distribution. This leads to the following form of the infinitesimal transformation associated to a rotation with angle $\theta \sim \epsilon$,

$$\begin{aligned} A_{\perp}^{L'} &= A_{\perp}^L + \epsilon A_{\perp}^{R*}, \\ A_{\parallel}^{L'} &= A_{\parallel}^L - \epsilon A_{\parallel}^{R*}, \\ A_0^{L'} &= A_0^L - \epsilon A_0^{R*}, \\ A_{\perp}^{R'} &= A_{\perp}^R - \epsilon A_{\perp}^{L*} - i\epsilon A_{\perp}^R k, \\ A_{\parallel}^{R'} &= A_{\parallel}^R + \epsilon A_{\parallel}^{L*} - i\epsilon A_{\parallel}^R k, \\ A_0^{R'} &= A_0^R + \epsilon A_0^{L*} - i\epsilon A_0^R k, \\ |A_t^{L'}|^2 &= |A_t^L|^2 - 2\epsilon [\text{Re}(A_0^{L2}) - \text{Re}(A_0^{R2}) + k \text{Im}(A_0^{L*} A_0^R)], \end{aligned} \quad (\text{A.10})$$

where $k = [(\text{Re}(A_{\parallel}^{L2}) - \text{Re}(A_{\parallel}^{R2})) - (\parallel \leftrightarrow \perp)] / [\text{Im}(A_{\parallel}^L A_{\parallel}^{R*}) + (\parallel \leftrightarrow \perp)]$. Eq. (A.10) together with some important observations will guide us in the construction of the corresponding continuous transformation, namely:

- I. The structure of the distribution and the absence of lepton masses in the infinitesimal transformation informs us that the symmetries of the massive distribution should be also symmetries of the massless case; consequently, the form of the rotation matrices should respect the form of the transformations in the massless case.
- II. The infinitesimal form shows that while the left components transform linearly, the right components transform non-linearly. Moreover, in the limit of $k \rightarrow 0$, the linear transformations of the massless case are recovered.
- III. All J_i , except for J_{1s} and J_{1c} , are invariant under this infinitesimal transformation independently of the explicit form of k . This last remark is, indeed, connected to point I.

These considerations taken together imply that the continuous symmetry transformations $U_1(\theta)$ and $U_2(\tilde{\theta})$ should take the form:

$$U_1(\theta) = \begin{bmatrix} \cos \theta & -\sin \theta \\ e^{-i\delta(\theta)} \sin \theta & e^{-i\delta(\theta)} \cos \theta \end{bmatrix}, \quad U_2(\tilde{\theta}) = \begin{bmatrix} \cosh i\tilde{\theta} & -\sinh i\tilde{\theta} \\ -e^{-i\tilde{\delta}(\tilde{\theta})} \sinh i\tilde{\theta} & e^{-i\tilde{\delta}(\tilde{\theta})} \cosh i\tilde{\theta} \end{bmatrix}. \quad (\text{A.11})$$

The last step to determine these rotation matrices completely is to obtain the phases $\delta(\theta)$ and $\tilde{\delta}(\tilde{\theta})$. These are non-linear functions of the transversity amplitudes and the angles θ and $\tilde{\theta}$, respectively. In a certain sense, the goal of these non-linear pieces is to cure the breaking of the massless symmetry by the massive terms, while respecting the basic structure of the massless symmetry. Imposing that the mass term in J_{1s}

$$\text{Re} \left(A_{\perp}^L A_{\perp}^{R*} + A_{\parallel}^L A_{\parallel}^{R*} \right) \quad (\text{A.12})$$

should be invariant under the symmetry transformation, we obtain that $\sin \delta(\theta)$ and $\cos \delta(\theta)$ are just the result of a rotation of a unitary vector $(\sin v, \cos v)$ whose first component $(\sin v)$ is indeed proportional to the mass term. This rotation is

$$\begin{pmatrix} \sin \delta(\theta) \\ \cos \delta(\theta) \end{pmatrix} = \begin{pmatrix} \cos u & -\sin u \\ \sin u & \cos u \end{pmatrix} \begin{pmatrix} \sin v \\ \cos v \end{pmatrix}, \quad (\text{A.13})$$

where $\sin v = x_1/\sqrt{h(\theta)}$, $\cos v = \eta_{y_1} \sqrt{1 - x_1^2/h(\theta)}$ and η_{y_1} is the sign of the function y_1 . The sign function has been introduced to ensure that $\delta(0) = 0$, which implies that the transformation matrix becomes the identity matrix⁵ for $\theta \rightarrow 0$. The rotation (u) is defined by

$$\cos u = \frac{y_1 \cos 2\theta + y_2 \sin 2\theta}{\sqrt{h(\theta)}}, \quad \sin u = \frac{x_1 \cos 2\theta + x_2 \sin 2\theta}{\sqrt{h(\theta)}}, \quad (\text{A.14})$$

where

$$\begin{aligned} x_1 &= \text{Re}(A_{\parallel}^L A_{\parallel}^{R*}) + (\parallel \leftrightarrow \perp), & x_2 &= \frac{1}{2} \left[\text{Re}(A_{\parallel}^L{}^2) - \text{Re}(A_{\parallel}^R{}^2) \right] - (\parallel \leftrightarrow \perp), \\ y_1 &= \text{Im}(A_{\parallel}^L A_{\parallel}^{R*}) + (\parallel \leftrightarrow \perp), & y_2 &= \frac{1}{2} \left[\text{Im}(A_{\parallel}^L{}^2) + \text{Im}(A_{\parallel}^R{}^2) \right] - (\parallel \leftrightarrow \perp), \\ h(\theta) &= (x_1 \cos 2\theta + x_2 \sin 2\theta)^2 + (y_1 \cos 2\theta + y_2 \sin 2\theta)^2. \end{aligned} \quad (\text{A.15})$$

⁵Notice, however, that the $\cos v$ defined as $\cos v = -\eta_{y_1} \sqrt{1 - x_1^2/h(\theta)}$ is also a solution, even if not connected to the identity in the limit $\theta \rightarrow 0$.

x_1 is precisely the mass term of J_{1s} . Being an invariant, it can be expressed in terms of the coefficients J_i of the distribution:

$$x_1 = \frac{q^2}{m_\ell^2} \frac{(2 + \beta_\ell^2)}{4} \left(\frac{J_{1s}}{2 + \beta_\ell^2} - \frac{J_{2s}}{\beta_\ell^2} \right). \quad (\text{A.16})$$

Also the non-linear parameter k in eq. (A.10) can be rewritten as $k = 2x_2/y_1$. Notice that due to the non-linear form of the transformation

$$U_1(\theta_1) \cdot U_1(\theta_2) \neq U_1(\theta_1 + \theta_2).$$

This does not pose a problem since one can easily concatenate transformations, one after the other, always evaluating the corresponding $\delta(\theta_i)$ for each transformation. A final important remark is that the requirement of $\sqrt{1 - x_1^2/h(\theta)}$ to be real imposes a restriction for the range of validity of the transformation around $\theta = 0$, i.e., there is a maximum and a minimum allowed value for θ , given by the condition

$$\left| \frac{x_1}{\sqrt{h(\theta)}} \right| \leq 1. \quad (\text{A.17})$$

Inside this range of validity $\delta(\theta)$ is simply given by $\delta(\theta) = v - u$.

To complete the transformation of all amplitudes under $U_1(\theta)$ we still need to find the transformation of the amplitude A_t . This is obtained by imposing the invariance of the mass term in J_{1c}

$$|A'_t|^2 = |A_t|^2 + 2 \left(\text{Re}(A_0^L A_0^{R*}) - \text{Re}(A_0^{L'} A_0^{R'*}) \right), \quad (\text{A.18})$$

where the primed $A_0^{L,R}$ can be obtained easily from n'_0 .

Following exactly the same steps for the symmetry transformation $U_2(\tilde{\theta})$ we can also identify the corresponding $\tilde{\delta}(\tilde{\theta})$ by the rotation

$$\begin{pmatrix} \sin \tilde{\delta}(\tilde{\theta}) \\ \cos \tilde{\delta}(\tilde{\theta}) \end{pmatrix} = \begin{pmatrix} \cos \tilde{u} & -\sin \tilde{u} \\ \sin \tilde{u} & \cos \tilde{u} \end{pmatrix} \begin{pmatrix} \sin \tilde{v} \\ \cos \tilde{v} \end{pmatrix}, \quad (\text{A.19})$$

where $\sin \tilde{v} = \tilde{x}_1/\sqrt{\tilde{h}(\tilde{\theta})}$, $\cos \tilde{v} = \eta_{\tilde{y}_1} \sqrt{1 - \tilde{x}_1^2/\tilde{h}(\tilde{\theta})}$, $\eta_{\tilde{y}_1}$ is the sign of the function \tilde{y}_1 and

$$\cos \tilde{u} = \frac{\tilde{y}_1 \cos 2\tilde{\theta} + \tilde{y}_2 \sin 2\tilde{\theta}}{\sqrt{\tilde{h}(\tilde{\theta})}}, \quad \sin \tilde{u} = \frac{\tilde{x}_1 \cos 2\tilde{\theta} + \tilde{x}_2 \sin 2\tilde{\theta}}{\sqrt{\tilde{h}(\tilde{\theta})}}, \quad (\text{A.20})$$

with

$$\begin{aligned} \tilde{x}_1 &= x_1, & \tilde{x}_2 &= \frac{1}{2} \left[\text{Im}(A_{\parallel}^{L2}) - \text{Im}(A_{\parallel}^{R2}) \right] - (\parallel \leftrightarrow \perp), \\ \tilde{y}_1 &= y_1, & \tilde{y}_2 &= \frac{1}{2} \left[-\text{Re}(A_{\parallel}^{L2}) - \text{Re}(A_{\parallel}^{R2}) \right] - (\parallel \leftrightarrow \perp), \\ \tilde{h}(\tilde{\theta}) &= (\tilde{x}_1 \cos 2\tilde{\theta} + \tilde{x}_2 \sin 2\tilde{\theta})^2 + (\tilde{y}_1 \cos 2\tilde{\theta} + \tilde{y}_2 \sin 2\tilde{\theta})^2. \end{aligned} \quad (\text{A.21})$$

The same discussion about the range of validity can be applied to $U_2(\tilde{\theta})$ just by substituting in eq. (A.17) $x_i \rightarrow \tilde{x}_i$, $h(\theta) \rightarrow \tilde{h}(\tilde{\theta})$ and now $\tilde{\delta}(\tilde{\theta}) = \tilde{v} - \tilde{u}$. $|A'_t|^2$ can be computed from eq. (A.18) but using the corresponding primed $A_0^{L,R}$ amplitudes under the $U_2(\tilde{\theta})$ transformation.

A.3 Symmetries in the presence of scalar contributions

The last case to discuss here is the symmetry structure of the angular distribution in presence of scalar contributions to the decay channel $B_d \rightarrow K^{*0}(\rightarrow K\pi)\ell^+\ell^-$.

The infinitesimal transformation, too long to write it explicitly here, provides the following important information:

- A_\perp and A_\parallel transform exactly as in the massive case.
- A_0 and A_S get mixed in the transformation and, contrary to the massive case, an explicit dependence on the lepton mass appears in the symmetry transformation. This has an important consequence for the construction of observables: while the lepton mass terms in J_{1s} is invariant by itself, the mass terms in J_5 and J_7 are not.

Another fundamental difference with the previous cases, is that the use of the compact two-component complex vector n_i is no longer possible for A_0 and A_S . Consequently, we will introduce a new formalism in terms of four-component vectors

$$\vec{v}_\parallel = \begin{pmatrix} \text{Re}A_\parallel^L \\ \text{Im}A_\parallel^L \\ \text{Re}A_\parallel^R \\ \text{Im}A_\parallel^R \end{pmatrix}, \quad \vec{v}_\perp = \begin{pmatrix} \text{Re}A_\perp^L \\ \text{Im}A_\perp^L \\ -\text{Re}A_\perp^R \\ -\text{Im}A_\perp^R \end{pmatrix}, \quad \vec{v}_0 = \begin{pmatrix} \text{Re}A_0^L \\ \text{Im}A_0^L \\ \text{Re}A_0^R \\ \text{Im}A_0^R \end{pmatrix}, \quad \vec{v}_S = \begin{pmatrix} \text{Re}A_S \\ \text{Im}A_S \\ 0 \\ 0 \end{pmatrix} \quad (\text{A.22})$$

and two 4×4 matrices

$$C = \begin{pmatrix} \mathbb{I}_2 & \mathbb{I}_2 \\ \mathbb{I}_2 & \mathbb{I}_2 \end{pmatrix}, \quad \gamma = \begin{pmatrix} -i\sigma_2 & 0 \\ 0 & i\sigma_2 \end{pmatrix} \quad (\text{A.23})$$

and will describe the angular distribution in terms of them. Notice that $\gamma^T = -\gamma$ and $\gamma \cdot \gamma^T = \mathbb{I}_4$. We remind here the explicit form of the Pauli σ matrices:

$$\sigma_1 = \begin{pmatrix} 0 & 1 \\ 1 & 0 \end{pmatrix}, \quad \sigma_2 = \begin{pmatrix} 0 & -i \\ i & 0 \end{pmatrix}, \quad \sigma_3 = \begin{pmatrix} 1 & 0 \\ 0 & -1 \end{pmatrix}. \quad (\text{A.24})$$

The matrix C is needed to symmetrize the vector \vec{v}_S , which appears in the angular distribution as $v_{\vec{S}C} \equiv C \cdot \vec{v}_S$. In terms of the four vectors in eq. (A.22) and the two matrices in

eq. (A.23) one can rewrite the coefficients J_i including scalars as

$$\begin{aligned}
J_{1s} &= \frac{(2 + \beta_\ell^2)}{4} (\vec{v}_\perp \cdot \vec{v}_\perp + \vec{v}_\parallel \cdot \vec{v}_\parallel) + 2 \frac{m_\ell^2}{q^2} (\vec{v}_\parallel \cdot (C - \mathbb{I}_4) \cdot \vec{v}_\parallel - \vec{v}_\perp \cdot (C - \mathbb{I}_4) \cdot \vec{v}_\perp), \\
J_{1c} &= \vec{v}_0 \cdot \vec{v}_0 + 4 \frac{m_\ell^2}{q^2} (\vec{v}_0 \cdot (C - \mathbb{I}_4) \cdot \vec{v}_0 + |A_t|^2) + \frac{\beta_\ell^2}{2} (v_{\vec{S}C} \cdot v_{\vec{S}C}), \\
J_{2s} &= \frac{\beta_\ell^2}{4} (\vec{v}_\perp \cdot \vec{v}_\perp + \vec{v}_\parallel \cdot \vec{v}_\parallel), & J_{2c} &= -\beta_\ell^2 (\vec{v}_0 \cdot \vec{v}_0), \\
J_3 &= \frac{\beta_\ell^2}{2} (\vec{v}_\perp \cdot \vec{v}_\perp - \vec{v}_\parallel \cdot \vec{v}_\parallel), & J_4 &= \frac{1}{\sqrt{2}} \beta_\ell^2 (\vec{v}_\parallel \cdot \vec{v}_0), \\
J_5 &= \sqrt{2} \beta_\ell \left(\vec{v}_\perp \cdot \vec{v}_0 - \frac{m_\ell}{\sqrt{q^2}} \vec{v}_\parallel \cdot v_{\vec{S}C} \right), & J_{6s} &= 2 \beta_\ell (\vec{v}_\parallel \cdot \vec{v}_\perp), \\
J_{6c} &= 4 \beta_\ell \frac{m_\ell}{\sqrt{q^2}} (\vec{v}_0 \cdot v_{\vec{S}C}), & J_7 &= -\sqrt{2} \beta_\ell \left(\vec{v}_\parallel \cdot \gamma \cdot \vec{v}_0 - \frac{m_\ell}{\sqrt{q^2}} \vec{v}_\perp \cdot \gamma \cdot v_{\vec{S}C} \right), \\
J_8 &= -\frac{1}{\sqrt{2}} \beta_\ell^2 (\vec{v}_\perp \cdot \gamma \cdot \vec{v}_0), & J_9 &= -\beta_\ell^2 (\vec{v}_\parallel \cdot \gamma \cdot \vec{v}_\perp).
\end{aligned} \tag{A.25}$$

The angular distribution exhibits four symmetries:

- A global phase transformation⁶ for

$$\vec{v}_j = V_{(0)}(\phi) \vec{v}_j, \tag{A.26}$$

with $j = \parallel, \perp, 0, SC$, and where

$$V_{(0)} = \begin{bmatrix} \cos \phi & -\sin \phi & 0 & 0 \\ \sin \phi & \cos \phi & 0 & 0 \\ 0 & 0 & \cos \phi & -\sin \phi \\ 0 & 0 & \sin \phi & \cos \phi \end{bmatrix}. \tag{A.27}$$

- An independent phase transformation for the A_t amplitude: $A'_t = e^{i\phi t} A_t$.
- And the same two rotations of the massive case. However, there is an important difference between the transformation properties of $A_\perp^{L,R}$, $A_\parallel^{L,R}$ on one side and the transformation properties of $A_0^{L,R}$, A_S on the other, that will be detailed in the following.

On the one hand, $A_\perp^{L,R}$ and $A_\parallel^{L,R}$ transform exactly as in the massive case

$$\vec{v}_j = V_{(1)}(\theta) \vec{v}_j \quad \text{and} \quad \vec{v}'_j = V_{(2)}(\tilde{\theta}) \vec{v}_j \tag{A.28}$$

for $j = \perp, \parallel$ and the matrices $V_{(1)}(\theta)$ and $V_{(2)}(\tilde{\theta})$ are simply the mapping of the 2x2 matrices $U_1(\theta)$ and $U_2(\tilde{\theta})$ in the 4-d formalism and are defined by

$$V_{(1)}(\theta) = \begin{bmatrix} \cos \theta & 0 & -\sin \theta & 0 \\ 0 & \cos \theta & 0 & \sin \theta \\ \cos \delta \sin \theta & \sin \delta \sin \theta & \cos \delta \cos \theta & -\sin \delta \cos \theta \\ \sin \delta \sin \theta & -\cos \delta \sin \theta & \sin \delta \cos \theta & \cos \delta \cos \theta \end{bmatrix} \tag{A.29}$$

⁶Incidentally notice that the matrix γ can be interpreted also as a phase transformation of $\pi/2$ for the L components and $-\pi/2$ for the R components.

and

$$V_{(2)}(\tilde{\theta}) = \begin{bmatrix} \cos \tilde{\theta} & 0 & 0 & -\sin \tilde{\theta} \\ 0 & \cos \tilde{\theta} & -\sin \tilde{\theta} & 0 \\ -\sin \tilde{\delta} \sin \tilde{\theta} \cos \tilde{\delta} \sin \tilde{\theta} \cos \tilde{\delta} \cos \tilde{\theta} & -\sin \tilde{\delta} \cos \tilde{\theta} & & \\ \cos \tilde{\delta} \sin \tilde{\theta} \sin \tilde{\delta} \sin \tilde{\theta} \sin \tilde{\delta} \cos \tilde{\theta} & \cos \tilde{\delta} \cos \tilde{\theta} & & \end{bmatrix}. \quad (\text{A.30})$$

The non-linear structures $\delta(\theta)$ and $\tilde{\delta}(\tilde{\theta})$ in $V_{(1)}(\theta)$ and $V_{(2)}(\tilde{\theta})$ are the same as in eq. (A.13) and eq. (A.19) respectively. In this new formalism, the expression of x_i , y_i , \tilde{x}_i and \tilde{y}_i can be rewritten in a more compact way:

$$x_1 = (\vec{v}_{\parallel} \cdot (C - \mathbb{I}_4) \cdot \vec{v}_{\parallel} - \vec{v}_{\perp} \cdot (C - \mathbb{I}_4) \cdot \vec{v}_{\perp}) / 2, \quad (\text{A.31})$$

$$x_2 = (\vec{v}_{\parallel} \cdot C_{x2} \cdot \vec{v}_{\parallel} - \vec{v}_{\perp} \cdot C_{x2} \cdot \vec{v}_{\perp}) / 2, \quad (\text{A.32})$$

$$y_1 = (\vec{v}_{\parallel} \cdot C_{y1} \cdot \vec{v}_{\parallel} - \vec{v}_{\perp} \cdot C_{y1} \cdot \vec{v}_{\perp}) / 2, \quad (\text{A.33})$$

$$y_2 = (\vec{v}_{\parallel} \cdot C_{y2} \cdot \vec{v}_{\parallel} - \vec{v}_{\perp} \cdot C_{y2} \cdot \vec{v}_{\perp}) / 2 \quad (\text{A.34})$$

and

$$\tilde{x}_1 = x_1, \quad \tilde{y}_1 = y_1, \quad (\text{A.35})$$

$$\tilde{x}_2 = (\vec{v}_{\parallel} \cdot C_{\tilde{x}2} \cdot \vec{v}_{\parallel} - \vec{v}_{\perp} \cdot C_{\tilde{x}2} \cdot \vec{v}_{\perp}) / 2, \quad (\text{A.36})$$

$$\tilde{y}_2 = (\vec{v}_{\parallel} \cdot C_{\tilde{y}2} \cdot \vec{v}_{\parallel} - \vec{v}_{\perp} \cdot C_{\tilde{y}2} \cdot \vec{v}_{\perp}) / 2, \quad (\text{A.37})$$

with

$$C_{x2} = \begin{pmatrix} \sigma_3 & 0 \\ 0 & -\sigma_3 \end{pmatrix}, \quad C_{y1} = \begin{pmatrix} 0 & -i\sigma_2 \\ i\sigma_2 & 0 \end{pmatrix}, \quad C_{y2} = \begin{pmatrix} \sigma_1 & 0 \\ 0 & \sigma_1 \end{pmatrix},$$

$$C_{\tilde{x}2} = \begin{pmatrix} \sigma_1 & 0 \\ 0 & -\sigma_1 \end{pmatrix}, \quad C_{\tilde{y}2} = \begin{pmatrix} -\sigma_3 & 0 \\ 0 & -\sigma_3 \end{pmatrix}. \quad (\text{A.38})$$

On the other hand, in the scalar case the transformation of the amplitudes $A_0^{L,R}$ is different from the massive case, but shares the same structure than the transformation of A_S :

$$\vec{v}_0^j = V_{(j)} \left(\hat{v}_0^{(j)} + \vec{v}_0 \right), \quad \vec{v}_{SC}^j = V_{(j)} \left(\hat{v}_S^{(j)} + v_{SC} \right), \quad (\text{A.39})$$

where

$$\hat{v}_0^{(j)} = \begin{pmatrix} \hat{v}_{01}^{(j)} \\ \hat{v}_{02}^{(j)} \\ \hat{v}_{03}^{(j)} \\ \hat{v}_{04}^{(j)} \end{pmatrix}, \quad \hat{v}_S^{(j)} = \begin{pmatrix} \hat{v}_{S1}^{(j)} \\ \hat{v}_{S2}^{(j)} \\ \hat{v}_{S3}^{(j)} \\ \hat{v}_{S4}^{(j)} \end{pmatrix}, \quad (\text{A.40})$$

with $j = 1, 2$. These vectors contain the non-linear part of the transformation associated to $A_0^{L,R}$ and A_S and are functions of θ (for $j = 1$), $\tilde{\theta}$ (for $j = 2$), all amplitudes and the lepton mass m_ℓ .

The last remaining point is to determine $\hat{v}_0^{(j)}$ and $\hat{v}_S^{(j)}$. They are fixed by requiring the invariance of the angular distribution under the $V_1(\theta)$ and $V_2(\tilde{\theta})$ transformations. The

set of eight equations required to obtain the components of $\hat{v}_0^{(j)}$ and $\hat{v}_S^{(j)}$ arise from the coefficients J_4, J_5, J_7 and J_8 after imposing the invariance of the angular distribution under the transformations:

$$\begin{aligned} \vec{v}_{\parallel} \cdot \hat{v}_0^{(j)} &= 0, & v_{\perp} \cdot \gamma \cdot \hat{v}_0^{(j)} &= 0, \\ v_{\perp} \cdot \hat{v}_0^{(j)} - \frac{m_{\ell}}{\sqrt{q^2}} \vec{v}_{\parallel} \cdot \hat{v}_S^{(j)} &= 0, & \vec{v}_{\parallel} \cdot \gamma \cdot \hat{v}_0^{(j)} - \frac{m_{\ell}}{\sqrt{q^2}} v_{\perp} \cdot \gamma \cdot \hat{v}_S^{(j)} &= 0, \end{aligned} \quad (\text{A.41})$$

together with the ones derived from J_{2c} and J_{6c}

$$\hat{v}_0^{(j)} \cdot \hat{v}_0^{(j)} + 2\hat{v}_0^{(j)} \cdot \vec{v}_0 = 0, \quad \hat{v}_0^{(j)} \cdot \hat{v}_S^{(j)} + \hat{v}_0^{(j)} \cdot v_{\vec{S}C} + \vec{v}_0 \cdot \hat{v}_S^{(j)} = 0, \quad (\text{A.42})$$

and two more equations to impose that the first component of the vector $v_{\vec{S}C}'$ must equal the third while the second component should equal the fourth⁷

$$\vec{d}^{(j)} \cdot (\hat{v}_S^{(j)} + v_{\vec{S}C}) = 0, \quad \vec{e}^{(j)} \cdot (\hat{v}_S^{(j)} + v_{\vec{S}C}) = 0, \quad (\text{A.43})$$

where

$$\begin{aligned} \vec{d}^{(j)} &= (V_{(j)1,1} - V_{(j)3,1}, V_{(j)1,2} - V_{(j)3,2}, V_{(j)1,3} - V_{(j)3,3}, V_{(j)1,4} - V_{(j)3,4}), \\ \vec{e}^{(j)} &= (V_{(j)2,1} - V_{(j)4,1}, V_{(j)2,2} - V_{(j)4,2}, V_{(j)2,3} - V_{(j)4,3}, V_{(j)2,4} - V_{(j)4,4}). \end{aligned} \quad (\text{A.44})$$

The system can be solved as follows:

- I. Obtain $\hat{v}_0^{(j)}$ in terms of $\hat{v}_S^{(j)}$ from the first set of eqs. (A.41). The components of the vector $\hat{v}_0^{(j)}$ are then:

$$\begin{aligned} \hat{v}_{01}^{(j)} &= m_1^{(j)} \text{Re}X^{L,R} + m_2^{(j)} \text{Im}Y^{L,R}, & \hat{v}_{02}^{(j)} &= m_1^{(j)} \text{Im}X^{L,R} - m_2^{(j)} \text{Re}Y^{L,R}, \\ \hat{v}_{03}^{(j)} &= -m_1^{(j)} \text{Re}X^{R,L} - m_2^{(j)} \text{Im}Y^{R,L}, & \hat{v}_{04}^{(j)} &= -m_1^{(j)} \text{Im}X^{R,L} + m_2^{(j)} \text{Re}Y^{R,L} \end{aligned} \quad (\text{A.45})$$

where

$$\begin{aligned} X^{a,b} &= A_{\parallel}^a A_{\perp}^{*b} A_{\parallel}^b + |A_{\parallel}^b|^2 A_{\perp}^a, \\ Y^{a,b} &= A_{\perp}^a A_{\parallel}^{*b} A_{\perp}^b + |A_{\perp}^b|^2 A_{\parallel}^a, \end{aligned} \quad (\text{A.46})$$

with

$$m_1^{(j)} = \frac{1}{\omega} \frac{m_{\ell}}{\sqrt{q^2}} \vec{v}_{\parallel} \cdot \hat{v}_S^{(j)}, \quad m_2^{(j)} = \frac{1}{\omega} \frac{m_{\ell}}{\sqrt{q^2}} v_{\perp} \cdot \gamma \cdot \hat{v}_S^{(j)} \quad (\text{A.47})$$

and $\omega = |A_{\perp}^L|^2 |A_{\parallel}^R|^2 + |A_{\perp}^R|^2 |A_{\parallel}^L|^2 + 2\text{Re}(A_{\parallel}^{L*} A_{\perp}^L A_{\perp}^R A_{\parallel}^{R*})$.

- II. Use eq. (A.43) to express the components $\hat{v}_{S3}^{(j)}$ and $\hat{v}_{S4}^{(j)}$ in terms of $\hat{v}_{S1}^{(j)}$ and $\hat{v}_{S2}^{(j)}$:

$$\begin{aligned} \hat{v}_{S3}^{(j)} &= \frac{d_1^{(j)} e_4^{(j)} - d_4^{(j)} e_1^{(j)}}{d_4^{(j)} e_3^{(j)} - d_3^{(j)} e_4^{(j)}} \left[\hat{v}_{S1}^{(j)} + \text{Re}A_S \right] + \frac{d_2^{(j)} e_4^{(j)} - d_4^{(j)} e_2^{(j)}}{d_4^{(j)} e_3^{(j)} - d_3^{(j)} e_4^{(j)}} \left[\hat{v}_{S2}^{(j)} + \text{Im}A_S \right] - \text{Re}A_S \\ \hat{v}_{S4}^{(j)} &= \frac{d_3^{(j)} e_1^{(j)} - d_1^{(j)} e_3^{(j)}}{d_4^{(j)} e_3^{(j)} - d_3^{(j)} e_4^{(j)}} \left[\hat{v}_{S1}^{(j)} + \text{Re}A_S \right] + \frac{d_3^{(j)} e_2^{(j)} - d_2^{(j)} e_3^{(j)}}{d_4^{(j)} e_3^{(j)} - d_3^{(j)} e_4^{(j)}} \left[\hat{v}_{S2}^{(j)} + \text{Im}A_S \right] - \text{Im}A_S \end{aligned} \quad (\text{A.48})$$

⁷Therefore $v_{\vec{S}C}' = (\text{Re}A_S', \text{Im}A_S', \text{Re}A_S', \text{Im}A_S')$.

III. Determine $\hat{v}_{S_1}^{(j)}$ and $\hat{v}_{S_2}^{(j)}$. Using eqs. (A.42) together with eq. (A.45) we find the last two equations. The first of eqs. (A.42) gives

$$[|X^{L,R}|^2 m_1^{(j)2} + |Y^{L,R}|^2 m_2^{(j)2} + 2m_1^{(j)} m_2^{(j)} \text{Im}(X^{L,R*} Y^{L,R})] + (L \leftrightarrow R) = [-2\text{Re}(A_0^{L*} X^{L,R}) m_1^{(j)} - 2\text{Im}(A_0^{L*} Y^{L,R}) m_2^{(j)}] - (L \leftrightarrow R) \quad (\text{A.49})$$

where $m_i^{(j)}$ are functions of $\hat{v}_S^{(j)}$ as given in eq. (A.47).

The second of eqs. (A.42) gives rise to

$$[m_1^{(j)} \text{Re}(A_S^* X^{L,R}) + m_2^{(j)} \text{Im}(A_S^* Y_{L,R})] - (L \leftrightarrow R) = -\hat{v}_{S_1}^{(j)} (\text{Re}A_0^L + m_1^{(j)} \text{Re}X^{L,R} + m_2^{(j)} \text{Im}Y^{L,R}) -\hat{v}_{S_2}^{(j)} (\text{Im}A_0^L + m_1^{(j)} \text{Im}X^{L,R} - m_2^{(j)} \text{Re}Y^{L,R}) -\hat{v}_{S_3}^{(j)} (\text{Re}A_0^R - m_1^{(j)} \text{Re}X^{R,L} - m_2^{(j)} \text{Im}Y^{R,L}) -\hat{v}_{S_4}^{(j)} (\text{Im}A_0^R - m_1^{(j)} \text{Im}X^{R,L} + m_2^{(j)} \text{Re}Y^{R,L}). \quad (\text{A.50})$$

IV. Substituting eqs. (A.47) and eqs. (A.48) in eq. (A.49) and eq. (A.50) we end up with a system of two coupled quadratic equations which are function of $\hat{v}_{S_1}^{(j)}$ and $\hat{v}_{S_2}^{(j)}$. This system can be solved numerically and typically provides two complex solutions (to be discarded) and two real ones. The real solutions for $\hat{v}_{S_1}^{(j)}$ and $\hat{v}_{S_2}^{(j)}$, once inserted in eq. (A.39), generate two sets of transformed amplitudes \vec{v}_0' and \vec{v}_{SC}' that leave the angular distribution invariant. One of them is connected to the identity whereas the other is not, exactly as it occurred with $\delta(\theta)$ and $\tilde{\delta}(\tilde{\theta})$. This completes the definition of the symmetry transformation of the $A_0^{L,R}$ and A_S amplitudes.

B Large recoil limit expressions

In this appendix we present the expressions of the observables P_i and M_i in the large recoil limit. These are useful to study qualitative properties of the observables as well as for

rough quantitative estimates.

$$|n_0|^2 = 2Q_1^2 Q_2^2 \xi_{\parallel}^2 \left(|\mathcal{C}_{10} - \mathcal{C}'_{10}|^2 + |(F\hat{s} \mathcal{C}_7^{\text{eff}} + \mathcal{C}_9^{\text{eff}}) - (F\hat{s} \mathcal{C}_7^{\text{eff}'} + \mathcal{C}_9^{\text{eff}'})|^2 \right), \quad (\text{B.1})$$

$$|n_{\parallel}|^2 = 2Q_1^2 \xi_{\perp}^2 \left(|\mathcal{C}_{10} - \mathcal{C}'_{10}|^2 + |(F\mathcal{C}_7^{\text{eff}} + \mathcal{C}_9^{\text{eff}}) - (F\mathcal{C}_7^{\text{eff}'} + \mathcal{C}_9^{\text{eff}'})|^2 \right), \quad (\text{B.2})$$

$$|n_{\perp}|^2 = 2Q_1^2 \xi_{\perp}^2 \left(|\mathcal{C}_{10} + \mathcal{C}'_{10}|^2 + |(F\mathcal{C}_7^{\text{eff}} + \mathcal{C}_9^{\text{eff}}) + (F\mathcal{C}_7^{\text{eff}'} + \mathcal{C}_9^{\text{eff}'})|^2 \right), \quad (\text{B.3})$$

$$\text{Re}(n_{\perp}^{\dagger} n_{\parallel}) = 4Q_1^2 \xi_{\perp}^2 \text{Re}[(F\mathcal{C}_7^{\text{eff}} + \mathcal{C}_9^{\text{eff}})\mathcal{C}_{10}^* - (F\mathcal{C}_7^{\text{eff}'} + \mathcal{C}_9^{\text{eff}'})\mathcal{C}'_{10}^*], \quad (\text{B.4})$$

$$\text{Im}(n_{\perp}^{\dagger} n_{\parallel}) = -4Q_1^2 \xi_{\perp}^2 \text{Im}[\mathcal{C}_{10}\mathcal{C}'_{10}^* + (F\mathcal{C}_7^{\text{eff}} + \mathcal{C}_9^{\text{eff}})(F\mathcal{C}_7^{\text{eff}'} + \mathcal{C}_9^{\text{eff}'})^*], \quad (\text{B.5})$$

$$\begin{aligned} \text{Re}(n_0^{\dagger} n_{\parallel}) &= 2Q_1^2 Q_2 \xi_{\parallel} \xi_{\perp} \left(|\mathcal{C}_{10} - \mathcal{C}'_{10}|^2 + |\mathcal{C}_9^{\text{eff}} - \mathcal{C}_9^{\text{eff}'}|^2 + F^2 \hat{s} |\mathcal{C}_7^{\text{eff}} - \mathcal{C}_7^{\text{eff}'}|^2 \right. \\ &\quad \left. + F(1 + \hat{s}) \text{Re}[(\mathcal{C}_7^{\text{eff}} - \mathcal{C}_7^{\text{eff}'})(\mathcal{C}_9^{\text{eff}} - \mathcal{C}_9^{\text{eff}'})^*] \right), \end{aligned} \quad (\text{B.6})$$

$$\text{Im}(n_0^{\dagger} n_{\parallel}) = -2Q_1^2 Q_2 \xi_{\parallel} \xi_{\perp} \text{Im}[F(1 - \hat{s})(\mathcal{C}_7^{\text{eff}} - \mathcal{C}_7^{\text{eff}'})(\mathcal{C}_{10} - \mathcal{C}'_{10})^*], \quad (\text{B.7})$$

$$\begin{aligned} \text{Re}(n_0^{\dagger} n_{\perp}) &= 2Q_1^2 Q_2 \xi_{\parallel} \xi_{\perp} \text{Re}[\left((F(1 + \hat{s})\mathcal{C}_7^{\text{eff}} + \mathcal{C}_9^{\text{eff}}) + (F(1 - \hat{s})\mathcal{C}_7^{\text{eff}'} + \mathcal{C}_9^{\text{eff}'}) \right) \mathcal{C}_{10}^* \\ &\quad - \left((F(1 - \hat{s})\mathcal{C}_7^{\text{eff}} + \mathcal{C}_9^{\text{eff}'}) + (F(1 + \hat{s})\mathcal{C}_7^{\text{eff}'} + \mathcal{C}_9^{\text{eff}'}) \right) \mathcal{C}'_{10}^*], \end{aligned} \quad (\text{B.8})$$

$$\begin{aligned} \text{Im}(n_0^{\dagger} n_{\perp}) &= 2Q_1^2 Q_2 \xi_{\parallel} \xi_{\perp} \left(2\text{Im}[\mathcal{C}_{10}\mathcal{C}'_{10}^* + F^2 \hat{s} \mathcal{C}_7^{\text{eff}} \mathcal{C}_7^{\text{eff}'*} + \mathcal{C}_9^{\text{eff}} \mathcal{C}_9^{\text{eff}'*}] - \text{Im}[F((1 - \hat{s})\mathcal{C}_7^{\text{eff}} \right. \\ &\quad \left. + (1 + \hat{s})\mathcal{C}_7^{\text{eff}'})\mathcal{C}_9^{\text{eff}*} - F((1 + \hat{s})\mathcal{C}_7^{\text{eff}} + (1 - \hat{s})\mathcal{C}_7^{\text{eff}'})\mathcal{C}_9^{\text{eff}'*}] \right), \end{aligned} \quad (\text{B.9})$$

$$|n_{\perp}|^2 - |n_{\parallel}|^2 = 8Q_1^2 \xi_{\perp}^2 \left(\text{Re}[\mathcal{C}_{10}\mathcal{C}'_{10}^*] + \text{Re}[(F\mathcal{C}_7^{\text{eff}} + \mathcal{C}_9^{\text{eff}})(F\mathcal{C}_7^{\text{eff}'} + \mathcal{C}_9^{\text{eff}'})^*] \right), \quad (\text{B.10})$$

$$|n_{\parallel}|^2 + |n_{\perp}|^2 = 4Q_1^2 \xi_{\perp}^2 \left(|\mathcal{C}_{10}|^2 + |\mathcal{C}'_{10}|^2 + |F\mathcal{C}_7^{\text{eff}} + \mathcal{C}_9^{\text{eff}}|^2 + |F\mathcal{C}_7^{\text{eff}'} + \mathcal{C}_9^{\text{eff}'}|^2 \right), \quad (\text{B.11})$$

$$M_1 = -\frac{2m_{\ell}^2}{q^2 \beta_{\ell}^2} \frac{|\mathcal{C}_{10}|^2 + |\mathcal{C}'_{10}|^2 - |F\mathcal{C}_7^{\text{eff}} + \mathcal{C}_9^{\text{eff}}|^2 - |F\mathcal{C}_7^{\text{eff}'} + \mathcal{C}_9^{\text{eff}'}|^2}{|\mathcal{C}_{10}|^2 + |\mathcal{C}'_{10}|^2 + |F\mathcal{C}_7^{\text{eff}} + \mathcal{C}_9^{\text{eff}}|^2 + |F\mathcal{C}_7^{\text{eff}'} + \mathcal{C}_9^{\text{eff}'}|^2}, \quad (\text{B.12})$$

$$M_2 = \frac{4m_{\ell}^2}{q^2}. \quad (\text{B.13})$$

where the following short-hand notation has been used

$$F \equiv \frac{2\hat{m}_b}{\hat{s}}, \quad Q_1 \equiv \sqrt{2} N m_B (1 - \hat{s}), \quad Q_2 \equiv \frac{1}{2\sqrt{2}\hat{m}_{K^*}\sqrt{\hat{s}}} (1 - \hat{s}). \quad (\text{B.14})$$

References

- [1] BABAR collaboration, B. Aubert et al., *Measurements of branching fractions, rate asymmetries and angular distributions in the rare decays $B \rightarrow K\ell^+\ell^-$ and $B \rightarrow K^*\ell^+\ell^-$* , *Phys. Rev. D* **73** (2006) 092001 [[hep-ex/0604007](#)] [[INSPIRE](#)].
- [2] BELLE collaboration, J.-T. Wei et al., *Measurement of the Differential Branching Fraction and Forward-Backward Asymmetry for $B \rightarrow K^{(*)}\ell^+\ell^-$* , *Phys. Rev. Lett.* **103** (2009) 171801 [[arXiv:0904.0770](#)] [[INSPIRE](#)].

- [3] CDF collaboration, T. Aaltonen et al., *Observation of the Baryonic Flavor-Changing Neutral Current Decay $\Lambda_b \rightarrow \Lambda\mu^+\mu^-$* , *Phys. Rev. Lett.* **107** (2011) 201802 [[arXiv:1107.3753](#)] [[INSPIRE](#)].
- [4] CDF collaboration, T. Aaltonen et al., *Measurements of the Angular Distributions in the Decays $B \rightarrow K^{(*)}\mu^+\mu^-$ at CDF*, *Phys. Rev. Lett.* **108** (2012) 081807 [[arXiv:1108.0695](#)] [[INSPIRE](#)].
- [5] F. Krüger and J. Matias, *Probing new physics via the transverse amplitudes of $B^0 \rightarrow K^{(*)}(\rightarrow K^-\pi^+)\ell^+\ell^-$ at large recoil*, *Phys. Rev.* **D 71** (2005) 094009 [[hep-ph/0502060](#)] [[INSPIRE](#)].
- [6] U. Egede, T. Hurth, J. Matias, M. Ramon and W. Reece, *New observables in the decay mode $\bar{B}_d \rightarrow \bar{K}^{(*)}\ell^+\ell^-$* , *JHEP* **11** (2008) 032 [[arXiv:0807.2589](#)] [[INSPIRE](#)].
- [7] LHCb collaboration, R. Aaij et al., *Differential branching fraction and angular analysis of the decay $B^0 \rightarrow K^{*0}\mu^+\mu^-$* , [arXiv:1112.3515](#) [[INSPIRE](#)].
- [8] U. Egede, T. Hurth, J. Matias, M. Ramon and W. Reece, *New physics reach of the decay mode $\bar{B} \rightarrow \bar{K}^{*0}\ell^+\ell^-$* , *JHEP* **10** (2010) 056 [[arXiv:1005.0571](#)] [[INSPIRE](#)].
- [9] D. Becirevic and E. Schneider, *On transverse asymmetries in $B \rightarrow K^{*0}\ell^+\ell^-$* , *Nucl. Phys.* **B 854** (2012) 321 [[arXiv:1106.3283](#)] [[INSPIRE](#)].
- [10] C. Bobeth, G. Hiller and D. van Dyk, *The Benefits of $\bar{B} \rightarrow \bar{K}^*l^+l^-$ Decays at Low Recoil*, *JHEP* **07** (2010) 098 [[arXiv:1006.5013](#)] [[INSPIRE](#)].
- [11] A.Y. Korchin and V.A. Kovalchuk, *Asymmetries in $\bar{B}_d^0 \rightarrow \bar{K}^{*0}e^+e^-$ decay and contribution of vector resonances*, [arXiv:1111.4093](#) [[INSPIRE](#)].
- [12] C. Bobeth, G. Hiller and D. van Dyk, *More Benefits of Semileptonic Rare B Decays at Low Recoil: CP-violation*, *JHEP* **07** (2011) 067 [[arXiv:1105.0376](#)] [[INSPIRE](#)].
- [13] A.K. Alok et al., *New Physics in $b \rightarrow s\mu^+\mu^-$: CP-Violating Observables*, *JHEP* **11** (2011) 122 [[arXiv:1103.5344](#)] [[INSPIRE](#)].
- [14] E. Lunghi and A. Soni, *An improved observable for the forward-backward asymmetry in $B \rightarrow K^*\ell^+\ell^-$ and $B_s \rightarrow \phi\ell^+\ell^-$* , *JHEP* **11** (2010) 121 [[arXiv:1007.4015](#)] [[INSPIRE](#)].
- [15] A.K. Alok et al., *New Physics in $b \rightarrow s\mu^+\mu^-$: CP-Conserving Observables*, *JHEP* **11** (2011) 121 [[arXiv:1008.2367](#)] [[INSPIRE](#)].
- [16] A.Y. Korchin and V.A. Kovalchuk, *Contribution of low-lying vector resonances to polarization observables in $\bar{B}_d^0 \rightarrow \bar{K}_0^{*0}e^+e^-$ decay*, *Phys. Rev.* **D 82** (2010) 034013 [[arXiv:1004.3647](#)] [[INSPIRE](#)].
- [17] A. Bharucha and W. Reece, *Constraining new physics with $B \rightarrow K^*\mu^+\mu^-$ in the early LHC era*, *Eur. Phys. J.* **C 69** (2010) 623 [[arXiv:1002.4310](#)] [[INSPIRE](#)].
- [18] A.K. Alok et al., *New-physics contributions to the forward-backward asymmetry in $B \rightarrow K^*\mu^+\mu^-$* , *JHEP* **02** (2010) 053 [[arXiv:0912.1382](#)] [[INSPIRE](#)].
- [19] E. Lunghi and J. Matias, *Huge right-handed current effects in $B \rightarrow K^*(K\pi)\ell^+\ell^-$ in supersymmetry*, *JHEP* **04** (2007) 058 [[hep-ph/0612166](#)] [[INSPIRE](#)].
- [20] C. Bobeth, G. Hiller and G. Piranishvili, *CP Asymmetries in $\bar{B} \rightarrow \bar{K}^*(\rightarrow \bar{K}\pi)\bar{\ell}\ell$ and Untagged $\bar{B}_s, B_s \rightarrow \phi(\rightarrow K^+K^-)\bar{\ell}\ell$ Decays at NLO*, *JHEP* **07** (2008) 106 [[arXiv:0805.2525](#)] [[INSPIRE](#)].

- [21] W. Altmannshofer et al., *Symmetries and Asymmetries of $B \rightarrow K^* \mu^+ \mu^-$ Decays in the Standard Model and Beyond*, *JHEP* **01** (2009) 019 [[arXiv:0811.1214](#)] [[INSPIRE](#)].
- [22] M. Beneke and T. Feldmann, *Symmetry breaking corrections to heavy to light B meson form-factors at large recoil*, *Nucl. Phys.* **B 592** (2001) 3 [[hep-ph/0008255](#)] [[INSPIRE](#)].
- [23] T. Huber, E. Lunghi, M. Misiak and D. Wyler, *Electromagnetic logarithms in $\bar{B} \rightarrow X(s) \ell^+ \ell^-$* , *Nucl. Phys.* **B 740** (2006) 105 [[hep-ph/0512066](#)] [[INSPIRE](#)].
- [24] P. Gambino, M. Gorbahn and U. Haisch, *Anomalous dimension matrix for radiative and rare semileptonic B decays up to three loops*, *Nucl. Phys.* **B 673** (2003) 238 [[hep-ph/0306079](#)] [[INSPIRE](#)].
- [25] M. Gorbahn and U. Haisch, *Effective Hamiltonian for non-leptonic $|\Delta F| = 1$ decays at NNLO in QCD*, *Nucl. Phys.* **B 713** (2005) 291 [[hep-ph/0411071](#)] [[INSPIRE](#)].
- [26] C. Bobeth, P. Gambino, M. Gorbahn and U. Haisch, *Complete NNLO QCD analysis of $\bar{B} \rightarrow X_s \ell^+ \ell^-$ and higher order electroweak effects*, *JHEP* **04** (2004) 071 [[hep-ph/0312090](#)] [[INSPIRE](#)].
- [27] M. Misiak and M. Steinhauser, *NNLO QCD corrections to the $\bar{B} \rightarrow X_s \gamma$ matrix elements using interpolation in $m(c)$* , *Nucl. Phys.* **B 764** (2007) 62 [[hep-ph/0609241](#)] [[INSPIRE](#)].
- [28] S. Descotes-Genon, D. Ghosh, J. Matias and M. Ramon, *Exploring New Physics in the $C7-C7'$ plane*, *JHEP* **06** (2011) 099 [[arXiv:1104.3342](#)] [[INSPIRE](#)].
- [29] A. Khodjamirian, T. Mannel, A. Pivovarov and Y.-M. Wang, *Charm-loop effect in $B \rightarrow K^{(*)} \ell^+ \ell^-$ and $B \rightarrow K^* \gamma$* , *JHEP* **09** (2010) 089 [[arXiv:1006.4945](#)] [[INSPIRE](#)].
- [30] M. Beneke, T. Feldmann and D. Seidel, *Systematic approach to exclusive $B \rightarrow V \ell^+ \ell^-$, V gamma decays*, *Nucl. Phys.* **B 612** (2001) 25 [[hep-ph/0106067](#)] [[INSPIRE](#)].
- [31] M. Beneke, T. Feldmann and D. Seidel, *Exclusive radiative and electroweak $b \rightarrow d$ and $b \rightarrow s$ penguin decays at NLO*, *Eur. Phys. J.* **C 41** (2005) 173 [[hep-ph/0412400](#)] [[INSPIRE](#)].
- [32] H. Asatrian, H. Asatrian, C. Greub and M. Walker, *Two loop virtual corrections to $B \rightarrow X_s$ lepton+ lepton- in the standard model*, *Phys. Lett.* **B 507** (2001) 162 [[hep-ph/0103087](#)] [[INSPIRE](#)].
- [33] S. Descotes-Genon, D. Ghosh, J. Matias and M. Ramon, *Exploring New Physics in $C_7 - C_7'$* , *PoS(EPS-HEP2011)170* [[arXiv:1202.2172](#)] [[INSPIRE](#)].
- [34] W. Altmannshofer, P. Paradisi and D.M. Straub, *Model-Independent Constraints on New Physics in $b \rightarrow s$ Transitions*, *JHEP* **04** (2012) 008 [[arXiv:1111.1257](#)] [[INSPIRE](#)].
- [35] FOR THE LHCb collaboration, D. Martinez Santos, *Rare Decays in $LHCb$* , [arXiv:1201.5359](#) [[INSPIRE](#)].
- [36] FOR THE CMS collaboration, L. Martini, *Search for $B_s \rightarrow \mu\mu$ and $B_0 \rightarrow \mu\mu$ decays in CMS*, [arXiv:1201.4257](#) [[INSPIRE](#)].
- [37] LHCb collaboration, R. Aaij et al., *Strong constraints on the rare decays $B_s \rightarrow \mu^+ \mu^-$ and $B^0 \rightarrow \mu^+ \mu^-$* , [arXiv:1203.4493](#) [[INSPIRE](#)].
- [38] J. Matias, in preparation.

